THE GEOCHEMISTRY AND MINERALOGY OF GOSSANS OVERLYING NICKEL-COPPER SULPHIDE MINERALISATION

by

ROGER LAWRENCE BROTHERTON

A Thesis Submitted for the Degree
of Doctor of Philosophy
University of London

Department of Geology,
Imperial College of Science and Technology,
London

July 1979

ROGER LAWRENCE BROTHERTON

THE GEOCHEMISTRY AND MINERALOGY OF GOSSANS
OVERLYING NICKEL-COPPER SULPHIDE MINERALISATION

ABSTRACT

A petrographic and geochemical study of 17 oxidised nickel sulphide ore bodies from the semi-arid Archean Shield regions of southern Africa and Western Australia indicates that these deposits undergo qualitatively similar near surface alteration; the pentlandite-pyrrhotite primary assemblage of each being progressively replaced by one of secondary violarite and iron disulphides. The latter give way abruptly to iron oxide-rich gossans above recent water table levels. The resulting zoned alteration sequences are very similar to those observed in the Kambalda and other Western Australian deposits by previous workers. Each is the mineralogical expression of an electrochemical corrosion (oxidation) cell that is developed within the ore body due to its differential aeration by oxygenated near surface ground waters.

Quantitative inter-deposit variation in alteration zone development is explained by a conceptual model that relates the initiation and subsequent growth of secondary (supergene) alteration to a progressive exhumation of the parent ore profile under near surface lateratisation conditions. The formation environment of nickel gossans is inferred in terms of Eh, pH and aqueous metal concentrations from a genetic interpretation of the principal mineralogical and geochemical features of these rocks and of their associated oxidate minerals. The characteristic occurrence of silica enrichment in nickel gossans is explained by an extension of the supergene formation model. This relates silica influx to the progressive exhumation of the gossan zone above the dry season water table associated with the active lateratisation of adjacent silicate rocks. The detailed arrangement of silica content and of textural forms in the Pikwe (Botswana) gossan is explained by a geological model which relates the observed depth distribution of these phenomena to a gradual replacement of laterite-forming conditions by a semi-arid climate in the late Tertiary.

The principal features of surface nickel gossans - geochemistry, relic sulphide textures and bulk mineralogy, are utilised to develop new quantitative techniques for sulphide ore tenor prediction. These techniques are based on Multiple Linear Regression Analysis. Near massive to massive sulphide nickel and copper tenor values, and overall nickel grade values are accurately predicted by the development of a battery of ore metal tenor predictor equations. These statistically relate linear combinations of surface gossan variables to the metal tenor of the equivalent sulphide ore. The closeness of predictive fit (accuracy) values, (at the 90 percent confidence level), of the equations relating surface gossan geochemistry to sulphide metal tenor are as follows: Near massive to massive sulphide nickel tenor, $\pm$ 15 percent; near massive to massive sulphide copper tenor, $\pm$ 20 percent; overall nickel grade, $\pm$ 35 percent. The devised method has several important methodological and economic advantages over previously available nickel sulphide prediction techniques.

ACKNOWLEDGEMENTS

ABBREVIATIONS

The following abbreviations apply throughout this thesis

General		Mineral Names	
m.	metres	Po	Pyrrhotite
Km.	kilometres	Pn	Pentlandite
ppm	parts per million	Vl	Violarite
gm.	gramme	Vpn	Violarite after pentlandite
equv.	equivalents	Vpo	Violarite after pyrrhotite
SHE	Standard Hydrogen Electrode	Cp/ccp	Chalcopyrite
Acc	Accessory	Cov	Covellite
N/A	not analysed	Mc	Marcasite
n.d.	not detected	Py	Pyrite
B.P.	before present	Cub	Cubanite
b.s.	below surface	Val	Valeriite
v'l'e	value	Mil	Millerite
W.A.	Western Australia	Mt	Magnetite
Rhod.	Rhodesia	FCr/Cr	Ferrochromite
Bots.	Botswana	Sil	Silicate
		Goe/Gt	Goethite
		Hem/Hm	Hematite
		SiO_2/Sl	Silica
		Carb/Cab	Carbonate
		Sid	Siderite
		Mag/Mgs	Magnesite
		Ca	Calcite
		Dol	Dolomite
		Hun	Huntite
		Gyp	Gypsum
		Njr	Natrojarosite
		Nal	Natroalunite
		Pact	Paratacamite

CONTENTS

CONTENTS (CONTINUED)

CONTENTS (CONTINUED)

CONTENTS (CONTINUED)

CONTENTS (CONTINUED)

CONTENTS (CONTINUED)

CONTENTS (CONTINUED)

CONTENTS (CONTINUED)

CONTENTS (CONTINUED)

CONTENTS (CONTINUED)

CONTENTS (CONTINUED)

CONTENTS (CONCLUDED)

LIST OF FIGURES

FIGURES (CONTINUED)

FIGURES (CONTINUED)

FIGURES (CONTINUED)

FIGURES (CONTINUED)

FIGURES (CONCLUDED)

LIST OF TABLES

TABLES (CONTINUED)

TABLES (CONCLUDED)

CHAPTER 1 - INTRODUCTION

Introduction and review of previous work on base metal sulphide alteration

Sulphide minerals are chemically unstable in near surface weathering environments and oxidise to form iron oxide-rich mineral assemblages. These oxidised rocks crop out as gossans. Strictly, gossans are rocks derived from sulphide assemblages of economic significance, (Nelson and Nelson, 1967). Exploration geologists have long been interested in these rocks because they are commonly the only visible surface expression of underlying mineralisation. The problem of gossan recognition is, therefore, of considerable economic importance.

For the geologist, however, this problem is complicated by the practical difficulty of distinguishing true gossans from other, unrelated, iron oxide-rich rocks. These other types include : (i) sedimentary ironstones and laterites, (non-gossans); (ii) iron-rich outcrops derived from sulphides of generally low economic value - notably pyrite and pyrrhotite, and termed pseudogossans, (Hawkes and Webb, 1962); and (iii) oxidised gossan-like rocks derived from disseminated sulphide deposits, (leached cappings). Initially, therefore, it is important to be able to distinguish true gossans from these unrelated rocks of superficially similar appearance.

Once the significance of the outcrop has been established, however, the principal problem facing the economic geologist is one of interpretation. Here, evaluation of the gossan outcrop in terms of the underlying sulphide mineralisation is the chief method of approach. In this way, it may be possible to obtain qualitative and, potentially, quantitative information on the nature of the sulphide ore. In consequence, the recognition of all types of leached rock outcrops and the subsequent evaluation of true gossan occurrences form two critical aspects of mineral exploration technology.

The oxidation of primary sulphide to gossan is a complex process and recognisable intermediate stages are generally exhibited. Several important base metal ore types in fact, exhibit conspicuous near surface alteration zoning.

Oxidising copper - zinc sulphide ores of acid volcanic affiliation ideally possess the following vertical alteration sequence : primary chalcopyrite - sphalerite ore at depth; a supergene enriched assemblage containing copper-rich secondary sulphides; a narrow earthy precious metal-rich lower oxide zone; a sulphate zone; and a

carbonate-rich upper oxide zone, (Blain and Andrew, 1977).

In contrast, oxidising lead - zinc ores of carbonate affiliation generally show the following vertical alteration sequence: primary galena - sphalerite ore at depth; an enriched lead and zinc carbonate assemblage with remnant sulphides; an oxide zone containing zinc carbonates and sulphates; and a siliceous hematite - manganese gossan, (Heyl and Bozion, 1962).

Oxidising lead - zinc ores of non-carbonate association likewise generally possess well-developed alteration profiles, (Blain and Andrew, op.cit.). These profiles typically consist of primary galena - sphalerite ore overlain by a thick (20 - 30m.) cerussite enriched zone that also comprises variable quantities of smithsonite, anglesite, silver sulphosalts and persistent sulphides. This enriched zone is overlain in turn by a thick (up to 50m.) oxide zone. This typically consists of cerussite, smithsonite and silver halides. The top of the oxide zone is capped by a siliceous cerussitic gossan of between 5 and 10m. thickness.

Conspicuous zoned alteration sequences are also exhibited by oxidising lead - zinc - silver vein deposits such as those at Keno Hill, (Yukon). Both the zonal configurations and the mineralogy of these sequences are, however, typically complex. In general though, the vertical alteration profile consists of primary ore; a silver enriched zone of variable thickness, and an overlying oxide zone.

Zoned near surface alteration occurs in oxidising nickel sulphide ores of ultramafic association. In these ores, the generalised vertical profile commences with primary pyrrhotite - pentlandite ore at depth. It then passes via an overlying transition zone into a secondary sulphide assemblage of violarite and pyrite and/or marcasite. This violarite - secondary iron disulphide assemblage remains chemically stable up to the level of the water table. A thin, typically patchy development of supergene enrichment may be present somewhat below this horizon.

An oxide zone characteristically overlies the secondary sulphides and extends upwards from the water table. It may be up to 45m. thick, and consists chiefly of goethite and silica with generally minor but variable proportions of hematite and oxidate minerals; principally carbonates and sulphates. The oxide zone may be capped by a siliceous gossan. This is especially true of the deeply-weathered Western Australian nickel deposits.

The secondary alteration of sulphide ore has long been considered to have an electrochemical basis, (Wells, 1914), and supergene alteration is now generally considered to be caused by slow exhumation of the ore body relative to the Eh gradient of the investing groundwater regime, (Blain and Brotherton, 1975). Profile exhumation causes disequilibrium between the Eh of the primary ore assemblage and that of the groundwater. In consequence, the equilibrium Eh necessary for supergene alteration to occur is exceeded, and the primary sulphides become chemically unstable with respect to the local Eh environment. Alteration to secondary (supergene) sulphides will, hence, occur in an attempt to restore Eh equilibrium with the investing groundwater.

These alteration reactions take place as oxidation half-cells, and as a result, electrons are released and are conducted away to be consumed elsewhere in complimentary reduction half-cell reactions. Continuous exhumation of the ore body causes a progressive development of supergene alteration, with electrons being conducted through the ore profile to the sites of these half-cell reduction reactions.

It is likely that the sulphide alteration process is driven by the reduction of oxygen-containing species in air-saturated groundwaters at the water table, and that oxygen or oxy-compounds are probably directly involved in these reduction half-cell reactions (Sato and Mooney, 1960). However, Thornber and Nickel, (1976) indicate that these species are not necessarily involved in the complementary oxidation reactions. In any event, the oxidation-reduction reactions produce an electrical polarisation of the ore body. This occurs because the release of electrons at depth leads to the formation of a positively-charged anode in that region, while the replenishment of oxygen at the water table – caused by continuous electron consumption, leads to the formation of a negatively-charged cathode region therein. In consequence, electrical current flows from the deep anode towards the shallow cathodic region, and the profile acts as a large electrochemical corrosion cell, (Thornber, 1975A). The overall electrical neutrality of the system is maintained by a complementary downward movement of positively charged species from cathode to anode, and occurs through the agency of groundwater circulation.

Thus, a continual development of supergene alteration is likely to occur as long as the prevailing Eh regime of investing groundwater causes electrical polarisation and current flow in the ore profile. In geological terms, this implies a generally

continuous exhumation of the ore body relative to the water table, (Blain and Brotherton, op.cit.).

The principal features of sulphide alteration zoning have been recognised for many years, (Penrose, 1894). It was not until 1900 however, that the closely-related phenomenon of supergene enrichment was independently explained by three workers: Emmons, (1901); Van Hise, (1901); and Weed, (1901). These authors indicated that supergene enrichment of oxidising sulphide assemblages was due to the reaction of sulphide with metal species carried down by groundwater from the corresponding zone of sulphide leaching.

This concept was supported by early laboratory work on copper sulphide enrichment by Winchell, (1903), and by studies of the chemical mechanisms of the enrichment process for copper sulphide ores made by Zies, et.al., (1916).

Several early reviews of the chemistry and field relations of supergene copper enrichment were made – notably by Kemp, (1906); Ransome, (1910); and Emmons, (1917). A more recent review and summary of copper oxidation phenomena is given by Anderson, (1955). Modern work on copper enrichment features, (Sillitoe and Clark, 1969), indicates that chalcopyrite – bornite – pyrite assemblages react with descending soluble species to give assemblages rich in chalcopyrite, djurleite, digenite and anilite.

Supergene alteration of lead – zinc orebodies is also common – Brown, (1936); Taylor, (1958); and Takahashi, (1960). Typically, however, primary lead and zinc sulphides exhibit a conspicuous lack of supergene enrichment, and give way to stable secondary assemblages of carbonates and sulphates.

The supergene alteration of nickel sulphide ores was first documented by Woodall and Travis, (1969) at Kambalda, Western Australia. Similar sequences have since been described at other Western Australian deposits, namely; Redross (Dalgarno, 1972), Mt. Windarra (Watmuff, 1974), Spargoville (Wilmshurst, 1975) and Agnew (Nickel et.al., 1976). The physico-chemical implications of the generalised alteration sequence have been developed by Thornber (1972), Nickel (1973), and Nickel et.al. (1974). An electrochemical model of nickel sulphide alteration, based on Kambalda, is presented by Thornber (1975A, op.cit.). This model is based on the existence of a galvanic corrosion cell that is driven by the reduction of

oxygen species in the zone of sulphide leaching at the water table. The principal mineralogical features of the Thornber model are now explained.

Pentlandite is the first sulphide to undergo alteration and does so because it possesses the lowest (most negative) oxidation potential in the primary ore assemblage. It undergoes an in situ replacement by violarite. The violarite forms as a direct pseudomorphic replacement and the external form of the pentlandite is retained. The reaction also brings about a substantial volume reduction which is characteristically manifested as an exaggerated development of the pentlandite octahedral cleavage structure. As a result of this alteration, excess nickel and iron are released from the pentlandite lattice. The iron typically precipitates as siderite. The nickel however, generally combines with adjacent pyrrhotite to form a second violarite phase. Up to one third of the nickel content of pentlandite may be released through this reaction. The second violarite phase (Vpo) is both chemically and texturally distinct from that after pentlandite (Vpn). It is iron-rich and nickel-poor relative to Vpn and replaces pyrrhotite in a feather-like lamellar form along the 001 parting directions.

Alteration of the remainder of the pyrrhotite takes place after pentlandite has been totally converted to violarite. The alteration occurs since pyrrhotite possesses the next lowest oxidation potential in the ore assemblage. Hence, it becomes chemically unstable and alters to secondary iron disulphide: pyrite and/or marcasite. In the Thornber model, alteration of pentlandite and pyrrhotite constitute deep anodic oxidation processes.

The resulting violarite – "pyrite" secondary sulphide assemblage, together with primary pyrite and chalcopyrite, remains chemically stable up to the level of the water table. At this point, the high Eh environment associated with oxygen saturated groundwater causes the sulphide assemblage to undergo rapid corrosive alteration, (shallow anodic oxidation). As a result, ore metals, iron and sulphur, are released into the groundwater environment as oxidised species. The ore metals may subsequently be trapped by co-precipitation with ferric oxides. Alternatively, they may retain a mobile aqueous form and percolate back down through the secondary sulphide ore profile. Here, they may react with the secondary sulphides to form enriched violarite, pyrite or other metal-rich phases. Alternatively, they may pass out of the ore zone and be precipitated as carbonates and sulphates in the

relatively high pH environment of the wall rocks, (Thornber and Nickel, op.cit.).

A chemical study of the pre-mining nickel sulphide alteration environment at Kambalda is presented by Thornber (1975B). A series of pH and Eh measurements are made on co-existing artifically prepared groundwaters and natural sulphide ores. The results indicate that the Eh – pH environment of primary ore approximates -0.3V (SHE), (Eh), and 8 – 9 (pH). In contrast, the results for the equivalent environment of shallow weathering (corroding supergene) ore respectively approximate +0.3V (SHE), and 5 – 6. These results agree favourably with the equivalent natural environments inferred from the alteration model briefly outlined above. Further, Thornber reports that the results of a series of leaching, simulation (Gel), and resistivity experiments on Kambalda ores similarly support his genetic model; namely, that galvanic corrosion due to differential aeration supplies the driving force behind near surface nickel sulphide alteration.

The brief review of previous work on the secondary (supergene) alteration of base metal ores is now concluded. The results of this work indicate that the formation of oxide zones above base-metal sulphide deposits represents the final stage in the near surface alteration of these ores. Thus gossans are derived from secondary assemblages and not from the primary sulphides. As a result, knowledge of the likely mineralogy, geochemistry and textural relations of secondary (supergene) ore assemblages is vital to any attempt at evaluation of the equivalent gossans.

A brief review of previous work on gossan discovery and evaluation

As previously noted, the evaluation of gossan outcrops in terms of the economic potential of equivalent sulphide presents a major problem in mineral exploration. The subject was first systematically investigated by Locke and his associates working in the porphyry copper province of the south-west United States, (Morse and Locke, 1924; Locke, 1926). These workers recognised that there were definite textural relationships between copper and iron sulphides and their oxidised derivatives. For instance, they were able to distinguish between limonites after disseminated chalcopyrite and pyrite on the basis of textural criteria. Thus, limonite after chalcopyrite was observed to form directly at the oxidation site, while that after pyrite was generally transported away before being precipitated. Consequently, recognition of the significance of limonite textures enabled Locke, within specified

geographical areas, to make empirical estimates of sulphide copper grade from oxidised outcrops.

Locke's early work on disseminated copper deposits was extended to gossans over massive sulphide by Blanchard and Boswell. These workers initially continued Locke's work on the textural recognition of limonite after chalcopyrite and pyrite, (Blanchard and Boswell, 1925). They recognised three types of limonite after these minerals: Indigenous – deposited in situ; Transported – deposited up to several centimetres from the oxidation site; and Exotic – deposited a relatively long distance from the oxidation site. Interpretation of the genetic significance of these limonite types allowed these workers to deduce the provenance of limonite in massive oxidised copper gossan outcrops and, subsequently, to make empirical estimations of the copper grade of the original sulphide ore.

A parallel study on the oxidation products of sphalerite and galena, however, (Boswell and Blanchard, 1927), indicated that few inferences about the nature of parent lead – zinc ores could be made from limonite textures.

The principal contribution of Blanchard and Boswell to the field of gossan evaluation was however, their work on relict sulphide textures, (Boswell and Blanchard, 1929). Here they noted that many sulphide minerals preferentially oxidise along cleavage and fracture planes to give a generally characteristic regular cell-like pattern or boxwork that is generally retained after the completion of leaching. Further, their work showed that boxwork retention was semi-quantitatively related to the proportion of supergene silica that is incorporated within the boxwork structure.

As a result of this discovery, these workers made a series of studies of boxwork textures after various ore minerals: bornite and tetrahedrite, (Blanchard and Boswell, 1930); galena and sphalerite, (Blanchard and Boswell, 1934); molybdenite, (Blanchard and Boswell, 1935); and arseno pyrite and chromite. (Blanchard, 1942). The results of this work promoted the textural evaluation of gossans to a new significance, and allowed a prediction of sulphide metal grade to be made directly from suitable gossan outcrops for several important base metal ore-types.

In continuation of this work, a detailed study of boxwork chemistry and mineralogy was made by Blanchard (1944). Here Blanchard notes that the compositional range of boxwork material is typically variable with respect to iron oxide and silica

contents. And he indicates that boxwork cell walls are generally composed of silicified limonite: a finding that confirms the importance of supergene silica in the preservation of boxwork structures during sulphide leaching.

The empirical field-based studies of Blanchard and his co-workers were significantly aided by parallel work on the supergene alteration of sulphide deposits and on laboratory studies of natural gossan-forming minerals. Chief among the latter were the investigations of sulphide leaching by Buehler and Gottschalk, (1910), of iron oxide mineralogy, chemistry and stability relations carried out by Posnjak and Merwin, (1919 and 1922), and Peacock (1942). And the studies of iron oxide and silica aqueous chemistry performed by Lovering (1923), Moore and Maynard (1929) and Roy (1945).

The work of Roland Blanchard, partly reviewed in 1939, (Blanchard, 1939), and summarised in the book "Interpretation of Leached Outcrops", published posthumously in 1968, remains a valuable contribution to research on the use of gossans in the prediction of parent sulphide metal grades.

The problems of outcrop evaluation were, however, also studied by other investigators in the pre-war period, notably by Schmitt, (1939). This worker advocated the development of more widely applicable structural, lithological and mineralogical evaluation criteria, rather than reliance on a small number of locally derived textural features.

In the early post-war period, however, little new work was done on base metal outcrop evaluation, apart from a rather inconclusive study of lead - zinc evaluation criteria by Kelley, (1958). The two reviews of base metal criteria that were published at this time - Kelley, et.al., (1958), and Whitten, (1966), present little new data of any significance and draw substantially on Blanchard's earlier work in this field.

The discovery, in 1966, of nickel gossan outcrops in the Eastern Goldfields region of Western Australia marked the commencement of investigations on this type of leached outcrop. From the outset, work on nickel gossans was orientated towards the development of recognition and evaluation criteria based on geochemistry and on pseudomorphed sulphide textures. This was principally because the typically highly siliceous Western Australian nickel gossans were unsuited to the classic "Locke -

Blanchard" methods of cellular leached texture evaluation, but also because rapid methods of chemical analysis were by now available.

The following review is concerned exclusively with investigations based on Australian nickel gossans, since no work has been published on nickel – copper gossans in southern Africa.

Work on the recognition of nickel gossans has concentrated chiefly on the development of statistics-based techniques permitting these rocks to be distinguished from other ironstones on the basis of rock geochemistry.

Clema and Stevens-Hoare, (1973), note that nickel gossans are typified by high nickel and copper contents, low manganese and chromium contents, and very low lead and zinc contents. Whereas in contrast, laterites are typified by high Ni and Cr, medium to low Mn and low Cu, Pb and Zn. Further, shales and cherts typically exhibit high to medium Ni, Zn and Mn, medium Cr, medium to low Cu and low Pb contents. Wad is characterised by very high Mn, medium Ni, Cu and Zn, and low Pb and Cr. Further, these authors indicate that veins and fault-associated rocks may exhibit high Cu, if sulphides are present, but are otherwise typified by medium Pb, Mn and Zn contents, and by medium to low Ni and Cr contents.

These workers subsequently devise an empirical method of distinguishing nickel gossans from the other ironstones types documented. They derive two significant metal combinations, These are ratioed against total metal content in Wt.% units and the two functions thereby obtained are then individually plotted against total metal content on two-dimensional scattergrams. The two derived functions are: $\frac{Ni + Cu}{M}$ and $\frac{Mn + Cr}{M}$, where M equals the total trace metal content of the rock, (Ni + Cu + Zn + Pb + Mn + Cr). The method is stated to differentiate between gossans and non-gossans with fair accuracy, but is held to be rather inaccurate for discriminating nickel gossans from high nickel – low copper lateritic rocks.

Bull and Mazzucchelli, (1975), subject trace metal data from 270 nickel gossans and non-gossans of various types to discriminant analysis. The functions derived from this treatment permit unknown samples to be allocated to one of five genetic groupings with known degrees of accuracy. Further, a trial classification of unknown ironstone sample data indicates that the technique gives a correct allocation for about 88 percent of these rocks.

Joyce and Clema, (1974), use principle components analysis of trace metal data to distinguish between nickel gossans and other Western Australian ironstones. These workers note that two principal components are required to explain about 67 percent of the total variance exhibited by their test data set of 96 samples. The first component, P_I, consists chiefly of a linear combination of Log Ni and Log Cu, and is thought to be related to nickel gossans. The second component, P_{II}, consists principally of Log Cr and is probably related to nickeliferous laterites. The authors indicate that a plot of P_I versus P_{II} misclassifies 9 out of 176 gossan samples and 11 out of 224 samples of other ironstones – a five percent misallocation error. Further, they indicate that these results are also obtained from a more practical s cattergram produced by plotting the product (nickel x copper) in p.p.m. units against chromium (p.p.m.) on log-log graph paper.

Work on the evaluation of nickel gossans in terms of sulphide metal grade falls into two categories : geochemical and textural. The published work on geochemical evaluation has, up to the present, been restricted to the use of platinum group metals.

The use of platinum group metals as geochemical discriminators of nickel gossans was first put forward by Keays, (1972). In a more detailed study, Travis et.al., (1976), indicate that palladium and iridium exhibit a positive correlation with nickel in primary nickel sulphide assemblages. They note that these two platinoids persist through the sequence of secondary sulphide alteration and are retained in the gossan at generally unchanged or enriched levels. Further, they indicate that the generally low level of Pd and Ir in non-gossan ironstones enables these metals to be used as discriminators of nickel sulphide mineralisation. Finally, these workers suggest that the absolute content of the more inert iridium in nickel gossans can provide a fairly reliable semi-quantitative guide to the nickel grade of the parent sulphide ore.

Very little work has been published on the textural evaluation of nickel gossans. The microscopic examination of these rocks is, however, a potentially important technique. This is because nickel gossans typically retain a proportion of the ore textures of their parent supergene sulphide assemblages as pseudomorphs in iron oxide. The replacement of violarite by goethite is especially significant in this respect. Mineragraphic analysis of nickel gossans is, therefore, a potentially powerful tool in the evaluation of former sulphide grades, as is indicated by Whittle, (1972), Roberts and Travis, (1974) and Groves and Whittle, (1976).

Published reviews of the current "state of the art" concerning nickel gossan studies have been made by the following workers: Hancock and Wilmshurst, (1972); Pontifex, (1972); Cochrane, (1973); Wilmshurst, (1976); and Moeskops, (1977). A more general review of base metal sulphide alteration and gossan evaluation is presented by Blain and Andrew, (op.cit.).

Critical evaluation of previous work on gossans

The forgoing review indicates the · research effort that has gone into the study of base metal gossans over the last sixty years. The early work in this field (1920 - 1930) was confined to the copper porphyry province of the south-west United States, and to mining districts in other parts of that country. This period saw the development of Locke's work on textural evaluation which was to have a fundamental influence on leached outcrop interpretation until the mid nineteen-sixties.

Locke's investigations were empirical and based on an experienced and accurate observation of limonite precipitation textures after disseminated copper ore. By this means he was able to predict the copper grade of the underlying ore with accuracy. The technique, however, was localised in its application. It could not be applied to other areas, even within the same mining district, without prior orientation work in these localities. The general technique was, however, highly suited to individual ore types cropping out in the kind of arid conditions in which it was developed.

Locke's work on limonite texture evaluation was initially extended by Blanchard. The principal contribution of this worker, however, was in the development of relic sulphide textures as ore grade predictors.

During the period 1930 - 1945, Blanchard investigated and described the boxwork textures of several important ore minerals. The technique that he developed had several advantages over Locke's method. Foremost of these was the fact that boxwork textures were ideally specific to each mineral and did not vary appreciably. The technique was, therefore, of much wider applicability and could be used wherever the boxwork was present in outcrop. Further, the structure could be examined in situ, and rapid estimates could hence be made of both the nature of the original ore assemblage, and, (ideally), the absolute proportions of its component minerals.

The disadvantages of boxwork evaluation were essentially practical ones. Considerable experience was needed to recognise the various boxwork textures, especially where these reflected local effects such as post-depositional structural deformation. Care was therefore also required in evaluating the significance of the structures in the outcrop because of this recognition problem. Further, the technique could only be used easily on coarse or medium grained ore relics because of the difficulties involved in direct field observation of replicate textures after fine grained ores. More importantly, though, boxwork evaluation was totally unusable in deeply-weathered laterised terrains where pervasive silification completely obliterates any leached skeletal relics after sulphide. Despite these disadvantages however, the techniques of boxwork evaluation developed principally by Blanchard were extensively used as both a qualitative and, in ideal cases, a quantitative guide to ore during the period 1930 - 1960.

The discovery and evaluation of surface gossans in Western Australia created new problems since here the mineralisation crops out in deeply lateratised terrain and the near surface environment is characterised by pervasive silification. In consequence, the now well-proven boxwork evaluation methods of Blanchard could not be used. By the 1960's, however, significant advances had been made in the field of rapid chemical analysis and these new methods formed the basis of much of the subsequent work on nickel gossan recognition. The principal problem involved in the recognition of nickel gossans in this region was the difficulty of distinguishing these rocks from other ironstones of similar appearance but of unrelated origin.

Three investigations of this problem have been published, (Moeskops, op.cit.). The recognition technique of Clema and Stevens-Hoare, (op.cit.) is empirically based. The technique has several advantages, principally speed and simplicity. Further, it utilises chemical data on Ni, Cu, Zn, Pb, Mn and Cr contents of ironstones, which should be readily available as part of any contemporary prospect appraisal programme. In addition, the technique is acceptably accurate with a misallocation rate of about 10 percent. Finally, the use of two sets of chemical parameters to define chemical discriminant fields helps in the correct allocation of possible border-line cases.

One disadvantage of the method is that it utilises acid-soluble and not total Cr data. Thus it is satisfactory only if the original samples have been prepared using a nitric/perchloric acid leaching technique. In consequence, the method does not

allow Cr data obtained from hydrofluoric acid leaching techniques or from "total analysis" methods such as XRF analysis to be used with confidence. A second disadvantage is that the method does not distinguish between types of non-gossans – information that would be beneficial to a primary recognition of non-gossan types. Finally, the technique cannot effectively separate nickel gossans from high nickel – high copper laterites, and its use may hence create recognition problems for gossans cropping out within lateratised rocks.

The recognition technique of Joyce and Clema (op.cit.) is based on a principal components analysis of ironstone chemical data. It has several slight advantages over the empirical method of Clema and Stevens-Hoare. Thus, it is statistically sounder: Only data from three metals are required, namely Ni, Cu and Cr. Further, the method is slightly more accurate with an estimated misallocation rate of around five percent. The method is otherwise, as easy to use; the data being plotted on a simple scatter plot.

The disadvantages are the same as those of the empirical technique. In addition, however, the authors state that the use of total extraction as opposed to acid soluble Cr data actually invalidates the technique, rather than impairing its efficiency.

The gossan recognition technique of Bull and Mazzucchelli (op.cit.) is based on discriminant analysis. These workers devise a scatterplot that allocates ironstone data to one of five groupings on the basis of a series of discriminant equations. This is one principal advantage of the technique over the other two discussed. A second advantage is that the derived discriminant functions can be updated and improved as further data becomes available. The method otherwise gives a comparable misallocation rate, (about 12 percent), and is easy to use in the field. The principal disadvantage is again that it utilises acid-soluble and not "total extraction" chromium data.

All three methods discussed afford relatively simple, rapid and accurate ways of recognising nickel gossans on the basis of their trace metal geochemistry. They were devised for the express purpose of distinguishing gossans from other ironstones in the deeply laterised terrain of the Yilgarn Shield. In consequence, the accuracy of these techniques in the recognition of nickel gossans in other semi-arid regions, such as central-southern Africa, may not be as significant as in the region for which they

were devised.

A small amount of published work has sought to predict the metal grade of the original nickel sulphide ore from the characteristics of the equivalent gossan. The study by Travis et.al. (1976, op.cit.) of the use of palladium and iridium as discriminators and predictors of nickel sulphide mineralisation is the first full study of its kind to be attempted on this ore type.

The technique as documented has, however, several disadvantages. The analytical method used for the determination of the platinoids, i.e. neutron activation, is both time consuming and costly. It is therefore, impractical for routine outcrop evaluation studies. This point is especially relevant when it is realised that reliable assessment of ore grade from gossans can only be potentially made through the rapid analysis of a reasonable number of representative samples from each occurrence. Further, the use of iridium at best gives only a semi-quantitative assessment of sulphide nickel grade, the accuracy range being 3 to 16 weight percent. In addition, gossan samples corresponding to sulphide nickel grades below 3 percent are not easily distinguished from barren rocks by this technique. The method as it stands is hence not very useful as an accurate predictor of sulphide nickel grade, although it is very reliable as a non-routine discriminant technique for the recognition of nickel gossans in Western Australia.

In contrast, the microscopic evaluation of gossan pseudomorph textures gives a potentially accurate indication of the minimum expected nickel grade of former ore. This is especially true of Western Australian nickel gossans since these typically retain the textures of their parent sulphide assemblages as recognisable iron oxide pseudomorphs.

The principal disadvantage of this type of evaluation is that it is best performed on polished sections. These take time to prepare and are relatively costly, and require description by an experienced mineralogist. Further, each section covers only a relatively small area and, hence, a reasonable number are needed in order to accurately evaluate a single gossan occurrence. However, under certain circumstances, (i.e. the presence of large well-preserved pseudomorphs), the use of cut, lapped slabs may be substituted. These have the advantage of being quicker to prepare, and they provide a larger, more representative area for visual inspection.

Research objectives

The present study has four principal research objectives. The first is the description of previously undocumented super-gene altered nickel sulphide deposits and occurrences in southern Africa and Western Australia. The second is a re-assessment and possible further development of the Thornber supergene alteration model in the light of this work and of that from a parallel study of previously documented nickel sulphide deposits. The third objective is an interpretation of the geology and chemistry of nickel gossan genesis based on data made available by the descriptive study. The fourth objective is the further development of techniques for the evaluation of nickel gossans in terms of the economic metal grade of equivalent sulphide ore.

Research approach

Well developed oxide zones are present over oxidising nickel sulphide deposits of middle Archaen age in the present-day semi-arid regions of Western Australia and central-southern Africa. Access to suitable occurrences is possible in these areas because of currently active commercial development.

The sampling strategy adopted for the present study was devised to achieve two objectives. Firstly, to obtain information on the range of near surface alteration phenomena occurring in Archaen nickel sulphide ore bodies within present-day semi-arid climatic environments. Secondly, to obtain as much information as possible about the style of alteration occurring within individual ore bodies.

The first objective was achieved by sampling as many suitable nickel sulphide alteration sequences as was logistically practicable. The second objective was achieved by a programme of detailed representative sampling that was carried out, wherever possible, at each location.

A sampling strategy of this type has several advantages in the present instance. It allows a generalised approach to be made to the problems of sulphide alteration, gossan genesis and gossan evaluation that form a substantial part of the research objectives of the present study. In addition, detailed work on individual occurrences allows the documentation of previously undescribed alteration sequences to be carried out. It also permits the adoption of a potentially fruitful comparative

approach in pursuance of the genetic and outcrop evaluation objectives of the study.

Two sets of field sampling were undertaken. The first was conducted in Western Australia by the present author's research supervisor, Dr. C.F. Blain, in July – August, 1973, before the start of the study proper. The second was conducted jointly by the present author and Dr. Blain in central-southern Africa during the period April – May, 1974.

In both areas direct sampling was carried out wherever possible at each mine or prospect that was visited, and wherever practicable, a suite of samples was taken from spatially-controlled representative locations down the supergene altered profile from surface gossan to primary ore. Samples of the adjacent host rocks were also taken where possible. Alternatively, representative material was sampled from documented drill core, metallurgical test drums and dumps. In all, 28 occurrences of oxidising massive nickel sulphide mineralisation were sampled in the two areas visited. The material from these profiles forms the basis of the present study.

A standardised procedure was adopted for the initial stages of the laboratory study: All samples were documented, visually examined, and two replicate specimens were removed from each. One of these specimens was sent for polished section preparation. The other was utilised for chemical analysis. This duplicate technique was used in the initial sample preparation so that the mineralogy and geochemistry of each sample could be determined from as near identical specimen-pairs as possible.

Mineragraphic work was subsequently carried out on a set of 17 profile sample suites. These formed a sub-set of the best documented profiles in the original study set of 28 occurrences. Standard mineragraphic techniques were used in a descriptive and interpretive analysis of these oxidation profiles. Confirmatory tests of mineralogy were, when necessary, performed using standard X-ray diffraction powder analysis techniques.

A study of the mineral chemistry of sulphide supergene alteration in several southern African deposits was carried out by Electron Microprobe Analyser. This work was performed as a complement to the petrological study of sulphide alteration in these occurrences.

The bulk chemical analysis of all samples in the study suite was carried out by X-ray Fluorescence Analysis. Samples were initially prepared for analysis using standard crushing and pelletisation techniques. The X.R.F. method was used for several reasons: Firstly, to facilitate the analysis of silica in the typically silica-rich nickel gossan suite; Secondly, because the method gave, in theory, acceptable accuracy and precision limits for all elements in the proposed analytical suite, and Thirdly, because it was both rapid and non-destructive. The use of X.R.F. therefore permitted an integrated, relatively simplified approach to be made to the principal analytical problem in hand, namely, the rapid and accurate chemical analysis of a large number of specimens of several distinct petrological types for a suite of 12 metallic and non-metallic elements.

A considerable amount of analytical development work was necessary, however, before acceptable bulk chemical data could be produced. Details of this work appear in Appendix One.

The bulk chemical data obtained from the X.R.F. analysis were subsequently utilised in four principal ways: In the description of sulphide alteration sequences performed on the study suite of 17 occurences; In the sulphide alteration and gossan genesis studies; and as the basis of work on the geochemical evaluation of nickel gossans.

A study of the mineralogy and geochemistry of oxidate minerals in gossans and host rocks was made using respectively, X.R.D. and Atomic Absorption Spectroscopy. This work was undertaken in order to document these phenomena and to allow the results to be subsequently utilised in the genetic and evaluation studies.

Specific gravity and porosity measurements were made on all specimens in the study suite. A technique based on the Walker's Steelyard method was developed for this purpose. The measurements were made in order to document these physical parameters within the specimen set, and hence to provide data on their variation within individual sulphide alteration sequences. These parameters were also measured to enable bulk chemistry to be expressed in weight equivalents per unit volume. Chemical data in these units are independent of density and porosity considerations. They can therefore be used to document true bulk chemical changes across rock types of differing density and porosity, as for example, between sulphide and oxide in the leaching zone of oxidising sulphide orebodies.

Full technical and methodological details of sampling techniques and of laboratory work programmes are   set out in Appendix One.

Form of presentation of subject matter

The present study is divided into three parts. The first part is descriptive and deals with the documentation of near surface oxidation in nickel-copper sulphide occurrences in central-southern Africa and Western Australia. It is divided into five sections (Chapters Two to Six). Chapter Two is a general introduction to the geology and geomorphology of the study areas and summarises the geology of each deposit. Chapter Three is a description of near-surface alteration in the Pikwe nickel – copper sulphide deposit, Botswana. Chapter Four is a description of near-surface alteration at five other undocumented nickel – copper sulphide deposits in central-southern Africa. Chapter Five is a description of near surface alteration in eleven mostly undocumented nickel-copper sulphide deposits in Western Australia. Chapter Six takes the form of a descriptive inter-comparison of all 17 altered nickel sulphide profiles that together comprise the present study suite.

The second part of the work deals with sulphide oxidation and gossan formation in nickel – copper sulphide ore bodies within present-day semi-arid climatic environments. It is divided into two sections (Chapters Seven and Eight). Chapter Seven re-assesses recent concepts of nickel sulphide supergene alteration in the light of data made available by the descriptive work of the present study. Chapter Eight deals with an interpretation of the geology and chemistry of nickel gossan genesis similarly based on data made available by the present work.

The third part of the study concerns the development of better techniques for the prediction of sulphide metal grades from measurable features of the corresponding nickel gossans. It is divided into three sections, (Chapters Nine to Eleven). Chapter Nine deals with the development of sulphide metal predictor techniques based on the mineralogy of nickel gossans. Chapter Ten deals with the prediction of sulphide metal grades based on the evaluation of nickel gossan textures. Finally, Chapter Eleven documents the development of techniques for the prediction of sulphide metal grades from nickel gossan geochemistry.

Chapter Twelve comprises a summary of the work encompassed by the study, its principal conclusions, and recommendations for further work.

The written text of the work is supplemented by two appendices. Appendix One provides methodological and technical details of all techniques employed in the course of the study. Appendix Two sets out the chemical and physical data generated during the work.

PART ONE
DESCRIPTIVE GEOLOGY

CHAPTER TWO

THE GEOLOGY AND GEOMORPHOLOGY OF THE STUDY AREAS

2.1. GEOLOGICAL SETTING

This chapter firstly outlines the general geological and geomorphological setting of the study deposits. The geology of the individual deposits is then briefly described prior to more detailed consideration of selected examples in Chapters Three to Five.

The Yilgarn Block of Western Australia is exposed over a roughly triangular area of approximately 620,000 Km^2., (Fig.2.1.1.). The Eastern Goldfields province forms the eastern half of this region and contains generally N.N.W. trending "Greenstone belts" of Archean age that are intruded by slightly younger granites, (Knight, 1975).

These greenstone belts are commonly composed of sequences of ultramafic, mafic and felsic volcanics/intrusives. Volcanoclastic sediments, cherts and banded ironstones are also common within the greenstone sequences, (Gee, 1975). The nickel sulphide deposits studied in this region are associated with the ultramafic units of these greenstone successions.

In the southern African Shield, the Archean Rhodesian and Kaapvaal cratons are separated by the elongate, slightly younger (Archean) Limpopo mobile belt, (Anhaeusser, 1976), (Fig.2.1.2.). All but one of the nickel – copper sulphide deposits sampled in central-southern Africa occur within either the Rhodesian craton or the Limpopo mobile belt.

The Rhodesian craton is exposed over an area of about 320,000 Km^2. It consists of a scattered, commonly elongate, early basement schist series that consists of numerous greenstone successions. These greenstones are intruded by slightly younger Precambrian granites, (Phaup, 1973). Much of the nickel sulphide mineralisation is associated with mafic and ultramafic units within the greenstone belts.

The slightly younger Limpopo mobile belt consists of a broad zone, (about 900 Km. long and up to 250 Km. wide), of deformed and metamorphosed granitic gneiss and paragneiss that is interposed on an east-west axis between the adjacent cratons. Van Breeman and Dobson, (1972), give the age of the main folding and metamorphism

KEY

☷ Post – Archean platform cover

▥ Precambrian mobile belts

☐ Granitoid and gnessic terrain

☰ Supracrustal (greenstone) belts

▦ Late Precambrian metasediments

▨ Precambrian ultramafic intrusives

Sample Deposits

1 Mount Windarra

2 Carr Boyd

3 Scotia

4 Nepean

5 Mount Monger

6 Jan Shoot

7 Kambalda Deposits – Lunnon Shoot / Silver Lake
ore body

– Otter Shoot

– McMahon Mine

– Durkin Shoot

8 Spargoville 5A

9 Widgiemooltha Area – Mount Edwards

– Dordie North

– Widgiemooltha No. 3

10 Redross

11 Ravensthorpe No. 5

23

Fig.2.1.1. The Locations of the sampled Western Australian Deposits
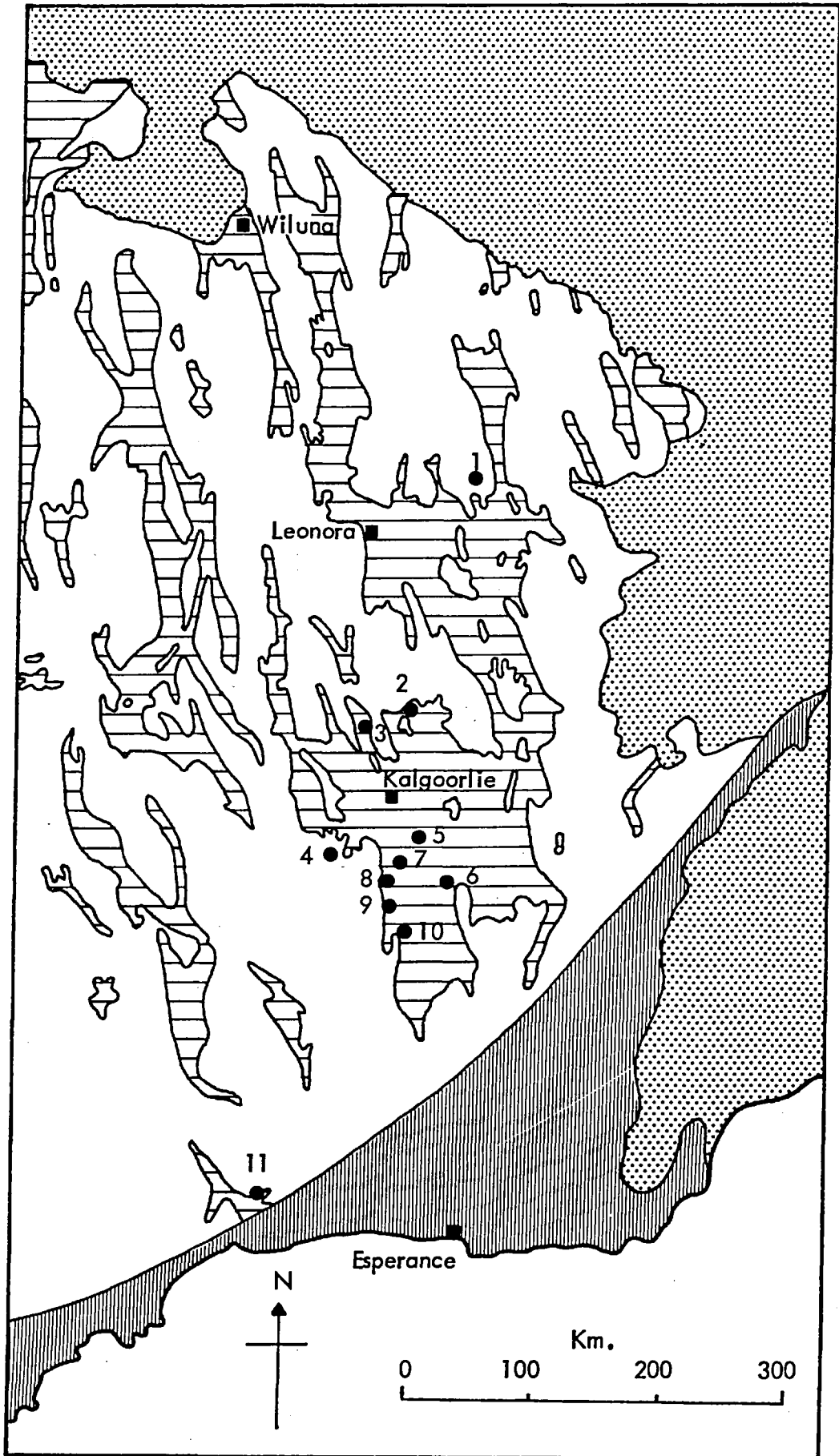
Fig.2.1.2.   The Locations of the sampled southern African deposits
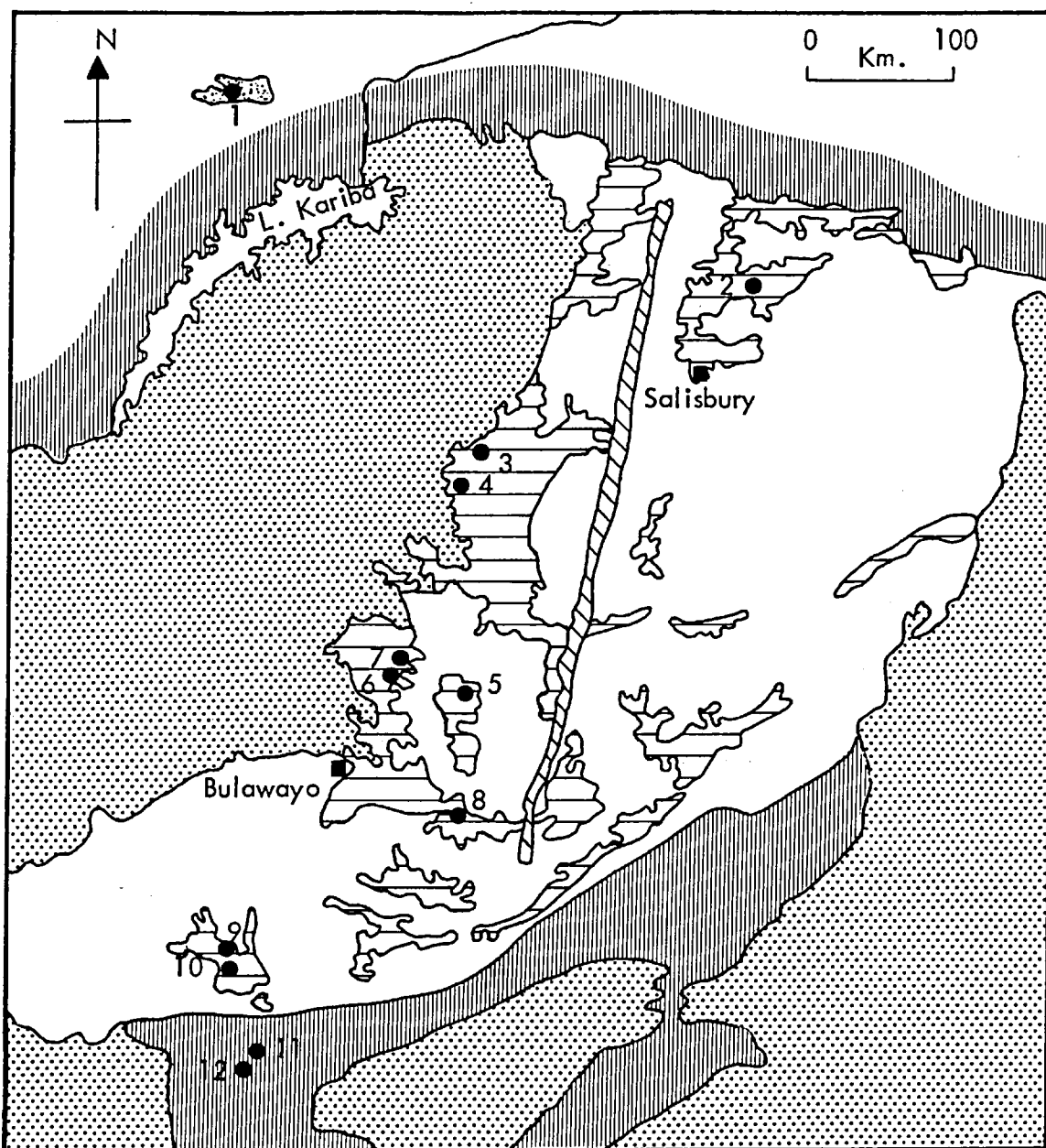
KEY - as per Fig.2.1.1.

Sample Deposits

1	Munali	7	Fibre
2	Trojan	8	Epoch
3	Perserverance	9	Phoenix
4	Empress	10	Selkirk
5	Shangani	11	Pikwe
6	Damba	12	Selibi

as between 2,690 and 2,000 m.y. Three structural zones are recognised within the Limpopo belt, (Cox et.al., 1965) : north and south marginal zones; two intermediate linear zones with trends parallel to the belt long axis; and a highly disturbed central zone. In north-east Botswana, the northern segment of this central zone contains several nickel sulphide deposits associated with metamorphosed ultramafic intrusive rocks, (Gordon, 1973).

A nickel deposit with an atypical metallogenic setting occurs in association with a probable late Precambrian metagabbro in south-central Zambia. The metagabbro is intruded into Proterozoic metasediments of Katanga age. The deposit is clearly younger than the other sampled occurrences because the Katangian rocks lie unconformably on a Precambrian basement gneiss complex.

In general, the metallogenic setting of nickel sulphide mineralisation within the Rhodesian craton in southern Africa is broadly comparable to that of the deposits in the Yilgarn Block region of Western Australia. No mineralisation with settings analogous to those of the Limpopo belt or the cover sequences in Zambia, however, are recognised in the Eastern Goldfields nickel province of Western Australia.

2.2. GEOMORPHOLOGY

The Yilgarn Block in Western Australia is situated within a present-day semi-arid climatic environment. Similar climatic conditions exist in the western parts of the Southern African Shield. In contrast, the central and eastern parts of this latter region currently possess a rather more temperate, humid climate. Despite these climatic variations, however, all the deposits studied in these areas exhibit deep weathering in the aerated zone above recent water table levels. These weathered zones typically consist of iron oxide-rich mineral assemblages that crop out as ferruginous gossans. The generally deep development of these zones indicates that sulphide weathering has been taking place over a considerable period of time in both regions. It is relevant, therefore, to briefly consider the climatic and geomorphological history of the Yilgarn and Southern African Shields.

Climate and Vegetation

The Yilgarn Shield today forms part of the Great Central Desert of Australia. Annual rainfall in the Eastern Goldfields region is generally below 30cm. per year and is

commonly less than 20cm. over much of the area, (Fig.2.2.1.). Precipitation is markedly seasonal, nearly all occurring in winter. The summers are typically dry and hot with maximum temperatures of between $30°$ and $36°C$, (Fig.2.2.2.). The winters are mostly dry and temperate, with mean maximum temperatures of between $15°$ and $18°C$, (Fig.2.2.3.). Zero rainfall conditions therefore persist for much of the year apart from the generally short wet season in winter. The region consequently possesses a typically dry hot semi-arid climate at the present time.

The vegetation cover of much of the Eastern Goldfields area is of Mediterranean shrub type, (Fig.2.2.4.). North of Kalgoorlie it consists chiefly of medium and short Eucalyptus. This gives way progressively northwards into Acacia shrubland that is principally developed on the arid hardpan soils of the northern Yilgarn region. The area south of Kalgoorlie is dominated by Eucalyptus and low shrub. South of Norseman this assemblage is progressively succeeded by zones of low Eucalyptus shrub. The vegetation of the Eastern Goldfields area is thus typical of that developed under recent dry semi-arid climatic conditions.

The climatic regime in the northern half of the Southern African Shield is rather more complex than that developed in the Yilgarn. Climate varies from semi-arid in the south-west through to warm temperate in the central and north-eastern parts of the region. Annual rainfall ranges between approximately 400mm. in south-western areas to over 800mm. in the north-east, (Fig.2.2.1.). Precipitation is markedly seasonal, most occurring in summer. The summers are warm to hot with mean maximum temperatures of approximately $30°$ to $32.5°C$ over much of the region, (Fig.2.2.2.). Maximum summer temperatures in north-central parts of the region are slightly cooler (around $27°C$). The winters are warm, with mean maximum temperatures of between about $22.5°$ in the south-west to around $25°C$ in the north-east, (Fig.2.2.3.).

As a consequence of the general north-easterly increase of rainfall and decrease in seasonal maximum temperature, the present climate of the region is appreciably zonal in character. The south-western part, which comprises the western portion of the Limpopo belt (N.E. Botswana), and the adjacent portion of the Rhodesian craton possesses a rather semi-arid climate. This is characterised by relatively low, strongly seasonal rainfall and mean maximum temperatures of about $31°$ and $23°C$ for summer and winter respectively.

Fig.2.2.1. Mean annual rainfall distribution in southern Africa and Western Australia (mm)
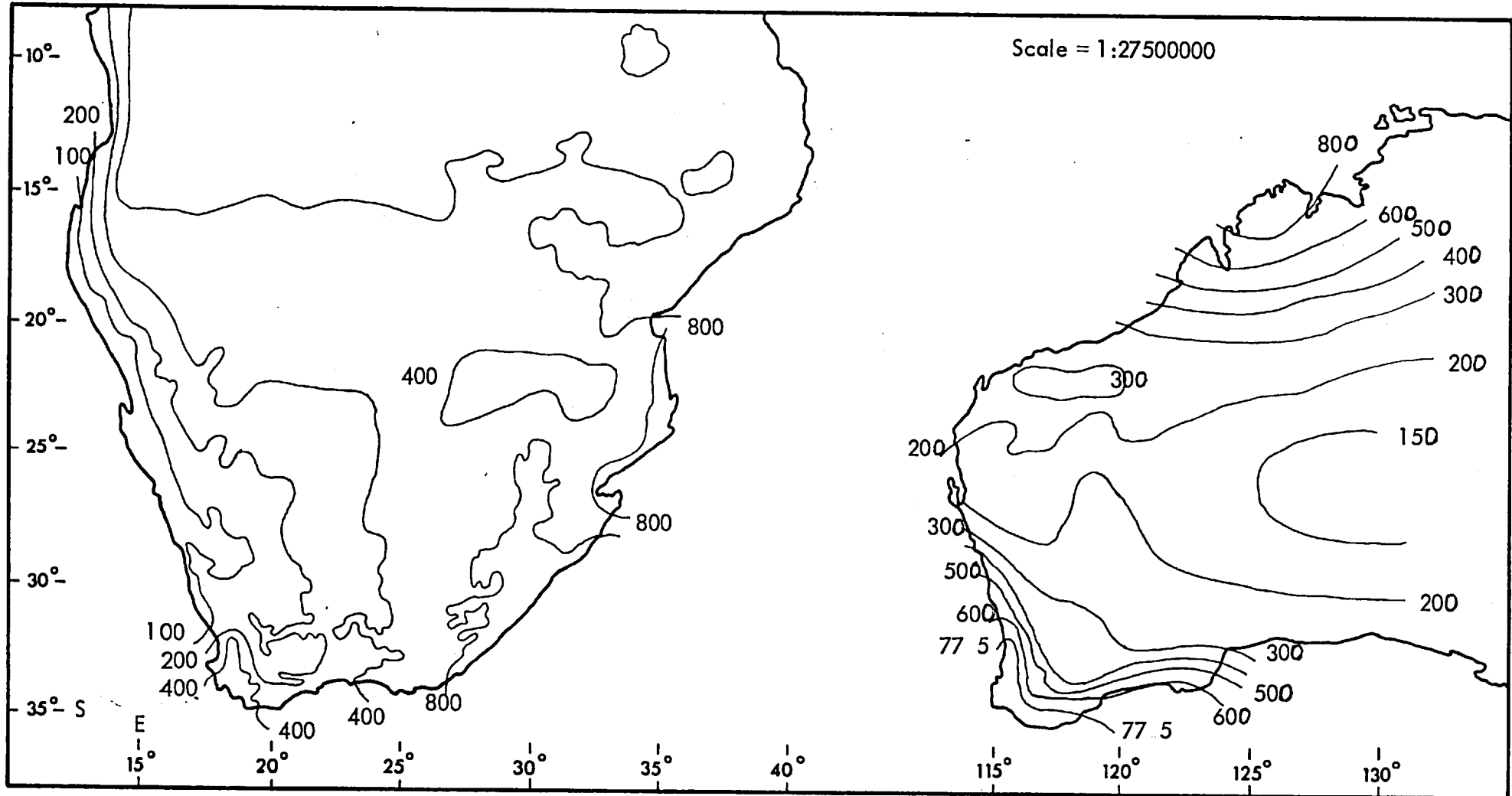
Fig. 2.2.2. Mean maximum summer temperature (°C) in southern Africa and Western Australia
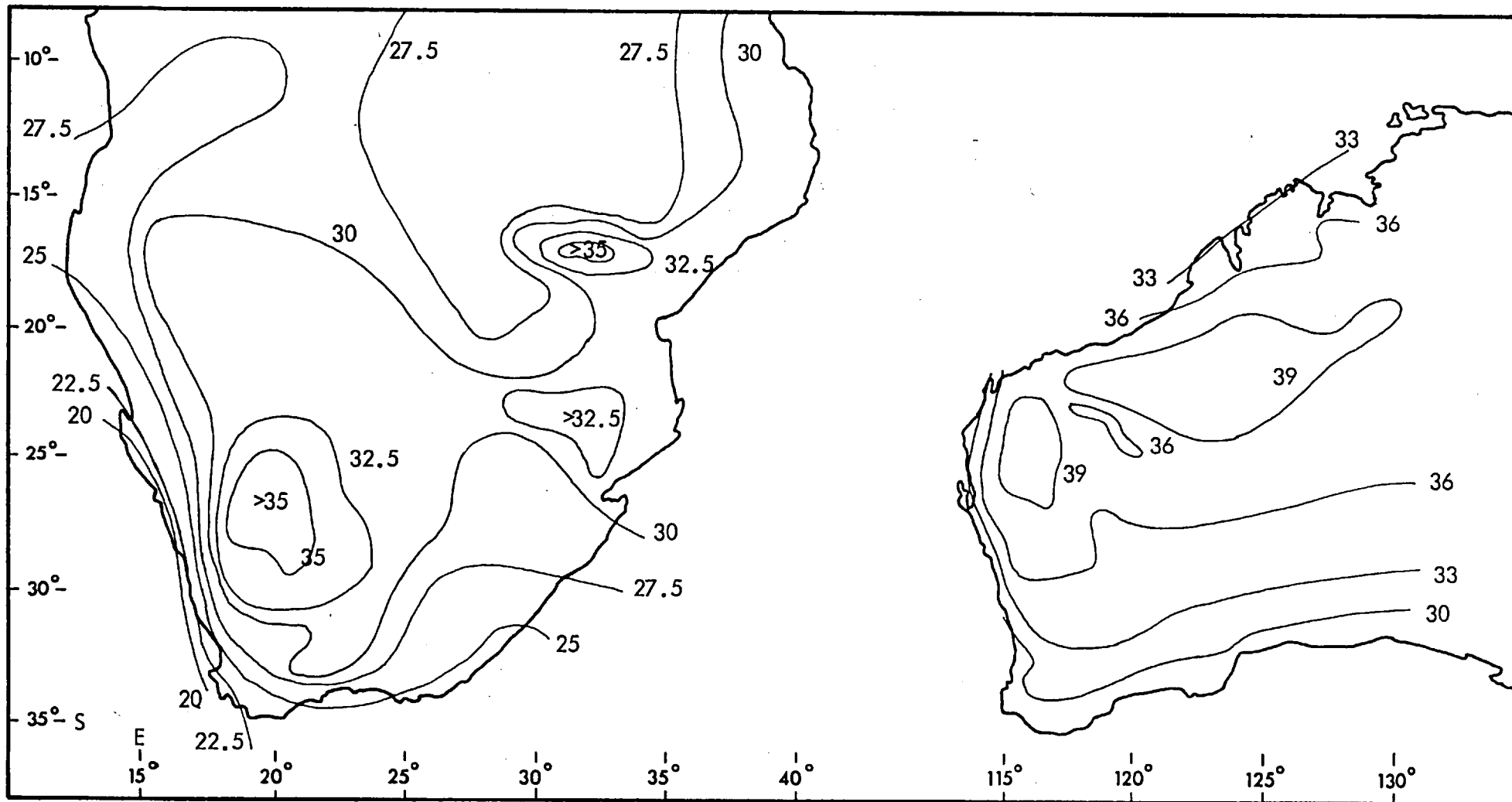
Fig.2.2.3. Mean maximum winter temperature (°C) in southern Africa and Western Australia
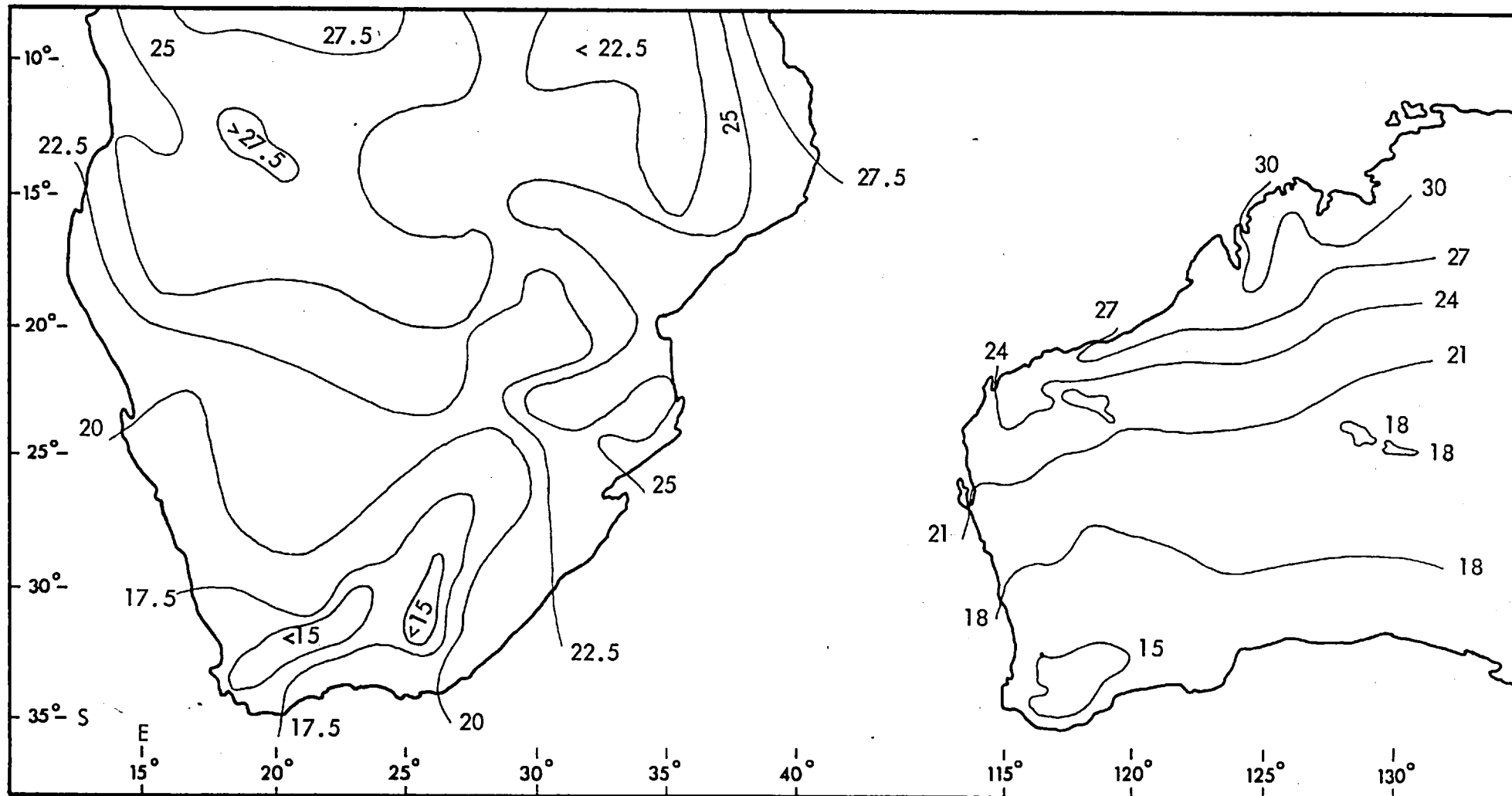
KEY

Dry tropical scrub and thorn forest

Steppe (short grass)

Desert vegetation (xerophytic shrub, grass, cactus)

Prairie (long grass)

Savanna (grass and shrub)

Tropical rainforest "Selva"

Mediterranean scrub (citrus, olive etc.)

Monsoon forest (moist deciduous)

Mountain vegetation

Sub-tropical forest - dry and wet hardleaf evergreen

Mixed broadleaf, mid-latitudes (broadleaf and conifer)

Fig.2.2.4. Vegetation types in southern Africa and Western Australia

Climatic conditions become progressively milder however towards the north-east. Annual rainfall values steadily increase, maximum summer temperatures progressively decrease and a concomitant rise in winter temperatures takes place. In consequence the climate in the north-eastern and northern parts of the region is warm temperate in character.

The distribution of vegetation types in the region reflects the climatic zonation outlined above, (Fig.2.2.4.). The semi-arid areas of the south-west are typified by dry tropical shrub and thorn forest. This assemblage gives way progressively to steppe-like grassland vegetation in the more temperate central and north-eastern areas of the region. Vegetation in the northern and north-western areas is similar to that in the south-west.

Geomorphology and Pedology

The physiography of much of the Yilgarn Shield approximates a typically flat or gently undulating plateau, (Prider, 1966). It is likely that it forms part of what was originally a continental-scale late Tertiary planation surface that was characterised by low relief, (David, 1950). The surface of the Yilgarn Shield is considered by Stephens (1971) to be a remnant of this late Tertiary surface that was not subsequently dissected by drainage rejuvenation due to later (Plio-Pleistocene) tectonic activity.

The drainage pattern of the shield is a scattered open system with salt lakes (Playas) occupying the main valleys. The system is inoperative except during exceptionally wet years when the contents of the playas are flushed out. Under normal semi-arid conditions though, some of the salt present in groundwaters accumulates in the playas, (Bettenay et.al., 1964).

The general drainage direction of the shield is eastwards towards the Nullarbor Plain and the Great Victoria Desert, (Mulcahy, 1973). Borehole data from the Coolgardie area indicate that the drainage system is pre-Eocene in age, (Balme and Churchill, 1959), and Johnstone et.al.(1973) consider that the system is a relic of a late Jurassic - early Cretaceous drainage pattern that became more or less defunct after the middle Cretaceous. It seems unlikely, therefore, that significant erosion of the Yilgarn surface has occurred since at least the Tertiary.

Climatic conditions become progressively milder however towards the north-east. Annual rainfall values steadily increase, maximum summer temperatures progressively decrease and a concomitant rise in winter temperatures takes place. In consequence the climate in the north-eastern and northern parts of the region is warm temperate in character.

The distribution of vegetation types in the region reflects the climatic zonation outlined above, (Fig.2.2.4.). The semi-arid areas of the south-west are typified by dry tropical shrub and thorn forest. This assemblage gives way progressively to steppe-like grassland vegetation in the more temperate central and north-eastern areas of the region. Vegetation in the northern and north-western areas is similar to that in the south-west.

Geomorphology and Pedology

The physiography of much of the Yilgarn Shield approximates a typically flat or gently undulating plateau, (Prider, 1966). It is likely that it forms part of what was originally a continental-scale late Tertiary planation surface that was characterised by low relief, (David, 1950). The surface of the Yilgarn Shield is considered by Stephens (1971) to be a remnant of this late Tertiary surface that was not subsequently dissected by drainage rejuvenation due to later (Plio-Pleistocene) tectonic activity.

The drainage pattern of the shield is a scattered open system with salt lakes (Playas) occupying the main valleys. The system is inoperative except during exceptionally wet years when the contents of the playas are flushed out. Under normal semi-arid conditions though, some of the salt present in groundwaters accumulates in the playas, (Bettenay et.al., 1964).

The general drainage direction of the shield is eastwards towards the Nullarbor Plain and the Great Victoria Desert, (Mulcahy, 1973). Borehole data from the Coolgardie area indicate that the drainage system is pre-Eocene in age, (Balme and Churchill, 1959), and Johnstone et.al.(1973) consider that the system is a relic of a late Jurassic – early Cretaceous drainage pattern that became more or less defunct after the middle Cretaceous. It seems unlikely, therefore, that significant erosion of the Yilgarn surface has occurred since at least the Tertiary.

The surface of the Eastern Goldfields region is deeply weathered and extensively lateratised. Laterite is typically present on the planated surfaces of Tertiary residuals. These residuals are commonly bounded by scarps (breakways), (Mulcahy, 1964). The planation surface may be covered by locally derived colluvial material of several   ages and in various states of aggragation. The colluvial cover may vary from very young undifferentiated sands to older types possessing air-hardened iron oxide segregations, (Mulcahy, 1973, op.cit.). These younger colluvial deposits originate by erosion of the ferruginous duricrust of pre-existing laterites, (Brewer and Bettanay, 1973).

A typical laterite profile has a near surface zone of ferruginous ironstone or aluminous laterite up to 5m. thick, (Prider, op.cit.). This is generally underlain by a typically thicker zone that is characterised by prominent red and brown ferruginous mottling – the Mottled Zone. This, in turn, overlies a thick zone of bleached kaolinised material – the Pallid Zone, (Stephens, op.cit.). In the Eastern Goldfields this pallid zone is thickest, (up to 30m.), beneath the trunk valleys of the drainage system. It is also extensively, though in general, more thinly developed beneath the planated surfaces (residuals) that divide these valleys, (Mulcahy, 1973, op.cit.).

Formation of laterite is thought likely to occur in association with a seasonally fluctuating water table, (Prescott and Pendleton, 1952). Lateratisation takes place as a result of the precipitation of hydrated oxides of iron and aluminium under oxidising conditions within the upper zone of water table fluctuation. The iron and aluminium are precipitated at the formation site after mobilisation from the parent material which corresponds to the underlying pallid zone. Iron is mobilised under reducing conditions and aluminium subsequently dissolves out under organically induced oxidation conditions. The iron and aluminium are not however mobilised or precipitated by the same chemical processes. Because of this, segregation of the two metals may take place during laterite formation, (Owen, 1954).

The mottled zone represents the site of water table fluctuation where localised oxidising conditions cause the precipitation of iron oxides in characteristic mottled textures. The pallid zone is the leached, kaolinised parent material from which the laterite is derived. It may retain wholly or in part the structure of the unaltered parent rock. Such a relationship indicates the residual nature of much of the Western Australian lateratisation.

Sivarajasingham et.al., (1962), indicate that these features of laterite formation, coupled with an associated loss of silica and bases from the profile, imply that progressive breakdown and desilicification of parent silicate play an important part in the lateratisation process. It is thus probable that an absolute loss of both silica and bases occurs by groundwater solution during the development of the laterite profile.

The climatic regime under which the Yilgarn Shield laterites formed is, by analogy probably very similar to that of modern deposits. At present, modern laterite profiles form in temperate regions with a moderate to high strongly seasonal rainfall. Johnstone et.al. (op.cit.) cite evidence indicating that the regional lateratisation of Western Australia was restricted to Oligocene – Miocene time. These workers indicate that younger periods of laterisation in Western Australia occur solely in south-western coastal areas of moderate but strongly seasonal rainfall. There is therefore, little doubt that laterites could not have formed under the semi-arid climatic conditions at present pertaining over much of the Yilgarn Shield region.

In a recent study of the Perserverence nickel deposit at Agnew in Western Australia, Nickel et.al., (1977, op.cit.), cite evidence relating the development of sulphide alteration and near-surface oxide formation to this late Tertiary lateratisation episode. The occurrence of other oxidised nickel sulphide deposits within lateratised terrain of this age in Western Australia may therefore indicate a similar relationship.

The soil cover of much of the Eastern Goldfields region consists chiefly of sandy yellow earths, (Fig.2.2.5.). These commonly overlie ironstone gravels. Thin alluvial deposits may however be associated with the gravels on valley floors. These deposits consist of sodic brown soils underlain by calcareous subsoils. Silty calcareous earths are associated with Playas in the eastern part of the region. Mulcahy, (1973 op.cit.) indicates that these calcareous soils may be directly derived from adjacent salt playas by aeolian action. Alternatively this worker suggests that they may be related to regionally developed fine-grained mafic and ultramafic rocks.

In all parts of the Eastern Goldfields the soil cover is underlain by thickly developed pallid zones indicating extensive laterisation. The character of the soil

types developed is, in contrast, typical of that associated with recent semi-arid to arid climatic environments.

The Southern African Shield corresponds broadly with the north-eastern portion of the Southern African Plateau, (Wellington, 1955). In the area corresponding to the northern half of the shield the plateau proper ranges in elevation from about 920m. to 1,850m. It is divided into a number of physiographic regions on the basis of altitude and landform.

The middle Limpopo basin forms part of the Limpopo - Sabi depression. This region corresponds to the area of the Limpopo mobile belt and the adjacent southern margin of the Rhodesian craton. The central area of the Limpopo basin in north-east Botswana consists of a rather even peneplain broken only by infrequent granitic outliers. Elevation is approximately 900 to 950m. It is likely that the Limpopo - Sabi depression formed as a result of subsidence following extensive post-Karroo trough faulting in the region, (Truter, 1945).

The greater part of the Rhodesian craton corresponds with the physiographic region of the Rhodesian uplands. This unit consists of a central axis of highveld that is flanked by two areas of middleveld. The highveld area is elongate and trends approximately NE - SW. It's elevation is typically between 1,200 and 1,800m., but is significantly higher in the extreme east. The highveld is typified by a flat pre-Kalahari peneplain of probable Miocene age that has not been appreciably affected by later erosion, (Maufe, 1935).

The flanking areas of middleveld undergo increasing dissection away from the central plateau. This is probably due to slight tilting associated with post-Karroo faulting in the Zambesi trough to the north. In the south the middleveld passes rather gradually into the flat terrain of the middle Limpopo basin. In the north, middleveld gives way to the Zambesi trough zone via the step-faulted Zambesi escarpment. The area of south-central Zambia bordering the northern edge of the Zambesi trough consists chiefly of middleveld similar to that in the south.

The relatively mild climate of much of the northern half of the Southern African Shield is reflected in the widespread development of yellow ferrallitic soils over most of the central and eastern areas of this region, (Fig.2.2.5.). These soils are

SOUTHERN AFRICA

a = brown and reddish-brown soils of tropical savannahs, thorny scrubs

T = reddish-brown and red soils of dry savannahs and dry deciduous forests = fersiallitic soils and alferritic soils

R = ferrallitic soils - strongly laterised of moist semi-deciduous forests and moist savannahs

K = hydromorphic soils, mineral hydromorphic soils - wet meadow, alluvial meadow, humic gley, gley and alluvial soils

U = mountain dry forest soils

WESTERN AUSTRALIA

X = red and brown hardpan (and zone soils)

Y = desert soils with sparse or without any vegetation

y = dunes and areas of shifting sands of dry regions - arid

W = gray desert-steppe soils (sierotzems) and gray cinnamon soils of dry steppes and shrub-steppes

S = solenetz soils (non-saline alkali soils)

R = red and yellow podzolic soils of moist subtropical forests (lateritic podzolic)

T = brown mediterranean soils

H = gray-brown pozdols

E = podzolised sols and non-podzolised frost-taiga soils of boreal coniferous forests

a = brown and reddish soils of thorny savannahs

Z = skeletal soils (lithosols)

Fig.2.2.5.   Soil types in southern Africa and Western Australia
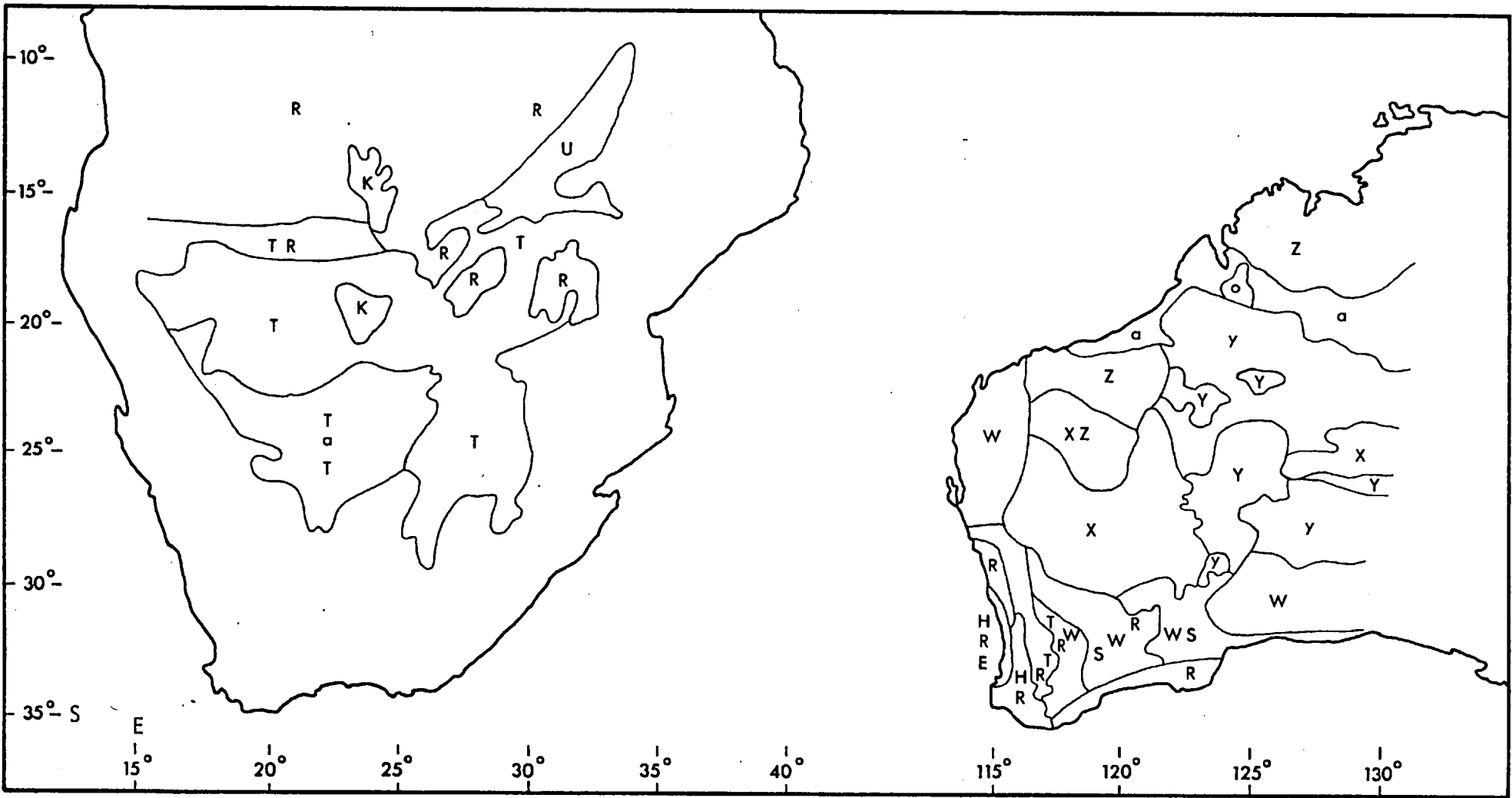
strongly leached and indicate the existence of a seasonally moist temperate climatic regime in these areas. Deep rock weathering is also typical in this region with the widespread development, (commonly down to 20 - 30m.), of kaolinised zones of weathered bedrocks. The long term establishment of seasonally humid, temperate climatic conditions in these parts of the shield region is therefore indicated.

The semi-arid climate of the south-western areas of the Shield (NE Botswana – SW Rhodesia) probably reflects the rather more recent climatic influence of the adjacent Kalahari region. The soils in this area of the Shield are typically those associated with progressive aridity of climate towards the Kalahari desert. Semi-arid fersialtic soils and halomorphic soils of solonetz type are common in the south-western areas of the Rhodesian craton, (Fig.2.2.5.). These soil types reflect the consequences of progressively lower rainfall and of increased aridity of climate in these areas. Further west in the extreme south-west of the craton and in the adjacent Limpopo belt these semi-arid soils give way to arid brown and reddish soils of hardpan type. These soils are indicative of an effectively hot dry climatic regime in operation along the western margins of the Shield. The presence of deep (40 - 50m.) kaolinised mantles over this region however indicates the relatively recent imposition of this present day semi-arid climate.

2.3. THE GEOLOGY AND WEATHERING OF INDIVIDUAL DEPOSITS

Principal features of the geology, primary ore mineralogy, weathering and surface expression of the sampled nickel deposits are summarised individually below. The location of each deposit is shown in Fig.2.1.1., (Western Australian deposits), and Fig.2.1.2., (southern African deposits).

The Western Australian deposits

Mount Windarra   The Mount Windarra deposit occurs as seven connected sheet-like, partly folded and nearly vertical lenses, (Roberts, 1975). These lenses or shoots are associated with a north-south striking sill-like ultramafic body that lies conformably between an older metasedimentary banded ironstone formation and a younger metabasalt unit, (Fig.2.3.1.). Ore is located at or near the contact of the ultramafic and the ironstone unit. Ore distribution is related to the drag-folding

Fig.2.3.1. The area geology of the Mt. Windarra nickel deposit (after Roberts,1975)

Lineated biotite adamellite and granodiorite

Amphibolite with minor amphibole-chlorite schist

Serpentinite and talc carbonate rock

Metasediments including banded iron formation

Gossan after nickel-sulphide mineralization

----- Mineralized horizon
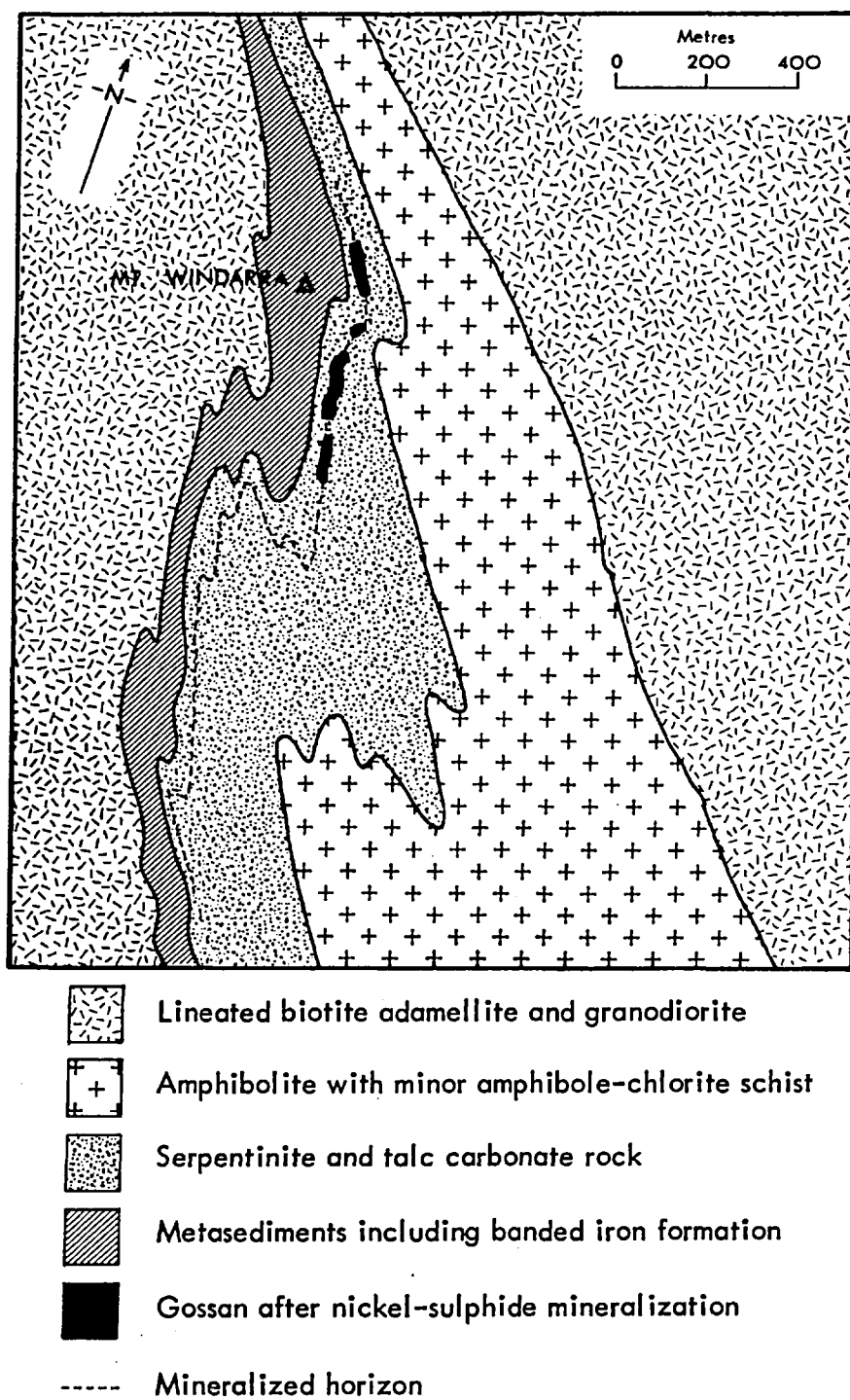
that affects the succession. Sampling for the present programme was done from a winze in the Shirley or A shoot.

The primary sulphide assemblage is one of pyrrhotite and pentlandite with accessory cobaltiferous pyrite and minor chalcopyrite and magnetite. There are several ore types at Windarra, the most important being the massive, breccia and disseminated sulphide - oxide varieties. Estimated probable reserves are 11.3 million tonnes at 1.46 percent nickel and 0.14 percent copper.

Sulphide alteration is well-developed and has been described by Watmuff (op.cit.). The gossan zone extends to about 40 metres below surface. Surface expression of the deposit consists of small gossanous outcrops among ferruginous float that is situated near the contact of a conspicuous banded ironstone unit with a poorly exposed ultramafic.

Carr Boyd   The Carr Boyd deposit occurs as an intrusive bronzite - sulphide pegmatoid breccia pipe complex near the western end of a lobate-shaped layered mafic-ultramafic succession, (Fig.2.3.2.). Three ore shoots are known, and these are situated within an east-north-easterly trending pegmatoid zone, (Purvis et.al., 1972). The two most easterly pipes, (numbers One to Two) break surface and extend down to depths of plus 200m. and 120m. respectively. Sampling for the present study was done in the open pit developed on No. One pipe.

The ore pipes average about 30 percent of massive to disseminated sulphides that enclose, or are interstitial to silicate. Up to 30 percent of unmineralised host xenoliths may also be present. The primary sulphide assemblage consists of : pentlandite (4%), nickeliferous pyrrhotite (20%) and minor pyrite, chalcopyrite and magnetite. Estimated probable reserves are 1.3 million tonnes at 1.65 percent nickel and 0.57 percent copper, (Schultz, 1975).

The surface intersection of the oxidation profile was first indicated by a small area of green carbonate staining on mafic outcrops. Later costeening however revealed gossans associated with ultramafic material, (Fig.2.3.3A).

Scotia   The sulphide mineralisation comprising the Scotia deposit occurs as a small lens at the base of a thick ultramafic pile and is separated from underlying volcanics by a thin sedimentary band, (Fig.2.3.4.). The orebody and its associated rocks

Fig.2.3.2. Geological sketch map of the Carr Boyd nickel deposit
(after Moeskops, 1973)

layered mafic and felsic rocks

layered ultramafic rocks

basic volcanic rocks

late stage bronzites and harzburgites

fault
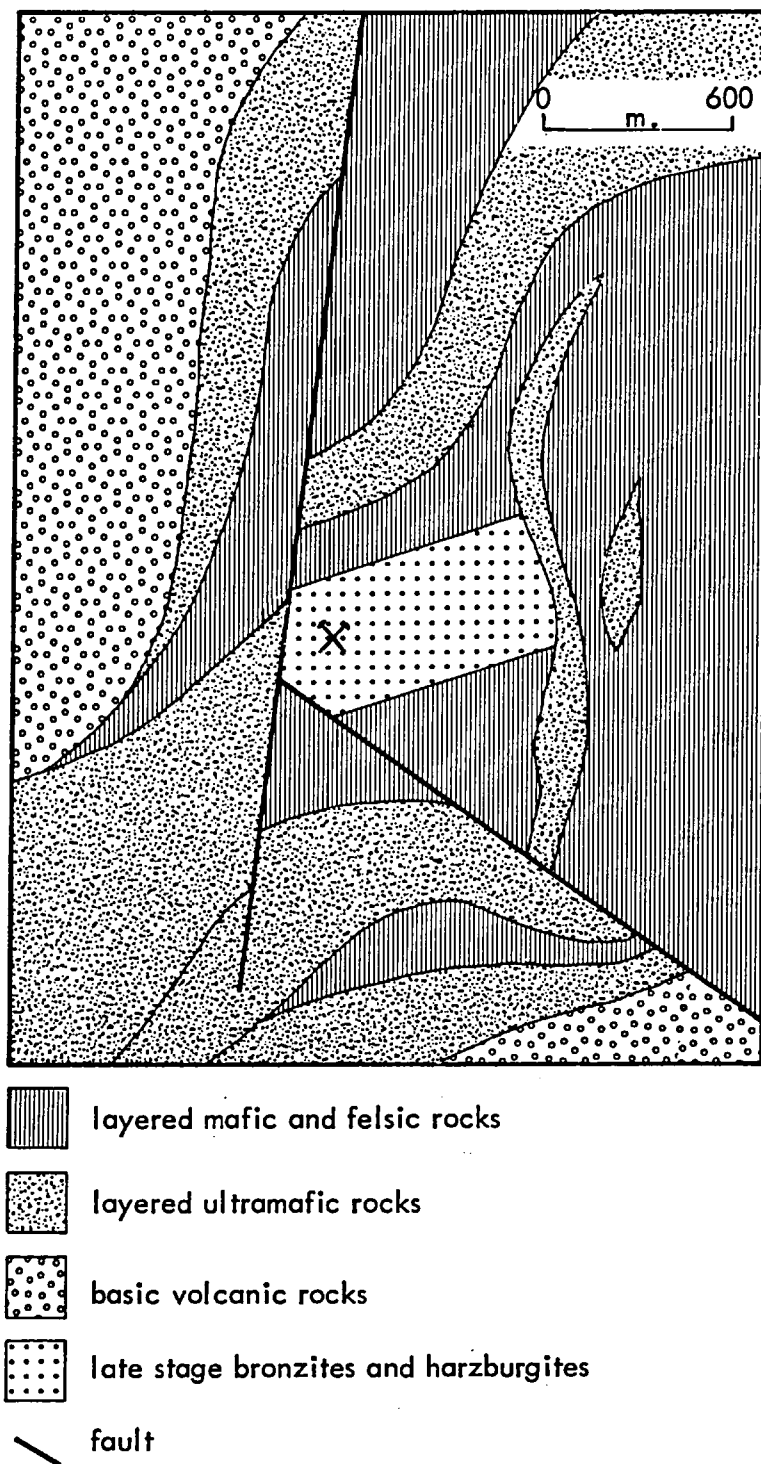
Fig.2.3.3   Surface Expressions of Nickel Ore (1)

A   Carr Boyd, W.A.
(Gossan profile)

B   Mount Monger, W.A.

Fig.2.3.3 Continued

C   Durkin Shoot, W.A.

D   Mount Edwards, W.A.

Fig.2.3.3   Continued

E   Widgiemooltha No 3,W.A.

F   Dordie North,W.A.

Fig.2.3.4.   The area geology of the Scotia nickel deposit
(after Christie, 1975)
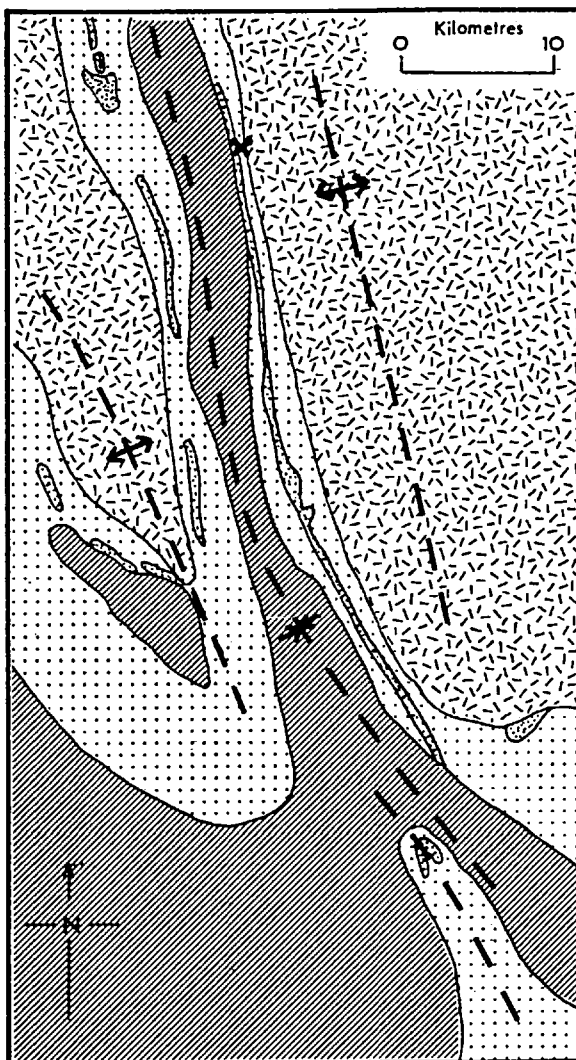
Metasediments

Ultramafics

Mafic rocks

Granite

Major fold axes

Scotia mine

form the eastern limb of a tightly folded greenstone syncline that has a N.N.W. axial strike and a southward axial plunge. The ore-bearing host is a lens-shaped dunitic unit with a N.N.E. surface strike. The orebody is located in a structural embayment in the footwall.

The Scotia orebody contains about 10 percent sulphide and is in two parts : an upper disseminated sulphide layer, and a discontinuous massive footwall layer. The average mineral proportions of the massive ore are : pentlandite 60%, pyrrhotite 30%, pyrite and magnetite 5% each, and chalcopyrite 0.5%. The relative proportion of pentlandite to pyrrhotite increases towards the top of the disseminated layer. Trace amounts of chromite are also present. The estimated probable reserves of the deposit are 1.13 million tonnes at 3.07 percent nickel and 0.25 percent copper, (Christie, 1975).

A brown siliceous caprock outcrops along the length of the ore-bearing ultramafic. Rare gossan shows are also present. Oxidation of the ore-bearing ultramafic extends down to the water table at 43m.

Nepean   The Nepean deposit occurs in the form of two closely associated overlapping and steeply-dipping tabular orebodies. These are located in the footwall contact zones of serpentinised sill-like peridotitic intrusives overlying metabasalts. These host rocks form part of a greenstone inlier in granite, (Fig.2.3.5.). Ore zones typically average about 1.5m. in thickness and consist of the sequence : Basal massive ore; "triangular" disseminated ore; and fine disseminated sulphide in serpentinite.

There is evidence of remobilisation of massive ore near the footwall contacts. Two mutually normal post-depositional warping events may be responsible for this phenomenon and for the shearing that has also affected the orebodies.

The primary sulphide assemblage is : pentlandite 60%, pyrite 20%, pyrrhotite 18%, with trace amounts of chalcopyrite, cubanite, valleriite and mackinawite. Estimated ore reserves are about 0.6 million tonnes at not less than 3.0 percent nickel, (Sheppy and Rowe, 1975).

No recognisable surface gossans were noted during surface exploration at Nepean,
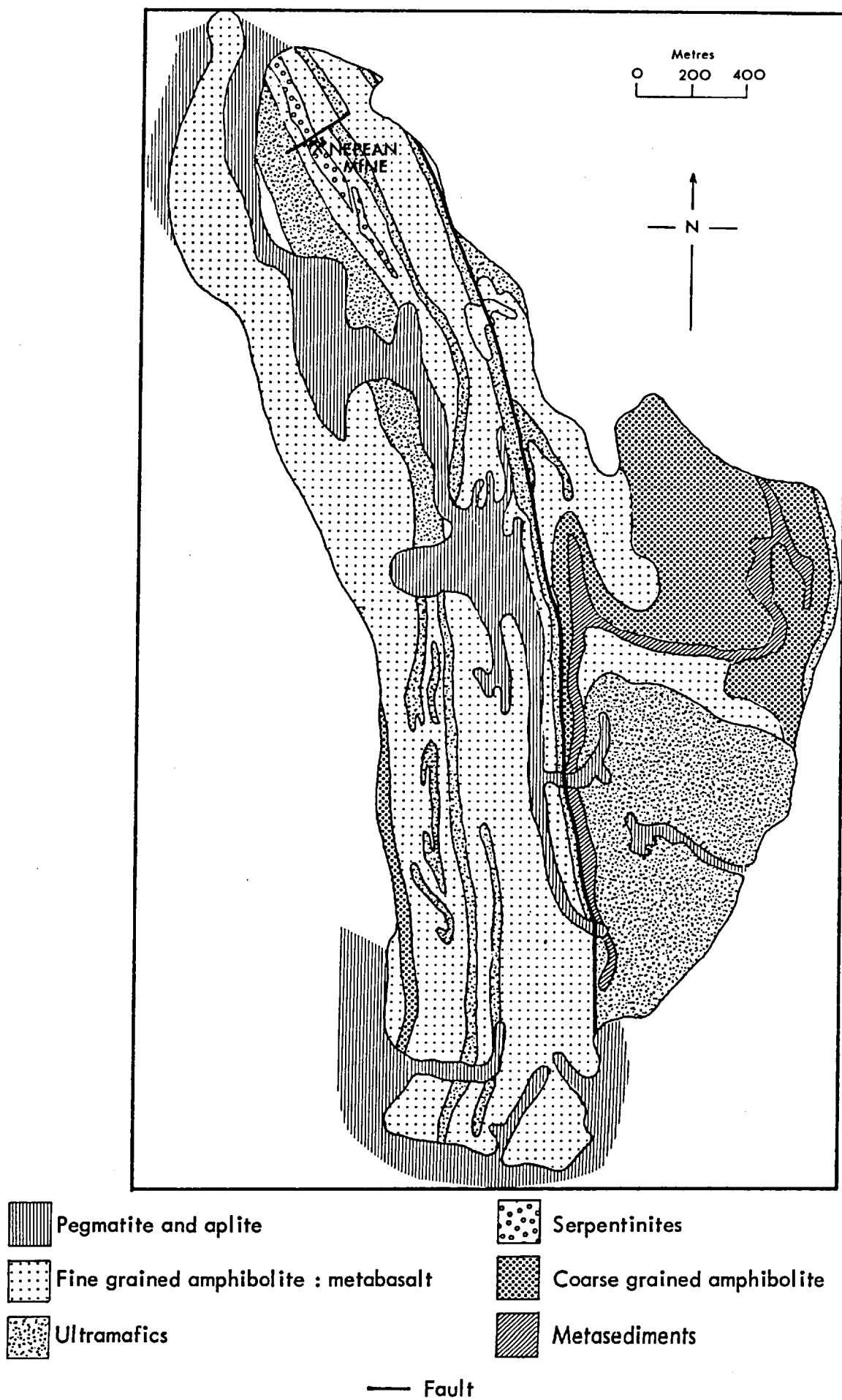
Fig.2.3.5. The area geology of the Nepean nickel deposit (after Sheppy and
Rowe, 1975)

probably because of deep soil formation. A typical Kambalda type sulphide
alteration sequence is developed in the deposit.

Mount Monger   The Mount Monger (Carnilya Hill) occurrence consists of a number
of closely spaced orebodies located within a sequence of altered ultramafic and
mafic rocks. These host rocks range in composition from serpentinites to talc-
carbonates and amphibolites. Extensive shale bands are also present and the
succession is almost certainly of greenstone affinity.

The actual host rock is an amphibolite and has a hornblende – chlorite assemblage.
Massive sulphide ore occurs at or near the basal contact with underlying serpentinite.
The massive zones are generally overlain by zones of disseminated sulphide. The
mineralogy of the primary ore comprises pyrrhotite, pentlandite with minor
amounts of chalcopyrite. A typical supergene alteration sequence of Kambalda
type is developed in the massive to semi-massive ore zones.

The deposit is represented at surface by patches of ferruginous gossan float. These
occur at or near basal contacts between host amphibolite and underlying
serpentinite, (Fig.2.3.3B.).

The Kambalda Deposits   Five of the eleven known sulphide occurrences at Kambalda
were sampled as part of the present study : Otter Shoot, McMahon, Durkin Shoot,
Jan Shoot (St. Ives), and the combined Silver Lake and Lunnon Shoots, (Fig.2.3.6.).

The ore deposits are associated with a thick sequence of ultramafic submarine lavas
interposed between two series of metabasalts. Generally, ore occurs as either lenses
in the ultramafic units – Hanging-wall mineralisation, or at the basal contact
between the ultramafic and the underlying footwall metabasalts – Contact
mineralisation. Hanging-wall ore is rarer than the footwall type. Of the deposits
sampled, all but the Lunnon Shoot and McMahon represent contact ore mineralisation.
Dislocation of the basal contact is a constant feature of all contact ore.

The broad doming of the Kambalda area is the sole local expression of major
folding. The dome itself is about seven kilometres long by three kilometres wide,
and plunges N.N.W. and S.S.E. at between 20 and 25°. The flanks commonly

Fig.2.3.6.   The geology of the Kambalda dome (after Ross and Hopkins,1975)
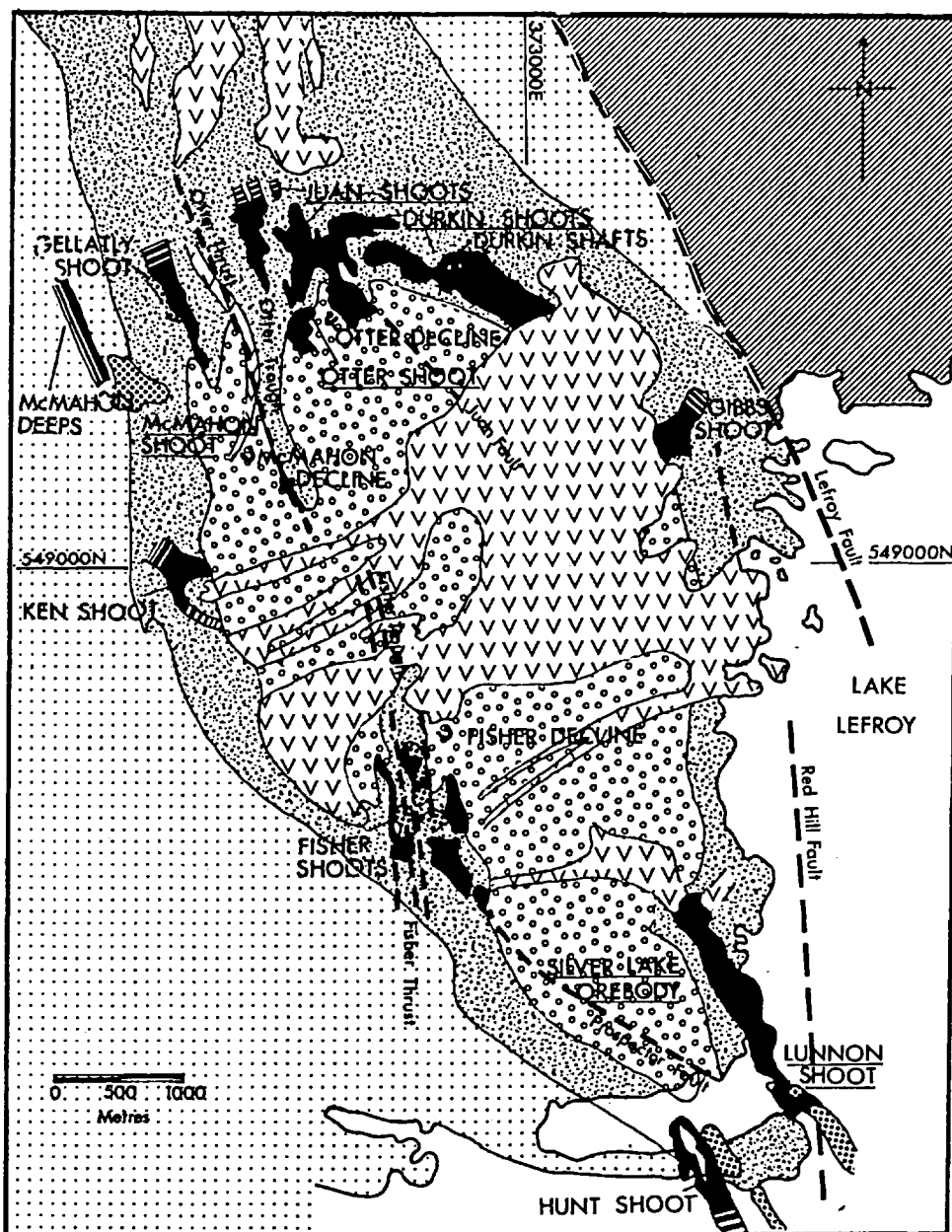
Footwall nickel sulphide mineralisation

Hanging wall nickel sulphide mineralisation

Ultramafic

Footwall metabasalt

Hanging wall metabasalt

Metasediments

Acid – Intermediate intrusives

—— Fault

dip away at 40° but dip angles are distally controlled by local and regional fault patterns. Small-scale irregularities in dome outline are also caused by faulting.

Contact ore commonly exists as narrow elongate bodies with N.N.W. trends, and is controlled by fault-bounded depressions in the footwall contact. A typical contact ore sequence averages 3m. in thickness, and consists of massive sulphides overlain by thicker, more continuous disseminated mineralisation.

Ross and Hopkins, (1975) state that the dominant components of primary mineralisation at Kambalda are monoclinic pyrrhotite and pentlandite. The ratio of these two minerals is variable however :- between 2.3 : 1 (8.5% Ni) at the Lunnon Shoot to 0.8 : 1 (20% Ni) at the Durkin Shoot. Pyrite usually froms less than 10 percent of the total ore content, with chalcopyrite at less than two percent. Millerite is an important constituent of the Otter Shoot primary assemblage.

Overall mean nickel : copper and nickel : cobalt ratios are 13 : 1 and 54 : 1 respectively. Estimated reserves for the five producing mines on the dome are 19.85 million tonnes at 3.3 percent nickel.

All the deposits sampled have well-defined sulphide alteration sequences and crop out as siliceous gossans at ultramafic contacts, (Figs. 2.3.3C, 2.3.7A).

Spargoville   Four sulphide occurrences are known at Spargoville. These are associated with a greenstone sequence that crops out at surface as a slightly arcuate north-south trending belt, (Andrews, 1975). The mineralisation occurs in discontinuous dunite lenses in three separate tremolite – talc – chlorite bodies. This dunite is commonly located at ultramafic – amphibolite (wall-rock) contacts.

In the present study, Location 5a was sampled. Here the mineralisation is localised on the western (? lower) contact of amphibolite with a narrow westerly dipping ultramafic lens, (Fig.2.3.8.). The host rock is probably a thin dunite selvage that grades into talc – tremolite – chlorite. The orebody is a small pod of massive violarite – pyrite and is located in a structural embayment in the dunite – amphibolite contact.

The upper 30m. of the orebody are completely oxidised and crops out as small discrete gossans. The mineralisation is thought to pinch out at about 80m.

Fig.2.3.7   Surface Expression of Nickel Ore (2)

A   Silver Lake Ore Body, W.A.

B   Redross, W.A.

Fig.2.3.7   Continued

C   Empress, Rhodesia

D   Shangani, Rhodesia

Fig.2.3.7 Continued

E   Selkirk, Botswana

Fig.2.3.8.   The area geology of the Spargoville 5A prospect
             (after Andrews, 1975)
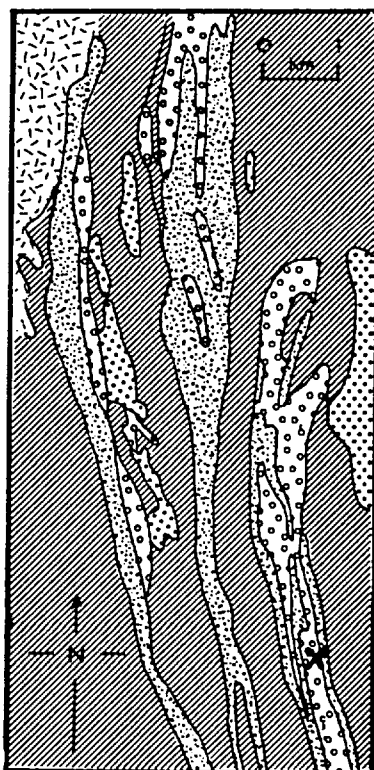
[ ] Granite

[ ] Porphyry

[ ] Ultramafics

[ ] Metasediments

[ ] Metabasalt

✗ 5A

Andrews suggests that it may represent the eroding distil end of a once larger deposit.

The Widgiemooltha deposits   Four occurrences were sampled in the Widgiemooltha area: The Widgiemooltha No.3 prospect, the Dordie North prospect, Redross and Mount Edwards. The first three of these are located on the eastern flank of the Widgiemooltha dome, (Fig.2.3.9.). Mount Edwards is located in the northern linear extension of the latter structure.

The area comprises three greenstone formations that are folded about a N.N.W. trending axis, and which contain at least four separate ultramafic units. In the southern part of the area the Widgiemooltha dome is formed by the intrusion of a younger granite into a major anticlinal structure within the greenstones. North of the dome the greenstones extend as sub-parallel belts.

Mineralisation is primarily associated with the oldest (lower) greenstone series. This consists of basal ultramafics overlain by a thick sequence of tholeiitic and magnesium-rich basalts. These are in turn overlain by a complex ultramafic volcanic suite containing sedimentary intercalations. Mineralisation occurs at the basal contact of this upper volcanic unit. The younger (middle and upper) greenstone series contain no mineralised ultramafic units.

The Mt. Edwards deposit occurs on the western limb of the Mt. Edwards anticline on the northward extension of the lower greenstone series, (Fig.2.3.10.). The "Widgie 3" prospect exists as a lens in the northern part of an ultramafic-dolerite contact embayment, which is also located in the lower greenstone series, (Fig.2.3.11.).

The Dordie North prospect occurs on the southern extension of the "Widgie 3" ultramafic, and is located in a contact embayment between that ultramafic and the footwall amphibolite, (Fig.2.3.12.). The Redross deposit forms a planar zone on a basal contact between an ultramafic unit and footwall amphibolite, (Fig.2.3.13.).

All four sampled occurrences have similar primary sulphide assemblages. Pyrrhotite and pentlandite are dominant and chalcopyrite is also present, but

its proportion is variable. In addition, nickel arsenides and arsenosulphides occur as minor constituents at Widgie 3 and Dordie North.

Reserves and mean grades are quoted by Dalgarno, (1975) as follows : Widgie 3, 0.9 million tonnes at 1.23 percent nickel and 0.9 percent copper; Dordie North, 1.2 percent nickel; Redross, 3.5 percent nickel and 0.32 percent copper. Grades for Mt. Edwards quoted in a paper by INAL staff (1975) are : 2.2 percent nickel and 0.2 percent copper. All four deposits show conspicuous sulphide alteration sequences of Kambalda type.

The individual surface expressions of the sampled profiles are as follows : Mt. Edwards − spasmodic, highly siliceous gossans within zones of mafic/ultramafic rubble, (Fig.2.3.3D); Widgie 3 − two narrow silicified gossans separated by a narrow shear zone, (Fig.2.3.3E.); Dordie North − a restricted zone of silicified gossan rubble, (Fig.2.3.3F.) ; and Redross − a restricted zone of spasmodic gossan float, (Fig.2.3.7B.).

Ravensthorpe   The Ravensthorpe Number Five prospect is located near the southern edge of the Yilgarn Shield. The mineralisation, which is present as massive, disseminated and vein types, occurs at or near the basal contact of a serpentinised ultramafic unit with an underlying quartzite. The ultramafic host is overlain by an altered ultramafic/mafic sequence that uncommonly exhibits thin mineralised bands.

The sulphide assemblage is rather variable but in general consists of pyrite, nickeliferous pyrrhotite and minor chalcopyrite. Small but variable amounts of violarite may also be present, and is associated with pyrite or pyrrhotite.

The mineralisation crops out as non-silicified gossan with minor silcrete present at the basal contact with the host ultramafic.

Fig.2.3.9.   The geology of the Widgiemooltha area (after Dalgarno, 1975)
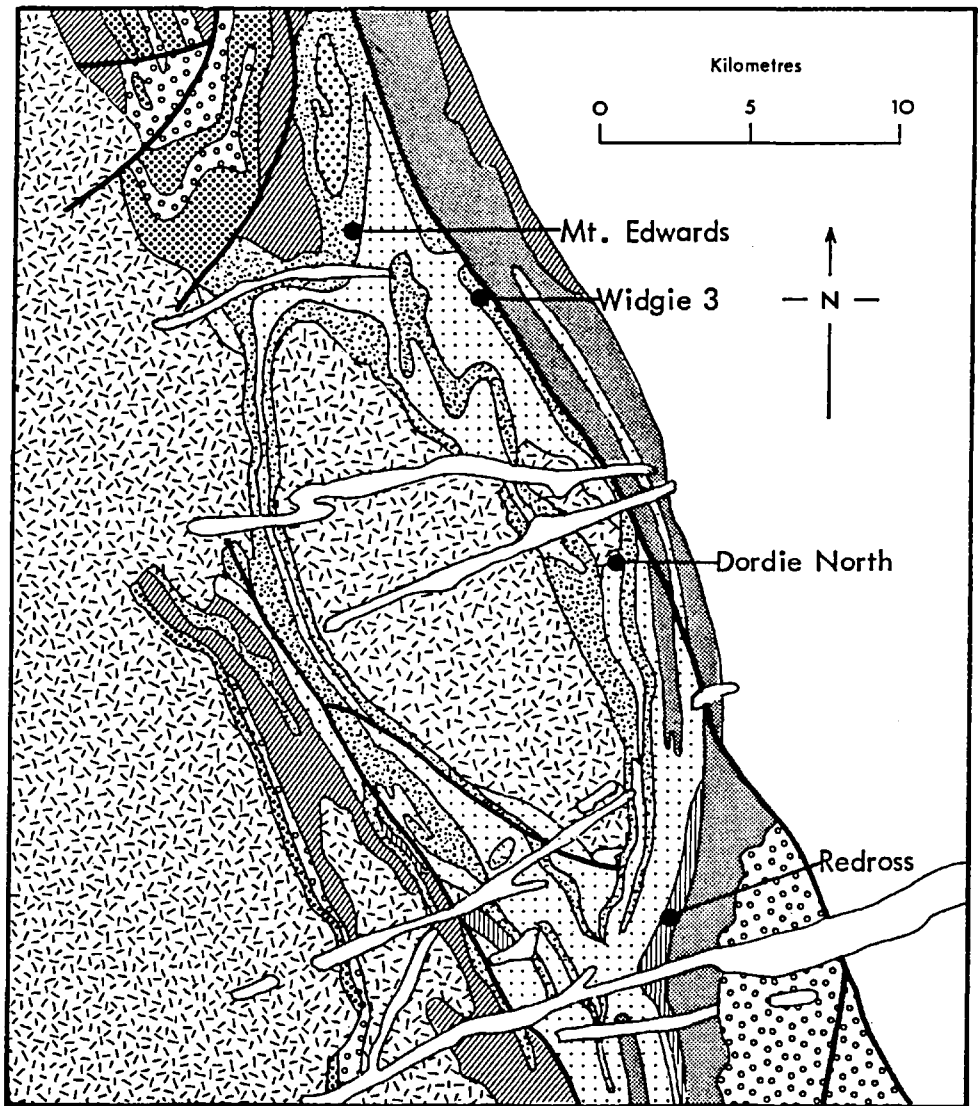
Metasediments

Acid extrusive rocks

Ultramafic : serpentinite

Thoeiitic basalt

Granite

Ultramafic : high magnesium basalt

Tholeiitic basalt

Layered mafic intrusive rocks

Porphyry

Norite dyke suite

Fault

Metres
0   50   100

- N -

Nickel sulphide mineralisation

Ultramafic : talc-tremolite

Ultramafic : serpentinite

Metasediments

Meta-tholeiitic basalt
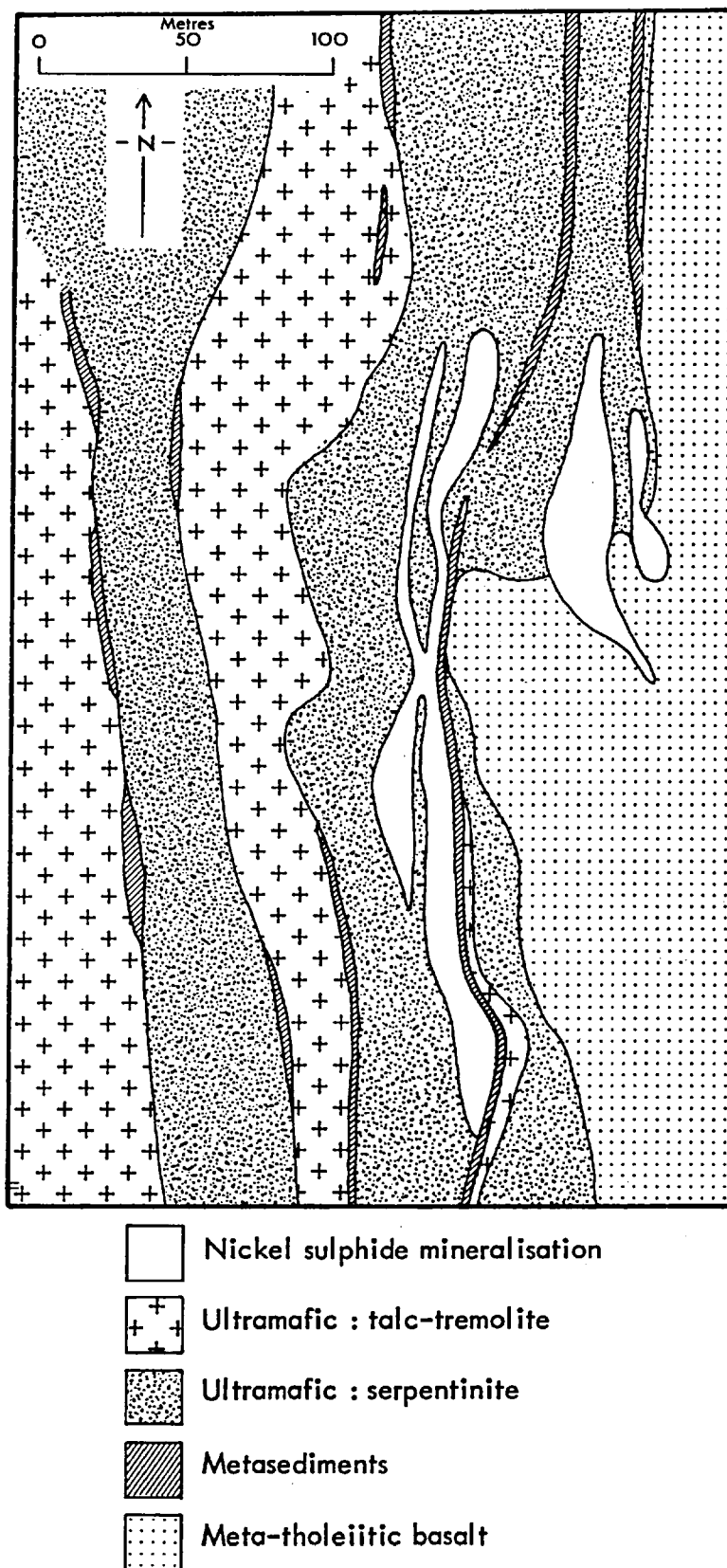
Fig.2.3.10.   The local geology of the Mt. Edwards nickel prospect
(after INCO staff, 1975)

SW   NE

300 m RL

200 m RL

100 m RL

Amphibolite

Widgie ultramafic : serpentinite

Nickel sulphide mineralisation

Porphyry dyke

— — Limit of oxidation
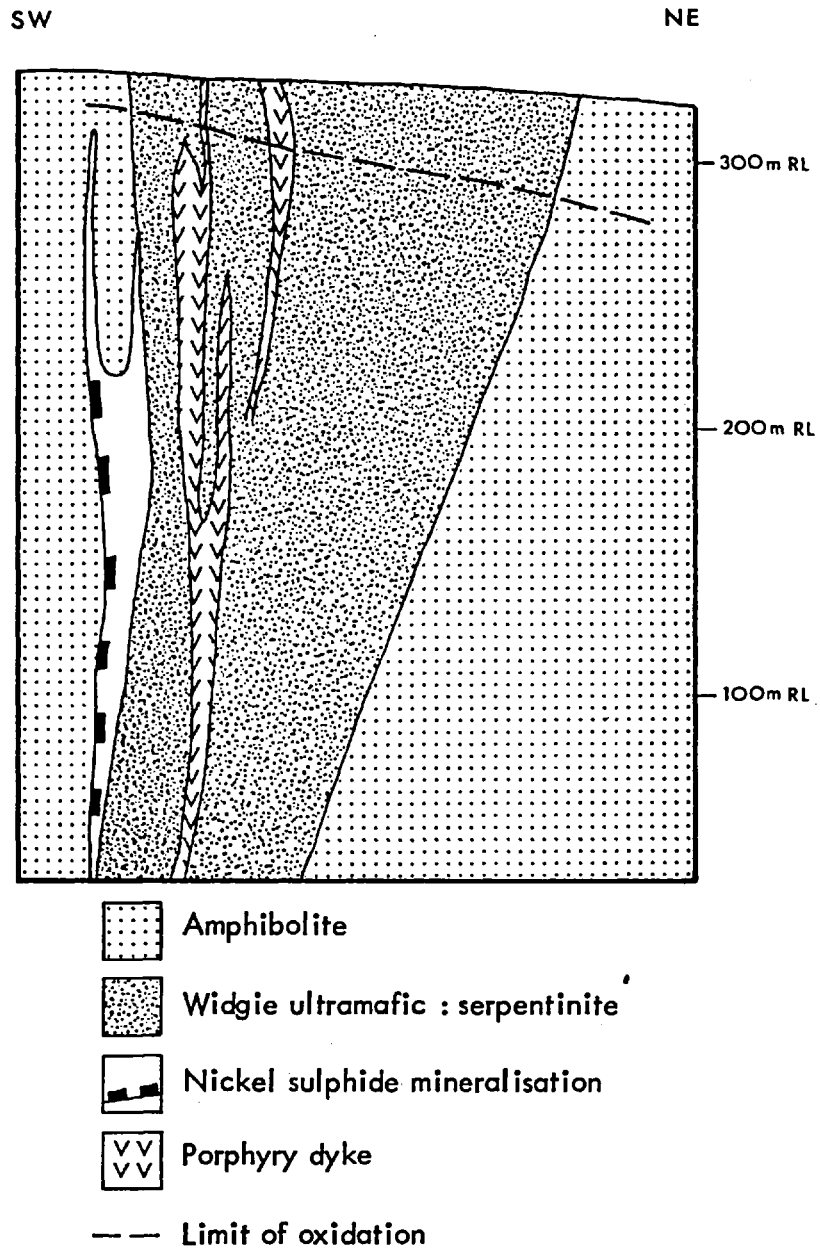
Fig.2.3.11.   Geological section through the Widgiemooltha No.3
prospect (after Dalgarno, 1975)

W   E

                                                              —200m RL

                                                              —100m RL

                                                              —O RL

▦ Footwall amphibolite

▦ Dordie ultramafic : serpentinite

▦ Porphyry dyke

▬ Nickel sulphide mineralisation

— — Limit of oxidation
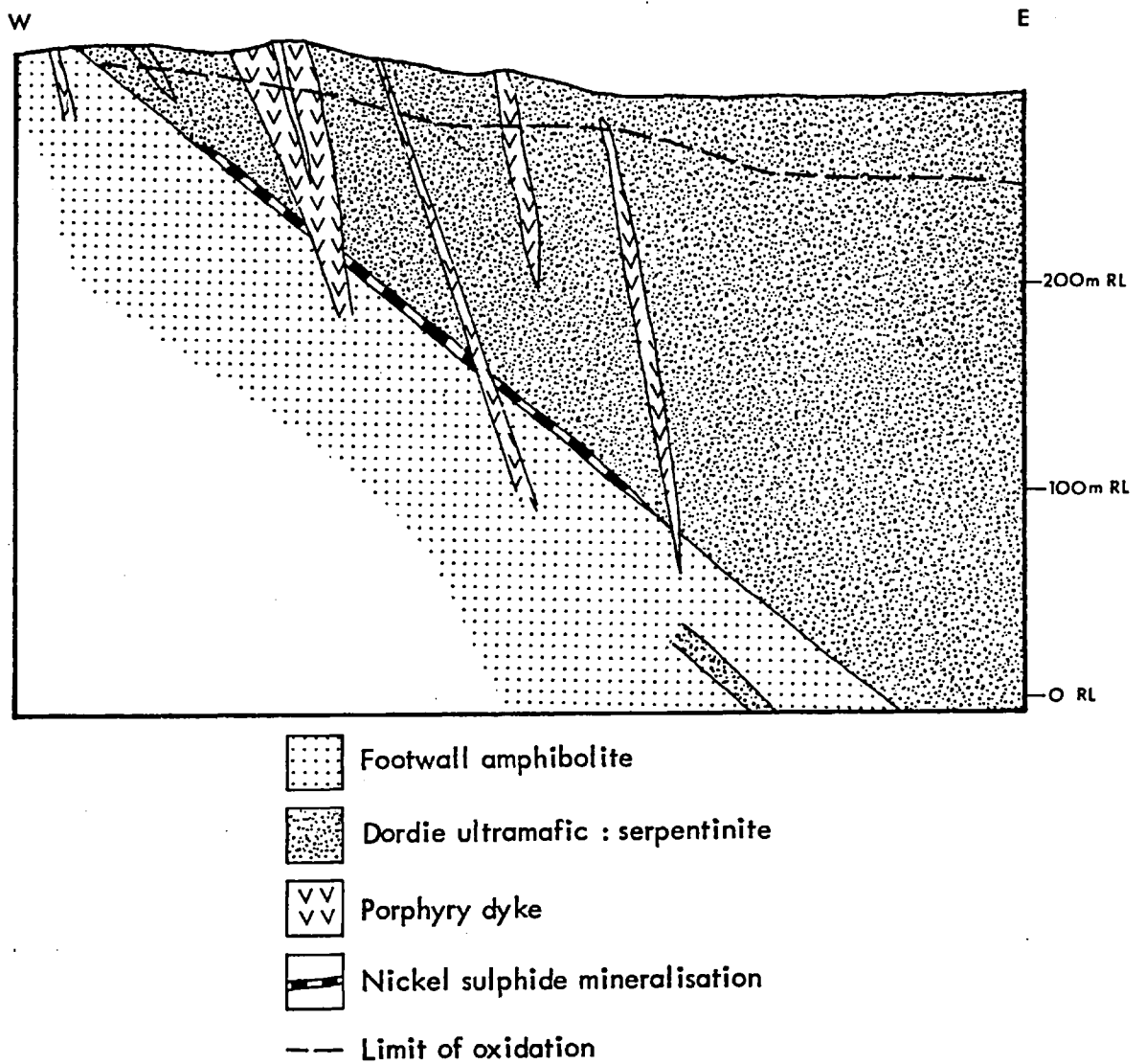
Fig.2.3.12. Geological section through the Dordie North nickel prospect
            (after Dalgarno, 1975)

Footwall amphibolite

Eastern amphibolite

Redross ultramafic

Metasediments

Nickel sulphide mineralisation
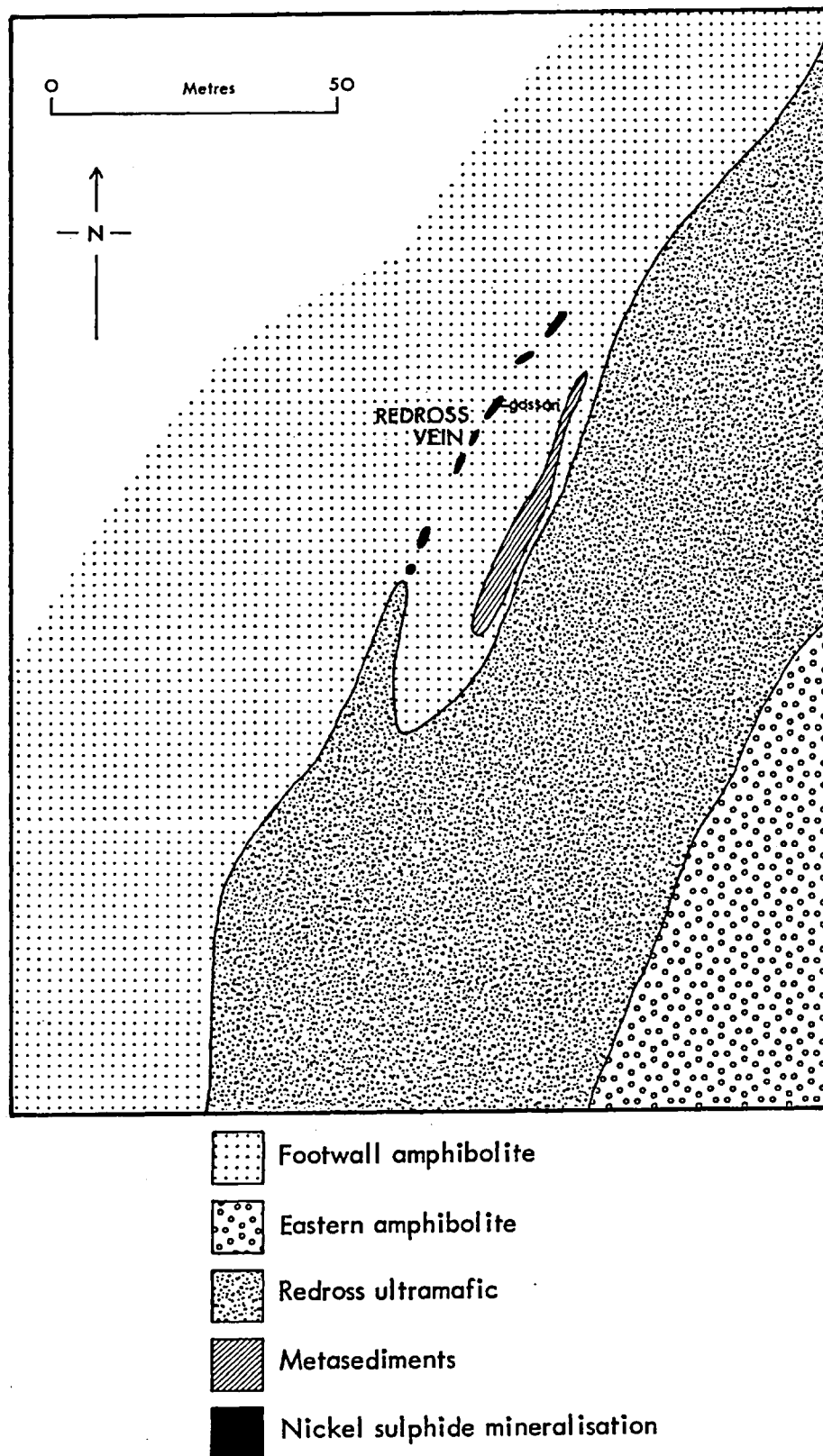
Fig.2.3.13. Local geology of the Redross nickel deposit
(after Dalgarno, 1975)

62
The central-southern African deposits

<u>Munali</u> At the Munali Hills nickel anomaly, mineralisation is associated with a
small elongate (5 by 1 Km.) metagabbro stock intruded into a N.W. dipping late
Proterozoic (Early Katangan) banded calc-silicate and carbonate sequence, (after
Smith, 1963).

Ore occurs in both massive and disseminated forms and is located at or near the
basal contact of the metagabbro with a local limestone/siltstone/quartzite
sequence, (Fig.2.3.14.). Mineralisation extends to at least 150m. below surface.
The primary sulphide assemblage comprises pyrrhotite and pentlandite with minor
chalcopyrite. A Kambalda-type supergene alteration sequence is present.

The deposit crops out as partly silicified gossan in weathered host at or near the
basal contact with altered limestone.

<u>Trojan</u> The Trojan deposit comprises three significant sulphide concentrations.
These occur in arcuate sill-like ultramafic units within an Archean greenstone
succession, (Fig.2.3.15.). The ultramafics consist of either dunite or serpentinite
after dunite. They are commonly separated by thin sedimentary intercalations.
Further, they may contain laterally extensive bands of thin ferruginous graphitic
slate and banded ironstone.

In both ultramafic types mineralisation is commonly disseminated and is
concentrated towards the centre of the unit, (Le Roex, 1964). Local massive
sulphide may however be present in serpentinite and is then generally located at
or near the basal contact with graphitic slate. Le Roex notes that the ore
assemblages differ in the two ultramafic host types: dunite commonly shows a
pentlandite, pyrite and nickeloan magnetite assemblage, with minor millerite
after pentlandite. In contrast, serpentinite generally has variable amounts of
pentlandite, pyrrhotite and magnetite, with minor pyrite and chalcopyrite.

Mineralised dunite is represented at surface by fairly fresh rock with earthy
magnesite and green nickel hydrosilicate staining. Mineralised serpentinite crops
out as spongy gossan containing nests of talc and carbonate.

<u>Perserverence</u> The Perserverence deposit occurs within a greenstone belt of
Bulawayan (Archean) age. The greenstone succession comprises a complex sequence

Metres

0   250   500

N

	Gabbro		Altered contact limestone
	Quartzite		Quartz-mica schist
	Gossan after nickel sulphide mineralisation		Scapolite-biotite schist
	Limestone		Contact zone : gabbro-limestone

Fig.2.3.14.   Local geol ⋅ of the Munali Hills nickel de osit

Kilometres

0   1   2

— N —

TROJAN HILL

CARDIFF HILL

▦ Granite   ▦ Mineralised ultramafic intrusives

▯ Greenstone succession   ▨ Metasediments
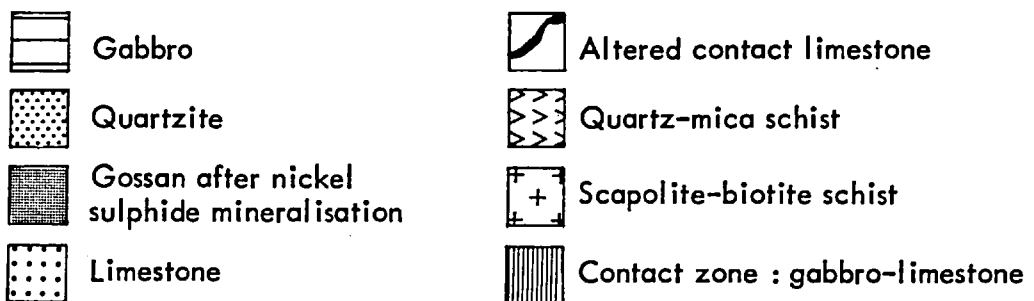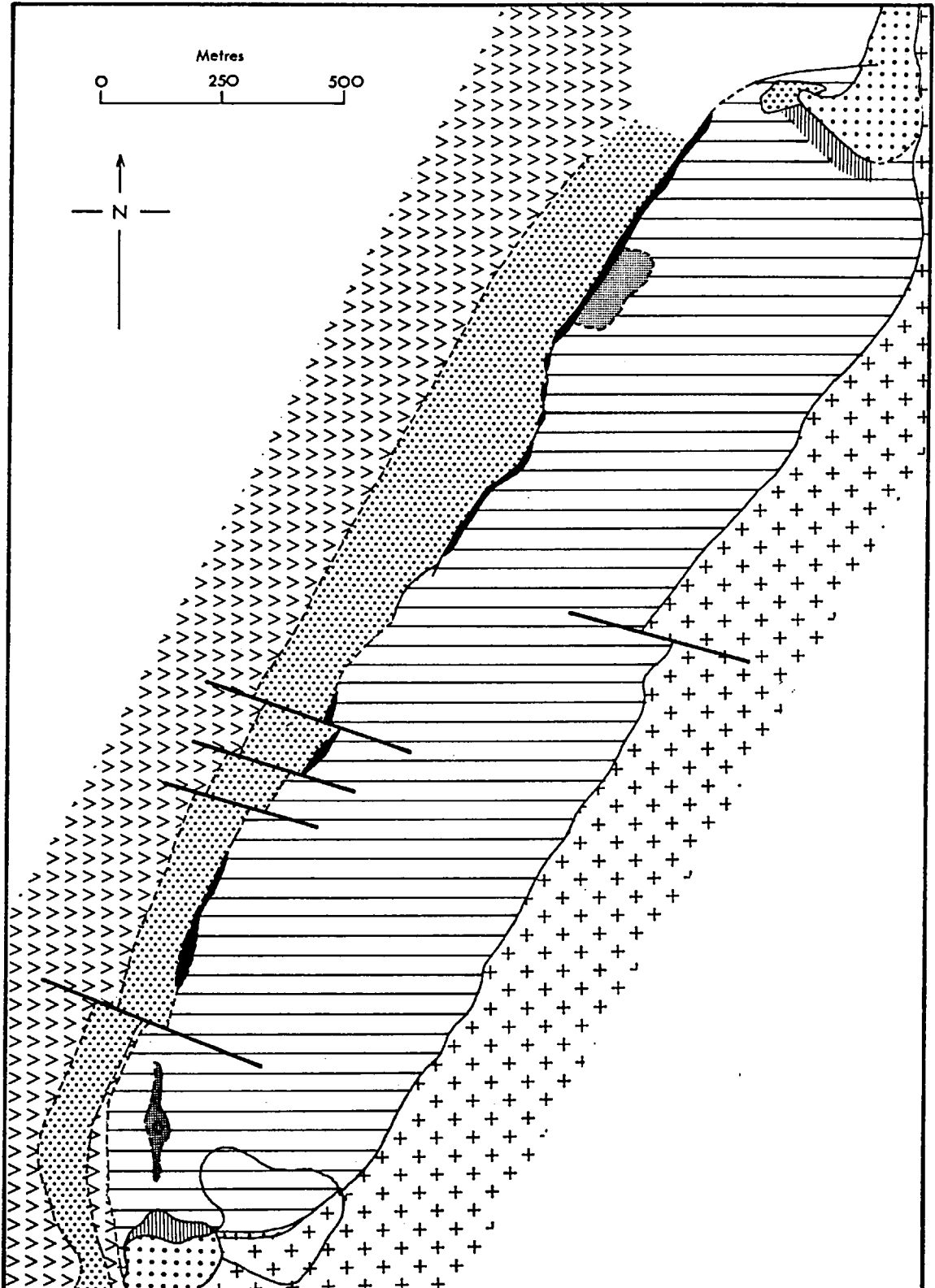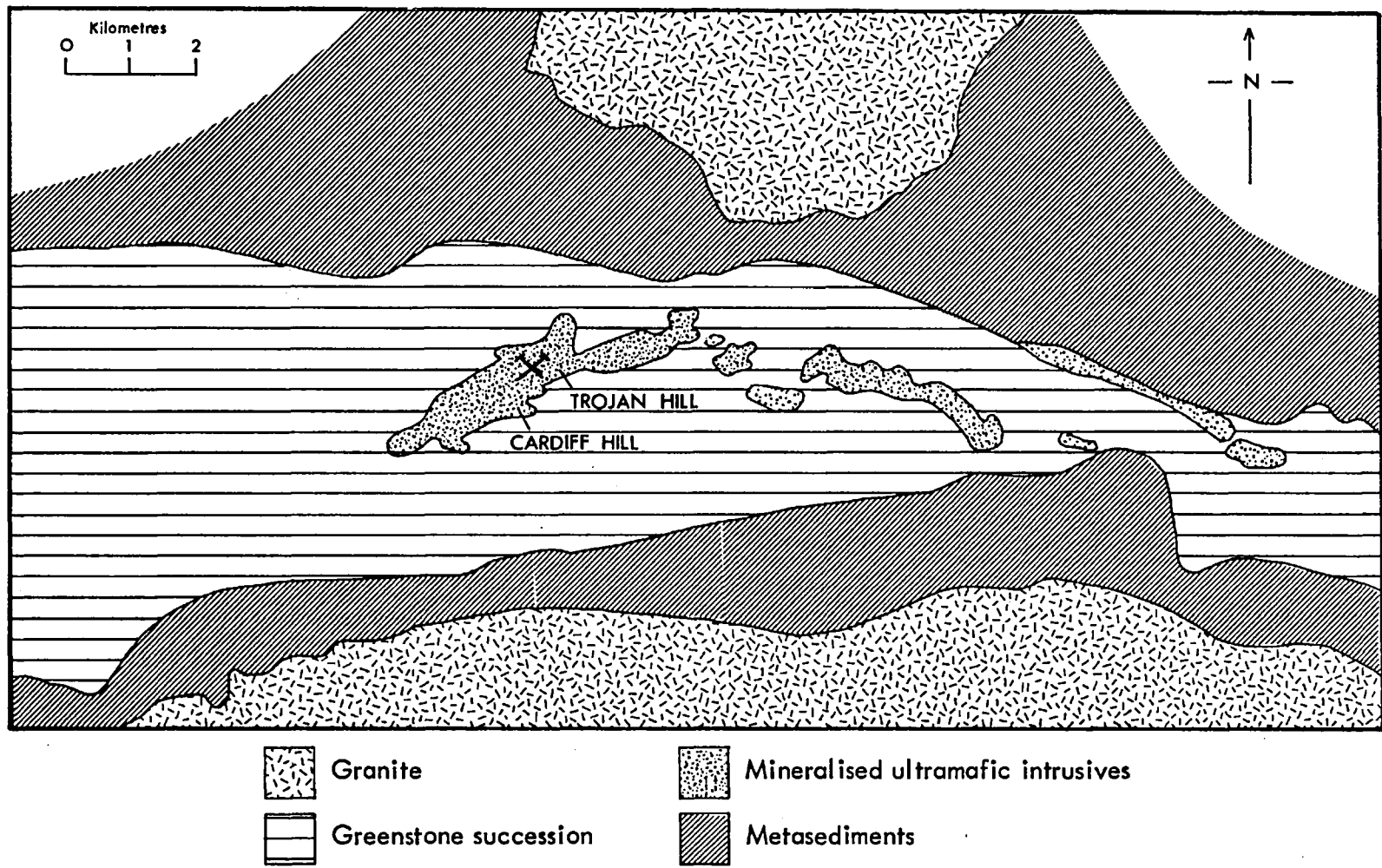
Fig.2.3.15.   The area geology of the Trojan nickel deposit (after Le Roex, 1964)

of acid and intermediate metavolcanics, metasediments, and small intrusive ultramafic bodies. The Perserverence mineralisation occurs within a sill-like amphibolite in one of these ultramafic units.

The orebody is lensoid in form. It occurs at or near the basal contact of host amphibolite with footwall serpentinite. Contact ore is typically massive and passes into progressively more disseminated sulphide away from the footwall contact. The primary ore assemblage comprises pyrrhotite and pentlandite, with accessory chalcopyrite. A supergene alteration sequence, similar to that at Kambalda is well developed at Perserverence.

The vertically inclined ore profile is overlain by a deep (40m.) oxide zone, and crops out as a linear zone of siliceous gossan rubble approximately 20m. wide.

Empress In the Empress nickel deposit the economic mineralisation is contained within the central zone of a dyke-like amphibolite after metagabbro/peridotite extending along the south-west edge of a small granodiorite stock, (Fig.2.3.16.). The stock is ovoid in outline and is surrounded by an Archean (Bulawayan) greenstone succession, (Sharpe, 1964). There is present a transition or "mixed zone" between the stock and the host amphibolite and which consists of alternating diorite and amphibolite bands.

The mineralisation may occur as blebs, masses or veinlets of sulphide in the host, and comprises pyrrhotite and pentlandite with subordinate chalcopyrite and minor pyrite and violarite. Traces of chalcocite are also present. The pentlandite is intimately associated with pyrrhotite in the form of granular intergrowths. More rarely it forms minute ex-solution flammes in the latter. Chalcopyrite is present as either discrete grains or as intergrowths.

Indicated reserves (1964) are 20.0 million tonnes at 0.7 percent nickel and 0.3 percent copper.

The orebody crops out as a clay-like rock with only rare minute malachite specks to indicate the buried mineralisation. Ferruginous gossans are present however, along the strike of the mineralised zone at Barebottom Hill, (Fig.2.3.7C.)

Shangani The Shangani deposit occurs within the northern part of the Shangani greenstone belt, (Viljoen et.al., 1976), (Fig.2.3.17.). Mineralisation is

66

see
below

Metres 500

N

Metres
0   100   200

N

Granodiorite
Greenstone succession
Dykes

Meladiorite (mixed zone)
Gabbro
Ore zone amphibolite
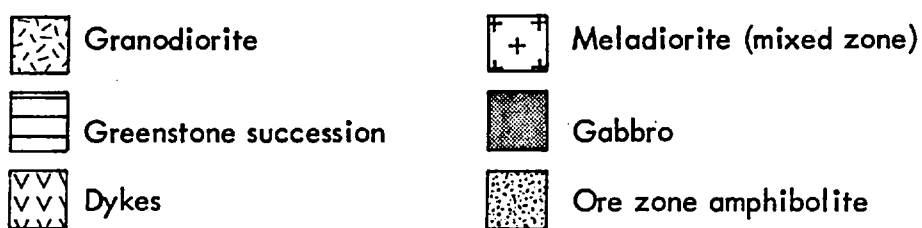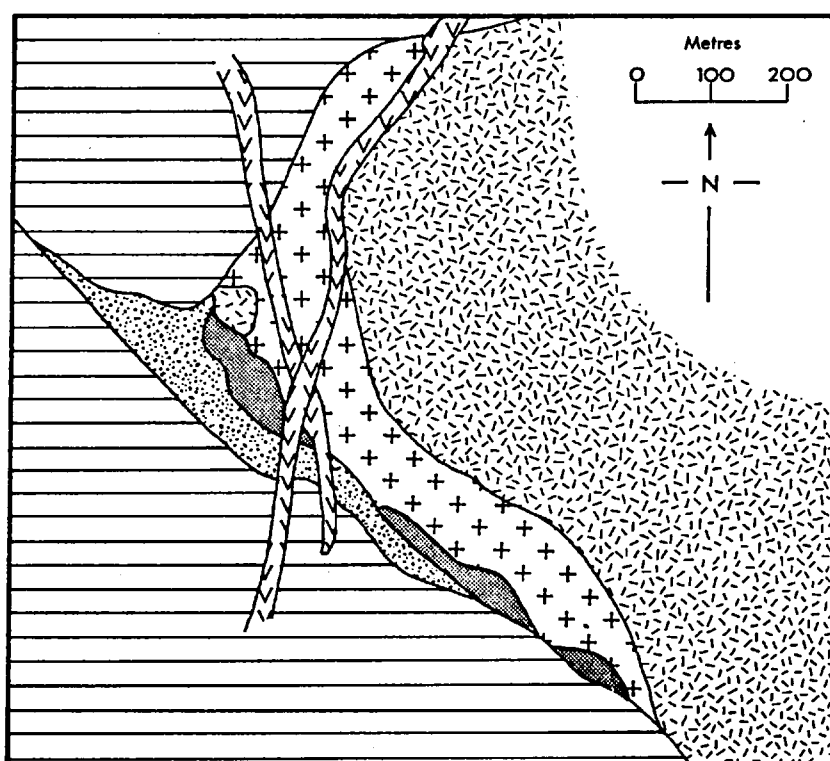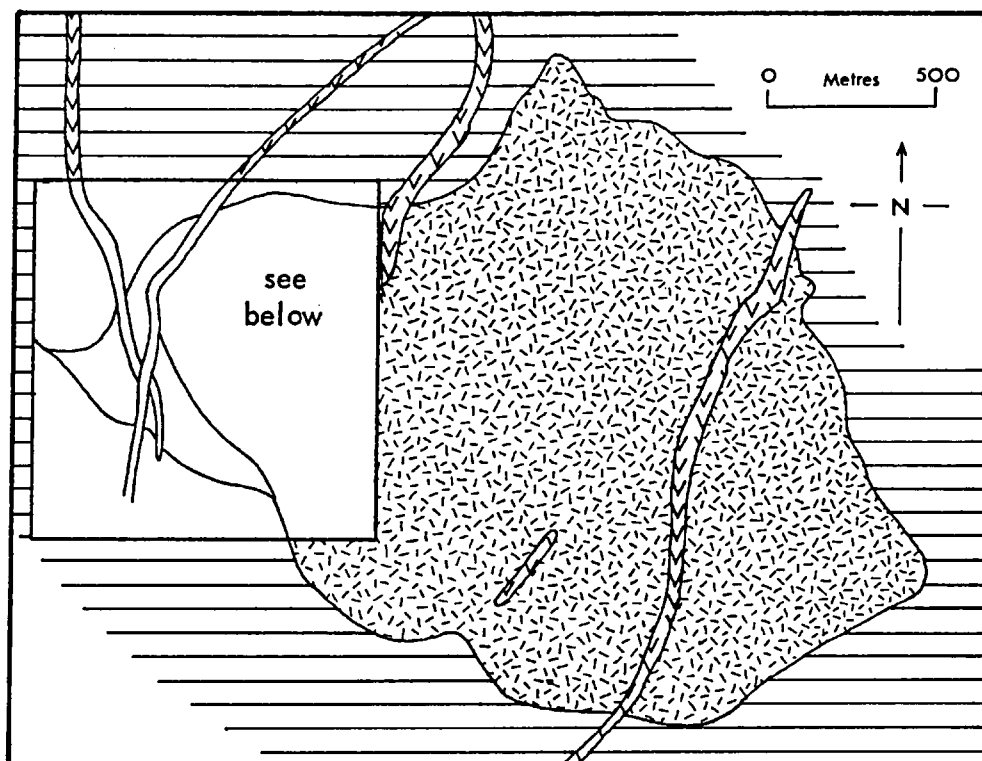
Fig.2.3.16. The local geology of the Empress nickel deposit
(after Sharpe, 1964)
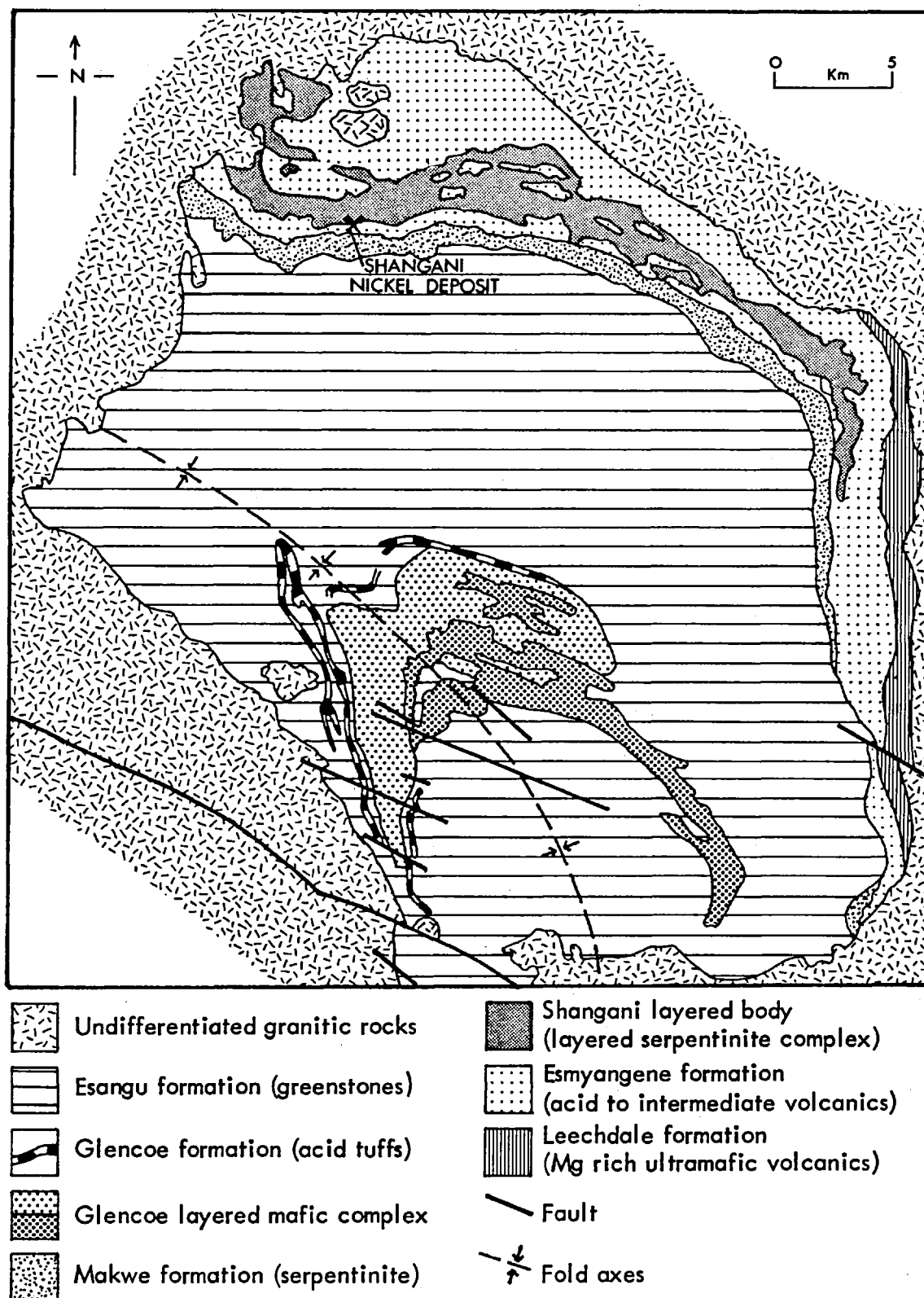
Fig.2.3.17. The area geology of the Shangani nickel deposit
(after Viljoen et al. ,1976)

associated with each of two south-east plunging lobes of an intrusive mushroom-shaped serpentinite complex.

The ore mineral assemblage is pyrrhotite-pentlandite. Two types of mineralisation are recognised: a massive pyrrhotite-rich type that occurs along the basal contact of the ultramafic lobes; and a volumetrically predominant disseminated pentlandite-rich type that occurs within the lobes themselves. Chalcopyrite and pyrite are minor constituents of both ore types.

Indicated reserves are approximately 16 million tonnes at 0.92 percent nickel.

The deposit crops out as three small patches of gossan of about 50m. total length, (Fig.2.3.7D.). These gossans, which are the outcrop of basal massive ore occur along the contact zone between footwall acid tuff and overlying metapyroxenite selvege.

The Damba area   There are three nickel prospects in this area: Damba, Damba South and Fibre. All three prospects are situated within a linear extrusive peridotite sequence that is associated with a north-south trending greenstone succession, (Fig.2.3.18.). The mineralisation occurs chiefly as interstitial blebs or fine disseminations of violarite and millerite, and is located towards the basal parts of serpentinised extrusive units. Minor to trace amounts of pentlandite, pyrite and chalcopyrite are generally also present.

The occurrences crop out as patches of ferruginous gossan rubble. The gossans at Fibre are located at the footwall contact of peridotite with metasediments, and probably represent thin units of locally massive ore, (Fig.2.3.19A.).

Epoch   Mineralisation at the Epoch prospect is associated with a talcose ultramafic complex that may be derived from a more extensive layered ultramafic sequence of Sebakian (early Archean) age.

The ore consists of pyrrhotite-pentlandite, mostly as disseminations in talc carbonate and talcose metadolerite. There are two ore zones. These occur at different stratigraphic levels in the host sequence, (Fig.2.3.20.). Both ore zones crop out as massive ferruginous gossan, (Fig.2.3.19B.).
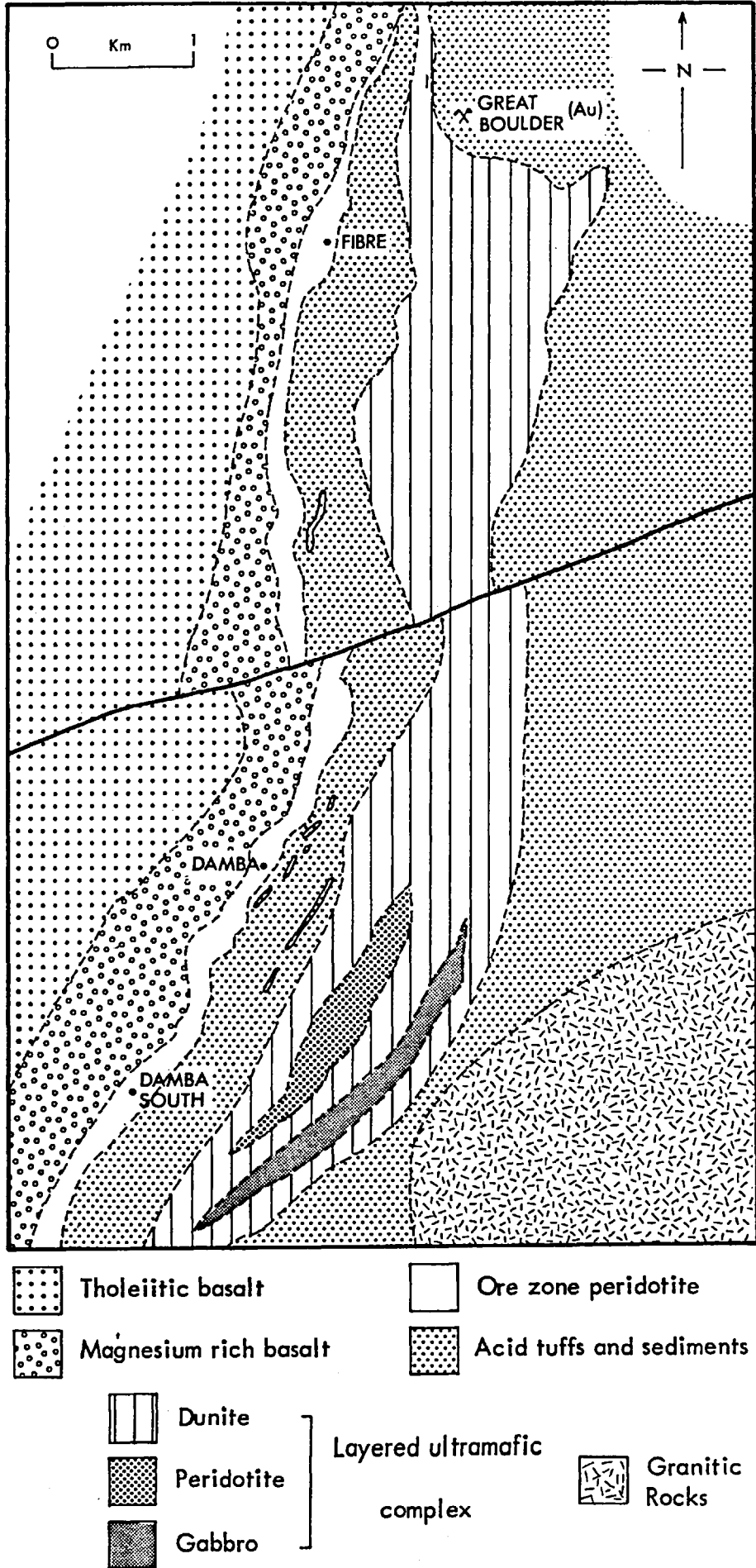
Fig.2.3.18. The geology of the Damba area

Fig.2.3.19 Surface expressions of Nickel Ore (3)

A   Fibre (Damba Area), Rhodesia
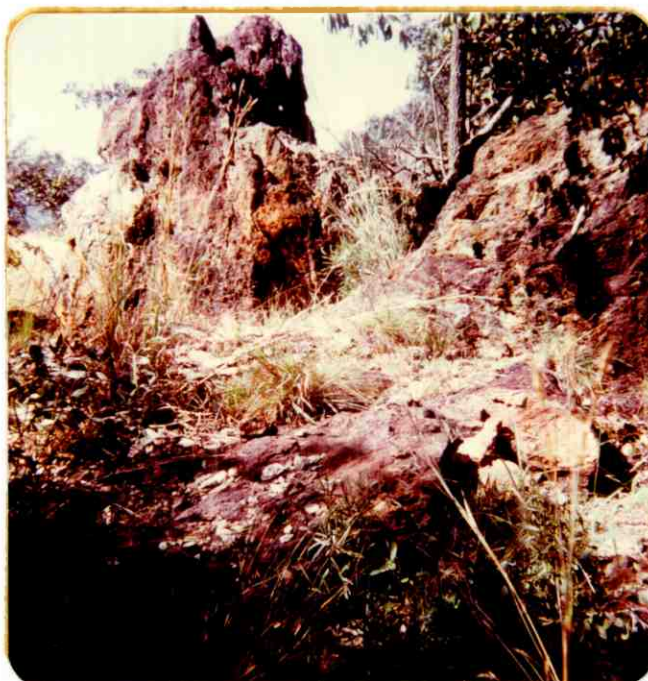
B   Epoch, Rhodesia

Fig.2.3.19 Continued

C   Pikwe, Botswana (Gossan profile)

D   Selibi, Botswana

Metres

0   50   100

S   N

TALC

CARBONATE

QUARTZ-AMPHIBOLE

ROCK

NORTH ZONE

MAIN ZONE
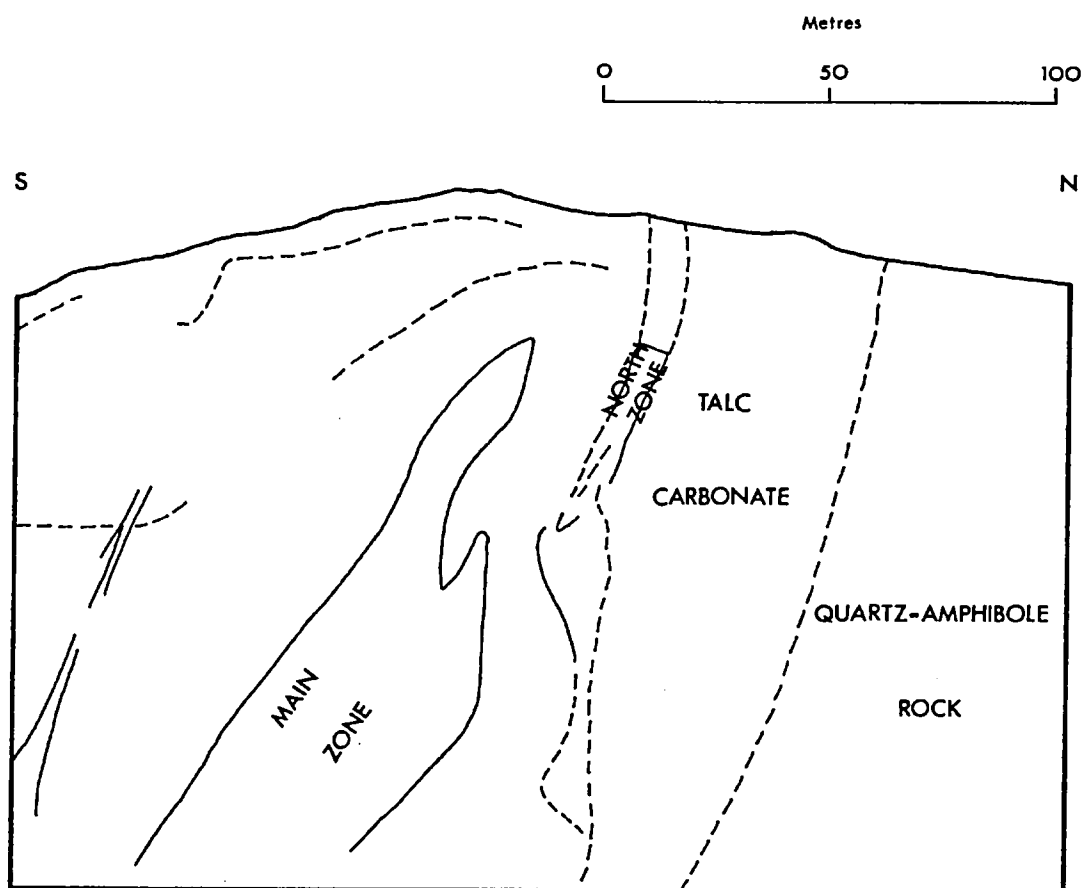
Fig.2.3.20.   Sketch section through the Epoch nickel prospect

Phoenix   The Phoenix deposit occurs within the Tati Schist Belt on the periphery of the Rhodesian craton in N.E. Botswana. The mineralisation is associated with intrusions of pegmatite and granite and occurs as shear and fracture fillings in a keel-shaped felspathic amphibolite body. The amphibolite host is surrounded and probably underlain by granite. It is likely that the present form of the mineralisation was caused by the remobilisation of a pre-existing orebody due to either emplacement or in situ formation of the investing granite, (S. Marsh, Pers.Comm.).

Economic (massive) mineralisation is confined to impersistent vein-like bodies situated within the vertical shear zones, and discontinuous, steeply plunging narrow ore shoots are localised at shear intersections. The ore assemblage consists of nickeliferous pyrrhotite, pentlandite – chiefly as ex-solution lamellae, chalcopyrite and minor pyrite. Estimated reserves are around 4.5 million tonnes at 2.1 percent nickel and 0.8 percent copper, (Baldock et.al.,1976).

The mineralisation at Phoenix crops out as a series of narrow linear gossan zones. More massive outcrops, corresponding to the coalesence of vein-ore, are prevalent at shear intersections.

Selkirk   The Selkirk deposit is associated with an inclined elongate wedge-shaped metatroctolite stock that is faulted against quartz diorite, (Fig.2.3.21.). Mineralisation is concentrated in the nose of the plunging synform so formed, and consists of a massive sulphide core surrounded by disseminated sulphide in the layered metatroctolite host, (Baldock et.al., op.cit.).

The mineral assemblage consists of pyrrhotite, pentlandite, chalcopyrite and pyrite. Ore reserves are estimated at some 3.0 million tonnes at 0.9 percent nickel and 0.8 percent copper.

Surface expression of the Selkirk deposit consists of an arcuate massive gossan outcrop in the nose of the host plunging synform, (Fig.2.3.7E.).

Pikwe   The Pikwe deposit is associated with a probable pre-tectonic intrusive amphibolite sill within a strongly refolded amphibolite/gneiss succession in the central zone of the Limpopo mobile belt, (Fig.2.3.22.).

The mineralisation occurs in the south-westerly dipping inverted limb of a major refolded recumbent antiform. The orebody is L-shaped, with northern and eastern limbs. In the northern limb, ore is present as massive blebs in amphibolite. Hanging wall massive sulphide ore predominates in the central (hinge) zone. In the eastern limb this hanging wall sulphide extends out into the paragneiss country rock. Disseminated sulphides are commonly present across the complete width of the host amphibolite.

The ore assemblage consists predominately of pyrrhotite, with minor pentlandite and chalcopyrite. Indicted proved reserves (1971) are 22.1 million tonnes at 1.45 percent nickel and 1.14 percent copper.

The Pikwe deposit has a well-developed gossan (Fig.2.3.19C.) that crops out at the surface in weathered amphibolite and possesses an extensive arcuate pattern.

Selibi The Selibi deposit lies on the southern flank of a structural basin within a gneissic sequence equivalent to that at Pikwe, (Fig.2.3.22.). Mineralisation is associated with an analogue of the Pikwe amphibolite. At Selibi however, the amphibolite has been subjected to an additional (early) phase of isoclinal folding. In consequence, the deposit is composed of a major, upper (overturned) orebody, and a lower minor one. Mineralisation is concentrated in the hanging wall of the upper fold limb and in the foot wall of the lower. Massive and disseminated ore types are present in both bodies.

The primary ore assemblage is similar to that at Pikwe. Estimated proved reserves (1971) are 10.0 million tonnes at 0.70 percent nickel and 1.56 percent copper.

There is little or no surface expression of ore at Selibi, (Fig.2.3.19D.). Buried massive gossans were, however, located by trenching operations.

Quartz diorite

Metatrocotolite host rock

Dolerite

Acid porphyry dykes

Gossans after nickel sulphide mineralisation

Fault
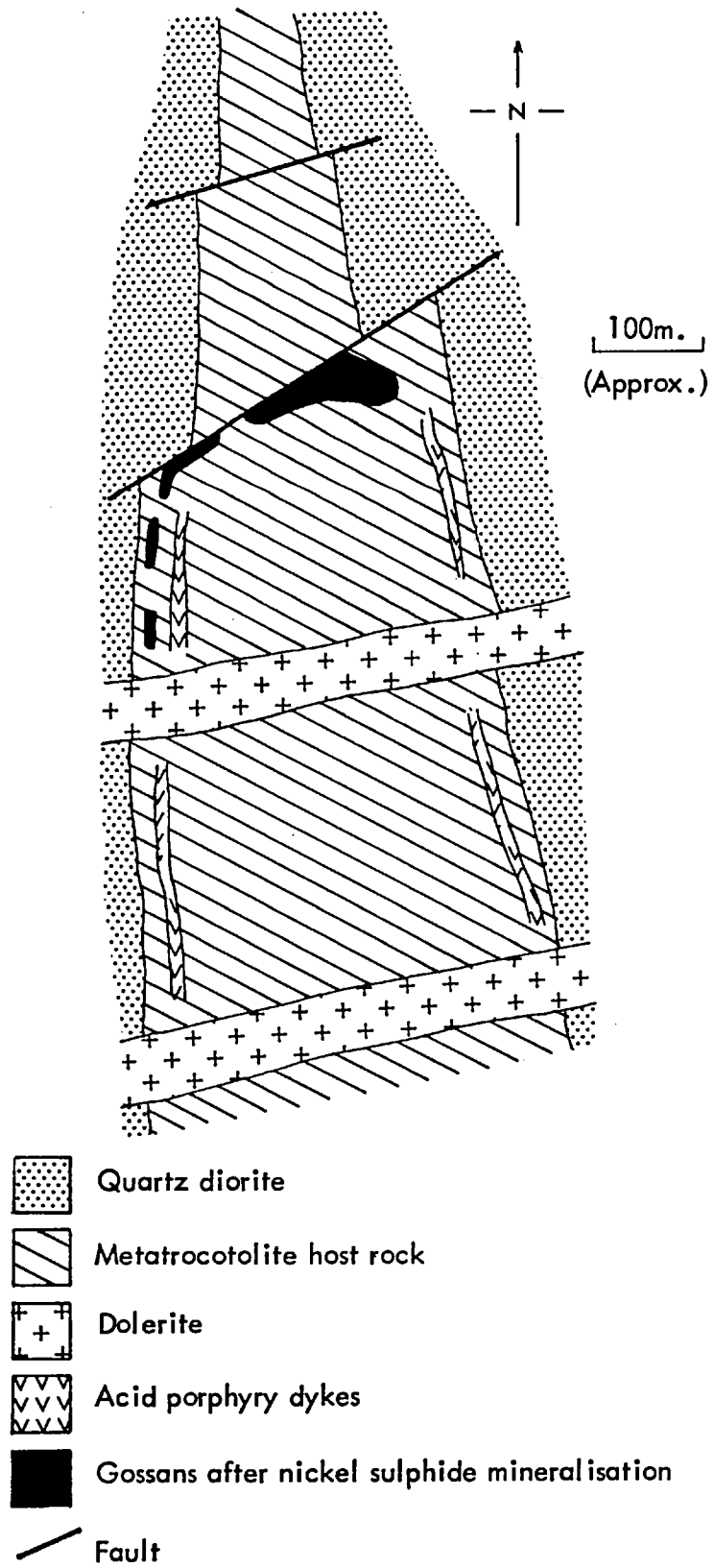
Fig.2.3.21. Geological sketch map of the Selkirk nickel prospect

Fig.2.3.22.   The geology of the Selibi -Pikwe area (after Wakefield, 1976)

Km

0   1   2   3

— N —

PIKWE

SELEBI
NORTH

SELEBI

[::::] Granitic gneiss   [ ] Undifferentiated gneiss

[||||] Sillimanite-cordierite gneiss   [/] Nickel sulphide mineralisation

[:::] Amphibolite   ⟋ Fault

[▓] Anorthositic gneiss   ∿ Structural trend
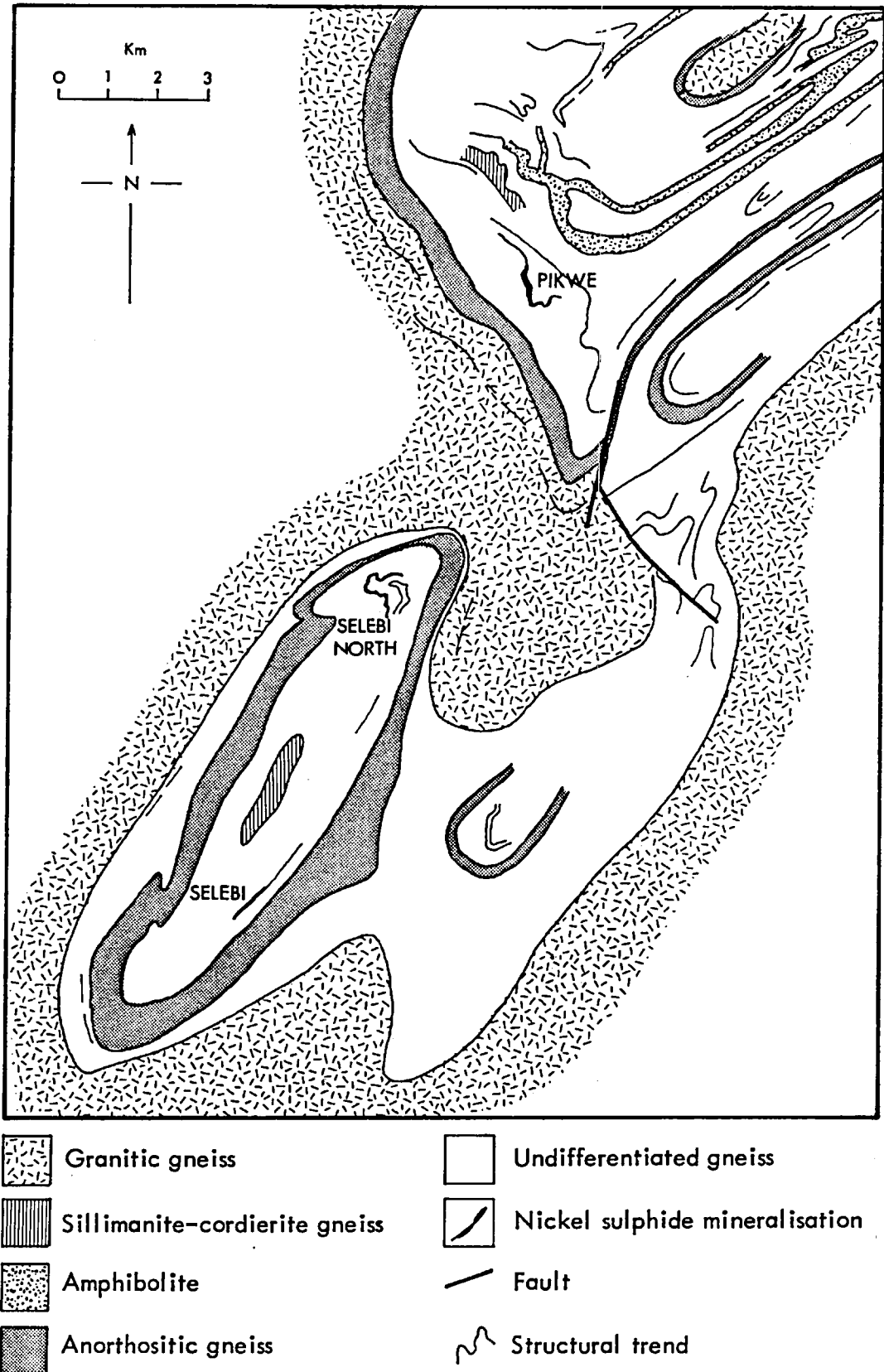
2.4. SUMMARY

The Archean Shield regions of Western Australia and southern Africa, in which the study deposits are located form essentially similar geological and metallogenic environments. Both regions contain typically elongate belts of volcanogenic/ metasedimentary successions of mafic – ultramafic affiliation. These "Greenstone belts" are typically invested and intruded by swarms of granitic plutons. Nickel sulphide mineralisation is associated with mafic, and more typically, ultramafic intrusive/extrusive rocks within these greenstone successions.

The recent climate of both Shield regions is in general semi-arid in nature. Rainfall is low, especially in the Yilgarn Shield, and is typically seasonal in character in both regions. In the Southern African Shield, however, the climate is not uniform. It varies from semi-arid in the south-western parts to warm temperate in the central and eastern areas. This zonal climatic configuration is reflected by vegetation and soil types. In the Yilgarn Shield, vegetation and soil type distributions are typical of a fairly uniform recent semi-arid to arid climatic environment.

In both regions the rocks are extensively and pervasively weathered. Work on the physiography of the Yilgarn indicates that the peneplained surface of the shield is Tertiary in age, with little active erosion occurring since that time. It is likely that the extensive deep lateratisation that characterises the surface of the shield was similarly developed in Tertiary times. The development of extensive alteration zones over the nickel deposits in this region is probably related to this lateratisation episode.

The corresponding physiography of the southern African Shield is rather more complex and consists of several somewhat linear, but more or less spatially distinct peneplain units developed at different altitudes. But here too, recent erosion appears to be at a minimum.

The widespread development of deep zones of silicate weathering and extensively leached soils in southern Africa indicates the long term development of temperate, seasonally humid conditions in this region. It is hence likely that the semi-arid climate prevalent in the southwestern area of the shield has been imposed only in relatively recent times. By analogy with the Yilgarn deposits, the development of extensive oxide zones above southern African nickel sulphide mineralisation is

probably related to a temperate seasonally humid paleoclimatic regime.

The essential geological features of the deposits comprising the study suite are indicated in Tables 2.4.1. and 2.4.2. for, respectively, the Western Australian and the southern African deposits.

Comparison of the regional geological settings of these deposits indicates that the majority occur within greenstone successions or equivalent lithologies of broadly similar age and locale. An exception is the Munali Pass deposit in Zambia. This occurrence is associated with a basic igneous intrusion, but is probably of Proterozoic age. In general though it is probable that the narrow range in regional settings exhibited by these deposits indicates a quite specific nickel metallogeny in the middle Archean. Further, this phenomenon appears to be confined to a narrow range of intrusive/extrusive igneous lithologies of mafic – ultramafic affiliation, and to have had quite narrow temporal limits.

The form of the orebodies appears to be remarkably consistent across the study suite. In general, the deposits are tabular or lensoid in form although all have been more or less affected by post-depositional deformation. There are, typically, significant concentrations of ore at, or near, the basal contacts of host silicates. Rarer hanging wall ore concentrations are also present in some instances.

These phenomena are probably related to the likely formation mode of these deposits: namely, as high temperature segregations of monosulphide solid solutions in silicate melts or crystal mushes of mafic to ultramafic composition.

There are however two exceptions to this generalised similarity of both host types and of orebody form. The first is the Carr Boyd Rocks deposit in Western Australia. Here, the sulphide mineralisation is developed in a bronzite-pegmatoid breccia pipe complex. The regional geological setting of the deposit is, however, of "normal" type. The second anamalous occurrence is the Phoenix deposit in Botswana. Here, the mineralisation is localised within vertical shear and fracture zones in a felspathic amphibolite host. The amphibolite forms a keel-like body and is invested in granite. The form of the Phoenix mineralisation and its structural setting indicate that the deposit probably results from the mobilisation of a pre-existing orebody. It is likely that the mobilisation was caused by the effects of local granitisation or granite emplacement.

Overall similarity between deposits is also apparent in terms of primary mineralogy and of ore type. The economic mineralisation typically consists of pyrrhotite and pentlandite with or without chalcopyrite. Accessory to trace amounts of pyrite and magnetite may also occur. Millerite is an important primary constituent at Otter Shoot, Kambalda. Minor amounts of nickel arsenides and sulpho-arsenides occur as primary constituents in two deposits of the Widgiemooltha Dome in Western Australia, (Widgie No.3 and Dordie North prospects).

Apart from these minor deviations however, the primary sulphide assemblages of the sampled deposits are consistent in their qualitative compositions. There is however, considerable quantitative variation between deposits, even between those in close spatial proximity: For example, the Lunnon and Durkin Shoots at Kambalda.

The ore minerals are typically in the form of disseminations in host silicate. These disseminations generally grade downwards into, or are closely associated with, zones of essentially massive to near-massive sulphides. These massive zones range from quite extensive formations (Lunnon Shoot), to small intermittent patches, (Epoch prospect, Rhodesia). However, massive sulphide is usually present to some extent in each ore deposit. Further, a zone of blebby, matrix or interstitial ore may be interposed between the two principal ore types. The generalised zonation of ore into disseminated, blebby and massive components is probably due to the generally accepted segregational origin of the parent sulphide material.

Deep weathering of primary ores has caused the development of secondary (supergene) sulphide assemblages, and ultimately, of extensive oxide zones above each deposit. These alteration sequences are, in general, qualitatively similar to those developed at Kambalda in Western Australia. Detailed descriptions of near-surface sulphide alteration in selected individual occurrences are set out in Chapters Three to Five.

The surface expressions of the sampled deposits exhibit a wide range of features: from conspicuous outcrops of massive gossan, (Epoch, Rhodesia), to small discrete patches or lenses of ferruginous oxide, (Shangani). Typically, however, the gossan zone occurs at or near the basal contact of the weathered host unit. It therefore generally represents the near-massive to massive component of the underlying footwall sulphide mineralisation.

In areas of deep soil formation there may be little or no direct outcrop of gossan at the surface. Here the deposit may be represented only by small patches of ferruginous rubble (float) as, for example, at Redross (W.A.). Alternatively, the soil cover may be deep enough to completely mask all physical manifestation of the underlying deposit, as at Nepean (W.A.), and Selibi (Botswana). At both these occurrences, ferruginous gossans were discovered only after trenching operations had been initiated.

Further information on the individual deposits comprising the study suite may be obtained from the literature cited in the summary Tables 2.4.1. and 2.4.2.

Deposit	Geographical Location Lat (S) Long (E)	Regional Geology	Host Rock Type(s)	Form of orebody	Ore types present	Primary sulphide mineralogy	Sulphide alteration	Depth of oxide zone	Surface expression of deposit	Published grade(s) and tonnage	References
Mount Windarra	Lat 28°29'S Long 122°14'E	greenstone succession	sill-like ultramafic at contact with B.I.F.	lenticular, related to drag folding	1) disseminated sulphide oxide 2) breccia 3) massive	Po Pn major cobaltiferous Py:Acc Ccp mag : trace	well-developed violarite and secondary pyrite	40m.	small gossan outcrops along ultramafic /B.I.F. contact	1.46% Ni 0.14% Cu 11.3 x 10⁶ tonnes	Roberts 1975 Watmuff 1975
Carr Boyd Rocks	Lat 30°04'S Long 121°38'E	lobate mafic – ultramafic complex	bronzite-pegmatoid complex	intrusive breccia pipes	massive to disseminated	Pn; Ni-ous Po 4% 20% Minor: Py Ccp Mag	partly developed violarite, pyrite;minor marcasite, greigite	25 - 30m.	malachite stains on umafics gossans revealed by costeaning	1.65% Ni 0.57% Cu 1.3 x 10⁶ tonnes	Purvis et al 1972 Schultz 1975
Scotia	Lat 30°12'S Long 121°16'E	in eastern limb of greenstone syncline	lens-shaped dunite	small lens in structural embayment in f/w	1) disseminated 2) discontinuous massive	Pn 60% Po 30% major Py Mag (5%) Acc Ccp (0.5%) minor	well developed violarite, pyrite	43m.	brown siliceous cap-rock on ore-bearing ultramafic gossan shows rare	3.07 % Ni 0.25% Cu 1.13 x 10⁶ tonnes	Christie 1975
Nepean	Lat 31°10'S Long 121°05'E	greenstone inlier in granite	serpentinised sill-like peridotitic intrusives	two overlapping steeply dipping tabular bodies in f/w zones	1) fine disseminated 2) triangular disseminated 3) basal massive	Pn 60% Py 20% Po 18% Ccp cub val : trace	well developed violarite, pyrite, marcasite	30m.	no surface expression	3.0% Ni 0.6 x 10⁶ tonnes	Sheppy and Rowe 1975
Mount Monger	Lat 31°04'S Long 121°58'E	greenstone succession	serpentinised ultramafic	probably lensoid or tabular	1) disseminated 2) massive	Pn Po : major Ccp : Acc Mag : trace	well developed violarite, pyrite	30 - 40m.	ferruginous gossan float	not available	–
Jan Shoot	Lat 31°11'S Long 121°41'E	greenstone succession in regional domed structure	serpentinised ultramafic volcanic succession	generally as elongate shoot along dislocated f/w contact of host	1) disseminated 2) basal massive	monoclinic Po, Pn Ccp Mag trace	well developed violarite, pyrite	30m.	well-defined siliceous gossans along f/w umafic contact	Composite for Kambalda Dome 3.3% Ni 0.25% Cu 19.85 x 10⁶ tonnes	Kambalda Deposits Ross & Hopkins 1975 Woodall & Travis 1969
Otter Shoot	as above	as above	as above	as above	as above	as above + millerite	as above	18m.	as above	–	as above
McMahon	as above	as above	as above	as above – also present as hanging wall ore	as above	as Jan Shoot	as above	50m. (H.W. ore)	as above	–	as above
Durkin Shoot	as above	as above	as above	as Otter Shoot	as above	as above	as above	25m.	as above	–	as above
Silver Lake / Lunnon	as above	as above	as above	as Otter Shoot but also hanging wall	as above	as above	as above	18m.	as above	–	as above
Spargoville 5A Prospect	Lat 31°20'S Long 121°30'E	arcuate greenstone succession	dunite lenses within tremolite-talc-chlorite bodies	podiform in structural embayment in f/w of thin dunite selvege	1) disseminated 2) basal massive	no primary sulphide assemblage present	violarite secondary pyrite	30m.	small discrete siliceous gossans	not available	Andrews 1975
Mount Edwards	Lat 31°38'S Long 121°32'E	NNW trending greenstone succession	ultramafic volcanic complex peridotite flows	elongate lenses at or near f/w contact with underlying volcanoclastic unit	1) disseminated 2) some massive	Po Pn : majors Ccp : minor	well developed violarite, pyrite	35m.	spasmodic siliceous gossans within laterised mafic/ umafic rubble zones	2.2% Ni 0.2% Cu 1.54 x 10⁶ tonnes	Inco Staff (In Knight 1975)
Widgiemooltha No.3 Prospect	as above	in domed greenstone anticline intruded by granite	ultramafic volcanics	lens-shaped or sigmoidal in f/w embayment in host	1) disseminated 2) basal massive	Pn Po minor arsenides	well developed violarite, pyrite, marcasite	30m.	two narrow zones of silicified gossans	1.23% Ni 0.9% Cu 0.9 x 10⁶ tonnes	Dalgarno 1975
Dordie North Prospect	as above	as above	southern extension of Widgie '3' umafic	two minor embayments in f/w contact	1) disseminated 2) narrow basal massive	Pn Po Ccp arsenides : minor	as above	20m.	restricted zone of silicified gossan rubble	1.2% Ni no tonnage data	Dalgarno 1975
Redross	as above	as above	narrow ultramafic differentiated sill	planar on f/w contact of host with underlying amphibolite	1) disseminated 2) matrix 3) irregular basal massive	Pn Po major Ccp minor	as above	25 - 30m.	restricted zone of spasmodic gossan float	3.5% Ni 0.32% Cu 1 x 10⁶ tonnes	Dalgarno 1975
Ravensthorpe No.5 Prospect	Lat 33°50'S Long 120°10'E	ultramafic sequence	serpentinised ultramafic volcanic unit	probably tabular at or near basal contact of host with underlying quartzite	1) vein 2) disseminated 3) massive	Py, nickeliferous Po Ccp minor	some alteration violarite, pyrite	25m.	non-silicified gossan along basal contact of host ultramafic	not available	–

Table 2.4.2. Geological summary of the sampled southern African nickel deposits

Deposit	Geographical Location Lat (S) Long (E)	Regional Geology	Host Rock Type(s)	Form of orebody	Ore types present	Primary sulphide mineralogy	Sulphide alteration	Depth oxide zone	Surface expression of deposit	Published grade(s) and tonnage	References
Munali Zambia	Lat 15°54'S Long 28°06'E	mafic intrusion in late Proterozoic metasediments	metagabbro	probably lensoid or tabular at f/w contact of host with metasediments	1) disseminated 2) massive	Pn, Po : major Ccp : Acc Mag : Minor	well-developed violarite pyrite	35m.	zones of partly silicified gossan at or near host contact with altered limestone	not available	Smith 1963
Trojan Rhodesia	Lat 17°18'S Long 31°20'E	greenstone succession	sill-like dunite and serpentinite	1) lensoid or tabular in centre of host unit 2) locally massive at/near host basal contact with slates	1) disseminated 2) massive	in dunite:Pn, Py nickeloan Mag in serp : Pn Po mag Ccp, Py = minor	violarite pyrite (marcasite)	30m.	spongy gossans containing nests of host material	not available	Le Roex 1964
Perserverence Rhodesia	Lat 17°59'S Long 29°50'E	greenstone succession	amphibolite after andesite	lensoid at or near basal contact of host with serpentinite	1) disseminated 2) basal massive	Pn Po Ccp	well-developed violarite pyrite	38m.	linear zone of siliceous gossan rubble	not available	–
Empress Rhodesia	Lat 18°28'S Long 29°25'E	granodiorite intrusion in greenstone succession	dyke-like "amphibolite" bordering stock margin	tabular within central zone of host	1) disseminated 2) semi-massive (blebby) 3) (rarer) massive	Pn Po Ccp Py minor	partially developed violarite pyrite	20m.	ferruginous gossans along line of mineralisation. clay-like outcrop over main ore zone	0.7% Ni 0.3% Cu 20 x 10^6 tonnes	Sharpe 1964
Shangani Rhodesia	Lat 19°42'S Long 29°15'E	greenstone succession	intrusive serpentinite complex	lensoid along and within plunging lobes of mushroom-shaped host	1) disseminated within host 2) massive at basal contacts	Pn Po major Py Ccp minor	probable partial development in massive violarite pyrite	20 – 40m.	small gossan patches along a restricted contact zone	0.92% Ni 16 x 10^6 tonnes	Viljoen et al 1976
Damba Area Rhodesia	Lat 19°40'S Long 28°53'E	linear extrusive (greenstone) sequence	serpentinised ultramafic extrusives (meta-peridotite)	probably tabular near host basal contacts	1) disseminated 2) blebby interstitial	Po Pn Ccp Py Mil	partly developed in blebby-coarsely disseminated material violarite (pyrite)	30m.	ferruginous gossan rubble patches	not available	–
Fibre Rhodesia	Lat 19°40'S Long 28°53'E	as above	northward extension of Damba host	tabular at f/w contact of host with metasediments	as above	probably as above	probably similar to Damba occurrences	30m.	ferruginous gossan rubble at host basal contact	not available	–
Epoch Rhodesia	Lat 20°29'S Long 29°20'E	layered ultramafic (greenstone) sequence	altered mafic and ultramafic units (talcose metadolerite and talc carbonate)	lensoid or tabular in host	mostly disseminated patchy basal massive	probably Pn Po	probable development in massive or coarse disseminated violarite (pyrite)	25 – 40m.	massive ferruginous gossans	not available	–
Phoenix Rhodesia	Lat 21°13'S Long 27°46'E	hetereogeneous metabasic zone in granite migmatite	heterogeneous felspathic amphibolite	impersistent vein-like bodies in shear zones	near-massive to massive in steeply-plunging narrow shoots	Ni-ous Po Pn Ccp Py : minor	well-developed violarite, pyrite	20 – 25m.	narrow linear gossan zones with broader outcrops at shear intersections	2.1% Ni 0.8% Cu 4.5 x 10^6 tonnes	Baldock et al 1976
Selkirk Botswana	Lat 21°19'S Long 27°43'E	metamorphosed intermediate to basic intrusive complex	wedge-shaped metatroctolite stock	tabular along fold nose and axis of host stock and adjacent quartz diorite	mainly massive (fold core) surrounded by disseminated in host stock	Po Pn Ccp Py minor	well developed in massive ore violarite pyrite	20 – 30m.	massive gossan outcrop in nose of host plunging synform	0.9% Ni 0.8% Cu 3.0 x 10^6 tonnes	Baldock et al 1976
Pikwe Botswana	Lat 21°54'S Long 26°53'E	granite-gneiss paragneiss, meta-volcanics/sediments	intrusive pre-tectonic amphibolite sill	tabular, L-shaped in inverted limb of refolded recumbent antiform	1) disseminated 2) massive blebby (N.limb) 3) massive (E.limb hanging-wall)	Po Pn Ccp Mag minor	well-developed violarite pyrite	40m.	massive gossan outcrop in arcuate pattern	1.45% Ni 1.14% Cu 22.1 x 10^6 tonnes	Gordon 1973 Baldock et al 1976 Wakefield 1976
Selibi Botswana	as above	as above	intrusive pre-tectonic amphibolite sill folded isoclinally	tabular folded (isoclinally) upper limb: hanging wall body lower limb: footwall body in folded host	1) disseminated 2) massive	Po Pn Ccp Mag minor	probably very similar to Pikwe	30 – 40m.	no direct surface expression (deep soil). massive ferruginous gossans in trenches (4 - 7m.)	0.70% Ni 1.56% Cu 10.0 x 10^6 tonnes	Gordon 1973 Baldock et al 1976

`CHAPTER THREE

SUPERGENE ALTERATION AT THE PIKWE NICKEL-COPPER SULPHIDE
DEPOSIT, BOTSWANA

3.1. INTRODUCTION

The sequence of near surface sulphide alteration that is developed in the Pikwe
nickel-copper sulphide deposit is now described. The study is based on the
oxidation sequence that is present within the northern limb of the ore body.
Sampling in this sector was carried out by documented drillcore, (for primary
and secondary sulphides), and within the open pit developed on the northern
limb, (for leaching sulphides and for the overlying oxide zone profile).

The petrology of progressive sulphide alteration (oxidation) is dealt with first,
and is set out as a descriptive synopsis in section 3.2. This work consists of
a mineralogical and textural documentation of each successive stage in the
observed alteration sequence that is developed in near-massive to massive
sulphide ore: that is, from unaltered primary sulphide, through secondary
sulphide development and subsequent oxidative leaching, to the formation and
succeeding development of the overlying oxide (gossan) profile.

The work is supplemented by mineral chemical data, where such information is
available. A more detailed chemical documentation of individual members of
the Pikwe suite is set out in the relevant part of Appendix Two.

The above work programme is performed in order to document the petrology of
this previously unreported supergene oxidation sequence. It is also carried out
to allow due comparison to be made with the previously undocumented oxidation
profiles developed in the other nickel sulphide deposits that comprise the
remainder of the present study suite, (Chapters Four, Five and Six). The results
of this descriptive work are subsequently utilised in the genetic investigations
that form Chapters Seven and Eight of the present study.

The petrological work on progressive sulphide oxidation at Pikwe is complemented
by a description of the petrology of associated host silicate alteration, and of
related oxidate minerals. These studies are made in order to document the effects
of sulphide leaching on adjacent silicate rocks at this deposit. But they are also
performed in order to aid a general investigation of the effect of silicate alteration

on oxide zone petrology and chemistry, (Chapter Eight).

The petrological work documented in section 3.2. is further supplemented by a description of true density and porosity variation within the observed oxidation profile, (section 3.3.). This work is performed in order to document the profile variation of these physical properties at Pikwe. But also, more importantly, because density and porosity act as semi-quantitative indicators of both mineralogical and chemical change within the alteration sequence.

The second major part of the present chapter, (section 3.4), comprises a description of the bulk mean chemistry of the Pikwe sulphide oxidation sequence. This work, hence, forms a natural complement to the petrological description in section 3.2 as it documents the behaviour of a suite of important major and minor elements during progressive sulphide alteration.

Chapter Three concludes with a brief summary, (section 3.5). Details of the techniques employed in the investigation are set out in Appendix One.

3.2 THE PETROLOGY OF THE ALTERATION SEQUENCE

The petrology of Pikwe massive primary sulphide ore

The following petrological description of near surface alteration at Pikwe is based on the oxidation sequence developed in the northern limb of the deposit, (Fig.3.2.1.). This limb of the ore body consists of a westerly-dipping sulphide zone of variable thickness and somewhat irregular distribution, (Gordon, op.cit.). The mineralisation is typically present as lenses of massive sulphide within a near monominerallic hornblende amphibolite, and generally occurs at or near the hanging wall contact of host and adjacent paragneiss, (Fig.3.2.2.). Unaltered primary massive sulphide ore extends to within 98 metres of the surface.

The primary mineral assemblage of near-massive to massive ore at Pikwe comprises pyrrhotite-pentlandite-chalcopyrite-magnetite and minor silicate, (Table 3.5.1.). It has been previously documented by several workers, (Gordon, op.cit.; Wakefield, 1974, 1976). In consequence, only those features of significance to the present study are now summarised.

Fig. 3.2.1. Sketch Plan of the Pikwe Ore Body

(Based on Wakefield 1976)
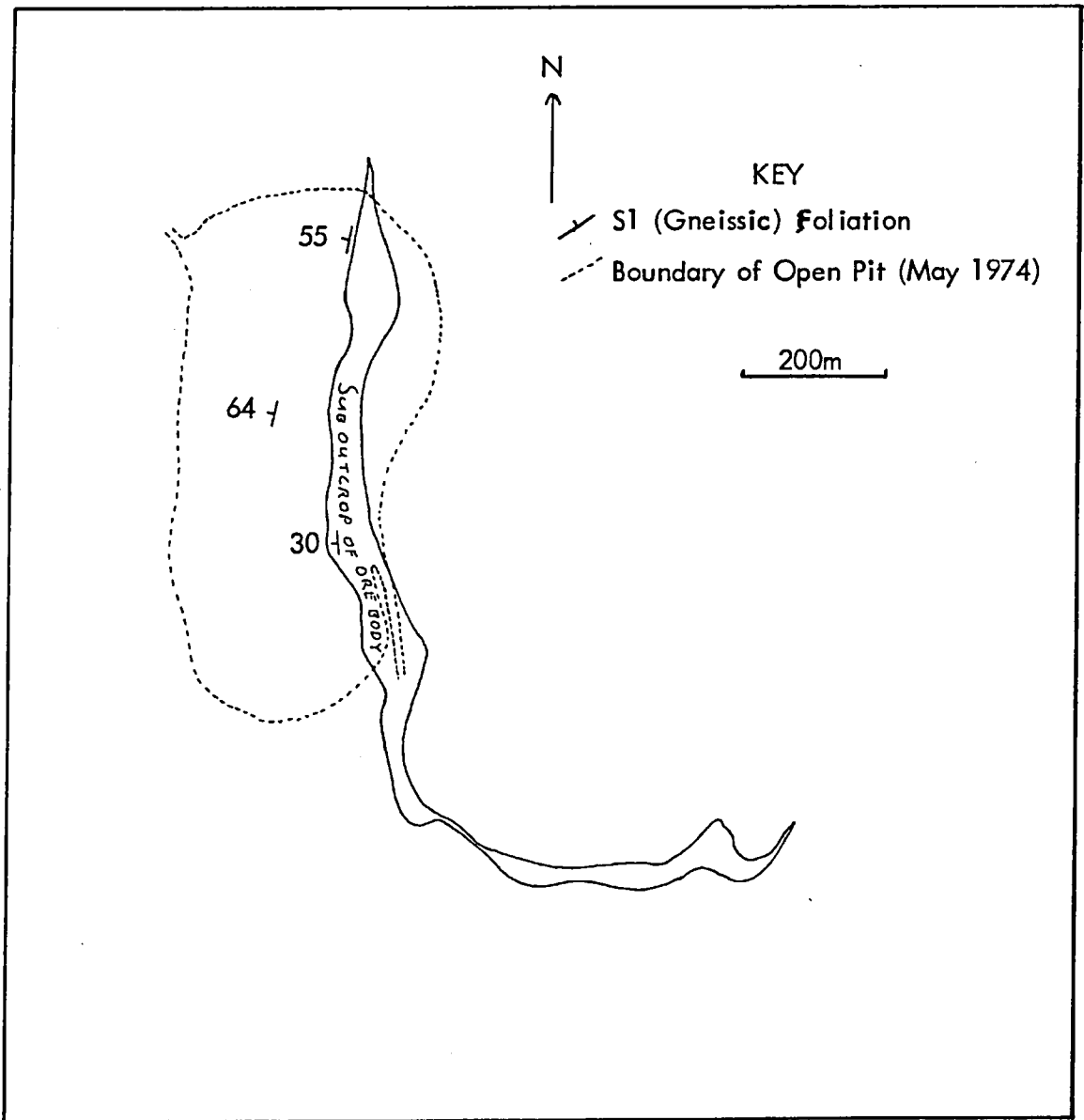
Fig. 3.2.2. Section through the North Limb of the Pikwe Ore Body

(Based on data supplied by B.C.L.)

W

E

Depth
(m)

0
20
40
60
80
100
120
140
160
180
200

g g g g
g g g g

1

8

4

6

3

1

5

7 5 7

2

4

500m

KEY

1 Massive Sulphide Ore

2 Host Amphibolite

3 Hanging Wall Grey Gneiss

4 Foot Wall Grey Gneiss

5 Grey Gneiss

6 Pink Gneiss

7 Pink Gneiss with Biotite

8 Interbedded Grey and Pink Gneiss

g Gossan after Sulphide Ore
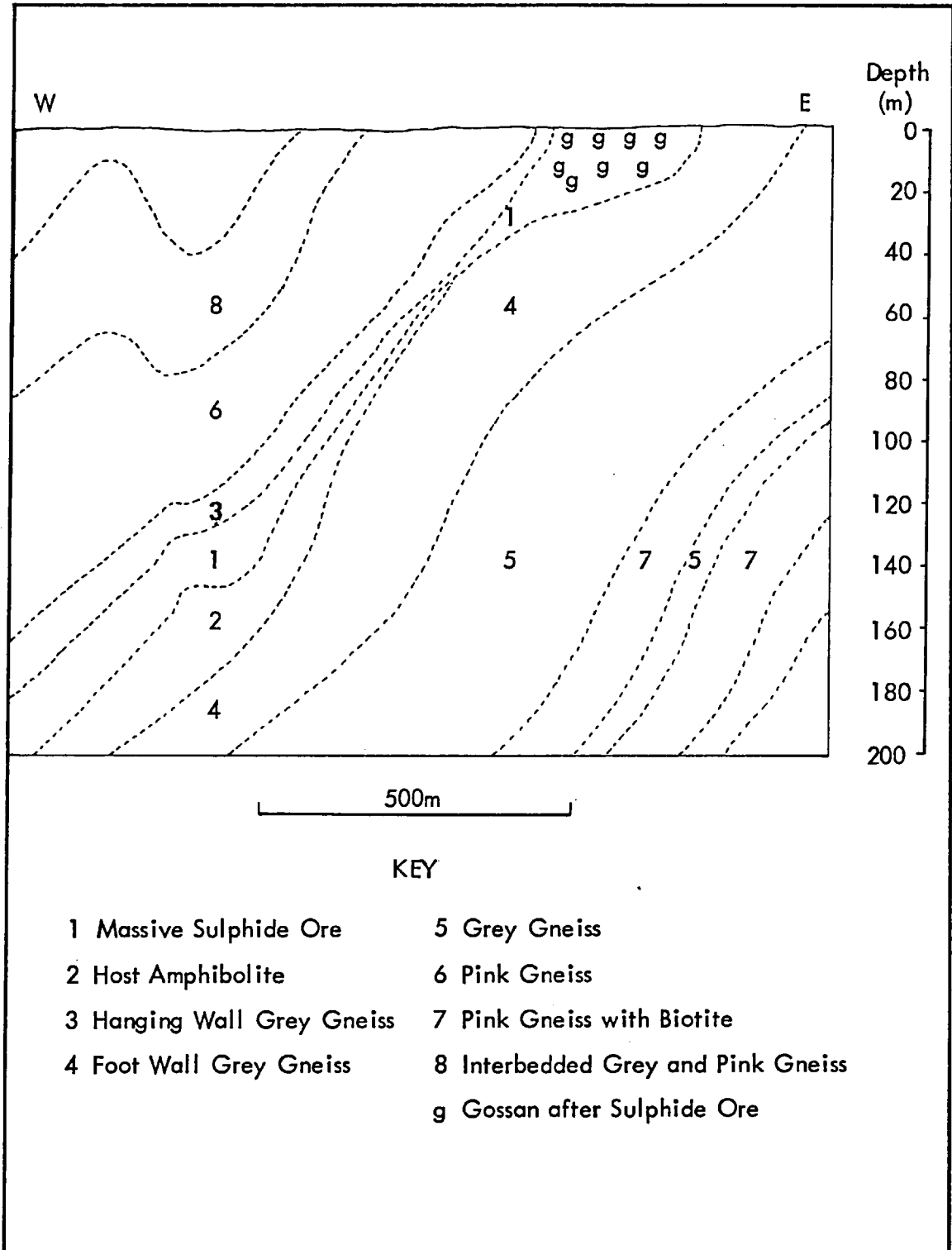
Pyrrhotite forms between 80 and 90 percent of the massive sulphide assemblage, (Fig.3.2.3.). The mineral is present in two forms: as large (6 to 8mm.) irregularly-shaped grains containing generally conspicuous deformation structures; and as rarer, more homogeneous polygonal form of mean size 1.5 to 2.0mm. The deformation structures in the large grain type take the form of elongate spindle twins or well-developed kink-zone forms, (Fig.3.2.4A.).

The five pyrrhotite compositions given in Table 3.2.1 indicate that monoclinic pyrrhotite (Fe_7S_8) characteristically occurs in the rim areas of the grains from which the data were obtained. Further, the data also indicate that Pikwe monoclinic pyrrhotite is typified by sub-detection ($<$ 200ppm) levels of both nickel and cobalt.

Pentlandite forms about five percent of Pikwe massive sulphide ore, (Fig.3.2.3.). It is present in two textural varieties; as an elongate interstitial form along pyrrhotite borders, (Fig.3.2.4B.), and as flamme aggregates within pyrrhotite, (Fig.3.2.4C.). The mean ratio of the two pentlandite forms is approximately four to one.

The chemical compositions of three interstitial pentlandite grains, (Table 3.2.2.), indicate that Pikwe pentlandite exhibits relatively little inter-sample variation in its major element proportions. In contrast however, the data show that an inter-sample complementary variation of cobalt and copper contents may occur in this pentlandite species.

Chalcopyrite forms about five percent of Pikwe massive ore, (Fig.3.2.3.), but is inhomogeneously distributed within the sampled ore material. The mineral exhibits several textural forms - from irregular equant grains, (Fig.3.2.4D.), through elongate stringer forms, (Fig.3.2.4E.), to bleb-like grains associated chiefly with silicates.

The chemical compositions of two Pikwe chalcopyrite grains are given in Table 3.2.3. These data indicate that the constituent major elements show little inter-sample variation, and that chalcopyrite is probably characterised by a near-theoretical stoichiometry. Further, Table 3.2.3. also demonstrates that the sampled chalcopyrites do not contain detectable quantities of either nickel or cobalt.

Fig.3.2.3. Mineralogical Profile of Pikwe Sulphide Alteration
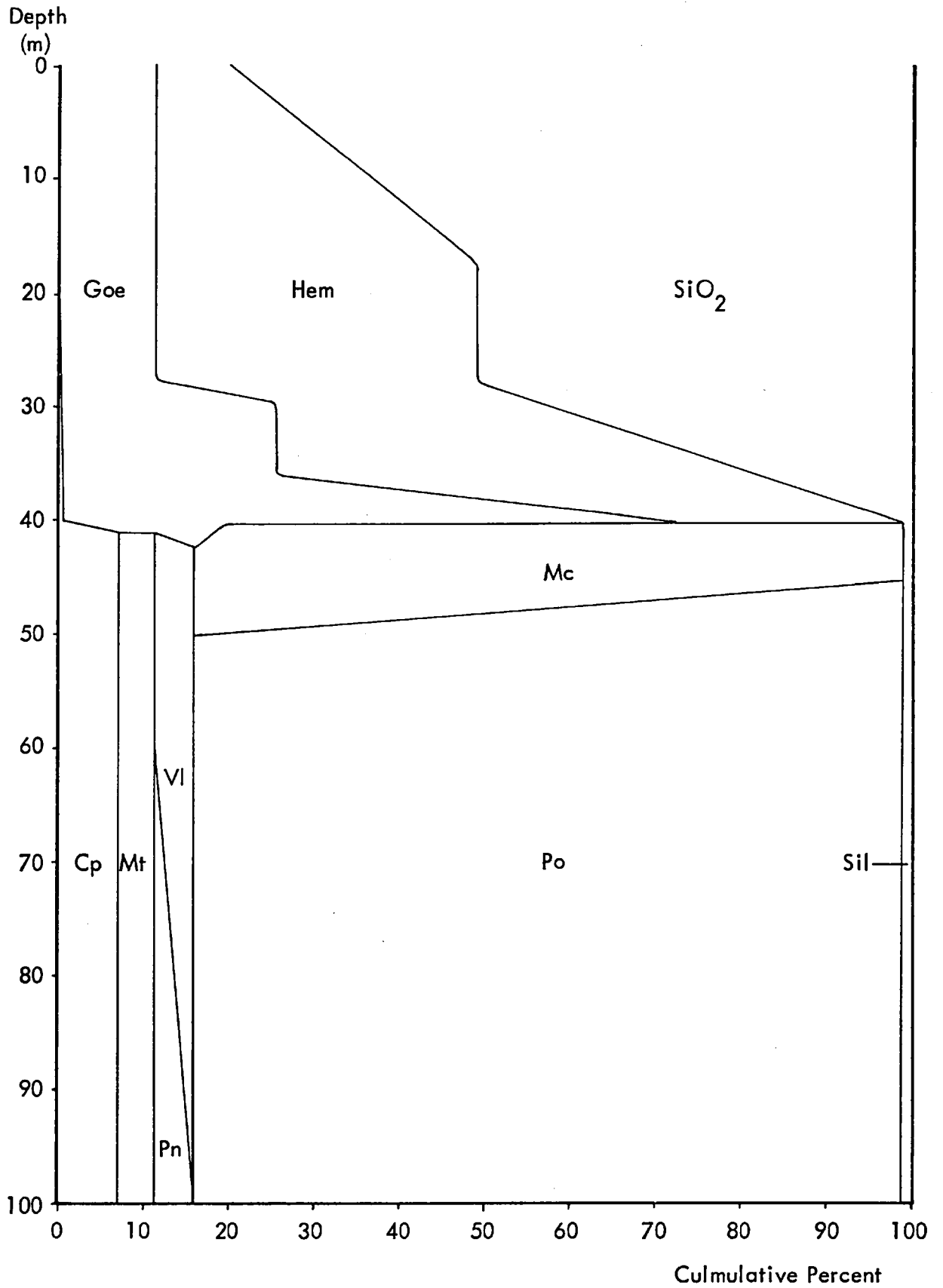
TABLE 3.2.1. PYRRHOTITE COMPOSITIONS – PIKWE

Sample	Fe	Ni	S	Co	Cu	Ti	Wt% Total	Atomic Formula $Fe_x S_8$	Atomic Formula $Me_x S_8$	Me:S ratio
2084/A4/8	59.70	n.d.	39.88	n.d.	0.17	0.04	99.79	-	-	-
	(46.15)	-	(53.70)	-	(0.12)	(0.04)	-	$Fe_{6.88}S_8$	$Me_{6.91}S_8$	0.86
2084/A7/3	60.02	n.d.	38.87	n.d.	0.06	0.05	99.00	-	-	-
	(46.95)	-	(52.97)	-	(0.04)	(0.04)	-	$Fe_{7.09}S_8$	$Me_{7.11}S_8$	0.89
2084/A8/18	60.23	n.d.	39.70	n.d.	0.08	0.04	100.05	-	-	-
	(46.51)	-	(53.40)	-	(0.05)	(0.04)	-	$Fe_{6.97}S_8$	$Me_{6.99}S_8$	0.87
2084/A9/26	59.74	n.d.	40.37	n.d.	0.10	0.04	100.25	-	-	-
	(45.88)	-	(54.01)	-	(0.07)	(0.04)	-	$Fe_{6.80}S_8$	$Me_{6.82}S_8$	0.85
2084/A8/15	60.36	n.d.	39.27	n.d.	0.18	0.03	99.84	-	-	-
	(46.81)	-	(53.05)	-	(0.12)	(0.03)	-	$Fe_{7.06}S_8$	$Me_{7.09}S_8$	0.89

Figures in brackets are in Atomic % units

68

TABLE 3.2.2. INTERSTITIAL PENTLANDITE COMPOSITIONS - PIKWE

Sample	Fe	Ni	S	Co	Cu	Ti	Wt% Total	Atomic Formula $Ni_nFe_mS_8$	Atomic Formula Me_xS_8	Me:S ratio
2084/A5/1	27.95	35.59	33.62	3.29	0.28	0.05	100.78	-	-	-
	(22.58)	(27.35)	(47.31)	(2.52)	(0.19)	(0.05)	-	$Ni_{4.63}Fe_{3.82}S_8$	$Me_{8.92}S_8$	1.12
2084/A5/11	28.27	34.99	34.12	2.58	0.73	0.03	100.72	-	-	-
	(22.78)	(26.81)	(47.88)	(1.98)	(0.52)	(0.03)	-	$Ni_{4.48}Fe_{3.81}S_8$	$Me_{8.72}S_8$	1.09
2084/A4/7	28.70	33.73	34.03	3.28	0.16	0.02	99.92	-	-	-
	(23.22)	(26.77)	(47.36)	(2.51)	(0.12)	(0.02)	-	$Ni_{4.52}Fe_{3.92}S_8$	$Me_{8.88}S_8$	1.11

TABLE 3.2.3.   CHALCOPYRITE COMPOSITIONS – PIKWE

Sample	Fe	Ni	S	Co	Cu	Ti	Wt% Total	Atomic Formula $Cu_nFe_mS_2$	Atomic Formula Me_xS_2	Me:S ratio
2084/A4/9	30.60	n.d.	34.96	n.d.	34.07	0.02	99.65	-	-	-
	(25.19)	-	(50.14)	-	(24.66)	(0.01)	-	$Cu_{0.99}Fe_{1.01}S_2$	$Me_{1.99}S_2$	1.00
2084/A9/27	30.59	n.d.	34.84	n.d.	34.95	0.07	100.45	-	-	-
	(25.06)	-	(49.72)	-	(25.16)	(0.07)	-	$Cu_{1.01}Fe_{1.01}S_2$	$Me_{2.02}S_2$	1.01

Fig. 3.2.4. Petrography of Pikwe Sulphide Ore (1)

Scale length = 100 μ

A.   Typical kink-zone pyrrhotite deformation (x 220) Oil

B.   Typical form of interstitial pentlandite (x 220) Oil

Pentlandite;light grey: Pyrrhotite;medium grey: Silicate;black

C.   Flamme-like lamellar pentlandite (x 600) Oil

Pentlandite;light grey: Pyrrhotite;medium grey: Voids/silicate;black

D.   Equant chalcopyrite grain form (x 600) Oil

Chalcopyrite;medium-dark, equant (right centre): Pentlandite;light grey:
Pyrrhotite;medium dark (top left): Smythite after pyrrhotite;light-medium
grey (right centre): Violarite after Pn;dark grey, circular in Pn.
Silicate:black

E.   Elongate chalcopyrite grain form (x 1000) Oil

Chalcopyrite;dark grey, mottled: Pentlandite;light - medium grey: Pyrrhotite;
medium grey

F.   Euhedral magnetite form (x 320) Oil

Magnetite; medium - dark grey: Ilmenite; dark grey rim: Pyrrhotite; medium
grey matrix: Lamellar pentlandite; light grey: Silicate; dark grey

G.   Chalcopyrite rimming magnetite (x 220) Oil

Chalcopyrite; light grey (top left, lower left): Magnetite; dark grey:
Pyrrhotite; light - medium grey (right)

H.   Ex-solution rim of Ilmenite in magnetite (x 110) Air

Magnetite; medium grey: Ilmenite; medium - dark grey rim: Pyrrhotite;
light - medium grey: Silicate; dark grey: Voids; black

Fig.3.2.4.
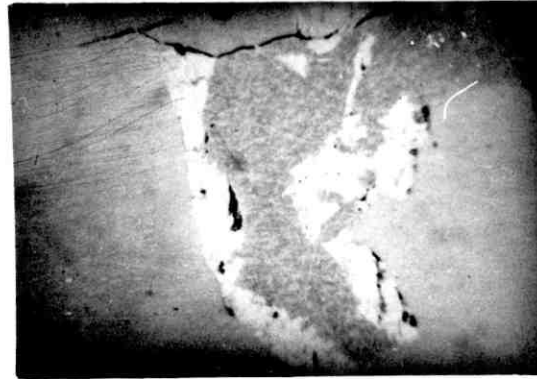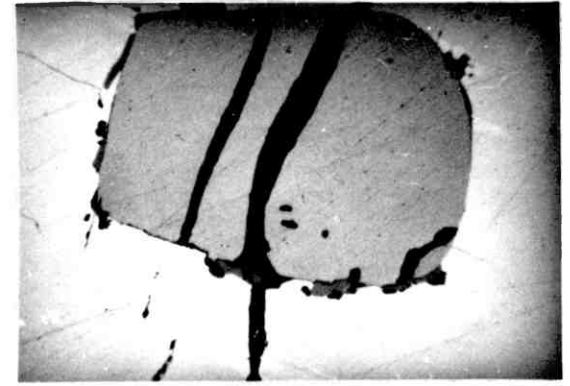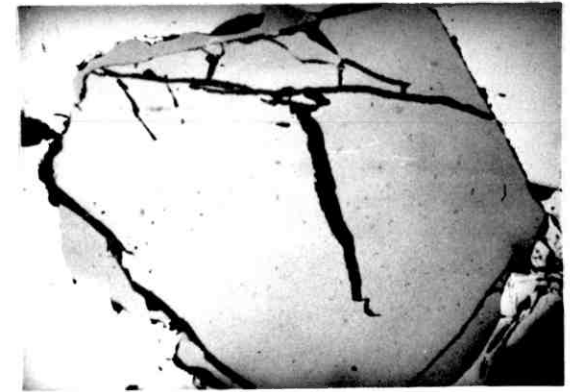
Magnetite averages about six percent in sampled massive ore, (Fig.3.2.3). It is typically subhedral in form, but more regular euhedral types are also common, particularly in the larger grain sizes, (Fig.3.2.4F.).Chalcopyrite and interstitial pentlandite are commonly associated with magnetite, and the spinel may be partially rimmed by these minerals - especially by chalcopyrite, (Fig.3.2.4G.).Ilmenite ex-solution structures are quite common in Pikwe magnetites and are present as either thin external rims, (Fig.3.2.4H.), or as elongate needle-like lamellae in the octahedral cleavage partings of the parent magnetite, (Fig.3.2.5A.).

The Petrology of the sulphide alteration sequence

The near surface alteration of massive sulphide ore at Pikwe is initiated by the pseudomorphic replacement of pentlandite by violarite. Incipient alteration of interstitial pentlandite typically occurs either proximal to octahedral cleavage, or at random within the grain, (Fig.3.2.5B.). In both instances the alteration forms as small (5-10μ) spheroids that comprise an outer (blue-grey) violarite zone surrounding a central porous core, (Fig.3.2.5C.).

Subsequent growth of violarite leads to the respective development of either thin linear zones, or to a progressive coalescence of isolated sites. Further alteration then occurs along broad fronts in directions normal to octahedral cleavage, which subsequently dilates due to an associated volume reduction. Uncommonly, violarite formation is preceded by the intermediate formation of brownish Bravoite, $((Fe,Ni)S_2)$, (Fig.3.2.5D.).

The chemical compositions of 17 violarite after interstitial pentlandite (Vpn) grains are presented in Table 3.2.4. The data indicate that the inter-grain variation in sulphur content shown by these violarite samples is rather small, but that the corresponding variations in both iron and nickel are significantly greater - as are those of the minor metals: cobalt, copper and titanium.

The data also indicate that the weight percent compositions of individual grains typically summate to totals that are significantly less than 100 percent - a finding that agrees with the results of previous workers, (Nickel et.al.,1974,op.cit.). This is thought to be due to a pronounced absorbance of secondary X-rays by the highly porous violarite grain surfaces during chemical analysis.

The observed stoichiometry of the sampled violarite suite typically approximates, or is

TABLE 3.2.4. VIOLARITE AFTER INTERSTITIAL PENTLANDITE COMPOSITIONS – PIKWE.

Sample	Fe	Ni	S	Co	Cu	Ti	Wt% Total	Atomic Formula $Ni_nFe_mS_4$	Atomic Formula Me_xS_4	Me:S ratio
2084/A7/2	24.95	29.53	42.26	1.13	0.18	0.03	99.12	-	-	-
	(19.50)	(21.96)	(57.55)	(0.86)	(0.10)	(0.03)	-	$Ni_{1.53}Fe_{1.36}S_4$	$Me_{2.94}S_4$	0.74
2084/A7/4	25.28	30.07	41.38	0.75	0.16	0.07	97.70	-	-	-
	(19.92)	(22.54)	(56.81)	(0.56)	(0.11)	(0.07)	-	$Ni_{1.59}Fe_{1.40}S_4$	$Me_{3.05}S_4$	0.76
2084/A7/7	24.48	28.21	41.27	2.80	1.25	0.02	98.15	-	-	-
	(19.50)	(21.38)	(57.29)	(1.94)	(0.89)	(0.02)	-	$Ni_{1.49}Fe_{1.36}S_4$	$Me_{2.98}S_4$	0.75
2084/A8/13	25.30	28.83	45.05	0.08	0.13	0.03	99.42	-	-	-
	(19.25)	(20.87)	(59.71)	(0.06)	(0.09)	(0.03)	-	$Ni_{1.40}Fe_{1.29}S_4$	$Me_{2.70}S_4$	0.68
2084/A8/16	22.49	29.71	41.18	4.11	0.14	0.02	97.72	-	-	-
	(17.71)	(22.31)	(56.63)	(3.07)	(0.09)	(0.02)	-	$Ni_{1.58}Fe_{1.25}S_4$	$Me_{3.07}S_4$	0.77
2084/A9/19	24.87	27.89	41.77	2.69	0.12	0.05	97.38	-	-	-
	(19.60)	(20.91)	(57.35)	(2.01)	(0.08)	(0.05)	-	$Ni_{1.46}Fe_{1.37}S_4$	$Me_{2.98}S_4$	0.75

TABLE 3.2.4. CONTINUED

Sample	Fe	Ni	S	Co	Cu	Ti	Wt% Total	Atomic Formula $Ni_n Fe_m S_4$	Atomic Formula $Me_x S_4$	Me:S ratio
2084/A9/20	23.89	30.55	42.40	0.71	0.42	0.05	98.01	-	-	-
	(18.68)	(22.72)	(57.74)	(0.53)	(0.29)	(0.04)	-	$Ni_{1.57} Fe_{1.29} S_4$	$Me_{2.92} S_4$	0.73
2084/A9/24	21.52	29.75	40.50	6.94	0.16	0.06	98.92	-	-	-
	(16.92)	(22.26)	(55.48)	(5.17)	(0.11)	(0.06)	-	$Ni_{1.60} Fe_{1.22} S_4$	$Me_{3.20} S_4$	0.80
2084/A10/31	19.75	32.54	41.34	3.30	0.21	0.01	97.65	-	-	-
	(15.61)	(24.46)	(56.91)	(2.84)	(0.14)	-	-	$Ni_{1.72} Fe_{1.10} S_4$	$Me_{3.03} S_4$	0.76
2084/A10/34	24.24	29.14	43.19	1.54	0.34	0.05	98.47	-	-	-
	(18.80)	(21.50)	(58.30)	(1.14)	(0.22)	(0.04)	-	$Ni_{1.48} Fe_{1.29} S_4$	$Me_{2.87} S_4$	0.72
2084/A5/2	21.46	31.30	41.67	3.61	0.20	0.04	98.25	-	-	-
	(16.82)	(23.37)	(56.95)	(2.69)	(0.14)	(0.04)	-	$Ni_{1.64} Fe_{1.18} S_4$	$Me_{3.02} S_4$	0.76
2084/A5/3	19.53	31.97	41.72	3.82	0.37	0.04	97.44	-	-	-
	(15.43)	(24.02)	(57.40)	(2.86)	(0.26)	(0.03)	-	$Ni_{1.67} Fe_{1.08} S_4$	$Me_{2.95} S_4$	0.74

TABLE 3.2.4. CONCLUDED

Sample	Fe	Ni	S	Co	Cu	Ti	Wt% Total	Atomic Formula $Ni_nFe_mS_4$	Atomic Formula Me_xS_4	Me:S ratio
2084/A5/4	21.65	30.96	41.08	3.89	0.35	0.03	97.97	-	-	-
	(17.05)	(23.19)	(56.60)	(2.90)	(0.24)	(0.03)	-	$Ni_{1.64}Fe_{1.21}S_4$	$Me_{3.08}S_4$	0.77
2084/A5/5	19.68	31.61	42.68	3.51	0.24	0.03	97.75	-	-	-
	(15.42)	(23.55)	(58.23)	(2.60)	(0.17)	(0.03)	-	$Ni_{1.62}Fe_{1.06}S_4$	$Me_{2.87}S_4$	0.72
2084/A5/6	19.43	33.33	42.11	2.34	0.82	0.01	98.03	-	-	-
	(15.42)	(24.88)	(57.56)	(1.74)	(0.54)	(0.01)	-	$Ni_{1.73}Fe_{1.07}S_4$	$Me_{2.96}S_4$	0.74
2084/A5/7	20.86	32.06	40.85	3.27	0.36	0.05	97.46	-	-	-
	(16.56)	(24.21)	(56.47)	(2.47)	(0.25)	(0.05)	-	$Ni_{1.72}Fe_{1.17}S_4$	$Me_{3.08}S_4$	0.77
2084/A5/8	20.96	32.38	41.89	2.50	0.33	0.02	98.07	-	-	-
	(16.46)	(24.18)	(57.27)	(1.86)	(0.22)	(0.01)	-	$Ni_{1.69}Fe_{1.15}S_4$	$Me_{2.99}S_4$	0.75

slightly poorer in metal than the theoretical value of Me_3S_4. Thus these values do not agree with those noted by several workers – notably Desborough and Czamanske, (1973), who indicate that secondary violarites typically possess metal-rich, non-stoichiometric molecular formulae.

A comparison of the mean compositions of Pikwe interstitial pentlandite and replacement violarite is presented in Table 3.2.5. The data indicate that a significant increase in the relative proportions of nickel to iron occurs as a result of the alteration process, and that absolute losses of nickel, iron, cobalt and copper also take place.

In contrast, the simultaneous increase in sulphur that appears to occur is very probably a relative change only, as pseudomorphic (constant sulphur) replacement conditions characterise the pentlandite-violarite alteration phenomenon. The likely (oxidation) reaction corresponding to the above pentlandite-violarite mineralogical alteration is indicated in Equation 1, Fig.3.2.10.

Incipient formation of violarite in lamellar pentlandite occurs within the central cores of individual flammes and is indicated by the development of blue-violet, porous, fracture-bordered areas within these structures. Subsequent alteration occurs both normal and sub-parallel to flamme long axes, and the resulting violarite faithfully pseudomorphs the parent pentlandite form, (Fig.3.2.5E.).

The chemical compositions of three violarite after lamellar pentlandite grains, (Table 3.2.6), indicate, on available data, that this species is probably typified by considerable inter-sample variation in its constituent major and minor metals. Further, in common with interstitial Vpn, lamellar Vpn at Pikwe exhibits both low analytical totals and approximates near-stoichiometric anomalous molecular proportions.

A comparison of mean interstitial and lamellar violarite compositions is made in Table 3.2.7. The data indicate that lamellar Vpn is typically richer in iron and poorer in both nickel and the minor ore metals than the interstitial form, with marked differences occuring in respect of iron and cobalt content. Further, it is likely that these overall differences broadly reflect similar primary compositional differences in the parent pentlandite species.

Petrographic observations indicate that localised alteration of flamme pentlandite is already in progress at about the 100m. level, at which depth interstitial pentlandite

Table 3.2.5. Comparison of interstitial pentlandite and violarite compositions

	INTERSTITIAL PENTLANDITE (n = 3)	VIOLARITE AFTER INTERSTITIAL PENTLANDITE (n = 17)
Fe	28.31	22.37
	(22.62)	(17.56)
Ni	34.77	30.55
	(26.49)	(22.81)
S	33.59	41.90
	(48.25)	(57.28)
Co	3.05	2.81
	(2.34)	(2.09)
Cu	0.39	0.34
	(0.27)	(0.23)
Ti	0.03	0.04
	(0.03)	(0.04)
TOTAL (Wt%)	100.15	98.00
Ni:Fe	1.17	1.29
Me:S	1.11	0.75

DATA GIVEN IN BRACKETS IN ALL CHEMICAL TABLES ARE IN ATOMIC % UNITS

TABLE 3.2.6.   VIOLARITE AFTER LAMELLAR PENTLANDITE - PIKWE

Sample	Fe	Ni	S	Co	Cu	Ti	Wt% Total	Atomic Formula $Ni_nFe_mS_4$	Atomic Formula Me_xS_4	Me:S ratio
2084/A9/22	25.33	29.39	42.69	0.44	0.14	0.06	98.06	-	-	-
	(19.74)	(21.80)	(57.98)	(0.33)	(0.10)	(0.06)	-	$Ni_{1.50}Fe_{1.36}S_4$	$Me_{2.89}S_4$	0.72
2084/A9/23	29.73	26.38	41.96	0.02	0.18	0.05	98.32	-	-	-
	(23.20)	(19.58)	(57.04)	(0.01)	(0.13)	(0.05)	-	$Ni_{1.37}Fe_{1.63}S_4$	$Me_{3.01}S_4$	0.75
2084/A9/25	26.09	28.60	42.46	0.14	0.11	0.04	97.42	-	-	-
	(20.46)	(21.34)	(57.99)	(0.10)	(0.08)	(0.03)	-	$Ni_{1.47}Fe_{1.41}S_4$	$Me_{2.90}S_4$	0.73

Table 3.2.7. Comparison of interstitial and lamellar violarite compositions

	VIOLARITE AFTER INTERSTITIAL PENTLANDITE (n = 17)	VIOLARITE AFTER LAMELLAR PENTLANDITE (n = 3)
Fe	22.37	27.05
	(21.14)	(20.40)
Ni	30.55	28.17
	(22.81)	(20.91)
S	41.90	42.37
	(57.28)	(57.68)
Co	2.81	0.20
	(2.09)	(0.15)
Cu	0.34	0.15
	(0.23)	(0.07)
Ti	0.04	0.05
	(0.04)	(0.05)
TOTAL (Wt%)	98.00	97.91
Ni:Fe	1.29	0.99
Me:S	0.75	0.73

first undergoes alteration. Further, these data also indicate that flamme pentlandite is completely altered to violarite by about the 80m. level. In contrast to which, the interstitial type exhibits a rather irregular alteration pattern within the depth profile – remnants of unaltered sulphide persisting up to the 45m. level.

It is likely that this difference in oxidation response is due to a combination of factors, namely, the aggregation state of the mineral, its accessibility to oxygenated groundwater, and the effects of larger scale geological factors such as shearing and general ground-water movement.

The oxidation of pentlandite to violarite is paralleled by the alteration of adjacent monoclinic pyrrhotite to smythite. This latter mineral characteristically takes the form of red-brown anisotropic feather-like fringes that are developed along interstitial pentlandite-pyrrhotite borders. The long axes of the feathers are typically orientated sub-parallel to pyrrhotite 001 cleavage, (Fig.3.2.5F.). In contrast, smythite typically develops around lamellar violarite as elongate sheaths that enclose the flamme aggregates.

The chemical compositions of two smythite grains are presented in Table 3.2.8. These data indicate that Pikwe smythite is probably typified by rather variable nickel and copper contents, and that it contains no detectable cobalt. Further, the sampled data indicate that the corresponding molecular formula is slightly metal-rich, but that it approximates the theoretical stoichiometric value of Me_9S_{11}.

The existence of smythite in the Pikwe alteration sequence supplements previously reported occurrences of this mineral by Taylor, (1970); Taylor and Williams, (1972); and Nickel, (1972).

The presence of nickel in smythite has important implications, as Table 3.2.8. indicates that this metal is effectively absent from its parent sulphide, i.e. monoclinic pyrrhotite. It is therefore likely that the formation of smythite from monoclinic pyrrhotite is initiated by the nickel that is released during the formation of violarite from adjacent pentlandite. Further, Table 3.2.8 also demonstrates that smythite formation leads to a significant loss of iron, but takes place at constant sulphur – as is also evidenced petrographically by the observed replacement texture. These features are incorporated into the corresponsing smythite formation reaction that constitutes Equation Two, Fig.3.2.10.

TABLE 3.2.8. SMYTHITE COMPOSITIONS – PIKWE

Sample	Fe	Ni	S	Co	Cu	Ti	Wt% Total	Atomic Formula $Fe_m Ni_n S_{11}$	Atomic Formula $Me_x S_{11}$	Me:S ratio
2084/A7/5	55.03	3.99	40.99	n.d.	0.09	0.05	100.15	–	–	–
	(42.22)	(2.91)	(54.78)	–	(0.06)	(0.04)	–	$Fe_{8.50} Ni_{0.58} S_{11}$	$Me_{9.10} S_{11}$	0.83
2084/A10/33	54.72	3.18	40.11	n.d.	0.21	0.06	98.28	–	–	–
	(42.79)	(2.37)	(54.65)	–	(0.14)	(0.05)	–	$Fe_{8.61} Ni_{0.58} S_{11}$	$Me_{9.13} S_{11}$	0.83

Fig. 3.2.5. Petrography of Pikwe Sulphide Ore (2)

Scale length = 100 μ

A.   Ilmenite exsolved along magnetite leavage (x 220) Oil

Magnetite; medium-dark grey: Ilmenite; light-medium grey: Pyrrhotite;
light grey: Silicate; black

B.   Random nucleation of violarite in pentlandite (x 600) Oil

Pentlandite; light-medium grey: Violarite; dark grey, spheroidal associated
with small voids (black):   Pyrrhotite; medium-dark grey: Silicate; grey-black

C.   Violarite nucleation along pentlandite cleavage (x 600) Oil

Pentlandite; light grey: Violarite; medium-dark grey, linear: Pyrrhotite;
medium-dark grey, (lower right):   Smythite; light-medium grey (lower right)

D.   Formation of violarite after bravoite (after pentlandite) (x 600) Oil

Bravoite; medium-dark grey: Pentlandite; light-medium grey: Violarite;
black, speckled spheroidal: Pyrrhotite; dark grey (lower margin) :
Voids; black

E.   Pseudomorphic replacement of pentlandite by violarite (x 220) Oil

Interstitial violarite; medium-dark grey, granular: Pyrrhotite; dark grey,
homogeneous: Smythite; light grey, fringe on Vpn: Voids/Silicate;
black

F.   Well-developed smythite after pyrrhotite (x 600) Oil

Smythite; light grey fringes: Pyrrhotite; medium-dark grey: Violarite (Vpn)
dark grey, granular: Silicate; black

G.   Replacement of smythite by violarite after pyrrhotite (x 1000) Oil

Smythite; light grey, finger-like: Pyrrhotite; medium-dark grey:
Vpo; light-medium grey, granular

H.   Direct corrosive replacement of pyrrhotite by violarite (Vpn) (x 600) Oil

Pyrrhotite; medium grey: Vpo; light-medium grey, fringe-like: Vpn;
light-medium grey, spindle-shaped: Voids; black

Fig.3.2.5.
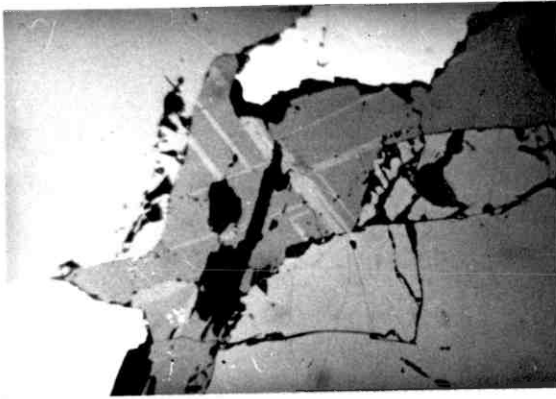
A
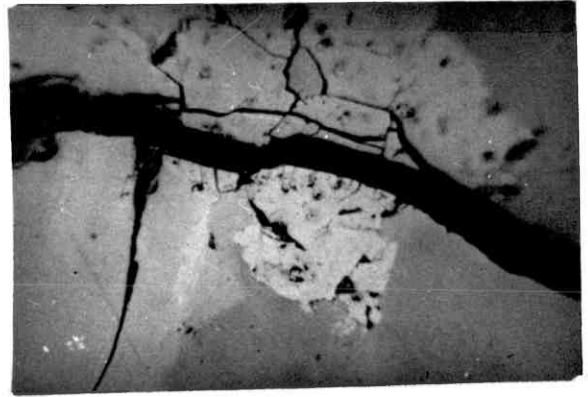
B
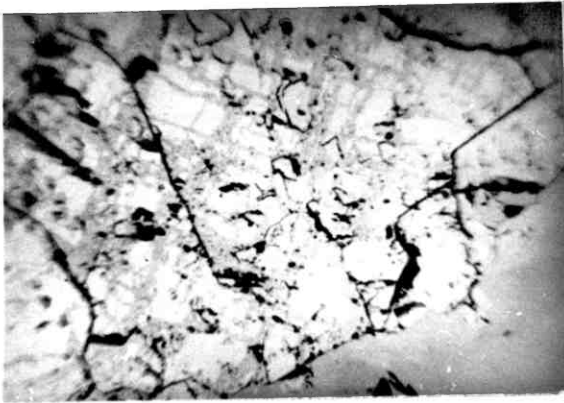
C
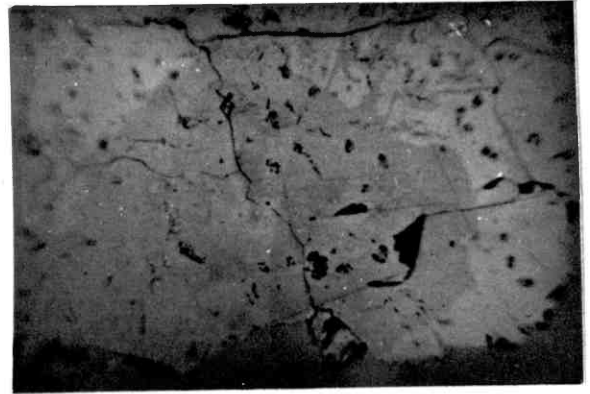
D
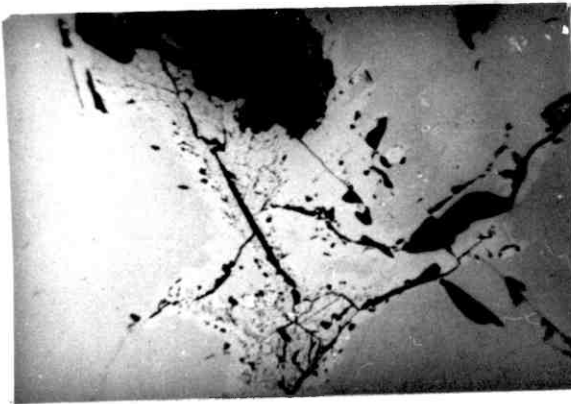
E
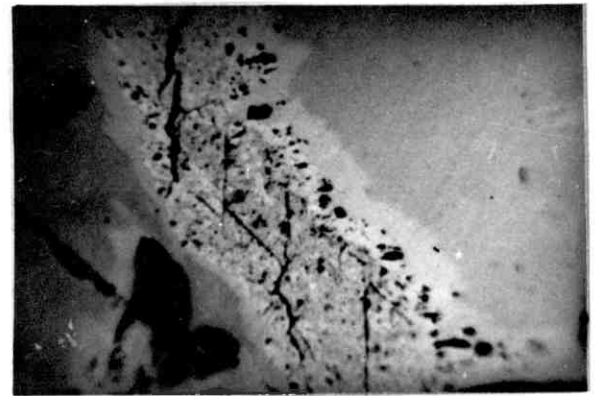
F
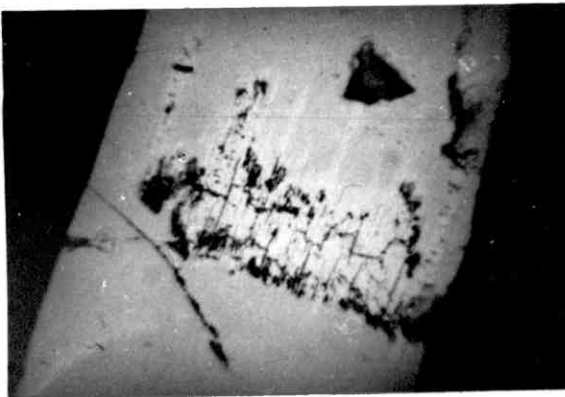
G
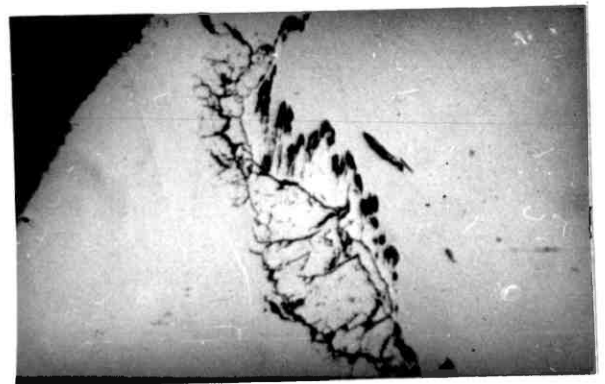
H

The formation of smythite constitutes however, only the first stage in pyrrhotite alteration at Pikwe, as smythite is itself subsequently replaced by pink-violet to pinkish-blue feather-like fringes of violarite after pyrrhotite (Vpo), (Fig.3.2.5G.).

This violarite species is generally porous, and it grows into and replaces smythite from pentlandite-pyrrhotite grain borders. Further, its lamellae are orientated sub-parallel to the long axes of the smythite grain aggregates and are typically bordered by small linear fractures. The development of Vpo around lamellar pentlandite/violarite, however, generally takes the form of elongate sheaths interposed between the nickel sulphide flamme aggregate and its enclosing smythite envelope.

The chemical compositions of six sampled Vpo grains, (Table 3.2.9) indicate that this mineral appears to be typified by considerable inter-sample variation in iron, nickel and, (especially), cobalt contents. Further, the data also demonstrate that the analytical totals of Pikwe Vpo, as with Vpn, characteristically summate to considerably less than 100 percent.

In contrast to both the interstitial and lamellar Vpn species however, Pikwe Vpo appears to possess a wide range of metal-to-sulphur ratios, but has a probable bias, on available evidence, towards slightly metal-rich (non-stoichiometric) values.

A comparison of mean smythite and Vpo compositions, (Table 3.2.10), indicates that the smythite-violarite alteration phenomenon is accompanied by a dramatic absolute decrease in iron content, and by a concommitant absolute increase in both nickel and cobalt content. Table 3.2.10 also indicates however, that Vpo formation probably occurs under constant sulphur conditions. Further, the corresponding reaction equation, (Equation 2a, Fig.3.2.10), demonstrates that the process constitutes an oxidation phenomenon.

Petrographic data indicate that the pentlandite-violarite conversion process is closely paralleled by the sequential development of smythite and Vpo. Smythite growth typically ceases at a relatively early stage however, and it is generally overgrown by Vpo before pentlandite conversion is terminated. Further, Vpo may continue to grow once it has completely replaced smythite if free nickel is still available. It then commonly replaces pyrrhotite directly, as is evidenced by conspicuous corrosion fronts between the two minerals, (Fig.3.2.5H.).

TABLE 3.2.9. 'VIOLARITE AFTER PYRRHOTITE COMPOSITIONS – PIKWE

Sample	Fe	Ni	S	Co	Cu	Ti	Wt% Total	Atomic Formula $Ni_n Fe_m S_4$	Atomic Formula $Me_x S_4$	Me:S ratio
2084/A7/1	27.25	28.05	41.87	0.04	0.12	0.02	97.34	–	–	–
	(21.45)	(21.01)	(57.42)	(0.03)	(0.08)	(0.02)	–	$Ni_{1.46}Fe_{1.49}S_4$	$Me_{2.96}S_4$	0.74
2084/A7/6	24.34	28.12	40.65	4.09	0.15	0.02	97.38	–	–	–
	(19.33)	(21.24)	(56.23)	(3.08)	(0.10)	(0.02)	–	$Ni_{1.5}Fe_{1.38}S_4$	$Me_{3.12}S_4$	0.78
2084/A7/8	24.87	29.50	41.73	1.82	0.12	0.03	98.07	–	–	–
	(19.51)	(22.01)	(57.02)	(1.35)	(0.08)	(0.03)	–	$Ni_{1.54}Fe_{1.37}S_4$	$Me_{3.04}S_4$	0.76
2084/A7/10	26.77	27.57	39.37	3.25	0.11	0.04	97.11	–	–	–
	(21.45)	(27.52)	((54.96)	(2.47)	(0.08)	(0.04)	–	$Ni_{1.53}Fe_{1.56}S_4$	$Me_{3.28}S_4$	0.82
2084/A7/11	23.23	27.47	40.44	6.14	0.11	0.04	97.43	–	–	–
	(18.47)	(20.78)	(56.01)	(4.62)	(0.08)	(0.04)	–	$Ni_{1.48}Fe_{1.33}S_4$	$Me_{3.14}S_4$	0.79
2084/A9/21	25.94	28.27	43.19	0.33	0.26	0.04	98.04	–	–	–
	(20.16)	(20.90)	(58.48)	(0.24)	(0.18)	(0.04)	–	$Ni_{1.43}Fe_{1.38}S_4$	$Me_{2.84}S_4$	0.71

Table 3.2.10. Comparison of pyrrhotite, smythite and Vpo compositions

	PYRRHOTITE (n = 5)	SMYTHITE (n = 2)	VIOLARITE AFTER PYRRHOTITE (n = 6)
Fe	60.05	54.88	25.40
	(46.47)	(42.50)	(20.06)
Ni	n.d.	3.59	28.17
	-	(2.64)	(21.16)
S	39.62	40.55	41.21
	(53.41)	(54.71)	(56.70)
Co	n.d.	n.d.	2.61
	-	-	(1.96)
Cu	0.12	0.15	0.14
	(0.09)	(0.10)	(0.10)
Ti	0.04	0.05	0.03
	(0.04)	(0.04)	(0.03)
TOTAL (Wt%)	99.83	99.21	97.56
Ni:Fe	-	0.06	1.05
Me:S	0.87	0.83	0.76

A mineralogical analysis of the sampled massive ore profile at Pikwe indicates that the 'transition' assemblage; pyrrhotite-Vpo-pentlandite-Vpn-magnetite-chalcopyrite, is present between the 98m. and 45m. levels, (Fig.3.2.3.). Towards the latter horizon however, the remaining pyrrhotite becomes rapidly converted to secondary marcasite and a full secondary sulphide assemblage based on violarite and marcasite is established. This secondary alteration zone is present as a rather erratic development between, (approximately), the 45m. and 40m. levels.

The secondary sulphide assemblage is dominated by pseudomorphic replacements of marcasite after large structurally-deformed pyrrhotite grains. These structures take the form of large areas of sub-parallel kink-zone textures, (Fig.3.2.6A.). The style of the parent pyrrhotite textures is typically exaggerated by the marcasite due to a volume reduction of about 30 percent, but the external borders of former pyrrhotite grains are commonly recognisable, (Fig.3.2.6A.).

Marcasite is also present as various types of bird's eye structures, (Ramdour, 1960). These may be large, comprise two zones, and exhibit polygonal outlines after pyrrhotite, (Fig.3.2.6B.). Alternatively, they may be small, single-zoned structures developed within kink-zone pseudomorphs, (Fig.3.2.6A.).

Violarite is typically present as actively oxidising grains, (Fig.3.2.6C.). Whereas, in contrast, chalcopyrite remains relatively unaltered in this zone, (Fig.3.2.6D.).

Oxidation of the violarite-marcasite assemblages is generally initiated towards the top of the secondary sulphide zone at about 43m., (Fig.3.2.3.). The gross texture of the sampled zone of active sulphide leaching consists chiefly of large oxidising blocks of marcasite that are intimately invested in drusy goethite, (Fig.3.2.6E.).

Both forms of violarite after pentlandite may undergo in situ alteration to goethite, (Fig.3.2.6F.). Alternatively, these minerals may be completely or partially leached, (Fig.3.2.6C.). Chalcopyrite alteration commonly takes the form of an in situ replacement by goethite, but an intermediate rim alteration to covellite may also occur, (Fig.3.2.6G.). Magnetite is generally represented by grain pseudomorphs containing drusy goethite or silica, (Fig.3.2.6H.)

The observed pattern of marcasite oxidation is rather complex. In summary, however,

Fig. 3.2.6. Petrography of Pikwe Sulphide Ore (3)

Scale length = 100 μ

A. Marcasite mimics after kink-zoned pyrrhotite (x 600) Oil

Marcasite; light grey: Chalcopyrite; light-medium grey (equant): Goethite after chalcopyrite; dark grey

B. Marcasite bird's eye structure (x 220) Oil

Marcasite; light grey: Goethite; medium-dark greys

C. Oxidising violarite (x 1000) Oil

Violarite; medium grey: Marcasite, light grey: Goethite; grey-black

D. Unaltered chalcopyrite in sulphide leaching zone (x 110) Air

Chalcopyrite; light-medium grey: Oxidising violarite; light-medium grey, granular: Oxidising marcasite; light grey

E. Typical block texture of sulphide leaching zone (x 110) Air

Chalcopyrite; light grey homogeneous (top centre): Violarite; medium-dark grey (left and right margins): Marcasite; medium grey (lower margin): Voids; black

F. In situ replacement of violarite by goethite (x 1000) Oil

Marcasite; light grey: Violarite; light-medium grey: Goethite; dark grey

G. Alteration sequence: chalcopyrite-covellite-goethite (x 1000) Oil

Chalcopyrite; white-grey: Covellite; medium-dark grey, thin rimming on Cp: Goethite; grey-black rimming on covellite: Marcasite; light-medium grey: Voids: black

H. Silica filling leached magnetite cavity (x 1000) Oil

Silica; medium-dark grey: Hematite; grey-black showing relic magnetite cleavage directions: Marcasite; light greys

Fig.3.2.6.
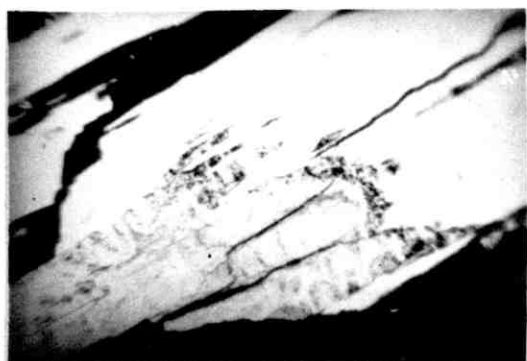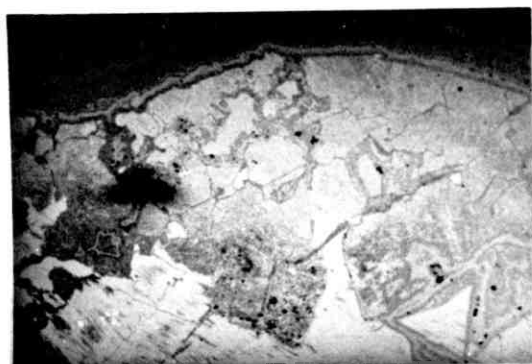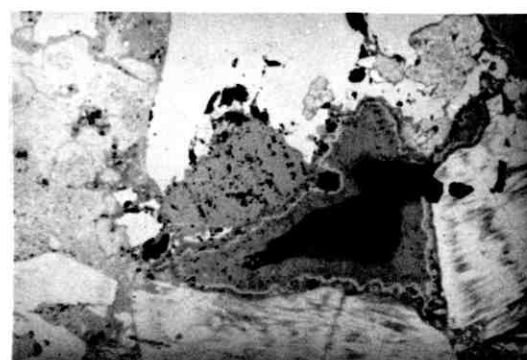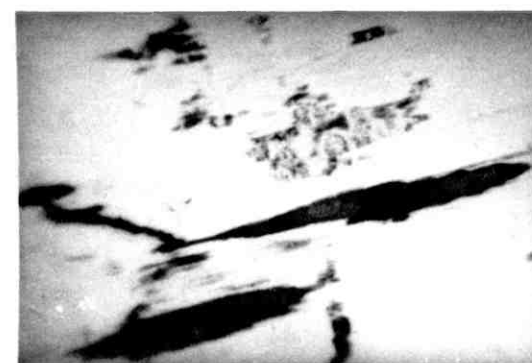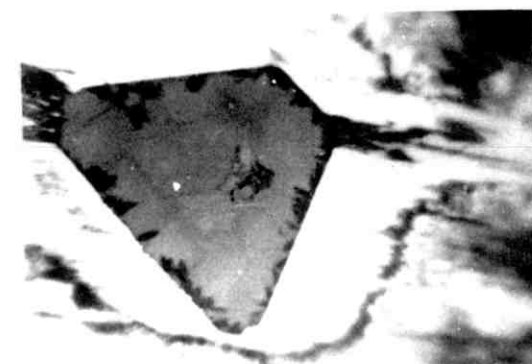
the mineral undergoes a zoned oxidation, with progressive alteration occurring outwards from the centre of each kink-zone pseudomorph. This phenomenon causes the formation of a series of sub-parallel linear zones, (Fig.3.2.6E.). Further, the alteration process may bring about direct leaching, or the in situ formation of goethite. Marcasite bird's-eye textures are however relatively unaffected by oxidation in available sample material.

The chemistry of sulphide leaching and iron oxide formation

The above petrographic summary data indicate that each member of the secondary sulphide assemblage may undergo both pseudomorphic replacement by iron oxide and pervasive leaching at the water table horizon. In order to document these phenomena comprehensively, the likely reaction equations corresponding to these observed mineralogical changes are set out in equations 4 to 18 in Fig.3.2.10. The data that form the basis of these reactions are drawn from the available mineral chemical information generated during the present work.

The reactions corresponding to the observed pervasive leaching of the five constituent sulphide minerals of the secondary assemblage; namely, interstitial and lamellar Vpn, Vpo, marcasite and chalcopyrite are set out in equations four to eight in Fig.3.2.10. All these equations indicate that sulphide leaching at Pikwe is oxidative in nature and produces excess acid species. In addition, the reaction mechanisms corresponding to the subsequent precipitation, as goethite and hematite, of the iron mobilised by these sulphide leaching reactions are respectively set out in equations 17 and 18 in the same figure.

The equivalent pseudomorphic replacement mechanisms of the five secondary sulphides are set out in equations 9 to 16 in Fig.3.2.10. These equations indicate that acid oxidising conditions are also produced during pseudomorphic replacement. They also demonstrate, however, that all or most of the constituent sulphide iron is retained as oxide during this process. The individual equations correspond to the type of oxide that is observed to replace specific sulphide minerals. Further, the complete release of ore metals indicated in equations 9 to 16 is necessarily an oversimplification as it is highly probable that appreciable quantities of these elements remain entrapped within their original loci as a result of the pseudomorphic replacement process.

The petrology of the oxide zone: Mineralogy

At Pikwe, the rather narrow secondary sulphide zone is succeeded vertically by a deep profile of iron oxides and silica. This oxide zone extends from the pre-mining water table level at about 40 metres through to the surface, (Fig.3.2.3.).

The following petrological description of the Pikwe oxide zone is based on material sampled in a series of bench traverses taken across this oxidised profile as exposed in the Pikwe open pit in May 1974. Samples were obtained between 40m. and 18m. levels within the pit, and from surface outcrops along strike from this latter feature.

The gross mineralogy of the Pikwe oxide zone consists principally of hematite, goethite and silica. The mean proportions of this assemblage, based on a sample size of 51 specimens, are: hematite 33.7 percent; goethite 25.5 percent and silica 39.6 percent.

The relative proportions of these minerals are not constant within the sampled profile however and Fig.3.2.3. implies that two principal types of mineralogical variation occur within the Pikwe oxide zone. These are: firstly, a depth variation in the relative mean proportion of goethite to hematite; secondly, a systematic relationship between depth and mean silica content.

Mineralogical evidence indicates that goethite is the predominant iron oxide formed as a result of sulphide oxidation at the 40m. level, (Fig.3.2.3.). Between this horizon and the 36m. level however, the relevant data indicate that hematite becomes the dominant iron mineral, and that the absolute quantities of the two phases actually become reversed, (Table 3.2.11.).

A further change in iron oxide relations takes place however between the 36m. and 30m. levels. Here the mean amount of goethite present remains roughly constant, but is accompanied by a decrease in the absolute quantity of co-existing hematite. This phenomenon coincides with a steady increase in the mean silica content of the oxide zone, (Fig.3.2.3.).

The ratio of goethite to hematite again decreases dramatically between the 30m. and 28m. levels. Whereas the mean absolute contents of both oxides remain relatively constant above the 28m. horizon, and persist in this relationship up to the top of

Table 3.2.11.   Depth variation of Hematite:Goethite ratios in the Pikwe Gossan

Mean depth (m)	Hematite:Goethite ratio	No of Samples
0.0	1.09	5
19.2	2.61	6
28.2	2.50	12
29.8	0.84	13
33.6	1.73	6
35.9	2.40	5
39.8	0.42	4

115

the sampled open pit profile at 18m. below surface.

The mean iron oxide ratio of the sampled surface gossan exhibits a goethite: hematite ratio of around unity. These data thus indicate an apparent substantial decrease in the absolute quantity of hematite present compared to that of the 18m. level, (Fig.3.2.3.). The significance of this result cannot however be quantitatively assessed as the sampled surface gossans are not directly developed above the sampled oxide profile, and may not hence constitute fully representative surface analogues.

Fig.3.2.3. further indicates that the distribution of mean silica content within the sampled Pikwe profile exhibits a marked depth-controlled distribution. Thus mean silica contents at the base of the oxide zone are low, but increase linearly up to around 50 percent between this horizon and the 28m. level. Above 28m., in contrast, the proportion of silica remains constant at about 50 percent through to the top of the sampled oxide profile at 18m. below surface.

Contrastingly, the surface gossan suite has a mean silica content of about 80 percent. This figure is a substantial increase over that of the 18m. level, and probably indicates the existence of significant additional silicification in the top 18 metres of the Pikwe oxide profile. Interpretation of silica contents in the surface gossans is however subject to similar constraints as that of iron oxide proportions in these rocks.

The petrology of the oxide zone: Textures

The oxide zone immediately overlying the sulphide leaching horizon is characterised by the development of iron oxide pseudomorphic textures after sulphide minerals. Much of this stratum consists of discrete blocks of iron oxide after 'oxidation zoned' marcasite set within a matrix of drusy goethite, (Fig.3.2.7A.) . A high proportion of these ex-marcasite structures have been replaced solely by fine-grained goethite and typically contain well-preserved hematite pseudomorphs after lamellar violarite (Vpn), (Fig.3.2.7B.).

Less commonly however, marcasite block pseudomorphs are defined in a combination of goethite and hematite, and where this replacement mode occurs, goethite (or void space) typically defines the central portions of the block with hematite typically occupying the marginal parts of the structures, (Fig.3.2.7C.). Pseudomorph bird's eye textures are also commonly present in this basal horizon and are typically defined in fine grained goethite with hematite marking out the sulphide shrinkage

cracks, (Fig.3.2.7D.).

Recognisable pseudomorphs after other component sulphide minerals also occur in the basal part of the oxide zone. Thus, interstitial violarite is generally represented by goethite mimic textures, and the octahedral cleavage patterns are, in general, clearly defined by goethite or hematite, (Fig.3.2.7E.). In addition, former chalcopyrite grains are typically represented by boxwork structures in goethite, (Fig.3.2.7F.), or more rarely in hematite. They are also present as complete, though rather rare hematite pseudomorphs, (Fig.3.2.7G.).

Work on silica textures in the bottom five metres of the Pikwe oxide zone (40-36m.) indicates that this mineral is present therein chiefly as colloidal or cryptocrystalline layered fillings in cavities and fractures within ex-marcasite mimic blocks or investing drusy goethite, (Fig.3.2.7H.). No evidence of silica replacing iron oxide structures was noted in this sub-zone. In consequence, it is likely that silica has been introduced into the basal part of the oxide zone by percolating ground water, and has, subsequently, been precipitated from solution in suitable cavities.

Textural evidence of the in situ alteration of goethite to hematite becomes significant at about the 37-38m. level in the oxide zone, and available data indicate that the replacement may occur in one of two ways, both of which generally result in the retention of sulphide mimic textures. In the most common replacement form, goethite is directly superceded by hematite in a single stage process. This involves the gradual replacement of fine-grained goethite by advancing fronts of fine-grained hematite, (Fig.3.2.8A.). Alternatively, a two stage replacement may occur. Here, goethite undergoes a preliminary recrystallisation to a coarser, typically bright yellow variant before being replaced by fine-grained hematite, (Fig.3.2.8B.).

Sulphide mimic textures are also preserved between the 36 and 30m. levels: which sub-zone overlies the basal region of the oxide profile. In this vertical interval however, sulphide pseudomorphs are defined chiefly by hematite, and goethite generally fulfills a subordinate role. In this respect, ex-marcasite kink zone pseudomorphs are present as fine-grained hematite, and those forms quite commonly contain remnant patches of goethite within the central areas of the mimic structure, (Fig.3.2.8C.). In contrast, bird's eye relics are generally present as goethite that

exhibits only a partial replacement by hematite, (Fig.3.2.8D.).

Relic textures after violarite species and chalcopyrite are also commonly observed in the 36-30m. sub-zone. Thus both interstitial Vpn and Vpo are preserved as goethite mimics, (Fig.3.2.8E.), and lamellar Vpn is also recognisable as goethite pseudomorphs within hematite after marcasite, (Fig.3.2.8F.). In contrast, chalcopyrite is represented by boxworks in goethite or in composite goethite / hematite, and small interstitial remnants of copper sulphides are quite commonly associated with these structures, (Fig.3.2.8G.).

The assemblage of sulphide mimic textures present within the 36-30m. sub-zone is, however, progressively modified above about the 33m. level as increasing proportions of the parent rock become affected by a large scale influx of silica. This latter phenomenon appears to cause a widespread dissolution and partial re-precipitation of iron oxides, and, moreover, results in the development of a pervasive matrix of cryptocrystalline silica. Former textural relations are, hence, totally obliterated as a result of this replacement process. Further, the re-precipitated iron oxides generally form discreet patches of randomly distributed hematite spherulites, although extensive areas of similar structures in goethite are also noted, (Fig.3.2.8H.).

Textural evidence of a second phase of goethite alteration is also present at about the 29-28m. level. This takes the form of an in situ replacement of goethite sphulites by hematite, and commonly occurs as a broad rather diffuse zone that is interposed between the two oxide types, (Fig.3.2.9A.).

The overlying 28-18m. vertical sub-zone is though characterised by the possession both of extensive matrix silicification, and by the existence of well-preserved relic sulphide textures in iron oxides after marcasite and lamellar violarite (Vpn), (Fig. 3.2.9B.). Further a noted overall constancy in mean proportions of these two textural assemblages over this vertical interval infers a probable constancy of silica influx in this portion of the oxide profile.

No data are available for the 18-0m. vertical interval due to sample inaccessibility, but textural relations in the surface gossans are similar to those present in the 28-18m. sub-zone. These rocks, hence, consist principally of spheroidal hematite aggregates set within a pervasive matrix of colloidal or cryptocrystalline silica. No relic sulphide textures were observed, however, in the sampled surface gossans.

Fig. 3.2.7. Petrography of the Pikwe Gossan (1)

Scale length = 100 μ

A. Goethite mimics after secondary marcasite structures (x 220) Oil
    Blue-white filter

    Goethite; medium greys: Voids; black

B. Hematite mimics after lamellar violarite (Vpn) (x 220) Oil

    Hematite; light greys: Goethite; medium to dark greys

C. Composite iron oxide mimic after marcasite (x 110) Air. Blue-white filter

    Hematite; light grey: Goethite; medium grey

D. Goethite mimic after marcasite bird's eye structure (x 220) Oil

    Goethite; medium grey: Hematite; light grey

E. Goethite mimic after interstitial violarite (Vpn) (x 220) Oil. Blue-white
    filter

    Goethite; medium-dark grey: Hematite; light grey

F. Goethite boxworks after chalcopyrite (x 220) Oil. Blue-white filter

    Goethite; medium grey: Hematite; light grey: Voids; black

G. Hematite boxwork after chalcopyrite (x 220) Oil. Blue-white filter

    Hematite; light-medium grey: Voids; black

H. Silica as void filling (x 600) Oil

    Goethite; medium grey: Silica; dark grey

Fig.3.2.7.
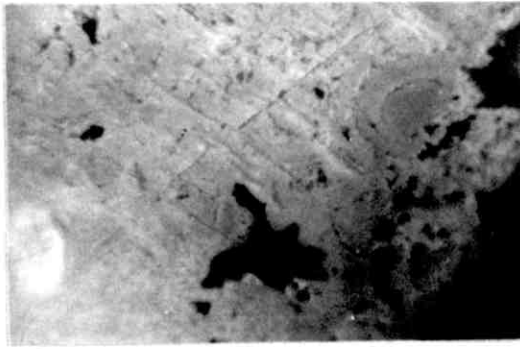
A

B
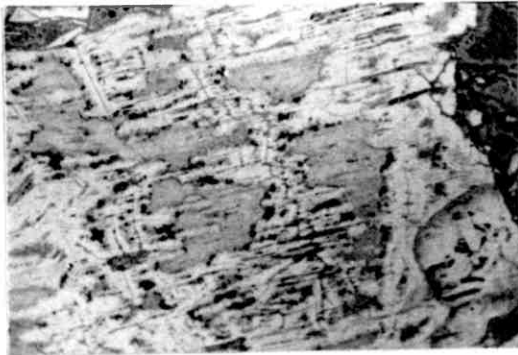
C

D

E
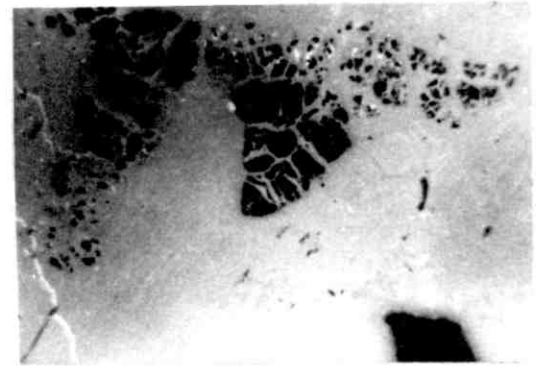
F
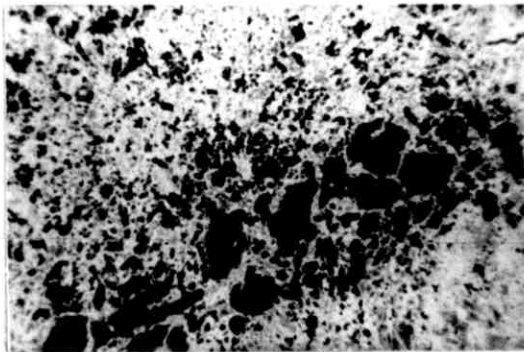
G
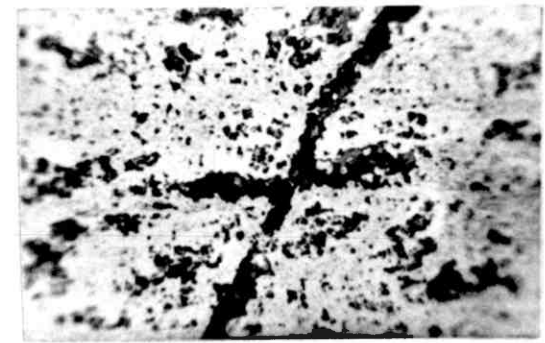
H

Fig. 3.2.8.   Petrography of the Pikwe Gossan   (2)

Scale length = 100 μ

A.   Single stage replacement of goethite by hematite (x 220) Oil

      Goethite; dark grey: Hematite; light grey

B.   Two-stage replacement of goethite by Hematite (x 220) Oil

      'Goethite One'; dark grey, homogeneous (lower left):   'Goethite Two';
      medium grey (centre):   Hematite; medium-dark grey (top left)

C.   Composite iron oxide mimic after marcasite (x 110) Air. Blue-white filter

      Hematite; light grey: Goethite; medium to dark greys

D.   Partial replacement of goethite by hematite in bird's eye mimic (x 110) Air
      Blue-white filter

      Goethite; dark grey: Hematite; light to medium greys: Voids; black

E.   Goethite mimic after interstitial violarite at 36 - 30m. level (x 320) Air
      Blue-white filter

      Goethite; medium greys: Hematite; light grey

F.   Goethite mimics after lamellar violarite (Vpn) (x 320) Air

      Goethite; dark grey: Hematite; light-medium grey: Voids; black

G.   Chalcopyrite remnant in goethite boxwork after the same (x 110) Air
      Blue-white filter

      Chalcopyrite; white-grey (lower centre):   Goethite; medium grey

H.   Goethite recrystallisation texture (x 1000)Oil

      Goethite; medium grey, spherulitic: Silica matrix; grey-black:
      Relic marcasite; white-grey

Fig.3.2.8.
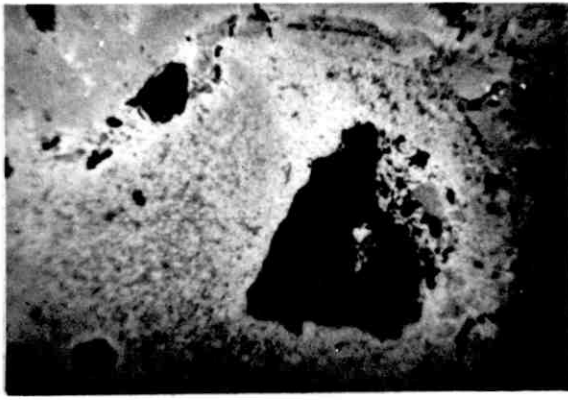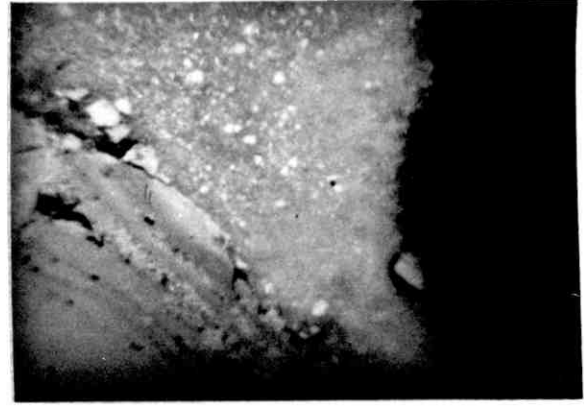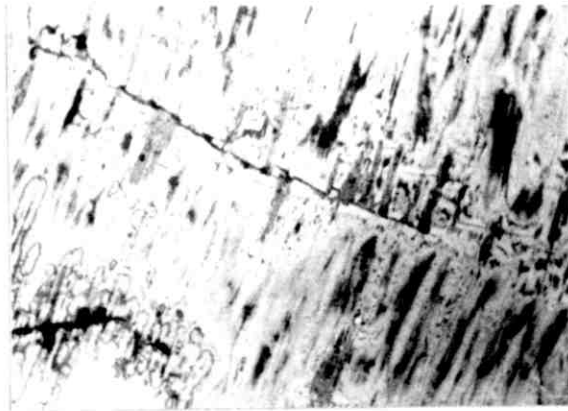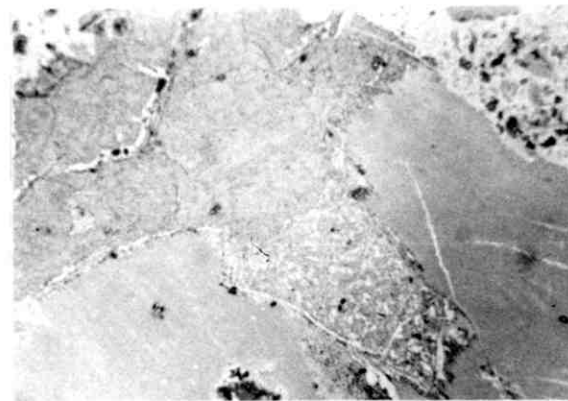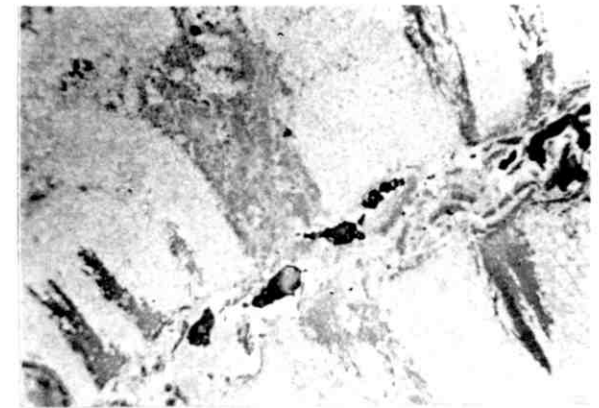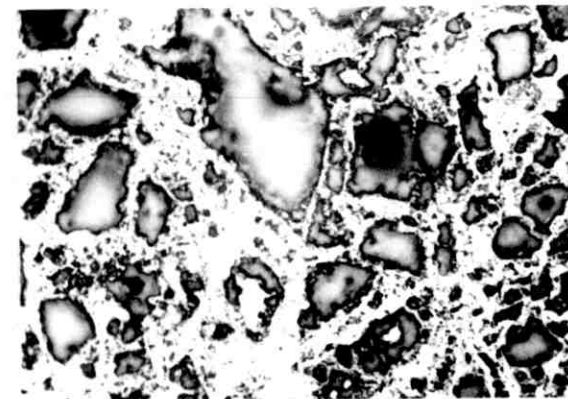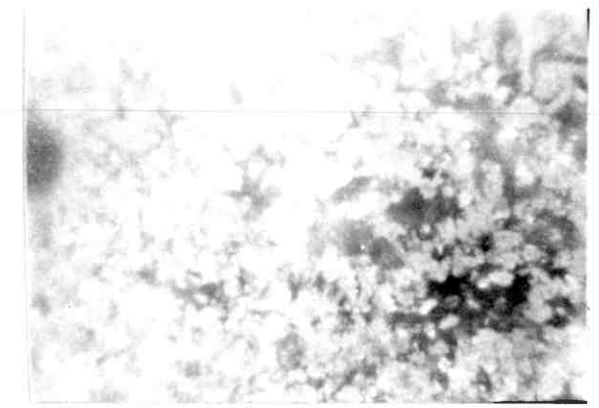
Fig. 3.2.9. Petrography of Pikwe Gossan and Host Amphibolite

Scale length = 100 μ

A. Replacement of goethite by hematite (x 40) Air

   Goethite; medium-dark grey: Hematite; light grey: Voids; black

B. Hematite mimic after marcasite bird's eye structure (28 - 18m. level) (x 600) Oil

   Hematite; light-medium grey, spherulitic: Silica; dark grey

C. Typical goethite lineations after amphibolite (x 220) Air. Blue-white filter

   Goethite; medium grey: Silica; medium-dark grey

D. Replacement of goethite by hematite in amphibole lattice structure (x 220) Air

   Goethite; medium grey: Hematite; light-medium grey:
   Silica matrix; dark grey

E. Relic amphibole grain outlines (x 600) Oil

   Silica; medium greys

F. α - cristobalite replacement of original silicate lattice (x 1000) Oil

   α - cristobalite; light-medium grey (left half):   Goethite; medium grey:
   spherulitic (right half):   Silica matrix; grey-black

Fig.3.2.9.
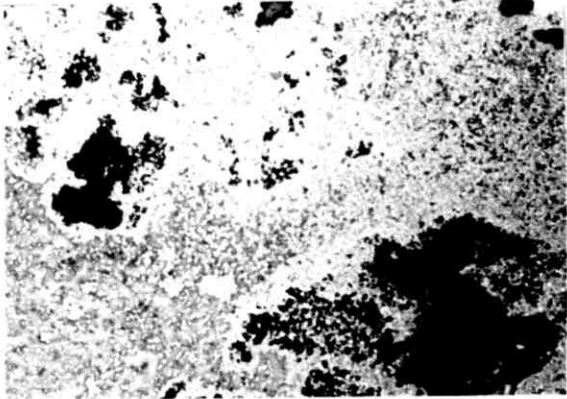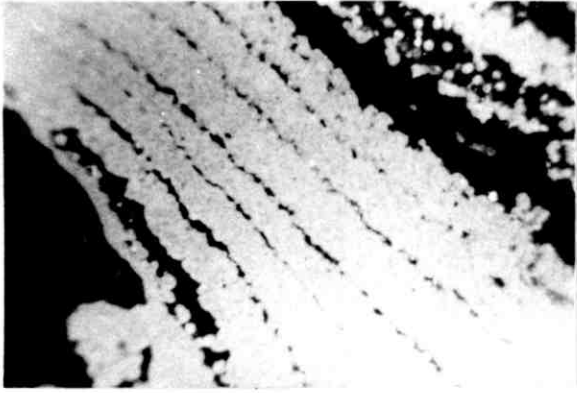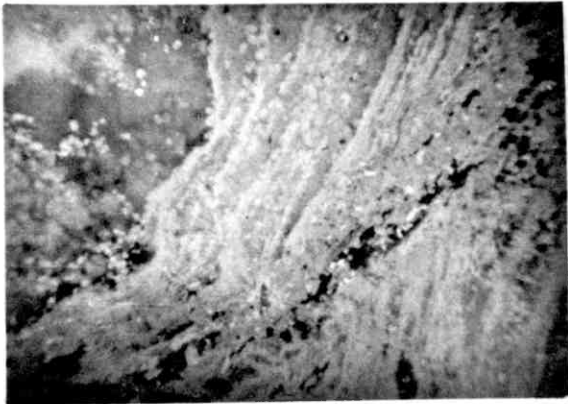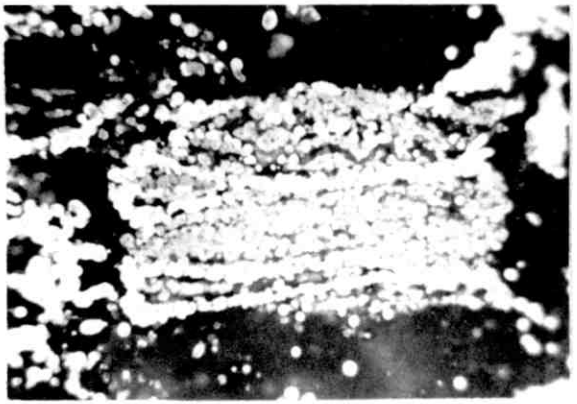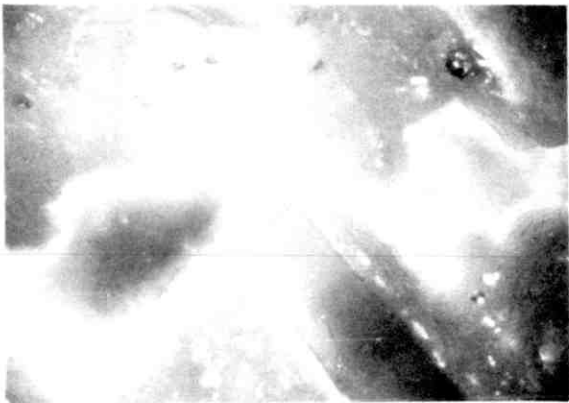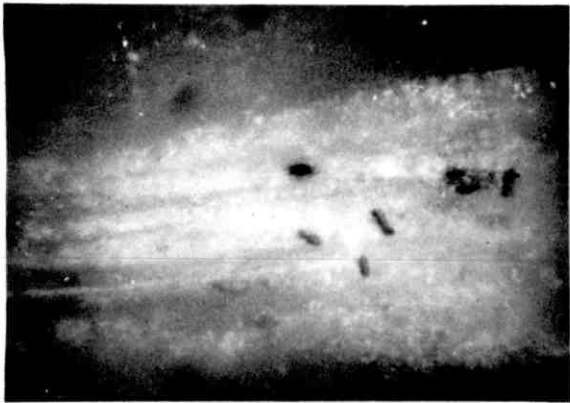
Chemical processes within the oxide zone profile

The previously documented sulphide leaching and iron oxide precipitation reactions take place within the narrow horizon defined by the zone of active sulphide leaching that occurs at the pre-mining water table. In consequence, this zone forms a generally well-defined stratum of intense chemical activity within the oxidation profile.

In contrast, the overlying oxide profile comprises a zone of low chemical activity, and hence chemical changes within it are rarer and occur at characteristically slower rates. In fact, petrographic observations indicate that chemical change in the Pikwe oxide profile is most probably limited to the large-scale progressive alteration of goethite to hematite.

Equation 19, (Fig.3.2.10.), indicates however that this alteration is not a redox process, but that it appears to be a simple dehydration reaction. It is likely, though, that the goethite – hematite transformation occurs due to slight differences in thermodynamic stability between the two oxides in the chemical environment of the Pikwe oxide profile. A discussion of the chemical implications of this alteration reaction is not, however, presented here, but is postponed until the subject of nickel gossan genesis and evolution is more fully treated in Chapter Eight of the present work.

The petrology of associated oxidate minerals

In general, oxidate minerals comprise only a small proportion of the oxide zone mineral assemblage in any oxidised nickel sulphide deposit. These minerals are formed from the chemical products of near-surface weathering of these sulphide deposits and of their adjacent silicate rocks; which overall process comprises sulphide leaching, acid hydrolysis of adjacent wall rock, and normal near surface deep weathering of proximal silicate rocks. As such, oxidate minerals are generally located either within the oxide zone of the deposit, or in adjacent altered wall rocks. Further they typically possess textures which indicate their formation as precipitants from aqueous solution. Because of their origins, therefore, the recognition and interpretation of oxidate minerals and their chemistries and textures, can supply information of use in both genetic and outcrop evaluation studies of nickel gossans.

In view of these considerations, the descriptive petrology of the Pikwe oxidation

profile is now supplemented by brief summary descriptions of oxidate minerals recognised in this deposit. The full descriptive data are given in Appendix Two, and details of the research methods used in this study appear in Appendix One. Interpretation of the data in terms of chemical formation conditions and of nickel gossan recognition and evaluation are made in Chapters Eight and Nine respectively of the present work.

Five oxidate minerals have been recognised at Pikwe during the present study. These are: Natroalunite, Natrojarosite, transported Hematite, transported Goethite and Calcite.

Natroalunite, $(NaAL_3(SO_4)_2(OH)_6)$ occurs in both the oxide zone and in immediately adjacent weathered amphibolite, (Table A2/7, Appendix Two). It is by far the commonest oxidate mineral in the Pikwe oxidised profile. The mineral is typically white to pale green or yellow-green in colour, and is generally both very soft and fine grained, (Table A2/7, Appendix Two). It occurs in three textural forms: as isolated botryoids or more extensive drusy growths on the walls of solution cavities: as more extensive coverings on joint and fracture surfaces: or as locally massive, rather indurate veining within weathered amphibolite. Further, Table A2/7, (Appendix Two) also indicates that the nickel and copper contents of natroalunite are typically high and somewhat variable, but that they respectively average 2943ppm and 5566ppm.

Natrojarosite, $(NaFe_3(SO_4)_2(OH_6)$, (Table A2/8, Appendix Two) is rarer than natroalunite at Pikwe and has been principally noted in the weathering amphibolite host. Where present, this mineral occurs chiefly as botryoidal or drusy growths along the walls of solution cavities and on joint faces. It ranges in colour from yellow through yellow-buff to medium brown, and is typically fine grained and soft, (Table A2/8, Appendix Two).

Hematite, $(\propto Fe_2O_3)$, is present as a distinct oxidate phase in both the oxide zone proper and in adjacent weathered amphibolite. It is chiefly noted in two textural forms: firstly as generally patchy lining to solution cavities and joint faces: and, secondly, as vein-like intrusions in amphibolite. The mineral is typically fine grained and is generally soft unless silicified. Its colour ranges from light chocolate brown through dark red to black.

Both nickel and copper contents of sampled Pikwe oxidate hematite

are typically variable, but respectively average 4308 ppm and 7615 ppm.

Goethite, (α-FeOOH), occurs as a rare oxidate mineral within the Pikwe oxide zone and is generally present as thin, patchy, commonly botryoidal cavity or joint face lining. Oxidate goethite is characteristically fine grained and soft, and its colour ranges from pale yellow through yellow-brown to orange. The mean nickel and copper contents of this goethite form are respectively 8223 ppm and 5565 ppm.

A rare occurrence of Calcite ($CaCO_3$) is noted in the weathering host amphibolite. The mineral is present as thin, transparent, rather indurate varnish-like deposits on the surface of silicified joints, (Table A2/3, Appendix Two).

The petrology of host amphibolite weathering

The petrological description of the Pikwe sulphide oxidation profile is now concluded with short summary expositions of the petrology and chemistry of host amphibolite alteration. These studies complement the profile investigation by documenting the effects of sulphide oxidation on host silicate weathering processes. But perhaps more importantly, such work allows the effects of silicate weathering on the mineralogy and chemistry of the oxide profile to be subsequently elucidated and utilised in the understanding of nickel gossan genesis and development.

Unaltered host amphibolite consists principally of hornblende with minor amounts of andesine plagioclase and chloritised phlogopite mica. Incipient weathering is present at the 40m. level, and takes the form of montmorillonite replacement in plagioclase, and as a partial alteration of chlorite to goethite.

In deeply weathered samples from the 23-18m. sub-zone of the oxidation profile, the original silicate mineralogy has been replaced by an oxidised assemblage that is dominated by silica and iron oxides. Mimic replacements of amphibolite lattice structures are common in this material and take the form of lineations of small ($<1\mu$) goethite corpuscles set within a colloidal silica matrix, (Fig.3.2.9C.). It is thought likely that these textures originate from an in situ oxidation of iron in the Y^{vi} lattice sites of the parent amphibole. Local alteration of goethite to hematite is also a common feature of these mimicked hornblende textures, and progressive transformation commonly occurs along the goethite lamellae, (Fig.3.2.9D.).

The cryptocrystalline silica forming the matrix of the oxidised silicate is not however completely structureless, and definite outlines of former hornblende grains are quite commonly observed within it. Where present, these grains are typically defined by thin septae of silica or goethite, (Fig.3.2.9E.). More rarely, the silica matrix carries linear trains of small whitish corpuscular inclusions that may exhibit a local continuity with corpuscular goethite lamellae, (Fig.3.2.9F.). These linear forms are hence also thought likely to be related to lattice structures in the original amphibole. These inclusions may consist of low temperature (α) cristobalite. More detailed work is required however before the presence of this phase is definitely established.

The chemistry of host amphibolite weathering

The acid that is released in the zone of sulphide leaching as a result of Equations 4 to 18, (Fig.3.2.10.), is highly active chemically and tends to react with any suitable substrate within its immediate environment. The effect of such reactions, however, is to neutralise this acid as the latter is effectively removed from the environment as a result of its chemical combination with the substrate material.

All reactions leading to the removal of acid species from the sulphide leaching zone can thus be regarded as acid-buffering processes. At Pikwe, the principal material available for such buffering reactions is the host amphibolite wall rock, and Equation 21. (Fig.3.2.10.), indicates that the near monominerallic amphibolite assemblage probably reacts with free hydrogen ion by a process of acid hydrolysis. In consequence, the constituent hornblende undergoes chemical degradation and effectively neutralises large quantities of acid species.

The form of Equation 21 is partly based on petrographic observations of acid hydrolysed host amphibolite. These data indicate that the hornblende is typically replaced by silica and by small, but variable amounts of iron oxides. It is therefore likely that much of the cation content of the hornblende is oxidised and leached out during hydrolysis, (Equation 21). It is also probable that these mobile cations subsequently form a part of the metal source for the oxidate minerals that are present within the Pikwe weathered profile.

FIG. 3.2.10. CHEMISTRY OF THE PIKWE ALTERATION SEQUENCE

ACID BUFFERING REACTION

21 $(Na, K, Ca)_{2.09}(Mg\ Fe^{II}Fe^{III}Al)_{5.56}(Si_{6.48}Al_{1.52}O_{22})(OH)_{1.20} + 13.44H_2O + 17.87H^+ = 0.46Na^+ + 0.15K^+ +$

$1.50Ca^+ + 2.78Mg^{2+} + 1.17Fe^{2+} + 2.63(Al(H_2O)_6)^{3+} + 3.48H_4SiO_4 + 3SiO_2 + 0.47FeOOH + 1.5e^-$

CATHODIC REDUCTION OF OXYGEN

20 $O_2 + 2H_2O + 4e^- = 4OH^-$

DEHYDRATION OF GOETHITE

19 $2FeOOH = Fe_2O_3 + H_2O$
   Goethite   Hematite

SHALLOW ANODIC WEATHERING REACTIONS

18 $2Fe^{2+} + 3OH^- = Fe_2O_3 + 3H^+ + 2e^-$
                 Hematite

17 $Fe^{2+} + 2OH^- = FeOOH + H^+ + e^-$
                 Goethite

16 $CuS + 4H_2O + Fe^{2+} + 2OH^- = FeOOH + SO_4^{2-} + Cu^{2+} + 9H^+ + 9e^-$
   Covellite   Goethite

15 $Cu_{1.00}Fe_{1.01}S_2 + 8.00H_2O + 2.02OH^- = 1.01FeOOH + 2.0SO_4^{2-} + Cu^{2+} + 17.01H^+ + 17.03e^-$
   Chalcopyrite   Goethite

14 $FeS_2 + 8H_2O + 2OH^- = FeOOH + 2SO_4^{2-} + 17H^+ + 15e^-$
   Marcasite

13 $Ni_{1.63}Fe_{1.26}Co_{0.15}S_4 + 16.00H_2O + 1.89OH^- = 0.63Fe_2O_3 + 4SO_4^{2-} + 1.63Ni^{2+} + 0.15Co^{2+} + 33.89H^+$
   Violarite (after inst. Pn)   Hematite $+ 31.34e^-$

12 $Ni_{1.49}Fe_{1.42}Co_{0.10}S_4 + 16.00H_2O + 2.84OH^- = 1.42FeOOH + 4SO_4^{2-} + 1.49Ni^{2+} + 0.10Co^{2+} + 33.42H^+$
   Violarite (after Po)   Goethite $+ 31.44e^-$

11 $Ni_{1.45}Fe_{1.47}Co_{0.01}S_4 + 16.00H_2O + 2.94OH^- = 1.47FeOOH + 4SO_4^{2-} + 1.45Ni^{2+} + 0.01Co^{2+} + 33.47H^+$
   Violarite (after lam. Pn) $+ 31.33e^-$

10 $Ni_{1.63}Fe_{1.26}Co_{0.15}S_4 + 16.00H_2O + 2.52OH^- = 1.26FeOOH + 4SO_4^{2-} + 1.63Ni^{2+} + 0.15Co^{2+} + 33.26H^+$
   Violarite (after inst. Pn) $+ 31.34e^-$

9   $Cu_{1.00}Fe_{1.01}S_2 + 4H_2O = CuS + SO_4^{2-} + 1.01Fe^{2+} + 8H^+ + 8.02e^-$
   Chalcopyrite   Covellite

8   $Cu_{1.00}Fe_{1.01}S_2 + 8H_2O = 1.01Fe^{2+} + Cu^{2+} + 2SO_4^{2-} + 16H^+ + 16.02e^-$

7   $FeS_2 + 8H_2O = Fe^{2+} + 2SO_4^{2-} + 16H^+ + 14e^-$
   Marcasite

6   $Ni_{1.49}Fe_{1.42}Co_{0.10}S_4 + 16.00H_2O = 1.49Ni^{2+} + 1.42Fe^{2+} + 0.10Co^{2+} + 4SO_4^{2-} + 32H^+ + 30.02e^-$
   Violarite (after Po)

5   $Ni_{1.45}Fe_{1.47}Co_{0.01}S_4 + 16.00H_2O = 1.45Ni^{2+} + 1.47Fe^{2+} + 0.01Co^{2+} + 4SO_4^{2-} + 32H^+ + 29.86e^-$
   Violarite (after lam. Pn)

4   $Ni_{1.63}Fe_{1.26}Co_{0.15}S_4 + 16.00H_2O = 1.63Ni^{2+} + 1.26Fe^{2+} + 0.15Co^{2+} + 4SO_4^{2-} + 32H^+ + 30.08e^-$
   Violarite (after inst. Pn)

DEEP ANODIC WEATHERING REACTIONS

3   $Fe_{6.89}S_8 = 4FeS_2 + 2.89Fe^{2+} + 5.78e^-$
   Monoclinic Po Marcasite

2A $0.73Fe_{8.55}Ni_{0.53}S_{11} + 2.60Ni^{2+} + 0.28Co^{2+} = 2Ni_{1.49}Fe_{1.42}Co_{0.14}S_4 + 3.36Fe^{2+} + 0.96e^-$
   Smythite   Violarite (after Po)

2   $Fe_{6.89}S_8 + 0.39Ni^{2+} = 0.73Fe_{8.55}Ni_{0.53}S_{11} + 0.67Fe^{2+} + 0.57e^-$
   Monoclinic Po   Smythite

1   $Ni_{4.52}Fe_{3.87}Co_{0.40}S_8 = 2Ni_{1.59}Fe_{1.23}Co_{0.15}S_4 + 1.34Ni^{2+} + 1.41Fe^{2+} + 0.16Co^{2+} + 5.70e^-$
   Interstitial Pentlandite Violarite (after inst. Pn)

In addition though, acid hydrolysis causes the destruction of the amphibole network structure and appreciable quantities of silica are released from the host rock. Much of this silica subsequently precipitates in the adjacent oxide profile, but it is likely that a second, somewhat more abundant silica source than the relatively low-silica host amphibolite is necessary to fully explain the observed large-scale silicification of the Pikwe oxide zone.

It is hence probable that a substantial part of the silica component is derived from the near-surface weathering of proximal (silica-rich) gneisses. This is because the influx of large quantities of mobile silica from sub-surface levels by descending groundwater that such a source implies would do much to explain both the form of the silica depth profile at Pikwe and the occurrence of wholesale silica replacement textures above the 33 metre level.

3.3 DENSITY AND POROSITY VARIATION WITHIN THE PIKWE OXIDATION PROFILE

The variations of mean true density and mean porosity in the Pikwe oxidation profile are indicated in Fig.3.3.1. These depth profiles indicate that definite variations in both density and porosity occur within the documented oxidation sequence. The form of both profiles in the 92-42m. sub-zone demonstrates however, that no significant mean variation probably occurs in these two physical properties within the Transition zone or in the lower part of the overlying violarite-marcasite zone.

It is likely that this lack of variation is caused by a combination of relatively low pentlandite-pyrrhotite primary ratio and a vertically extensive transition zone. This is because both of these features act to dilute the changes in density and porosity that are caused by the progressive development of the lighter, more porous violarite from pentlandite between the 98 and 45 metre levels.

In contrast, Fig.3.3.1. also demonstrates that dramatic changes in both density and porosity occur in the upper part of the violarite-marcasite zone and across the sulphide-oxide transition at 40m. In this respect, mean density falls from $4.4 gm.cc.^{-1}$ to $3.1 gm.cc.^{-1}$ across the 42.5-39m. vertical interval, and mean porosity values increase sharply from three percent to about twenty percent over the same vertical distance. These changes are brought about by the wholesale leaching of sulphide

Fig.3.3.1. Mean True Density and Porosity profiles – Pikwe
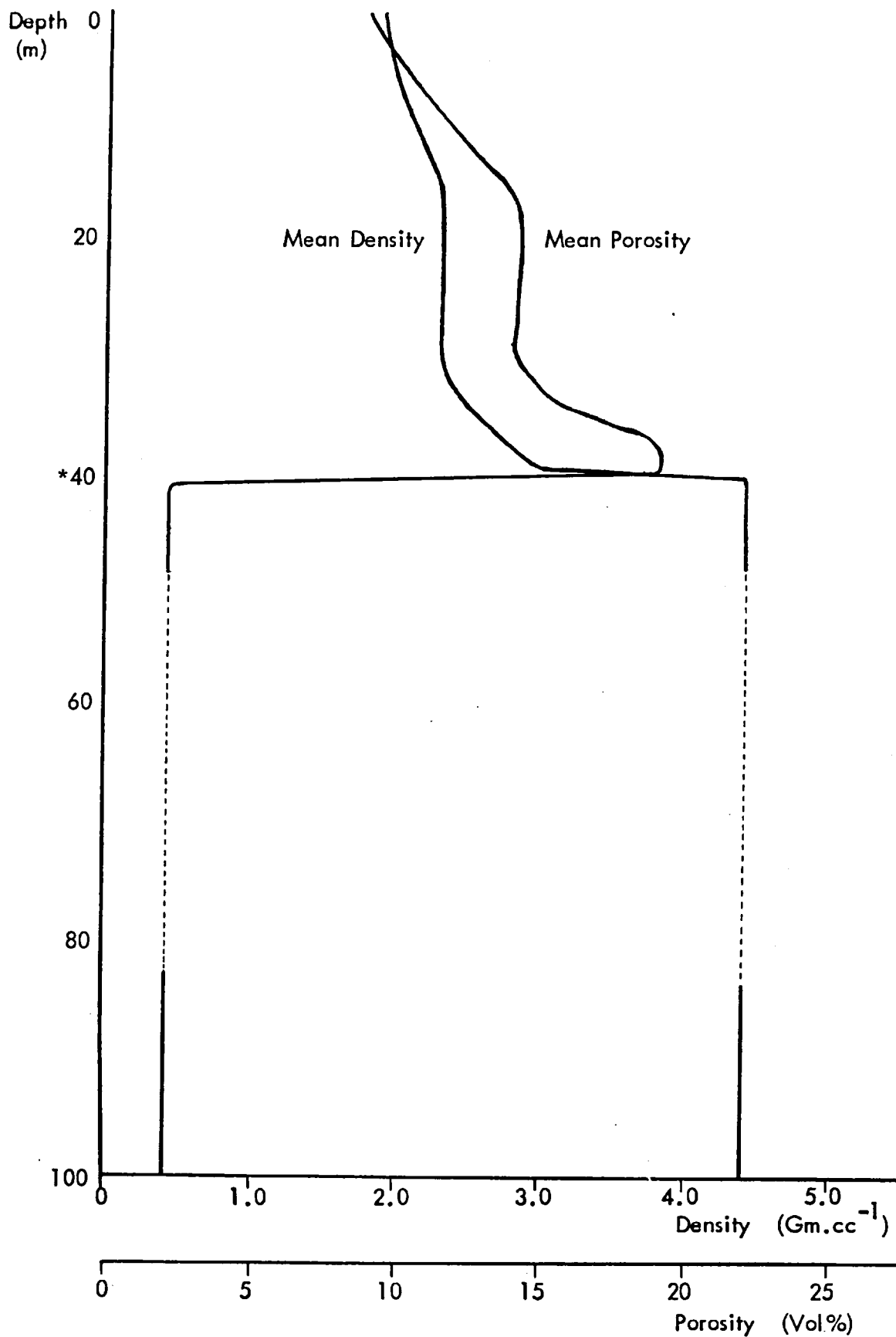
* Approximate position of the Water table

and concomitant precipitation of iron oxides that occurs at the 40m. level.

In the basal part of the oxide zone, mean density values continue to decrease progressively up to about the 28m. level, where they stabilise at around $2.3gm.cc.^{-1}$. The mean density of the oxide zone mineral assemblage then remains relatively constant up to about the 18m. level, and an interpolation between the 18m. and surface levels indicates that a further mean density decrease probably takes place over this vertical interval.

Mean porosity variation within the Pikwe oxide zone profile broadly parallels that of mean density, (Fig.3.3.1.). High mean values of about 20 percent are typical of the basal five metres of the oxide zone, but a progressive decrease in porosity takes place across the overlying 35-28m. vertical interval, with mean values gradually falling to about 12 percent at the 28m. level. Mean values are relatively constant in the 28-18m. sub-zone, but undergo a probable further decrease between 18m. and the surface.

Variations in mean true density and mean porosity within the oxide depth profile hence closely reflect the vertical sequence of mineralogical changes that have been described in section 3.2 More specifically, it is probable that the observed changes in these physical variables are directly related to the vertical variation in absolute mean silica content within the oxide zone profile at Pikwe.

3.4 THE BULK GEOCHEMISTRY OF THE PIKWE SULPHIDE ALTERATION SEQUENCE

The bulk geochemistry of the progressive oxidation sequence developed in the Pikwe deposit is now described. The account is based on two summary diagrams. Fig.3.4.1. illustrates the vertical variation, within the oxidation profile, of mean iron,sulphur, silicon, nickel and copper contents, and Fig.3.4.2. indicates the corresponding variations of mean cobalt, manganese, chromium and titanium contents within this same vertical depth zone. All chemical data are cast in units of gramme equivalents per cc in order that absolute variations in element contents may be documented and described.

A comparison of Figs. 3.2.3. and 3.4.1. indicates that the chemical variations of the major elements iron, sulphur and silicon in the Pikwe oxidation profile closely parallels the distribution of the principal phases containing these elements in the

mineralogical alteration sequence. In this respect, the behaviour of iron is directly related to the fate of the primary iron-rich sulphide minerals· pyrrhotite, pentlandite, chalcopyrite and their secondary equivalents during progressive oxidation.

In consequence, the small but definite gradual loss of iron that occurs between the 95m. and 45m. levels in the oxidation profile, (Fig.3.4.1.) probably corresponds to the progressive alteration of pentlandite to violarite that takes place across this vertical interval as this phenomenon results in a release of excess iron, (Fig.3.2.10.).

Contrastingly, the more notable drop in mean iron values that occurs between the 42m. and 39m. levels demonstrates that a substantial quantity of this metal is lost from the oxidation profile as a result of pervasive sulphide leaching at the water table horizon, (40m. level). The relatively small absolute difference in iron values that exists across this vertical interval indicates however, that a considerable proportion of this metal is retained in the profile. This feature is almost certainly due to the precipitation of iron as iron oxide. Further, the subsequent variation of iron contents within the oxide zone profile correlates closely with the variation in mean iron oxide content in this depth zone, as iron is exclusively located within goethite and hematite above the 39m. level.

The variation of mean sulphur content within the oxidation profile, (Fig.3.4.1.), exactly matches the gross distribution of sulphide phases in the mineralogical alteration sequence, (Fig.3.2.3.). The overall form of the mean sulphur depth profile therefore acts as an index of sulphide behaviour during progressive oxidation. In this respect, the constancy of mean sulphur values in the 95-42m. vertical interval,(Fig.3.4.1.), demonstrates that the progressive alteration of pyrrhotite and pentlandite to violarite and marcasite occuring within this sub-zone takes place without net loss of sulphur.

In contrast, the almost total depletion in sulphur, ($>99.9\%$), that occurs across a narrow vertical interval at the 40m. level is indicative of the restrictive vertical extent of sulphide leaching and of the dramatic effect that this process has on the chemistry of the oxidation profile. Further, the form of the sulphur profile across the 40m. level actually indicates that the sulphide assemblage undergoes total degradation at this horizon, and that, in consequence, sulphur is removed from the ore profile probably as soluble, highly mobile, oxidised species.

The vertical variation of mean silicon contents observed within the oxidation profile, (Fig.3.4.1.), not unexpectedly parallels similar variations in the mean contents of silicon-bearing phases within the mineralogical alteration sequence, (Fig.3.2.3.). The constancy of silicon mean contents between the 98m. and 40m. levels hence implies that a relatively uniform mean proportion of silicate minerals is associated with the oxidising primary massive sulphide assemblage.

In contrast, the form of the silicon depth profile above the sulphide leaching horizon, (40m.), corresponds closely with the documented vertical variation in mean silica contents that occurs in the oxide zone, (Fig.3.2.3.). It is therefore, entirely due to the observed phases of silica influx that are known to have affected the Pikwe oxide zone, (Section 3.2.).

The overall constancy of mean nickel contents in the 98-42m. sub-zone, (Fig.3.4.1.), indicates that the oxidising primary sulphide assemblage effectively forms a closed system with regard to this metal. Thus the appreciable quantities of nickel that are released from pentlandite during the formation of violarite (Vpn), (Fig.3.2.10.), must be utilised principally in the formation of violarite after pyrrhotite (Vpo), and not removed from the ore profile in significant amounts.

In contrast, the marked drop in mean nickel content that occurs across the 40m. level demonstrates that the metal is actively released as a result of sulphide leaching. These relations also indicate, however, that the mobilised nickel must subsequently be rapidly removed from the viscinity of the mineralisation zone, and it is likely that this operation occurs due to the formation of soluble, oxidised cationic species.

Comparison of the depth profiles of nickel and iron for the sub-zone above the 40m. level, (the oxide zone), demonstrates that marked similarities occur in the distribution of the two metals in this part of the oxidation profile, (Fig.3.4.1.). This close parallelism of form consequently implies that residual nickel is chiefly associated with iron oxide minerals in the Pikwe oxide zone, and it is, hence, likely that nickel is present as either a co-precipitant trapped within oxide mineral lattices, or else as adsorbed species on iron oxide grain surfaces. These types of association seem the most likely since nickel undergoes several further episodes of

depletion within the oxide zone, (Fig.3.4.1.), and the metal must, therefore, be present in a chemically mobile form for this phenomenon to occur.

The uniformity of copper mean values in the 98-42m. sub-zone, (Fig.3.4.1.), indicates that no significant quantities of this metal are lost during supergene sulphide alteration at Pikwe. In contrast, the marked copper depletion that occurs across the sulphide-oxide transition at 40m. demonstrates that a substantial proportion of the metal is removed from the ore zone as a result of sulphide leaching processes.

The shape of the mean copper profile above the 40m. level shows that the metal does not undergo further significant depletion until the 25m. level is attained, and, hence, mean copper contents remain essentially stable within the bottom 15 metres of the oxide zone. Above about 25m. though, Fig.3.4.1. indicates that a further episode of copper depletion takes place, and available data imply that this feature probably persists through to the surface outcrop.

A comparison of the copper and nickel depth profiles, (Fig.3.4.1.), shows that the two metals behave somewhat differently during progressive oxidation. In this respect, nickel undergoes a significantly greater degree of depletion across the sulphide leaching horizon than does copper, even though the two metals are present in similar quantities within the sulphide ore assemblage. Further, since both metals would be expected to possess comparable mobilities under the acid oxidising conditions characteristically associated with sulphide leaching, it is unlikely that the observed depletion difference is due to this latter factor.

The most likely cause of this phenomenon is, hence, thought to be that due to the differential occurrence of the two ore metals within sulphide minerals of significantly different chemical stabilities. In this respect, chemical data,(Section 3.2.), demonstrate that nickel and copper are respectively concentrated in violarite and chalcopyrite within the Pikwe secondary sulphide assemblage. Further, petrographic studies of the behaviour of these minerals during sulphide oxidation indicate that chalcopyrite tends to be preferentially retained across the sulphide-oxide transition, and that it subsequently persists in either unaltered or secondary forms, for some vertical distance into the overlying oxide zone, (Section 3.2.).

Fig. 3.4.1. Mean Profile Variations of Fe, S, Si, Ni and Cu – Pikwe

*. Approximate position of the water table

Element content (Gm. Equivs.cc^{-1})
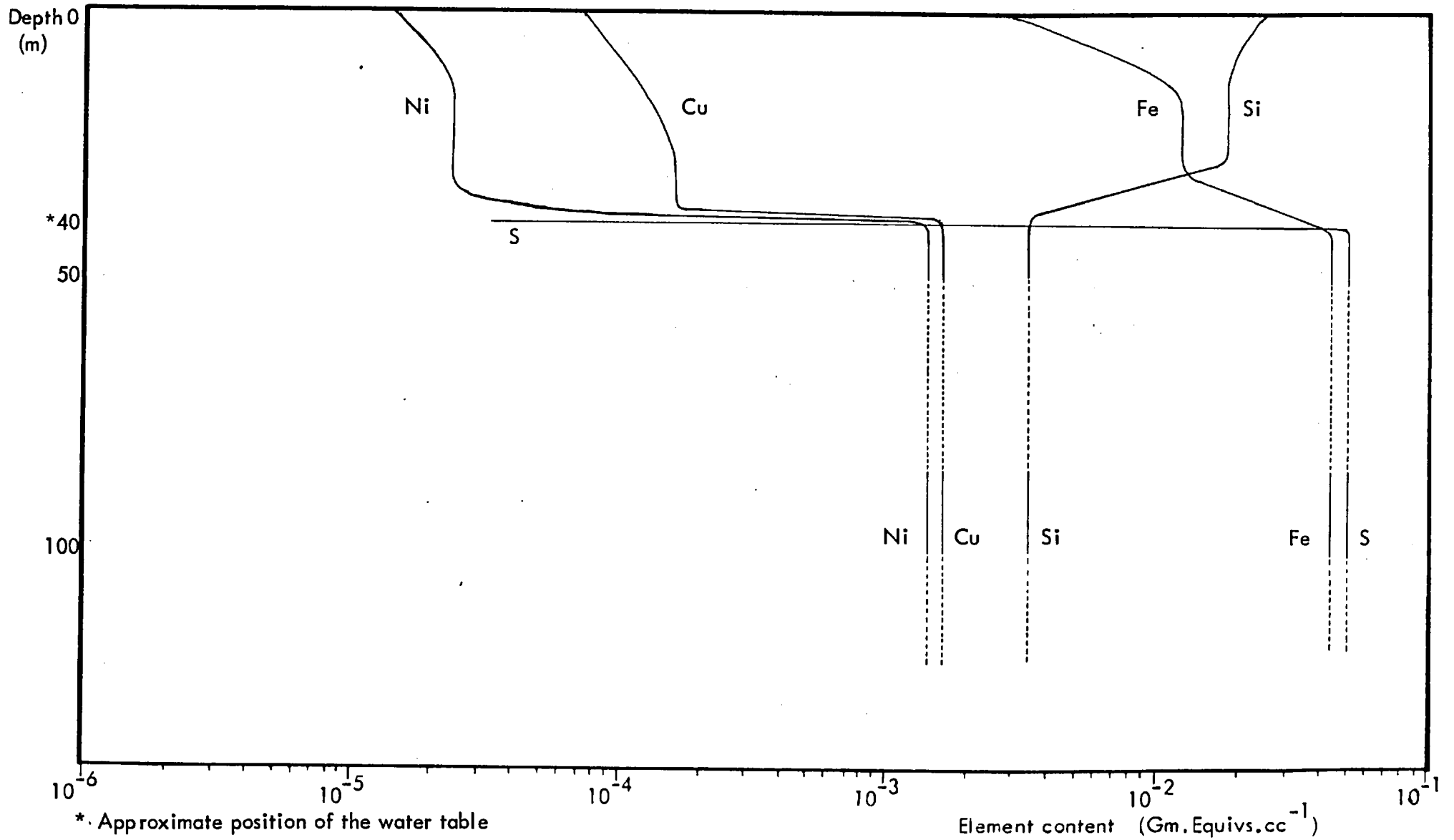
It is likely, therefore, that the observed differences in behaviour of copper and nickel in the upper part of the Pikwe oxidation profile are, in fact, due to the differential retention of copper within persistent copper sulphide relics in the bottom portion of the oxide zone profile.

The mean variations of the four metals cobalt, manganese, chromium and titanium within the Pikwe oxidation profile are presented in Fig.3.4.2. In common with the economic metals nickel and copper, each of these minor metals exhibits little significant variation in mean content within the 98-42m. sub-zone, and it is very probable that no net loss of these elements occurs during the formation of the secondary sulphide mineral assemblage at Pikwe.

In common with nickel, both cobalt and manganese undergo conspicuous depletion across the sulphide-oxide transition zone (42-39m.sub-zone) and all three metals subsequently demonstrate very similar variations in profile pattern within the overlying oxide zone, (Figs.3.4.1. and 2). In addition, chemical data, (Section 3.2.), indicate that cobalt, (and probably manganese), are concentrated with nickel in violarite species. This close mineralogical association, coupled with the well-known similarity in chemical behaviour of these three first row transition metals, strongly implies that these elements are simultaneously released during sulphide leaching.

These features further imply that the non-leached portions of each metal are simultaneously trapped in, or adsorbed on precipitating iron oxides, and that, the closely parallel variation patterns that they exhibit within the oxide profiles are therefore likely to be caused by similar chemical behaviour during the subsequent history of the iron oxide assemblage.

The form of the chromium and titanium profiles in the top 45 metres of the Pikwe oxidation sequence is characteristically different from each other and from those of the other trace metals, (Fig.3.4.2.). The depth distribution of mean chromium contents within the Pikwe oxidation profile demonstrates that this metal is enriched in the oxide zone relative to the parent sulphide assemblage. It must be, therefore, that chromium is introduced into the oxide zone from an external source, and the most likely provenence is the ultramafic succession enclosing the ore body, - more specificically, the adjacent host amphibolite.

Fig. 3.4.2.   Mean Profile Variations of Co, Mn, Cr and Ti – Pikwe

* Approximate position of the water table

Element content   (Gm. Equivs. cc^{-1})

137
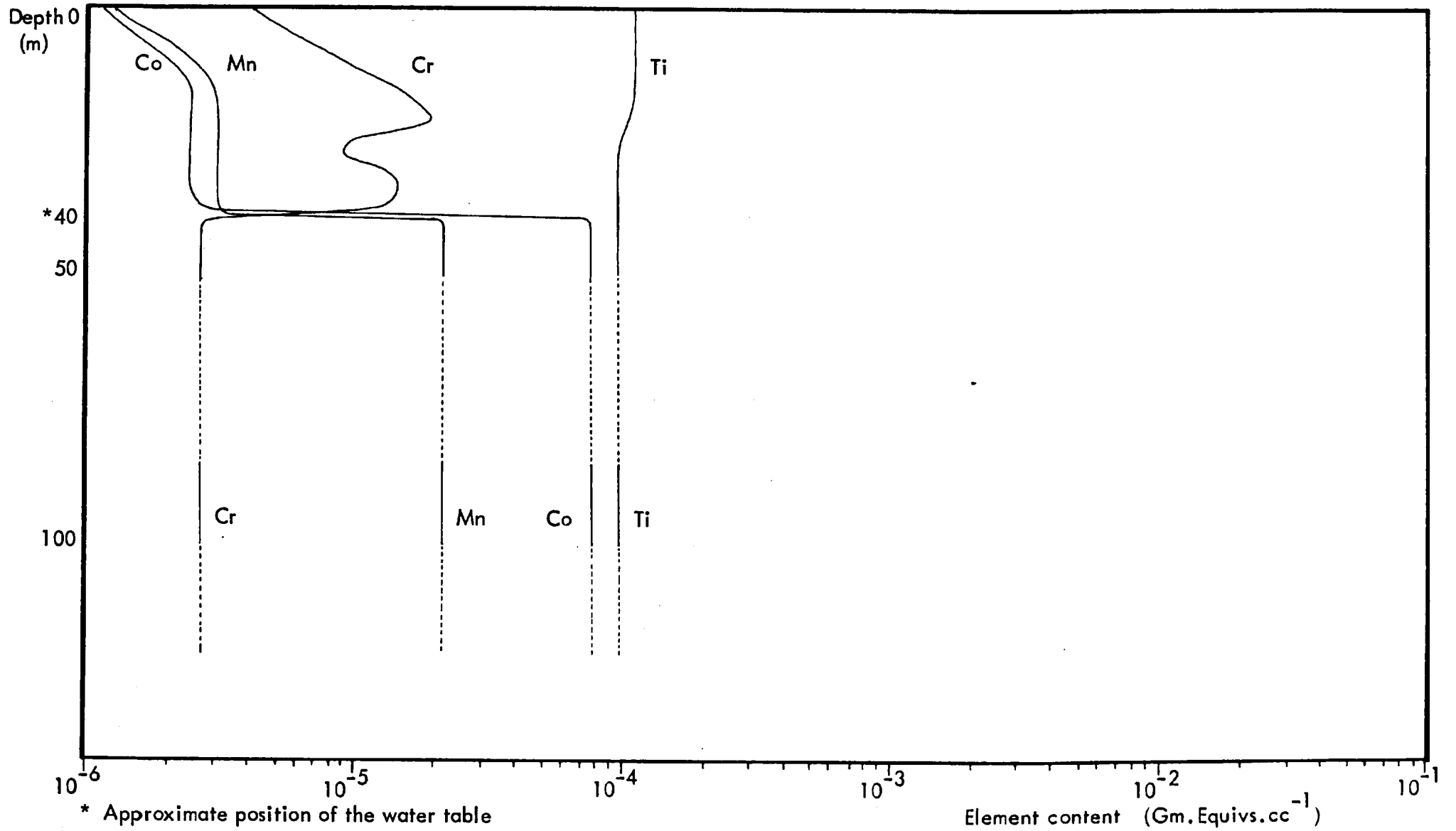
Fig.3.4.2. demonstrates that no significant change in titanium mean values occurs across the 40m. level or within the 40 - 25m. vertical interval. A slight increase in titanium content may, however, take place between the 25m. and 18m. levels, but the small size of this feature more likely reflects small-scale sample variation.

The overall uniformity of the titanium mean profile therefore demonstrates that this metal is not appreciably affected by the progressive oxidation of the Pikwe sulphide assemblage, and relevant petrographic and chemical data indicate that this passivity is probably due chiefly to the predominant location of titanium within the residuate mineral ilmenite ($FeTiO_3$).

3.5 SUMMARY

Work on a depth profile through near-massive to massive nickel sulphide ore at Pikwe demonstrates that a near-surface progressive sulphide alteration sequence is established in this deposit. The principal features of this observed sequence are summarised in Table 3.5.1. These data indicate that the principal constituents of the primary sulphide assemblage pyrrhotite and pentlandite, undergo progressive alteration to a secondary assemblage of violarite and marcasite between the 100m. and 45m. depth levels.

Sulphide alteration is initiated at about 90 to 100 metres below surface when interstitial and lamellar pentlandite undergo pseudomorphic replacement by chemically distinct violarite species. Excess iron, nickel and cobalt are released as a result of this alteration process.

Petrographic data demonstrate that alteration of adjacent monoclinic pyrrhotite takes place once pentlandite conversion has been initiated. At Pikwe, pyrrhotite alteration is a two stage process. Initial modification takes the form of pseudomorphing fringes of smythite. These structures are developed along grain borders and replace the parent sulphide along the 001 cleavage directions.

This intermediate smythite is however, itself subsequently superceded by violarite (Vpo). Replacement is again pseudomorphic in character and occurs along the mimicked 001 pyrrhotite cleavage in the smythite. Further, chemical data show that the formation of both smythite and violarite require the incorporation of nickel released by altering pentlandite, and it is hence likely that this mode of pyrrhotite is fundamentally influenced, if not actually controlled, by the alteration of adjacent

pentlandite.

Chemical and textural data demonstrate that the alteration of both pentlandite and pyrrhotite take place under conditions of constant sulphur. The data also indicate, that these primary sulphide alteration phenomena comprise oxidation processes.

With reference to Table 3.5.1., the vertical sub-zone between the 100m. and 45m. levels in the Pikwe massive sulphide profile is characterised by an assemblage of violarite after both interstitial and lamellar pentlandite, violarite after pyrrhotite, unaltered pyrrhotite, chalcopyrite, magnetite, and associated silicates. Available data imply, though, that violarite formation does not occur uniformly within this profile, and it is probable that this heterogeneity of alteration response is due to the combined effect of both small- and large-scale geological factors on local chemical conditions within the Pikwe ore zone.

This rather gradual change in sulphide assemblage is, however, also reflected in density and porosity, and in bulk chemical variation within the 100 - 45m.sub-zone. In this respect, both mean density and porosity show no significant change between the 100 and 45m. levels, and the bulk chemistry of the ore assemblage, with the exception of iron is likewise unaffected during the development of violarite. The small loss of iron that does occur is, however, probably due to its expulsion from the ore profile. This loss of iron hence contrasts significantly with the retention of nickel simultaneously released by the process of pentlandite alteration and which implies that most of this released ore metal is subsequently taken up during pyrrhotite alteration.

At about 45m., unaltered pyrrhotite undergoes a rapid, typically pseudomorphic, replacement by marcasite. This reaction is oxidative in character, and probably occurs under constant sulphur conditions. The resultant secondary sulphide assemblage of violarite and marcasite is present as a relatively narrow, erratically distributed zone between the 45m. and 40m. levels in Pikwe massive ore.

Between the 42m. and 40m. levels, though, the relevant data indicate that the violarite-marcasite assemblage undergoes pervasive leaching. In this respect, violarite species are generally the first sulphides to be effected, and are either replaced by goethite pseudomorphs or else undergo complete dissolution. Marcasite leaching generally occurs at about 40m. and very commonly takes the form of a mimicked replacement by iron oxides - typically goethite, but more uncommonly by a combination of goethite and hematite.

Chalcopyrite similarly exhibits oxidation in this narrow sub-zone, and it is commonly replaced by goethite: either as complete grain pseudomorphs or else as boxwork structures. A proportion is, however, generally unaffected by leaching or alters to secondary covellite. In contrast, magnetite typically undergoes total removal at this level, although ex-solved daughter ilmenite zones or lamellae generally remain unaffected by oxidation.

A substantial decrease in mean density and a very large increase in mean porosity take place as a result of sulphide leaching. Gross chemical modifications also accompany these fundamental mineralogical changes. In this respect, sulphur exhibits an almost total removal across the sulphide leaching zone - most probably as sulphate ion. Whereas iron is only partially removed, a large proportion being retained and subsequently precipitated as (ferric) oxides. Contrastingly, nickel, cobalt and manganese show strong depletion, and this feature is probably due to their release as highly mobile oxidised species. Copper also exhibits a substantial although anomalously low depletion in the sulphide leaching zone. But both chromium and titanium, contrastingly, remain unaffected by sulphide dissolution.

The secondary sulphide assemblage is replaced above the 40m. level by one composed of iron oxides. Goethite is the principal oxide present, although substantial quantities of hematite also occur. Further, this fundamental change in mineral assemblage is reflected in a zone of high porosity and by subsequently lower mean density values in this region of the oxidation profile, (Fig.3.3.1.).

Pseudomorphed sulphide textures are very common in the basal part of the oxide zone, and both 'kink-zone' and bird's eye marcasite structures are preserved as goethite, or, less commonly as goethite/hematite composites. Violarite mimic textures are commonly present as goethite, and chalcopyrite is generally noted as goethite pseudomorphs or boxworks.

Chemical data indicate that the mimicked replacement of sulphide by iron oxide generates large quantities of hydrogen ion, and it is likely that much of this acid is subsequently neutralised by buffering reactions involving the acid hydrolysis of adjacent host amphibolite wall rock. This hydrolytic attack on hornblende-rich silicate leads to the degradation of the amphibole mineral lattice. In consequence, the component metals are oxidised and leached out, and substantial quantities of silica are released.

It is likely that these released metals subsequently precipitate in various combinations,

with or without sulphate ion, to provide part of the suite of oxidate minerals observed in the Pikwe oxide and weathered amphibolite zones. In contrast, the mobilised silica is mainly precipitated in the basal part of the oxide zone as cavity and void fillings.

Petrological studies demonstrate that progressive mineralogical changes occur within the oxide zone depth profile. In this respect, a large-scale dehydration of goethite to hematite occurs in the 39 - 35m. sub-zone, and in consequence, much of the relic sulphide textures present above the 35m. level are defined in hematite. Available data also indicate, however, that goethite alteration effectively ceases in the overlying 35 - 30m. sub-zone and that mean goethite contents consequently stabilise in this vertical interval. It is likely, though, that a second, vertically restricted, episode of goethite dehydration occurs within the 30 - 28m. sub-zone.

A progressive linear increase in mean silica content occurs between the 39m. and 30m. levels in the oxide profile. This phenomenon is caused by an influx and subsequent precipitation of silica probably released during the deep weathering of proximal silica-rich gneissic units.

The effect of silica enrichment on the incumbent mineral assemblage is fundamental. It leads to the development of a pervasive matrix of colloidal silica and to the partial replacement of the iron oxide assemblage, with a consequent obliteration of relic sulphide textures. In addition, a concomitant decrease in both mean density and mean porosity values occurs between the 39m. and 30m. levels as a direct result of the increased proportion of silica in the oxide zone mineral assemblage.

Available data for the overlying 28m. - 18m. vertical interval demonstrate that the mean proportions of goethite, hematite and silica remain effectively constant in this sub-zone, and this phenomenon probably indicates that no net mineralogical changes are occuring in this part of the oxide profile. In contrast, the overlying top 18 metres of the oxide zone appear to manifest a second major phase of silicification, and this feature probably results in a further episode of relic sulphide texture obliteration taking place within this sub-zone.

The bulk chemistry of the Pikwe oxide profile is, in general, closely related to the gross mineralogical features outlined above. Thus, iron and silicon variation are directly related to respective changes in iron oxide and silica content within the

profile. The mean variations of nickel, cobalt and manganese closely parallel that of iron. These transition metals are, hence, probably associated with iron oxides as co-precipitated material. In contrast, copper exhibits rather anomalous behaviour in the oxide profile as it displays constant mean values within the bottom 15 metres of the zone after initial depletion due to sulphide leaching. It is likely, however, that this copper retention phenomenon is chiefly due to the presence of residual chalcopyrite or secondary covellite within this part of the oxide profile.

The behaviour of both chromium and titanium within the oxide profile differs markedly from the other documented metals. In this respect, the distribution of chromium contents exhibits a definite depth-controlled enrichment pattern.

In contrast, titanium exhibits very little significant mean variation within the entire sulphide oxidation sequence, and it is very probable that this phenomenon is due chiefly to the principal location of this relatively immobile metal in the stable mineral ilmenite.

The sequence of mineralogical change that occurs within the massive sulphide ore profile is qualitatively similar to that documented in several Western Australian nickel sulphide deposits, (Nickel et.al., 1974, 1977, op.cit. Watmuff, op.cit. Dalgarno, op.cit.; Wilmshurst, op.cit.). It is, hence, likely that the development of sulphide alteration at Pikwe can be similarly explained in terms of a chemical model based on the Kambalda deposits as developed by Thornber, (1975a, op.cit.).

TABLE 3.5.1. SUMMARY DATA OF SULPHIDE ALTERATION - PIKWE

Depth (m)	Alteration Zone	No. of Samples (n)	MINERALOGY (Means and ranges) Volume % Units							Den gm/cc	Por %	S	Fe	SiO$_2$	MgO	Al$_2$O$_3$	CO$_3$	Ni	Cu	Mn	Cr	Co	Ti
	Oxide	52	**Hm** 1.0	**Gt** 2.0	**Si** 1.0	**Nal**	**Njr**	**Ca**		1.20	1.0		6.04	0.11	0.10	0.20		102	30	25	25	30	42
			33.7	25.5	39.6	trace	trace	trace		2.43	12.0	-	37.89	36.45	0.22	1.50	-	836	3918	69	201	73	1723
40			80.0	90.0	90.0					3.50	48.0		61.87	89.79	0.50	5.90		4353	10592	316	910	477	12601
	Violarite - Marcasite	3	**Gt** 7.5	**Vl** 0.5	**Mc** 75.0	**Cp** 1.0	**Il**																
			17.5	0.7	80.0	1.7	0.1			3.80	3.6	39.71	56.39	1.05	0.10	0.40	-	17445	2412	126	25	3121	1007
~45			7.5	0.5	75.0	1.0																	
	Transition	5	**Po** 30.0	**Pn** 2.5	**Vl** 2.5	**Mc**	**Cp** 0.0	**Mt** 0.0	**Sl** 1.0	2.90	1.2	23.54	36.17	0.10	0.10	0.10		11080	4833	119	25	543	276
			63.0	2.1	3.1		11.5	7.0	13.0	3.94	4.5	30.43	49.27	8.51	0.96	2.58	-	15810	41085	504	63	874	1285
			85.0	4.5	4.5		45.0	15.0	25.0	4.80	10.6	37.09	58.61	19.15	2.70	10.40		21916	79800	1005	1269	1269	3039
90 - 100	Primary	2	**Po** 60.0	**Pn** 3.0			**Cp** 2.0	**Mt** -	**Sl** 5.0	3.80	-	31.08	46.05	0.10	0.10	0.10		14152	4665	193	-	859	689
			75.0	4.0			4.5	2.0	15.0	4.15	1.0	33.95	52.25	8.64	0.30	0.35	-	17472	14455	223	25	1020	1121
			90.0	5.0			7.0	-	25.0	4.50	-	36.83	58.45	17.23	0.50	0.60		20792	24244	253	-	1180	1553

Physical data (mean/ranges) = Den gm/cc, Por %. GEOCHEMISTRY (Means and ranges): Wt.% Units = S, Fe, SiO$_2$, MgO, Al$_2$O$_3$, CO$_3$; p.p.m. Units = Ni, Cu, Mn, Cr, Co, Ti.

CHAPTER FOUR

NEAR SURFACE OXIDATION IN FIVE ADDITIONAL NICKEL SULPHIDE

DEPOSITS IN SOUTHERN AFRICA

4.1. INTRODUCTION

The petrology and geochemistry of five additional supergene-altered nickel sulphide deposits in southern Africa are now described. The format of the present chapter is similar to that used in the description of the sulphide oxidation sequence at Pikwe, Botswana, (Chapter Three).

In the present chapter, each deposit is described in turn. The petrology of the observed sequence of sulphide alteration - including mineral chemistry - is firstly set out. The bulk chemistry of progressive sulphide oxidation is then presented. In order to avoid unnecessary repetition, however, the descriptions of each alteration sequence are in synoptic form and much of the relevant data is condensed in summary figures and/or tables that accompany the text. More detailed data are presented in the relevant parts of Appendix Two.

The chapter concludes with a brief summary section that comprises a short resume of the presented material. Detailed descriptive comparison of the deposits is, however, deferred until Chapter Six.

4.2 SUPERGENE SULPHIDE ALTERATION IN THE MUNALI HILLS DEPOSIT, ZAMBIA

The location and known geology of the Munali Hills nickel deposit has been previously outlined in section four of Chapter Two. In summary, the deposit occurs as an elongate tabular ore body located at or near the foot wall zone of a gabbro that is intruded into a late Precambrian sequence, (Table 2.4.2.).

The petrology of the primary sulphide assemblage

The mineral assemblage of unaltered near-massive to massive sulphide ore consists principally of pyrrhotite and pentlandite, (Table 4.2.1.). Minor quantities of both chalcopyrite and magnetite are also present however, as are trace amounts of hypogene marcasite. Pyrrhotite is the dominant (matrix) sulphide and forms about

80 percent of the primary assemblage, (Table 4.2.1.). The constituent grains are commonly rather equant in form and typically exhibit mutual boundary textures. Spindle deformation twinning is also generally present in Munali pyrrhotite, (Fig. 4.2.1A.).

Pentlandite comprises about eight percent of the ore assemblage, (Table 4.2.1.). It typically occurs as elongate stringers along pyrrhotite-pyrrhotite grain borders, (Fig.4.2.1B.). Chalcopyrite averages about two percent of massive ore, but is inhomogeneously distributed within the assemblage, (Table 4.2.1.). Where present, though, it is typically elongate in form and may partly replace other minerals.

Magnetite forms about two percent of unaltered massive ore, (Table 4.2.1.). It is generally present as smooth, rounded, semi-hedral to euhedral grains that commonly contain lamellae or patches of ex-solved ilmenite, (Fig.4.2.1C.). Incipient oxidation of magnetite in primary ore may manifest itself as patchy rims of maghemite, (Fig.4.2.1D.). Marcasite is characteristically present in primary ore as a localised hypogene replacement of pyrrhotite, (Fig.4.2.1E.).

The petrology of the sulphide alteration sequence

Available data indicate that supergene alteration of the Munali primary sulphide assemblage is initiated at about 140 - 150 metres b.s. At this level pentlandite undergoes incipient replacement by violarite. The alteration takes the form of spherical nucleii that typically consist of an outer zone of violarite surrounding a central, highly porous core, (Fig.4.2.1F.). Progressive growth of violarite generally takes place by the gradual coalescence of point nucleii and leads to the early replacement of pentlandite octahedral cleavage zones, (Fig.4.2.1G.).

Replacement of adjacent pyrrhotite occurs soon after violarite after pentlandite (Vpn) begins to nucleate. Initial alteration takes the form of feathery lamellar patches of reddish-brown smythite. This mineral replaces pyrrhotite along the 001 cleavage and nucleates on the grain borders between pyrrhotite and altering pentlandite, (Fig.4.2.1H.).

Continued development of Vpn is, however, paralleled by the initiation and subsequent development of a second episode of pyrrhotite alteration. This occurs as blue-violet porous feather-like fringes of violarite after pyrrhotite, (Vpo). This mineral replaces smythite along the mimicked 001 pyrrhotite cleavages, (Fig.4.2.2A.)

146

Fig. 4.2.1. Petrography of Munali Sulphide Ore (1)

Scale length = 100 μ

A.   Spindle deformation twinning in pyrrhotite. (x 110) Air

B.   Typical texture of interstitial pentlandite (x 110) Air

Pentlandite; white-light grey: Pyrrhotite; medium grey: Smythite fringes; medium dark grey

C.   Ilmenite lamella associated with magnetite (x 320) Air

Carbonate; dark grey: Thin hematite rim; mid-grey: Ilmenite; medium-dark grey elongate: Pyrrhotite; light grey: Voids and silicates; dark

D.   Maghemite rimming magnetite (x 110) Air

Magnetite; medium-dark grey (top half):   Maghemite; light grey rim: Carbonate; dark grey mottled: Pyrrhotite; very light grey (left)

E.   Localised replacement of pyrrhotite by hypogene marcasite (x 110) Air

Hypogene marcasite; white: Pyrrhotite; medium grey: Carbonate; dark grey

F.   Incipient growth of violarite after pentlandite (x 1000) Oil

Pentlandite; light grey: Violarite; medium-dark grey: Voids; black

G.   Replacement of pentlandite cleavage by violarite (x 320) Air. Blue-white filter

Pentlandite; light grey: Violarite; medium-dark grey: Voids; black

H.   Typical replacement texture of smythite (x 320) Air

Pentlandite; light grey: Violarite; medium-dark grey, granular: Smythite; medium-dark grey fringes: Pyrrhotite; mid-grey (top):   Voids; black

Fig.4.2.1.
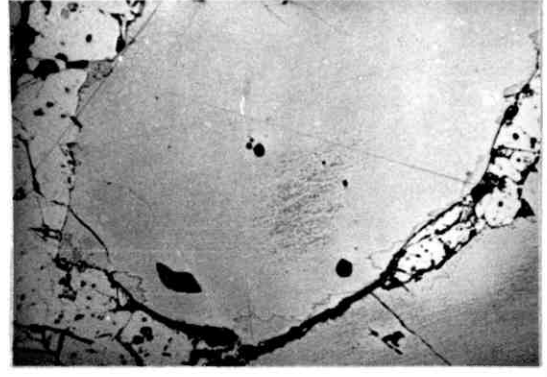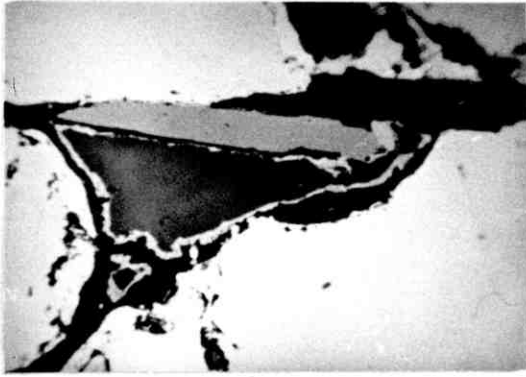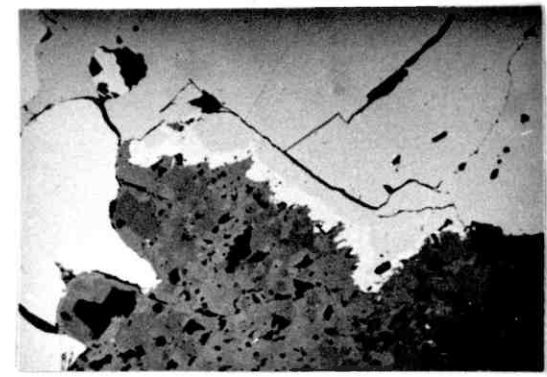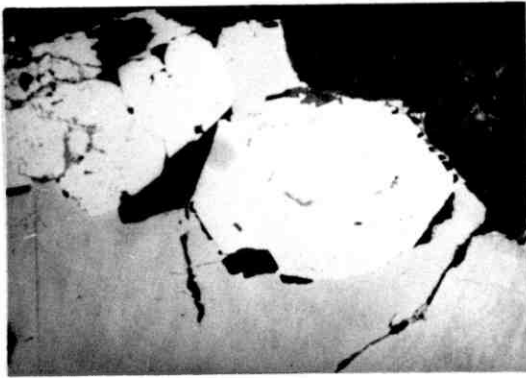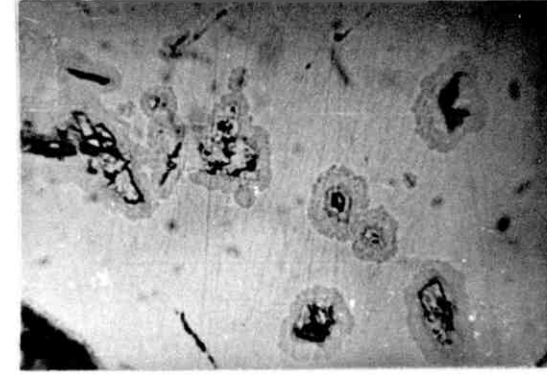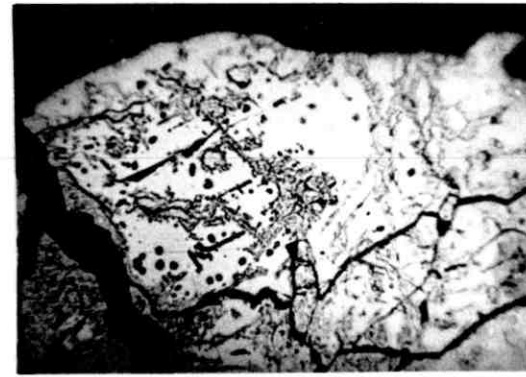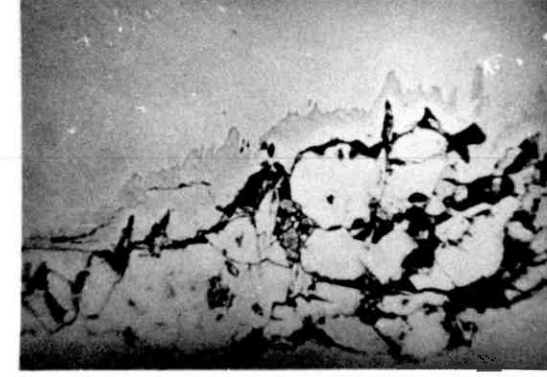
The subsequent growth of Vpn and Vpo from their parent minerals occurs simultaneously. Eventually though, pentlandite is completely replaced by Vpn, and Vpo growth consequently ceases due to the termination in the supply of free nickel necessary for its formation, (Fig.4.2.2B.). In many instances however, cessation of Vpo growth occurs after the complete replacement of smythite by Vpo, with the result that this latter mineral may show textural evidence of direct formation from pyrrhotite, (Fig.4.2.2C.).

Available data indicate that the assemblage Vpn, pyrrhotite and Vpo is present up to about the 40 - 45m. level in the Munali alteration profile, (Table 4.2.1.). Above about 60 metres however, pyrrhotite exhibits an increasing tendency to be replaced by secondary iron disulphides.

Petrological observations demonstrate that pyrrhotite typically alters to fine-grained marcasite that very commonly undergoes a subsequent recrystallisation to massive pyrite, (Fig.4.2.2D.). The pyrite commonly exhibits discrete zones of pinkish-brown bravoite, and has the superficial appearance of a primary hypogene mineral. The secondary nature of this massive mineral is, however, indicated by its characteristic passive interdigitation with violarite after pyrrhotite, (Fig.4.2.2E.). Further, it is likely that the nickel in the bravoite lamellae is chiefly derived from the parent pyrrhotite, although no chemical data are available to confirm this supposition.

Available data indicate that the observed sulphide assemblage is subjected to an active replacement by carbonate above the 60m. level. The replacing mineral is an iron-rich calcite, and preferentially supercedes both violarite, (Fig.4.2.2F.) and chalcopyrite, (Fig.4.2.2G.). It is very probable that the iron component of this calcite is derived from that released during the formation of violarite after both pentlandite and pyrrhotite, and as a result of the formation of marcasite from pyrrhotite. In contrast, the calcium and carbonate components very likely result from the weathering of adjacent host metagabbro.

No sulphide material is available for study above the 50m. level, but it is likely that the secondary sulphide assemblage of violarite and marcasite/pyrite is fully established at about the 40-45m. level and subsequently persists up to the water table at approximately 30 to 35 metres below surface.

Fig. 4.2.2. Petrography of Munali Sulphide Ore (2)

Scale length = 100μ

A. Replacement of smythite by violarite after pyrrhotite (x 600) Oil

Partly altered pentlandite; whitish-grey: Violarite after pyrrhotite; medium-dark grey, granular: Smythite; dark grey: Pyrrhotite; mid-grey

B. Fully developed secondary violarite texture (x 110) Air

Violarite after pentlandite fringed by violarite after pyrrhotite; mid-grey, granular: Pyrrhotite; light-medium grey: Carbonate; dark grey-black

C. Corrosion front between violarite (Vpo) and pyrrhotite (x 320) Air

Violarite (Vpn and Vpo); mid-grey, granular: Pyrrhotite; mid-grey: Voids; black

D. Recrystallisation of fine-grained marcasite pyrite (x 110) Air

F - G secondary marcasite; medium-dark grey, granular: Probably Ni-rich pyrite; mid-grey, rimming fringe: Zoned pyrite; light grey: Pyrrhotite; mid-grey (top left): Vpn; mid-grey, granular (top left): Voids; black Carbonate; dark grey (extreme right)

E. Super-position of Vpo and massive secondary pyrite (x 1000) Oil

Violarite; medium grey, granular: Pyrite; mid-grey: Carbonate; dark grey (top)

F. Replacement of violarite after pentlandite by iron-rich calcite (x 600) Oil

Fe-rich calcite; dark grey: Residual Vpn; medium grey, granular: Pyrrhotite; mid-grey

G. Replacement of chalcopyrite by iron-rich calcite (x 110) Air

Fe-rich calcite; dark grey: Chalcopyrite; light grey invested with calcite: Pyrrhotite; light grey surround: Violarite, medium-dark grey, granular

Fig.4.2.2.

A

B

C

D

E

F

G
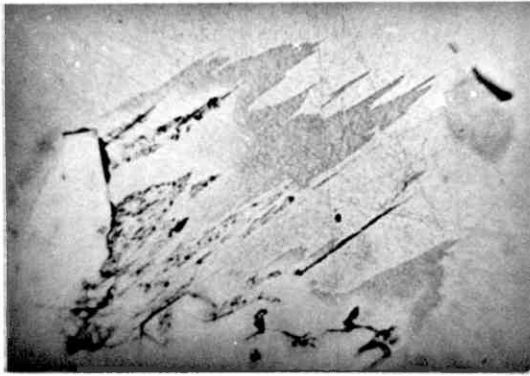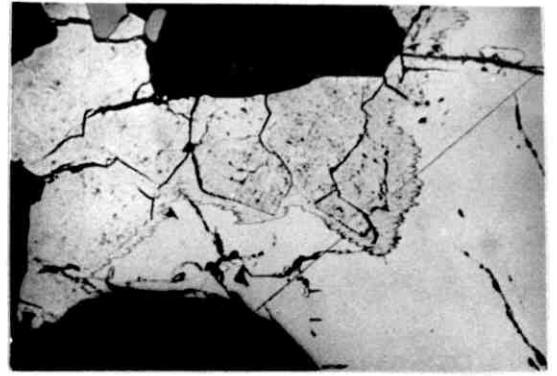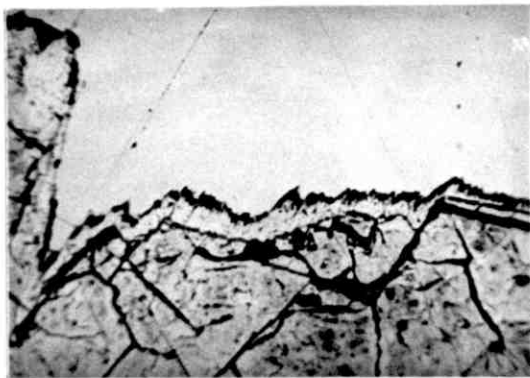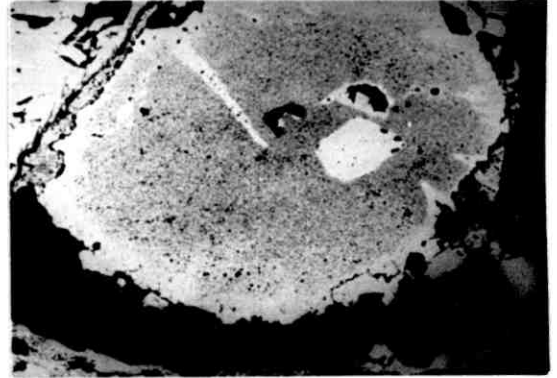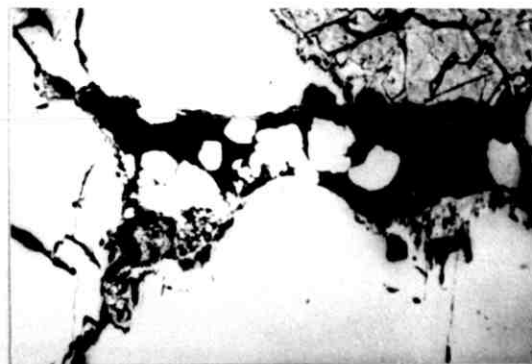
The petrology of the oxide zone

The sulphide alteration sequence at Munali is represented above the water table by a zone of iron oxide-rich rocks that extend upwards from about the 35m. level and crop out at the surface as discrete areas of ferruginous gossan, (Section 2.4.). In the present study, sample material was available solely from the surface outcrop, and hence no attempt to analyse vertical variation within the oxide zone profile at Munali has been possible. The following summary description of oxide zone petrology is therefore based entirely on the mineralogical and textural relations observed in the sampled surface gossan suite. It is, however, very likely that such features typify the Munali oxide zone as a whole.

The mineralogy of the Munali oxide zone consists of goethite, hematite and silica. Goethite averages about 55 percent in the study material, but its mean content exhibits large inter-sample variation, (Table 4.2.1.). It is present in several textural configurations and is important in the preservation of pseudomorphic textures after the secondary sulphide assemblage in the Munali gossan. In this respect, goethite is commonly present as well-preserved pseudomorphs after Vpn and Vpo, (Figs.4.2.3A and 4.2.3B, respectively). More rarely, the mineral occurs in the following configurations: Linear pyrrhotite cleavage mimics, (Fig.4.2.3C.); bird's eye structures after secondary marcasite, (Fig.4.2.3D.); (rare) massive structures after secondary pyrite, (Fig.4.2.3E.); and as (quite rare) boxworks after chalcopyrite, (Fig.4.2.3F.). Uncommonly, goethite is also observed as a direct replacement of ilmenite, (Fig.4.2.3G.), or as a late cavity growth mineral, (Fig.4.2.3H.).

Hematite averages approximately 25 percent in the sampled gossan suite, but characteristically exhibits a wide range of contents therein, (Table 4.2.1.). The mineral is present in several textural configurations and importantly occurs as mimic structures after several members of the secondary sulphide assemblage. In this connection, hematite very commonly occurs as pseudomorphs after marcasite-mimicked pyrrhotite cleavage structures, (Fig.4.2.4A.); as direct mimic textures after secondary marcasite, (Fig.4.2.4B.), and secondary pyrite, (Fig.4.2.4C.); and as boxworks after chalcopyrite, (Fig.4.2.4D.). More rarely, the mineral occurs as pseudomorphic replacements of violarite after pentlandite grains, (Fig.4.2.4C.), and quite commonly defines the octahedral cleavage traces in goethite mimics after Vpn, (Fig.4.2.3A.). Further, the mineral is observed as a

Fig. 4.2.3. Petrography of the Munali Gossan (1)

Scale length = 100 μ

A. Violarite after interstitial pentlandite as goethite mimic (x 220) Oil.
Blue-white filter

Goethite; medium grey: Colloidal goethite; medium-dark grey: Voids;
dark,structure fringed by goethite after Vpo. Goethite lineations also mimic
Po cleavage

B. Goethite after Vpo (x 220) Oil   Blue-white filter

Outline of interstitial Vpn. Vpn internal cleavage structure. Fringing Vpo
in goethite

C. Goethite after secondary mimicked pyrrhotite cleavage (x 220) Oil
Blue-white filter

Sub-parallel ribbing after Po cleavage well preserved. Broad linear zones
are after deformation (kink-zone) borders

D. Goethite mimics after marcasite bird's eye structures (x 220) Oil
Blue-white filter

Bird's eye mimics in goethite with some retention of internal structure; dark
grey. Fine-grained hematite (light grey) as principal matrix component
(after secondary marcasite)

E. Goethite mimic after massive secondary pyrite (x 220) Oil. Blue-white filter

Zoned structure well shown.   Small pyrite relic (light grey) at lower left

F. Goethite as chalcopyrite boxworks (x 220) Oil. Blue-white filter

Boxworks defined in goethite (medium-dark grey) rimmed by hematite (light
grey). Outline of former Cp grain is well preserved, with an adjacent small
marcasite bird's eye mimic in goethite. Boxwork interstites filled with
hematite or as voids (resin-filled dark grey)

G. Goethite as direct ilmenite replacement (x 320) Air. Blue-white filter

Ilmenite (medium grey) surrounded by goethite (medium-dark grey), the
latter invested by later drusy hematite (light-medium grey)

H. Goethite as late-stage drusy growth on hematite (x 320) Air
Partly crossed nicols

Goethite (dark grey) precipitation on hematite (light-medium) grey.
Voids in black

Fig.4.2.3.

A

B
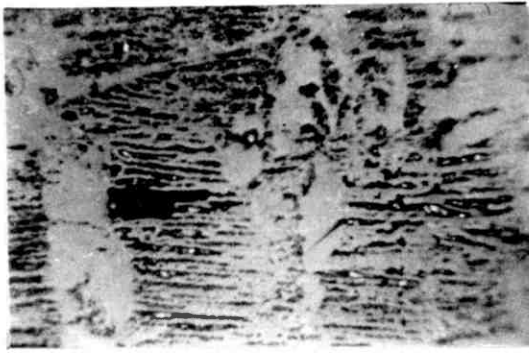
C

D

E
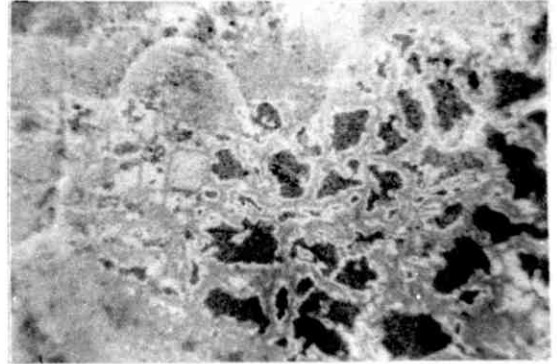
F
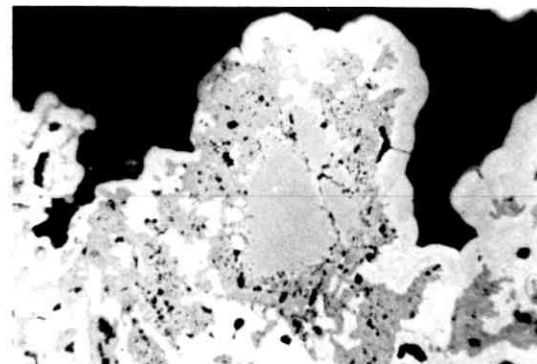
G
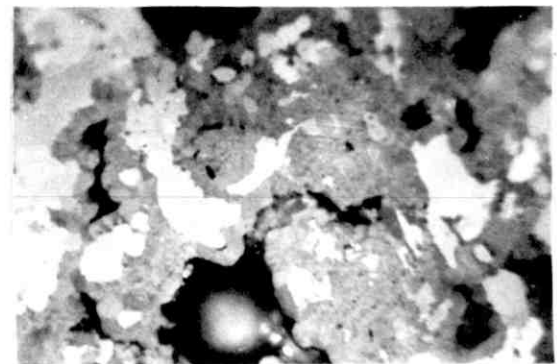
H

Fig. 4.2.4. Petrography of the Munali Gossan (2)

Scale length = 100μ Blue-white filter used throughout

A.   Hematite boxwork after composite pyrrhotite/secondary marcasite (x 110) Air

B.   Hematite mimic after marcasite bird's eye structure   (x 220) Oil

C.   Hematite mimic after massive secondary pyrite (x 600) Oil

D.   Hematite boxworks after chalcopyrite (x 320) Air

Typical quadrangular cell-form (LEFT). Adjacent mimiced pyrrhotite cleavage relic also in hematite (light grey). Goethite = medium-dark grey matrix (centre and right)

E.   Hematite mimics after magnetite (x 600) Oil

Hematite (light grey) defines the octahedral spinel cleavage. Relic magnetite (medium grey) is present in inter-cleavage blocks. Matrix (dark grey) is colloidal silica

F.   Hematite as late drusy growth (x 220) Oil

Hematite (light grey) precipitated on goethite mimics after violarite (Vpn) (dark grey)

G.   Silica as boxwork filling (1) (x 110) Air

Silica (dark grey) present in goethite boxworks after silicate (mid-grey)

H.   Silica as boxwork filling (2))x 110) Air

Silica (dark grey) as interstitial cell filling in goethite boxwork after chalcopyrite (mid-grey)

155
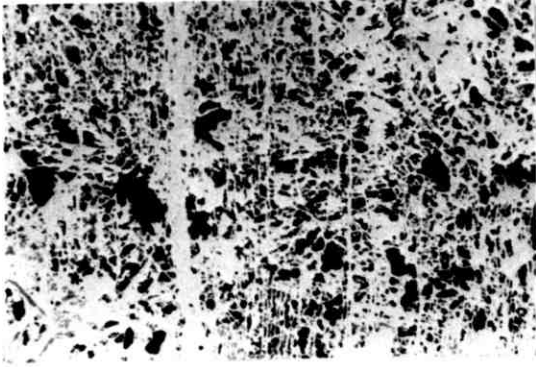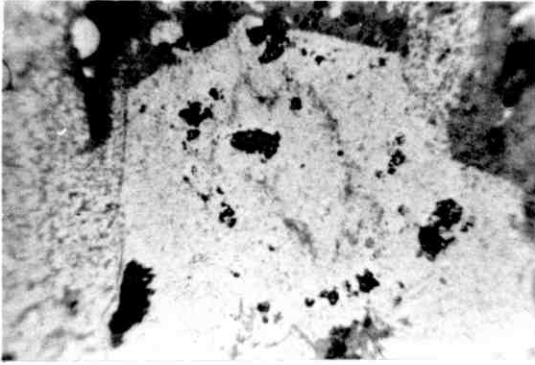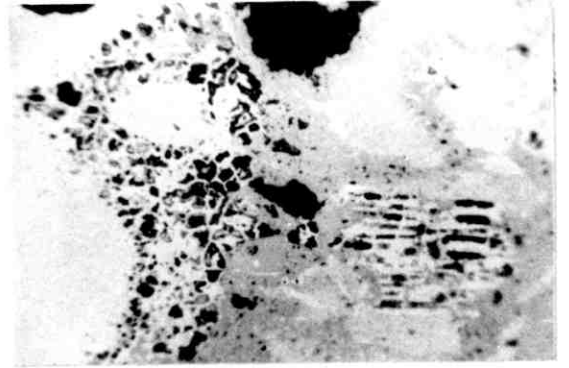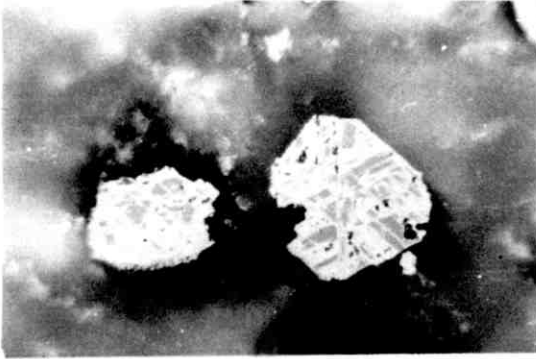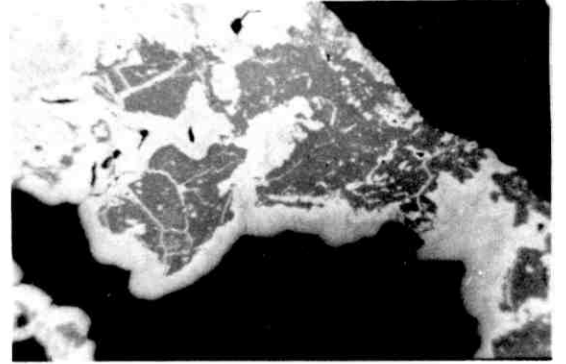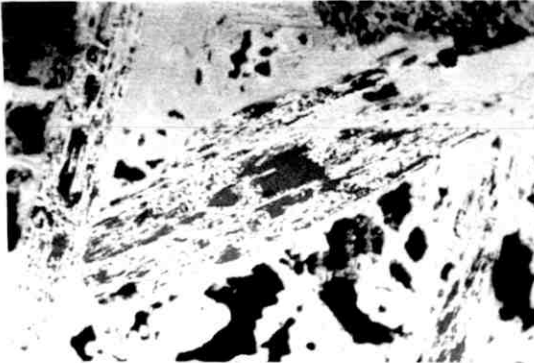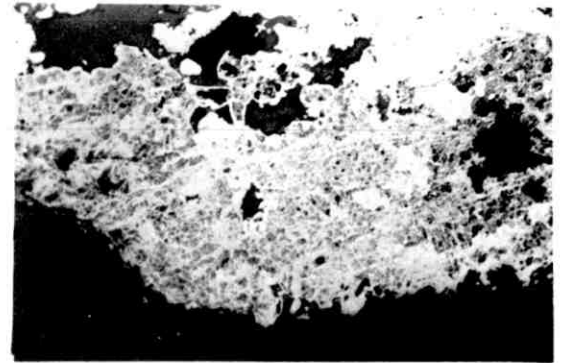
Fig.4.2.4.

direct replacement of magnetite, (Fig.4.2.4E.). It is also present in the Munali surface gossans as a late cavity filling, (Fig.4.2.4F.).

Silica averages about 20 percent of the sampled Munali gossan, but the contents of individual samples vary widely, (Table 4.2.1.). The mineral is typically present however as a late cavity filling and in this respect tends to invest the leached intersticies of boxworks and other leached structures after sulphide, (Figs.4.2.4G and 4H.)

The mean variation in both true density and porosity within the sampled oxidation profile is illustrated in Fig.4.2.5. The progressive change of both variables between the 150m. and 50m. levels very probably corresponds principally with the gradual alteration of pentlandite to less dense more porous violarite within this vertical interval. In contrast, the significant changes in both variables that occur at about 35m. indicate the fundamental physico-chemical changes that take place across the sulphide leaching horizon at the water table.

The host metagabbro exhibits conspicuous near surface alteration at Munali. The primary mineralogy of this rock consists principally of hornblende, plagioclase felspar and biotite. Available data indicate that this assemblage subsequently weathers to one rich in talc and containing trace to minor quantities of montmorillonite.

The bulk chemistry of the sulphide alteration sequence

The bulk mean chemical variation of a suite of important elements within the Munali oxidation profile is illustrated in Fig.4.2.6. Available data indicate that little significant variation in mean content occurs in this element suite within the sulphide alteration sequence proper, (150 - 38m. vertical interval). The observed progressive decrease in mean iron content is, however, exceptional in this respect, and is very likely due to loss of this metal during the gradual alteration of pentlandite to violarite within the sulphide alteration profile.

Fig.4.2.6. further indicates the dramatic chemical changes that occur as a result of sulphide leaching. In this respect, available data demonstrate that sulphur

undergoes effective total leaching and removal during sulphide degradation. In contrast, about 60 percent of the iron content of the oxidising sulphide assemblage is retained (as iron oxides) within the overlying oxide zone. Similarly, the two-fold increase in mean silicon content that occurs across the sulphide-oxide transition likely corresponds to the influx of this element into the oxide zone in the form of silica that is released by the acid hydrolysis and/or more normal near surface weathering process of adjacent silicate rocks.

The mean depth profiles of the transition metal suite typically exhibit conspicuous depletion across the sulphide leaching horizon, (35m. level). This feature is especially marked for nickel and cobalt and is likely due to the highly mobile oxidised forms of these metals that exist within such high Eh – low pH chemical environments. Available data also indicate that titanium also undergoes considerable depletion across the sulphide-oxide transition. This finding appears though, to be at variance with the typically immobile behaviour of titanium in this type of chemical environment, (Hawkes and Webb, op.cit.). It is probable however, that titanium depletion is related in this instance to a significant oxidation of parent ilmenite during sulphide leaching at Munali. In contrast, copper exhibits a relatively small depletion across the sulphide-oxide transition, and is likely that this feature is due chiefly to the retention of copper in pseudomorphs or as relic sulphide within the oxide zone.

The mean variation of chromium across the sulphide leaching horizon contrasts significantly with the behaviour of all other analysed transition metals in that this element exhibits an enrichment in the oxide zone. It is likely that this phenomenon is due to the net influx of this metal into the Munali oxide zone as a result of the weathering of adjacent ultramafic rocks.

Fig.4.2.5. Mean True Density and Porosity profiles — Munali

* Approximate position of the Water table
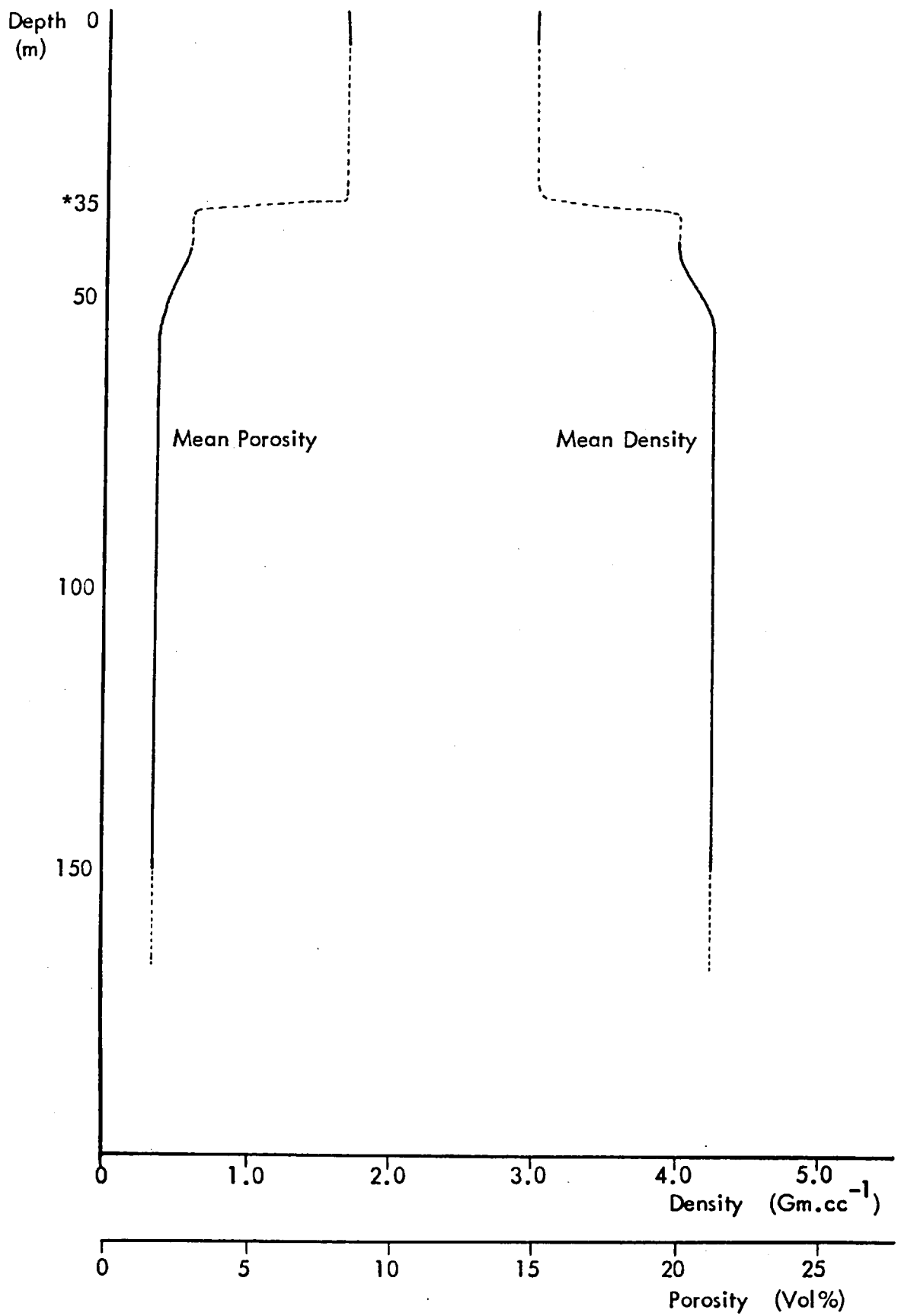
Fig. 4.2.6.   Chemical Variations in Alteration Profile – Munali

* Approximate position of the water table

TABLE 4.2.1. SUMMARY DATA OF SULPHIDE ALTERATION - MUNALI

Depth (m)	Alteration Zone	No. of Samples (n)	MINERALOGY (Means and ranges) Volume % Units									Physical data (mean/ranges) Den gm/cc	Por %	GEOCHEMISTRY (Means and ranges) Wt.% Units S	Fe	SiO$_2$	MgO	Al$_2$O$_3$	CO$_3$	p.p.m. Units Ni	Cu	Mn	Cr	Co	Ti
35 40 ~45 60	Oxide	8	Hm 3.0	Gt 1.0	Sl 1.0							2.50	3.5	no data	16.81	2.81	0.20	0.10	no data	1053	559	63	25	65	114
			25.5	55.5	19.5							3.05	8.3		49.79	18.43	1.04	1.11		6856	2463	327	191	327	5328
			60.0	88.0	75.0							3.20	13.4		61.63	68.45	3.10	2.60		15441	6095	708	766	991	38794
	Violarite - pyrite	no data																							
	Transition	3	Po 65.0	Pn 0.1	Vl 9.5	Cp 0.1	Mt 1.0	Sil 2.0	Ca 0.5	Mc		3.80	1.0	32.80	51.33	3.50	0.05	0.05		24761	30	74	-	1461	240
			68.3	0.2	10.5	0.7	6.0	7.0	7.0	trace		4.03	3.0	36.02	53.99	4.44	0.73	0.03	N/A	34408	824	423	30	1777	1351
			70.0	0.5	12.0	2.0	15.0	10.0	10.0			4.30	5.6	38.09	55.76	5.41	2.00	0.10		43510	2412	877	-	2023	3159
	Primary	3	Po 80.0	Pn 7.0		Cp 0.1	Mt 1.0	Sil 0.5		Mc		4.10	1.0	27.91	54.97	0.05	2.00	0.05		25436	30	297	-	1023	947
			81.7	8.3		2.3	3.0	3.3		trace		4.23	1.8	32.95	55.62	2.84	3.47	0.07		27851	2654	542	30	1307	1371
			85.0	10.0		4.0	4.0	5.0				4.30	2.3	35.89	56.50	7.08	5.40	0.10		30693	6918	1003	-	1538	2116

4.3. SUPERGENE SULPHIDE ALTERATION IN THE PERSERVERENCE DEPOSIT, RHODESIA

The Perserverence deposit occurs as an elongate vertically-inclined lens of massive to disseminated sulphide that is located at or near the basal (footwall) contact of host amphibolite with serpentinite, (Section 2.4.). The following oxidation profile description is based on material sampled within the open pit developed over the deposit, (oxide rocks and supergene-altered sulphides), and from that in underground developments, (primary sulphide).

The petrology of the primary sulphide assemblage

The primary massive sulphide assemblage comprises pyrrhotite and pentlandite, with minor amounts of chalcopyrite and traces of ferrochromite, (Table 4.3.1.). Variable, accessory quantities of silicate are also associated with massive sulphide ore.

Pyrrhotite forms about 80 percent of the massive primary sulphide assemblage. It is present as a matrix of generally equidimensional polygonal grains in which triple-point boundaries are commonly observed, (Fig.4.3.1A.). The presence of this texture indicates that the Perserverence ore assemblage has been subjected to low temperature annealing, probably in response to an episode of post-formational structural deformation. Chemical data on a suite of pyrrhotite grains, (Table 4.3.2.), indicate that the mineral is exclusively present as the monoclinic variety and contains appreciable quantities of cobalt.

Pentlandite forms about six percent of primary massive ore at Perserverence, (Table 4.3.1.). The mineral is present in two forms: As elongate blocky stringers along pyrrhotite borders, (Fig.4.3.1B.); and as aggregates of flamme lamellae in pyrrhotite, (Fig.4.3.1C.). No chemical data are available for primary pentlandite.

Chalcopyrite forms about 2.5 percent of the primary assemblage, but is rather heterogeneously distributed within the ore. It is generally present as elongate stringers along pyrrhotite borders, (Fig. 4.3.1D.), but may also rim and partly replace grains of ferrochromite, (Fig.4.3.1E.). The chemical compositions of a suite of chalcopyrite grains are presented in Table 4.3.3. These data show that Perserverence chalcopyrite contains appreciable, though typically variable quantities of nickel and cobalt.

TABLE 4.3.1. SUMMARY DATA OF SULPHIDE ALTERATION – PERSERVERANCE

Depth (m)	Alteration Zone	No. of Samples (n)	Mineralogy (Means and ranges) Volume % Units	Den gm/cc	Por %	S	Fe	SiO$_2$	MgO	Al$_2$O$_3$	CO$_3$	Ni	Cu	Mn	Cr	Co	Ti
~38	Oxide	8	Hm 0.0 Gt 3.0 Si 7.5	2.20	2.3	no data	2.56	1.77	0.10	0.20	no data	1422	30	97	89	30	30
			15.5 25.0 60.0	2.66	5.7		26.07	55.87	1.00	0.94		2464	1853	834	377	134	225
			60.0 50.0 80.0	3.20	14.0		61.50	94.86	6.00	2.40		5100	3099	1687	1970	246	1025
~45	Violarite – pyrite	4	Vl 2.0 Cp 1.3 Sil 2.0 Mc 60.0	3.00	2.0	33.37	51.62	0.00	0.90	0.10	N/A	21861	12030	624	363	537	180
			5.2 2.4 – 11.5 80.0	3.78	5.6	35.47	53.76	3.05	1.63	0.28		23118	16913	1005	409	665	260
			7.0 4.7 30.0 90.0	4.40	14.5	38.92	57.61	5.12	2.20	0.50		26277	20250	1375	452	844	384
~70	Transition	3	Po 5.0 Vl 7.0 Cp 1.0 Sil 5.0 Mc 0.0	3.60	2.8	36.09	50.42	0.00	0.30	0.00	N/A	22207	13460	795	287	60	114
			31.7 – 10.7 9.7 – 15.0 33.3	3.83	3.6	38.17	57.62	4.04	7.57	0.20		22411	34226	2256	347	358	158
			85.0 15.0 25.0 20.0 60.0	4.40	4.7	40.25	63.65	9.84	6.20	0.40		22615	68633	5097	486	545	198
	Primary	3	Po 80.0 Pn 5.0 Cp 2.0 FCr 0.0 Sil 5.0	3.80	0.0	33.44	57.16	0.00	0.20	0.00	N/A	17154	1446	327	281	97	108
			83.3 6.0 – 2.7 0.3 8.3 –	4.23	3.6	36.13	57.60	1.67	0.37	0.03		23254	6619	771	306	321	206
			85.0 8.0 3.0 1.0 15.0	4.60	5.6	37.61	58.07	4.99	0.70	0.10		27291	13276	1285	602	657	396

TABLE 4.3.2.   PYRRHOTITE COMPOSITIONS – PERSERVERANCE

Sample	Fe	Ni	S	Co	Cu	Ti	Wt% Total	Atomic Formula $Fe_x S_8$	Atomic Formula $Me_x S_8$	Me:S ratio
2301/A2/5	60.94	n.d.	39.45	0.87	0.04	0.01	101.67	-	-	-
	(46.69)	-	(52.65)	(0.64)	(0.03)	-	-	$Fe_{7.09} S_8$	$Me_{7.20} S_8$	0.90
2301/A3/14	60.38	n.d.	39.40	0.97	0.04	0.03	100.82	-	-	-
	(46.46)	-	(52.81)	(0.71)	(0.03)	-	-	$Fe_{7.04} S_8$	$Me_{7.15} S_8$	0.89
2301/A4/20	59.27	n.d.	39.10	0.76	0.04	0.01	99.18	-	-	-
	(46.26)	-	(53.15)	(0.56)	(0.03)	-	-	$Fe_{6.96} S_8$	$Me_{7.05} S_8$	0.88
2301/A6/26	59.45	n.d.	39.64	0.96	0.04	0.03	100.12	-	-	-
	(45.82)	-	(53.40)	(0.75)	(0.03)	-	-	$Fe_{6.86} S_8$	$Me_{6.98} S_8$	0.87
2301/A6/32	59.68	n.d.	39.77	1.03	0.05	0.04	100.57	-	-	-
	(45.92)	-	(53.30)	(0.75)	(0.03)	-	-	$Fe_{6.89} S_8$	$Me_{7.01} S_8$	0.88
2301/A8/38	59.52	n.d.	40.13	0.86	0.08	0.01	100.60	-	-	-
	(45.68)	-	(53.64)	(0.63)	(0.05)	-	-	$Fe_{6.81} S_8$	$Me_{6.91} S_8$	0.86

TABLE 4.3.3. CHALCOPYRITE COMPOSITIONS - PERSERVERANCE

Sample	Fe	Ni	S	Co	Cu	Ti	Wt% Total	Atomic Formula $Cu_nFe_mS_2$	Atomic Formula Me_xS_2	Me:S ratio
2301/A2/2	30.67	3.30	34.71	0.82	29.94	0.04	99.48	-	-	-
	(25.27)	(2.58)	(49.82)	(0.64)	(21.69)	-	-	$Cu_{0.87}Fe_{1.02}S_2$	$Me_{2.02}S_2$	1.01
2301/A3/13	30.76	0.95	34.24	0.71	32.68	0.01	99.35	-	-	-
	(25.48)	(0.75)	(49.41)	(0.56)	(23.80)	-	-	$Cu_{0.96}Fe_{1.01}S_2$	$Me_{2.05}S_2$	1.02
2301/A4/22	31.05	0.21	34.52	0.74	33.96	0.01	100.49	-	-	-
	(25.47)	(0.17)	(49.31)	(0.57)	(24.68)	-	-	$Cu_{0.99}Fe_{1.03}S_2$	$Me_{2.06}S_2$	1.03
2301/A6/33	30.53	0.17	35.07	0.77	33.98	0.02	100.54	-	-	-
	(24.95)	(0.13)	(49.92)	(0.60)	(24.41)	-	-	$Cu_{0.98}Fe_{1.00}S_2$	$Me_{2.01}S_2$	1.00
2301/A8/37	31.00	0.01	34.96	0.60	34.32	0.01	100.90	-	-	-
	(25.28)	(0.01)	(49.65)	(0.46)	(24.60)	-	-	$Cu_{0.99}Fe_{1.02}S_2$	$Me_{2.03}S_2$	1.01

TABLE 4.3.4.   FERROCHROMITE COMPOSITIONS - PERSERVERANCE

Sample	2303/1	2303/2	2303/3	2303/4	2305/1	2305/2
TiO2	1.69	2.40	1.85	2.36	1.38	3.33
Al2O3	2.27	1.85	2.48	0.56	1.73	2.61
Cr2O3	30.27	36.72	33.46	39.65	48.20	43.48
Fe2O3	31.30	21.64	31.99	22.22	15.65	15.68
FeO	30.31	29.89	32.47	31.26	30.22	32.36
MnO	0.43	0.48	0.38	0.53	0.50	0.49
MgO	0.00	0.11	0.00	0.00	0.00	0.00
NiO	0.00	0.00	0.00	0.00	0.00	0.00
ZnO	2.73	2.77	2.91	2.58	3.21	3.11
V2O5	0.56	1.25	0.59	2.92	0.75	0.71
TOTAL (Wt%)	99.56	97.11	106.13	102.07	101.63	101.78

Sample	2305/3	2305/4	2305/5	2300/1	2300/2	2300/3
TiO2	1.49	5.79	2.70	1.86	1.62	9.64
Al2O3	1.53	1.52	1.00	0.11	0.24	0.32
Cr2O3	49.53	36.56	36.84	31.57	40.39	42.62
Fe2O3	13.95	14.71	21.49	32.11	23.82	3.51
FeO	30.22	32.62	29.76	31.38	30.69	37.44
MnO	0.34	0.40	0.42	0.28	0.53	0.40
MgO	0.00	0.00	0.00	0.00	0.00	0.00
NiO	0.00	0.00	0.00	0.00	0.00	0.00
ZnO	3.27	3.09	3.15	1.56	2.17	2.09
V2O5	0.75	1.58	1.34	1.11	1.07	1.73
TOTAL (Wt%)	100.67	96.26	96.71	99.99	100.54	97.74

Sample	2300/4	2300/5	2300/6			
TiO2	2.10	5.85	1.96			
Al2O3	0.07	0.26	2.09			
Cr2O3	35.44	42.59	38.72			
Fe2O3	29.38	11.55	20.38			
FeO	31.86	34.24	30.42			
MnO	0.38	0.46	0.45			
MgO	0.00	0.00	0.00			
NiO	0.00	0.00	0.00			
ZnO	2.24	1.94	2.08			
V2O5	1.73	1.64	0.99			
TOTAL (Wt%)	103.19	98.53	97.09			

Ferrochromite averages less than one percent of the massive primary ore assemblage, (Table 4.3.1.). The mineral is typically present as equant grains and these commonly exhibit conspicuous rims or lamellae of magnetite, (Fig.4.3.1F.). Chemical analysis of these composite spinel grains, (Table 4.3.4.), confirms that the cores consist of ferrochromite, (Groves et.al.; 1977, 1979).

The petrology of the sulphide alteration sequence

Available data indicate that incipient alteration of massive primary ore at Perserverence occurs at about 70 metres below surface. At this depth both varieties of pentlandite undergo incipient replacement by violarite, (Fig.4.3.1G.). Pseudomorphic replacement of the original pentlandite structure is a characteristic feature of this process, (Fig.4.3.1H.).

The chemical compositions of a suite of violarite after pentlandite (Vpn) grains are presented in Table 4.3.5. These data show that the replacing violarite is very probably iron-rich and nickel-poor compared with pentlandite, although no concrete data on pentlandite composition is available in the present study. The corresponding (approximate) chemical reaction is, however, indicated in Equation 1 of Fig.4.3.3.

The compositions of violarite after pentlandite at Perserverence characteristically summate to totals significantly less than 100 percent. It is likely that this phenomenon is again due to the high surface porosity of the grains causing an inhibition of X-ray reflection during chemical analysis. Interestingly, the corresponding molecular formulae of sampled Vpn typically exhibit non-stoichiometric, high metal-to-sulphur ratios in agreement with the findings of Desborough and Czamaske, (op.cit.). This result is hence at variance with that noted in the corresponding violarite species at Pikwe, and indicates that the normal stoichiometric violarite compositions observed in that deposit are very likely real, and not due to analytical bias, as was thought possible.

The formation of violarite from pentlandite is accompanied by progressive alteration of adjacent pyrrhotite. This phenomenon is a two-stage process at Perserverence and leads to the consecutive formation of smythite and of violarite after pyrrhotite, (Vpo). Smythite forms as small discrete patches of red-orange feathers along the grain borders of pyrrhotite and altering pentlandite, and the mineral grows into the pyrrhotite in a direction parallel to the 001 cleavage direction, (Fig.4.3.2A.).

Fig. 4.3.1. Petrography of Perserverance Sulphide Ore (1)

Scale length = 100 μ

A. Pyrrhotite grain mosaic showing triple-point junctions (x 110) Air

Partly crossed nicols

B. Typical texture of interstitial pentlandite (x 110) Air

Pentlandite; light-medium grey: Pyrrhotite; dark grey: Silicate; dark

C. Typical texture of lamellar pentlandite (x 320) Air

Pentlandite; light grey: Pyrrhotite; medium grey: Silicate; dark

D. Typical texture of chalcopyrite (x 110) Air

Chalcopyrite; medium dark grey: Pyrrhotite; medium grey: Pentlandite;
light grey: Silicate; dark grey

E. Typical association of chalcopyrite with ferrochromite (x 110) Air

Chalcopyrite; light grey: Pyrrhotite; medium grey: Ferrochromite;
dark grey

F. Magnetite rim to ferrochromite (x 220) Oil

Ferrochromite; medium-dark grey: Magnetite; medium grey, rimming
central core. Some alteration of magnetite to hematite (light grey)- right

G. Incipient replacement of pentlandite by violarite (x 320) Air

Pentlandite; light grey: Violarite; dark grey: Pyrrhotite; medium grey

H. Typical violarite pseudomorphs after interstitial pentlandite (x 110) Air

Violarite; medium-dark grey, granular: Pyrrhotite; medium-dark grey:
chalcopyrite; medium grey (top left): Voids (resin); dark

Fig.4.3.1.
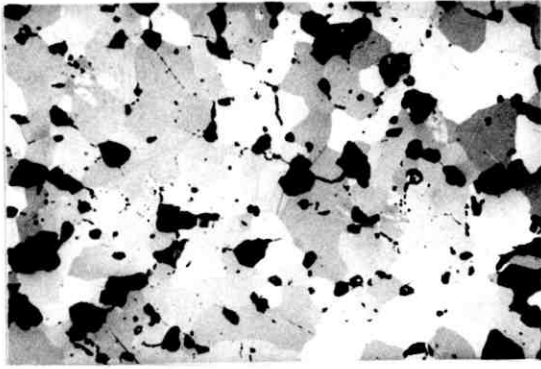
A
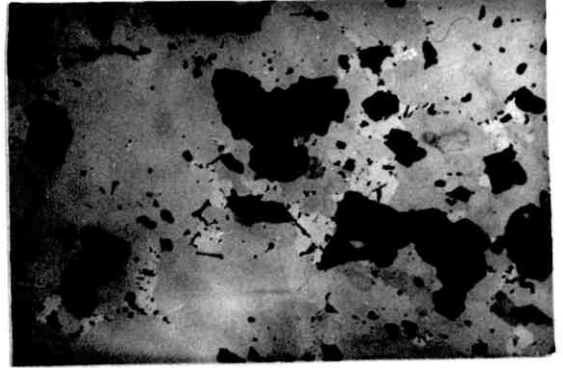
B
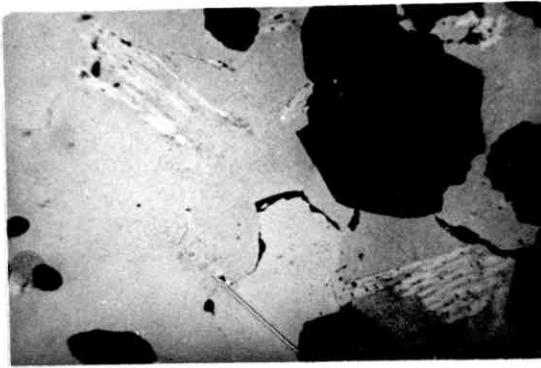
C
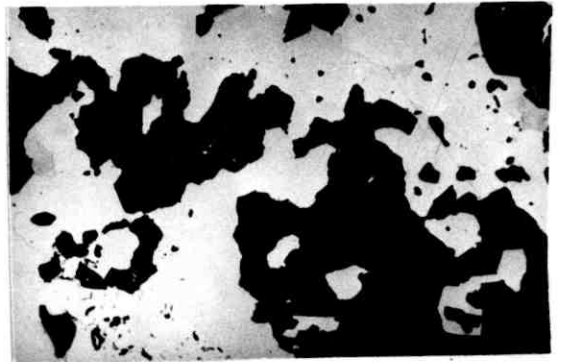
D

E
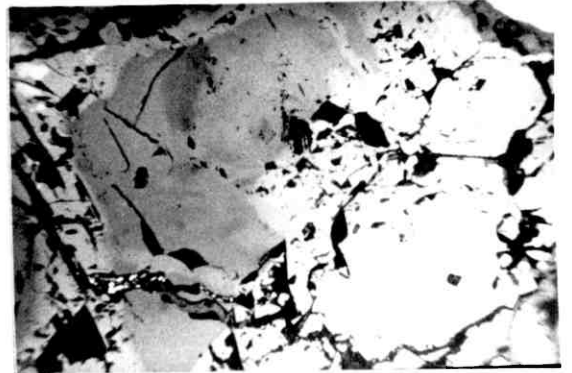
F
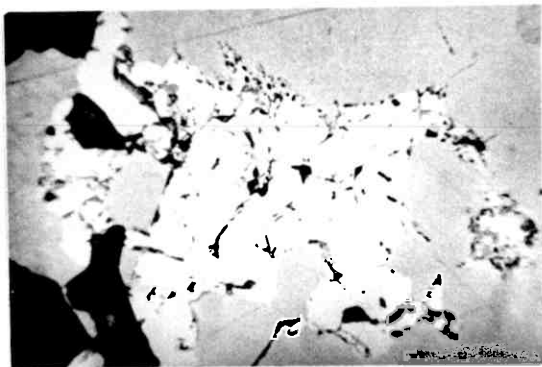
G

H

TABLE 4.3.5.   VIOLARITE AFTER PENTLANDITE COMPOSITIONS – PERSERVERANCE

Sample	Fe	Ni	S	Co	Cu	Ti	Wt% Total	Atomic Formula $Ni_n Fe_m S_4$	Atomic Formula $Me_x S_4$	Me:S ratio
2301/A2/4	24.53	28.97	40.59	2.47	0.12	0.03	96.71	-	-	-
	(19.59)	(22.01)	(56.45)	(1.87)	(0.08)	-	-	$Ni_{1.56}Fe_{1.39}S_4$	$Me_{3.09}S_4$	0.77
2301/A3/9	24.02	29.18	40.90	2.60	0.13	0.02	96.85	-	-	-
	(19.12)	(22.10)	(56.73)	(1.96)	(0.09)	-	-	$Ni_{1.56}Fe_{1.35}S_4$	$Me_{3.05}S_4$	0.76
2301/A3/12	24.15	28.68	40.41	2.47	0.13	0.02	95.86	-	-	-
	(19.43)	(21.95)	(56.66)	(1.89)	(0.09)	-	-	$Ni_{1.55}Fe_{1.37}S_4$	$Me_{3.06}S_4$	0.77
2301/A4/15	27.62	28.28	39.83	2.39	0.10	n.d.	98.22	-	-	-
	(21.87)	(21.31)	(54.96)	(1.80)	(0.09)	-	-	$Ni_{1.55}Fe_{1.59}S_4$	$Me_{3.28}S_4$	0.82
2301/A4/21	23.62	29.01	40.36	2.67	0.12	0.02	95.80	-	-	-
	(19.02)	(22.23)	(56.62)	(2.04)	(0.09)	-	-	$Ni_{1.57}Fe_{1.35}S_4$	$Me_{3.07}S_4$	0.77
2301/A6/23	24.10	28.37	40.53	2.43	0.11	0.02	95.56	-	-	-
	(19.42)	(21.75)	(56.90)	(1.86)	(0.08)	-	-	$Ni_{1.53}Fe_{1.37}S_4$	$Me_{3.03}S_4$	0.76

TABLE 4.3.5. CONTINUED

Sample	Fe	Ni	S	Co	Cu	Ti	Wt% Total	Atomic Formula $Ni_nFe_mS_4$	Atomic Formula Me_xS_4	Me:S ratio
2301/A6/27	23.86	27.65	40.25	2.42	0.11	0.02	94.31	-	-	-
	(19.45)	(21.46)	(57.16)	(1.87)	(0.08)	-	-	$Ni_{1.50}Fe_{1.36}S_4$	$Me_{3.00}S_4$	0.75
2301/A6/28	23.38	28.26	40.92	2.74	0.11	0.01	95.42	-	-	-
	(18.82)	(21.64)	(57.37)	(2.09)	(0.08)	-	-	$Ni_{1.51}Fe_{1.31}S_4$	$Me_{2.98}S_4$	0.74
2301/A6/31	24.46	27.99	41.16	2.68	0.12	0.02	96.43	-	-	-
	(19.50)	(21.23)	(57.16)	(2.02)	(0.09)	-	-	$Ni_{1.49}Fe_{1.37}S_4$	$Me_{3.00}S_4$	0.75
2301/A8/34	26.83	28.91	39.64	2.67	0.19	0.02	98.26	-	-	-
	(21.28)	(21.81)	(54.75)	(2.01)	(0.13)	-	-	$Ni_{1.59}Fe_{1.56}S_4$	$Me_{3.21}S_4$	0.80
2301/A8/35	25.57	29.01	40.19	2.50	0.49	0.02	97.78	-	-	-
	(20.30)	(21.90)	(55.57)	(1.88)	(0.34)	-	-	$Ni_{1.58}Fe_{1.46}S_4$	$Me_{3.20}S_4$	0.80
2301/A8/36	23.70	28.21	40.73	2.84	1.07	0.03	96.58	-	-	-
	(18.94)	(21.45)	(56.71)	2.15	0.75	-	-	$Ni_{1.52}Fe_{1.34}S_4$	$Me_{3.06}S_4$	0.77

TABLE 4.3.6.   SMYTHITE COMPOSITIONS - PERSERVERANCE

Sample	Fe	Ni	S	Co	Cu	Ti	Wt% Total	Atomic Formula $Fe_m Ni_n S_{11}$	Atomic Formula $Me_x S_{11}$	Me:S ratio
2301/A2/7	51.64	5.66	40.16	0.99	0.08	0.02	98.55	-	-	-
	(40.37)	(4.21)	(54.69)	(0.73)	(0.06)	-	-	$Fe_{8.12} Ni_{0.85} S_{11}$	$Me_{9.13} S_{11}$	0.83
2301/A4/17	58.11	n.d.	41.31	0.90	0.03	0.01	100.36	-	-	-
	(44.39)	-	(54.96)	(0.65)	(0.02)	-	-	$Fe_{8.89} Ni_{0.00} S_{11}$	$Me_{9.02} S_{11}$	0.82
2304/A4/18	57.44	0.14	41.32	0.97	0.05	0.06	99.98	-	-	-
	(44.03)	(0.10)	(55.17)	(0.71)	(0.03)	(0.03)	-	$Fe_{8.78} Ni_{0.02} S_{11}$	$Me_{8.96} S_{11}$	0.82
2301/A4/19	57.18	0.08	40.94	0.99	0.06	0.06	99.27	-	-	-
	(44.15)	(0.06)	(55.06)	(0.73)	(0.04)	-	-	$Fe_{8.82} Ni_{0.01} S_{11}$	$Me_{8.99} S_{11}$	0.82
2301/A6/25	56.53	0.79	41.08	0.90	0.06	0.03	99.39	-	-	-
	(43.59)	(0.58)	(55.18)	(0.66)	(0.04)	(0.01)	-	$Fe_{8.69} Ni_{0.12} S_{11}$	$Me_{8.95} S_{11}$	0.81
2301/A6/30	56.42	0.26	41.43	0.99	0.12	0.02	99.24	-	-	-
	(43.48)	(0.19)	(55.61)	(0.73)	(0.08)	-	-	$Fe_{8.60} Ni_{0.04} S_{11}$	$Me_{8.80} S_{11}$	0.80

TABLE 4.3.7. VIOLARITE AFTER PYRRHOTITE COMPOSITIONS - PERSERVERANCE

Sample	Fe	Ni	S	Co	Cu	Ti	Wt% Total	Atomic Formula $Ni_nFe_mS_4$	Atomic Formula Me_xS_4	Me:S ratio
2301/A2/3	28.22	26.05	38.66	1.17	0.10	0.02	94.22	-	-	-
	(23.22)	(20.39)	(55.41)	(0.91)	(0.07)	-	-	$Ni_{1.47}Fe_{1.68}S_4$	$Me_{3.22}S_4$	0.80
2301/A2/6	28.19	26.15	40.17	1.17	0.24	0.01	95.93	-	-	-
	(22.67)	(20.01)	(56.26)	(0.89)	(0.17)	-	-	$Ni_{1.43}Fe_{1.61}S_4$	$Me_{3.11}S_4$	0.78
2301/A2/11	28.83	26.83	40.97	1.74	0.15	0.03	98.15	-	-	-
	(22.37)	(20.08)	(56.15)	(1.29)	(0.10)	-	-	$Ni_{1.43}Fe_{1.60}S_4$	$Me_{3.12}S_4$	0.78
2301/A4/16	28.22	26.57	40.29	1.10	0.13	0.01	96.32	-	-	-
	(22.60)	(20.25)	(56.23)	(0.84)	(0.09)	-	-	$Ni_{1.44}Fe_{1.61}S_4$	$Me_{3.12}S_4$	0.78
2301/A6/24	25.64	27.63	40.74	2.81	0.11	0.02	96.95	-	-	-
	(20.40)	(20.92)	(56.48)	(2.12)	(0.08)	-	-	$Ni_{1.48}Fe_{1.45}S_4$	$Me_{3.08}S_4$	0.77
2301/A6/29	27.38	25.96	40.41	1.20	0.13	0.03	95.11	-	-	-
	(22.13)	(19.96)	(56.90)	(0.92)	(0.09)	-	-	$Ni_{1.41}Fe_{1.56}S_4$	$Me_{3.03}S_4$	0.76

Table 4.3.8. Comparison of pyrrhotite, smythite and Vpo compositions

	PYRRHOTITE (n = 6)	SMYTHITE (n = 6)	VIOLARITE AFTER PYRRHOTITE (n = 6)
Fe	59.87	56.22	27.68
	(45.92)	(43.31)	(22.22)
Ni	n.d.	1.16	26.53
	-	(0.85)	(20.26)
S	39.58	41.04	40.21
	(53.35)	(55.08)	(56.22)
Co	0.91	0.96	1.53
	(0.66)	(0.70)	(1.17)
Cu	0.05	0.07	0.14
	(0.04)	(0.04)	(0.10)
Ti	0.02	0.03	0.04
	(0.02)	(0.03)	(0.04)
TOTAL (Wt%)	100.43	99.46	96.12
Ni:Fe	-	0.02	0.91
Me:S	0.87	0.82	0.78

The chemical composition of a number of smythite grains are presented in Table 4.3.6. These data demonstrate that smythite contains small but significant quantities of nickel. It is probable that the metal is derived from that released during Vpn formation, since parent pyrrhotite does not contain detectable quantities, (Table 4.3.2.). The corresponding likely reaction mechanism for the formation of smythite from pyrrhotite is given in Equation 2 of Fig.4.3.3.

Available data indicate that smythite is replaced by violarite after pyrrhotite during the progressive alteration of pentlandite to Vpn. The Vpo takes the form of extensive fringes of brownish-violet porous lamellae that grow into and replace smythite along the mimicked 001 pyrrhotite cleavage directions, (Fig.4.3.2B.). Chemical data for a suite of Vpo grains are given in Table 4.3.7., and indicate that low analytical totals and high metal-to-sulphur ratios characterise violarite after pyrrhotite at Perserverence. The corresponding formation reaction of Vpo from smythite, based on observed mean composition data, is given in Equation 3, (Fig.4.3.3.).

A comparison of mean pyrrhotite, smythite and Vpo chemistries, (Table 4.3.8.), demonstrates that the observed two-stage pyrrhotite alteration process occurs at constant sulphur. The data also indicates that the nickel, together with cobalt and copper, released from pentlandite during Vpn formation, is critical to both the initiation and the development of this form of pyrrhotite alteration at Perserverence. Further, Equations 2 and 3 in Fig.4.3.3. demonstrate that the formation of violarite from pyrrhotite is an oxidation process.

The transitional mineral assemblage resulting from the above processes remains stable up to about the 45m. level. At about this latter horizon however, residual pyrrhotite undergoes further alteration. This phenomenon takes one of two forms: Pyrrhotite may be wholly or partially removed by leaching, (Fig.4.3.2C.); or, more commonly, it may be replaced by fine-grained marcasite, (Fig.4.3.2D.). The initial formation of marcasite is, however, typically superceded by a phase of zoned recrystallisation giving a more massive secondary marcasite in which the polygonal outlines of the original pyrrhotite grains are commonly preserved, (Fig.4.3.2E.). Further, the dissolution of pyrrhotite is commonly accompanied by the deposition of drusy siderite - the iron probably being derived from leached pyrrhotite, (Fig.4.3.2F.).

No chemical data are available for either secondary marcasite or siderite, but the probable reaction mechanisms involved in their formation are respectively presented

Fig. 4.3.2. Petrography of Perserverance Sulphide Ore (2)

Scale length = 100 μ

A. Typical smythite texture (x 220) Oil

Pyrrhotite; dark grey: Smythite; light-medium grey: Violarite; medium-dark grey, granular: Unaltered pentlandite; light grey

B. Replacement of smythite by violarite after pyrrhotite (x 600) Oil

Pyrrhotite; dark grey: Smythite; light-medium grey: Vpo; medium-dark grey, granular: Silicate; dark

C. Leached cavities after oxidised pyrrhotite (x 110) Air

Marcasite; dark grey, granular: Pyrrhotite; medium grey: Pyrite; medium grey, elongate (lower): Magnetite; dark grey (upper left): Voids; dark

D. In situ recrystallisation of marcasite to massive pyrite (x 320) Air

Secondary marcasite after pyrrhotite; dark grey: Massive pyrite; medium grey

E. Massive marcasite after fine grained secondary marcasite (x 320) Air

Carbonate; dark grey: Voids; dark

F. Typical precipitation texture of siderite (x 110) Air

Siderite; dark grey: Massive pyrite; medium grey: Voids; dark

G. In situ alteration of chalcopyrite to covellite (x 320) Air

Chalcopyrite; light grey: Covellite; medium dark grey: Siderite; dark grey: Voids; dark

Fig.4.3.2.
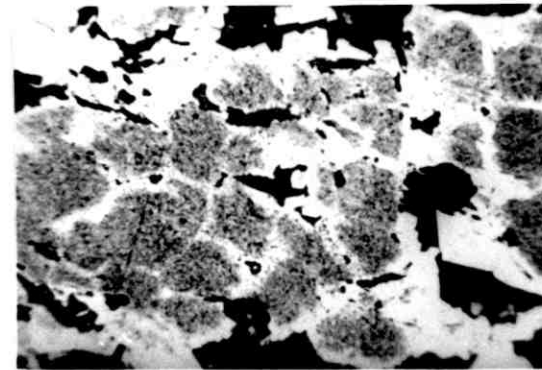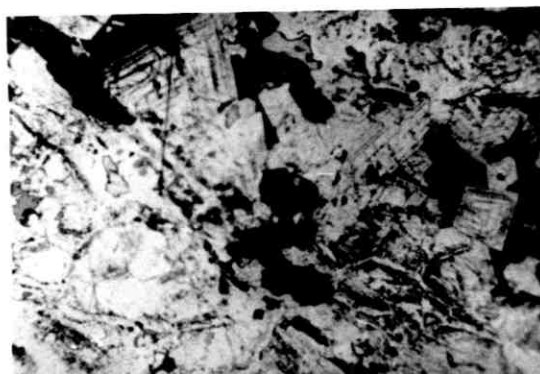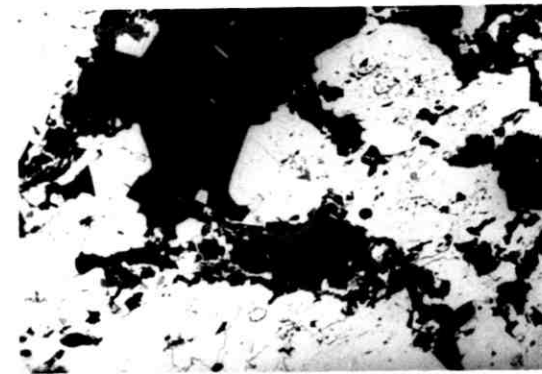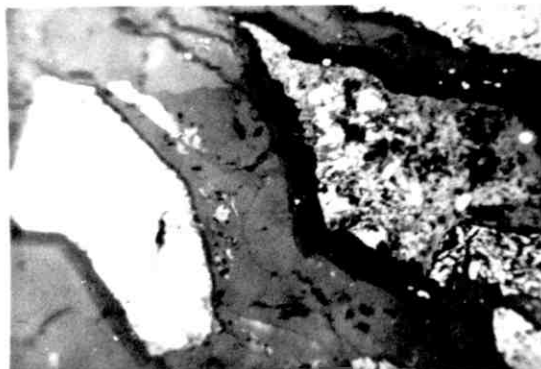
FIG. 4.3.3. CHEMISTRY OF THE PERSERVERANCE ALTERATION SEQUENCE

SHALLOW ANODIC WEATHERING REACTIONS

17 $FeS_2 + 8H_2O = Fe^{2+} + 2SO_4^{2-} + 16H^+ + 14e^-$
Marcasite

16 $Cu_{0.96}Fe_{1.02}S_2 + 8H_2O = 1.02Fe^{2+} + 0.96Cu^{2+} + 2SO_4^{2-} + 16H^+ + 15.96e^-$
Chalcopyrite

15 $Ni_{1.44}Fe_{1.58}Co_{0.08}S_4 + 16H_2O = 1.44Ni^{2+} + 1.58Fe^{2+} + 0.08Co^{2+} + 4SO_4^{2-} + 32H^+ + 30.20e^-$
Violarite (after Po)

14 $Ni_{1.54}Fe_{1.40}Co_{0.14}S_4 + 16H_2O = 1.54Ni^{2+} + 1.40Fe^{2+} + 0.14Co^{2+} + 4SO_4^{2-} + 32H^+ + 30.16e^-$
Violarite (after Pn)

13 $2Fe_3O_4 + H_2O = 3Fe_2O_3 + 2H^+ + 2e^-$
Magnetite   Hematite

12 $FeS_2 + 8H_2O + 1.50OH^- = 0.5Fe_2O_3 + 2SO_4^{2-} + 17.50H^+ + 15e^-$
Marcasite   Hematite

11 $Cu_{0.96}Fe_{1.02}S_2 + 8H_2O + 1.53OH^- = 0.51Fe_2O_3 + 0.96Cu^{2+} + 2SO_4^{2-} + 17.53H^+ + 16.98e^-$
Chalcopyrite   Hematite

10 $Ni_{1.54}Fe_{1.40}Co_{0.14}S_4 + 16H_2O + 2.10OH^- = 0.70Fe_2O_3 + 1.54Ni^{2+} + 0.14Co^{2+} + 4SO_4^{2-} + 34.10H^+ + 31.56e^-$
Violarite (after Pn)   Hematite

9 $FeS_2 + 8H_2O + 2OH^+ = FeOOH + 2SO_4^{2-} + 17H^+ + 15e^-$
Marcasite   Goethite

8 $Cu_{0.96}Fe_{1.02}S_2 + 8H_2O + 2.04OH^- = 1.02FeOOH + 0.96Cu^{2+} + 2SO_4^{2-} + 17.02H^+ + 16.98e^-$
Chalcopyrite   Goethite

7 $Ni_{1.54}Fe_{1.40}Co_{0.14}S_4 + 16H_2O + 2.80OH^- = 1.40FeOOH + 1.54Ni^{2+} + 0.14Co^{2+} + 4SO_4^{2-} + 33.40H^+ + 31.56e^-$
Violarite (after Pn)   Goethite

6 $Cu_{0.96}Fe_{1.02}S_2 + 4.16H_2O = 0.96CuS + 1.02Fe^{2+} + 1.04SO_4^{2-} + 8.32H^+ + 8.28e^-$
Chalcopyrite   Covellite

5 $Fe^{2+} + OH^- + HCO_3^- = FeCO_3 + H_2O$
Siderite

DEEP ANODIC WEATHERING REACTIONS

4 $Fe_{6.83}Co_{0.10}S_8 = 4FeS_2 + 2.83Fe^{2+} + 0.10Co^{2+} + 5.86e^-$
Monoclinic Po   Marcasite

3 $Fe_{8.65}Ni_{0.17}Co_{0.14}S_{11} + 3.79Ni^{2+} + 0.08Co^{2+} = 2.75Ni_{1.44}Fe_{1.58}Co_{0.08}S_4 + 4.31Fe^{2+} + 0.88e^-$
Smythite   Violarite (after Po)

2 $Fe_{6.83}Co_{0.10}S_8 + 0.10Ni^{2+} + 0.01Co^{2+} = 0.73Fe_{8.65}Ni_{0.17}Co_{0.14}S_{11} + 0.54Fe^{2+} + 0.88e^-$
Monoclinic Po   Smythite

1 $Ni_{4.52}Fe_{4.23}Co_{0.33}S_8 = 2Ni_{1.54}Fe_{1.40}Co_{0.14}S_4 + 1.44Ni^{2+} + 1.43Fe^{2+} + 0.05Co^{2+} + 5.84e^-$
Pentlandite   Violarite (after Pn)

in Equations 4 and 5 in Fig.4.3.3. Equation 4 indicates that the marcasite formation reaction is oxidative in nature.

The derived supergene sulphide assemblage of violarite species, marcasite and chalcopyrite is stable within the 45 - 38m. vertical interval, although available data infer that this secondary sulphide zone has a rather irregular development between these two levels. Chalcopyrite may however alter to covellite within this zone, (Fig.4.3.2G.). The likely reaction equation for this replacement phenomenon is presented in Equation 6 in Fig.4.3.3.

The petrology of the oxide zone

The supergene-altered sulphide profile is overlain by an extensively developed oxide zone. This zone extends upwards from the pre-miming water table (38 metres b.s.) and crops out as a narrow (20 metres wide) linear zone of ferruginous gossan, (Section 2.4.). The gross mineralogy of the Perserverence oxide zone comprises goethite, hematite and silica, (Table 4.3.1.).

Goethite averages about 25 percent of the Perserverence oxide zone assemblage, although it exhibits considerable inter-sample variation, (Table 4.3.1.). The mineral is present in several important textural forms. Chief among these are pseudomorph structures after massive secondary marcasite, (Figs.4.3.4A. and 4B.); and mimic (secondary) replacements after pyrrhotite polyhedra, (Fig.4.3.4C.). More rarely, goethite is noted as pseudomorphs after blocky Vpn, (Fig.4.3.4D.), or as boxwork structures after chalcopyrite, (Fig.4.3.4E.).

Hematite forms about 15 percent of the mean oxide zone assemblage, but likewise exhibits a very wide range of contents within the sampled rock suite, (Table 4.3.1.). It is present chiefly as mimicked replacements of former marcasite pseudomorphed pyrrhotite textures. In this respect, polyhedral pseudomorphs are quite common, (Fig.4.3.4F.), but rarer occurrences of both deformed and undeformed pyrrhotite cleavage structures, (Figs.4.3.4G. and 4H. respectively), are also noted. Hematite is also present as replacements to interstitial Vpn - typically as boxwork structures, (Fig.4.3.5A.), but also, more rarely, as complete grain replacements, (Fig.4.3.5B.), or as pseudomorphs after lamellar Vpn, (Fig.4.3.5C.). The mineral similarly defines boxwork structures after chalcopyrite, (Fig.4.3.5D.),

179

Fig. 4.3.4. Petrography of the Perserverance Gossan (1)

Scale length = 100 μ

A.   Goethite mimics after secondary marcasite (1) (x 320) Air. Blue-white filter

Angular grain borders are well-preserved along edge of block

B.   Goethite mimics after secondary marcasite (2) (x 110) Air. Blue-white filter

Zoned structure defined partly by hematite (light grey) in goethite (medium grey):   Silica; dark

C.   Goethite mimics after original pyrrhotite polyhedra (x 110) Air. Blue-white filter

Goethite; light - medium grey: Silica; medium - dark grey: Voids; dark

D.   Goethite mimic after interstitial Vpn (x 320) Air. Blue-white filter

Cleavages defined in silica (dark grey)

E.   Goethite as boxwork after chalcopyrite (x 110) Air. Blue-white filter

Goethite as cell walls and part of interstices, (light-medium to medium grey)
Silica as residual interstitial filling, (dark grey):   Voids; dark

F.   Hematite mimics after pyrrhotite polyhedra (x 320) Air. Partly crossed nicols

G.   Hematite mimic after deformed pyrrhotite cleavage (x 320) Air. Blue-white filter

Silica;   dark grey

H.   Hematite (boxwork) mimic after undeformed pyrrhotite cleavage (x 110) Air Blue-white filter

Silica matrix; dark grey: Voids; dark

Fig.4.3.4.

181
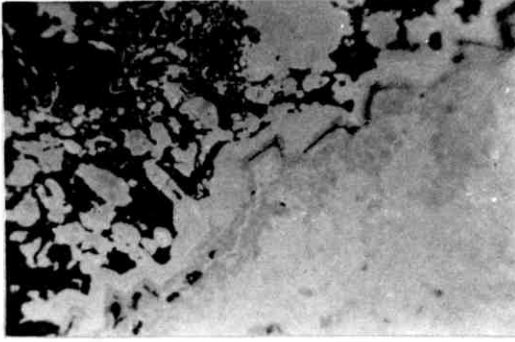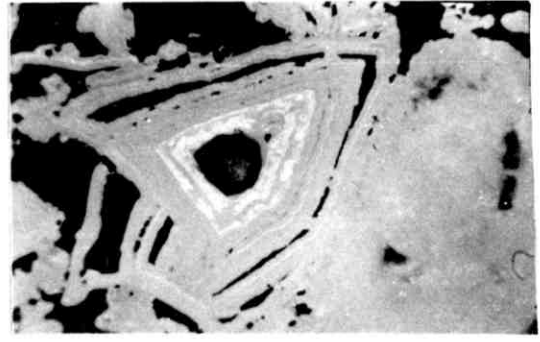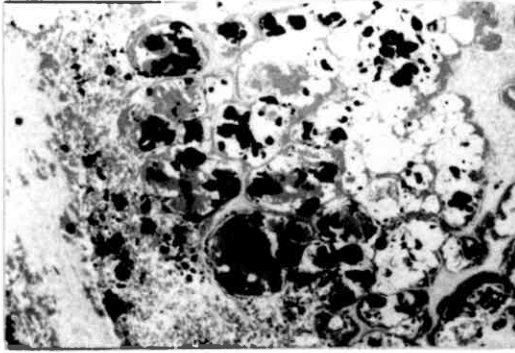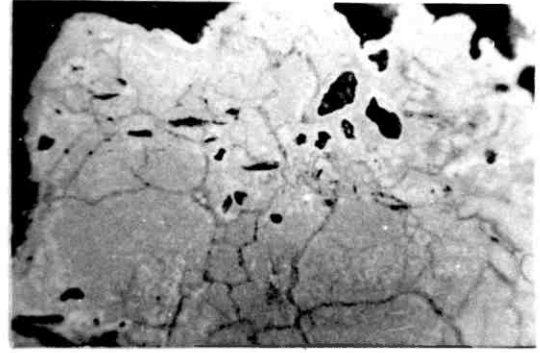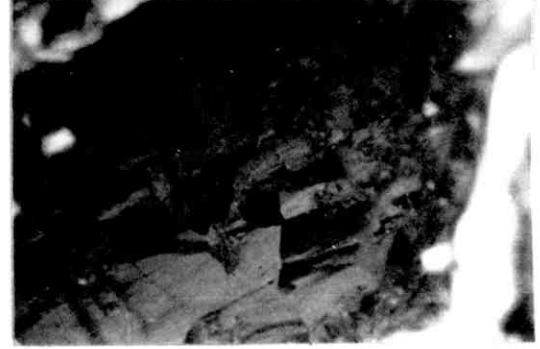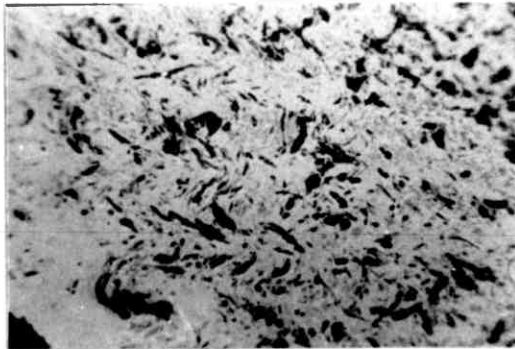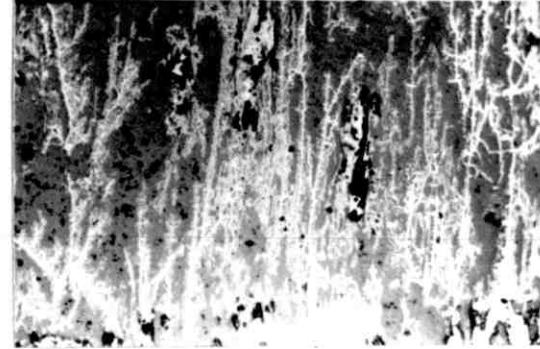
Fig. 4.3.5. Petrography of the Perserverance Gossan (2)

Scale length = 100 μ   Blue-white filter used throughout

A.   Hematite boxworks after interstitial violarite (Vpn) (x 320) Air

Hematite defines the retained blocky octahedral cleavage of the original
pentlandite

B.   Hematite mimic after interstitial violarite (Vpn) (x 110) Air

Silica; dark grey: Voids; dark: Internal structural details are not preserved

C.   Hematite mimics after lamellar violarite (Vpn) (x 110) Air

Silica; dark grey: Voids; dark

D.   Hematite boxworks after chalcopyrite (x 600) Air

Hematite (light-medium grey) defines cell walls and some interstices.
Silica (dark grey) fills the remainder of the structure

E.   Hematite mimic after spinel (x 320) Air

Hematite preserves the basal cleavage (light-medium) grey. Adjacent
chalcopyrite boxwork defined in goethite (medium-dark) grey. Silica;
dark grey matrix

F.   Silica as pervasive matrix (x 110) Air

Relic Vpn stringer preserved as hematite boxwork and solid mimic (light
grey):   Voids; dark

G.   Silica as preserver of sulphide mimics (1) (x 110) Air

Hematite boxwork after interstitial violarite (Vpn) (light grey)
Voids; dark

H.   Silica as preserver of sulphide mimics (2) (x 110) Air

Goethite outlines after massive secondary marcasite

182
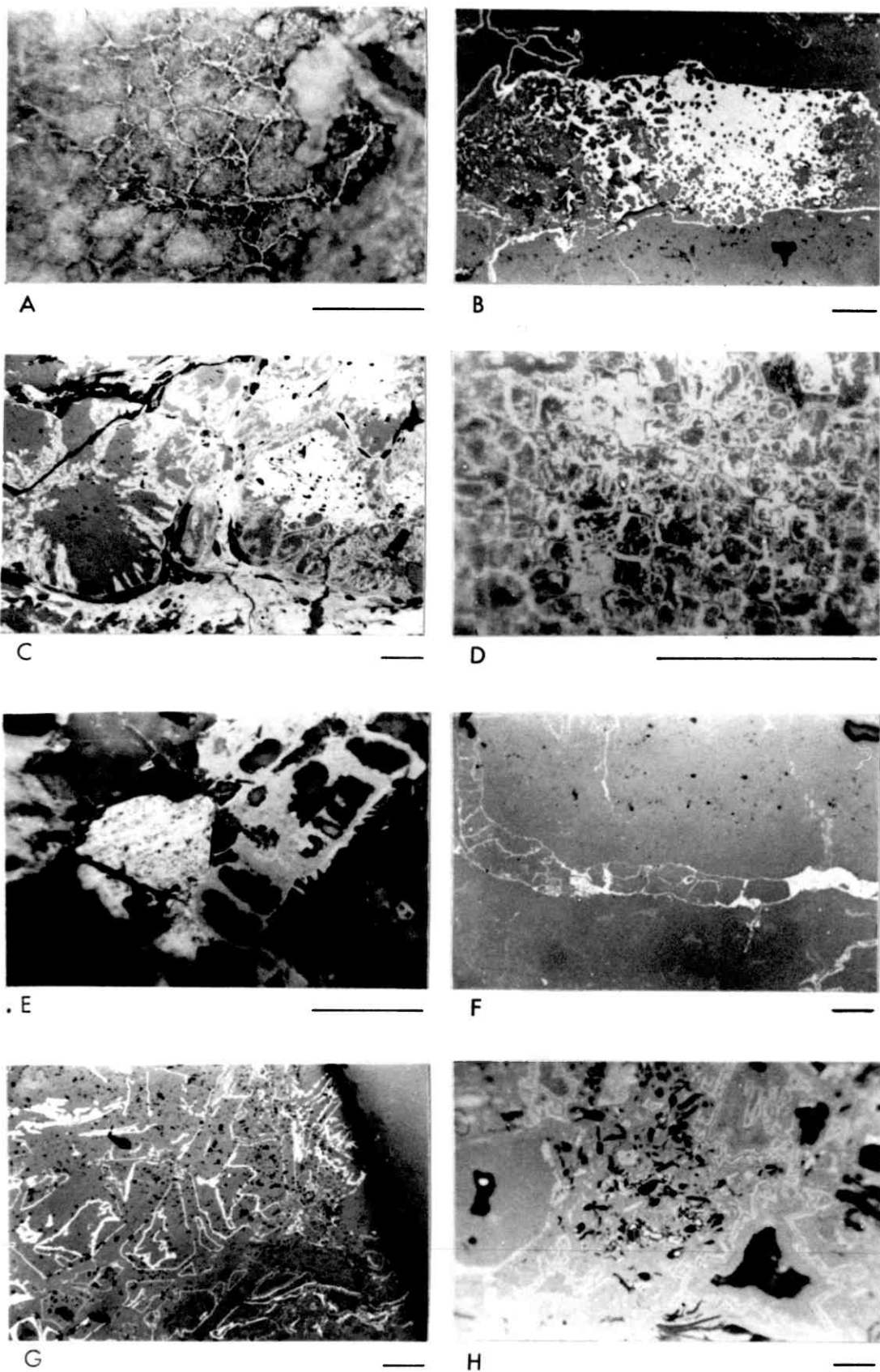
Fig.4.3.5.

and is noted as pseudomorphic replacements of spinel, (Fig.4.3.5E.). The likely reaction mechanisms corresponding to the mimicked replacement of individual ore minerals by goethite and hematite are set out in the appropriate Equations in Fig.4.3.3.

Silica averages 60 percent in the Perserverence oxide zone, although individual sample contents vary widely, (Table 4.3.1.). The mineral is present in three textural forms: As a pervasive colloidal matrix, (Fig.4.3.5F.); as pseudomorphic replacements of sulphide minerals, (Figs.4.3.5G. and 5H.); and as boxwork lattices to oxidised sulphides, (Fig.4.3.4D.). All three textural forms are, however, derived through the precipitation of soluble silica that is brought into the oxide zone by groundwater. It is very probable that near surface hydrolytic weathering of adjacent silicate rocks provides the ultimate source of this silica.

The likely vertical variations of mean true density and mean porosity within the Perserverence oxidation profile are indicated in Fig.4.3.6. The progressive changes in both physical properties in the 70 - 45m. vertical interval correspond with the gradual alteration of pentlandite and pyrrhotite to less dense porous violarite that occurs within this sub-zone. Further, the constancy of both variables between the 45 and 39m. levels indicates the mature development therein of the secondary sulphide assemblage of marcasite and violarite.

In contrast, the subsequent marked drop in mean density across the 38m. horizon directly reflects the dramatic change in mineral assemblage that occurs as a consequence of sulphide leaching. Whereas the form of the mean porosity profile in this sub-zone is consistent with the sequence of pervasive sulphide leaching and progressive silica influx that very likely occurs at or just above the pre-mining water table level.

The bulk chemistry of the sulphide alteration sequence

The bulk mean variation of a suite of important major and minor elements within the Perserverence oxidation profile are presented in Fig.4.3.7. The effectively constant depth profiles of all indicated elements, except iron, within the 140 - 40m. vertical interval demonstrates that little overall variation in chemistry occurs

Fig.4.3.6. Mean True Density and Porosity profiles – Perserverance
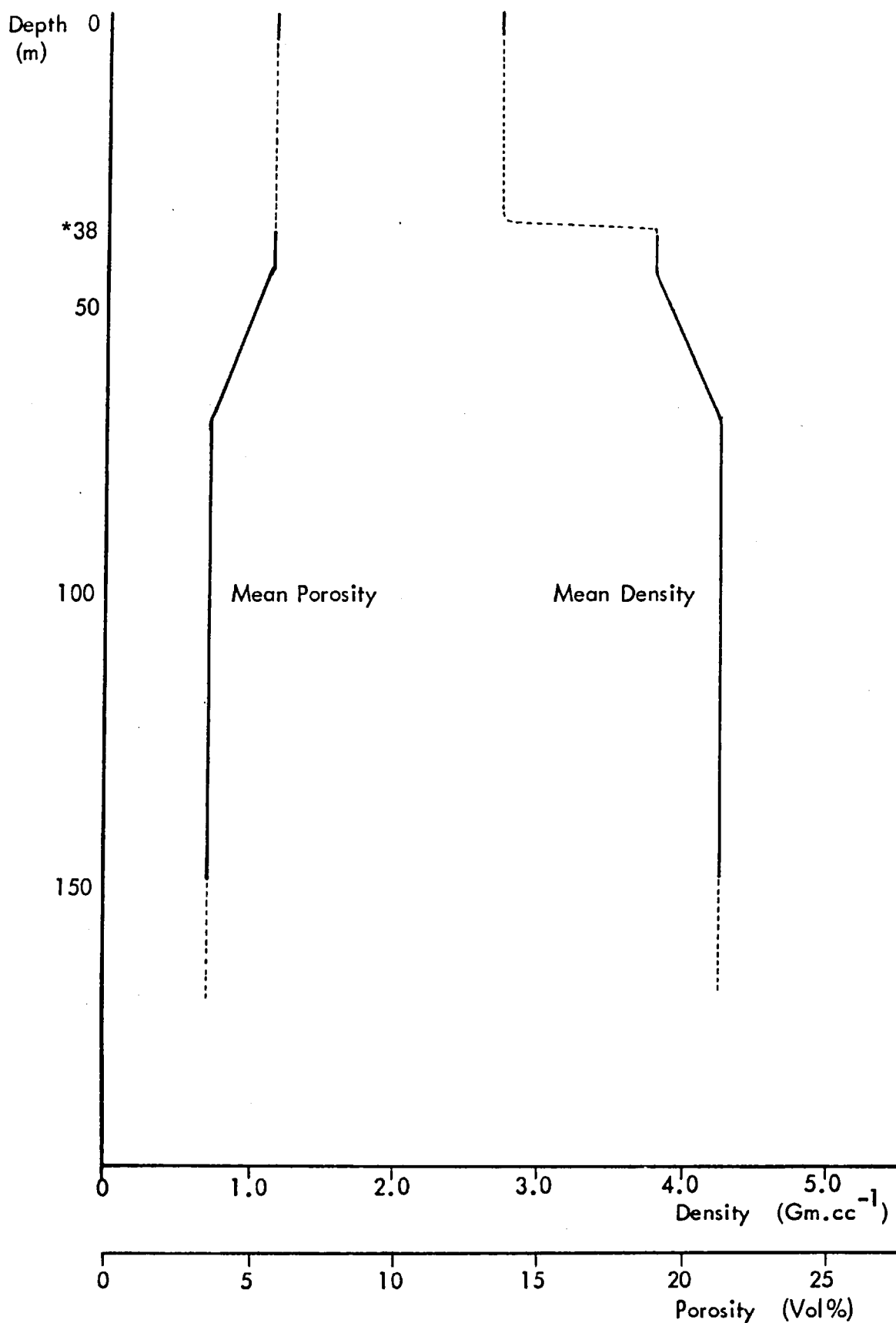
* Approximate position of the Water Table

Fig. 4.3.7.   Chemical Variations in Alteration Profile – Perserverance
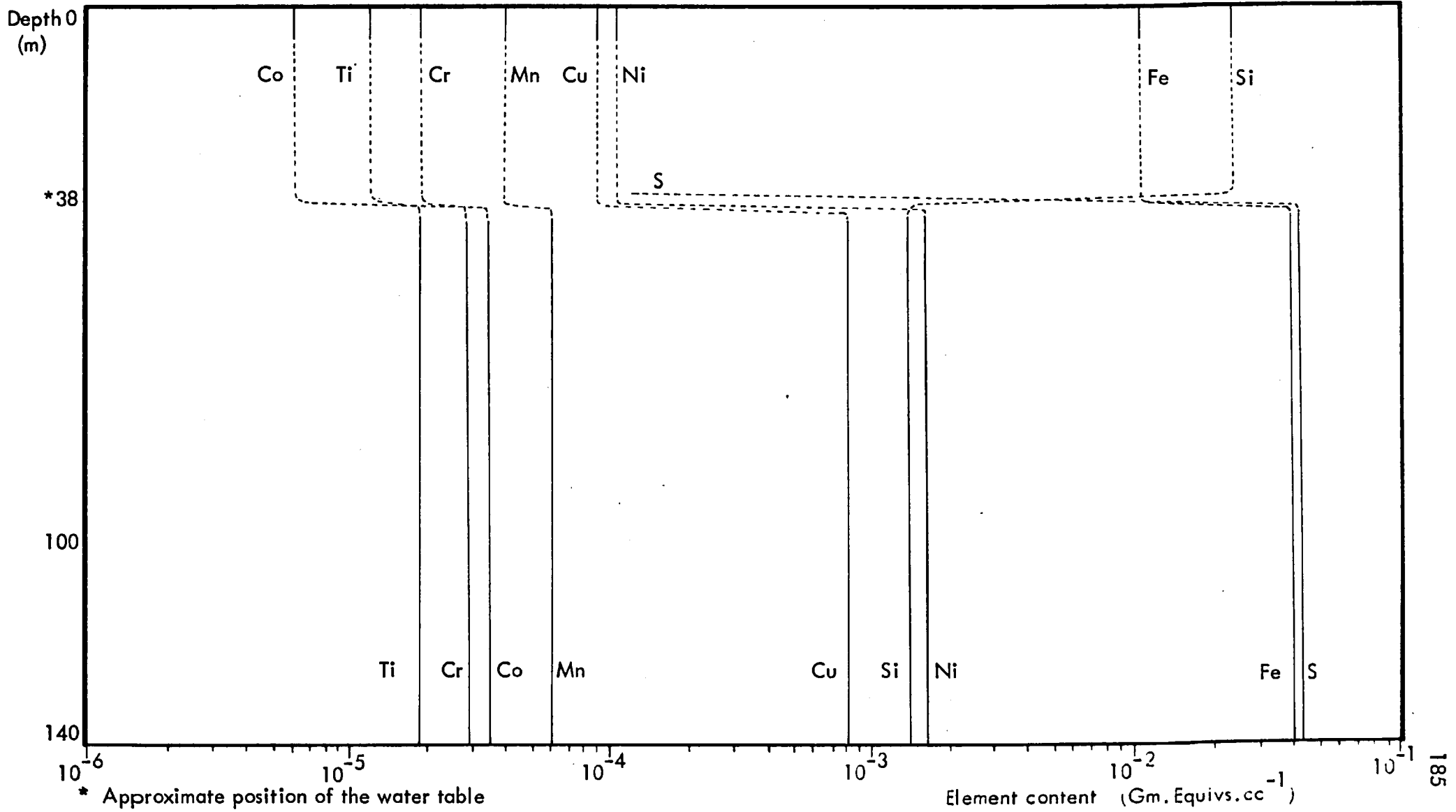
during the formation of the secondary sulphide assemblage in the Perserverence
deposit. In contrast, the slight loss of iron noted across the 70 - 40m. sub-zone
likely represents the small but progressive loss of this metal that occurs during the
oxidation of pentlandite and pyrrhotite, (Fig.4.3.3.).

The behaviour of the element assemblage across the sulphide-oxide transition at
about 38m. is consistent with the physico-chemical effects of the pervasive sulphide
leaching that takes place at that horizon. Hence, the retention of much of the iron
within the immediate basal horizon of the oxide zone (38m. level) is due to the
fixation of this metal in precipitated iron oxides. In contrast, the drastic
impoverishment of sulphur across the 38m. horizon is caused by the mobilisation
and removal of this element as highly soluble sulphate ion during sulphide leaching.
Further, the differential relative depletion of individual trace metals across the
sulphide-oxide transition closely parallels the expected behaviour of these elements
in the high Eh - low pH conditions typically created by pervasive sulphide leaching.

Little detailed evidence is on hand to indicate the variation of the element suite
within the overlying oxide zone. But available petrographic and chemical data
imply that appreciable quantitites of iron oxides are subsequently removed from the
basal 10 metres of the oxide zone due to the progressive influx of large quantities
of silica into that locality.

4.4. SUPERGENE SULPHIDE ALTERATION IN THE TROJAN DEPOSIT, RHODESIA

The Trojan deposit occurs as a series of vertically-inclined lensoid or tabular bodies
within a number of proximal sill-like dunite and serpentinite units in an Archean
greenstone succession. Disseminated mineralisation occurs towards the centres of
the host units, but massive ore is present at or near the host basal contact with
underlying slates, (Section 2.4.). The following description of near surface
sulphide alteration is based on underground sampling, (massive sulphides and some
oxide material), and on surface samples, (oxides), of the Cardiff Hill ore body.

The petrology of the primary massive sulphide assemblage

The mineral assemblage of sampled massive primary ore comprises pyrrhotite and

TABLE 4.4.1. SUMMARY DATA OF SULPHIDE ALTERATION - TROJAN

Depth (m)	Alteration Zone	No. of Samples (n)	MINERALOGY (Means and ranges) Volume % Units	Den gm/cc	Por %	S	Fe	SiO_2	MgO	Al_2O_3	CO_3	Ni	Cu	Mn	Cr	Co	Ti
~30 - 35	Oxide	3	Hm 1.0, Gt 50.0, Si 2.5	2.40	11.5	no data	42.61	2.42	0.40	0.40		8557	879	1776	30	54	330
			Hm 2.5, Gt 70.0, Si 25.0	2.67	13.4		49.61	13.68	1.37	1.90	N/A	12479	1148	11199	548	197	390
			Hm 5.0, Gt 98.0, Si 40.0	3.00	15.8		59.81	21.49	1.90	2.10		14467	1430	18820	1567	373	426
~65 - 70	Violarite - pyrite	1	Hm -, Gt -, Vl 10.0, Cp 1.0, Mt no data, Sil 5.0, Mc 85.0	4.10	2.4	36.46	52.08	3.69	1.00	0.40	N/A	38025	1438	1479	2648	978	192
~100	Transition	1	Po 87.0, Pn 2.0, Vl 4.5, Cp 1.0, Mt no data, Sil 7.0	4.30	3.7	29.40	53.52	6.28	3.06	2.92	N/A	25242	2787	6011	1151	477	576
	Primary	2	Po -, Pn 5.0, Cp -, Mt 1.0, Sil 7.5		1.9	31.07	48.24	4.22	0.60	0.20		22002	1654	728	267	411	108
			Po 80.0, Pn 7.5, Cp 1.0, Mt 1.5, Sil 8.8	4.40	2.8	33.91	52.63	6.16	4.45	0.50	N/A	28356	2117	1040	1783	572	147
			Po -, Pn 10.0, Mt 2.0, Sil 10.0		3.6	36.74	57.02	8.09	8.30	0.80		34709	2580	1352	3154	3154	186

TABLE 4.4.2. PYRRHOTITE COMPOSITIONS - TROJAN

Sample	Fe	Ni	S	Co	Cu	Ti	Wt% Total	Atomic Formula Fe_xS_{10}	Atomic Formula Me_xS_{10}	Me:S ratio
2309/A1/1	60.50	n.d.	38.61	n.d.	0.06	0.03	99.20	-	-	-
	(47.34)	-	(52.62)	-	(0.04)	(0.02)	-	$Fe_{9.02}S_{10}$	$Me_{9.05}S_{10}$	0.91
2309/A1/3	61.49	n.d.	38.78	n.d.	0.05	0.07	100.10	-	-	-
	(47.49)	-	(52.42)	-	(0.03)	(0.06)	-	$Fe_{9.04}S_{10}$	$Me_{9.06}S_{10}$	0.91
2309/A1/9	61.32	n.d.	39.25	n.d.	0.07	0.06	100.68	-	-	-
	(47.26)	-	(52.69)	-	(0.05)	(0.05)	-	$Fe_{8.98}S_{10}$	$Me_{9.03}S_{10}$	0.90

TABLE 4.4.3.   PENTLANDITE COMPOSITIONS - TROJAN

Sample	Fe	Ni	S	Co	Cu	Ti	Wt% Total	Atomic Formula $Ni_nFe_mS_8$	Atomic Formula Me_xS_8	Me:S ratio
2309/A1/5	30.74	34.20	32.55	0.39	0.15	0.04	98.08	-	-	-
	(25.50)	(26.99)	(47.05)	(0.31)	(0.11)	(0.04)	-	$Ni_{4.59}Fe_{4.34}S_8$	$Me_{9.01}S_8$	1.13
2309/A1/8	31.40	34.90	32.69	0.29	0.17	0.04	99.49	-	-	-
	(25.73)	(27.21)	(46.68)	(0.22)	(0.12)	(0.04)	-	$Ni_{4.66}Fe_{4.41}S_8$	$Me_{9.14}S_8$	1.14

TABLE 4.4.4.   FERROCHROMITE COMPOSITIONS – TROJAN

Sample	2311/1	2311/2	2311/3	2311/4	2311/5	2308/1
TiO2	0.97	0.90	2.11	1.64	0.94	0.89
Al2O3	2.66	3.11	3.32	0.05	0.23	1.97
Cr2O3	44.11	45.01	36.78	53.67	62.03	54.66
Fe2O3	16.02	16.94	22.16	10.04	3.57	9.14
FeO	25.80	26.64	28.49	27.23	25.98	27.51
MnO	2.37	2.23	2.03	1.97	2.03	1.36
MgO	0.00	0.00	0.00	0.00	0.00	0.10
NiO	0.00	0.00	0.00	0.00	0.00	0.00
ZnO	4.47	4.81	3.68	4.48	5.57	4.70
V2O5	1.97	1.82	1.41	1.31	0.74	1.15
TOTAL (Wt%)	98.36	101.46	100.00	100.40	101.09	101.48

Sample	2308/2	2308/3	2308/4	2308/5	2310/1	2310/2
TiO2	0.98	0.62	1.10	0.71	7.22	1.90
Al2O3	2.35	2.78	2.26	2.26	2.35	0.97
Cr2O3	51.74	52.12	51.95	51.09	39.92	36.69
Fe2O3	10.26	10.88	9.95	12.04	11.39	25.23
FeO	26.79	27.06	27.65	26.96	33.05	28.12
MnO	1.54	1.50	1.26	1.50	1.89	1.45
MgO	0.00	0.11	0.00	0.06	0.12	0.07
NiO	0.00	0.00	0.00	0.00	0.00	0.00
ZnO	4.98	4.62	4.53	4.70	4.24	3.65
V2O5	1.07	1.06	1.31	1.27	1.18	0.60
TOTAL (Wt%)	99.71	100.75	100.03	100.59	101.36	98.68

Sample	2310/3	2310/4	2310/5	2310/6	2310/7	
TiO2	0.97	0.74	1.26	1.92	1.26	
Al2O3	2.10	0.23	0.51	0.06	0.10	
Cr2O3	50.00	12.02	44.94	51.16	56.48	
Fe2O3	12.27	54.50	20.13	11.23	7.90	
FeO	25.65	30.42	27.62	26.37	25.79	
MnO	1.55	0.57	1.52	1.65	1.60	
MgO	0.25	0.00	0.16	0.39	0.51	
NiO	0.00	0.00	0.00	0.00	0.00	
ZnO	5.58	0.91	4.22	4.94	5.20	
V2O5	0.91	0.44	1.02	1.53	1.34	
TOTAL (Wt%)	99.28	99.83	101.38	99.24	100.18	

pentlandite with minor amounts of chalcopyrite and ferrochromite, (Table 4.4.1.). Accessory quantities of silicates are also, however, associated with Trojan massive sulphide ore.

Pyrrhotite comprises about 80 percent of the sulphide assemblage. This mineral forms the matrix of the ore and is typically present as a mosaic of interlocking, generally rather equant grains, (Fig.4.4.1A.). The chemical composition of three pyrrhotite grains are presented in Table 4.4.2. These data indicate that hexagonal pyrrhotite predominates in the Trojan primary sulphide assemblage, and that this phase contains no detectable concentrations of nickel or cobalt.

Pentlandite comprises approximately 7.5 percent of primary massive ore, (Table 4.4.1.). It is present in two textural forms: Firstly as (commonly) elongate stringers along pyrrhotite grain borders, (Fig.4.4.1B.);and secondly, as rarer flamme lamellar aggregates within pyrrhotite, (Fig.4.4.1C.). The chemical data of two pentlandite grains, (Table 4.4.3.) indicate that this mineral is relatively poor in cobalt.

Chalcopyrite comprises approximately one percent of Trojan primary ore, (Table 4.4.1.), but is rather irregularly distributed within the assemblage. The mineral is commonly present as elongate stringers along pyrrhotite borders, but is also associated with pentlandite, (Fig.4.4.1D.).

Ferrochromite forms about 1.5 percent of the primary sulphide assemblage, (Table 4.4.1.). This mineral is commonly present as euhedral forms within the sulphide matrix, but rather more irregular elongate forms are typically associated with silicate inclusions, (Fig.4.4.1E.). Further, the mineral typically exhibits outer rims or zones of magnetite, (Fig.4.4.1E.). The chemistry of a number of ferrochromite grains are presented in Table 4.4.4., and these data confirm the identity of this spinel phase.

The petrology of the sulphide alteration sequence

Available data indicate that incipient alteration of primary massive ore occurs at about 100 metres below surface at Trojan, (Table 4.4.1.). Alteration commences with the formation of violarite from both varieties of pentlandite. Violarite formation in interstitial pentlandite is typically initiated in areas proximal to the octahedral cleavage traces and the alteration subsequently advances into the body

of the pentlandite along broad fronts, (Fig.4.4.1F .). In contrast, however, the alteration of lamellar pentlandite generally takes place outwards from the centres of the flamme aggregates, (Fig.4.4.1G.).

The chemical composition of two grains of violarite after interstitial pentlandite (Vpn) are presented in Table 4.4.5. These data indicate that Trojan violarite analyses summate to totals significantly less than 100 percent, but that the mean molecular formula corresponds closely with the theoretical (stoichiometric) value of Me_3S_4.

A comparison of mean pentlandite and violarite compositions is presented in Table 4.4.6. These data indicate that substantial absolute changes in iron, nickel and cobalt contents occur as a result of violarite formation. In addition, Table 4.4.6. also demonstrates that an appreciable increase in sulphur content occurs during the alteration process. It is, however, very probable that this sulphur enrichment is relative rather than absolute since the formation of violarite characteristically takes place as a pseudomorphic replacement process, (Fig.4.4.2A.). The corresponding reaction mechanism of violarite (Vpn) formation is set out in Equation 1, (Fig.4.4.3.), and indicates that pentlandite replacement is an oxidation process.

Petrographic data demonstrate that pyrrhotite alteration is initiated once violarite begins to replace pentlandite. The alteration takes the form of laterally extensive feather-like lamellar growths of brownish-violet porous violarite after pyrrhotite (Vpo) that develop along pyrrhotite/pentlandite mutual grain borders, (Fig.4.4.2B.). The lamellae are orientated with their long axes sub-parallel to the 0001 cleavage parting of the parent hexagonal pyrrhotite. A thin zone of void space precede the violarite growth front and indicates that active corrosion is associated with the violarite formation process, (Fig.4.4.2C.). The conspicuous absence of an intermediate smythite stage in the pyrrhotite-violarite alteration sequence at Trojan is likely to be related to the presence of hexagonal, (as opposed to monoclinic) pyrrhotite.

The chemical composition of a single analysed Vpo grain, (Table 4.4.7.), indicates that this mineral is relatively iron-rich and nickel-poor compared with violarite after interstitial pentlandite. It is likely that these chemical differences are due to the formation of Vpo from an ore metal-depleted parent, as is indicated by the mean composition of hexagonal pyrrhotite similarly presented in Table 4.4.7. It is hence very probable that the nickel and cobalt required for the formation of Vpo is derived

from that released during the alteration of adjacent pentlandite to violarite. This feature is incorporated in the likely reaction corresponding to the pyrrhotite-violarite alteration (oxidation) process presented in Equation 2 of Fig.4.4.3. The data in Table 4.4.7. also indicate however that Vpo likely approximates the theoretical stoichiometry of violarite.

Available data demonstrate that the transitional sulphide assemblage of Vpn, pyrrhotite, Vpo, chalcopyrite and ferrochromite is present between the 100m. and 70m. levels of the Trojan oxidation profile. At about 65 - 70 metres b.s., however, the remaining pyrrhotite is replaced by secondary marcasite, (Table 4.4.1.). Replacement typically occurs as fine-grained (colloidal) aggregates of marcasite, and these commonly contain pseudocolloform shrinkage cracks, (Fig.4.4.2D.). Local recrystallisation to a coarser grained form may, however, occur subsequently, (Fig.4.4.2E.).

Large bird's eye structures are also present in secondary marcasite, and probably develop within parts of former large pyrrhotite grains, (Fig.4.4.2F.). Whereas, in contrast, smaller equant mosaic pyrrhotite grain shapes are commonly well preserved by replacing iron disulphide, (Fig.4.4.2G.). The other members of the transition ore assemblage generally remain stable during marcasite formation, although chalcopyrite not uncommonly exhibits incipient in situ alteration to covellite at this level of the oxidation profile, (Fig.4.4.2H.).

The chemical composition of a single secondary marcasite grain is presented in Table 4.4.8. The low trace metal contents of this specimen reflect its derivation from ore metal-depleted pyrrhotite, (Table 4.4.2.). Further, a comparison of pyrrhotite and marcasite compositions, (Table 4.4.8.), indicates that marcasite formation results in the release of substantial quantities of iron, (Equation 3, Fig.4.4.3.).

Extensive sample data are lacking for the secondary (supergene) zone of violarite-marcasite at Trojan, (Table 4.4.1.). But such information that is available implies that this alteration zone is probably present between the 65m. and 30m. levels in the Trojan (Cardiff Hill) ore profile.

194

Fig. 4.4.1. Petrography of Trojan Sulphide Ore (1)

Scale length = 100 μ .

A. Typical pyrrhotite matrix mosaic (x 220) Oil   Partly crossed nicols

Lammellar pentlandite; light grey: Pyrrhotite; medium to medium-dark grey: Voids; dark

B. Interstitial pentlandite form (x 220) Oil   Partly crossed nicols

Pentlandite; light-medium grey, elongated: Pyrrhotite; medium to medium-dark grey: Voids; dark

C. Typical pentlandite flamme aggregate in pyrrhotite (x 220) Oil
Partly crossed nicols

Pentlandite; medium grey: Voids; dark

D. Typical chalcopyrite texture (x 220) Oil

Chalcopyrite; medium to dark grey (left margin and top):   Pentlandite; light-medium grey (centre):   Pyrrhotite; medium-dark grey (right margin):   Voids; dark

E. Typical ferrochromite texture (x 220) Oil

Central ferrochromite cores (dark grey) surrounded by magnetite ring (medium grey):   Pyrite; light grey: Voids; dark

F. Typical violarite replacement texture - interstitial pentlandite (x 220) Oil

Pentlandite; medium grey: Violarite; medium-dark grey, granular: Pyrrhotite; medium-dark grey: Voids; dark

G. Typical violarite replacement texture - lamellar pentlandite (x 220) Oil

Violarite; medium grey: Pyrrhotite; medium-dark grey: Voids; dark

195
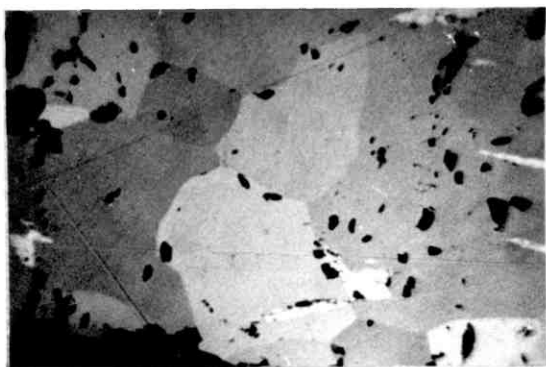
Fig.4.4.1.

A
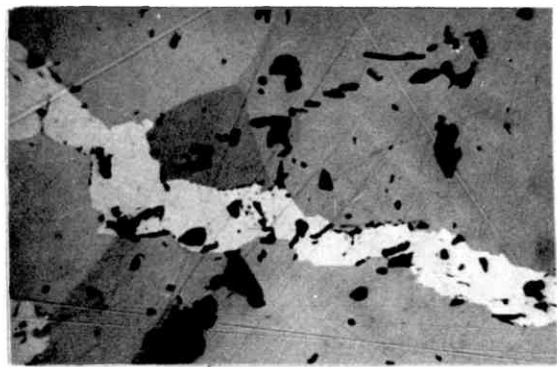
B

C
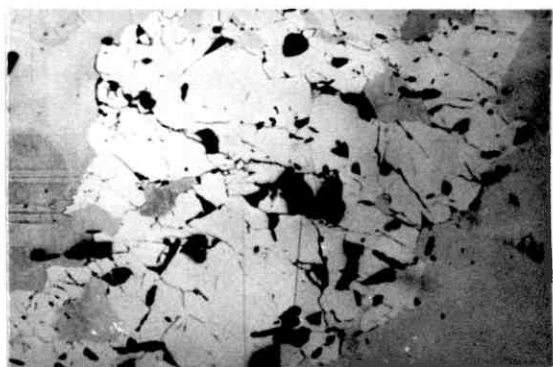
D
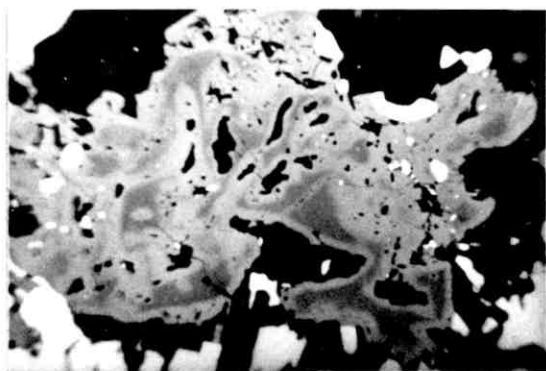
E
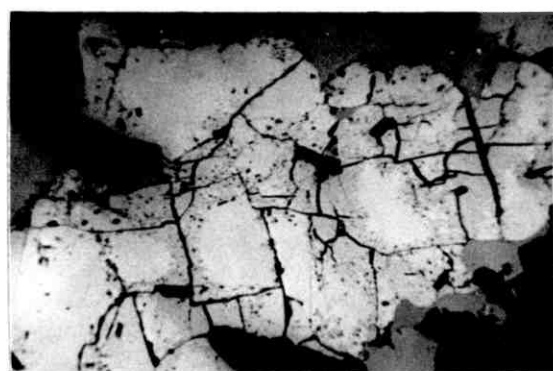
F
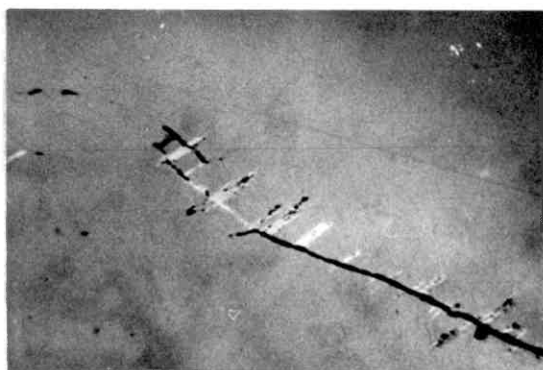
G

Fig. 4.4.2. Petrography of Trojan Sulphide Ore (2)

Scale length = 100 μ

A. Completed replacement of interstitial pentlandite by violarite (x 600) Oil

Violarite; medium grey: Pyrrhotite; medium-dark grey: Voids; dark

B. Violarite after pyrrhotite growth texture (x 600) Oil

Typical development of corrosion front between Vpo and pyrrhotite

C. Extensively developed Vpo corrosion front (x 600) Oil

Pentlandite; light grey: Violarite species; medium grey, granular:
Pyrrhotite; light to medium grey: Voids; dark

D. Typical pseudocolloform secondary marcasite texture (x 220) Oil

Marcasite; medium-dark grey, granular (top half): Violarite species; medium
grey, granular (lower half): Voids; dark

E. Recrystallisation of fine-grained marcasite to a coarser variety (x 220) Oil

Fine-grained secondary marcasite; medium-dark grey, granular: coarser
marcasite; medium grey: Violarite species; dark grey, granular:
Voids; dark

F. Typical marcasite bird's eye texture after pyrrhotite (x 220) Oil

G. Pyrrhotite mosaic mimicked by replacing marcasite (x 220) Oil

H. In situ alteration of chalcopyrite to covellite (x 600) Oil

Chalcopyrite; medium grey: Covellite; dark grey rimming cp: Violarite;
medium-dark grey, granular (lower left, top right): Marcasite; medium grey
(bottom right, centre left): Voids; dark

Fig.4.4.2.
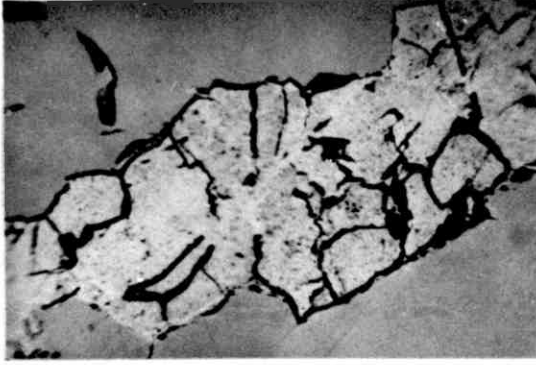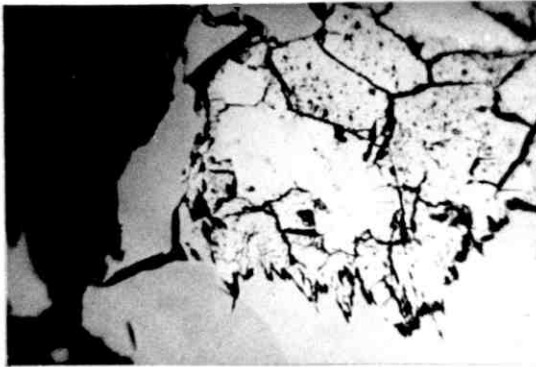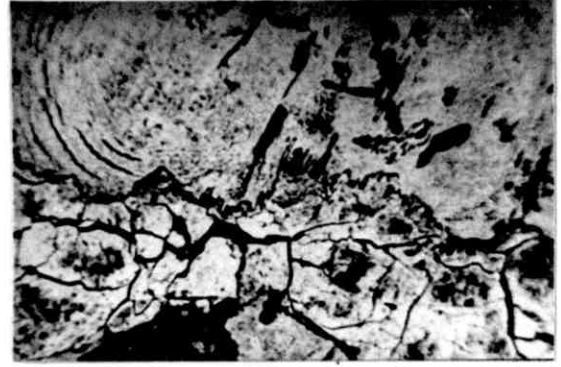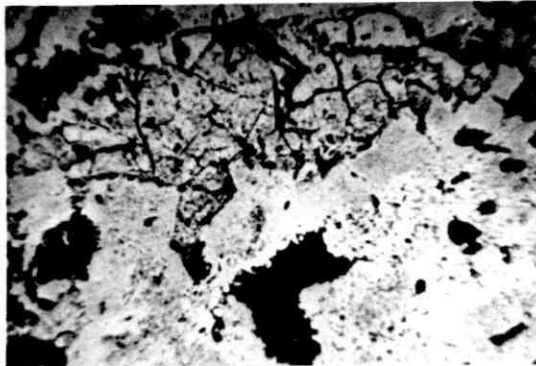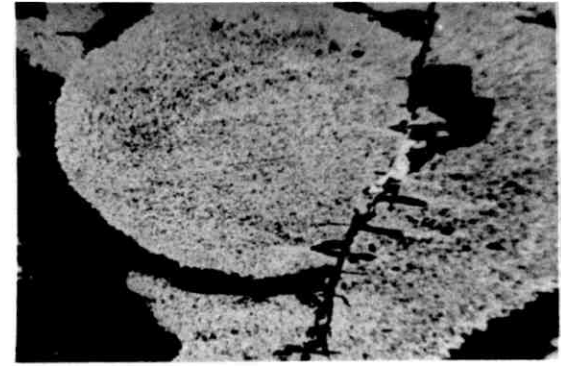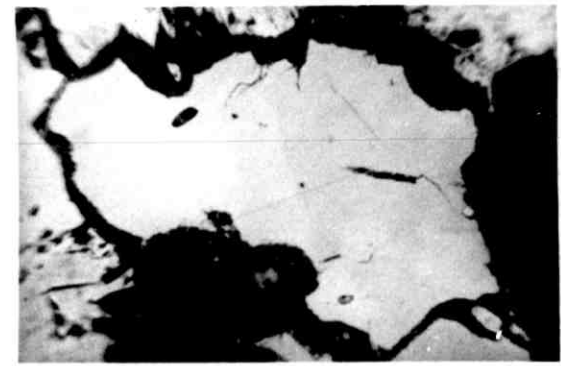
TABLE 4.4.5. VIOLARITE AFTER PENTLANDITE COMPOSITIONS - TROJAN

Sample	Fe	Ni	S	Co	Cu	Ti	Wt% Total	Atomic Formula $Ni_nFe_mS_4$	Atomic Formula Me_xS_4	Me:S ratio
2309/A1/2	23.64	30.59	41.31	0.16	0.12	0.04	95.86	-	-	-
	(18.92)	(23.29)	(57.59)	(0.12)	(0.08)	(0.03)	-	$Ni_{1.62}Fe_{1.32}S_4$	$Me_{2.95}S_4$	0.74
2309/A1/6	22.64	30.79	41.08	0.24	0.10	0.05	94.94	-	-	-
	(18.28)	(23.66)	(57.78)	(0.18)	(0.10)	(0.03)	-	$Ni_{1.64}Fe_{1.27}S_4$	$Me_{2.93}S_4$	0.73

Table 4.4.6.   Comparison of pentlandite and violarite (Vpn) compositions

	PENTLANDITE (n = 2)	VIOLARITE AFTER PENTLANDITE (n = 2)
Fe	31.07	23.14
	(25.62)	(18.60)
Ni	34.55	30.69
	(27.10)	(23.46)
S	32.62	41.19
	(46.86)	(57.66)
Co	0.34	0.20
	(0.27)	(0.15)
Cu	0.16	0.13
	(0.12)	(0.09)
Ti	0.04	0.04
	(0.04)	(0.04)
TOTAL (Wt%)	98.79	95.40
Ni:Fe	1.06	1.26
Me:S	1.14	0.98

Table 4.4.7. Comparison of pyrrhotite and violarite (Vpo) compositions

	PYRRHOTITE (n = 3)	VIOLARITE AFTER PYRRHOTITE (n = 1)
Fe	61.01	25.22
	(47.35)	(20.26)
Ni	n.d.	29.55
	-	(22.58)
S	38.88	40.75
	(52.56)	(57.02)
Co	n.d.	0.07
	-	(0.05)
Cu	0.06	0.13
	(0.04)	(0.09)
Ti	0.05	0.05
	(0.04)	(0.04)
TOTAL (Wt%)	100.00	95.76
Ni:Fe	-	1.11
Me:S	0.90	0.75

Table 4.4.8. Comparison of pyrrhotite and secondary marcasite compositions

	PYRRHOTITE (n = 3)	SECONDARY MARCASITE (n = 1)
Fe	61.01	45.44
	(47.35)	(33.23)
Ni	n.d.	0.01
	-	(0.01)
S	38.88	52.33
	(52.56)	(66.67)
Co	n.d.	0.03
	-	(0.02)
Cu	0.06	0.03
	(0.04)	(0.02)
Ti	0.05	0.07
	(0.04)	(0.07)
TOTAL (Wt%)	100.00	97.91
Ni:Fe	-	-
Me:S	0.90	0.50

FIG. 4.4.3. CHEMISTRY OF THE TROJAN ALTERATION SEQUENCE

SHALLOW ANODIC WEATHERING REACTIONS

14 $FeS_2 + 8H_2O = Fe^{2+} + 2SO_4^{2-} + 16H^+ + 14e^-$
Marcasite

13 $CuFeS_2 + 8H_2O = Cu^{2+} + Fe^{2+} + 2SO_4^{2-} + 16H^+ + 16e^-$
Chalcopyrite

12 $Ni_{1.44}Fe_{1.58}Co_{0.08}S_4 + 16H_2O = 1.44Ni^{2+} + 1.58Fe^{2+} + 0.08Co^{2+} + 4SO_4^{2-} + 32H^+ + 30.20e^-$
Violarite (after Po)

11 $Ni_{1.63}Fe_{1.29}Co_{0.01}S_4 + 16H_2O = 1.63Ni^{2+} + 1.29Fe^{2+} + 0.01Co^{2+} + 4SO_4^{2-} + 32H^+ + 29.86e^-$
Violarite (after Pn)

10 $FeS_2 + 8H_2O + 1.50OH^- = 0.5Fe_2O_3 + 2SO_4^{2-} + 17.50H^+ + 15.0e^-$
Marcasite   Hematite

9 $Ni_{1.44}Fe_{1.58}Co_{0.08}S_4 + 16H_2O + 2.37OH^- = 0.79Fe_2O_3 + 1.44Ni^{2+} + 0.08Co^{2+} + 4SO_4^{2-} + 34.37H^+$
Violarite (after Po)   Hematite $+ 31.78e^-$

8 $Ni_{1.63}Fe_{1.29}Co_{0.01}S_4 + 16H_2O + 1.94OH^- = 0.65Fe_2O_3 + 1.63Ni^{2+} + 0.01Co^{2+} + 4SO_4^{2-} + 33.94H^+$
Violarite (after Pn)   Hematite $+ 31.15e^-$

7 $FeS_2 + 8H_2O + 2OH^- = FeOOH + 2SO_4^{2-} + 17H^+ + 15e^-$
Marcasite   Goethite

6 $CuFeS_2 + 8H_2O + 2OH^- = FeOOH + Cu^{2+} + 2SO_4^{2-} + 17H^+ + 17e^-$
Chalcopyrite   Goethite

5 $Ni_{1.44}Fe_{1.58}Co_{0.08}S_4 + 16H_2O + 3.16OH^- = 1.58FeOOH + 1.44Ni^{2+} + 0.08Co^{2+} + 4SO_4^{2-} + 33.58H^+$
Violarite (after Po)   Goethite $+ 31.78e^-$

4 $Ni_{1.63}Fe_{1.29}Co_{0.01}S_4 + 16H_2O + 2.58OH^- = 1.29FeOOH + 1.63Ni^{2+} + 0.01Co^{2+} + 4SO_4^{2-} + 33.29H^+$
Violarite (after Pn)   Goethite $+ 33.73e^-$

DEEP ANODIC WEATHERING REACTIONS

3 $Fe_{9.01}S_{10} = 5FeS_2 + 4.01Fe^{2+} + 8.02e^-$
Hexagonal Po   Marcasite

2 $Fe_{9.01}S_{10} + 3.18Ni^{2+} = 2Ni_{1.59}Fe_{1.43}S_4 + 6.15Fe^{2+} + 5.94e^-$
Hexagonal Po   Violarite (after Po)

1 $Ni_{4.63}Fe_{4.37}Co_{0.05}S_8 = 2Ni_{1.63}Fe_{1.29}Co_{0.01}S_4 + 1.37Ni^{2+} + 1.79Fe^{2+} + 0.03Co^{2+} + 6.38e^-$
Pentlandite   Violarite (after Pn)

The petrology of the oxide zone

The oxide zone developed over the Trojan deposit extends from about the 30m. level to the surface where it crops out as spongy ferruginous gossan, (Section 2.4.). The mineralogy of the oxide zone mineral assemblage comprises goethite and silica with minor to trace amounts of hematite.

Goethite averages about 70 percent in the sampled oxide zone material. The mineral is present in several textural forms, and is typically noted as mimic replacements of several members of the secondary sulphide assemblage. In this respect, goethite is chiefly present as boxworks after large secondary mimicked hexagonal pyrrhotite grains, (Fig.4.4.4A.); as complete mimic replacements of polygonal secondary marcasite, (Fig.4.4.4B.), and marcasite bird's eye structures, (Fig.4.4.4C.). The mineral also commonly pseudomorphs all three noted violarite species; namely, interstitial Vpn, (Fig.4.4.4D.); lamellar Vpn, (Fig.4.4.4E.); and Vpo, (Fig.4.4.4F.). Goethite is also uncommonly present as boxworks after chalcopyrite, (Fig.4.4.4G.).

The presence of these secondary sulphide textures in goethite indicates that pseudomorphic replacement processes must commonly occur during the formation of the oxide zone assemblage at the water table in the Trojan deposit. Hence goethite can directly replace all three violarite species, marcasite and chalcopyrite. The likely chemistry of these reactions is indicated in Equations 4 to 7 in Fig.4.4.3. Whereas the relevant equations corresponding to direct leaching of the secondary sulphide assemblage comprise Equations 11 to 14 in the same figure.

Silica averages about 25 percent of the sampled oxide zone assemblage, and the mineral is present chiefly as well-preserved relic structures after amphibole grains, (Fig.4.4.4H.). More rarely, however, silica is noted as interstitial fillings to well-preserved pseudomorphs of interstitial Vpn, (Fig.4.4.4I).

Hematite is noted only in trace amounts in the sampled Trojan oxide zone, but where present may also form pseudomorphic structures after violarite species and marcasite. The likely formation reactions corresponding to these replacement phenomena are indicated in Equations 8 to 10 in Fig.4.4.3.

The mean variation in both true density and porosity in the Trojan sulphide oxidation sequence is presented in Fig.4.4.5. The diagram demonstrates that the depth

Fig. 4.4.4. Petrography of the Trojan Gossan

Scale length = 100µ unless otherwise stated

A.   Goethite boxworks after hexagonal pyrrhotite (x 40) Air   Blue-white filter

Voids; dark: Goethite; light-medium grey

B.   Goethite mimics after polygonal secondary marcasite (x 220) Oil

Violarite mimics; medium grey: Pyrrhotite mimics; light-medium grey:
Altered silicates; medium-dark to dark grey

C.   Goethite mimics after marcasite bird's eyes (x 220) Oil

Altered silicates; dark grey: Voids; dark

D.   Goethite mimic after interstitial violarite (x 220) Oil

Altered silicate; dark grey, lineated.   Internal Vpn cleavage is recognisable
– defined as voids

E.   Goethite mimics after lamellar violarite (x 220) Oil

Lamellar Vpn mimics in goethite (bottom left). Well preserved Vpn mimics with
goethite filled cleavages.   Silicate; dark grey

F.   Goethite mimics after Vpo (x 600) Oil

Silicates; dark grey

G.   Goethite boxworks after chalcopyrite (x 110) Air Blue-white filter

Voids- dark grey (resin)

H.   Silica as relics after amphibole grains (x 220) Oil   Blue-white filter

Non-specific goethite; light grey

I.   Silica interstitial filling of violarite relic (x 110) Air Blue-white filter

Silica; dark grey : Non-specific goethite; light-medium grey: Voids; dark

Fig.4.4.4.
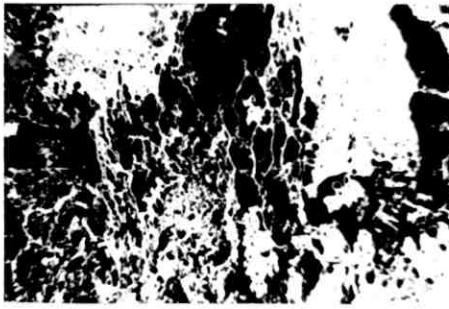
A   1000μ
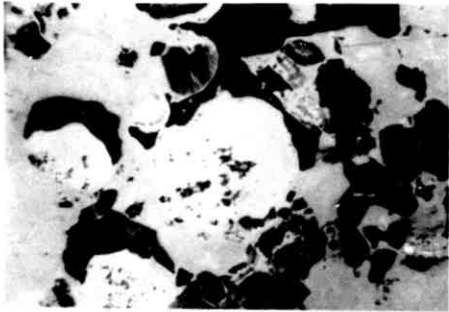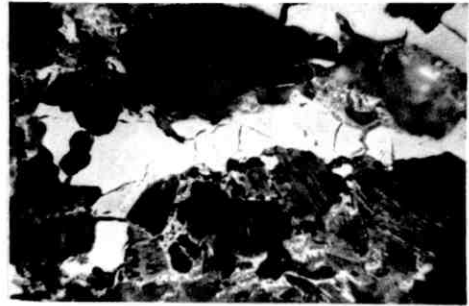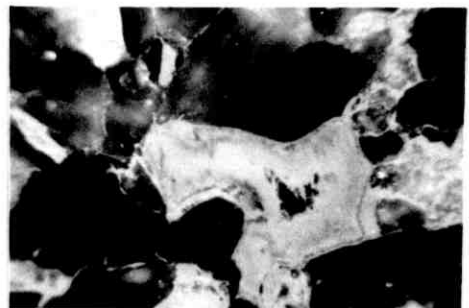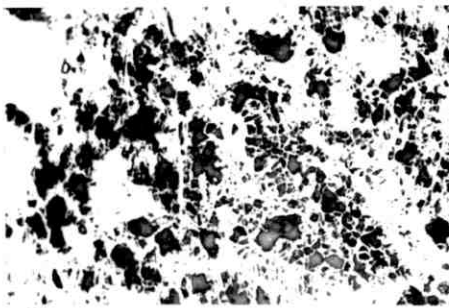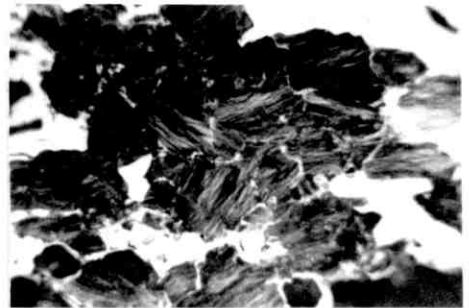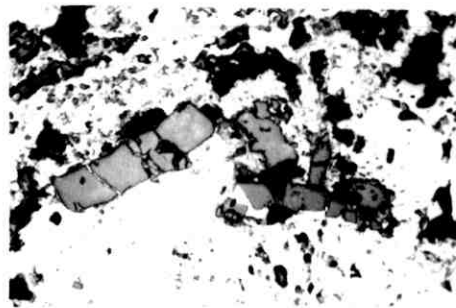
Fig. 4.4.5. Mean True Density and Porosity profiles — Trojan
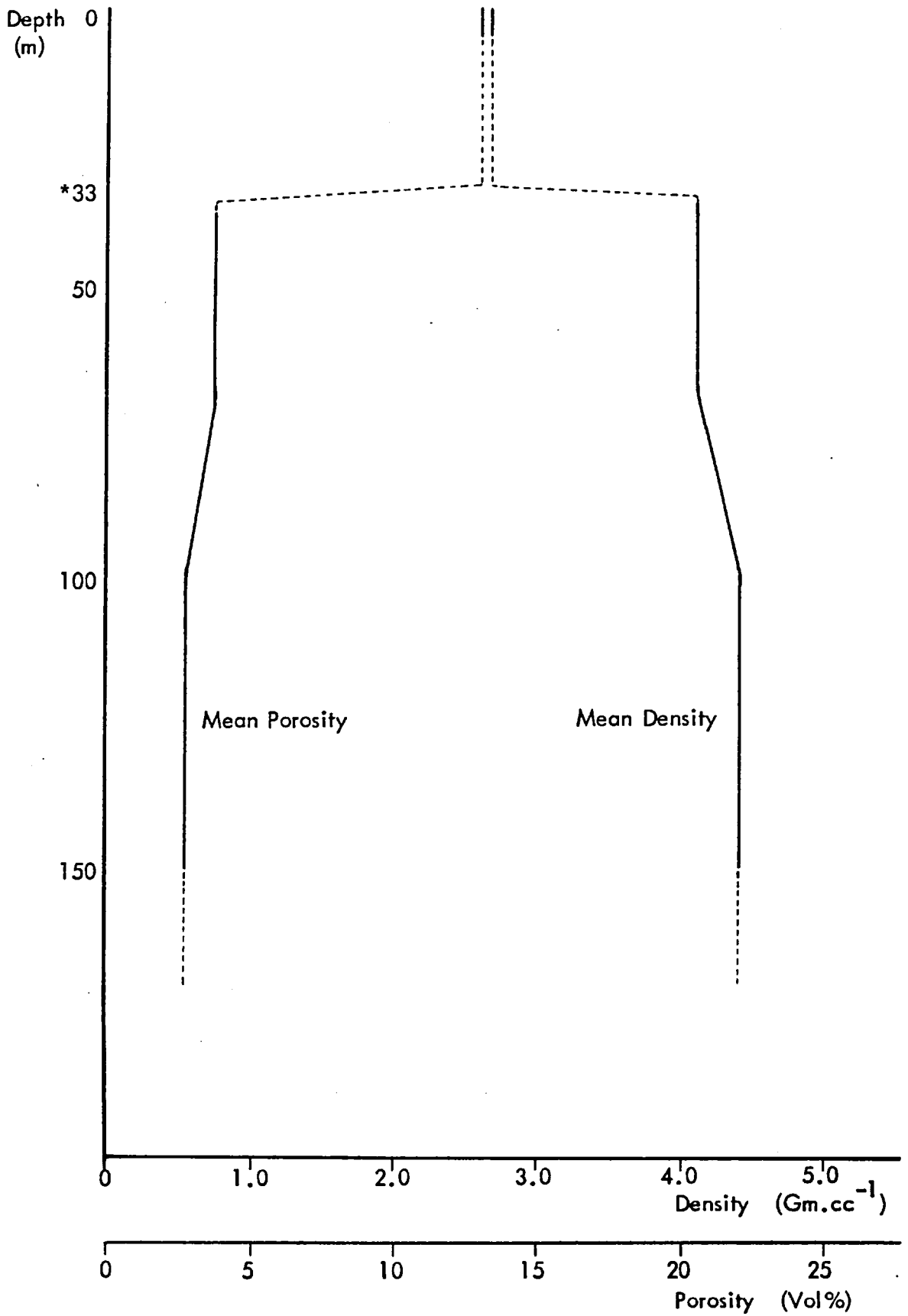
* Approximate position of the Water table

Fig. 4.4.6. Chemical Variations in Alteration Profile – Trojan

* Approximate position of the water table

Element content (Gm.Equivs.cc^{-1})
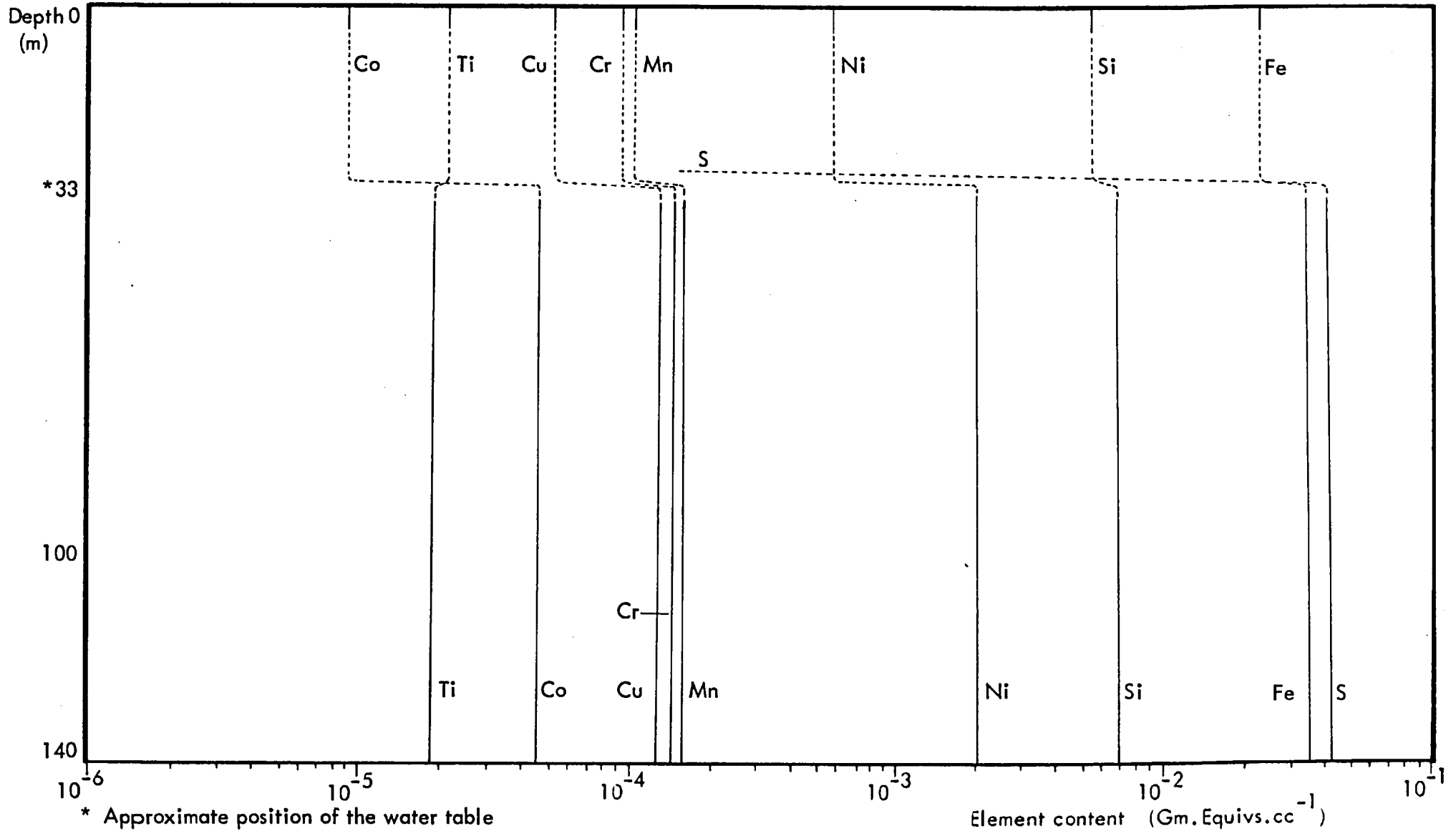
variation of both physical properties closely parallels the sequence of physico-
chemical changes documented in the sulphide alteration profile.

The bulk chemistry of the sulphide alteration sequence

The bulk mean chemical variation of a suite of constituent major and minor elements
within the sampled sulphide alteration profile at Trojan is presented in Fig.4.4.6.
The effective constancy of all element profiles between the 70m. and 30m. levels
indicates, on available data, that no overall chemical change occurs during the
development of the secondary (supergene) sulphide assemblage of violarite and
marcasite. Further, the indicated modification in individual element contents across
the sulphide-oxide transition at 30m. corresponds in general both with petrographic
observations of the oxide zone minera assemblage, and with the likely behaviour
of these elements under the high Eh – low pH conditions imposed by sulphide
leaching.

4.5. SUPERGENE ALTERATION IN THE PHOENIX DEPOSIT, BOTSWANA

The Phoenix deposit occurs as a series of steeply-dipping, impersistent bodies of
massive sulphide that are located in shear zones within a heterogeneous felspathic
amphibolite host, (Section 2.4.). The following description of the sulphide
alteration profile developed in this deposit is based on drillcore data (sulphides)
and on surface sampling of the overlying oxide zone.

The petrology of the primary sulphide assemblage

The mineralogy of primary massive sulphide ore consists of pyrrhotite and pentlandite
with minor amounts of chalcopyrite and magnetite, (Table 4.5.1.). Pyrrhotite
comprises about 75 percent of primary ore and forms the matrix of the assemblage,
(Table 4.5.1.). It is present as a mosaic of interlocking rather equant grains that
exhibit a distinctly polygonal tendency, (Fig.4.5.1A.).

The chemical compositions of two pyrrhotite samples are presented in Table 4.5.2.
These data indicate that the mineral is cobalt-rich, but that it also contains
substantial quantities of nickel. Further, data also indicate that Phoenix pyrrhotite

TABLE 4.5.1. SUMMARY DATA OF SULPHIDE ALTERATION - PHOENIX

Depth (m)	Alteration Zone	No. of Samples (n)	Mineralogy (Means and ranges) Volume % Units							Physical data (mean/ranges) Den gm/cc	Por %	Geochemistry (Means and ranges) Wt.% Units S	Fe	SiO$_2$	MgO	Al$_2$O$_3$	CO$_3$	p.p.m. Units Ni	Cu	Mn	Cr	Co	Ti
~20	Oxide	8	Hm 2.0	Gt 12.0	Si 3.0					2.80	1.9		58.01	2.60	0.30	0.40		676	1286	74	27	45	174
			31.0	64.5	4.5					3.10	10.9	N/A	59.37	4.30	0.35	2.05	N/A	1999	10743	95	283	161	751
			82.0	93.0	5.0					3.50	15.9		60.43	6.59	0.40	4.00		6051	25186	126	944	747	1876
~25	Violarite - pyrite	no data																					
~90 -100	Transition	3	Po 75.0	Pn 0.0	Vl 3.0	Cp 0.5	Mt	Sil 0.0	Mc/Py 2.0	3.30	0.4	28.74	42.81	10.43	0.00	0.00		39007	375	409	96	627	234
			80.0	2.3	8.5	2.0	N/A	4.3	2.3	3.70	2.6	31.40	44.43	13.47	1.67	1.57	N/A	44995	3895	582	237	926	512
			85.0	7.0	12.5	5.0		10.0	3.0	3.90	4.3	33.08	48.66	17.29	2.70	3.50		49120	9026	869	465	1165	887
	Primary	5	Po 70.0	Pn 12.5	-	Cp 0.5	Mt 0.0	Sil 0.0		3.50	0.5	29.35	36.95	0.43	0.20	0.00		36296	30	74	30	911	90
			75.0	15.5	-	1.6	4.0	0.4		4.26	2.8	34.78	50.11	5.32	0.38	0.90	N/A	51963	23453	114	52	1127	252
			80.0	20.0		5.0	7.5	2.0		4.60	6.0	37.46	55.23	19.72	0.60	3.30		59037	79879	171	103	1560	420

Fig. 4.5.1. Petrography of Phoenix Sulphide Ore (1)

Scale length = 100μ

A.   Polygonisation in pyrrhotite (x 110) Air   Partly crossed nicols

   Lamellar Pentlandite; light to medium grey

B.   Etched pyrrhotite showing compositional differentiation (x 110) Air

   Hexagonal pyrrhotite; dark grey (etched):. Monoclinic pyrrhotite;
   medium grey (unetched): Pentlandite (interstitial and lamellar);
   light grey

C.   Typical interstitial pentlandite with associated lamellar variety (x 320) Air

   Pentlandite; medium grey: Pyrrhotite; medium-dark grey

D.   Triangularly disposed pentlandite lamellar texture (x 110) Air

   Lamellar pentlandite; light grey: Pyrrhotite; medium-dark grey:
   Voids; dark

E.   Typical patch-like chalcopyrite grain (x 320) Air

   Chalcopyrite; medium-dark grey: Pentlandite; medium grey: Voids; dark

F.   Chalcopyrite rimming magnetite (x 110) Air

   Magnetite; dark grey: Chalcopyrite; 'pinky'-grey: Pentlandite; light grey
   (bottom left):   Pyrrhotite; light grey (left side, bottom right)

G.   Typical idiomorphic magnetite grain (x 110) Air

   Magnetite; dark grey: Pyrrhotite, medium grey (bottom):   Pentlandite;
   light grey (left margin)

H.   Initial nucleation of violarite in interstitial pentlandite (x 600) Oil

   Pentlandite; medium grey: Violarite; dark grey, spherical: Pyrrhotite;
   medium-dark grey (bottom right):   Voids; dark

Fig.4.5.1.
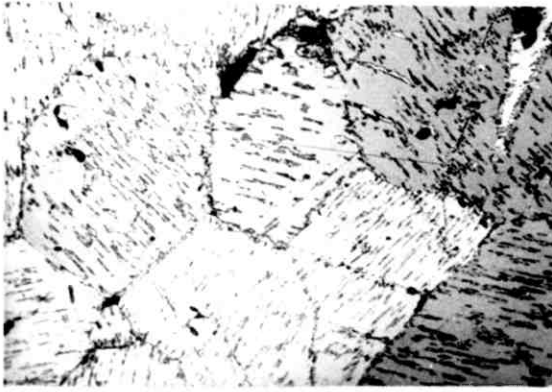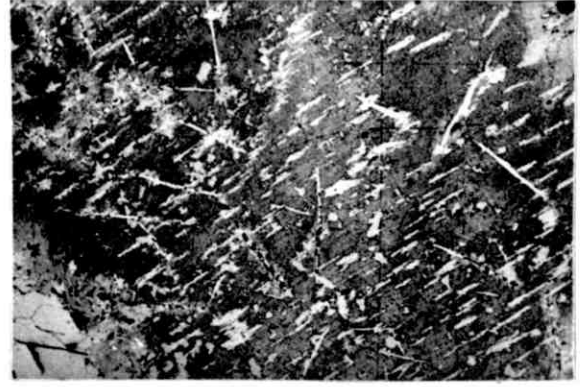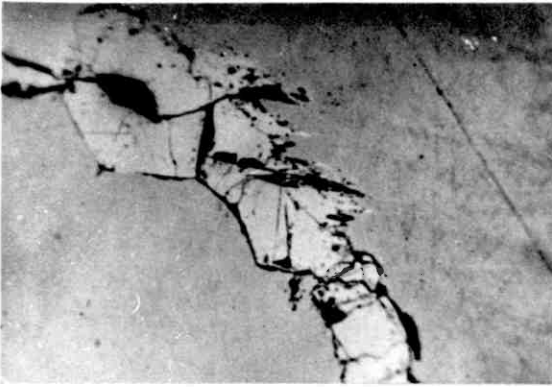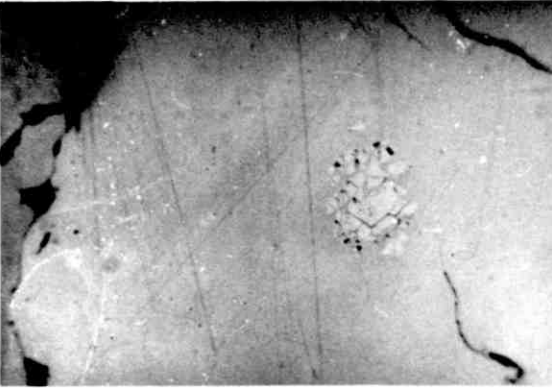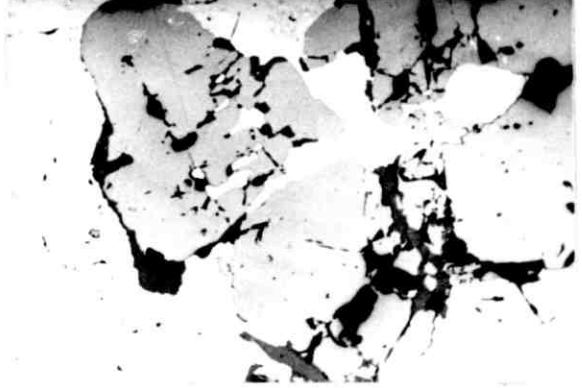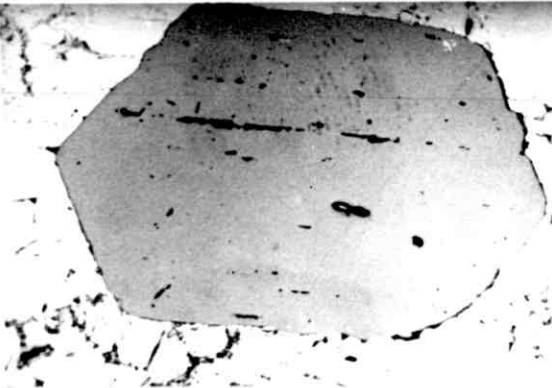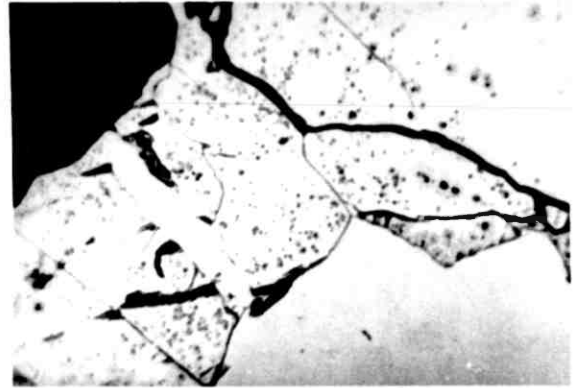
TABLE 4.5.2.   PYRRHOTITE COMPOSITIONS - PHOENIX

Sample	Fe	Ni	S	Co	Cu	Ti	Wt% Total	Atomic Formula Fe_xS_8	Atomic Formula Me_xS_8	Me:S ratio
2138/A3/1	59.89	0.24	39.76	0.88	0.05	0.04	100.84	-	-	-
	(45.99)	(0.18)	(53.17)	(0.64)	(0.03)	(0.02)	-	$Fe_{6.92}S_8$	$Me_{7.05}S_8$	0.88
2138/A5/9	58.51	0.06	39.64	0.80	0.04	0.05	99.10	-	-	-
	(45.56)	(0.05)	(53.77)	(0.59)	(0.03)	(0.03)	-	$Fe_{6.78}S_8$	$Me_{6.88}S_8$	0.86

212

TABLE 4.5.3. PENTLANDITE COMPOSITION – PHOENIX

Sample	Fe	Ni	S	Co	Cu	Ti	Wt% Total	Atomic Formula $Ni_nFe_mS_8$	Atomic Formula Me_xS_8	Me:S ratio
2138/A3/5	30.02	35.37	32.81	1.98	0.13	0.01	100.33	-	-	-
	(24.47)	(27.42)	(46.58)	(1.53)	(0.09)	-	-	$Ni_{4.71}Fe_{4.20}S_8$	$Me_{9.18}S_8$	1.15

TABLE 4.5.4. VIOLARITE AFTER PENTLANDITE COMPOSITIONS – PHOENIX

Sample	Fe	Ni	S	Co	Cu	Ti	Wt% Total	Atomic Formula $Ni_nFe_mS_4$	Atomic Formula Me_xS_4	Me:S ratio
2138/A3/4	24.73	30.87	39.67	1.80	0.10	0.01	97.18	-	-	-
	(19.79)	(23.50)	(55.29)	(1.36)	(0.07)	-	-	$Ni_{1.70}Fe_{1.43}S_4$	$Me_{3.24}S_4$	0.81
2138/A5/6	24.09	29.52	40.39	1.90	0.11	0.02	96.03	-	-	-
	(19.37)	(22.57)	(56.54)	(1.44)	(0.08)	(0.01)	-	$Ni_{1.59}Fe_{1.37}S_4$	$Me_{3.07}S_4$	0.77
2138/A5/10	24.60	28.76	39.93	1.85	0.12	0.02	95.28	-	-	-
	(19.94)	(22.18)	(56.38)	(1.42)	(0.08)	(0.01)	-	$Ni_{1.52}Fe_{1.41}S_4$	$Me_{3.10}S_4$	0.78

214

Fig. 4.5.2. Petrography of Phoenix Sulphide Ore (2)

Scale length = 100 μ

A.   Coalescence of violarite nucleii in pentlandite (x 320) Air

Pentlandite; medium grey: Violarite; dark grey: Voids; black

B.   Violarite fronts growing into pentlandite cleavage blocks (x 110) Air

Pentlandite; light grey: Violarite; medium grey, granular: Pyrrhotite;
medium-dark grey: Voids; black

C.   Typical lamellar growth texture (x 320) Air

Pentlandite/Violarite; light grey: Smythite; medium-grey feather-like
fringes (bottom left, right centre bottom)

D.   Typical mature violarite replacement of interstitial pentlandite (x 220) Air
      Blue-white filter

Violarite species (Vpn and Vpo); light-medium grey, granular: Pyrrhotite;
light grey: Voids; black

E.   Typical smythite development in pyrrhotite (x 220) Oil   Blue-white filter

Smythite; white (right bottom):   Pyrrhotite, light grey: Voids; black

F.   Typical texture of Vpo replacing smythite (x 600) Oil   Blue-white filter

Vpo; medium grey, granular: Smythite, light grey: Pyrrhotite; medium
grey: Voids; black

G.   Fully developed violarite after pyrrhotite (x 320) Air

Violarite species (Vpn and Vpo); light-medium grey, granular: Pyrrhotite;
medium grey: Voids; black

Fig.4.5.2.
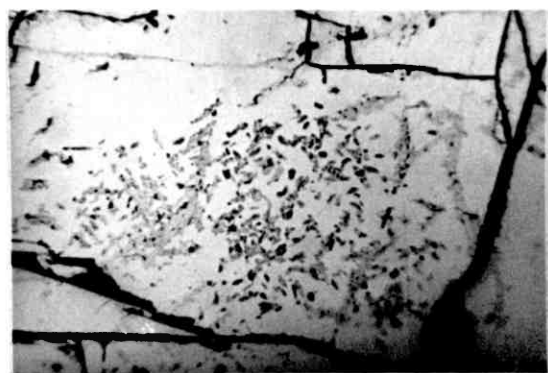
A
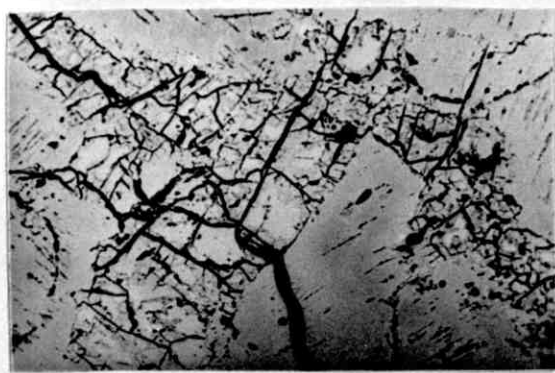
B

C
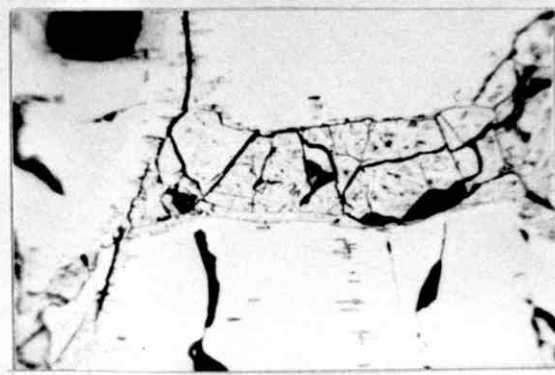
D
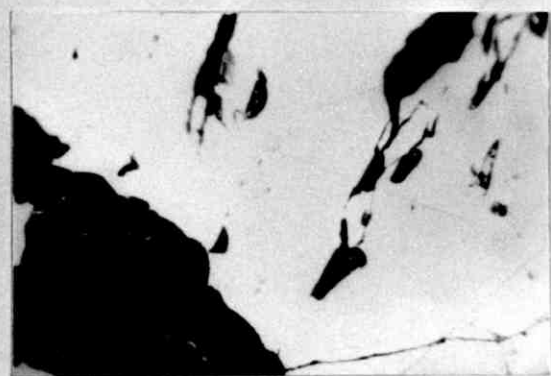
E
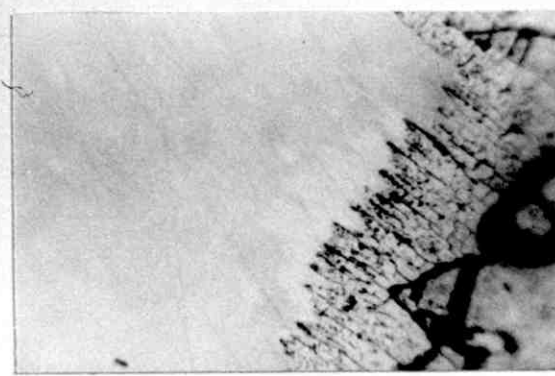
F
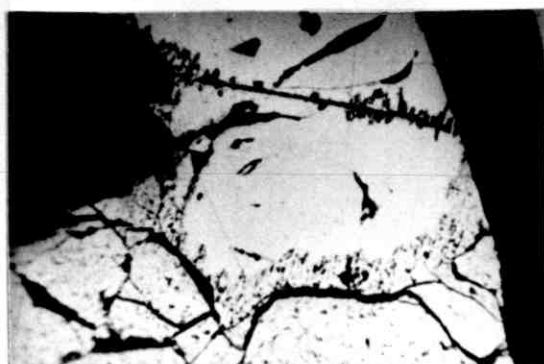
G

generally comprises an outer zone of monoclinic type surrounding a hexagonal core, (Fig.4.5.1B.). This observation is substantiated by the monoclinic composition of the two analysed samples of 'rim' pyrrhotite noted in Table 4.5.2.

Pentlandite averages about 15 percent of Phoenix massive sulphide ore, (Table 4.5.1.). The mineral is present in two textural forms: As a blocky elongate variety interstitial to the pyrrhotite grain matrix, (Fig.4.5.1C.); and as elongate aggregates of flamme lamellae orientated along the 001 cleavage partings in pyrrhotite, (Fig.4.5.1A.). Lamellar pentlandite is however, also commonly present as sets of triangularly-disposed lamellae that exhibit a mutual 60° orientation to each other, (Fig.4.5.1D.). This texture is likely a frozen high temperature ex-solution phenomenon wherein lamellar pentlandite has separated out from a high symmetry (cubic) iron sulphide phase. The two pentlandite varieties occur in approximately equal overall proportions in the sampled massive sulphide material.

The chemical composition of a typical blocky pentlandite grain, (Table 4.5.3.), indicates that the mineral contains appreciable quantities of cobalt, and that the molecular formula corresponds reasonably closely to the theoretical value of Me_9S_8.

Chalcopyrite comprises about 1.5 percent of the primary massive sulphide assemblage, (Table 4.5.1.). The mineral tends however, to be rather heterogenously distributed within the ore. It may be present as large patch-like grains, (Fig.4.5.1E.). More commonly though, chalcopyrite is noted as rims to magnetite grains, and may exhibit extensive replacement of the latter mineral, (Fig.4.5.1F.).

Magnetite comprises about four percent of massive ore, (Table 4.5.1.), although the mineral is rather erratically distributed within the assemblage. It is however, present as rather euhedral, often idiomorphic grains, (Fig.4.5.1G.).

The petrology of the sulphide alteration sequence

Available data indicate that alteration of the Phoenix massive sulphide assemblage is initiated at about 100 metres below surface where pentlandite exhibits incipient alteration to violarite. Both pentlandite varieties are affected by this phenomenon. Replacement of the interstitial form occurs as a gradual coalescence of spherical violarite nucleii developed along the octahedral partings of the parent mineral,

217

(Figs.4.5.1H, and 2A.). Subsequent growth of violarite occurs along broad fronts into the interstitial blocks of pentlandite created by this initial replacement process, (Fig.4.5.2B.). Lamellar pentlandite typically alters to violarite by outward growth from the centre of the individual flammes, (Fig.4.5.2C.).

The chemical compositions of a number of violarite after interstitial pentlandite grains (Vpn) are presented in Table 4.5.4. These data indicate that the analytical totals of this violarite type characteristically summate to less than 100 percent. Further, the corresponding molecular formulae demonstrate the metal-rich non-stoichiometry of interstitial Vpn in the Phoenix deposit.

A comparison of interstitial pentlandite and violarite chemistry is presented in Table 4.5.5. These data demonstrate that the formation of interstitial Vpn at Phoenix is characterised by the release of substantial quantities of both nickel and iron. Further, the significant increase in sulphur that also occurs in consequence of violarite formation very likely constitutes only a relative change since the alteration reaction probably occurs at constant sulphur; as is evidenced by the pseudomorphic replacement texture that is characteristically involved, (Fig.4.5.2D.). The corresponding likely reaction mechanism is set out as Equation 1 in Fig.4.5.3.

The alteration of pentlandite to violarite in Phoenix massive sulphide ore is closely paralleled by a two-stage alteration of pyrrhotite to violarite. In this respect, pyrrhotite undergoes an initial alteration to orange-red anisotropic smythite. This mineral is typically developed as extensive featherlike fringes along pyrrhotite grain borders and grows into the parent mineral along the 001 cleavage partings, (Fig.4.5.2E.)

The chemistry of sampled Phoenix smythite is remarkable in that it contains no detectable nickel, (Table 4.5.6.). Further, it is likely that this nickel deficiency – a phenomenon previously unreported in the literature, is compensated for by a slightly increased iron content. In contrast, though, a comparison of pyrrhotite and smythite chemistry, (Table 4.5.7.), indicates that the replacing mineral faithfully reflects the cobalt content of its parent. The likely reaction mechanism corresponding to the pyrrhotite-smythite alteration process is given in Equation 2 of Fig. 4.5.3.

Progressive formation of violarite (Vpo) from pentlandite is accompanied by the parallel development of violarite from smythite. The replacing violarite is developed as commonly bluish-violet porous feather lamellar fringes that overgrow

Table 4.5.5.   Comparison of pentlandite and violarite (Vpn) compositions

	INTERSTITIAL PENTLANDITE (n = 1)	VIOLARITE AFTER INTERSTITIAL PENTLANDITE (n = 3)
Fe	30.02	24.47
	(24.44)	(19.69)
Ni	35.37	29.72
	(27.39)	(22.75)
S	32.81	40.00
	(46.54)	(56.06)
Co	1.98	1.85
	(1.53)	(1.41)
Cu	0.13	0.11
	(0.10)	(0.08)
Ti	0.01	0.02
	(0.01)	(0.02)
TOTAL (Wt%)	100.33	96.16
Ni:Fe	1.12	1.16
Me:S	1.15	0.79

TABLE 4.5.6. SMYTHITE COMPOSITIONS – PHOENIX

Sample	Fe	Ni	S	Co	Cu	Ti	Wt% Total	Atomic Formula $Fe_m Ni_n S_{11}$	Atomic Formula $Me_x S_{11}$	Me:S ratio
2138/A3/2	58.35	n.d.	41.34	0.75	0.05	0.04	100.53	–	–	–
	(44.52)	–	(54.94)	(0.50)	(0.04)	(0.03)	–	$Fe_{8.91} Ni_{0.00} S_{11}$	$Me_{9.02} S_{11}$	0.82
2138/A5/8	57.61	n.d.	41.36	0.70	0.04	0.03	99.74	–	–	–
	(44.21)	–	(55.28)	(0.51)	(0.03)	(0.02)	–	$Fe_{8.80} Ni_{0.00} S_{11}$	$Me_{8.90} S_{11}$	0.80

Table 4.5.7.   Comparison of pyrrhotite, smythite and Vpo compositions

	PYRRHOTITE (n = 2)	SMYTHITE (n = 2)	VIOLARITE AFTER PYRRHOTITE (n = 3)
Fe	59.20	57.98	26.57
	(45.79)	(44.33)	(21.15)
Ni	0.15	n.d.	28.35
	(0.11)	-	(21.47)
S	39.70	41.35	40.72
	(53.48)	(55.08)	(56.47)
Co	0.77	0.73	1.07
	(0.57)	(0.53)	(0.81)
Cu	0.04	0.04	0.11
	(0.03)	(0.03)	(0.08)
Ti	0.02	0.04	0.04
	(0.02)	(0.03)	(0.03)
TOTAL (Wt%)	99.84	100.13	96.85
Ni:Fe	-	-	1.02
Me:S	0.85	0.82	0.77

TABLE 4.5.8. VIOLARITE AFTER PYRRHOTITE COMPOSITIONS - PHOENIX

Sample	Fe	Ni	S	Co	Cu	Ti	Wt% Total	Atomic Formula $Ni_n Fe_m S_4$	Atomic Formula $Me_x S_4$	Me:S ratio
2138/A3/3	26.68	29.02	40.65	0.96	0.09	0.03	97.43	-	-	-
	(21.16)	(21.89)	(56.16)	(0.72)	(0.07)	(0.02)	-	$Ni_{1.56}Fe_{1.50}S_4$	$Me_{3.13}S_4$	0.78
2138/A5/7	26.75	27.91	40.82	1.12	0.09	0.02	96.72	-	-	-
	(21.31)	(21.15)	(56.63)	(0.85)	(0.07)	(0.01)	-	$Ni_{1.50}Fe_{1.50}S_4$	$Me_{3.07}S_4$	0.77
2138/A5/11	26.30	28.13	40.68	1.13	0.12	0.05	96.40	-	-	-
	(21.02)	(21.39)	(56.65)	(0.85)	(0.08)	(0.03)	-	$Ni_{1.51}Fe_{1.48}S_4$	$Me_{3.07}S_4$	0.77

Table 4.5.9.   Comparison of Vpn and Vpo compositions

	VIOLARITE AFTER PENTLANDITE (n = 3)	VIOLARITE AFTER PYRRHOTITE (n = 3)
Fe	24.47	26.57
	(19.69)	(21.15)
Ni	29.72	28.35
	(19.69)	(21.47)
S	40.00	40.72
	(56.06)	(56.47)
Co	1.85	1.07
	(1.41)	(0.81)
Cu	0.11	0.11
	(0.08)	(0.08)
Ti	0.02	0.04
	(0.02)	(0.03)
TOTAL (Wt%)	96.16	96.85
Ni:Fe	1.16	1.02
Me:S	0.79	0.77

FIG. 4.5.3. CHEMISTRY OF THE PHOENIX ALTERATION SEQUENCE

SHALLOW ANODIC WEATHERING REACTIONS

12 $FeS_2 + 8H_2O = Fe^{2+} + 2SO_4^{2-} + 16H + 14e^-$
Marcasite

11 $Ni_{1.52}Fe_{1.50}Co_{0.06}S_4 + 16H_2O = 1.52Ni^{2+} + 1.50Fe^{2+} + 0.06Co^{2+} + 4SO_4^{2-} + 32H^+ + 30.16e^-$
Violarite (after Po)

10 $Ni_{1.62}Fe_{1.41}Co_{0.10}S_4 + 16H_2O = 1.62Ni^{2+} + 1.41Fe^{2+} + 0.10Co^{2+} + 4SO_4^{2-} + 32H^+ + 30.26e^-$
Violarite (after Pn)

9 $FeS_2 + 8H_2O + 1.50OH^- = 0.50Fe_2O_3 + 2SO_4^{2-} + 17.5H^+ + 15e^-$
Marcasite   Hematite

8 $CuFeS_2 + 8H_2O + 1.50OH^- = 0.5Fe_2O_3 + 2SO_4^{2-} + Cu^{2+} + 17.5H^+ + 17e^-$
Chalcopyrite   Hematite

7 $FeS_2 + 8H_2O + 2OH^- = FeOOH + 2SO_4^{2-} + 17H^+ + 15e^-$
Marcasite   Goethite

6 $Ni_{1.52}Fe_{1.50}Co_{0.06}S_4 + 16H_2O + 3.0OH^- = 1.50FeOOH + 1.52Ni^{2+} + 0.06Co^{2+} + 4SO_4^{2-} + 33.50H^+$
Violarite (after Po)   Goethite $+ 31.66e^-$

5 $Ni_{1.62}Fe_{1.41}Co_{0.10}S_4 + 16H_2O + 2.82OH^- = 1.41FeOOH + 1.62Ni^{2+} + 0.10Co^{2+} + 4SO_4^{2-} + 33.41H^+$
Violarite (after Pn)   Goethite $+ 31.67e^-$

DEEP ANODIC WEATHERING REACTIONS

4 $Fe_{6.85}Co_{0.09}S_8 = 4FeS_2 + 2.85Fe^{2+} + 0.09Co^{2+} + 5.88e^-$
Monoclinic Po   Marcasite

3 $Fe_{8.85}Co_{0.11}S_{11} + 4.18Ni^{2+} + 0.06Co^{2+} = 2.75Ni_{1.52}Fe_{1.50}Co_{0.06}S_4 + 4.73Fe^{2+} + 0.98e^-$
Smythite   Violarite (after Po)

2 $Fe_{6.85}Co_{0.09}S_8 = 0.73Fe_{8.85}Co_{0.11}S_{11} + 0.42Fe^{2+} + 0.82e^-$
Monoclinic Po   Smythite

1 $Ni_{4.71}Fe_{4.20}Co_{0.26}S_8 = 2Ni_{1.62}Fe_{1.41}Co_{0.10}S_4 + 1.47Ni^{2+} + 1.38Fe^{2+} + 0.06Co^{2+} + 5.82e^-$
Pentlandite   Violarite (after Pn)

smythite inwards from pyrrhotite grain borders, (Fig.4.5.2F.). Progressive growth of this violarite mineral eventually leads to the total replacement of the smythite, (Fig.4.5.2G.).

The chemistry of a suite of violarite after pyrrhotite (Vpo) grains is presented in Table 4.5.8. These data indicate that low analysis totals and metal-rich stoichiometries typify this violarite species at Phoenix. Contrastingly, however, a chemical comparison of the two types of analysed violarite, (Table 4.5.9.), demonstrates that the ore metal-impoverished provenence of Vpo is reflected in its relatively low content of nickel and cobalt compared with that of interstitial Vpn.

This point is further emphasised when a direct comparison of pyrrhotite, smythite and Vpo chemistry is made, (Table 4.5.7.). Here, the dependence of Vpo formation on the availability of nickel released during pentlandite alteration is apparent from the compositional differences of the three genetically related minerals, and is further shown in the form of the corresponding reaction mechanism for the smythite-violarite alteration process, (Equation 3, Fig.4.5.3.).

Present data indicate that the transition assemblage of Vpn, pyrrhotite, Vpo, chalcopyrite and magnetite is present up to at least the 27m. level in the oxidation profile. No sulphide data are however to hand above this level, but it is likely, on the textural evidence available from oxide material, that pyrrhotite undergoes a general alteration to secondary iron disulphides before the water table is reached at about 20-25 metres b.s., (Equation 4, Fig.4.5.3.).

The petrology of the oxide zone

Available data indicate that the supergene-altered sulphide profile at Phoenix is overlain by an extensive oxide zone. This extends to the surface outcrop from the water table which is situated at about 20-25 metres b.s.

The Phoenix oxide zone mineral assemblage comprises goethite, hematite and silica, (Table 4.5.1.). Goethite averages about 65 percent of this assemblage, but exhibits wide variability within the sample set, (Table 4.5.1.). The mineral, however, forms a very important part of the oxide zone material, and this promenence is reflected by the textural relationships in which it is observed. In this respect, goethite is important in the preservation of relic and skeletal textures after all

principal members of the Phoenix secondary sulphide suite. It is noted as pseudomorphic replacements of interstitial Vpn, (Fig.4.5.4A.), and in one instance has been observed forming from co-existing violarite, (Fig.4.5.4B.). Further, goethite is also present as mimic replacements to both lamellar Vpn, (Fig.4.5.4C.), and Vpo, (Fig.4.5.4D.).

Goethite commonly also forms boxwork and pseudomorphic structures after mimicked primary pyrrhotite and secondary iron disulphide textural forms. Here, it is quite commonly observed as pseudomorphs after; pyrrhotite cleavage structures, (Fig.4.5.4E.); bird's eye forms, (Fig.4.5.4F.); and polygonal pyrrhotite grains, (Fig.4.5.4G.). Rather more rarely, goethite occurs associated with hematite as boxwork structures after chalcopyrite, (Fig.4.5.4H.).

Pseudomorphed sulphide textures are not however ubiquitously present in Phoenix massive oxide. Goethite is hence quite commonly noted as massive amorphous developments after secondary sulphides, (Fig.4.5.5A.); and as late stage precipitation and recrystallisation textures, (Figs.4.5.5B. and 5C. respectively.).

Hematite comprises about 30 percent of the sampled Phoenix oxide zone, although it too exhibits considerable inter-sample variation, (Table 4.5.1.). Where present, this mineral typically occurs as relic structures after the secondary sulphide assemblage. In this respect, hematite is most commonly noted as pseudomorphs after mimicked pyrrhotite and secondary iron disulphide structures. Hence it chiefly and most commonly occurs as boxworks after secondary pyrite, (Fig.4.5.5D.); as bird's eye structures, (Fig.4.5.5E.); as secondary mimicked pyrrhotite boxworks, (Fig.4.5.5F.), and cleavage, (Fig.4.5.5G.); and as relic pyrrhotite twinning structures, (Fig.4.5.5H.). In addition, hematite is also present as boxworks after chalcopyrite, (Fig.4.5.5I.). Hematite is not observed as replacements of violarite species at Phoenix, although it does very commonly occur as octahedral cleavage mimics in goethite pseudomorphs after interstitial Vpn, (Fig.4.5.4A.) The likely reaction mechanisms corresponding to the pseudomorphic replacement of individual ore minerals by goethite and hematite are set out in the appropriate Equations in Fig.4.5.3.

Silica forms only a minor part of the Phoenix oxide zone and represents about three to five percent of the mineral assemblage, (Table 4.5.1.). Where present it typically forms as cavity fillings and may pseudomorphically preserve leached sulphide grains, (Fig.4.5.5J.). The mineral is probably derived from the in situ

226

Fig. 4.5.4. Petrography of the Phoenix Gossan (1)

Scale length = 100 μ

A.   Goethite mimics after interstitial violarite (x 600) Oil   Blue-white filter

Goethite; dark grey: Hematite; light grey. Hematite defines the relic pentlandite cleavage

B.   In situ formation of goethite from violarite (x 220) Oil

Oxidising violarite; grey-black: Goethite; medium greys: Voids; black

C.   Goethite mimics after lamellar violarite (x 220) Oil   Partly crossed nicols

Goethite; medium greys: Voids; black

D.   Goethite mimics after violarite after pyrrhotite (x 600) Oil   Blue-white filter

Goethite; greys: Voids; black. Vpo feathering well preserved (top and right borders)

E.   Goethite mimics after mimicked pyrrhotite cleavage (x 220) Oil   Blue-white filter

goethite; greys: Voids; black

F.   Goethite mimic after marcasite bird's eye structure (x 220) Oil
Partly crossed nicols

Goethite; medium grey: Hematite; light grey: Voids; black

G.   Goethite mimic after pyrrhotite (x 220) Oil   Blue-white filter

Goethite; medium grey: Marcasite; whitish: Hematite; light grey:
Voids; black.
Sub-parallel kink-zone traces are recognisable

H.   Composite goethite/hematite boxwork after chalcopyrite (x 220) Oil
Blue-white filter

Goethite; medium grey: Hematite; light grey: Voids; black. A small chalcopyrite relic is present (right centre) . Cell walls are goethite sheathed with hematite.

Fig.4.5.4.

228
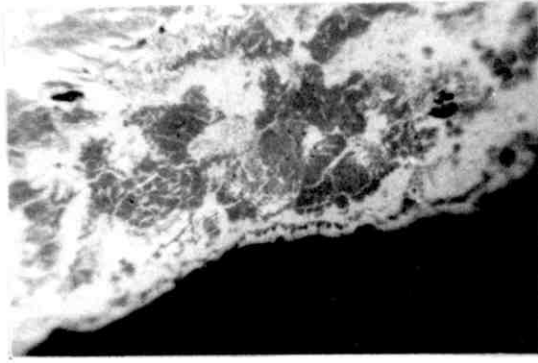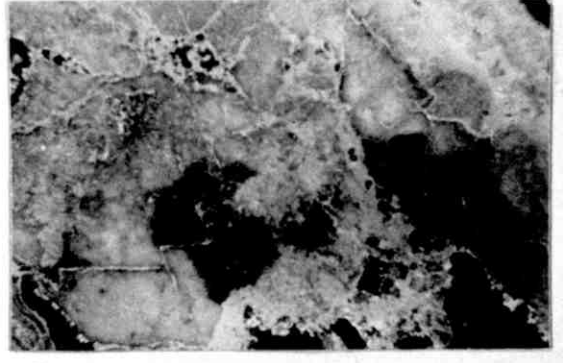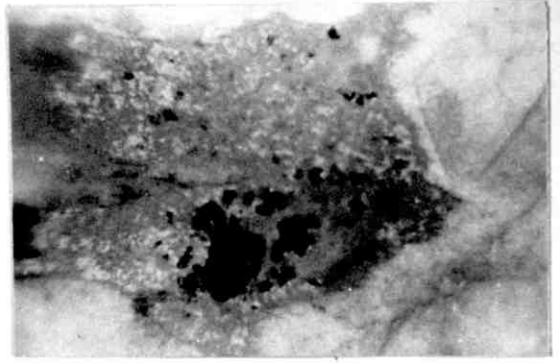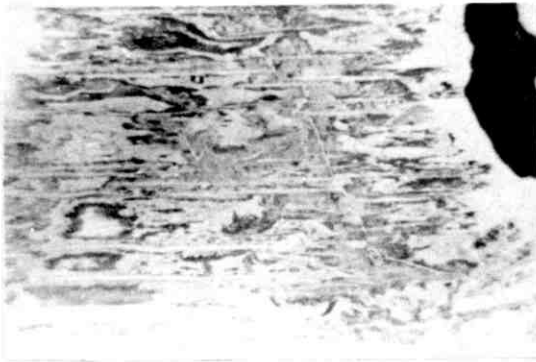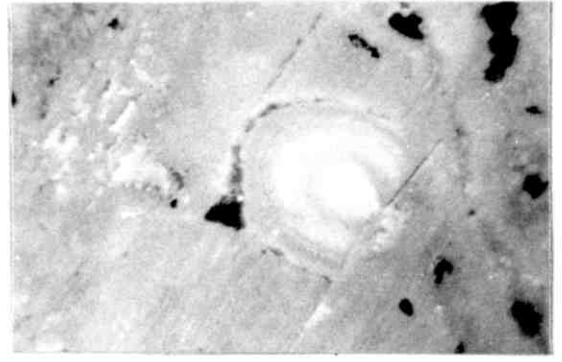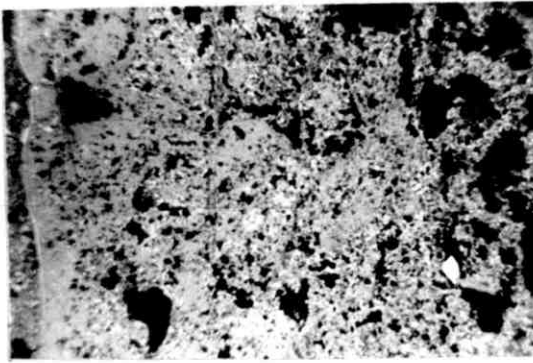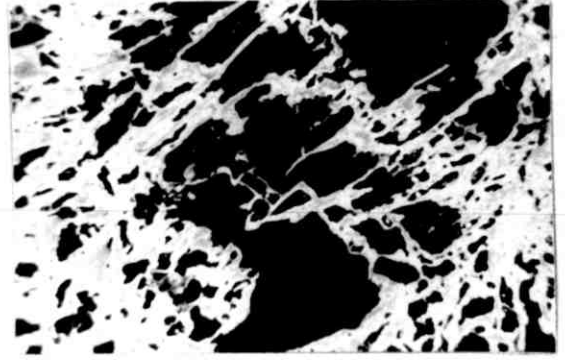
Fig. 4.5.5. Petrography of the Phoenix Gossan (2)

Scale length = 100 μ

A.   Goethite after secondary pyrite (x 220) Oil

    Goethite; medium grey: Pyrite; white: Voids black

B.   Typical late-stage drusy goethite (x 220) Oil   Partly crossed nicols

C.   Recrystallisation textures of goethite and hematite (x 220) Oil   Blue-white filter

    Goethite; dark grey: Hematite; light grey: Voids; black

D.   Hematite boxwork after secondary pyrite (x 220) Oil   Blue-white filter

    Pyrite relics; white: Goethite; medium grey: Hematite; light grey

E.   Hematite mimic after marcasite bird's eye structure (x 220) Oil

    Hematite; light grey: Goethite; medium grey: Voids; black

F.   Hematite boxwork after mimicked pyrrhotite (x 220) Oil   Blue-white filter

G.   Hematite mimics after mimicked pyrrhotite cleavage (x 110) Oil

    Hematite; light grey: Goethite; medium grey: Voids; black

H.   Hematite mimics after mimicked pyrrhotite twinning (x 220) Oil   Blue-white filter

    Hematite; light grey: Goethite; medium grey: Voids; Black

I.   Hematite boxwork after chalcopyrite (x 220) Oil   Blue-white filter

    Hematite; light-medium grey: Chalcopyrite relics; white: Voids; black

J.   Silica interstitial filling to leached cavities (x 220) Oil

    Goethite; medium grey: Silica; dark grey, blotchy

Fig.4.5.5.
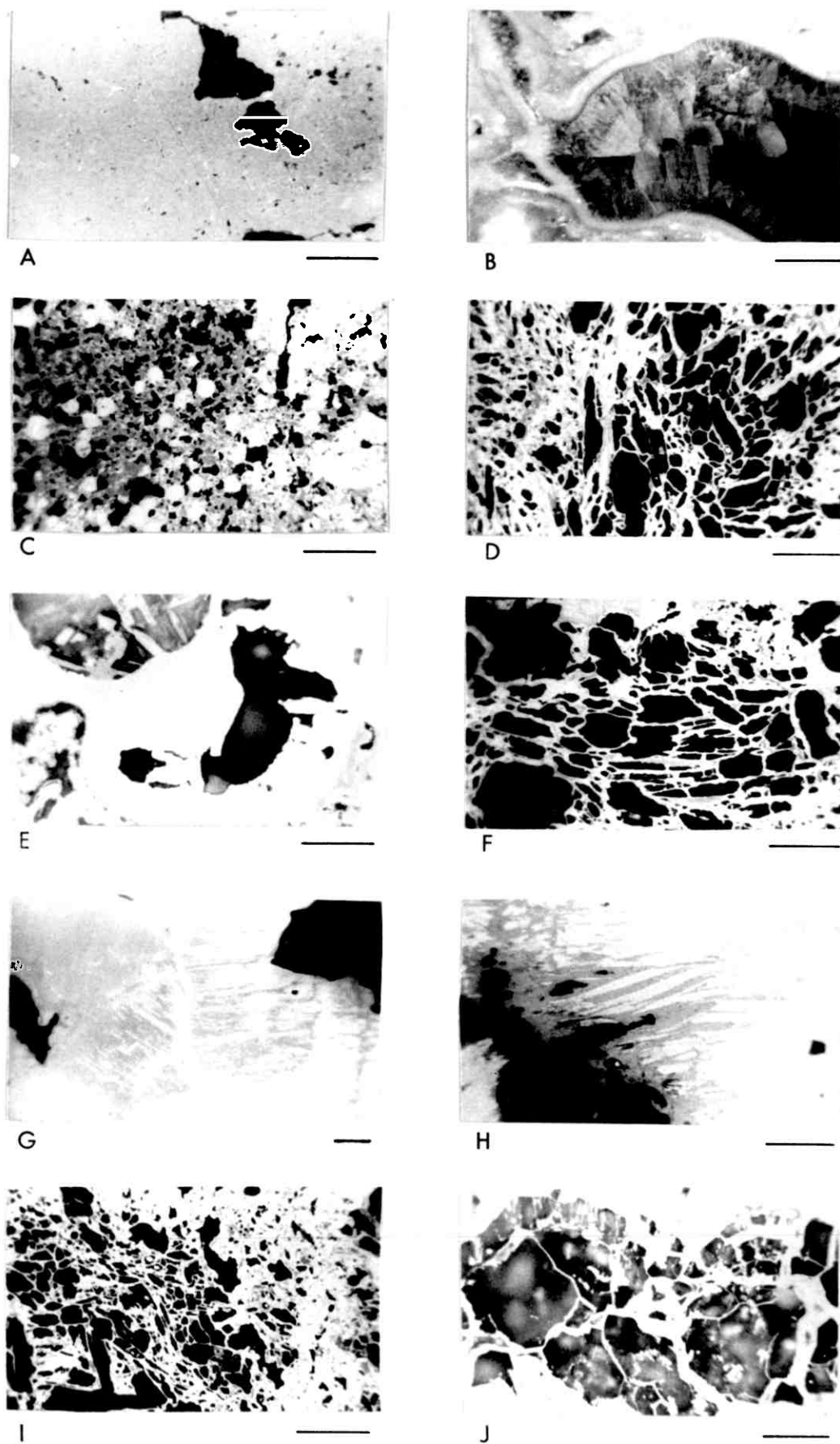
weathering of silicates that are associated with the former massive sulphide assemblage.

The above documentary evidence of goethite and hematite textural relations in the Phoenix oxide zone indicates that the secondary sulphide assemblage is commonly replaced in situ by these minerals during pervasive leaching at the water table. It is hence possible to formulate the likely reaction mechanisms corresponding to these mineral replacement phenomena, and these are set out in the appropriate equations within Fig.4.5.3.

The likely variation of mean density and porosity within the Phoenix alteration sequence is presented in Fig.4.5.6. The forms of both mean profiles closely parallel the physico-chemical changes that occur during the progressive oxidation of the Phoenix primary sulphide assemblage. In this respect the changes in mean density and porosity that occur across the 100-25m. vertical interval correspond with the gradual development of the secondary assemblage of violarite and marcasite. The alteration across the 20m. horizon corresponds to the dramatic changes brought about by pervasive sulphide leaching and by the subsequent development of the equivalent iron oxide assemblage.

The bulk chemistry of sulphide alteration

The mean variation of the analysed suite of important major and minor elements within the Phoenix massive sulphide profile is given in Fig.4.5.7. The constancy of element mean contents between the 100m. and 25m. levels indicates that the primary sulphide suite acts as an effectively closed chemical system during its gradual alteration to the secondary assemblage of violarite and marcasite. In contrast, the documented changes that occur across the sulphide-oxide transition (Approx. 20m. level), typically demonstrate the individual chemical response of each element to the high Eh-Low pH environment produced by the oxidative leaching of the secondary sulphide assemblage at this level.

Fig. 4.5.6. Mean True Density and Porosity profiles – Phoenix
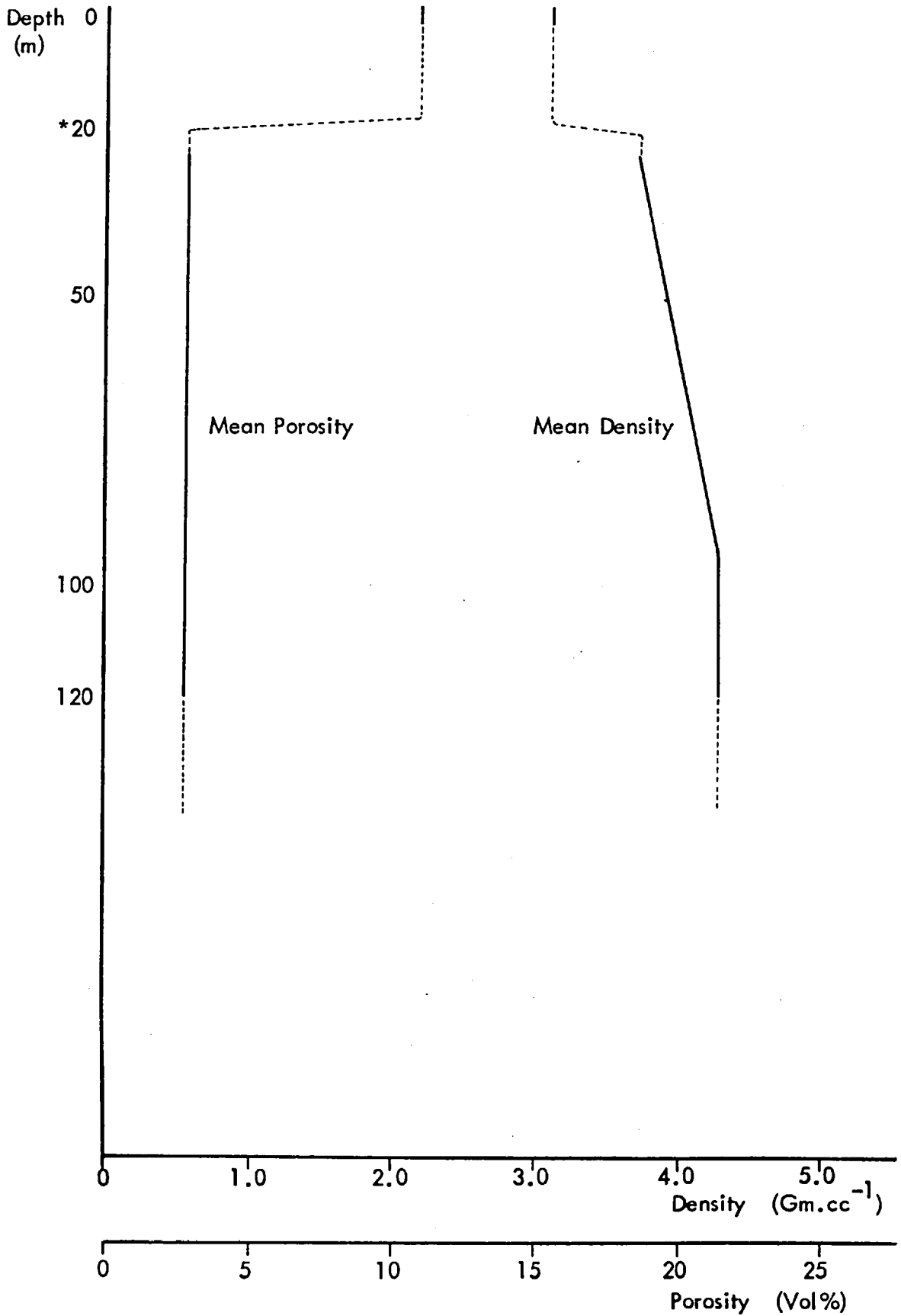
* Approximate position of the Water table

Fig. 4.5.7. Chemical Variations in Alteration Profile – Phoenix

* Approximate position of the water table

Element content (Gm.Equivs.cc^{-1})
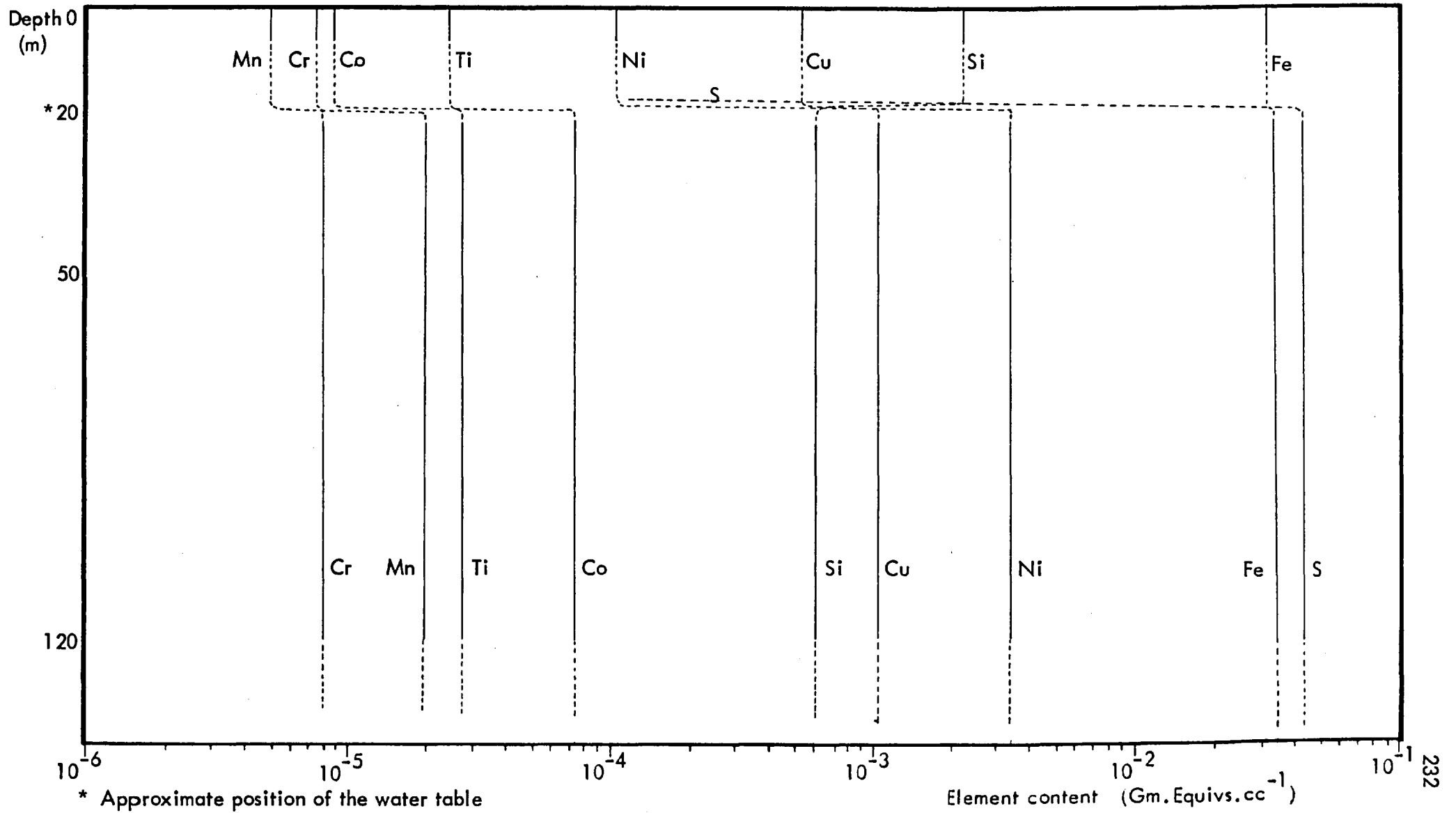
4.6. SUPERGENE ALTERATION IN THE SELKIRK DEPOSIT,,BOTSWANA

The Selkirk deposit occurs as a tabular ore body that is located within the fold nose and along the steeply plunging axis of a wedge-shaped (folded) metatroctolite stock. Massive sulphide is located in the fold core and is surrounded by disseminated ore within the host metatroctolite, (Section 2.4.). The near surface sulphide alteration sequence documented in the present study is derived from sampled drillcore material, (sulphides), and from surface specimens, (oxide material).

The petrology of the primary sulphide assemblage

The Selkirk primary sulphide assemblage consists of pyrrhotite and pentlandite with minor amounts of chalcopyrite, magnetite and silicates, (Table 4.6.1.). Pyrrhotite comprises about 80 percent of the primary ore and is present as an interlocking. mosaic matrix of generally equant grains, (Fig.4.6.1A.). Chemical data on a suite of pyrrhotites, (Table 4.6.2.), indicate that this mineral generally contains variable amounts of cobalt but no detectable nickel. Further, the metal-to-sulphur ratios of this grain suite demonstrate that pyrrhotite is exclusively present as the monoclinic variety in the Selkirk deposit.

Pentlandite forms eight percent of the primary sulphide assemblage, (Table 4.6.1.). It is present in two textural varieties; as a predominant elongate stringer type located along pyrrhotite grain borders, (Fig.4.6.1B.); and as a less common flamme lamellar form present as orientated aggregates within the pyrrhotite grains themselves, (Fig.4.6.1C.). The chemical compositions of a suite of interstitial (stringer) pentlandite grains are presented in Table 4.6.3. These data show that Selkirk pentlandite is typified by relatively constant absolute and relative proportions of iron and nickel, but that cobalt contents exhibit considerable inter-grain variation. Further, the equivalent metal-to-sulphur ratios demonstrate that this mineral possesses a typically metal-rich non-stoichiometric molecular formula in the Selkirk deposit.

Chalcopyrite averages about three percent of primary ore, although its distribution within the sulphide assemblage is typically heterogeneous, (Table 4.6.1.). The mineral is present in a variety of textural forms but is most commonly associated with magnetite as peripheral rims and it typically exhibits a partial replacement of the spinel, (Fig.4.6.1D.). Further, the chemical composition of a single representative chalcopyrite grain, (Table 4.6.4.), indicates that the mineral

TABLE 4.6.1. SUMMARY DATA OF SULPHIDE ALTERATION - SELKIRK

Depth (m)	Alteration Zone	No. of Samples (n)	MINERALOGY (Means and ranges) Volume % Units								Physical data Den gm/cc	Por %	GEOCHEMISTRY Wt.% Units S	Fe	SiO$_2$	MgO	Al$_2$O$_3$	CO$_3$	p.p.m. Units Ni	Cu	Mn	Cr	Co	Ti
	Oxide	15	Hm 2.0	Gt 0.0	Si 1.0						3.10	0.5	N/A	44.22	0.85	0.20	0.40	N/A	126	399	45	30	30	66
20			50.0	37.5	13.0						3.59	5.0		56.12	9.91	0.27	1.13		696	2279	73	709	53	462
			92.0	97.0	30.0						4.10	9.3		62.07	28.04	0.30	2.30		2365	5296	119	1643	164	1733
	Violarite – pyrite	no data																						
25	Transition	4	Po 80.0	Pn 0.00	Vi 1.50	Cp 0.50	Mt 0.50	Sil N/A	Py 0.00		4.20	0.8	35.87	56.20	0.00	0.10	0.00	N/A	25091	232	104	30	1172	114
			82.0	2.75	4.25	3.75	5.80	N/A	0.75		4.35	4.3	36.88	57.37	0.28	0.13	0.10		26609	16128	158	33	1249	275
			85.0	8.50	7.00	7.50	8.00		3.00		4.60	8.4	38.37	57.91	0.62	0.20	0.20		27275	22902	290	41	1351	582
~45	Primary	3	Po 80.0	Pn	–	Cp 0.50	Mt 0.00	Sil 0.0			4.20	2.3	35.19	57.08	0.23	0.10	0.00	N/A	21712	30	201	30	709	312
			81.7	8.00		3.00	5.20	1.7			4.35	3.8	36.66	58.41	0.55	0.17	0.10		22586	11896	733	66	941	529
			85.0			5.00	8.00	5.0			4.50	5.5	39.02	59.37	0.99	0.30	0.20		23605	23948	1709	137	1015	653

TABLE 4.6.2. PYRRHOTITE COMPOSITIONS - SELKIRK

Sample	Fe	Ni	S	Co	Cu	Ti	Wt% Total	Atomic Formula Fe_xS_8	Atomic Formula Me_xS_8	Me:S ratio
2162/A1/4	60.31	n.d.	39.90	0.71	0.03	0.03	101.06	-	-	-
	(46.21)	-	(53.26)	(0.52)	(0.02)	(0.02)	-	$Fe_{6.94}S_8$	$Me_{7.02}S_8$	0.88
2164/A2/9	59.98	n.d.	39.64	0.83	0.05	0.01	100.51	-	-	-
	(46.19)	-	(53.17)	(0.60)	(0.04)	-	-	$Fe_{6.95}S_8$	$Me_{7.05}S_8$	0.88
2172/A4/45	60.17	n.d.	39.22	n.d.	0.13	0.05	99.58	-	-	-
	(46.77)	-	(53.10)	-	(0.09)	(0.05)	-	$Fe_{7.05}S_8$	$Me_{7.07}S_8$	0.88
2172/A4/48	59.51	n.d.	40.37	n.d.	0.06	0.06	98.55	-	-	-
	(47.26)	-	(52.69)	-	(0.05)	(0.04)	-	$Fe_{7.18}S_8$	$Me_{7.19}S_8$	0.90

TABLE 4.6.3.   INTERSTITIAL PENTLANDITE COMPOSITIONS – SELKIRK

Sample	Fe	Ni	S	Co	Cu	Ti	Wt% Total	Atomic Formula $Ni_n Fe_m S_8$	Atomic Formula $Me_x S_8$	Me:S ratio
2172/A2/40	30.50	32.93	32.29	2.57	0.17	0.04	98.50	–	–	–
	(25.04)	(25.71)	(47.09)	(2.00)	(0.12)	(0.04)	–	$Ni_{4.37}Fe_{4.25}S_8$	$Me_{8.99}S_8$	1.12
2172/A3/41	30.34	32.91	32.61	2.48	0.16	0.04	98.54	–	–	–
	(25.08)	(25.88)	(46.96)	(1.94)	(0.11)	(0.04)	–	$Ni_{4.41}Fe_{4.28}S_8$	$Me_{9.08}S_8$	1.14
2172/A4/43	30.44	33.42	31.95	2.99	0.16	0.02	98.98	–	–	–
	(25.18)	(26.31)	(46.03)	(2.35)	(0.12)	(0.02)		$Ni_{4.57}Fe_{4.38}S_8$	$Me_{9.38}S_8$	1.17
2172/A4/44	29.65	34.65	32.48	2.54	0.15	0.05	99.09	–	–	–
	(24.43)	(26.98)	(46.62)	(1.82)	(0.11)	(0.05)	–	$Ni_{4.63}Fe_{4.19}S_8$	$Me_{9.16}S_8$	1.15
2172/A4/46	31.25	33.55	32.17	2.01	0.16	0.05	99.19	–	–	–
	(25.76)	(26.31)	(46.20)	(1.57)	(0.12)	(0.05)	–	$Ni_{4.56}Fe_{4.46}S_8$	$Me_{9.32}S_8$	1.17
2172/A4/47	30.84	33.72	32.43	1.90	0.16	0.01	99.06	–	–	–
	(25.41)	(26.43)	(46.55)	(1.49)	(0.12)	–	–	$Ni_{4.18}Fe_{4.02}S_8$	$Me_{9.19}S_8$	1.15

TABLE 4.6.3. CONCLUDED

Sample	Fe	Ni	S	Co	Cu	Ti	Wt% Total	Atomic Formula $Ni_n Fe_m S_8$	Atomic Formula $Me_x S_8$	Me:S ratio
2162/A1/1	30.84	33.36	32.86	3.70	0.14	n.d.	100.90	-	-	-
	(24.98)	(25.71)	(46.37)	(2.84)	(0.10)	-	-	$Ni_{4.44} Fe_{4.31} S_8$	$Me_{9.26} S_8$	1.16
2162/A2/6	30.31	32.70	32.65	3.80	0.22	0.02	99.68	-	-	-
	(24.83)	(25.48)	(46.59)	(2.95)	(0.16)	(0.01)	-	$Ni_{4.38} Fe_{4.26} S_8$	$Me_{9.18} S_8$	1.15
2162/A2/12	29.64	32.29	32.62	3.55	0.13	0.02	98.25	-	-	-
	(24.56)	(25.45)	(47.08)	(2.79)	(0.10)	(0.02)	-	$Ni_{4.33} Fe_{4.17} S_8$	$Me_{8.99} S_8$	1.12

TABLE 4.6.4. CHALCOPYRITE COMPOSITION - SELKIRK

Sample	Fe	Ni	S	Co	Cu	Ti	Wt% Total	Atomic Formula $Cu_n Fe_m S_2$	Atomic Formula $Me_x S_2$	Me:S ratio
2162/A2/8	30.77	0.01	34.91	0.62	34.26	0.02	100.58	-	-	-
	(25.16)	-	(49.72)	(0.48)	(24.63)	(0.01)	-	$Cu_{0.99} Fe_{1.01} S_2$	$Me_{2.02} S_2$	1.01

contains measurable cobalt, but that little nickel is present. The corresponding molecular formula does not deviate significantly from the theoretical value.

Magnetite averages about five percent of Selkirk massive primary ore but is rather heterogenously distributed within the ore assemblage, (Table 4.6.1.). The spinel is commonly present as typically equant grain forms and these commonly exhibit smooth rounded outlines, (Fig.4.6.1A.).

The petrology of the sulphide alteration sequence

Available data indicate that initial sulphide alteration at Selkirk occurs at about the 45m. level with the incipient alteration of pentlandite to violarite. Both pentlandite grain types are affected by this replacement process. In the interstitial variety, violarite nucleation typically occurs as small spherules located along the external grain borders or in the vicinity of the octahedral cleavage traces, (Fig. 4.6.1E.). Subsequent growth of violarite generally takes place as broad advancing alteration fronts within the pentlandite cleavage blocks, (Fig.4.6.1F.). This phenomenon eventually leads to the complete pseudomorphic replacement of pentlandite by violarite, (Fig.4.6.1G.). Lamellar pentlandite typically alters to violarite within the centres of individual lamellae and gradually replaces the parent phase in directions both parallel and normal to the flamme long axis.

The chemical compositions of a suite of five violarite after interstitial pentlandite grains (Vpn) are presented in Table 4.6.5. These data indicate that considerable variation in the absolute and relative contents of both nickel and iron typify this violarite species at Selkirk. In contrast, though, cobalt contents remain relatively constant within the sample suite. Further, analytical totals characteristically summate to less than 100 percent in Selkirk interstitial Vpn, and the metal-to-sulphur ratios displayed by the sample suite indicate that metal-rich non-stoichiometric molecular formulae typify this violarite type in the Selkirk deposit.

A comparison of mean interstitial pentlandite and violarite chemistry is presented in Table 4.6.6. The data indicate that pentlandite-violarite alteration at Selkirk is typified by a large absolute and relative iron loss and by a large relative gain in nickel, and further, that there is no significant absolute change in nickel content during the formation of interstitial Vpn. These features are also indicated by the chemistry of in situ violarite formation cited in Table 4.6.7, which also demonstrate

Fig. 4.6.1. Petrography of Selkirk Sulphide Ore

Scale length = 100μ unless otherwise indicated

A.   Typical pyrrhotite matrix mosaic (x 40) Air   Partly crossed nicols

Magnetite; dark grey: Pyrrhotite; light and medium greys

B.   Typical interstitial pentlandite texture (x 110) Air

Pentlandite; white: Pyrrhotite; light grey: Voids; black

C.   Typical lamellar pentlandite texture (x 320) Air

Pentlandite; whitish grey: Pyrrhotite; medium grey: Voids; black

D.   Rimming and partial replacement of magnetite by chalcopyrite (x 110) Air

Magnetite; dark Grey: Chalcopyrite; medium grey (left and centre right border):   Pyrrhotite; medium-dark grey (centre):   Altering pentlandite; light to medium grey, granular (bottom right and right centre border)

E.   Nucleation of violarite in interstitial pentlandite (x 320) Air

Pentlandite; light grey: Violarite; medium grey, spot-like: Pyrrhotite; medium grey: Voids; black

F.   Advanced stage of violarite formation in pentlandite (x 110) Air

Pentlandite; light grey: Violarite; medium-dark grey, granular: Pyrrhotite; light-medium grey: Magnetite; dark grey: Voids; black

G.   Completed pseudomorphic replacement of pentlandite by violarite (x 110) Air

Violarite; dark grey, granular: Pyrrhotite; light to dark grey: Magnetite; dark grey (lower margin):   Voids; black

H.   Corrosion front between pyrrhotite and developing violarite (after Po) (x 600) Oil

Violarite species; light greys; granular: Pyrrhotite, whitish grey: Voids; black

I.   Mimicked pyrrhotite cleavage in secondary pyrite (x 110) Air

Secondary pyrite; light to dark greys, granular: Pyrrhotite; light grey: Magnetite; dark grey (centre):   Carbonate veining; dark grey (lower margin):   Voids; black

240

Fig.4.6.1.
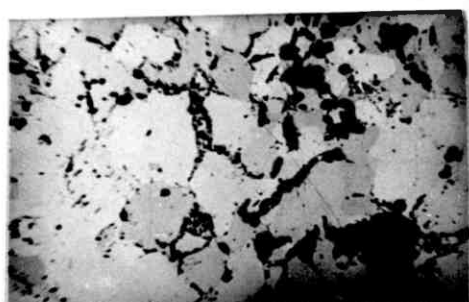
A 1000 μ

B

C
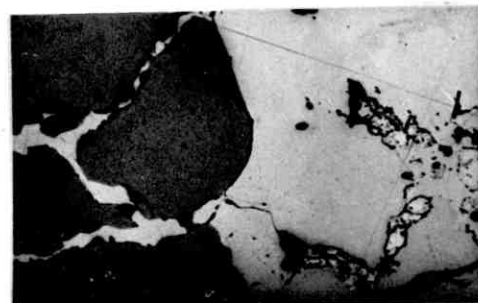
D

E
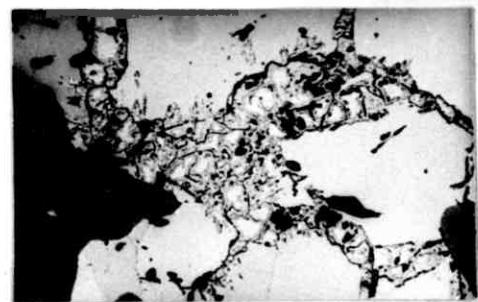
F
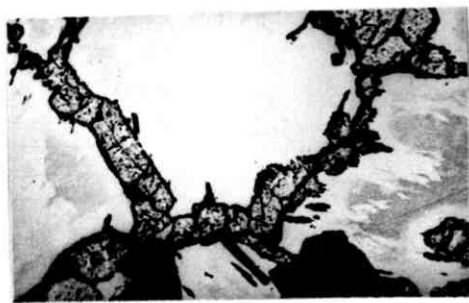
G
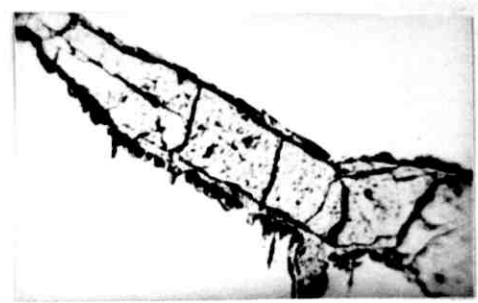
H

I

TABLE 4.6.5.   VIOLARITE AFTER INTERSTITIAL PENTLANDITE COMPOSITIONS - SELKIRK

Sample	Fe	Ni	S	Co	Cu	Ti	Wt% Total	Atomic Formula $Ni_n Fe_m S_4$	Atomic Formula $Me_x S_4$	Me:S ratio
2162/A1/2	19.28	34.59	39.22	3.54	0.10	0.02	96.74	-	-	-
	(15.55)	(26.55)	(55.12)	(2.70)	(0.07)	(0.01)	-	$Ni_{1.92}Fe_{1.13}S_4$	$Me_{3.25}S_4$	0.81
2162/A1/3	21.84	31.39	38.36	3.52	0.12	0.02	95.23	-	-	-
	(17.91)	(24.49)	(54.79)	(2.73)	(0.08)	(0.01)	-	$Ni_{1.79}Fe_{1.31}S_4$	$Me_{3.15}S_4$	0.79
2162/A2/7	19.30	32.60	38.26	3.63	0.21	0.02	94.02	-	-	-
	(16.00)	(25.72)	(55.27)	(2.86)	(0.15)	(0.01)	-	$Ni_{1.86}Fe_{1.16}S_4$	$Me_{3.24}S_4$	0.81
2162/A2/11	19.79	32.89	38.62	2.76	0.11	0.02	94.19	-	-	-
	(16.34)	(25.85)	(55.57)	(2.16)	(0.08)	(0.01)	-	$Ni_{1.86}Fe_{1.17}S_4$	$Me_{3.20}S_4$	0.80
2162/A2/13	16.78	36.03	39.41	3.42	0.12	0.01	95.77	-	-	-
	(13.64)	(27.85)	(55.79)	(2.63)	(0.09)	(0.01)	-	$Ni_{1.99}Fe_{0.98}S_4$	$Me_{3.17}S_4$	0.79

Table 4.6.6.   Comparison of pentlandite, interstitial Vpn and lamellar Vpn compositions

	INTERSTITIAL PENTLANDITE (n = 9)	VIOLARITE AFTER PENTLANDITE (n = 5)	VIOLARITE AFTER PYRRHOTITE (n = 1)
Fe	30.42	19.40	23.07
	(25.05)	(15.88)	(18.39)
Ni	33.26	33.50	29.53
	(26.05)	(26.09)	(22.44)
S	32.45	38.78	39.57
	(46.55)	(55.30)	(54.96)
Co	2.82	3.37	3.23
	(2.20)	(2.62)	(2.44)
Cu	0.16	0.13	2.56
	(0.15)	(0.10)	(1.80)
Ti	0.03	0.02	0.02
	(0.02)	(0.02)	(0.02)
TOTAL (Wt%)	99.13	95.19	97.99
Ni:Fe	1.04	1.64	1.22
Me:S	1.15	0.81	0.82

Table 4.6.7. Composition comparison of in situ pentlandite-violarite alteration

	PENTLANDITE	DAUGHTER VIOLARITE
Fe	29.64	16.78
	(24.59)	(13.64)
Ni	32.29	36.03
	(25.48)	(27.85)
S	32.62	39.41
	(47.14)	(55.79)
Co	3.55	3.42
	(2.79)	(2.63)
Cu	0.13	0.12
	(0.10)	(0.09)
Ti	n.a.	n.a.
	-	-
TOTAL (Wt%)	98.25	95.77
Ni:Fe	1.04	2.04
Me:S	1.12	0.79

that most of the original cobalt is retained in the replacing violarite.

The likely reaction mechanism corresponding to the interstitial pentlandite alteration reaction is given in Equation 1, Fig.4.6.3. This indicates that substantial quantities of iron are released during oxidation of interstitial pentlandite to Vpn, and that a smaller but significant amount of nickel is simultaneously expelled during this process.

The chemical compositions of two violarite after lamellar pentlandite grains, (Table 4.6.8.), demonstrate that this violarite type probably exhibits quite a wide variation in both absolute and relative metal contents. Available data on this species indicate however that it is also characterised by low analytical totals and by a metal-rich (though variable) non-stoichiometric molecular formula.

Further, a comparison of interstitial and lamellar Vpn chemistries, (Table 4.6.6.) demonstrates on available data that the interstitial variety is relatively nickel-rich compared with the lamellar form. It is likely that the difference is due chiefly to the parent lamellar pentlandite having ex-solved late from an ore-metal depleted pyrrhotite (Table 4.6.2.).

Incipient alteration of pyrrhotite occurs once Vpn formation has been initiated. Current data indicate that pyrrhotite is directly replaced by violarite (Vpo) and that no intermediate smythite transition phase is present in the alteration sequence developed at Selkirk. This replacement takes the form of laterally extensive bluish porous feather lamellae that typically develop along pyrrhotite/pentlandite grain borders and grow into the parent pyrrhotite along the 001 cleavage partings. Vpo growth is typically preceded by a corrosion front, (Fig.4.6.1H), and indicates that pyrrhotite undergoes dissolution during this alteration process.

The chemical composition of a single Vpo grain, (Table 4.6.9.), indicates that this violarite species is probably iron-rich compared to the two documented forms after pentlandite. Further, it appears likely that Vpo is relatively poor only in nickel since available data indicate that cobalt contents are comparable for the three violarite species at Selkirk. The very high copper content of the sampled Vpo grain is however, unlikely to be generally significant. But it probably indicates that Vpo composition can vary with the concentration of suitable metals available during the growth of the mineral lattice. In addition, Table 4.6.9. also indicates that Selkirk Vpo shares with interstitial and lamellar Vpn the possession of low

TABLE 4.6.8. VIOLARITE AFTER LAMELLAR PENTLANDITE COMPOSITIONS - SELKIRK

Sample	Fe	Ni	S	Co	Cu	Ti	Wt% Total	Atomic Formula $Ni_nFe_mS_4$	Atomic Formula Me_xS_4	Me:S ratio
2164/A1/5	24.29	31.88	39.06	3.13	0.11	n.d.	98.46	-	-	-
	(19.32)	(24.12)	(54.12)	(2.36)	(0.08)	-	-	$Ni_{1.78}Fe_{1.43}S_4$	$Me_{3.39}S_4$	0.85
2162/A2/10	19.52	34.24	41.58	2.95	0.11	0.02	98.42	-	-	-
	(15.32)	(25.56)	(56.83)	(2.19)	(0.08)	(0.02)	-	$Ni_{1.80}Fe_{1.08}S_4$	$Me_{3.04}S_4$	0.76

246

Table 4.6.9.   Comparison of pyrrhotite and violarite (Vpo) compositions

	PYRRHOTITE (n = 4)	VIOLARITE AFTER PYRRHOTITE (n = 1)
Fe	59.99	23.07
	(46.46)	(18.39)
Ni	n.d.	29.53
	-	(22.44)
S	39.42	39.57
	(53.18)	(54.96)
Co	0.39	3.23
	(0.28)	(2.44)
Cu	0.07	2.56
	(0.05)	(1.80)
Ti	0.04	0.02
	(0.04)	(0.02)
TOTAL (Wt%)	99.82	97.99
Ni:Fe	-	1.22
Me:S	0.87	0.82

analytical totals and a metal-rich non-standard stoichiometry.

A comparison of pyrrhotite and violarite after pyrrhotite compositions, (Table 4.6.9.), demonstrates the large quantities of free ore metals that are required to form violarite from nickel - and cobalt-poor Selkirk pyrrhotite. It is however very probable that the required material is derived from that expelled during the alteration of adjacent pentlandite to violarite. The reaction mechanism corresponding to Vpo formation is presented in Equation 2 of Fig.4.6.3.

Available data imply that the assemblage Vpn, pyrrhotite, Vpo, chalcopyrite and magnetite is probably present between the 50m. and 25m. levels in the Selkirk alteration profile. Above about 40m. however, residual pyrrhotite exhibits an increasing tendency to be replaced by secondary pyrite, (Table 4.6.1.). This alteration process is localised within the sampled material and generally only affects a single grain or group of grains. Typically, however, the replacing pyrite pseudomorphs the parent pyrrhotite and g enerally retains the latters cleavage structure in an exaggerated form, (Fig.4.6.11.) No chemical data are available for secondary pyrite after pyrrhotite, but the likely reaction mechanism for its formation is set out in Equation 3, (Fig.4.6.3.).

No data are available on the fully developed secondary sulphide assemblage of violarite and pyrite present.at Selkirk. But it is likely that this extends as a relatively narrow zone between (approximately) the 25m. level and the water table at about 20 metres b.s., (Table 4.6.1.).

The petrology of the oxide zone

Available data show that the Selkirk sulphide profile is overlain by a zone of iron oxide-rich rocks that extend from the water table level at about 20 metres b.s. to the surface, (Table 4.6.1.). The mineralogy of this overlying oxide zone comprises hematite, goethite and silica.

Hematite averages about 50 percent of the sampled oxide zone mineral assemblage, but exhibits considerable inter-sample variation, (Table 4.6.1.). It occurs in several textural forms within the Selkirk oxide zone and is chiefly present as mimic replacement structures after the secondary (supergene) sulphide assemblage. In this respect, hematite is very commonly noted as replacements to secondary pyrite after pyrrhotite - generally as large areas of fine-grained material containing numerous

248

Fig. 4.6.2. Petrography of the Selkirk Gossan (1)

Scale length = 100 μ

A. Hematite after massive secondary pyrite (x 600) Oil

Hematite; light-medium grey: Relic pyrite, white: Silica-filled cubic voids; dark grey, mottled

B. Hematite mimic after bird's eye structure (x 220) Oil Blue-white filter

Voids; dark grey

C. Hematite mimics after pyrrhotite grain outlines (x 110) Air Blue-white filter

Hematite; light to medium grey: Goethite; dark grey: Voids; black. Goethite defines inter-granular boundaries

D. Hematite mimics after mimicked pyrrhotite cleavage partings (x 220) Oil

Partly crossed nicols

E. Hematite mimic after interstitial violarite (x 110) Air Blue-white filter

Hematite; light-medium grey: Silica, dark grey: Voids; grey-black

F. Hematite mimics after lamellar violarite (x 220) Oil Blue-white filter

Hematite Vpo relics at right centre. Pyrrhotite scissor twinning is mimicked by goethite

G. Hematite boxwork after chalcopyrite (x 110) Air Blue-white filter

Hematite; light-medium grey: Silica matrix; dark grey: Voids; grey-black

H. Hematite mimic after magnetite (x 220) Oil blue-white filter

Fig.4.6.2.
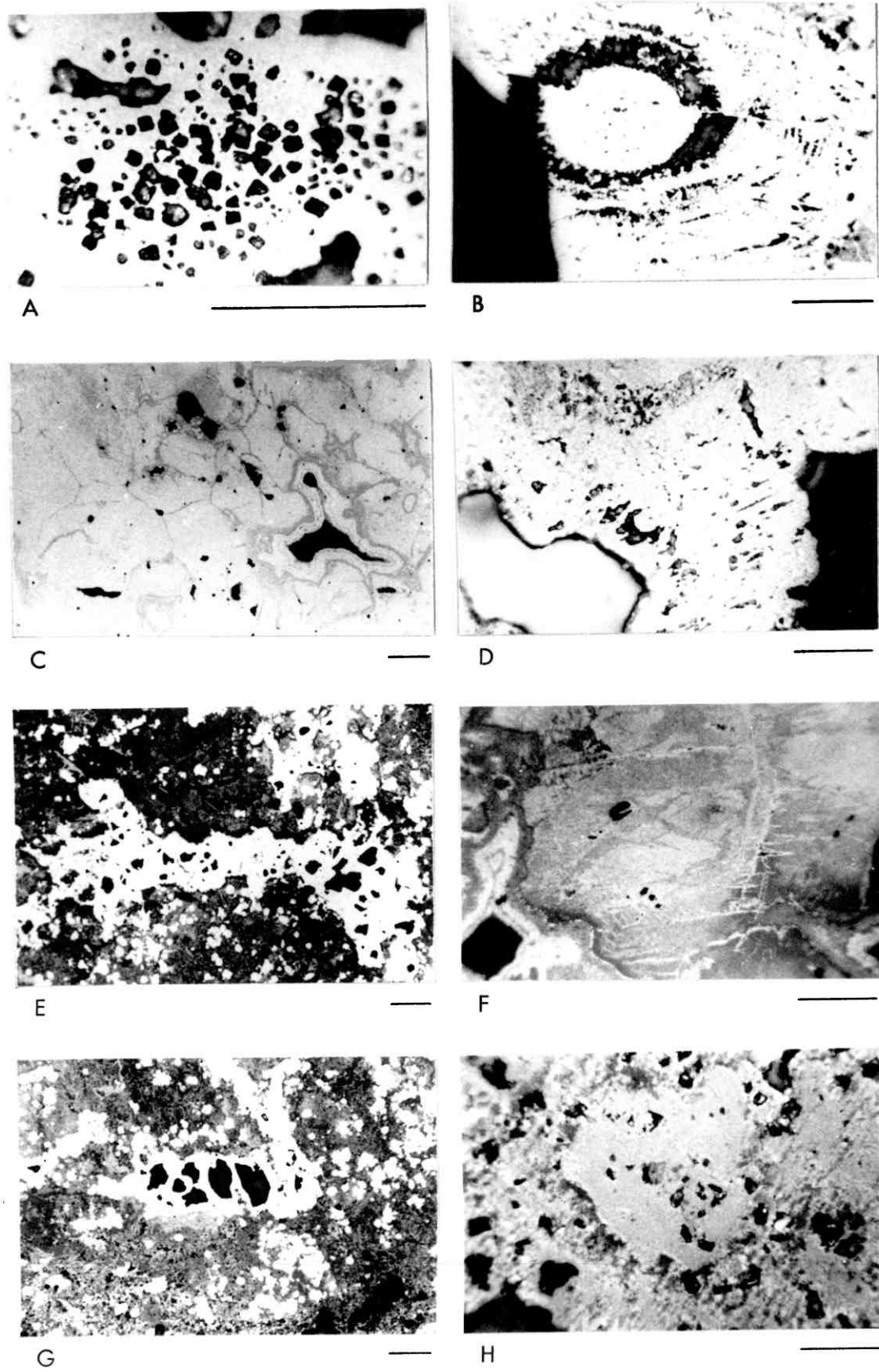
cubic leached voids, (Fig.4.6.2A.); but also as mimicked bird's eye structures, (Fig.4.6.2B.). Hematite is however, also present as secondary mimicked structures after pyrrhotite, and is observed both as grain pseudomorphs, (Fig. 4.6.2C.), and (less commonly) as relic structures after the 001 cleavage partings, (Fig.4.6.2D.). More rarely, hematite occurs as mimicked textures after violarite species, and is noted as pseudomorphs after both interstitial and lamellar varieties of Vpn, (Figs. 4.6.2E. and 2F. respectively).

The minor components of the ore assemblage chalcopyrite and magnetite are preferentially preserved as hematite structures. The former existence of chalcopyrite is typically indicated by characteristic hematite boxwork forms, (Fig.4.6.2G.). Whereas the former presence of magnetite is commonly noted by pseudomorphic, (Fig.4.6.2H.), or boxwork replacement structures, (Fig.4.6.4A.), in hematite.

Goethite averages about 38 percent of the sampled oxide zone material, and like hematite exhibits a wide range of contents across the specimen suite, (Table 4.6.1.). A considerable portion of goethite is present within relic structures after silicate, (4.6.4B.), but the mineral also typically forms pseudomorphic replacements after the component minerals of the secondary sulphide assemblage. In this respect, goethite may occur as extensive areas of fine-grained material containing cubic (ex-pyrite) voids, (Fig.4.6.4C.), and as large colloform structures also after secondary pyrite, (Fig.4.6.4D.). Pseudomorphic structures after original pyrrhotite textures are not uncommonly noted however, and these phenomena generally take the form of 001 cleavage mimics, (Fig.4.6.4E.); whole grain relics, (Fig.4.6.4F.); or as preserved deformation twinning, (Fig.4.6. 2F .)

Goethite is also commonly observed as pseudomorphs after several violarite species, and these sulphides are preferentially replaced by it in the Selkirk oxide zone. Thus interstitial Vpn is typically preserved as goethite mimic structures, (Fig.4.6.4G.), and rare manifestations of Vpo are present as goethite pseudomorphs, (Fig.4.6.5A.). Further, goethite similarly occurs as uncommon mimic replacements of magnetite, (Fig.4.6.5B.)

The likely reaction mechanisms corresponding to the pseudomorphic replacement of individual ore minerals by hematite and goethite are represented in the appropriate Equations in Fig.4.6.3.

Silica content exhibits a fairly wide variation within the Selkirk oxide zone, but averages about 13 percent in the sampled suite, (Table 4.6.1.). The mineral is

FIG. 4.6.3. CHEMISTRY OF THE SELKIRK ALTERATION SEQUENCE

SHALLOW ANODIC WEATHERING REACTIONS

19    $FeS_2 + 8H_2O = Fe^{2+} + 2SO_4^{2-} + 16H^+ + 14e^-$
Marcasite/
Pyrite

18    $Cu_{0.99}Fe_{1.01}Co_{0.02}S_2 + 8H_2O = 0.99Cu^{2+} + 1.01Fe^{2+} + 0.02Co^{2+} + 2SO_4^{2-} + 16.04H^+ + 12.04e^-$
· Chalcopyrite

17    $Ni_{1.63}Fe_{1.34}Co_{0.18}S_4 + 16H_2O = 1.63Ni^{2+} + 1.34Fe^{2+} + 0.18Co^{2+} + 4SO_4^{2-} + 32H^+ + 30.30e^-$
Violarite (after Po)

16    $Ni_{1.79}Fe_{1.25}Co_{0.16}S_4 + 16H_2O = 1.79Ni^{2+} + 1.25Fe^{2+} + 0.16Co^{2+} + 4SO_4^{2-} + 32H^+ + 30.40e^-$
Violarite (after lam. Pn)

15    $Ni_{1.89}Fe_{1.15}Co_{0.19}S_4 + 16H_2O = 1.89Ni^{2+} + 1.15Fe^{2+} + 0.19Co^{2+} + 4SO_4^{2-} + 32H^+ + 30.46e^-$
Violarite (after inst. Pn)

14    $Fe_3O_4 + 2H_2O = 3FeOOH + H^+ + e^-$
Magnetite   Goethite

13    $FeS_2 + 8H_2O + 2OH^- = FeOOH + 2SO_4^{2-} + 17H^+ + 13e^-$
Marcasite   Goethite

12    $Ni_{1.63}Fe_{1.34}Co_{0.18}S_4 + 16H_2O + 2.68OH^- = 1.34FeOOH + 1.63Ni^{2+} + 0.18Co^{2+} + 4SO_4^{2-} + 33.34H^+$
Violarite (after Po)   Goethite $+ 31.64e^-$

11    $Ni_{1.79}Fe_{1.25}Co_{0.16}S_4 + 16H_2O + 2.50OH^- = 1.25FeOOH + 1.79Ni^{2+} + 0.16Co^{2+} + 4SO_4^{2-} + 33.25H^+$
Violarite (after lam. Pn)   Goethite $+ 31.65e^-$

10    $Ni_{1.89}Fe_{1.15}Co_{0.19}S_4 + 16H_2O + 2.30OH^- = 1.15FeOOH + 1.89Ni^{2+} + 0.19Co^{2+} + 4SO_4^{2-} + 33.15H^+$
Violarite (after inst. Pn)   Goethite $+ 31.61e^-$

9    $2Fe_3O_4 + H_2O = 3Fe_2O_3 + 2H^+ + 2e^-$
Magnetite   Hematite

8    $Cu_{0.99}Fe_{1.01}S_2 + 8H_2O + 1.53OH^- = 0.51Fe_2O_3 + 0.99Cu^{2+} + 4SO_4^{2-} + 17.53H^+ + 13.08e^-$
Chalcopyrite   Hematite

7    $FeS_2 + 8H_2O + 1.5H_2O = 0.5Fe_2O_3 + 2SO_4^{2-} + 17.5H^+ + 15e^-$
Marcasite   Hematite

6    $Ni_{1.63}Fe_{1.34}Co_{0.18}S_4 + 16H_2O + 2.01OH^- = 0.67Fe_2O_3 + 1.63Ni^{2+} + 0.18Co^{2+} + 4SO_4^{2-} + 34.01H^+$
Violarite (after Po)   Hematite $+ 31.64e^-$

5    $Ni_{1.79}Fe_{1.25}Co_{0.16}S_4 + 16H_2O + 1.89OH^- = 0.63Fe_2O_3 + 1.79Ni^{2+} + 0.16Co^{2+} + 4SO_4^{2-} + 33.89H^+$
Violarite (after lam. Pn)   Hematite $+ 31.68e^-$

4    $Ni_{1.89}Fe_{1.15}Co_{0.19}S_4 + 16H_2O + 1.68OH^- = 0.56Fe_2O_3 + 1.89Ni^{2+} + 0.19Co^{2+} + 4SO_4^{2-} + 33.68H^+$
Violarite (after inst. Pn)   Hematite $+ 31.52e^-$

DEEP ANODIC WEATHERING PROCESSES

3    $Fe_{6.97}Co_{0.04}S_8 = 4FeS_2 + 2.97Fe^{2+} + 0.04Co^{2+} + 6.02e^-$
Monoclinic Po   Marcasite

2    $Fe_{6.97}Co_{0.04}S_4 + 3.26Ni^{2+} + 0.32Co^{2+} = 2Ni_{1.63}Fe_{1.34}Co_{0.18}S_4 + 4.29Fe^{2+} + 1.42e^-$
Monoclinic Po   Violarite (after Po)

1    $Ni_{4.48}Fe_{4.31}Co_{0.38}S_8 = 2Ni_{1.89}Fe_{1.15}Co_{0.19}S_4 + 0.70Ni^{2+} + 2.01Fe^{2+} + 5.42e^-$
Pentlandite   Violarite (after inst. Pn)

Fig. 4.6.4. Petrography of the Selkirk Gossan (2)

Scale length = 100μ   Blue-white filter used throughout

A.   Hematite boxwork after magnetite (x 220) Oil

B.   Goethite mimics after silicate (x 110) Air

      Goethite; medium-dark grey: Silica matrix; dark grey: Hematite; light-
      medium grey

C.   Goethite after secondary pyrite (x 110) Air

      Silicified goethite; dark grey: Hematite; light grey.   Cubic voids well shown

D.   Goethite mimics after secondary pseudocolloform texture (x 110) Air

      Goethite; medium-dark grey: Hematite; light grey.   Hematite defines
      the presolved shrinkage cracks.   Voids; black

E.   Goethite mimics after mimicked pyrrhotite cleavage (x 220) Oil

      Silicified goethite; dark greys: Hematite; light grey

F.   Goethite mimics after pyrrhotite grain structures (x 110) Air

      Goethite; medium-dark to dark greys: Hematite; light grey: Voids; black

G.   Goethite mimic after interstitial violarite (x 110) Air

      Goethite; medium grey: Silicified goethite after silicate; dark greys, mottled:
      Voids; grey-black to black

Fig.4.6.4.
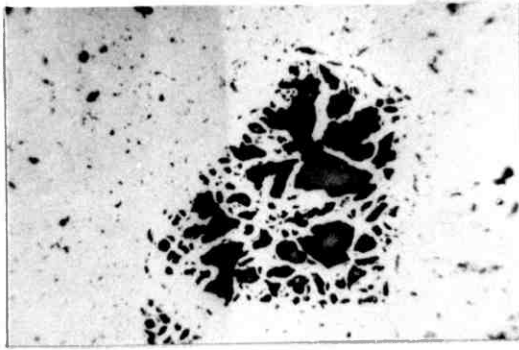
A
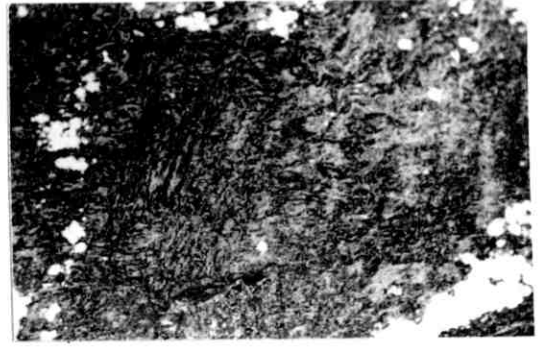
B
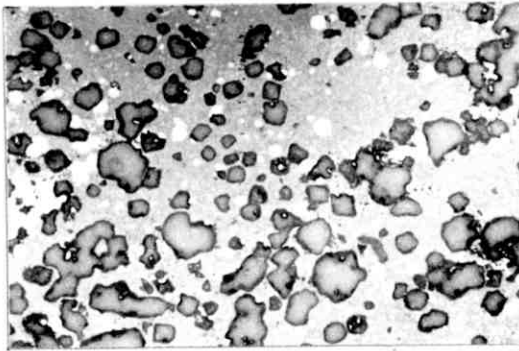
C
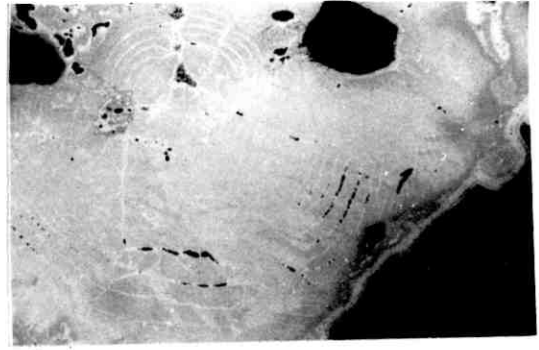
D
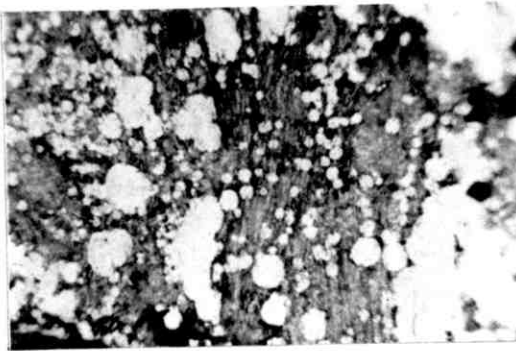
E
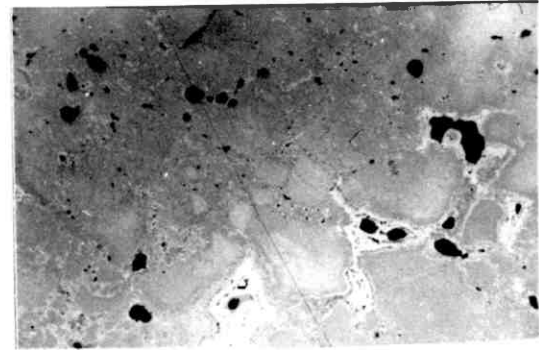
F
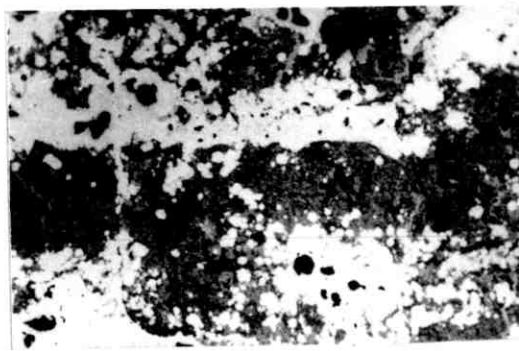
G

Fig. 4.6.5. Petrography of the Selkirk Gossan (3)

Figure scale = 100 μ

A. Goethite mimics after Vpo (x 600) Oil   Blue-white filter

Goethite· medium to dark grey: Voids; black

B. Goethite mimic after magnetite (x 110) Air   Partly crossed nicols

Goethite: medium to medium-dark greys: Silica: dark grey: Voids; white

C. Interstitial silica mimicking magnetite (x 110) Air

Silica; dark grey: Hematite; light grey: Goethite; medium grey (centre)

D. Interstitial silica mimicking violarite (x 110) Oil Blue-white filter

Silica; black, mottled: Hematite; light-medium grey: Silicified goethite after silicate; dark grey, mottled

Fig.4.6.5.
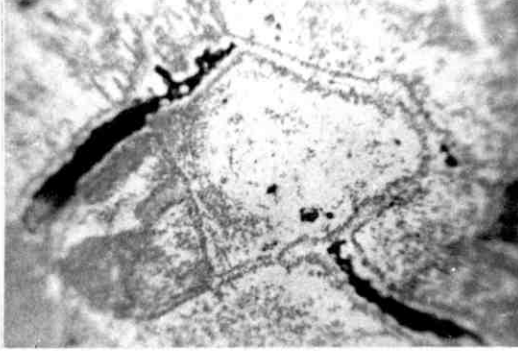
A
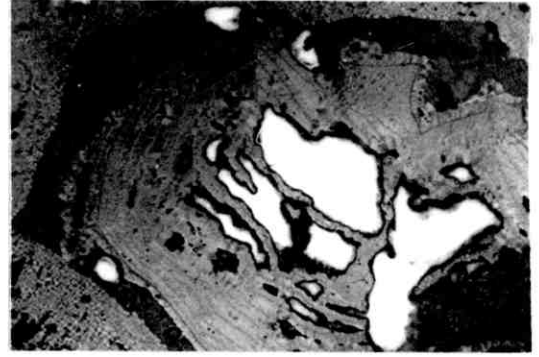
B
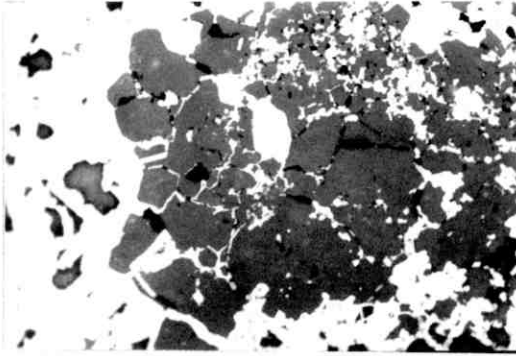
C
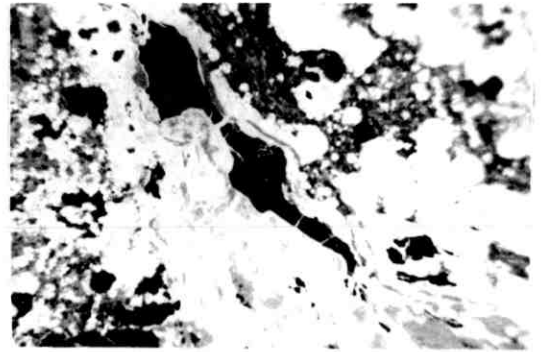
D

generally present as a pervasive matrix to areas of oxidised silicate, (Fig.4.6.4B.).
It is also however commonly noted as cavity fillings within leached out ore mineral
grains, and in this respect is chiefly present as interstitial fillings of ex-magnetite
and ex-interstitial violarite forms, (Figs. 4.6.5C. and 5D. respectively).

The likely depth variations of mean true density and of mean porosity within the
Selkirk oxidation profile are presented in Fig.4.6.6. The form of the mean density
profile indicates, on the basis of available data, that little significant mean
variation occurs in this physical variable during the development of the secondary
sulphide assemblage. Further, the relatively small mean density decrease that
subsequently takes place across the sulphide-oxide transition at about 20 metres b.s.
reflects the high degree of iron retention in the form of oxide minerals that occurs
in the Selkirk oxide zone, (Table 4.6.1.). The form of the mean porosity depth
profile similarly reflects the progressive development of the more porous secondary
sulphide minerals violarite and pyrite below the water table, and, further, concurs
with the wholesale precipitation of massive iron oxides that takes place above this
level.

Host silicate alteration

Table 4.6.10. indicates that the silicate host to the Selkirk mineralisation is very
probably a metagabbro. Further, petrographic and X-ray diffraction work on
weathered equivalents of this rock, demonstrates that the gabbro mineral assemblage
alters to one chiefly composed of kaolinite and quartz. This assemblage indicates
that the near surface alteration of the Selkirk host metagabbro probably occurred
under the influence of a long term regionally humid climatic regime, (Krauskopf,
1967). It is, in consequence, highly probable that the adjacent oxide zone develop-
ed above the Selkirk ore body also developed under these conditions. These infer-
ences thus support and extend Nickel's contention, (1977 op.cit.), that the oxide
zone at the Agnew deposit in Western Australia evolved during the former develop-
ment of humid climatic conditions.

Table 4.6.10. Chemical composition of host silicate - Selkirk

Oxide	Wt %
SiO_2	40.39
Al_2O_3	16.65
Fe_2O_3	2.31
FeO	9.40
CaO	6.89
MgO	15.72
Na_2O	1.28
K_2O	0.04
MnO	0.08
TiO_2	0.01
P_2O_5	0.08
Loss on Ignition	6.44
TOTAL	99.29

Based on data supplied by S.Marsh

258

Fig. 4.6.6.   Mean True Density and Porosity profiles – Selkirk
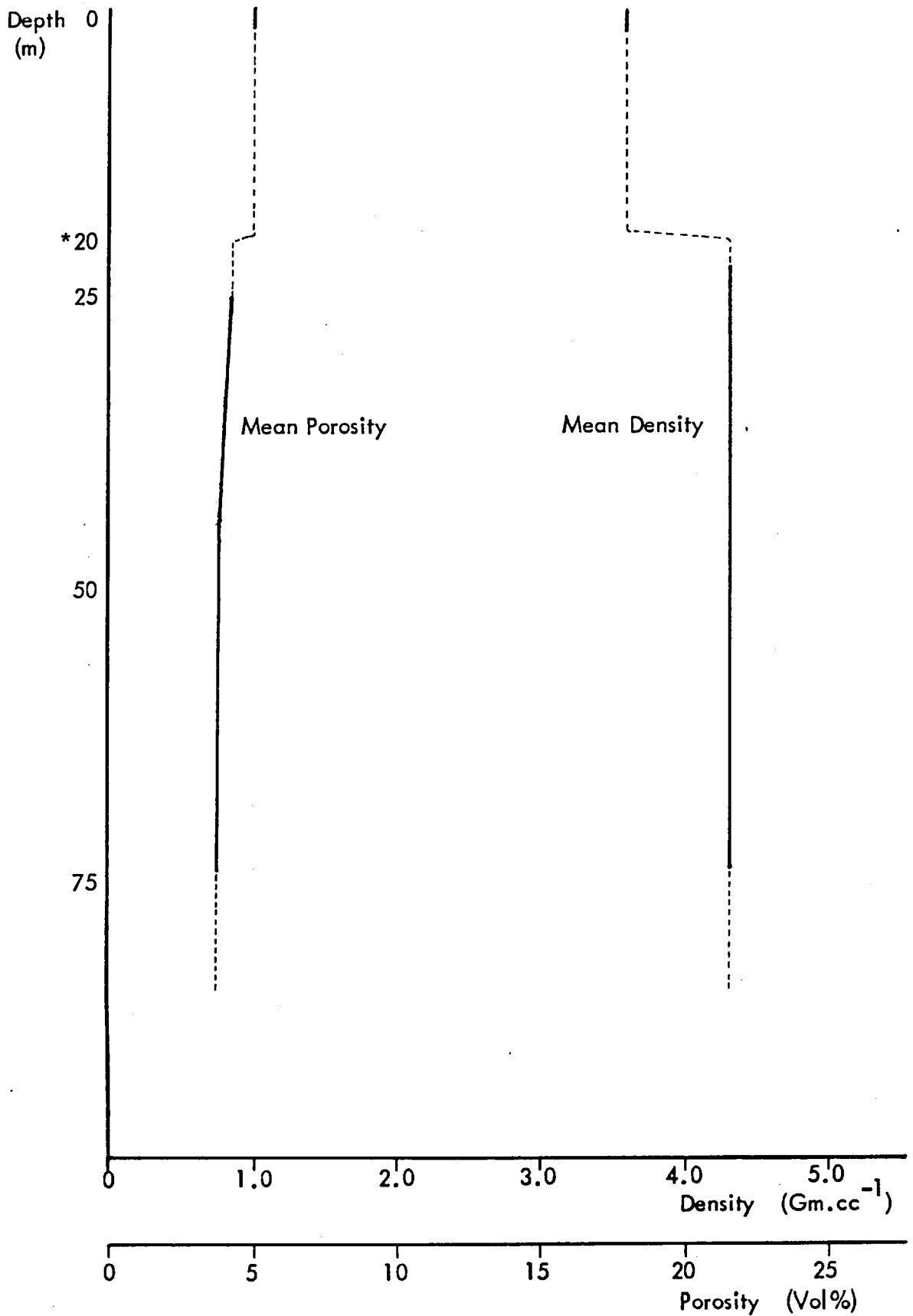
*   Approximate position of the Water table

Fig. 4.6.7.   Chemical Variations in Alteration Profile — Selkirk
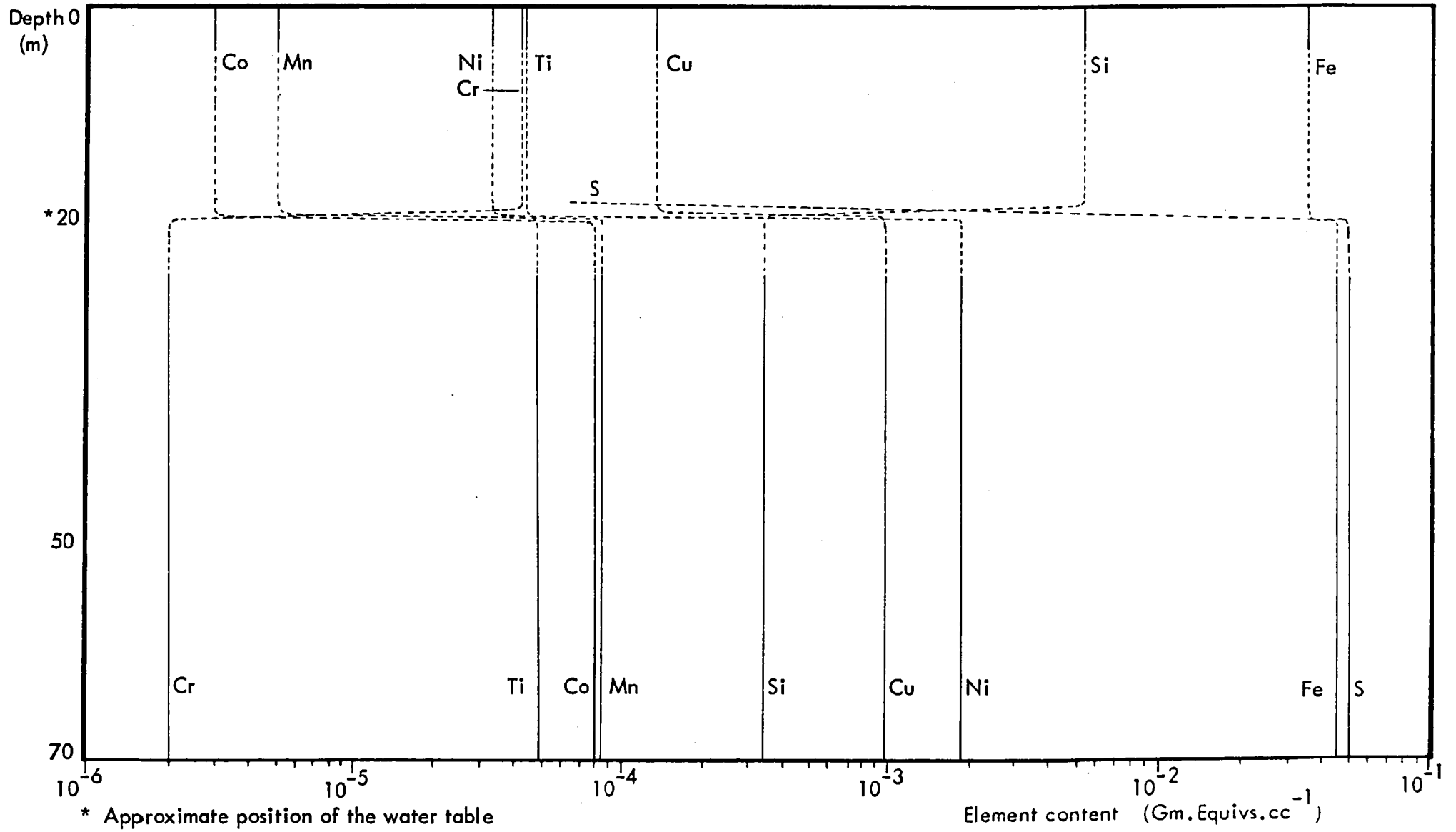
* Approximate position of the water table

Element content   (Gm.Equivs.cc^{-1})

The bulk chemistry of the sulphide alteration sequence

The mean depth variation of the constituent suite of major and minor elements within the Selkirk oxidation profile is presented in Fig.4.6.7. The overall mean constancy, (on available data), of all element profiles between the 60m. and 20m. levels indicates that the developing secondary sulphide assemblage at Selkirk effectively forms a closed chemical system. In contrast, the behaviour of the element suite across the sulphide-oxide transition at about 20 metres b.s. demonstrates the fundamental change in chemical environment that takes place as a result of wholesale leaching of the secondary sulphide assemblage at this level.

In this respect, the varying modification in mean content of sulphur and almost all the analysed trace metals across the 20m. level closely reflects the chemical behaviour of these individual elements under the acid, oxidising conditions imposed by the sulphide leaching process. Contrawise, the relatively small observed decrease in mean iron content reflects the large scale (pseudomorphic) oxidative precipitation of this metal as hematite and goethite that occurs at the water table. Further, the noted 15-fold increase in mean silicon content across the water table horizon at least partially reflects the influx of silica into the oxide zone from adjacent weathering silicate rocks , and the large mean increase in chromium that occurs within the Selkirk oxide zone must similarly indicate the influx of this metal into the ore profile as a result of silicate weathering.

4.7. SUMMARY

Chapter four has presented synoptic descriptions of the near surface sulphide alteration sequences that are developed in five major nickel-copper sulphide deposits in Southern Africa. This task has been achieved for each deposit by documentation of the petrological and bulk chemical changes that occur during the progressive oxidation of the primary massive sulphide ore assemblage through secondary (supergene) sulphide development to the establishment of the equivalent oxide zone. The results of this work indicate that qualitatively similar mineralogical, textural and bulk chemical changes occur during the progressive oxidation of primary ore in each deposit, but that there is considerable quantitative petrological and chemical variation between individual profiles.

For all but one of the deposits, (Munali), the petrological descriptions have included

details of mineral chemistry for representative primary and secondary ore minerals. These data have allowed the formulation of likely chemical reaction mechanisms for each of the mineralogical alteration phenomena observed within the relevant profile sequence.

The documentation of progressive sulphide alteration has been supplemented by descriptions of mean true density and mean porosity variation within each oxidation profile. This work has indicated that variations in mineralogy and bulk chemistry during sulphide alteration are generally reflected by parallel changes in the values of these two physical variables.

Brief outlines of the petrology of host rock alteration have also been appended for each deposit where this information is available. These data indicate the nature of the deep silicate weathering that characteristically accompanies the formation of iron oxide-rich zones above these deposits.

A full descriptive comparison of the five documented southern African oxidising nickel sulphide deposits, together with the Australian deposits forming the subject of chapter five, and the Pikwe deposit previously described in chapter three is made in chapter six.

CHAPTER FIVE

NEAR SURFACE OXIDATION IN ELEVEN WESTERN AUSTRALIAN

NICKEL SULPHIDE DEPOSITS

5.1. INTRODUCTION

The petrology and geochemistry of eleven supergene-altered nickel sulphide deposits in Western Australia is now set out. The first part of the chapter comprises synoptic descriptions of seven previously undocumented deposits. This work is then supplemented by brief descriptions of four already documented deposits from Kambalda that are based on investigations carried out during the present study. More detailed data on these deposits are located in the relevant sections of Appendix Two.

5.2. SUPERGENE SULPHIDE ALTERATION IN THE MT.EDWARDS DEPOSIT

The Mount Edwards deposit occurs as a steeply inclined elongate lens of massive to disseminated sulphide that is located at or near the footwall contact of host peridotite with underlying tholeiitic and magnesium-rich basalts, (Section 2.3. and Table 2.4.1.).

The petrology of the primary sulphide assemblage

The mineralogy of primary near-massive to massive sulphide comprises pyrrhotite and pentlandite with minor amounts of chalcopyrite and variable quantities of silicates, (Table 5.2.1.). Pyrrhotite averages about 75 percent of the sulphide assemblage and forms the matrix of the ore. It is typically present as an interlocking matrix of equant grains that commonly exhibit polygonal forms, (Fig.5.2.1A.).

Pentlandite forms about 15 percent of the Mt.Edwards primary sulphide assemblage, (Table 5.2.1.). It is typically present as elongate stringers located along pyrrhotite borders, (Fig.5.2.1B.). Chalcopyrite comprises approximately one percent of near-massive to massive primary ore, (Table 5.2.1.), and is present chiefly as small stringers or as blebs along pyrrhotite grain borders.

The petrology of the sulphide alteration sequence

Available data indicate that significant alteration of the Mt. Edwards primary sulphide assemblage occurs between about 95 and 80 metres below surface, (Table 5.2.1.). The alteration characteristically occurs as a progressive replacement of pentlandite by violarite. Initial nucleation of violarite takes place along the grain borders and cleavage traces of the parent sulphide. Progressive replacement then generally occurs as broad fronts into the adjacent cleavage blocks of the surrounding pentlandite, (Fig.5.2.1C.). It is likely that complete replacement of primary sulphide by violarite (Vpn) occurs below the 60 metre level.

The replacement of pentlandite by Vpn is paralleled by the alteration of pyrrhotite to violarite (Vpo). This violarite type takes the form of laterally extensive fringes of feathery lamellae that typically grow into the parent pyrrhotite along the 001 cleavage direction from grain borders adjacent to actively altering pentlandite, (Fig.5.2.1D.).

No intermediate smythite product was noted in the Mt. Edwards sample material, but this apparent absence is thought more likely due to a lack of study material from the corresponding depth sub-zone than to the non-formation of this mineral during the alteration of pyrrhotite to Vpo.

The full development of secondary violarite is accompanied by the deposition of siderite along the external borders and within the distended octahedral cleavage of Vpn, (Fig.5.2.1E.). This phenomenon also commonly results in the partial replacement of the secondary sulphide assemblage, (Fig.5.2.1F.).

Available data demonstrate that the transition assemblage of pyrrhotite, Vpo, Vpn and chalcopyrite is stable up to about the 60m. level in the Mt. Edwards ore profile, (Table 5.2.1.). Above this horizon, however, residual pyrrhotite quite abruptly alters to either marcasite or pyrite – the iron disulphide characteristically occuring as fine-grained (colloidal) material. The replacing mineral may be structureless, but it may also however contain pseudocolloform shrinkage cracks, (Fig.5.2.1E.). More commonly, though this secondary alteration exhibits sub-parallel lineations – typically defined by void trains, that mimic the 001 cleavage of the parent pyrrhotite, (Fig.5.2.1G.). These initial replacement textures are subsequently affected by a recrystallisation to massive structureless forms however, and this typically leads to the partial obliteration of these phenomena within the higher levels of the sulphide profile.

Fig. 5.2.1. Petrography of Mt.Edwards Sulphide Ore

Scale length = 100μ

A.   Pyrrhotite polygonal matrix texture (x 110) Air Partly crossed nicols

B.   Interstitial pentlandite texture (x 40) Air

Pentlandite: light-medium grey: Pyrrhotite; medium to medium-dark greys:
Silicates: black

C.   Replacement of pentlandite by violarite (x 600) Oil

Pentlandite: light grey: Violarite; medium-dark grey: Silicates; black

D.   Typical violarite after pyrrhotite texture (x 320) Air

Vpn; dark grey, granular: Vpo; medium grey, granular: Marcasite;
whitish-grey: Carbonate; grey-black

E.   Fully developed secondary assemblage (x 220) Oil

Secondary marcasite: light-medium grey, striated, granular (centre):
Violarite (Vpn); medium-dark grey, granular: Violarite (Vpo); light to
medium grey, fringe-like: Carbonate; dark grey

F.   Partial replacement of violarite by siderite (x 110) Air

Violarite; dark grey, granular: Siderite; dark grey: Marcasite; light-
medium grey, granular. Complete replacement of Vpn by siderite - lower
left. Partial replacement - upper right.

G.   Pyrrhotite cleavage mimicked in secondary marcasite (x 40) Air

Fine-grained marcasite: medium-dark grey: Coarse marcasite; medium
grey: Carbonate: dark grey

Fig.5.2.1.

A

B

C

D

E

F

G
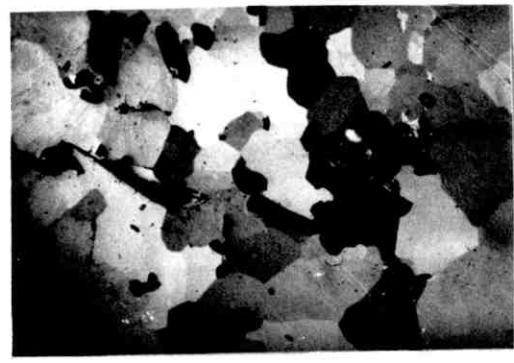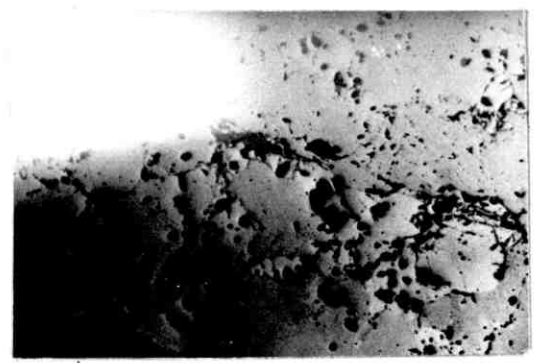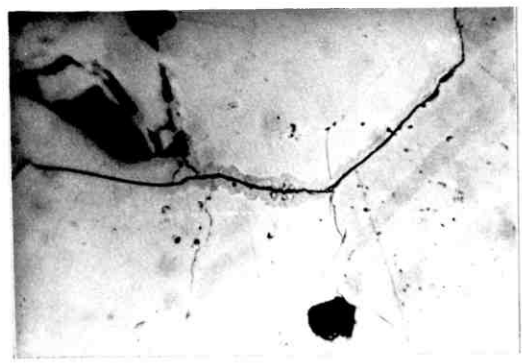
The petrology of the oxide zone

Present data indicate that the secondary sulphide assemblage of violarite, marcasite and pyrite extends between the 60m. and 35m. depth horizons. At the latter level however, the sulphides undergo pervasive oxidation and are replaced by an assemblage rich in iron oxides – principally goethite. This overlying oxide zone extends from the 35m. level to the surface where it crops out as rather spasmodic siliceous rubble, (Section 2.3.).

No analysis of depth variation within the Mt. Edwards oxide profile was possible in the present study because of the inaccessibility of all but the top ten metres of the profile. It is however likely that the near surface horizons are representative of at least the top 25 metres of the oxide zone due to the uniform deep weathering that occurs in the Widgiemooltha area, (Section 2.2.).

The mineralogy of the sampled Mt. Edwards gossan comprises goethite and silica. Variable but typically minor to trace amounts of hematite are also present, (Table 5.2.1.). Goethite comprises about 50 percent of the gossan mineral assemblage. It forms several important textural configurations and is present as mimic structures after secondary pyrite, (Figs. 5.2.2A. and 2B.); after secondary marcasite, (Figs. 5.2.2C. and 2D.); and as secondary mimic structures after pyrrhotite, (Fig. 5.2.2E.). Goethite is also the principal replacement mineral of both violarite after pentlandite, (Fig. 5.2.2F.), and of violarite after pyrrhotite, (Fig. 5.2.2G.). In contrast, hematite is present almost entirely as pseudomorphs after magnetite, (Fig. 5.2.2F.). Whereas silica is typically noted as a pervasive matrix and intimately invests goethite pseudomorph and boxwork structures, (Fig. 5.2.2H.).

The corresponding mean true density and mean porosity profiles

The mean variation of true density and of porosity within the sampled Mt. Edwards oxidation profile are indicated in Fig. 5.2.3. The depth variations of both physical properties closely reflect the mineralogical changes that occur during progressive sulphide alteration as pentlandite alters to less dense, more porous violarite. Further, the density and porosity changes across the 35m. level closely parallel the dramatic physico-chemical transformation that occurs at this horizon as a result of wholesale sulphide leaching.

Fig. 5.2.2. Petrography of the Mt. Edwards Gossan

Scale length = 500 μ

A.   Goethite mimics after secondary pyrite (x 110) Air Blue-white filter

Goethite; medium grey: Hematite; light grey: Silica; dark grey: Voids: black

B.   Goethite boxwork after secondary pyrite (x 220) Oil Blue-white filter

Goethite; medium grey: Residual pyrite; white-grey: Voids; black

C.   Goethite mimic after secondary marcasite (1) (x 220) Oil

Goethite; medium grey (centre): Hematite; light grey: Silicified goethite after violarite: medium-dark grey, mottled: Voids; grey-black

D.   Goethite mimic after secondary marcasite (2) (x 220) Oil

Goethite; light to medium grey: Voids; grey-black

E.   Goethite mimics after mimicked pyrrhotite (x 110) Air Blue-white filter

Goethite; medium greys: Silica; dark greys. Silica defines relic Vpo textures. Voids; black

F.   Goethite mimic after interstitial violarite (Vpn). Hematite mimics after Magnetite (x 80) Air   Blue-white filter

Goethite (after Vpn); dark grey (mottled): Hematite (after magnetite); white-grey: Silicified goethite matrix; medium greys, mottled: Silica; dark grey

G.   Goethite mimics after violarite violarite species (Vpn and Vpo) (x 110) Air Blue-white filter

Goethite: medium grey: Silica; dark grey: Voids; black. Fringe of Vpo texture preserved at centre lower

H.   Typical form of silica matrix (x 80) Air

Silica; dark grey: Goethite; light-medium to dark-medium greys

Fig.5.2.2.
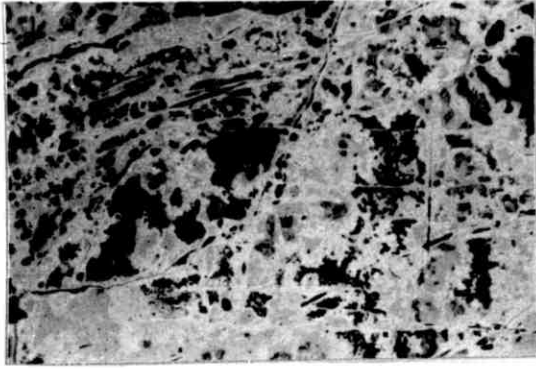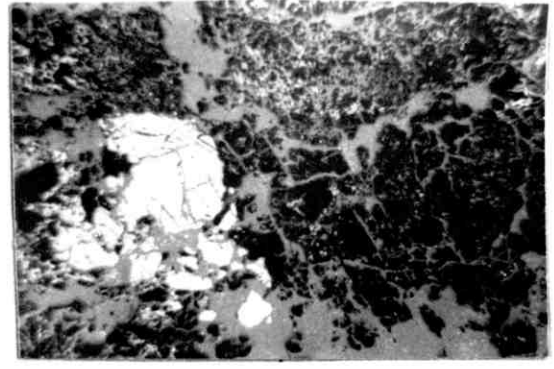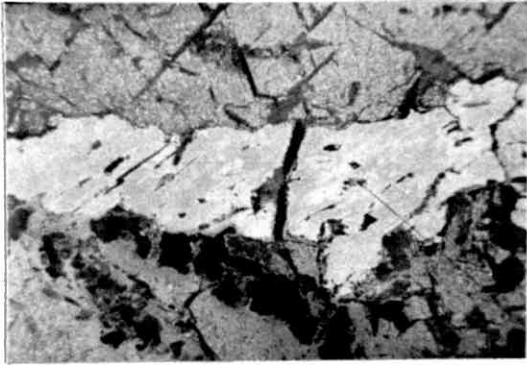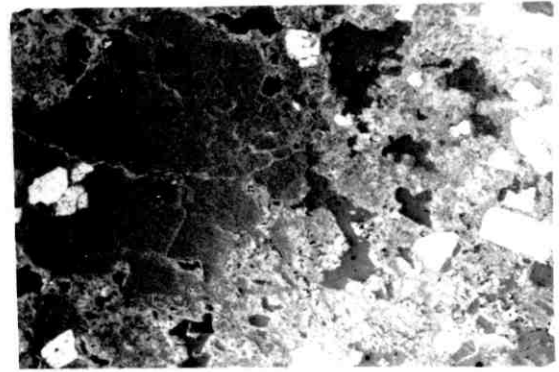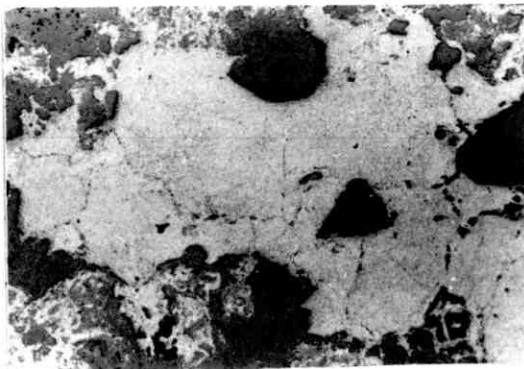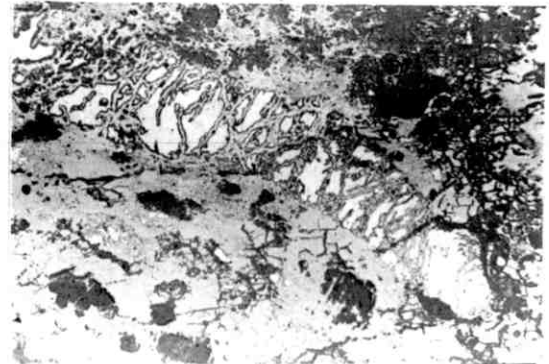
Fig. 5.2.3. Mean True Density and Porosity profiles – Mt. Edwards
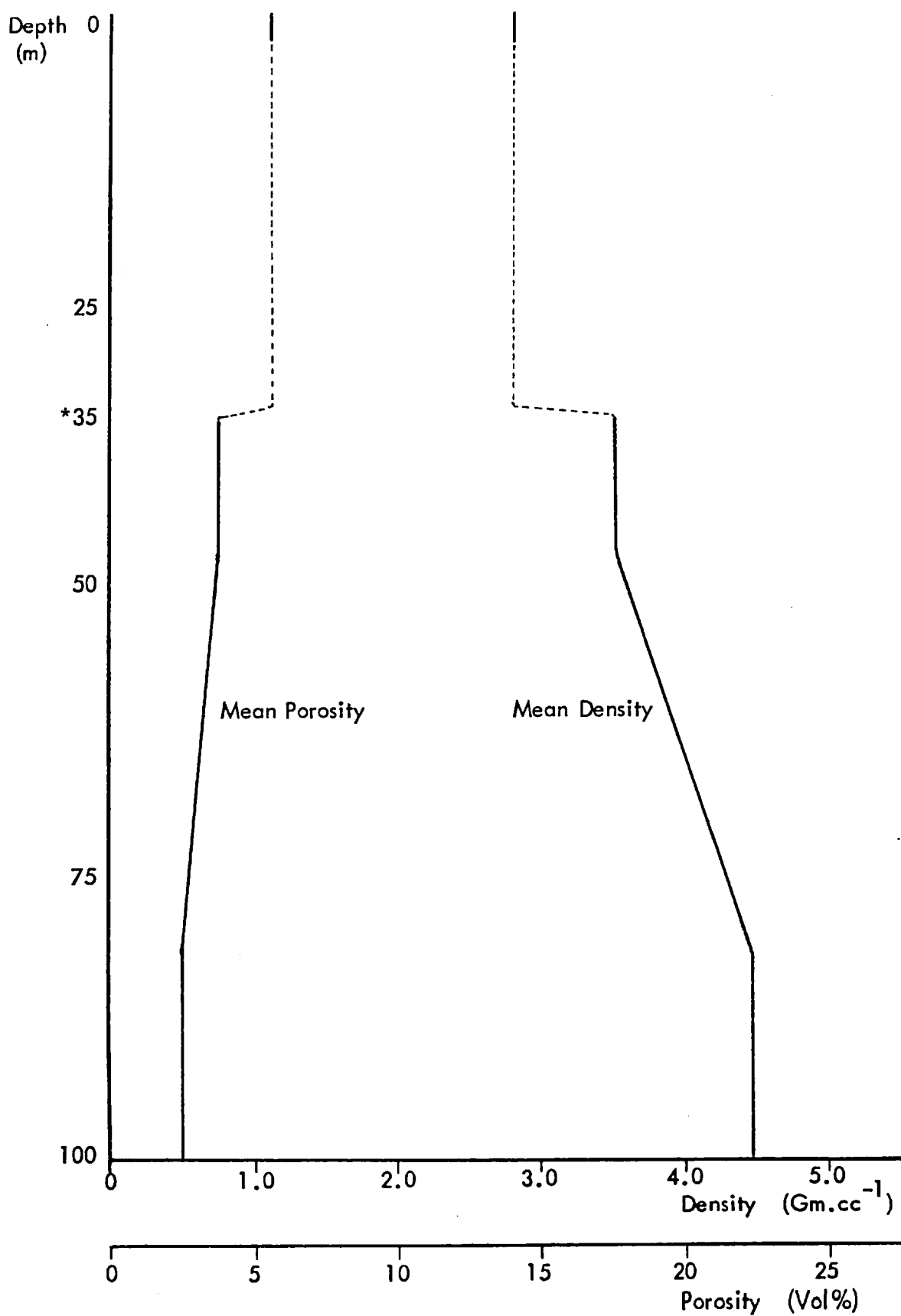
* Approximate position of the water table

The bulk chemistry of the sulphide alteration sequence

The bulk chemistry of the observed sulphide alteration sequence at Mt.Edwards is presented in Fig.5.2.4. The indicated mean constancy of all major and trace elements except iron between the 90m. and 35m. levels demonstrates that the supergene alteration of primary sulphide in this deposit effectively occurs as a closed chemical system. In contrast, the observed progressive loss of iron during supergene alteration is almost certainly related to its release from pentlandite and pyrrhotite during the gradual development of the secondary assemblage of violarite, marcasite and pyrite. Part of this released iron is subsequently precipitated locally as siderite, but a substantial proportion is removed from the ore profile , probably in aqueous solution.

The dramatic changes in element contents that occur across the 35m.level indicate the significant chemical effect of pervasive sulphide leaching at that horizon.In this respect, sulphur is oxidised and totally removed from the ore profile as highly mobile sulphate ion. Whereas up to one third of the mean iron content of the former sulphide assemblage is retained as iron oxide (goethite). Further the transition from sulphide to oxide zone assemblage is also marked by a three-fold increase in mean silicon content, the element being derived from precipitated silica brought into the oxide zone by groundwaters and ultimately derived from the weathering of proximal silicate rocks.

The behaviour of the trace metal suite across the sulphide-oxide transition generally corresponds to that expected from the known chemical response of these elements to the high Eh-low pH conditions associated with active sulphide leaching. The observed anomalous immobility of copper is, however, probably related to its presence largely in chalcopyrite, which mineral likely remains relatively unaffected by the initial sulphide leaching process. In comparison, the much less marked though recognisable retention of nickel within the oxide zone is probably related to the retention of this metal in pseudomorphic structures after violarite species.

The large depletion in normally immobile titanium across the sulphide-oxide transition infers that this element is probably not associated with a residual mineral such as chromite in the Mt.Edwards ore assemblage. In contrast, the observed two-fold increase in mean chromium content across the sulphide leaching zone indicates that the retention of this typically immobile metal is probably supplemented by an influx of chromium derived from the weathering of proximal ultramafic rocks.

Fig. 5.2.4.   Chemical Variations in Alteration Profile – Mt. Edwards

* Approximate position of the water table

Element content   (Gm. Equivs.cc^{-1})
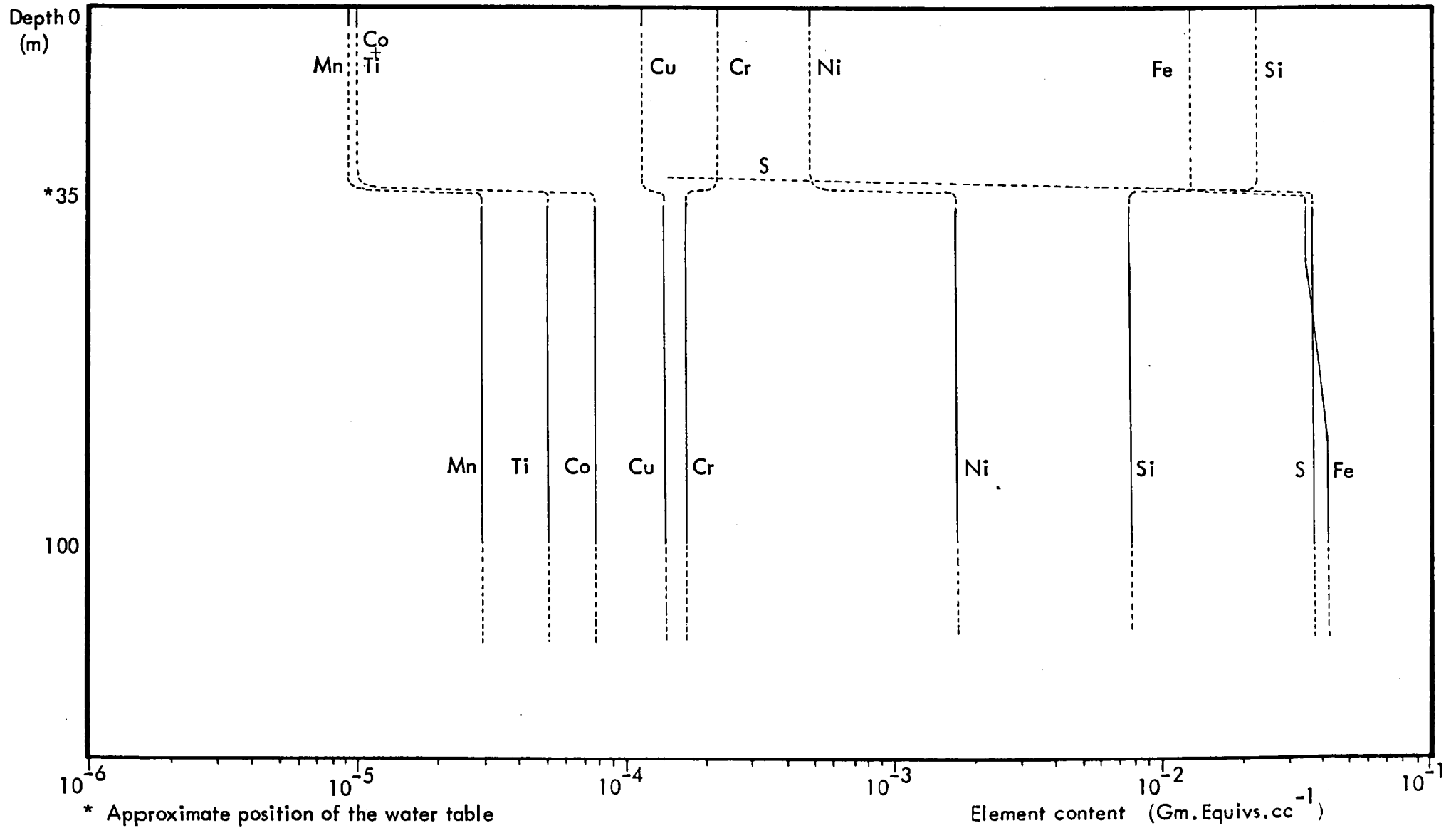
TABLE 5.2.1. SUMMARY DATA OF SULPHIDE ALTERATION – Mt. EDWARDS

Depth (m)	Alteration Zone	No. of Samples (n)	MINERALOGY (Means and ranges) Volume % Units							Den gm/cc	Por %	S	Fe	SiO$_2$	MgO	Al$_2$O$_3$	CO$_3$	Ni	Cu	Mn	Cr	Co	Ti
35	Oxide	14	Hm	Gt	Si			Cr	Gyp														
			1.0	5.0	25.0					1.90	1.3	N/A	5.82	7.68	0.00	0.00	N/A	959	104	30	48	30	28
			1.0	48.0	52.0			trace	trace	2.79	5.6		38.89	51.80	1.03	0.66		10166	2773	183	7084	225	182
			5.0	80.0	75.0					3.10	20.5		75.89	88.60	6.00	4.00		54794	9697	461	45205	963	462
45–50	Violarite – pyrite	5	Mc	Py	Vl	Cp	Mt	Sil	Sid														
			1.0	1.0	3.0	0.2	0.5	1.0	0.5	3.10	1.9	19.15	35.79	11.80	0.10	0.10	N/A	7709	583	111	965	859	66
			30.0	47.0	4.3	0.8	2.5	15.0	2.0	3.50	3.8	32.27	41.43	16.07	2.73	1.53		19944	4212	431	5207	1841	312
			85.0	95.0	5.0	1.0	10.0	40.0	7.0	3.70	6.0	42.84	46.57	22.51	6.40	4.70		28611	7660	784	16120	3800	641
	Transition	1	Po	Mc		Vl	Cp		Sil														
			70.0	17.0		7.0	0.5		5.0	3.70	1.3	27.34	51.40	10.58	2.60	4.80	N/A	4306	2844	790	157	580	1637
80–95	Primary	5	Po		Pn	Cp		Sil															
			65.0		5.0	0.1		1.0		4.00	1.0	18.44	43.23	1.16	0.10	0.10	N/A	17264	64	82	62	433	62
			76.0		14.5	1.0		10.0		4.42	2.6	20.31	52.49	8.81	1.15	1.63		32401	356	310	197	637	657
			85.0		20.0	2.0		30.0		4.60	8.9	35.35	58.18	23.71	3.50	5.60		49089	719	645	363	836	2272

Column groupings:
- MINERALOGY (Means and ranges) — Volume % Units
- Physical data (mean/ranges): Den gm/cc, Por %
- GEOCHEMISTRY (Means and ranges) — Wt.% Units: S, Fe, SiO$_2$, MgO, Al$_2$O$_3$, CO$_3$; p.p.m. Units: Ni, Cu, Mn, Cr, Co, Ti

5.3. SUPERGENE ALTERATION IN THE MT.MONGER DEPOSIT

The Mt.Monger (Carnilya Hill) deposit occurs as a series of steeply-dipping massive sulphide lenses overlain by disseminated ore and occurring at or near the basal contact of host amphibolite with underlying serpentinite, (Section 2.3.).

The petrology of the primary sulphide assemblage

The mineralogy of Mt.Monger primary massive sulphide comprises pyrrhotite (76 percent), pentlandite (11 percent), and minor amounts of magnetite/ferrochromite, (seven percent), chalcopyrite (three percent), and silicates (three percent), (Table 5.3.1.). Pyrrhotite forms the matrix of the ore and is present as a network of interlocking grains that commonly exhibit polygonal grain relations. Pentlandite is typically present as rather equant blocky grains, or as elongate stringers situated along pyrrhotite grain borders, (Fig.5.3.1A.). Ferrochromite generally occurs as rather elongate irregular grains that possess smoothed rounded outlines, (Fig.5.3.1B.), and chalcopyrite is commonly present as irregularly-shaped grains having rounded outlines, (Fig.5.3.1C.).

The petrology of the sulphide alteration sequence

Available data demonstrate that primary sulphide oxidation is initiated between the 80 and 60m. levels in the ore profile. At this depth pentlandite undergoes incipient alteration to violarite. Further, petrographic work indicates that violarite formation is typically initiated as thin elongate fingers developed sub-parallel to octahedral cleavage, (Fig.5.3.1D.). Subsequent development of violarite takes place both parallel and normal to pentlandite cleavage and eventually results in the complete pseudomorphic replacement of the parent mineral. No direct evidence is available in the present study to indicate a parallel development of violarite (Vpo) in adjacent pyrrhotite, and further, no data are offered to demonstrate the formation of an intermediate smythite stage during this likely alteration process. Iron oxide pseudomorphs after Vpo are, however, present in the equivalent overlying oxide material, and these confirm the existence of this type of pyrrhotite alteration in Mt.Monger sulphide ore, (Fig.5.3.2A.).

Direct mineragraphic evidence is available though to indicate the subsequent

Fig. 5.3.1. Petrography of Mt.Monger Sulphide Ore

Scale length = 100 μ unless otherwise indicated

A.   Typical interstitial pentlandite texture (x 40) Air

Pentlandite; light-medium grey: Pyrrhotite; medium grey: Spinel; dark grey

B.   Typical ferrochromite grain forms (x 110) Air

Ferrochromite: dark grey: Chalcopyrite; medium-dark grey: Pyrrhotite; medium grey: Pentlandite; light-medium grey, granular: Voids; black

C.   Typical chalcopyrite grain forms (x 320) Air

Chalcopyrite; medium grey: Pyrrhotite; light-medium grey: Spinel; dark grey: Pentlandite; light grey, mottled

D.   Initial alteration of pentlandite to violarite (x 600) Air

Pentlandite; medium grey: Violarite; dark-medium to dark grey: Voids; black: Spinel; dark grey (right).   Violarite shows diffuse borders with pentlandite

E.   In situ replacement of chalcopyrite by covellite (x 220) Oil

Chalcopyrite; light-medium grey (lower left):   Covellite; medium-dark grey, mottled: Pyrite· white: Rosin; dark grey

Fig.5.3.1.
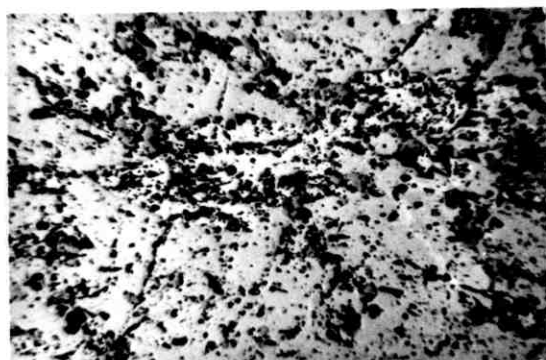
A

1000 μ
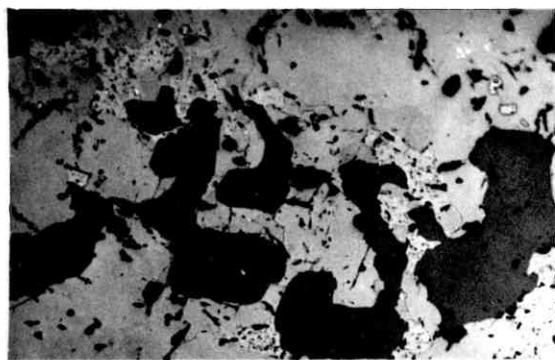
B

C
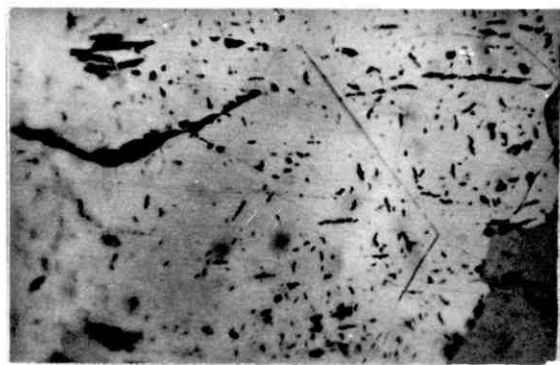
D
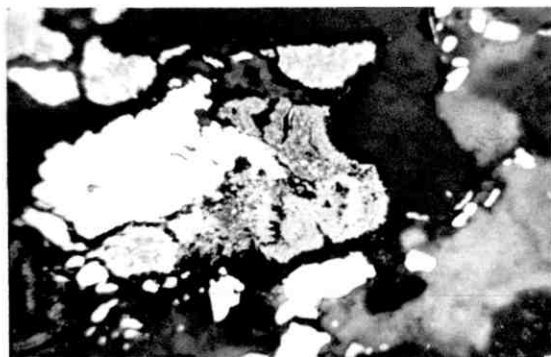
E

alteration of residual pyrrhotite to secondary iron disulphide. The depth horizon
at which this phenomenon occurs cannot however be directly determined on
currently available data, but is most likely to be situated within the 55 to 50m.
vertical interval, (Table 5.3.1.).

The petrology of the oxide zone

Pervasive oxidation of the secondary sulphide assemblage occurs at about the 40m.
level. Here the violarite-pyrite assemblage is replaced by one of goethite (42
percent), silica (49 percent), and hematite (10 percent), (Table 5.3.1.). At this
horizon violarite may be partially leached to form boxworks, (Fig.5.3.2B.).
Alternatively, the nickel sulphide may be directly replaced by goethite, (Fig.
5.3.2C.). Secondary pyrite generally leaches to reveal secondary mimicked
textures after pyrrhotite, (Fig.5.3.2D.), or is otherwise replaced in situ by iron
oxides, (Fig.5.3.2E.). Chalcopyrite is commonly replaced in situ by covellite,
(Fig.5.3.1E.), but also forms extensive leached (boxwork) structures in the Mt.
Monger gossan, (Fig.5.3.2F.). Numerous small relic ferrochromite grains - in
general partly altered to hematite, are also present in the oxide zone, (Fig.5.3.2G.).
Finally, all of these relic ore textures are characteristically invested in a pervasive
matrix of cryptocrystalline silica, (Fig.5.3.2H.).

Calcite and dolomite are present as oxidate phases in the Mt.Monger gossan.
Both minerals characteristically occur as surficial coverings on massive oxide after
sulphide. Further, the trace element contents of both phases indicate that their
development is probably related to a former episode of silicate weathering and
sulphide leaching, (Tables A2/3 and A2/4; Appendix Two).

The corresponding mean true density and mean porosity profiles

The mean variation of true density and of porosity within the sampled alteration
profile at Mt.Monger are presented in Fig.5.3.3. The profile forms indicate, on
available data, that little significant variation in either mean density or mean
porosity occurs during the development of the secondary sulphide assemblage at
this deposit. In contrast, the indicated changes in both physical properties that
occur across the 40m. level correspond with the fundamental physico-chemical

Fig. 5.3.2. Petrography of the Mt.Monger Gossan

Scale length = 300 μ

A.   Goethite mimics after Vpn and Vpo (x 320)m Air Blue-white filter

Goethite; light-medium grey: Silica; dark grey: Voids; black

B.   Goethite boxwork after massive violarite (Vpn) (x 40) Air

Voids; black

C.   Goethite mimic after interstitial violarite (Vpn) (x 110) Air Blue-white filter

Goethite; medium grey: Silica; dark grey: Voids; black

D.   Goethite boxwork after mimicked pyrrhotite structure (x 110) Air   Blue-white filter

Goethite; light-medium grey: Silica; dark grey: Voids; black

E.   Hematite mimics after secondary pyrite (x 110) Air Blue-white filter

Hematite; white-grey: Silica; dark grey: Voids; black
Relic pyrrhotite cleavage defined in void trains

F.   Goethite boxwork after chalcopyrite (x 110) Air Blue-white filter

Silica; medium to dark-medium grey: Voids; dark grey: Goethite;
light grey

G.   Ferrochromite relic in goethite matrix (x 110) Air Blue-white filter

Ferrochromite: 'pink'-grey (centre): Goethite; medium to dark greys, mottled:
Silica; dark grey: Voids; black: Hematite; light grey.
Part of goethite forms Vpn mimic (left and top)

H.   Typical relations of silica matrix (x 110) Air

Goethite: white-grey to light grey: Silica; dark grey: Voids; black

Fig.5.3.2.
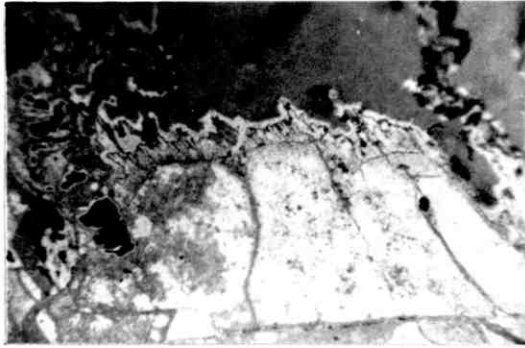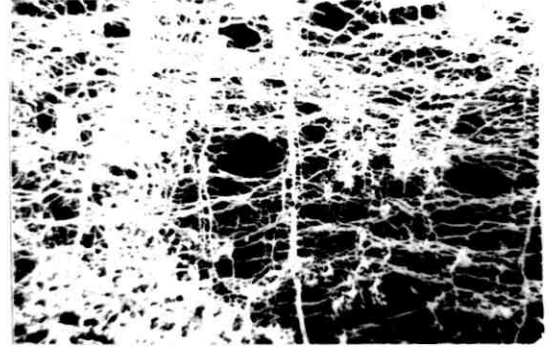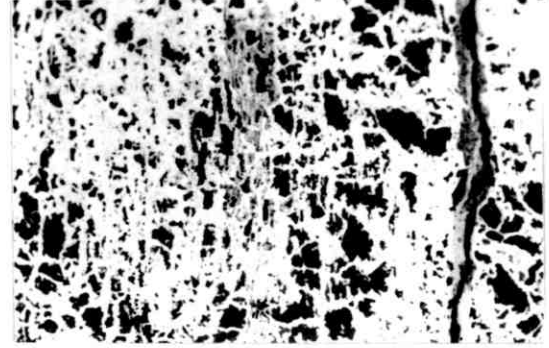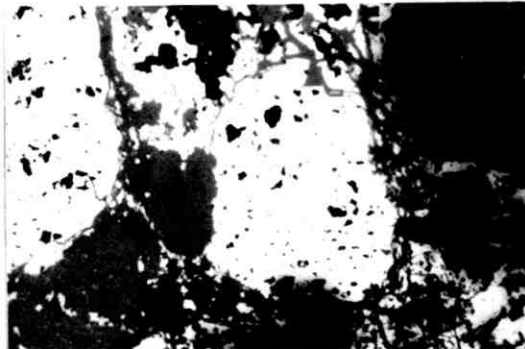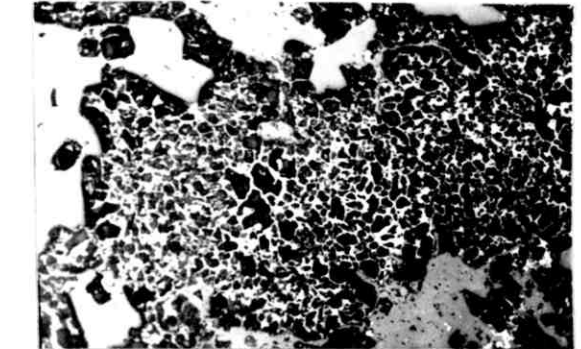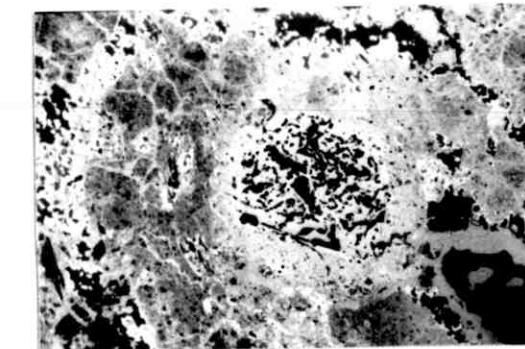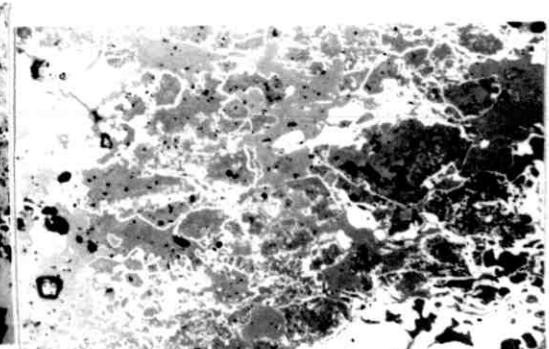
Fig. 5.3.3. Mean True Density and Porosity profiles – Mt.Monger
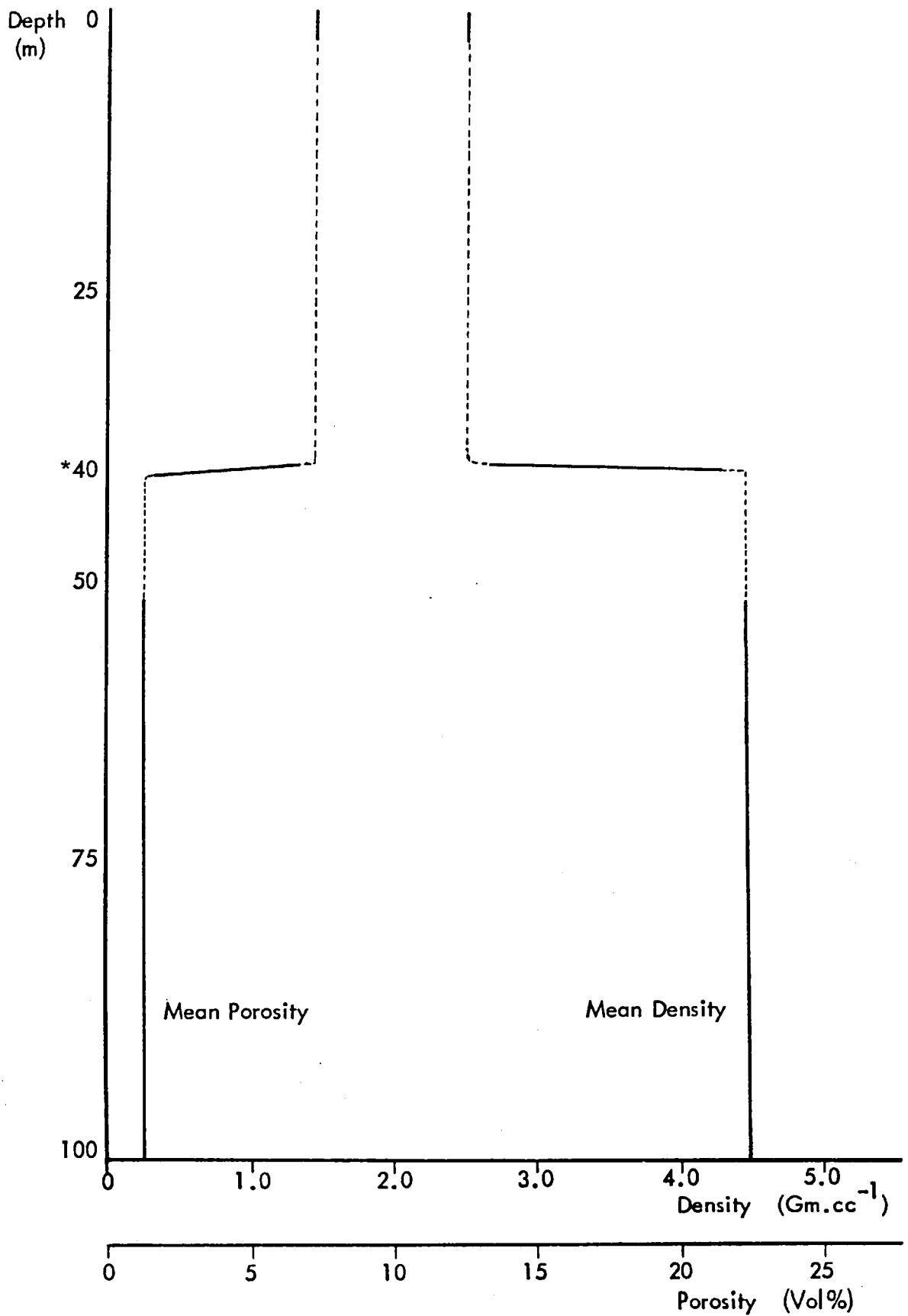
* Approximate position of the water table

Fig. 5.3.4.   Chemical Variations in Alteration Profile – Mt. Monger

Depth 0 (m)

Co Ti Mn   Cr Cu   Ni   Fe Si

S

*40

Mn Ti Cr   Co Cu   Si Ni   Fe S

100

10^{-6} 10^{-5} 10^{-4} 10^{-3} 10^{-2} 10^{-1}

* Approximate position of the water table

Element content (Gm. Equivs. cc^{-1})
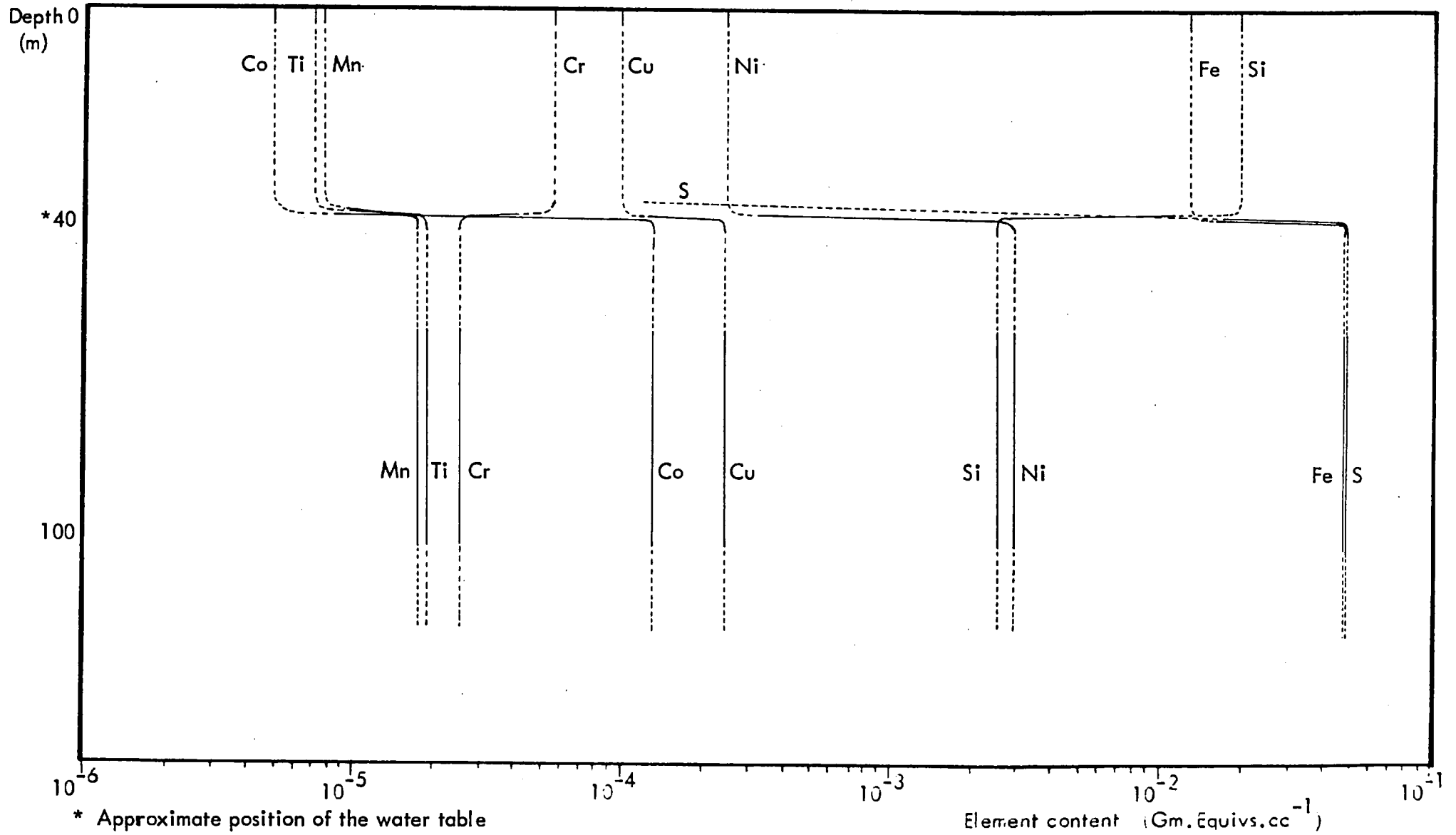
TABLE 5.3.1. SUMMARY DATA OF SULPHIDE ALTERATION - Mt.MONGER

Depth (m)	Alteration Zone	No. of Samples (n)	Mineralogy (Means and ranges) Volume % Units	Den gm/cc	Por %	S	Fe	SiO$_2$	MgO	Al$_2$O$_3$	CO$_3$	Ni	Cu	Mn	Cr	Co	Ti
	Oxide	18	Hm 1.0, Gt 5.0, Sl 1.5, FCr 0.0	1.90	0.5		3.06	1.32	0.00	0.10		110	479	30	62	62	36
			Hm 9.5, Gt 42.0, Sl 48.5, FCr 0.7, Ca 1.0, Dol trace	2.52	7.2	N/A	42.53	51.01	0.63	0.22	N/A	4512	2311	411	7374	101	137
40			Hm 42.0, Gt 92.0, Sl 85.0, FCr 3.0	3.10	16.8		86.71	99.24	4.20	0.60		23393	6638	4086	68419	314	552
	Sulphide - oxide transition	2	Py 33.0, Gt 15.0, Sl 33.0	2.50	0.9		20.65	40.67	0.10	0.10		3520	1134	59	171	709	72
			Py 34.0, Gt 24.0, Sl 41.5	2.80	4.5	14.12	24.50	52.23	0.30	0.30	N/A	5013	2049	2073	8115	952	213
			Py 35.0, Gt 33.0, Sl 50.0	3.10	8.1		38.35	63.79	0.50	0.50		6506	2964	4086	16058	1195	354
50 - 55	Violarite - pyrite	no data															
	Transition	1	Po 90.0, Pn 1.5, Vl 1.0, Cp 1.0, Mt 7.5	4.60	1.0	34.83	58.41	1.16	1.70	0.10	N/A	5383	7573	134	75	986	90
60-80	Primary	3	Po 75.0, Pn 5.0, Cp 1.0, Mt 4.0, Sil 2.0	4.30	0.5	30.54	50.34	3.58	2.80	0.20			919	245	68	1411	90
			Po 76.5, Pn 11.0, Cp 3.0, Mt 7.0, Sil 3.0	4.45	1.3	32.64	54.65	4.17	4.05	0.25	N/A	37577	1326	256	400	2087	261
			Po 80.0, Pn 17.5, Cp 5.0, Mt 10.0, Sil 5.0	4.60	2.0	34.75	58.96	4.76	5.30	0.30			7733	267	732	2762	432

transformation that takes place as a result of pervasive sulphide oxidation at this horizon.

The bulk chemistry of the sulphide alteration sequence

The bulk chemical variation within the sulphide oxidation profile sampled at the Mt.Monger deposit is presented in Fig.5.3.4. The overall constancy of all mean element contents within the 90 - 40 metre vertical interval indicates, on available data, that supergene sulphide development acts as a closed chemical system in this deposit.

In contrast, the variation of the major elements iron and sulphur across the zone of sulphide leaching at about 40 metres b.s. demonstrates the expected chemical behaviour of these elements in the high Eh - low pH environment created by sulphide degradation. The retention of about 30 percent of this mobilised iron above the sulphide leaching horizon is due to the precipitation of the metal as ferric oxides. Whereas, the increase in mean silicon content across the 40m. horizon is caused by the influx of silica into the oxide zone from its source in proximal weathering silicates.

The behaviour of the complementary suite of trace elements across the sulphide-oxide transition in general corresponds with the mobility differences existing between these elements in the acid oxidising conditions associated with sulphide leaching. Significantly though the observed relative immobility of typically mobile copper is probably due chiefly to the location of this metal in relatively resistant copper sulphide minerals. In contrast to which the substantial noted increase in chromium across the 40m.horizon is probably related to the influx of significant quantities of this metal into the oxide zone after its release through the chemical weathering of proximal Cr-rich ultramafic rocks.

5.4. SUPERGENE SULPHIDE ALTERATION IN THE JAN SHOOT, KAMBALDA

The Jan shoot occurs as an elongate lensoid orebody that is situated along the dislocated footwall contact of its steeply-dipping host serpentinite with under-lying metabasalt, (Section 2.3.). The ore consists of basal massive sulphide that grades upwards into disseminated material, (Table 2.4.1.). Sampling for the

present study was confined to the supergene altered horizons and to the surface gossans due to a shortage of underground development during initial fieldwork in July 1973.

The petrology of the supergene-altered sulphide assemblage

The secondary massive sulphide assemblage sampled at Jan Shoot comprises violarite after both pentlandite and pyrrhotite, (10 percent combined); secondary pyrite, (60 percent); secondary marcasite, (17 percent); chalcopyrite, (1.5 percent); and silicates, (10 percent); (Table 5.4.1.). These mineral proportions infer that the equivalent primary massive ore contains approximately 80 percent pyrrhotite and about 10 percent pentlandite.

Secondary pyrite is present as a massive matrix of generally interlocking, rather equant grains that surround irregular, commonly elongate aggregates of violarite after pentlandite, (Fig.5.4.1A.). The secondary nature of the pyrite is denoted by its passive fringing by feather lamellae of violarite after pyrrhotite, (Fig.5.4.1B.)

Secondary marcasite is rather heterogeneously distributed within the sampled secondary ore. Where present it usually occurs as fine-grained (colloidal) aggregates after pyrrhotite that quite commonly pseudomorph the cleavage traces of the parent sulphide, (Fig.5.4.1C.). This fine-grained marcasite generally undergoes in situ recrystallisation to a coarse bladed variety, (Fig.5.4.1D.). More typically however the fine-grained sulphide recrystallises either directly or indirectly to the massive pyrite forming the matrix of the secondary ore, (Fig.5.4.1E.). In both instances the relic pyrrhotite cleavage texture is apparently obliterated as a result of the replacement process.

Violarite after pentlandite (Vpn) occurs both as quite massive fine-grained aggregates, (Fig.5.4.1A.), and as discreet generally equant blocky forms within the secondary pyrite matrix, (Fig.5.4.1B.). Interestingly, the octahadral cleavage fillings of Jan Shoot Vpn exhibit considerable mineralogical variation. In this respect, violarite containing solely pyrite, (Fig.5.4.1B.); pyrite plus magnetite, (Fig.5.4.1F.); magnetite alone, (Fig.5.4.1G.); and siderite alone, (Fig.5.4.1H.) are commonly noted in the sampled material. It is likely that this variation in iron mineralogy indicates the presence of variable localised chemical conditions during the formation of violarite from pentlandite. However, it is possible that the

Fig. 5.4.1. Petrography of Jan Shoot Sulphide Ore

Scale length = 300 μ

A. Typical secondary ore texture (x 40) Air

Secondary pyrite: medium grey: Violarite: dark grey: Voids; black

B. Composite supergene alteration texture (x 110) Air

Vpn; grey-black, granular: Vpo; medium-dark grey, granular: Pyrite; medium grey: Carbonate; dark grey. Violarite (Vpn) cleavages invested in Pyrite

C. Secondary marcasite showing mimicked pyrrhotite cleavage structure (x 110) Air

Fine-grained marcasite: dark-medium grey, mottled: Coarser recrystallised marcasite; medium grey: Carbonate; grey-black

D. Marcasite recrystallising to coarser variety (x 320) Air

F.G. marcasite; dark-medium grey, mottled: Coarse marcasite; medium-grey: Carbonate: grey-black

E. Recrystallisation of marcasite to pyrite (x 220) Oil
F.G. marcasite: dark-medium grey, mottled: Massive pyrite; light to medium greys: Carbonate: grey-black

F. Violarite cleavage filling: pyrite and magnetite (x 110) Air

Cleavage traces only: Pyrite; medium grey: Magnetite; dark grey

G. Violarite cleavage filling: magnetite (x 320) Air

Violarite; medium grey, granular: Magnetite, medium-dark grey: Carbonate: grey-black

H. Violarite cleavage filling: siderite (x 80) Oil

Violarite; medium grey, granular: Siderite; dark grey: Pyrite; light grey

Fig.5.4.1.
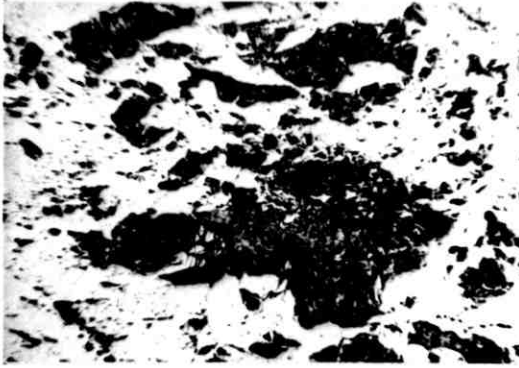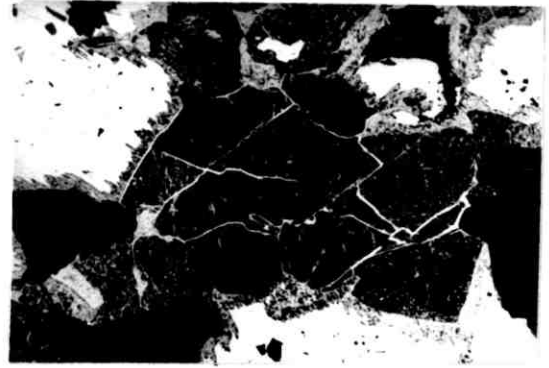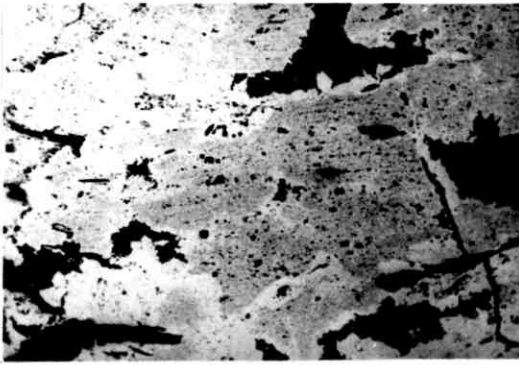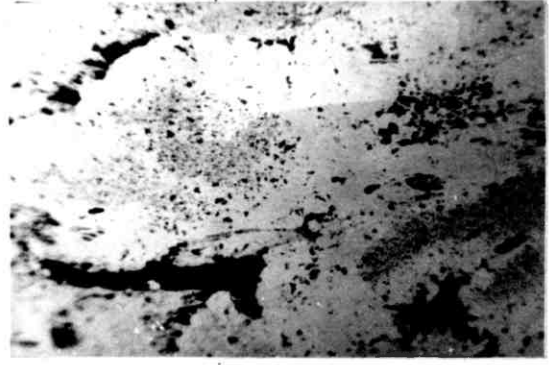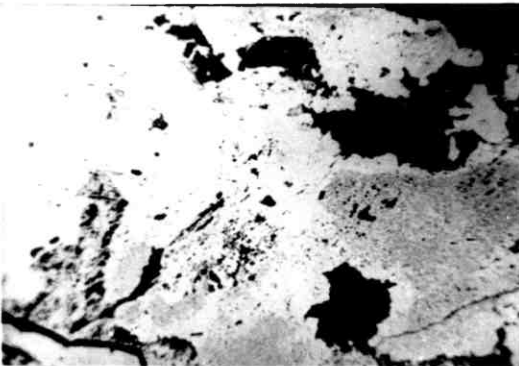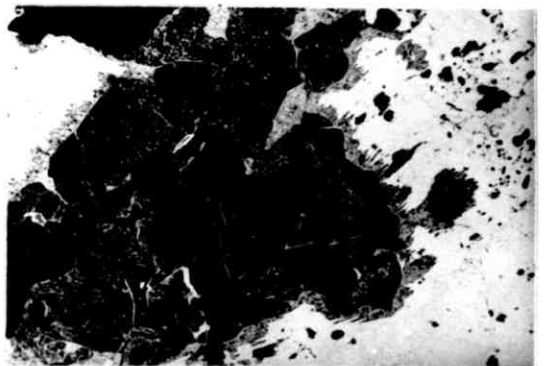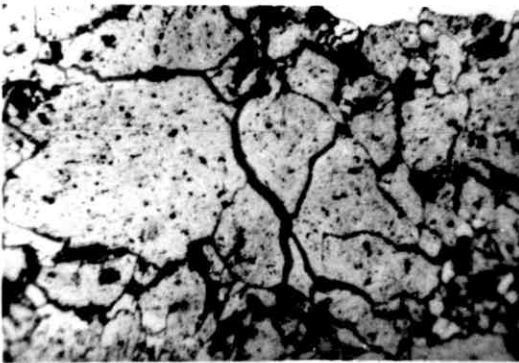
development of pyrite cleavage fillings may represent an intrusion of material rather than an in situ development. This is because there is some textural evidence of pyrite replacing magnetite within Vpn cleavage traces, (Fig.5.4.1F.).

The petrology of the oxide zone

Available data indicate that the secondary sulphide zone developed at the Jan Shoot extends from about the 75-80m. level up to approximately 30 metres b.s. The sulphides undergo pervasive leaching at this horizon and are superceded by an oxidised assemblage that comprises goethite (32 percent); silica (65 percent); and hematite, (1.5 percent), (Table 5.4.1.).

Goethite is noted in a number of significant textural relations in the Jan Shoot oxide zone. It is typically present as pseudomorphic replacements of violarite after pentlandite, (Fig.5.4.2A.); and violarite after pyrrhotite, (Fig.5.4.2B.). Further, goethite is also important in both relic and mimic structures after secondary iron disulphide. In this respect it is generally observed as boxwork structures after massive secondary pyrite, (Fig.5.4.2C.). Additionally, however, goethite also commonly occurs as secondary mimic structures after pyrrhotite in the form both of boxworks, (Fig.5.4.2D.), and of solid pseudomorphs, (Fig.5.4.2E.).

Silica is present as a pervasive cryptocrystalline matrix in the Jan Shoot oxide zone, (Fig.5.4.2F.). Further, it also directly invests solid goethite pseudomorph structures, (Fig.5.4.2G.), and typically fills the interstices of boxworks and other leached cavities after ore minerals, (Fig.5.4.2D.).

Hematite is rare in the Jan Shoot gossan. Where present, however, it is generally observed as pseudomorph structures after secondary marcasite, (Fig.5.4.2H.).

The corresponding mean true density and mean porosity profiles

The mean variation in true density and porosity within the sampled upper part of the Jan Shoot oxidation profile is indicated in Fig.5.4.3. The alteration in both physical properties across the water table horizon at about 30 metres b.s. directly reflects the fundamental mineralogical and chemical transformation that accompanies pervasive leaching of the secondary sulphide assemblage at this horizon.

Fig. 5.4.2. Petrography of the Jan Shoot Gossan

Scale length = 1000 μ Blue-white filter used throughout

A.   Goethite mimics after interstitial violarite (Vpn) (x 80) Air

  Goethite; light-medium grey: Silica; dark grey: Voids; black

B.   Goethite mimics after lamellar violarite (Vpo) (x 110) Air

  Goethite; light to medium greys: Silica; dark grey: Voids; black

C.   Goethite boxwork after secondary pyrite (x 110) Air

  Goethite; light to medium greys: Silica; dark grey: Voids; black

D.   Goethite boxworks after pyrite mimicked pyrrhotite cleavage structure
     (x 110) Air

  Goethite; light to medium greys: Silica; medium-dark grey: Voids; black

E.   Goethite mimic after mimicked pyrrhotite structure (x 110) Air

  Goethite; medium grey: Silica; dark grey: Hematite; light grey.
  Pyrrhotite cleavage lineations are well-preserved

F.   Silica as pervasive rock matrix (1) (x 40) Air

  Silicified goethite; medium grey: Goethite; light grey: Voids- black

G.   Silica as pervasive rock matrix (2) (x 80) Air

  Goethite; medium to dark greys, mottled: Silica; dark grey: Voids; black
  Goethite in violarite mimic structure is pervasively invested in silica

H.   Hematite mimics after secondary marcasite (x 110) Air

  Hematite; grey-white: Goethite; medium grey: Silica; dark grey:
  Voids; black
  Relic pyrrhotite cleavage structure is preserved

Fig.5.4.2.
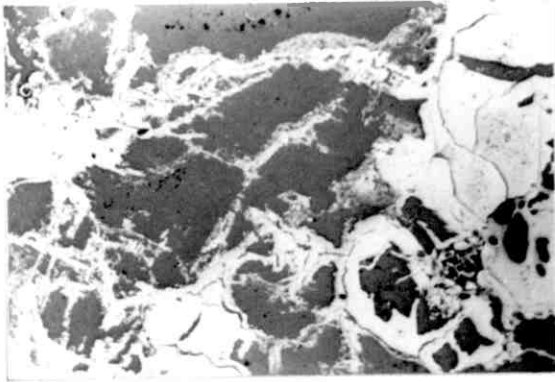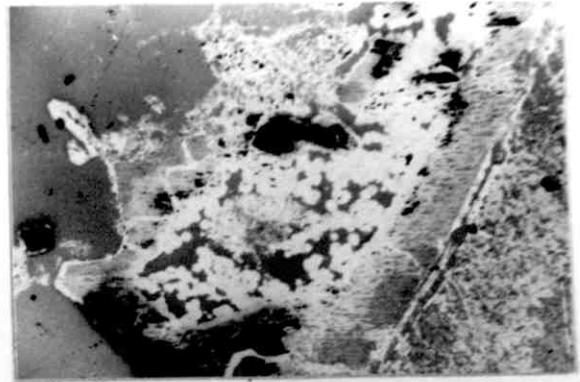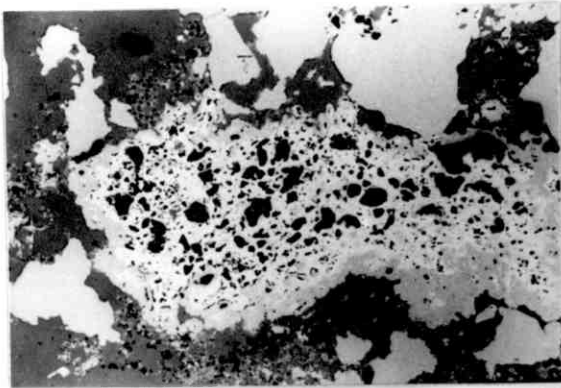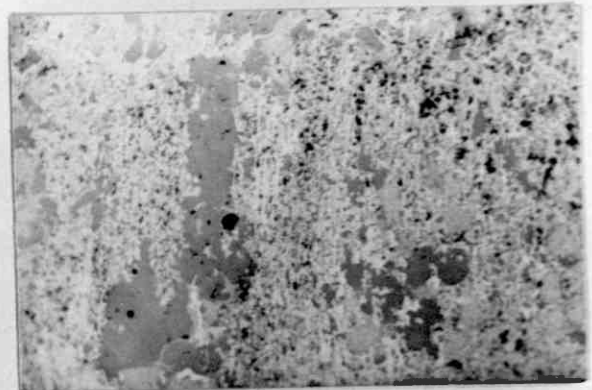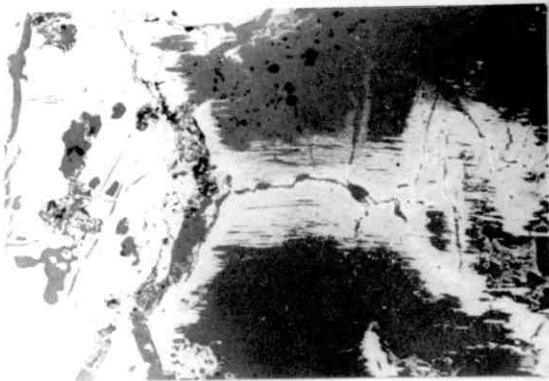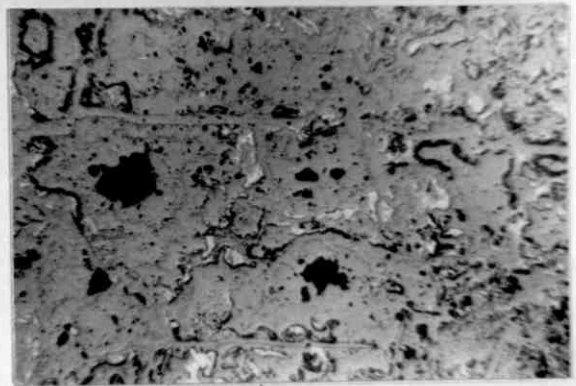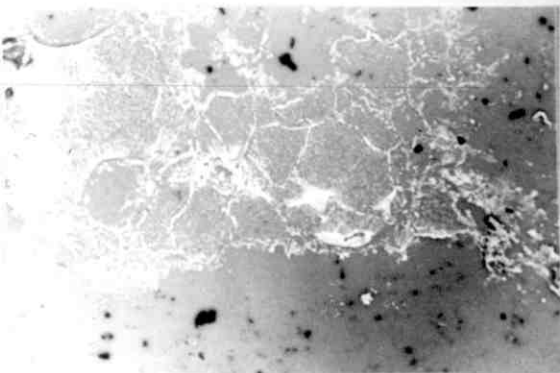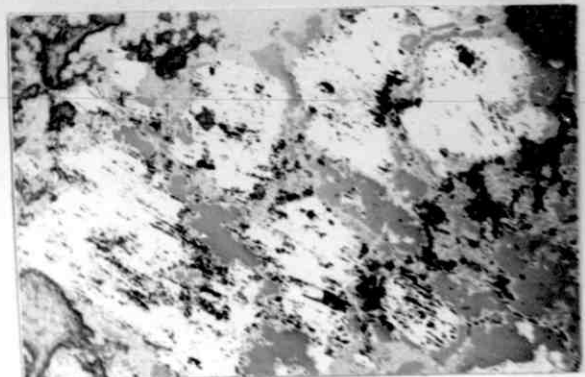
Fig. 5.4.3. Mean True Density and Porosity profiles – Jan Shoot
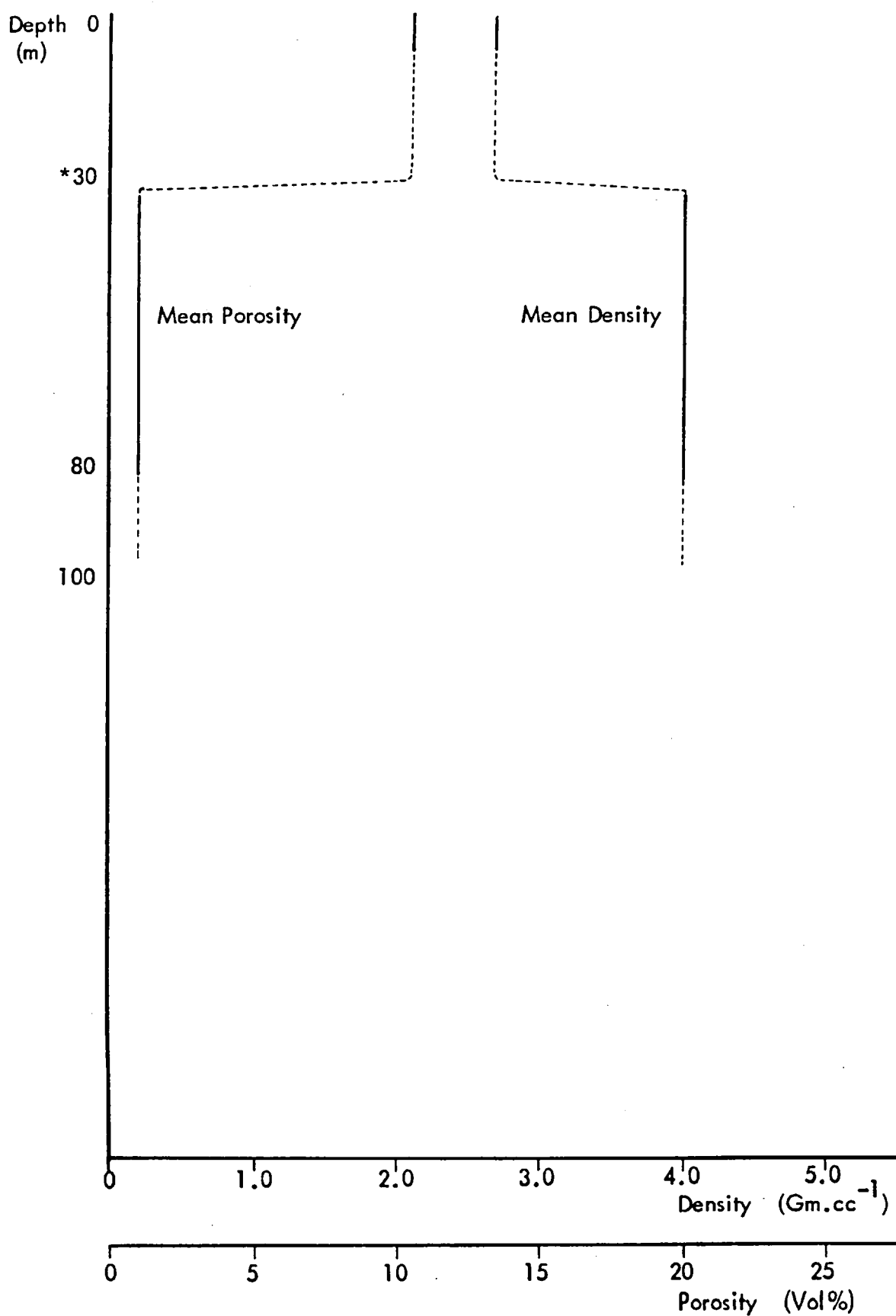
* Approximate position of the water table

Fig. 5.4.4. Chemical Variations in Alteration Profile – Jan Shoot

* Approximate position of the water table

Element content   (Gm. Equivs. cc^{-1})

290
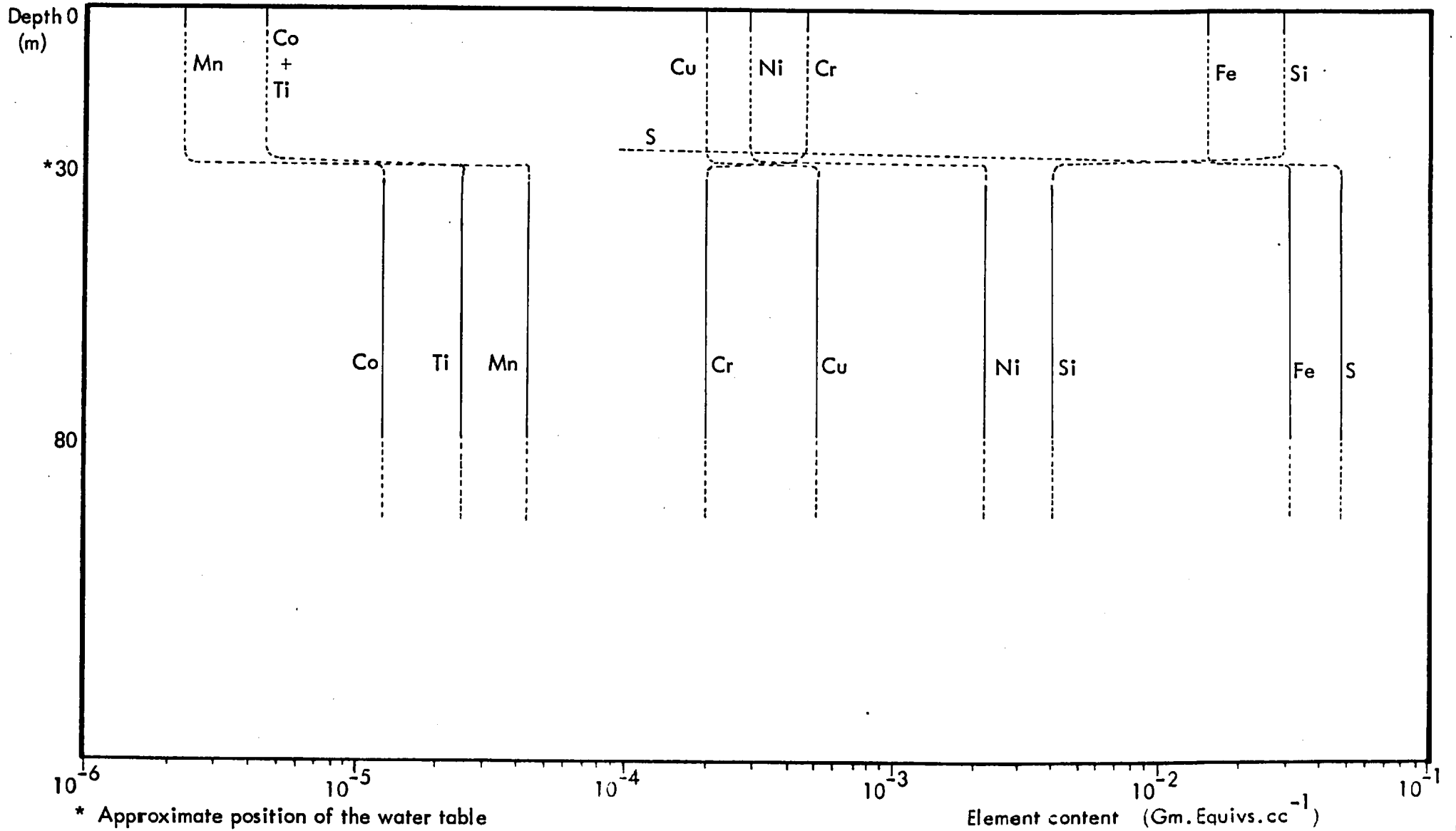
TABLE 5.4.1. SUMMARY DATA OF SULPHIDE ALTERATION - JAN SHOOT

Depth (m)	Alteration Zone	No. of Samples (n)	MINERALOGY (Means and ranges) Volume % Units						Physical data (mean/ranges) Den gm/cc	Por %	GEOCHEMISTRY (Means and ranges) Wt.% Units S	Fe	SiO₂	MgO	Al₂O₃	CO₃	p.p.m. Units Ni	Cu	Mn	Cr	Co	Ti
30 / 75-80	Oxide	6	Hm 0.5	Gt 15.0	Sl 50.0				2.20	0.5		12.06		0.10		0.00	2742	1973	25	698	88	24
			1.5	32.0	65.0				2.70	10.5		22.07	61.43	0.18	0.10	0.22	5898	3304	77	10624	220	35
			6.0	50.0	75.0				3.10	26.4		32.04		0.40		1.50	8887	5624	177	23051	499	54
	Violarite – pyrite	4	Vl 4.0	Cp 0.0	Py 15.0	Mc 0.0	Sll 4.0		3.30	0.5	30.12	37.29	0.26	0.00	0.00		13736	112	141	1033	45	30
			10.0	1.5	60.0	17.5	10.0		3.98	1.0	37.81	42.73	6.41	3.25	0.43	N/A	34510	7944	589	4549	176	325
			15.0	2.5	78.5	70.0	25.0		4.20	2.9	49.66	46.10	12.20	5.30	0.80		49576	22646	795	5179	433	959
	Transition	no data																				
	Primary	no data																				

The bulk chemistry of the sulphide-oxide transition

The alteration in bulk chemistry across the top 75 metres of the Jan Shoot oxidation profile is presented in Fig.5.4.4. The change in iron and sulphur contents that occur across the sulphide-oxide transition (30m level) is consistent with the expected behaviour of these elements in the acid oxidising conditions characteristically associated with sulphide leaching. Fig.5.4.4. indicates, however, that approximately 50 percent of the released iron is retained in the oxide zone as iron oxide (principally goethite). In contrast,the high mean silicon content of the sampled Jan oxide zone is likely due to the large-scale influx of silica derived from the weathering of proximal silicates.

The chemical behaviour of individual trace metals across the sulphide leaching horizon generally conforms quite closely to that typically exhibited by these elements in a high Eh-low pH environment. Significant anomalies do however occur, and in this respect, the noted retention of copper is probably related to the persistence of chalcopyrite and/or covellite into the chemically quiescent oxide zone. In contrast, the noted increase in mean chromium content across the sulphide-oxide transition is likely related to an influx of this metal into the oxide profile from adjacent weathering ultramafic rocks.

5.5. SUPERGENE SULPHIDE ALTERATION AT THE RAVENSTHORPE NO.5 PROSPECT

The mineralisation at the Ravensthorpe No.5 prospect occurs as massive, disseminated and vein ore and is situated at or near the basal contact of steeply-dipping serpentinite and underlying quartzite, (Section 2.3.). The following description is based on the supergene-altered near-massive component present in the deposit. No samples of unaltered primary ore were available for the present study.

The petrology of near-surface sulphide alteration

The (sampled) partly-altered near-massive sulphide mineralisation comprises pyrrhotite (about 45 percent), marcasite after pyrrhotite (20 percent), violarite after pentlandite (four to five percent), magnetite (three percent), chalcopyrite (one percent), and silicates (about 25 percent), (Table5.5.1.). Pyrrhotite in near-

massive ore typically occurs as rather equant grain aggregates that form the matrix of the sulphide mineralisation, (Fig.5.5.1A.). In areas of more disseminated character however, the sulphide generally occurs as elongate stringers or patches within a silicate matrix, (Fig.5.5.2A.).

Initiation of pyrrhotite alteration occurs irregularly with respect to depth in the massive sulphide profile. Available evidence indicates however that all pyrrhotite grains exhibit incipient alteration above the 150m. level. This alteration characteristically takes the form of small elongate lamellae of red-orange smythite. The smythite develops internally along the grain borders of the pyrrhotite and around included violarite lamellae, and the mineral grows into the parent phase along the 001 cleavage direction, (Fig.5.5.1B.).

Smythite is subsequently replaced by laterally-extensive fringes of violarite after pyrrhotite. This latter mineral supercedes the (transitional) smythite along the retained pyrrhotite 001 cleavage direction and typically forms along grain borders adjacent to violarite after pentlandite, (Fig.5.5.1C.).

Violarite after pentlandite typically occurs as discrete euhedral to elongate blocky grains associated with pyrrhotite and secondary marcasite, (Fig.5.5.1C.). It is also present as aggregates of flamme lamellae in these minerals, (Fig.5.5.1B.). Available data indicate that all or most of the parent pentlandite is altered to violarite above the 150m. level, (Table 5.5.1.).

Magnetite occurs as generally equant to rather elongate grains that typically possess smooth rounded outlines, (Fig.5.5.1A.). The spinel is fairly evenly distributed within the ore matrix and occurs in both sulphide and silicate components.

On the basis of available data, alteration of residual pyrrhotite is well-established at the 150m. level in the massive sulphide profile, (Table 5.5.1.). The alteration generally occurs as an in situ replacement by fine-grained marcasite. Replacement is initiated within the central region of the parent grain and subsequently takes place along the 001 cleavage direction. This phenomenon leads to the mimic preservation of the pyrrhotite cleavage structure in the replacing marcasite, (Fig. 5.5.2A.).

Subsequent recrystallisation of the pseudomorphing secondary marcasite generally takes place however, and leads to the development of bladed aggregates of coarser-grained marcasite within the former pyrrhotite grain areas, (Fig.5.5.2B.). Further, indirect evidence from oxide zone textures infers that at least part of the secondary

294

Fig. 5.5.1.   Petrography of Ravensthorpe Sulphide Ore

Scale length = 100 μ

A.   Typical massive ore texture (x 80) Air

Secondary marcasite after pyrrhotite; light-medium grey: Violarite;
medium-dark grey, granular: Spinel; medium-dark grey: Carbonate;
dark grey: Voids; black

B.   Secondary alteration of pyrrhotite (x 600) Oil

Pyrrhotite; medium-dark grey (centre):   Smythite; medium grey, lamellar:
Altering pentlandite; medium grey, granular: Voids; black

C.   Mature secondary (supergene) mineral assemblage (x 320) Air

Violarite species (Vpn and Vpo - lower right); medium grey, granular:
Marcasite; light to medium-dark grey (lower right): Carbonate; grey-black

295
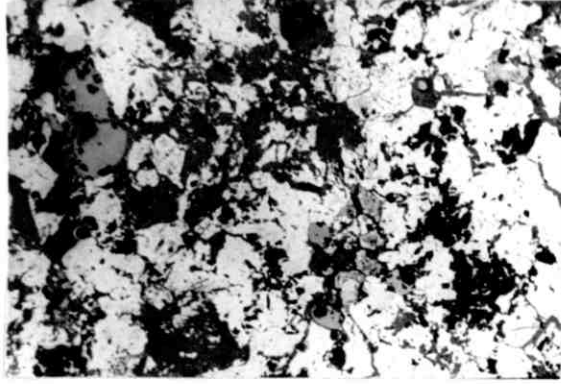
Fig.5.5.1.

A
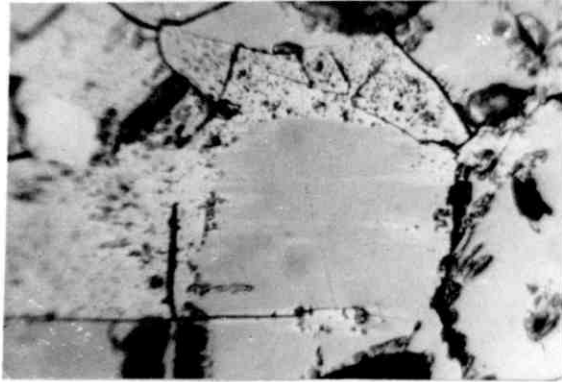
B
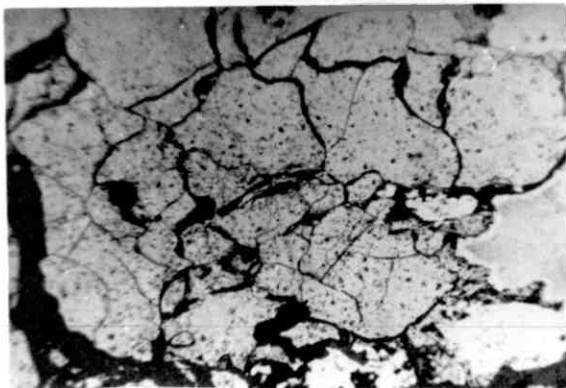
C

marcasite recrystallises to a massive pyrite, (Fig.5.5.2C.).

The petrology of the oxide zone

The mature massive secondary sulphide assemblage of violarite and marcasite is, on available evidence, present between (approximately) the 80m. level and the water table at 40 metres b.s. It is abruptly superceded at this latter level though by an oxidised assemblage that is composed principally of goethite (97 percent), but which also contains minor amounts of both hematite and silica (one percent each), (Table 5.5.1.).

Goethite forms the matrix of the oxide zone mineral assemblage after near-massive sulphide, (Fig.5.5.2C.). The iron oxide is present in several important textural configurations after the secondary sulphide assemblage. In this respect goethite occurs as pseudomorphs and residual structures after secondary iron dis-sulphides, and is present as bird's-eye textures after secondary marcasite, (Fig. 5.5.2D.); and as boxworks and solid aggregates after secondary pyrite, (Fig. 5.5.2C.). Goethite also occurs as less common secondary pseudomorphs after pyrrhotite, (Fig.5.5.2E.).

Goethite is, additionally, present as pseudomorphs after both violarite after pentlandite, (Fig.5.5.2F.), and violarite after pyrrhotite, (Fig.5.5.2E.), and it also occurs as rare replacements of chalcopyrite, (Fig.5.5.2G.).

Hematite is very rare in the sampled Ravensthorpe gossan, and where noted is present as a partial replacement of goethite. Silica is present as rare patches of interstitial and leached cavity filling in the gossan, (Fig.5.5.2H.).

Dolomite occurs as an oxidate mineral associated with the Ravensthorpe gossan. The carbonate mineral is present as a covering on joint faces, and its trace metal-rich chemistry, (Table A2/4 ,Appendix Two) indicates that it likely precipitated from solution during a previous episode of sulphide leaching when the oxide material now at the surface was situated at the level of the water table.

The corresponding mean true density and mean porosity profiles

The mean variations in true density and porosity within the sampled massive sulphide alteration sequence at Ravensthorpe are presented in Fig.5.5.3. Such

297

Fig. 5.5.2. Petrography of Ravensthorpe Ore (2) and Gossan

Scale length = 200μ   Blue-white filter used throughout

A.   Disseminated ore texture (x 320) Air

Pyrrhotite; grey-white: Secondary marcasite; grey-white, granular:
Silicate; grey-black. Pyrrhotite cleavage lineations are preserved by
replacing marcasite

B.   Recrystallisation of fine-grained to coarse bladed marcasite (x 320) Air

F.G. marcasite; medium-dark grey: Coarse marcasite; light-medium grey:
Silicate and voids: black

C.   Massive pyrite mimic in gossan (x 80) Air

Goethite after violarite; medium grey: Goethite after pyrite; light grey:
Voids; black

D.   Goethite mimic after marcasite bird's-eye structure (x 320) Air

Goethite; medium greys: Voids; dark grey

E.   Goethite mimic after mimicked pyrrhotite structure (x 320) Air

Goethite after pyrrhotite; medium-grey: Goethite after Vpo; medium-
dark grey: Voids and silica; grey-black

F.   Goethite mimics after interstitial violarite (Vpn) (x 110) Air

Goethite; light to medium greys: Voids; black: Mounting resin; dark grey

G.   Goethite boxwork after chalcopyrite (x 600) Air

Goethite; light to dark greys: Voids; black

H.   Silica as interstitial and cavity filling (x 110) Air

Silica; dark grey: Goethite; light to medium greys: Voids; black
Secondary marcasite pseudocolloform textures well preserved

Fig.5.5.2.
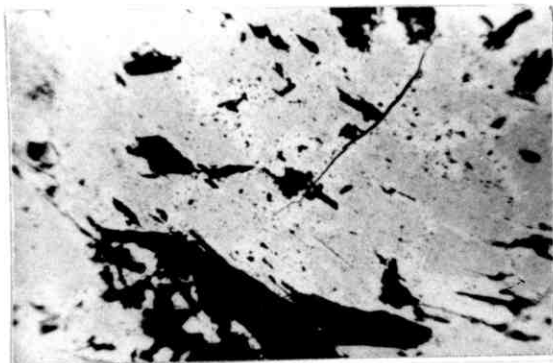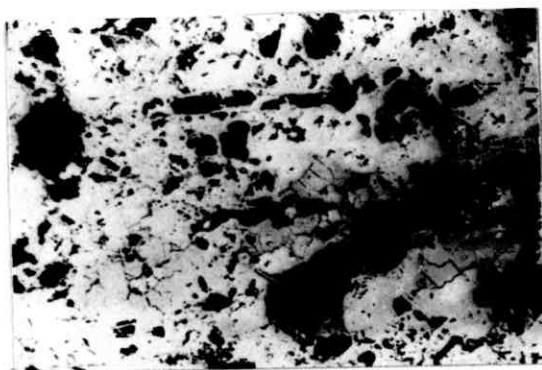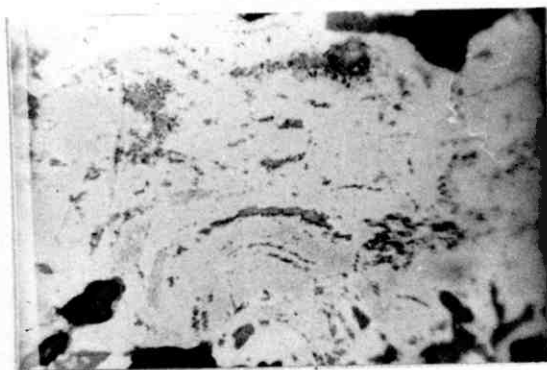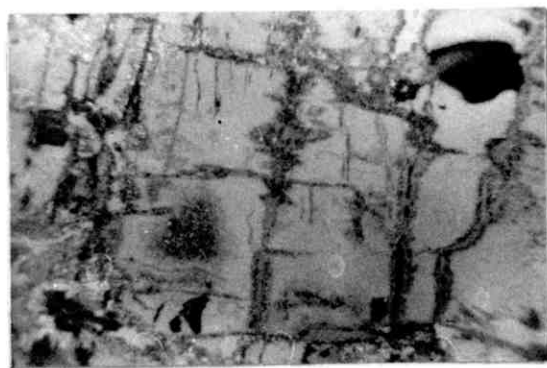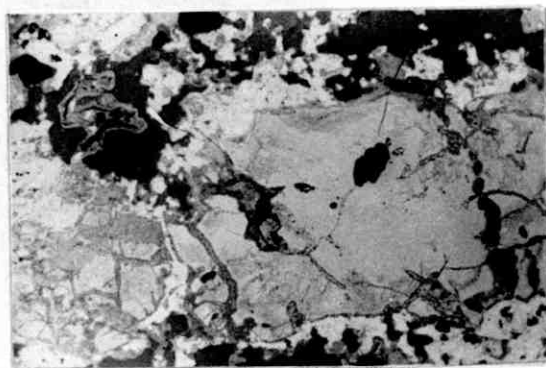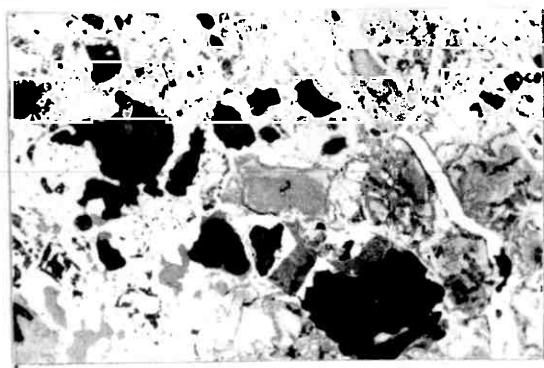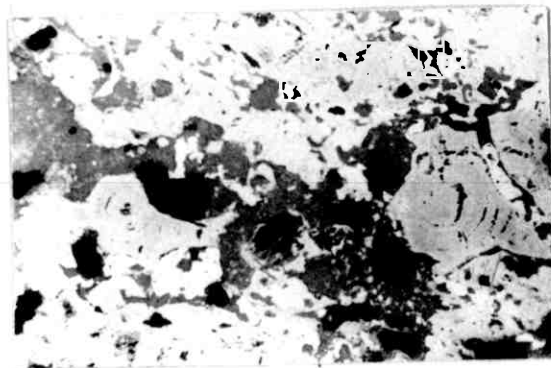
Fig. 5.5.3. Mean True Density and Porosity profiles - Ravensthorpe
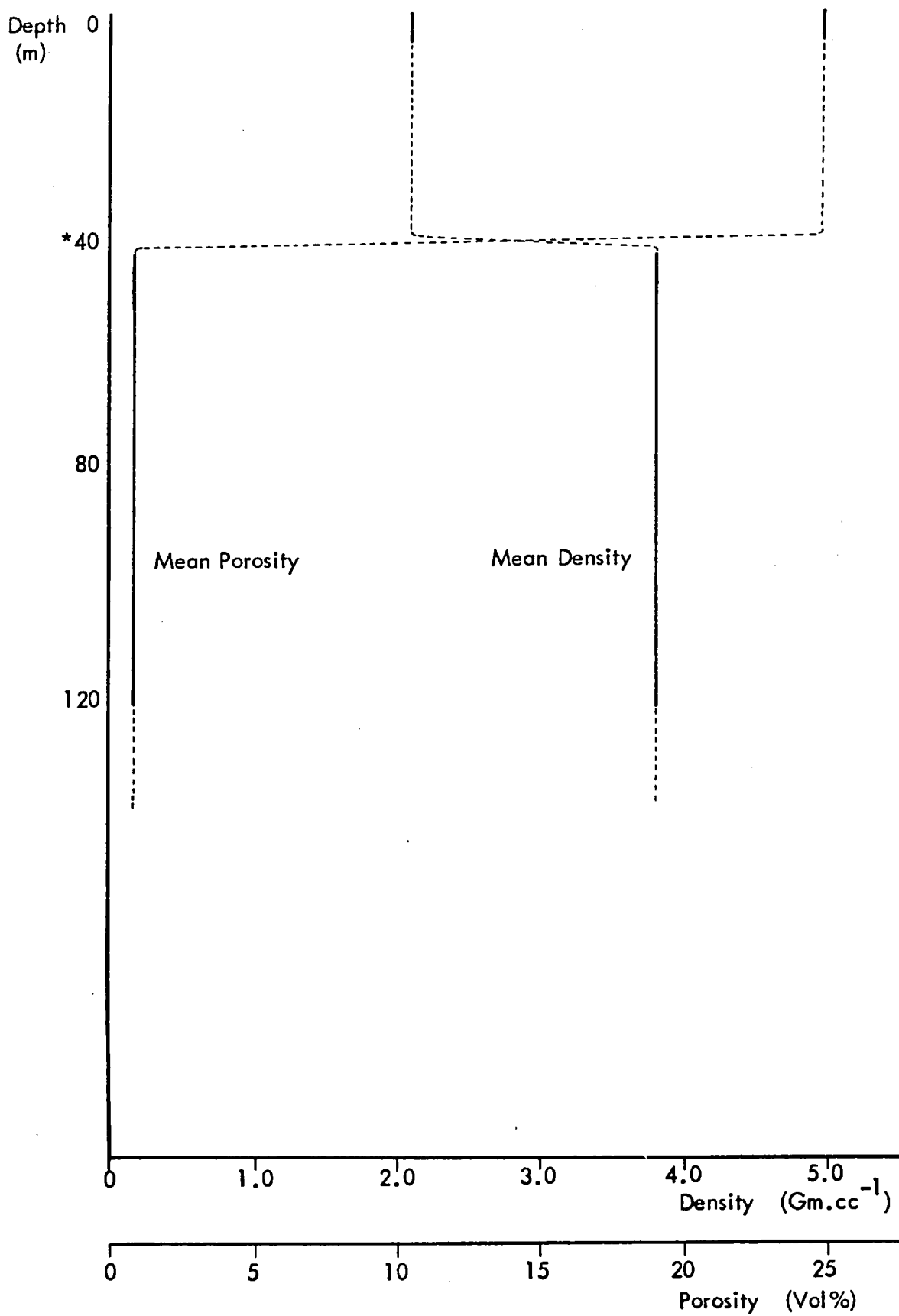
* Approximate position of the water table

data as are available demonstrate that little significant variation in either physical property occurs during the formation and subsequent occurrence of the secondary sulphide assemblage, (150-40m. levels). In contrast, the fundamental changes in mean density and porosity that occur across the 40m. horizon reflect the dramatic alterations in chemistry and mineralogy that occur as a result of sulphide leaching at this level.

The bulk chemistry of the Ravensthorpe sulphide alteration sequence

The bulk chemistry of the sampled near-massive sulphide alteration sequence is presented in Fig.5.5.4. The depth profiles set out in the figure cannot however be rigourously interpreted in a quantitative manner as they are based on rather small sample numbers. The data may be semi-quantitatively assessed though, and in this respect the individual constancy of all mean element profiles between the 150 and 40m. levels indicate the likely operation of an effectively closed chemical system during the formation of the secondary sulphide assemblage.

The behaviour of iron and sulphur across the sulphide-oxide transition (40m. level) demonstrates the wholesale oxidation and mobilisation of both these major elements under high Eh-low pH conditions, and the retention of substantial quantities of iron indicates, as in other nickel deposits, the subsequent precipitation of a proportion of this metal as iron oxides.

The effective (semi-quantitative) constancy of mean sulphide zone silicon contents across the sulphide leaching horizon indicates the likelihood that pervasive silification due to wall-rock silicate weathering is not a feature of the Ravensthorpe oxide zone.

The oxidation behaviour of the trace metal suite cannot be rigourously interpreted because of the sample size problem. In semi-quantitative terms though, individual metals, with the exception of cobalt and manganese exhibit variations that are reasonably compatible with their predicted mobilities within an acid oxidising (sulphide leaching) environment. The apparently immobile behvaiour of cobalt and manganese is however very likely due to bias induced by small sample numbers rather than to any significant deviation from expected chemical behaviour in these two metals.

Fig. 5.5.4. Chemical Variations in Alteration Profile – Ravensthorpe

* Approximate position of the water table

Element content (Gm.Equivs.cc^{-1})

TABLE 5.5.1. SUMMARY DATA OF SULPHIDE ALTERATION – RAVENSTHORPE No.5

Depth (m)	Alteration Zone	No. of Samples (n)	MINERALOGY (Means and ranges) Volume % Units								Physical data (mean/ranges)		GEOCHEMISTRY (Means and ranges) Wt.% Units						p.p.m. Units					
			Hm/Po	Gt	Sl/Vl	Cp	Mt	Dol	Mc	Sil	Den gm/cc	Por %	S	Fe	SiO$_2$	MgO	Al$_2$O$_3$	CO$_3$	Ni	Cu	Mn	Cr	Co	Ti
40	Oxide	3	1.0	95.0	0.5						2.00	15.5		56.71	2.67	0.30	0.50		22772	2061	752	123	1593	186
			1.0	97.0	1.0			trace			2.17	24.5		58.20	3.21	0.43	0.57	N/A	29525	2455	929	137	2029	236
			3.0	98.0	3.0						2.40	30.4		59.53	3.69	0.50	0.70		35062	2836	1131	144	2349	282
80	Violarite – pyrite	1			5.0		5.0		80.0	5.0	3.80	0.9	34.58	58.24	1.94	0.60	0.10	N/A	25028	3435	743	137	1195	78
	Transition	1	45.0		4.0	1.0	3.0		20.0	25.0	3.10	0.0	16.20	43.56	22.12	12.68	0.94	N/A	6852	895	945	438	367	600
120	Primary	no data																						

5.6. SUPERGENE SULPHIDE ALTERATION IN THE CARR BOYD DEPOSIT

The Carr Boyd deposit occurs as massive to disseminated sulphide ore within a vertical bronzite-pegmatoid intrusive breccia pipe complex. The complex itself is situated proximal to a lobate mafic-ultramafic layered succession, (Section 2.3.). The geology of the deposit has been described by Purvis et.al., (op.cit.), and by Schultz, (op.cit.). The supergene sulphide alteration present in the ore profile has not, however, previously been documented.

The present description is confined to the upper portion of the alteration sequence developed in near-massive ore; i.e. the secondary (supergene) sulphide zone and it's overlying oxide zone. This is because of the inaccessibility of the deeper portions of the ore body during sampling operations carried out in August 1973.

The petrology of the secondary (supergene) sulphide assemblage

The secondary sulphide assemblage of sampled near-massive ore comprises secondary marcasite after pyrrhotite (50 percent), secondary pyrite (12 percent), chalcopyrite (nine percent), violarite after pentlandite (two percent), and silicate (25 percent), (Table 5.6.1.).

Secondary marcasite occurs in the former grain locations of pyrrhotite. It is present in a fine-grained (colloidal) form that commonly retains the cleavage direction of the parent sulphide as elongate void trains, (Fig.5.6.1A.). Large (quite rare) pseudocolloform structures are also typically defined by fine-grained secondary marcasite, (Fig.5.6.1B.).

Secondary recrystallisation of colloidal marcasite is however typically observed in the sampled material. The mineral is generally replaced by a coarse bladed form (Fig.5.6.1D.), that not uncommonly exhibits thin bravoitic zoning, (Fig.5.6.1E.). The nickel in the bravoite probably derives from the parent pyrrhotite, as this is known to be nickel-rich, (Schultz, op.cit.).

Chalcopyrite is heterogeneously distributed within the sulphide assemblage. It is commonly associated with both primary and secondary pyrite, (Fig.5.6.1F.). Chalcopyrite not untypically exhibits localised partial alteration to covellite, (Fig.5.6.1G.).

Fig. 5.6.1. Petrography of Carr Boyd Sulphide Ore (1)

Scale length = 100μ   unless otherwise indicated

A.   Marcasite with relic pyrrhotite cleavage structure (x 110) Air

Marcasite; light-medium to medium grey: Violarite (after pyrrhotite); dark-medium grey, granular: Violarite after pentlandite; dark grey, granular: Silica; grey-black

B.   Pseudocolloform texture in secondary marcasite (x 110) Air

Fine-grained marcasite; medium-dark grey: Coarse-grained (recrystallised) marcasite; medium grey, mottled: Silica; grey-black: Magnetite; dark grey (top left):   Violarite; dark grey, granular (top left)

C.   Recrystallisation of marcasite to coarse, bladed variety (x 110) Air

F.G. marcasite; dark-medium grey, mottled (lower right):   Coarse marcasite; medium grey (centre):   Violarite species; dark grey, granular: Silica; black

D.   Recrystallisation of coarse marcasite to massive pyrite (x 320) Air   Partly crossed nicols

F.G. marcasite; medium-dark grey, mottled (left):   Coarse marcasite: light to medium-dark grey (lower margin):   Pyrite; light-medium grey, homogeneous: Violarite species: dark grey, granular: Silica; black

E.   Bravoite zoning in secondary pyrite (x 110) Air

Pyrite; medium grey: Bravoite; dark grey, linear: Violarite species; dark grey, granular: Voids; black

F.   Typical chalcopyrite texture and association (x 40) Air

Chalcopyrite; medium-dark grey: Pyrite; light to medium grey: Silicate; dark grey: Voids; black

G.   Partial alteration of chalcopyrite to covellite (x 320) Air

Chalcopyrite; medium grey, homogeneous: Covellite; dark-medium grey, fringing cp: Silica; black: Violarite; medium-dark grey, granular

H.   Typical secondary violarite texture (x 110) Air

Violarite species: dark grey, granular: Marcasite: dark-medium grey: Pyrite; medium grey in violarite cleavage: Silicate; grey-black

Fig.5.6.1.
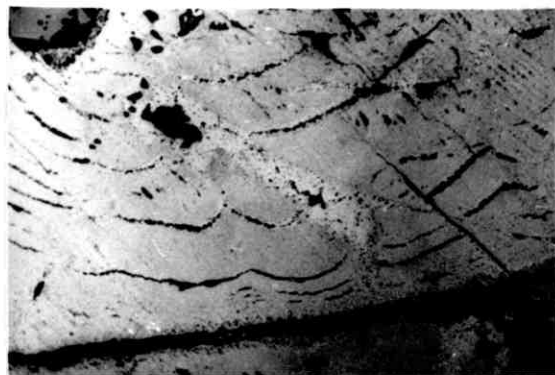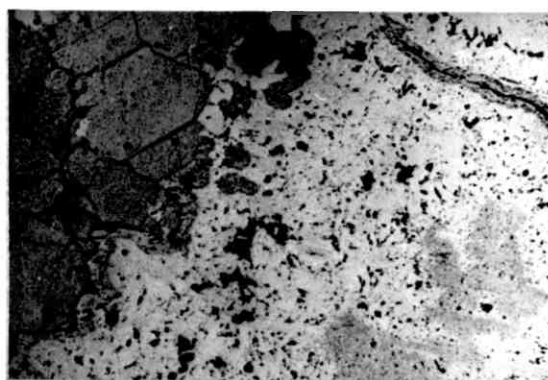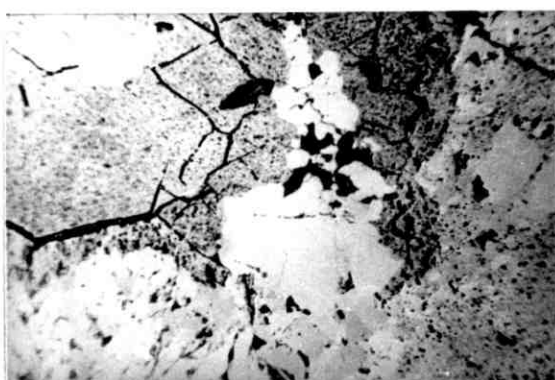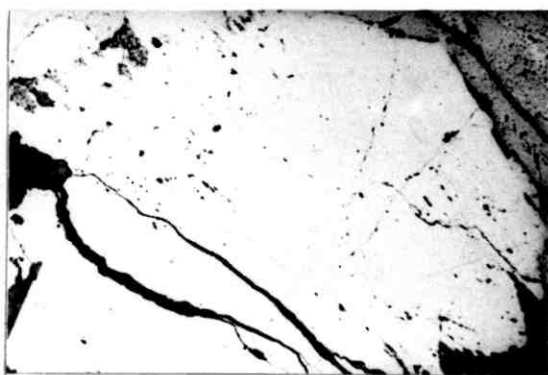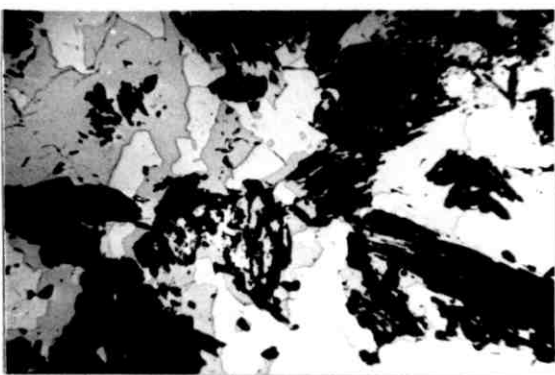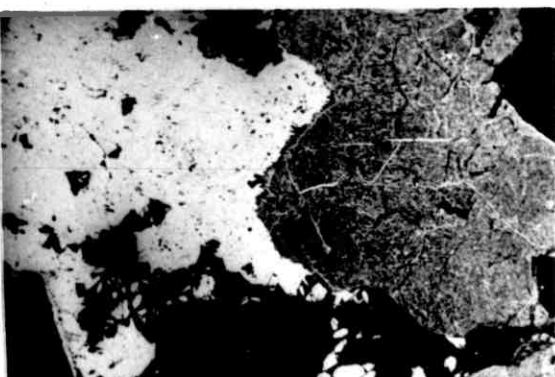
Fig. 5.6.2. Petrography of Carr Boyd Sulphide Ore (2)

Scale length = 100 μ

A. In situ replacement of iron disulphides by goethite (x 110) Air

Pyrite; white-grey: Goethite; dark-medium grey

B. Mimic replacement of chalcopyrite by covellite (x 110) Air

Covellite; light to medium greys, mimicking cp cleavage (centre): Goethite;
light-medium grey (top left): Silica; dark grey (right margin)

C. Mimic replacement of covellite by goethite (x 320) Air

Covellite; dark grey: Goethite; medium grey: Chalcopyrite relics; white-grey
Pyrite; white grey (lower margin)

D. In situ replacement of violarite by goethite (x 110) Air

Goethite after violarite; medium to dark grey, mottled: Pyrite; light grey:
Goethite after pyrite; light-medium grey: Voids; black

E. Partial replacement of violarite by covellite (x 600) Air

Covellite after Vpo; medium-dark grey, feather mimics: Goethite after
violarite (Vpn): dark grey, mottled (lower margin): Pyrite; light grey:
Silica; dark grey: Goethite after pyrite; medium-grey

F. Ilmenite relics in sulphide leaching zone (x 110) Air

Ilmenite ; medium to medium-dark grey, elongate, homogeneous: Pyrite;
light grey: Goethite after pyrite; medium grey: Goethite; medium-dark
grey: Silicate; grey-black

Fig.5.6.2.
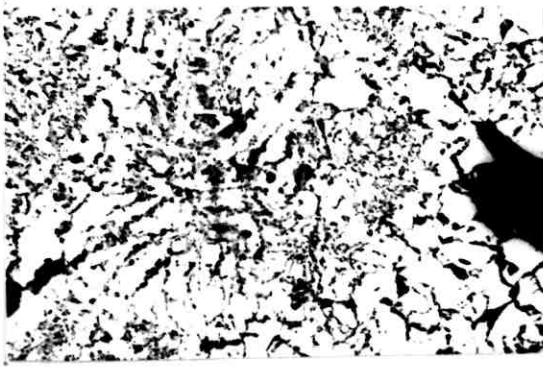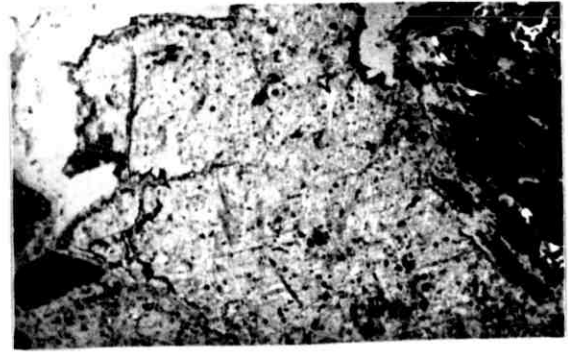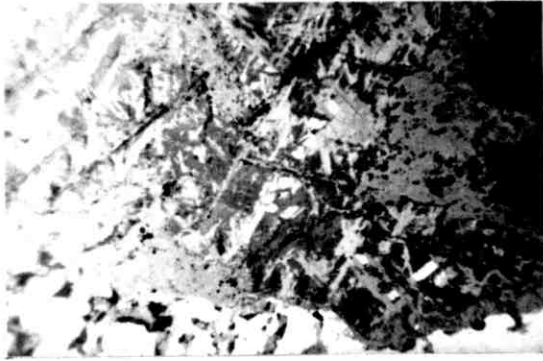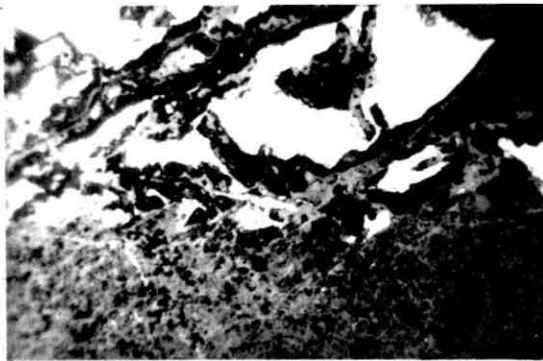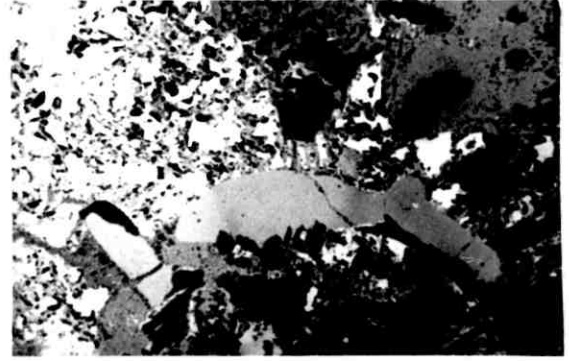
Violarite after pentlandite (Vpn) is present as discrete equant blocky grains that
are very commonly associated with secondary marcasite or pyrite, (Fig.5.6.1H.).
The octahedral cleavage partings are typically defined in amorphous silica,
(Fig.5.6.1C.), but are also noted as pyrite, (Fig.5.6.1H.). Violarite after
pyrrhotite (Vpo) occurs in association with Vpn and is characteristically developed
as feather-like fringes. These are present along grain borders between Vpn and
secondary iron disulphide, and are also located on relic fractures within the latter,
(Fig.5.6.1A.).

Available data indicates that the secondary sulphide assemblage is present from
about 35 - 40 metres b.s. up to (approximately) the 24m. level, (Table 5.6.1.).
At this latter horizon however, the sulphides undergo pervasive oxidation, and
secondary pyrite and marcasite are commonly replaced in situ by goethite,
(Fig.5.6.2A.).

Chalcopyrite exhibits a typical two-stage oxidation at the water table (24m.)
horizon. It undergoes an initial (pseudomorphic) alteration to covellite,
(Fig.5.6.2B.). The latter is subsequently replaced by goethite, (Fig.5.6.2C.).

Both violarite species commonly exhibit in situ replacement by goethite,
(Fig.5.6.2D.). But goethite formation may be preceded by an initial localised
partial alteration to covellite, (Fig.5.6.2E.).

The small amount of ilmenite present in the Carr Boyd secondary sulphide assemblage
is generally preserved during pervasive sulphide oxidation, (Fig.5.6.2F.).

The petrology of the oxide zone

The secondary sulphide zone is succeeded at about 24 metres b.s. by a zone rich
in iron oxides. The sampled mean mineralogy of this latter profile comprises
goethite (45 percent), hematite (15 percent) and silica (35 percent), (Table 5.5.1.).

Goethite occurs in a number of significant textural configurations in the Carr Boyd
oxide zone. It is present as pseudomorphic and boxwork structures after a number
of secondary ore minerals. Importantly, goethite forms pseudomorphs after Vpn
(Figs.5.6.3A. and 3B.) and Vpo (Fig.5.6.3C.). It is, however, also common as
boxworks after secondary pyrite, (Fig.5.6.3D.) and is similarly present in boxworks

structures after chalcopyrite, (Fig.5.6.3E.). Further, goethite also forms pseudomorphs after (rare) secondary marcasite birds-eye structures, (Fig.5.6.3F.).

Hematite is present chiefly as boxworks after several textural configurations of secondary pyrite, (Figs. 5.6.3G. and 3H.). Additionally it also occurs as extensive areas of pseudomorphs after coarse-grained bladed marcasite, (Fig.5.6.4A.). In contrast however, hematite mimicked replacements of violarite are not commonly observed, although both Vpn and Vpo do exhibit pseudomorph structures in hematite, (Figs. 5.6.4B. and 4C. respectively). Hematite also forms (rare) pseudomorphs after magnetite, (Fig.5.6.3G.).

There is some evidence for in situ replacement of goethite by hematite in the Carr Boyd oxide zone. Here, hematite is observed to nucleate as randomly distributed spherules within goethite matricies, (Fig.5.6.4D.), and gradually replaces the latter by the progressive growth and coalescence of these structures, (Fig.5.6.4E.). The development of hematite pseudomorphs after violarite and marcasite outlined above may, hence, be due to a late phase of hematite formation.

The bulk mineralogy of the oxide zone is complemented by a suite of oxidate minerals that occur within the oxide profile itself and in adjacent weathered host silicate. Magnesite is the commonest of these phases, (Table 5.6.1.). It occurs in a number of textural configurations, (Table A2/2;Appendix Two), all of which indicate that the mineral originated as a precipitant from metal-charged groundwaters. Further, the abnormally high nickel, copper and cobalt contents of these magnesites demonstrate their likely formation during former episodes of sulphide leaching, (Table A2/2 ; Appendix Two).

Traces of natroalunite and natrojarosite also occur in the oxide zone and in adjacent weathered host rocks, (Tables A2/7 and A2/8; Appendix Two). The textures of these minerals demonstrate that they similarly originate as groundwater precipitates. The inclusion of sulphate ion within their structures confirms their partial derivation as products of sulphide oxidation. In contrast, much of the alkali metals, aluminium and iron that they contain is likely derived from the chemical breakdown of proximal silicate mineral assemblages.

Trace amounts of blue-green paratacamite $(Cu_4Cl_2(OH)_6)$ occur in the Carr Boyd host silicate as botryoidal joint coverings and as late veinlets. The presence of this

Fig. 5.6.3. Petrography of the Carr Boyd Gossan (1)

Scale length = 100 μ Blue-white filter used throughout

A.   Goethite mimic after interstitial violarite (Vpn) (1) (x 110) Air

Silicified goethite; light grey, mottled: Goethite; medium grey (left margin)
Silica; medium-dark grey

B.   Goethite mimic after interstitial violarite (2) (x 320) Air

Goethite; light-medium grey: Silica; light-medium greys: Voids; blackedged

C.   Goethite mimics after Vpo (x 320) Air

Goethite after Vpo; light grey: Goethite after Vpn; medium grey, mottled:
Hematite (as Vpn cleavage relics); white-grey: Silica; medium-dark greys

D.   Goethite boxworks after secondary pyrite (x 110) Air

Goethite; medium grey: Hematite; light grey: Voids; black

E.   Goethite boxworks after chalcopyrite (x 110) Air

Goethite- medium grey, mottled: Peripheral hematite; light grey:
Silica; dark grey, mottled: Voids; black

F.   Goethite mimic after marcasite bird's-eye structure (x 320) Air

Goethite; medium grey: Hematite; light grey: Silica; dark grey:
Voids; black

G.   Hematite structures after pyrite (boxworks) and magnetite (mimics) (x 110) Air

Hematite; light grey: Silica; medium grey: Voids; black

H.   Hematite cubic boxwork after pyrite (x 110) Air

Hematite; light grey: Goethite; medium grey

Fig.5.6.3.
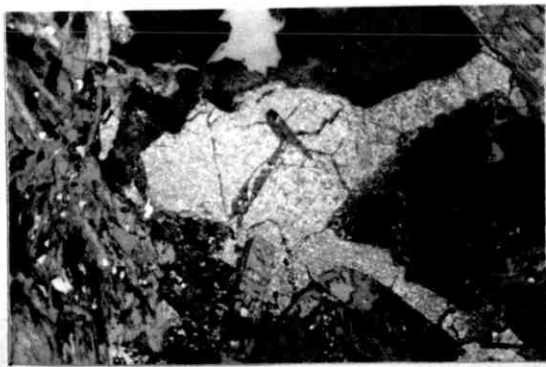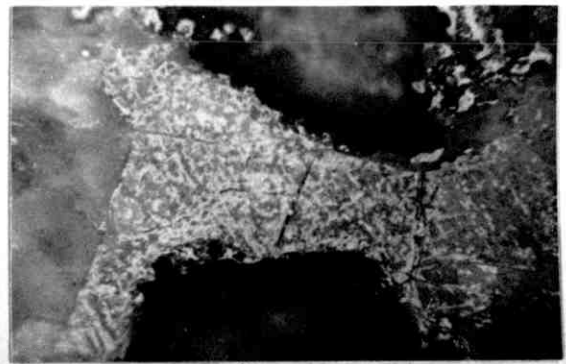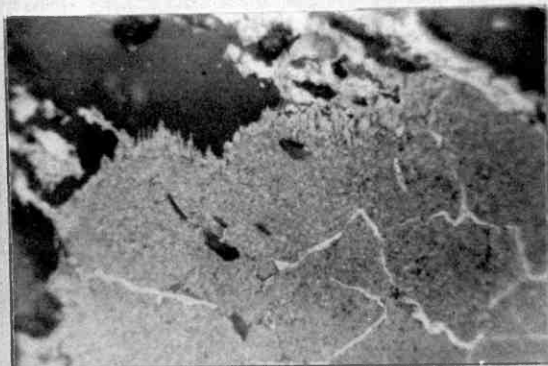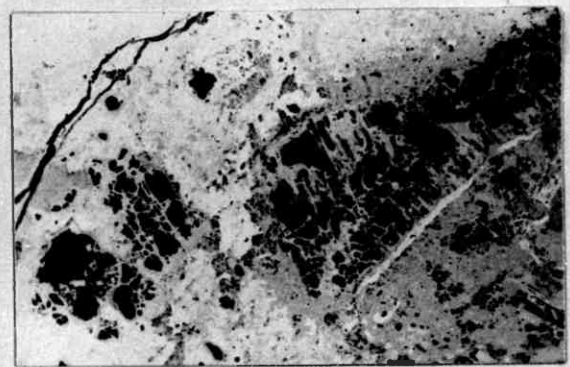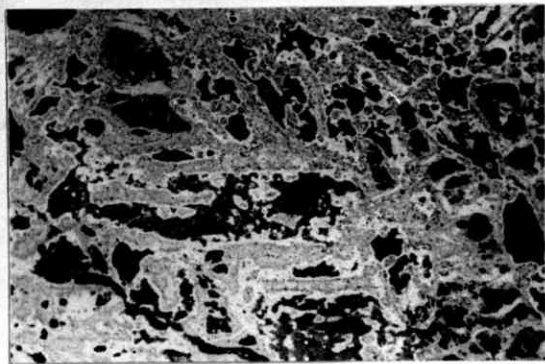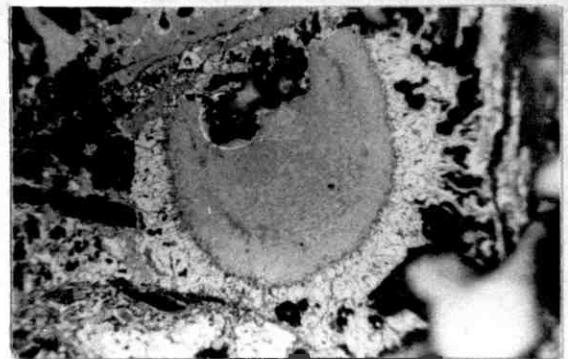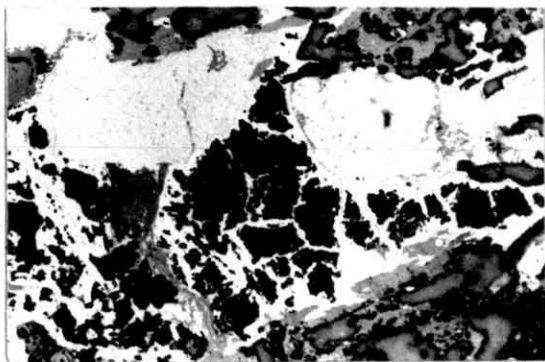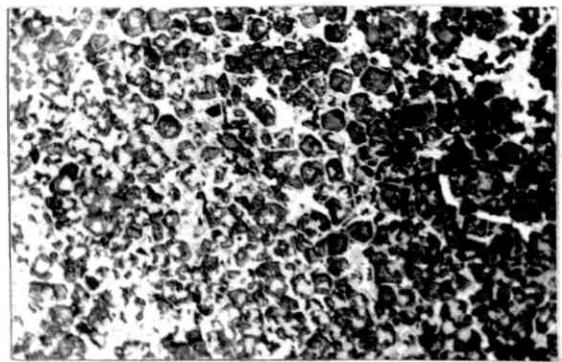
Fig. 5.6.4. Petrography of the Carr Boyd Gossan (2)

Scale length = 100 μ Blue-white filter used throughout

A.   Hematite mimics after coarse bladed marcasite (x 110) Air

Hematite; light-medium grey: Silica; dark grey: Voids; black

B.   Hematite mimic after interstitial violarite (Vpn) (x 110) Air

Hematite; grey-white: Goethite; light-medium grey – defines Vpn cleavages:
Voids; dark grey.   Hematite boxworks after pyrite also present (right)

C.   Hematite mimic after Vpo (x 110) Air

Hematite; white-grey: Goethite; medium greys: Voids; black:
Silica; dark grey. Adjacent pyrite boxwork also preserved in hematite (upper
left)

D.   In situ replacement of goethite by hematite (1) (x 320) Air

Goethite; medium-dark grey: Hematite; light-medium grey, spherulitic:
Voids; grey-black

E.   In situ replacement of goethite by hematite (2) (x 320) Air

Goethite; medium-dark greys: Hematite; medium grey, spherulitic:
Voids:black (edged)

Fig. 5.6.4.
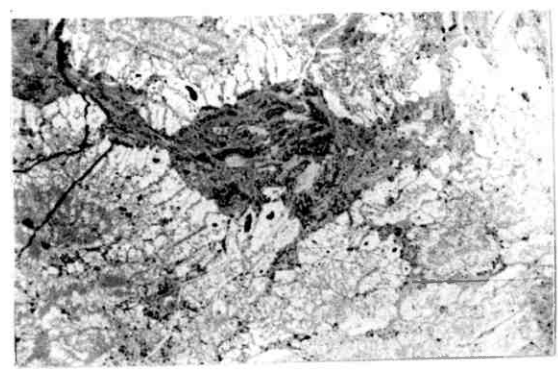
A
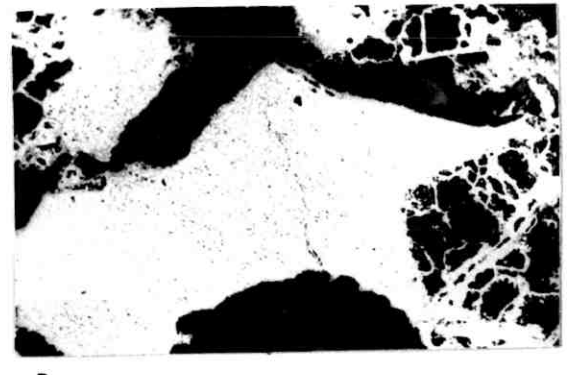
B
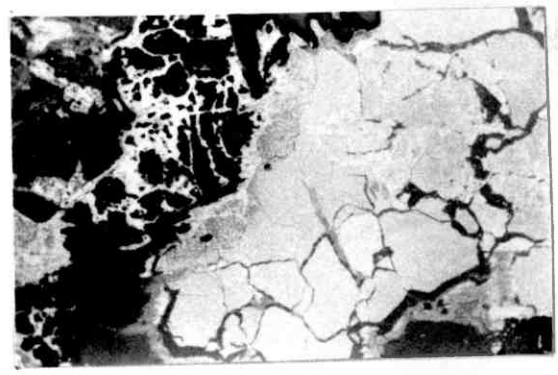
C
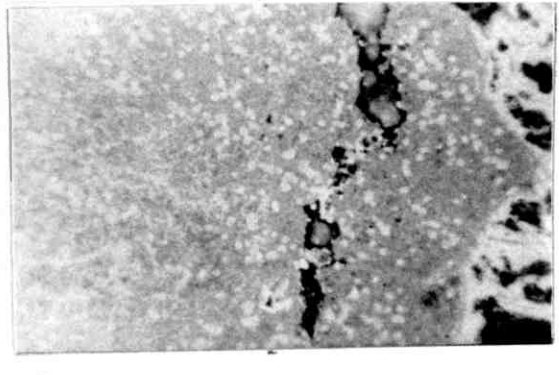
D
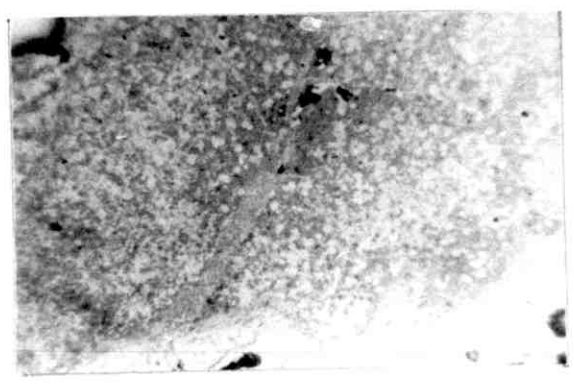
E

rare soluble mineral indicates the local occurrence of high concentrations of chloride ion, (in addition to copper species), in the groundwater from which it precipitated. Further, it is likely that this chloride is derived from the near-surface weathering of proximal silicate rocks.

The corresponding mean true density and mean porosity profiles

The mean variation in true density and porosity presented in Fig.5.6.5. closely reflects the progressive mineralogical changes that are observed in the top 40 metres of the Carr Boyd sulphide oxidation profile.

The bulk chemistry of sulphide oxidation and oxide formation

The bulk chemical variation of the standard suite of major and minor elements within the top 40 metres of the Carr Boyd oxidation profile is presented in Fig.5.6.6. The total depletion of sulphur across the sulphide-oxide transition horizon (24m. level) corresponds with the oxidation and consequent mobilisation of this element as sulphate ion. Whereas the 10 percent loss of iron that occurs across the same horizon indicates that most of this metal, released by sulphide leaching, is rapidly immobilised by precipitation as iron oxides. In contrast, the corresponding substantial increase in mean silicon content across the sulphide-oxide boundary is due to an influx of silica into the oxide zone from adjacent weathering silicates.

The relative variation of trace metals across the water table horizon corresponds in general with the expected differential chemical behaviour of these elements in the acid oxidising conditions characteristically associated with sulphide leaching. Further, the substantial mean increase in chromium probably relates to an influx of this metal into the oxide zone as a result of ultramafic silicate weathering.

In contrast, the four-fold increase in mean titanium noted in Fig.5.6.6. is unlikely to be due to a real enhancement of this metal in the oxide zone. Here, the enrichment phenomenon is more probably caused by the effects of a relatively small oxide sample population. This may be because parent ilmenite relics are rather heterogeneously distributed within available oxide zone material.

Fig. 5.6.5. Mean True Density and Porosity profiles – Carr Boyd
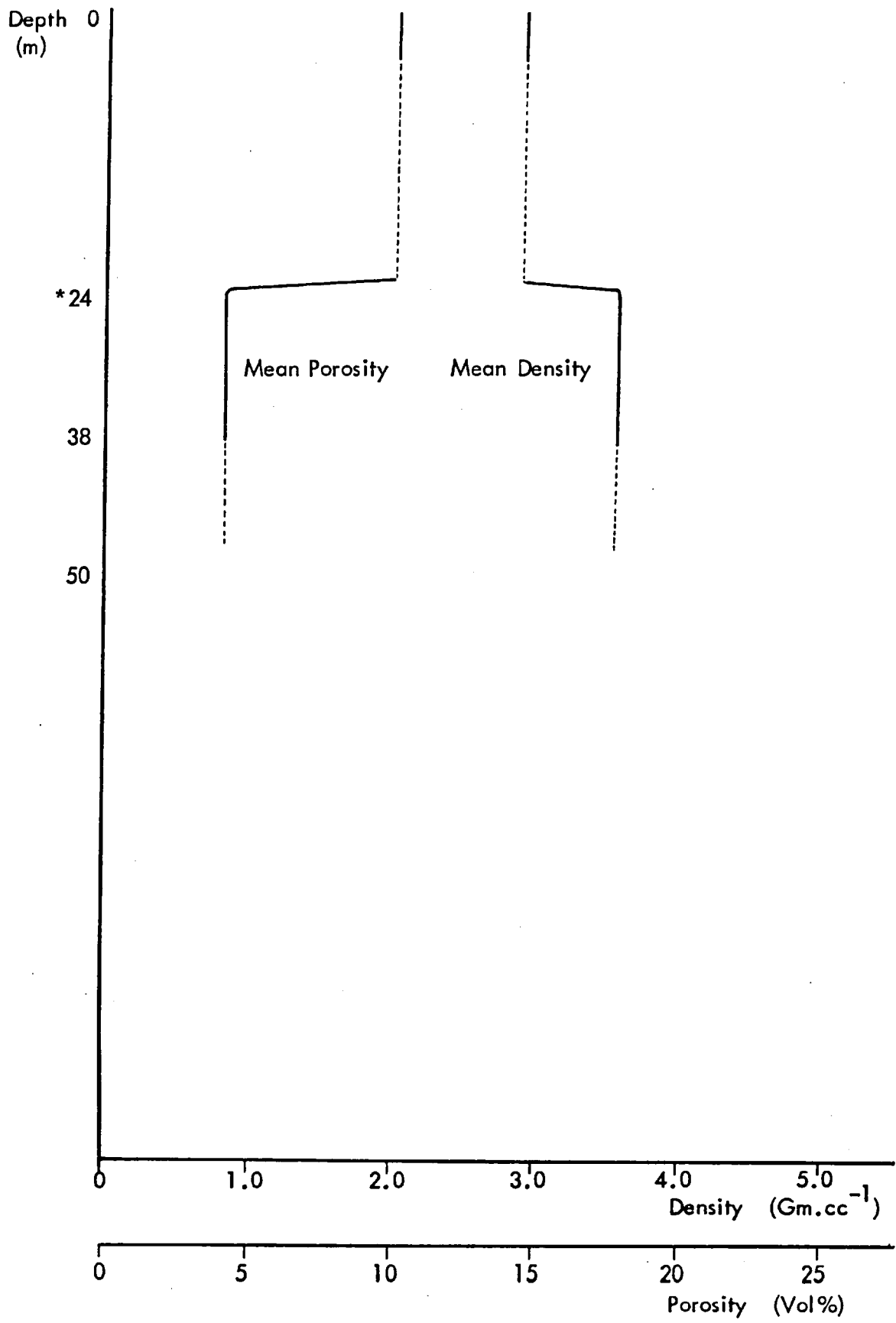
* Approximate position of the water table

Fig. 5.6.6. Chemical Variations in Alteration Profile – Carr Boyd

TABLE 5.6.1. SUMMARY DATA OF SULPHIDE ALTERATION - CARR BOYD

Mineralogy abbreviation columns are given by position: column 1 = Hm/Vl, column 2 = Gt/Cp, column 3 = SI/Mt, column 4 = MgS, column 5 = NJr/Cov/Py, column 6 = NaL, column 7 = Pact/Mc, column 8 = Sil.

Depth (m)	Alteration Zone	No. of Samples (n)	MINERALOGY (Means and ranges) Volume % Units Hm/Vl	Gt/Cp	SI/Mt	MgS	NJr/Cov/Py	NaL	Pact/Mc	Sil	Physical data (mean/ranges) Den gm/cc	Por %	GEOCHEMISTRY (Means and ranges) Wt.% Units S	Fe	SiO_2	MgO	Al_2O_3	CO_3	p.p.m. Units Ni	Cu	Mn	Cr	Co	Ti
24	Oxide	4	4.0	8.0	12.0						2.40	4.5	0.00	43.55	3.25	0.10	0.30		3701	631	59	89	30	629
			20.0	45.0	35.0	<0.5	trace	trace	trace		2.90	10.1	1.32	49.65	10.46	1.38	5.65	N/A	4630	2512	284	703	164	2044
			45.0	85.0	75.0						3.40	20.5	3.41	55.71	13.18	3.70	14.80		6522	4929	513	1526	269	3867
	Sulphide - oxide transition	1		25.0			3.0		55.0	20.0	3.30	6.2	no data											
35-40	Violarite - pyrite	3	1.0	0.5			0.0		12.5	7.0	3.30	1.8	30.81	35.14	7.40	0.20	0.10		2538	112	59	192	784	36
			2.2	8.8	<0.5		12.5		50.5	25.7	3.47	4.2	38.99	37.72	11.16	2.35	1.20	N/A	6616	28312	452	333	1268	358
			4.0	75.0			37.0		90.0	45.0	3.80	6.9	49.74	41.47	18.63	3.80	3.29		12714	79879	844	493	1520	654
	Transition	no data																						
	Primary	no data																						

5.7. SUPERGENE ALTERATION IN THE REDROSS DEPOSIT

The Redross deposit occurs as a steeply-dipping planar ore body that is located along the footwall contact of a differentiated ultramafic sill with underlying amphibolite, (Section 2.3). Massive sulphide occurs at the footwall contact but passes progressively into matrix and disseminated mineralisation away from the base of the host unit. The geology of the deposit has been outlined by Dalgarno, (op.cit.), but the supergene sulphide alteration developed in the orebody has not previously been documented.

Sampling for the present study was made from grab samples from the surface gossans and from near-massive sulphide material from metallurgical test drums. No direct depth control on sulphide alteration was hence possible, and the depth changes indicated in the following profile description are based on information obtained during the field visit to the deposit.

The petrology of supergene sulphide alteration

No unaltered (primary) massive sulphide was sampled at Redross. The mean mineralogy of the sampled partially altered ore however comprises pyrrhotite (52 percent), secondary marcasite (22.5 percent), pentlandite (four percent), violarite after pentlandite (six percent), magnetite (five percent), hypogene pyrite (1.5 percent) and silicates (10 percent), (Table 5.7.1.).

Pyrrhotite forms the matrix of the near-massive sulphide assemblage. It is present as localised areas of small equant polygonised grains, and as large (2-3mm.) rather irregular forms, (Fig.5.7.1A.).

Pentlandite occurs as typically elongate blocky stringers that are situated along pyrrhotite borders, (Fig.5.7.1B.). Whereas magnetite is present as rather equant grains that generally exhibit smoothed rounded outlines, (Fig.5.7.1A.). Pyrite is sparsely distributed within the partly altered sulphide assemblage and probably represents a localised early (hypogene) in situ alteration of pyrrhotite, (Fig.5.7.1C.).

Available data indicate that sulphide alteration is initiated with the incipient replacement of pentlandite by violarite at about 80 - 90 metres b.s. The violarite may randomly nucleate within the pentlandite, (Fig.5.7.1D.). But more commonly initial growth is confined to the cleavage traces, (Fig.5.7.1D.), and develops

319

Fig. 5.7.1. Petrography of Redross Sulphide Ore (1)

Scale length = 100 μ

A. Typical pyrrhotite matrix texture (x 110) Air

Pyrrhotite; light-medium to medium-dark grey, homogeneous: Pentlandite; light to medium grey, mottled: Magnetite; dark grey: Silicate; dark grey to grey-black

B. Typical form of interstitial violarite (Vpn) (x 110) Air

Pentlandite; light-medium grey: Violarite; medium-dark to dark grey, granular: Pyrrhotite; medium greys: Voids; black

C. Localised formation of hypogene pyrite from pyrrhotite (x 110) Air

Hypogene pyrite; light-medium grey (centre): Violarite/Pentlandite; medium grey, granular: Pyrrhotite; medium-dark grey: Spinel; medium-dark to dark grey, rounded: Silicate; black

D. Incipient growth of violarite along pentlandite cleavage zones (x 600) Oil

Pentlandite; medium grey: Violarite; dark grey, aphurulitic, associated with voids (black): Pyrrhotite; medium-dark grey (top centre)

E. Later stage replacement by violarite (x 600) Oil

Violarite; medium greys, mottled: Pyrrhotite; medium grey, homogeneous: Smythite after pyrrhotite; light-medium grey, lamellar: Violarite after pyrrhotite; light-medium grey, granular, lamellar: Silicates; dark grey to grey-black

F. Completed replacement of pentlandite by violarite (x 220) Oil

Violarite; medium-dark grey, granular: Siderite; dark grey cleavage filling: Spinel; dark grey (lower left corner)

G. Full development of violarite after pyrrhotite (x 220) Oil

Vpo; light-medium grey, granular, fringe-like: Vpn; dark grey, granular: Pyrrhotite; light-medium grey, homogeneous: Siderite; dark grey, in violarite cleavages: Spinel; dark grey (right): Voids; black

H. Marcasite mimicking cleavage structure of parent pyrrhotite (x 220) Oil

Secondary fine grained marcasite; light-medium grey, granular: Vpo; medium-dark grey, granular: Vpn; dark grey, granular (right margin): Siderite; dark grey Vpn cleavage filling: Voids; black: Spinel; dark grey (upper right corner)

Fig.5.7.1.

A

B

C

D

E

F

G

H

321
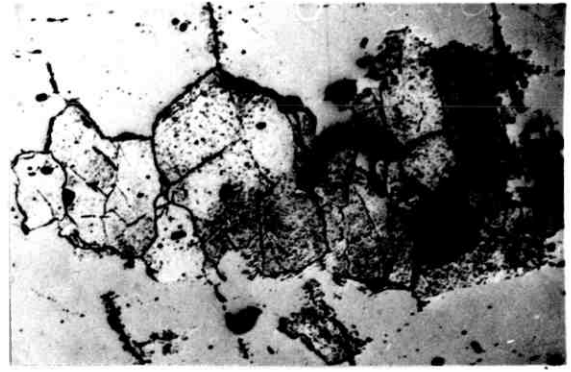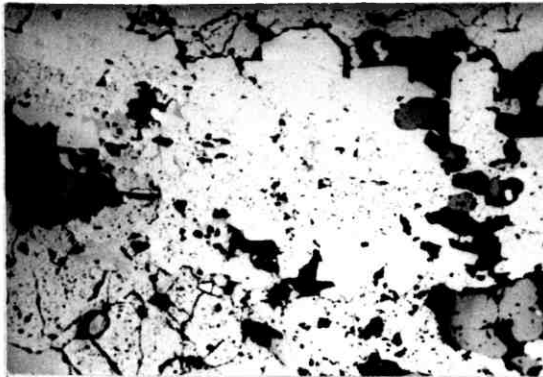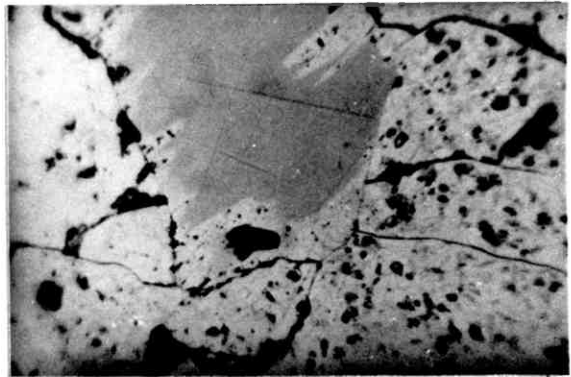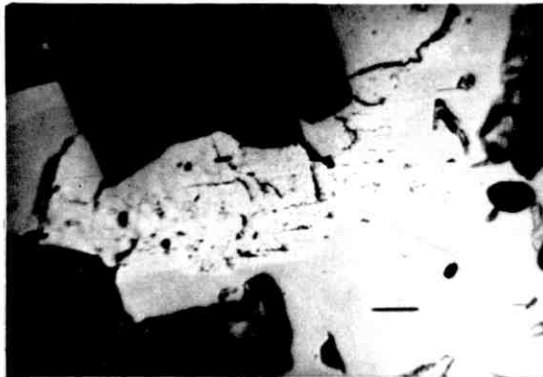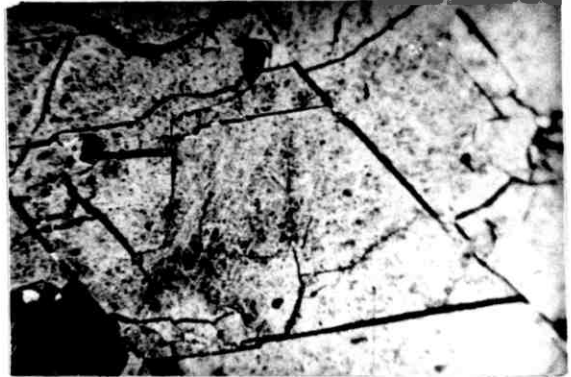
Fig. 5.7.2. Petrography of Redross Sulphide Ore (2)

Scale length = 100 μ

A.   Pseudocolloform structure in secondary marcasite (x 220) Oil

Marcasite; medium grey, granular: Vpn; dark grey, granular (right margin):
Vpo; medium-dark grey, granular, fringe-like (right):   Voids; black

B.   Recrystallisation of fine-grained to coarse bladed marcasite (x 220) Oil

Fine-grained marcasite; medium-dark grey, granular: Coarse marcasite;
light to medium grey, elongate: Voids; black: Violarite; dark grey, granular

C.   Massive pyrite after marcasite (x 110) Air

Pyrite; light grey: Violarite species; dark grey, granular: Spinel; medium grey,
rounded: Voids; black

Fig.5.7.2.

A

B
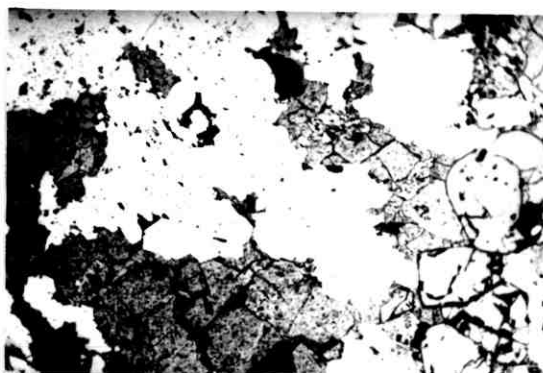
C

outwards from these zones along linear fronts, (Fig.5.7.1E.). Complete pseudomorphic replacement eventually occurs, and the distended octahedral cleavages of the parent pentlandite become filled with expelled iron in the form of siderite, (Fig.5.7.1F.).

Incipient alteration of adjacent pyrrhotite occurs once Vpn formation is under way. Alteration typically takes the form of small fingers of reddish smythite which develop along pentlandite/pyrrhotite borders and replace the parent iron sulphide along the 001 cleavage, (Fig.5.7.1E.).

The progressive alteration of pentlandite to violarite is accompanied by a concomitant development of violarite after pyrrhotite. This phase replaces smythite along the inherited 001 pyrrhotite cleavage and eventually forms laterally extensive feather-like fringes along the borders of many pyrrhotite grains, (Fig.5.7.1G.).

Available evidence demonstrates that residual pyrrhotite subsequently alters to secondary marcasite, but that this phenomenon does not occur uniformly within the sulphide profile. The replacing marcasite is however characteristically colloidal in nature and very commonly mimics the 001 cleavage of the parent pyrrhotite, (Fig.5.7.1H.). Moreover, shrinkage cracks may also develop within the marcasite due to de-watering and this causes the formation of pseudo-colloform structures, (Fig.5.7.2A.). Colloidal marcasite is however unstable due to its high surface area-to-volume ratio and recrystallisation to a coarser bladed form subsequently takes place, (Fig.5.7.2B.).

The secondary sulphide assemblage of violarite and secondary marcasite is fully developed above the 40-45m. level in the Redross ore profile, (Table 5.7.1.). Observational data indicate however that the marcasite undergoes a second recrystallisation to massive pyrite above this level, (Fig.5.7.2C.). This leads to the development of a secondary assemblage of violarite, pyrite and marcasite in the sub-zone immediately below the water table horizon at 25-30 metres b.s.

The petrology of the oxide zone

The secondary sulphide assemblage is superceded above the water table by an oxidised mineral assemblage that, on available information, comprises hematite

(20 percent),goethite (nine percent), silica (70 percent) and relic pyrite (1.5 percent), (Table 5.7.1.).

Hematite occurs mostly as boxwork forms after secondary pyrite, (Figs.5.7.3A and 3B.), but is also present as boxworks after Vpn, (Fig.5.7.3C.), and as rarer pseudomorphs of both violarite species, (Figs.5.7.3D. and 3E.). The oxide also occurs as relic structures after magnetite, (Figs.5.7.3F. and 3G.).

Goethite is present chiefly as skeletal structures after secondary pyrite, (Figs.5.7.3H. and 4A.). It also less commonly occurs in (composite) iron oxide boxworks after Vpn, (Fig.5.7.4B.), and as quite rare pseudomorphic replacements of both Vpn and Vpo, (Figs.5.7.4C. and 3E. respectively).

Silica occurs as a pervasive cryptocrystalline matrix to the indicated iron oxide textures and is typically present within the interstices of the sulphide boxwork structures, (Figs.5.7.3B. and 3C.). The mineral also preserves the external forms of totally leached grains as complete silica pseudomorphs, (Fig.5.7.4D.).

Calcite occurs as an oxidate mineral in the Redross gossan, (Table A2/3,Appendix Two). It is present as an extensively developed joint surface covering and as a leached cavity filling. These textures imply that the mineral formed from sulphate-rich solutions. But the relatively low ore metal content, (Table A2/3,Appendix Two) may indicate that the phase is a relatively late precipitant and not directly related to sulphide leaching.

The corresponding mean true density and mean porosity profiles

The likely mean variation in true density and porosity within the sampled Redross oxidation profile is presented in Fig.5.7.5. The form of both profiles between the 85 and 40-45m. levels is consistent with the progressive formation of violarite and marcasite from their denser, less porous respective parent minerals that occurs across this vertical interval. Similarly, the considerable vertically restricted changes in both physical properties that occur across the water table horizon at 25-30 metres b.s. reflect the corresponding fundamental transformation of profile mineralogy and chemistry at that level.

325

Fig. 5.7.3. Petrography of the Redross Gossan (1)

Scale length = 100 μ Blue-white filter used throughout

A.   Hematite boxwork after secondary pyrite (1) (x 110) Air

      Hematite; light grey: Silica; dark grey: Voids; black

B.   Hematite boxwork after secondary pyrite (2) (x 320) Air

      Hematite; light-medium grey: Silica; dark grey. Cube-like boxwork form

C.   Hematite boxwork after interstitial violarite (Vpn) (x 110) Air

      Hematite; light grey: Silica; dark grey: Voids; black

D.   Hematite mimic after interstitial violarite (Vpn) (x 110) Air

      Hematite; light grey: Silica; dark grey

E.   Hematite mimic after Vpo (x 320) Air

      Hematite; light grey: Silica; dark grey

F.   Hematite outline mimics after magnetite (x 110) Air

      Hematite; light grey: Silica; dark grey: Voids; black

G.   Hematite boxwork after magnetite (x 110) Air

      Hematite; light grey : Silica; dark grey: Voids; black

H.   Goethite boxwork after pyrite (x 110) Air

      Goethite; medium grey: Hematite; light grey: Silica; dark grey:
      Voids; black

Fig.5.7.3.

327
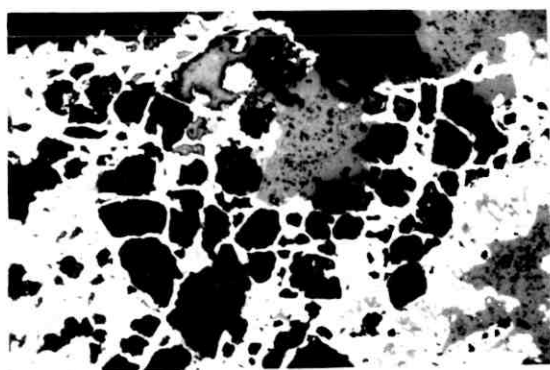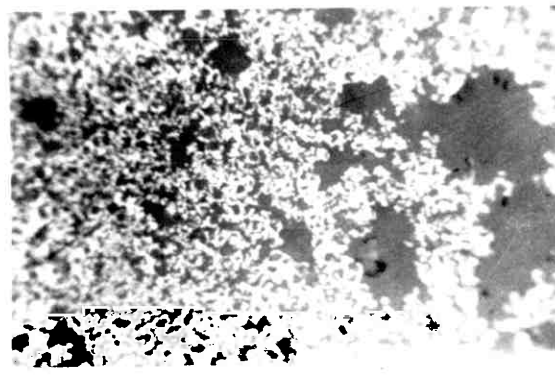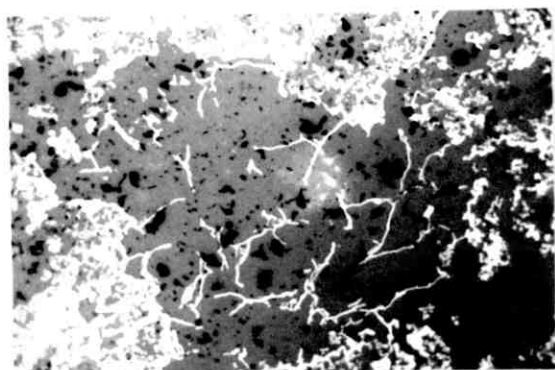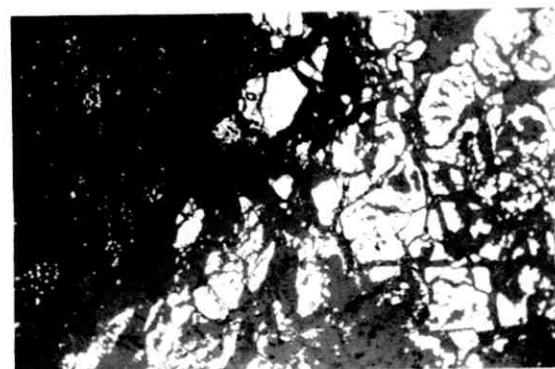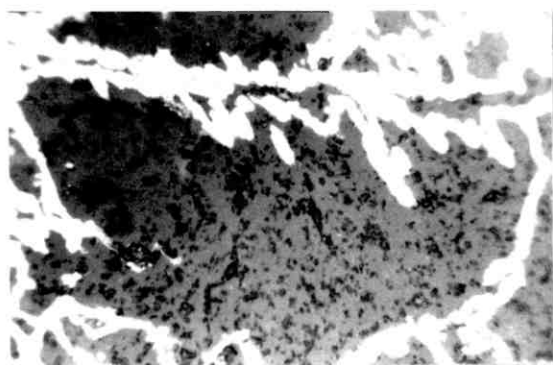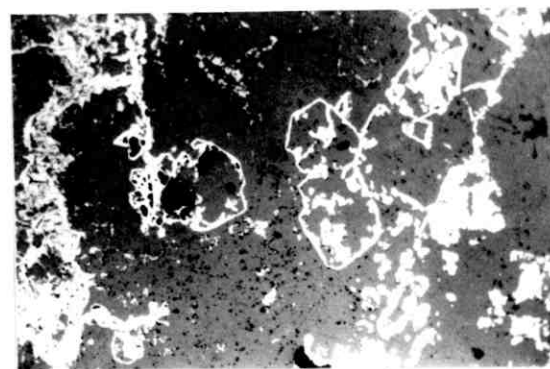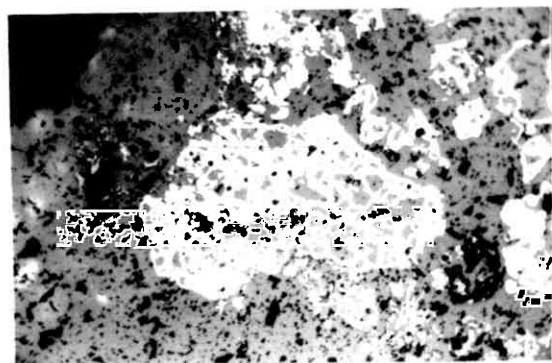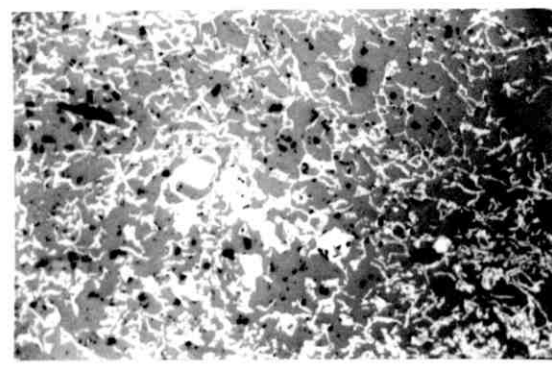
Fig. 5.7.4. Petrography of the Redross Gossan (2)

Scale length = 100 μ   unless otherwise indicated

Blue-white filter used throughout

A.   Goethite boxwork after secondary boxwork (x 40) Air

Goethite; light-medium grey: Silica; dark grey

B.   Composite iron oxide boxwork after interstitial violarite (x 110) Air

Goethite; medium grey – filament centres: Hematite; light grey –
filament edges: Silica; dark grey: Voids; black

C.   Goethite mimic after interstitial violarite (x 320) Air

Goethite after Vpn; medium grey, granular: Hematite; light grey:
Silica; dark grey

D.   Silica mimicking interstitial violarite grain form (x 110) Air

Silica; dark grey: Voids; black: Goethite; medium grey:
Hematite; light grey

328.

Fig.5.7.4.

A

1000 μ
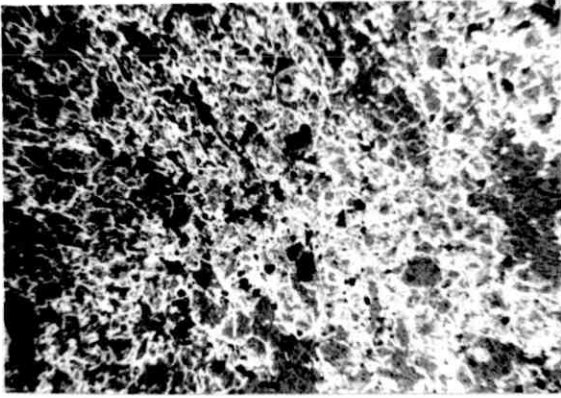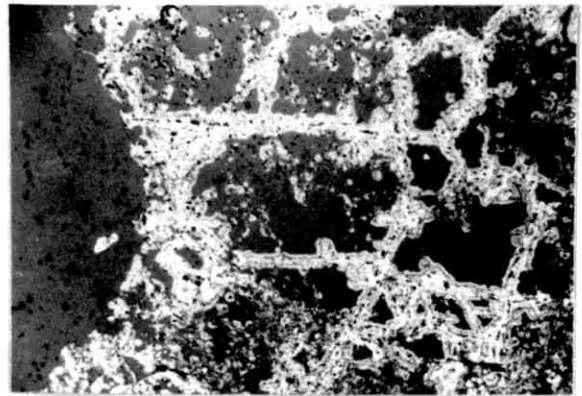
B
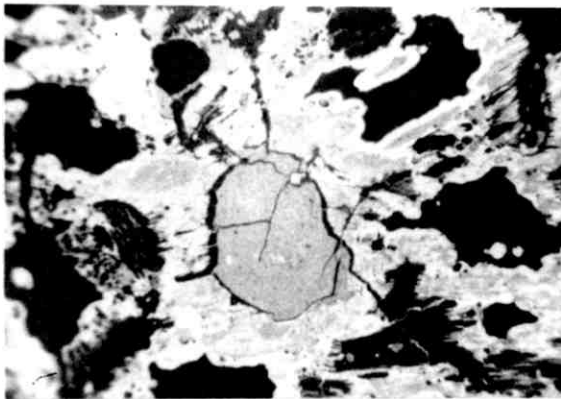
C
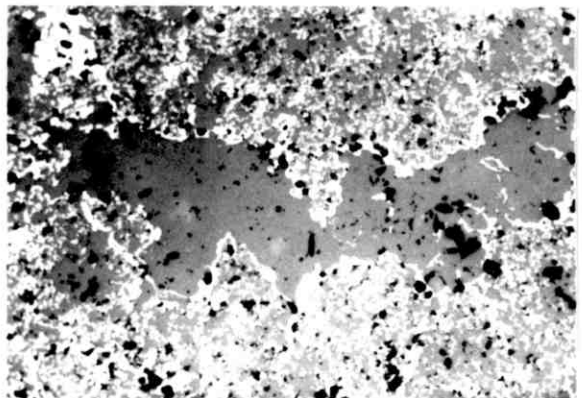
D

Fig. 5.7.5.   Mean True Density and Porosity profiles – Redross
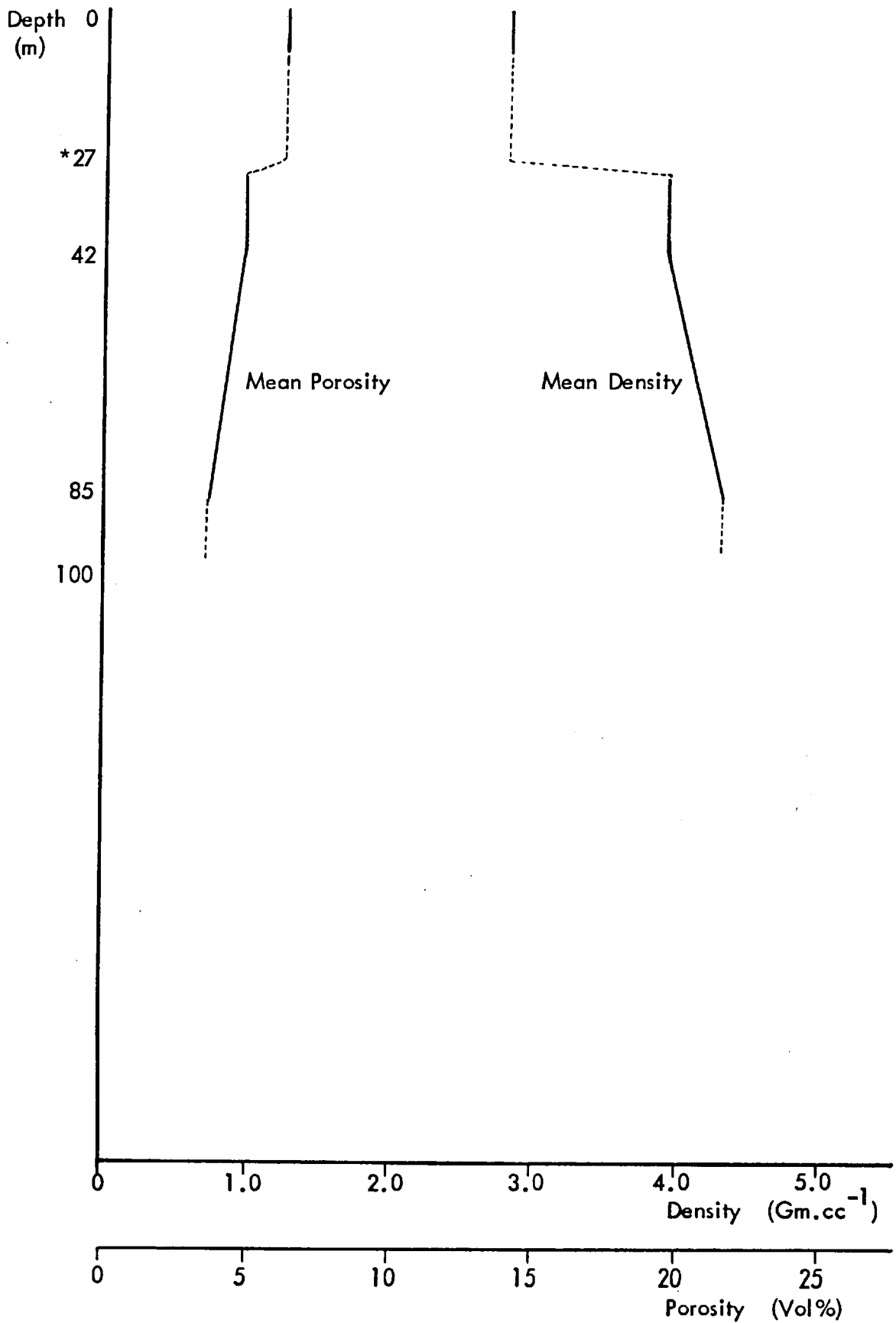
* Approximate position of water table

Fig. 5.7.6.   Chemical Variations in Alteration Profile – Redross

* Approximate position of the water table

Element content   (Gm.Equivs.cc^{-1})
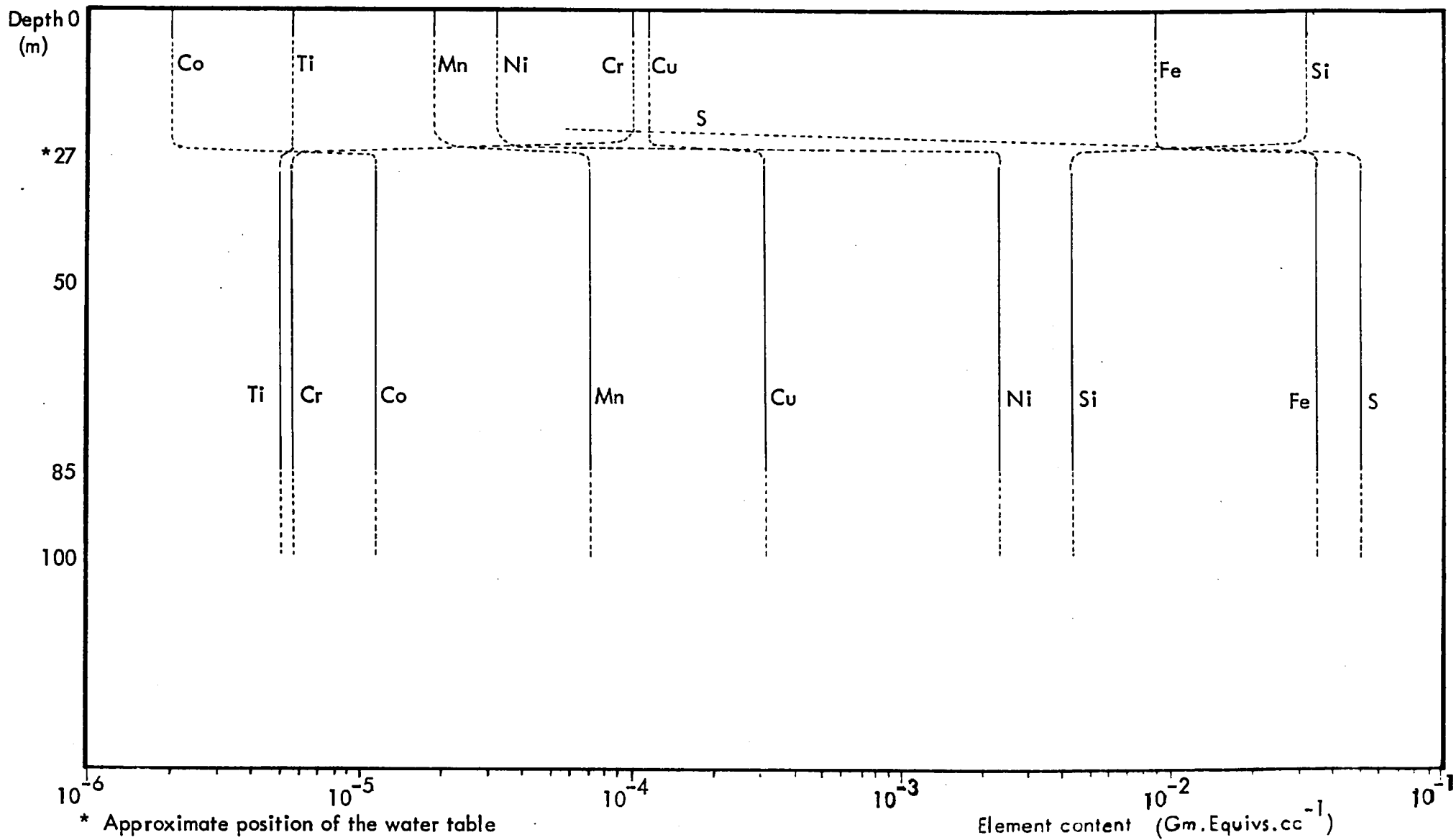
TABLE 5.7.1. SUMMARY DATA OF SULPHIDE ALTERATION - REDROSS

Depth (m)	Alteration Zone	No. of Samples (n)	MINERALOGY (Means and ranges) Volume % Units	Physical data (mean/ranges)		GEOCHEMISTRY (Means and ranges) Wt.% Units / p.p.m. Units

Oxide zone — Depth 25–30, n = 7

	Hm	Gt	Sl		Py		Ca	Den gm/cc	Por %	S	Fe	SiO₂	MgO	Al₂O₃	CO₃	Ni	Cu	Mn	Cr	Co	Ti
	7.5	1.0	60.0		0.0			2.40	1.1		5.71	43.10	0.10	0.10		173	935	119	294	30	30
	20.0	8.5	69.5		1.5		0.5	2.80	6.2		18.68	69.54	0.28	0.14	N/A	648	2555	391	1877	42	97
	35.0	27.0	85.0		3.0			3.10	17.5		34.69	89.66	0.80	0.20		1611	6950	869	3257	60	222

Violarite–pyrite zone — Depth 40–45, n = 2

	Vl	Cp	Mt	Py	Mc	Sil	Den gm/cc	Por %	S	Fe	SiO₂	MgO	Al₂O₃	CO₃	Ni	Cu	Mn	Cr	Co	Ti
	8.5		5.0	38.5	0.0	5.0	3.80	1.8	32.13	41.98	7.11	0.00	0.00		29609	775	684	30	120	36
	10.2	0.0	6.0	59.0	18.5	6.0	3.85	4.8	34.00	45.73	10.52	2.00	0.30	N/A	36666	7341	1282	145	333	87
	11.8		7.0	79.0	37.0	7.0	3.90	7.7	35.88	49.47	13.94	4.00	0.60		43722	13907	1880	260	545	138

Transition zone — Depth 80–90, n = 2

	Po	Pn	Vl	Cp	Mt	Py	Mc	Sil	Den gm/cc	Por %	S	Fe	SiO₂	MgO	Al₂O₃	CO₃	Ni	Cu	Mn	Cr	Co	Ti
	32.0	0.0	1.5	0.0	2.0	0.0	0.0	5.0	4.10	1.0	35.44	47.18	2.24	1.40			17806	519	267			
	52.0	4.0	6.2	0.5	5.0	1.5	22.5	10.0	4.25	3.5	38.54	52.22	2.45	1.50	0.00	N/A	30344	2229	617	30	30	30
	72.0	8.0	10.8	1.0	7.0	3.0	45.0	15.0	4.40	6.0	41.65	57.25	2.65	1.60			42881	3938	966			

Primary zone — no data

Bulk chemical variation within the Redross sulphide oxidation profile

The mean variation with depth of a suite of major and minor elements within the sampled Redross oxidation profile is presented in Fig.5.7.6. The constancy (based on available data) of all element profiles between the 80m. and 25-30m. levels indicates that supergene sulphide formation occurs as a closed chemical system in this deposit.

The behaviour of sulphur and iron across the sulphide-oxide transition signifies that all of the former and a large proportion of the latter are removed from the ore profile as a result of sulphide leaching. In contrast, the dramatic increase in silicon across the same horizon is probably due to the influx of large quantities of silica into the oxide zone as a result of silicate weathering.

Fig.5.7.6. also infers that the mean change in individual trace metal contents across the sulphide leaching horizon can be largely explained in terms of the chemical mobility of each element in the acid oxidising environment present at this level. The anomalous increase in chromium at this level is, however, likely due to an influx of this metal into the oxide zone as a result of ultramafic silicate weathering.

5.8. SUPERGENE ALTERATION IN THE SPARGOVILLE NO.5 DEPOSIT

The Spargoville 5A deposit occurs as a small pod of massive sulphide overlain by disseminated material. It is located within a structural embayment in the footwall contact of host dunite and underlying amphibolite, (Section 2.3.). No primary ore is present, and the deposit probably represents the distil remnant of a larger eroded orebody, (Andrews, op.cit.). For the present study, the deposit was sampled by means of drillcore (for sulphides), and by drillcore and surface grab samples (oxides).

The petrology of the secondary sulphide assemblage

The sampled secondary sulphide assemblage at Spargoville 5A comprises secondary pyrite (68 percent), secondary marcasite (18 percent), violarite (11 percent), chalcopyrite (0.5 percent), and siderite (2.5 percent), (Table 5.8.1.).

333

Fig. 5.8.1. Petrography of Spargoville 5A Sulphide Ore

Scale length = 300 μ

A. Typical secondary ore texture (x 80) Air

Violarite; medium grey - cleavages in siderite (black): Secondary pyrite; light-medium grey: Silicate; grey-black

B. Typical form of Vpo (x 110) Air

Violarite species; medium-dark grey, granular - Vpo feather-like fringes: Pyrite; light-medium grey: Silicate; grey-black

C. Direct recrystallisation ot fine grained marcasite to massive pyrite (x 220) Oil

Marcasite; medium to dark greys, granular: Pyrite; grey-white: Vpo; medium grey, granular, fringe-like: Voids; black

D. Pseudocolloform shrinkage cracks in marcasite (x 220) Oil

F.G. marcasite; light-medium to dark greys: Violarite; medium grey, granular (upper right corner): Carbonate; grey-black

E. Recrystallisation of fine grained to coarse marcasite (x 220) Oil

Fine grained marcasite; dark grey, granular: Coarse marcasite; medium grey, granular: Vpo; light-medium grey, granular, fringe-like: Vpn; medium-dark grey, granular: Siderite; dark grey, vein-like: Voids; black

Fig.5.8.1.
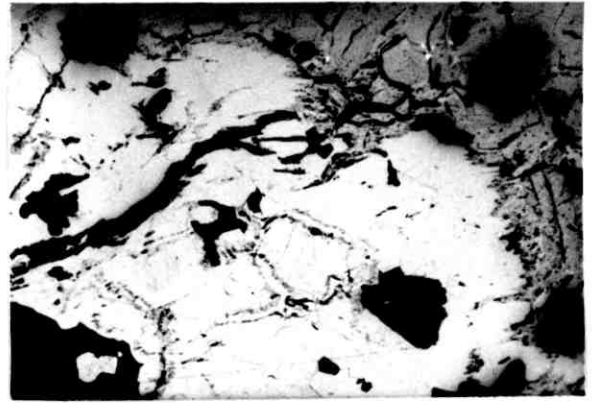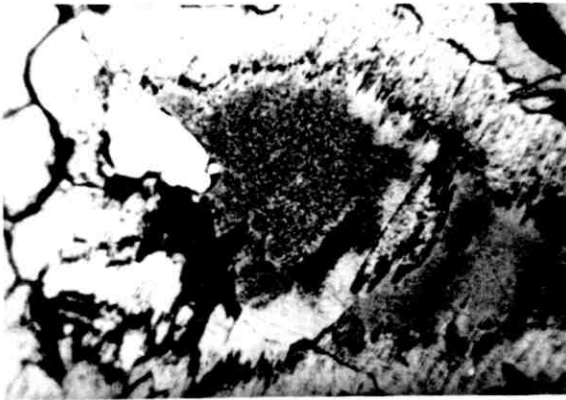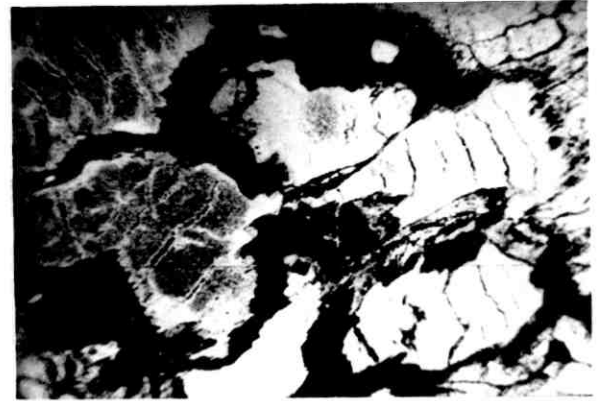
Both violarite after pentlandite and violarite after pyrrhotite are present in the sulphide assemblage. Vpn forms locally massive elongate aggregates within an ex-pyrrhotite matrix of iron disulphides, and siderite typically fills its octahedral cleavage partings, (Fig.5.8.1A.). Vpo is characteristically associated with Vpn and occurs as extensive feather lamellae in adjacent marcasite, (Fig.5.8.1B.).

Secondary pyrite and marcasite occur in locations formerly occupied by pyrrhotite. Textural evidence indicates that marcasite replaces pyrrhotite as structureless colloidal aggregates, (Fig.5.8.1C.), but pseudocolloform shrinkage may also be developed within the replacing phase, (Fig.5.8.1D.). The colloidal marcasite is, however, unstable and tends to recrystallise to either a coarser marcasite form, (Fig.5.8.1E.), or else directly to a massive secondary pyrite, (Fig.5.8.1C.). Further, mineragraphic observations demonstrate that total conversion to secondary pyrite may eventually take place within individual areas of marcasite, (Fig.5.8.1B.).

The petrology of the oxide zone

Available data indicate that the secondary sulphide assemblage is present from the base of the deposit (90m. +) up to the water table horizon at approximately 30-35 metres b.s. The sulphides are succeeded at this latter level by an oxidised assemblage that is composed of goethite (70 percent), hematite (1.5 percent) and silica (27 percent), (Table 5.8.1.). Minor quantities of relic ferrochromite (two percent) are also present.

Goethite occurs in several textural configurations after secondary ore minerals. It is present as relic forms after secondary iron disulphides - generally as large-scale silicified boxwork structures after secondary pyrite, (Figs.5.8.2A. and 2B.); but also as mimics after pseudocolloform marcasite, (Fig.5.8.2C.). It similarly occurs as (rare) secondary mimic structures after pyrrhotite, (Fig.5.8.2D.).

Textural relics after violarite are also typically preserved in goethite, and both Vpn and Vpo pseudomorphs are commonly observed within the Spargoville oxide zone material, (Fig.5.8.2E.).

Replacement of pyrite by magnesite occurs in the form of boxworks, (Fig.5.8.2F.). The noted occurrence of hematite mimics after Vpn is due to a late-stage dehydration of goethite within the oxide profile, (Fig.5.8.2G.).

Further, the existence of pseudocolloform marcasite textures in

Fig. 5.8.2.   Petrography of the Spargoville 5A Gossan

Scale length = 300 μ Blue-white filter used throughout

A.   Goethite boxwork after secondary pyrite (1) (x 80) Air

    Goethite; medium grey: Silica; dark grey

B.   Goethite boxwork after secondary pyrite (2) (x 220) Oil

    Goethite; medium grey: Silica; dark grey

C.   Goethite mimics after colloform marcasite (x 320) Air

    Goethite; medium grey: Silica; grey-black

D.   Goethite boxwork after mimicked pyrrhotite structure (x 110) Air

    Goethite; medium grey: Silica; dark grey. Sub-parallel filaments indicate former pyrrhotite structure

E.   Goethite mimics after Vpn and Vpo (x 110) Air

    Goethite; medium-dark grey: Hematite (after marcasite); light-medium grey

F.   Magnesite boxworks after pyrite (x 110) Air

    Magnesite; medium grey: Silica; dark grey: Hematite; light grey

G.   Hematite mimics after violarite species (x 110) Air

    Hematite; light to light-medium grey: Goethite; medium-dark grey (after marcasite):   Voids; black

H.   Hematite mimics after pseudocolloform marcasite (x 80) Air

    Hematite; light to dark greys: Silica; dark grey
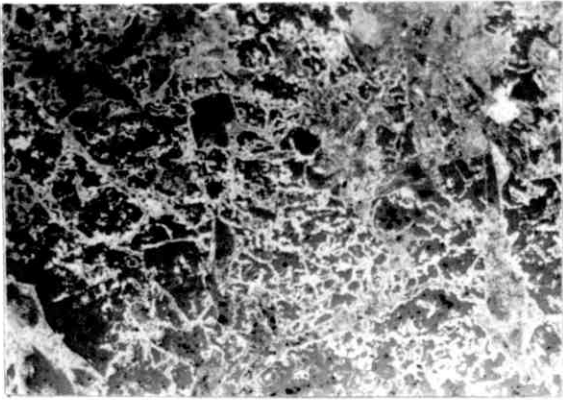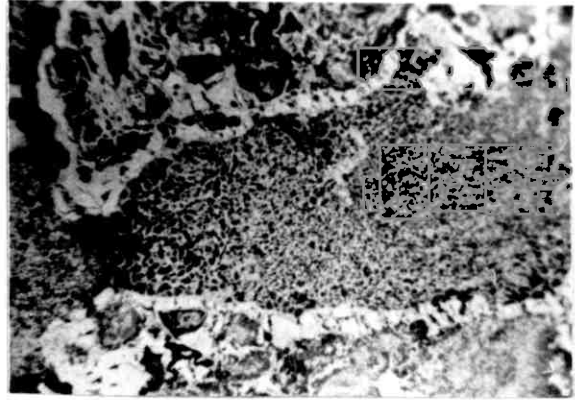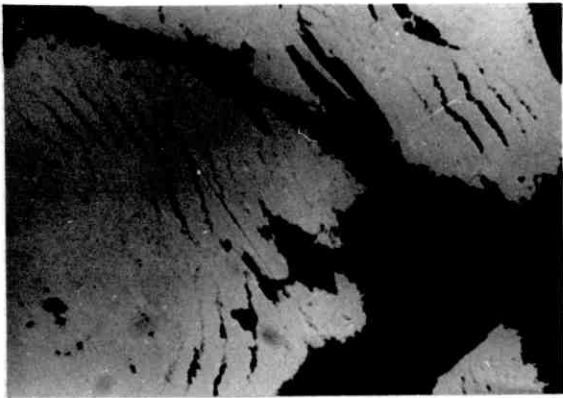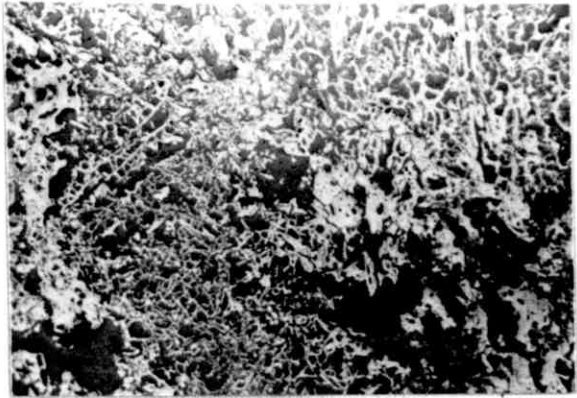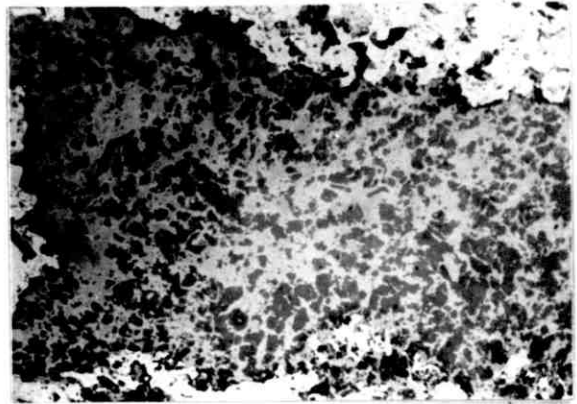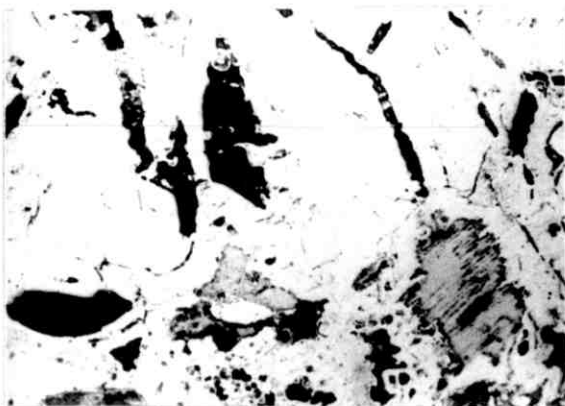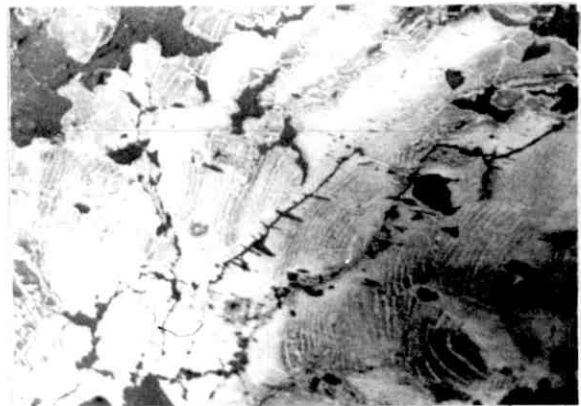
Fig.5.8.2.

hematite is also likely due to a late alteration of original mimic goethite, (Fig.5.8.2H.)

Silica occurs as a pervasive matrix in the Spargoville oxide zone and it typically invests boxworks and similar leached structures, (Fig.5.8.2A.)

Calcite and dolomite occur as oxidate minerals on joint planes in surface gossan material. In this locational setting, these carbonates are likely to be late derivations of silicate weathering and, hence, not directly related to sulphide leaching. This indication is borne out by the relatively low trace metal contents of sampled material, (Tables A2/3 and A2/4 ;Appendix Two).

Siderite occurs as patchy precipited deposits on fractures and joints in host silicate flanking the secondary sulphide zone. This textural and spatial relationship indicates that the constituent iron was likely released from the proximal ore during violarite formation. A contention that is supported by the high nickel content of analysed material.

The corresponding mean true density and mean porosity profiles

The likely mean variations in true density and porosity within the top 60 metres of the Spargoville oxidation profile are set out in Fig.5.8.3. The vertically restricted mean density decrease and porosity increase that take place across the 35m.horizon parallel the fundamental mineralogical and chemical changes that occur due to wholesale sulphide leaching at this level.

The bulk chemistry of the Spargoville sulphide-oxide transition

The individual mean variations of the standard element suite across the sulphide-oxide transition in the Spargoville 5A oxidation profile are presented in Fig.5.8.4. The form of the iron, sulphur and silicon mean profiles closely follow the expected behaviour of these elements under the chemical conditions existing at the water table, and the indicated changes in all three elements are well supported by minerographic evidence.

The changes in mean nickel, manganese and cobalt contents across the sulphide leaching horizon correspond to those expected from consideration of the aqueous chemistry of these metals in acid oxidising environments. Whereas the preferential

Fig. 5.8.3. Mean True Density and Porosity profiles – Spargoville 5A
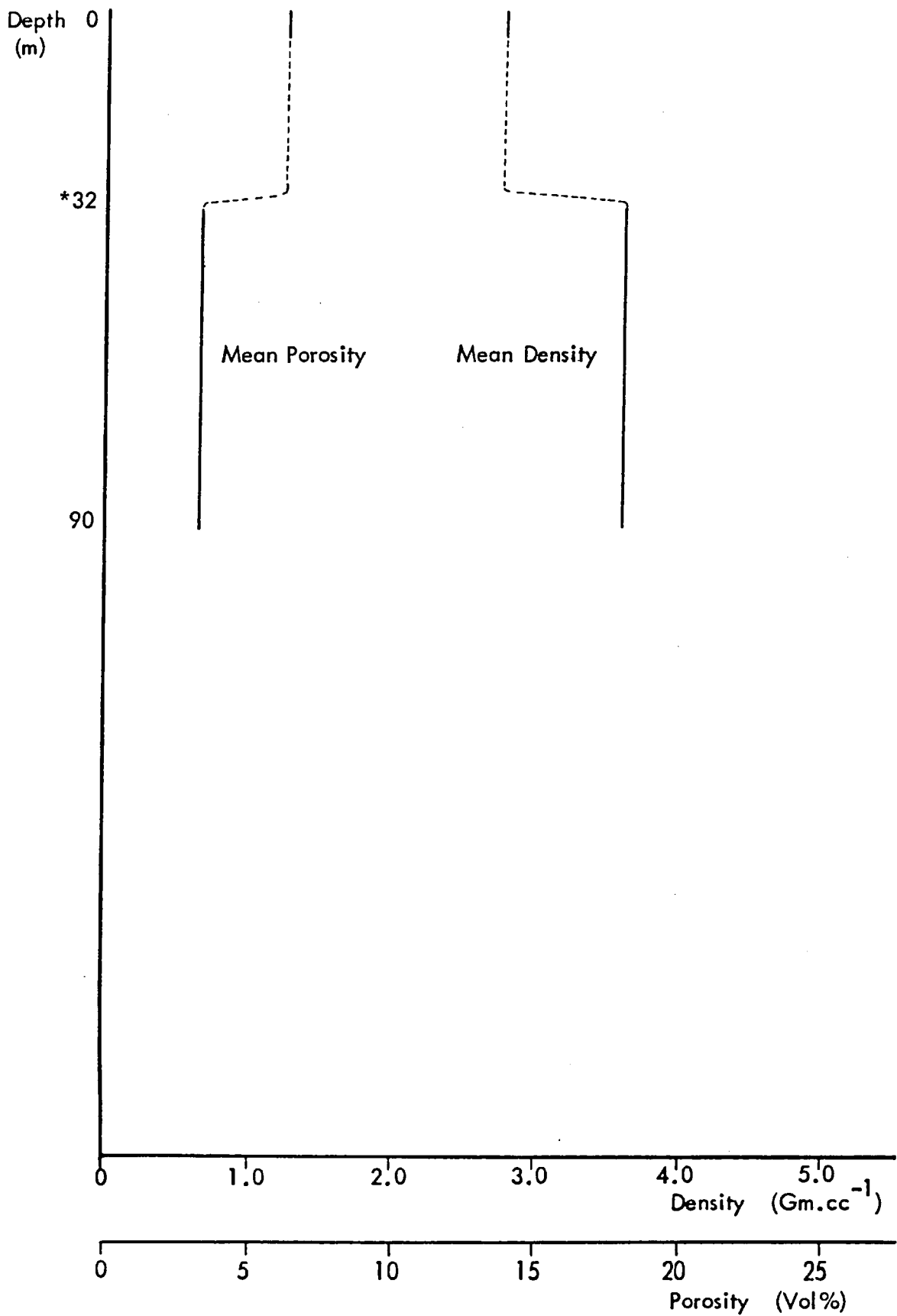
* Approximate position of the water table

Fig. 5.8.4. Chemical Variations in Alteration Profile — Spargoville 5A

TABLE 5.8.1. SUMMARY DATA OF SULPHIDE ALTERATION – SPARGOVILLE 5A

Depth (m)	Alteration Zone	No. of Samples (n)	Mineralogy (Means and ranges) Volume % Units										Physical data (mean/ranges)		Geochemistry (Means and ranges) Wt. % Units						p.p.m. Units					
			Hm	Gt	Sl	FCr	Ca	Vl	Cp	Py	Mc	Sid	Den gm/cc	Por %	S	Fe	SiO₂	MgO	Al₂O₃	CO₃	Ni	Cu	Mn	Cr	Co	Ti
30–35	Oxide	14	0.5	35.0	2.0	0.5	0.0						2.60	0.7		24.97	1.82	0.30	0.10	0.50	3874	2995	178	294	97	60
			1.5	70.0	27.0	2.0	0.5						2.78	6.2		39.12	26.34	0.81	0.45	1.13	32395	7429	894	18973	916	600
			5.0	85.0	60.0	15.0	7.0						3.00	14.6		52.04	39.04	2.80	0.90	8.60	71201	12062	3210	68419	1620	2206
	Violarite – pyrite	2						10.5	0.0	52.0	0.0	2.0														
								11.0	0.5	68.5	17.5	2.5	3.60	3.3	40.69	47.59	2.59	1.00	0.10	N/A	39628	7724	706	219	1217	54
~90								11.5	1.0	85.0	35.0	3.0														
	Transition	no data																								
	Primary	no data																								

341

retention (65%) of theoretically mobile copper may be related to the partial resistence of parent chalcopyrite or covellite to the initial stages of wholesale sulphide leaching.

The indicated large mean increases in chromium and titanium across the sulphide leaching horizon are anomalous in that both metals are typically immobile in acid oxidising environments. A proportion of the chromium enrichment may, as in other deposits, be due to an influx of this metal into the oxide profile in consequence of silicate weathering. But the 14-fold increase indicated in Fig.5.8.1. is probably too large to be more than partly explained by such an external enrichment phenomenon. More likely, the large increases in both metals are more apparent than real, and are due to the presence of substantial numbers of relic ferrochromite grains in the sampled oxide material - a mineral that is not present in the sampled equivalent sulphides in significant quantities, (Table 5.8.1.).

5.9.SUPERGENE SULPHIDE ALTERATION IN FOUR DEPOSITS OF THE KAMBALDA DOME

The petrology and geochemistry of four supergene altered nickel sulphide deposits from the Kambalda dome are now briefly described. The study suite comprises Lunnon Shoot/Silver Lake Ore Body (S.L.O.B.), Otter Shoot, McMahon and Durkin Shoot. The supergene alteration sequence developed in all four deposits have been previously described, (Woodall and Travis, op.cit., Nickel et.al., 1972 op.cit., Ross and Hopkins, op.cit., Keele and Nickel, 1974). The objective of the present section is the presentation of additional descriptive data on these deposits.

The Lunnon, Otter and Durkin Shoots occur as massive to disseminated sulphide at or near the footwall contact of host serpentinised ultramafic with underlying metabasalts. The sampled McMahon orebody is present at the hanging-wall contact of this host serpentinite, and all four deposits consist of basal massive ore progressively overlain by matrix and disseminated material, (Section 2.3.). Sampling for the present study was carried out in the underground developments, open pits and surface exposures present at the individual deposits.

The mineralogy and chemistry of the oxidation profiles sampled at each deposit are summarised in Tables 5.9.1. to 5.9.4. Sampling was in all cases except the Lunnon Shoot restricted to the higher parts of the oxidation sequence and

consisted of material from the secondary (violarite-pyrite) and overlying oxide zones only, (Tables 5.9.1. to 5.9.4.). Partly altered (Transition) sulphide material was however sampled at Lunnon/Silver Lake in addition to the overlying secondary sulphide and oxide zones, (Table 5.9.1.).

The petrology of the supergene-altered sulphide assemblages

Available data indicate that the secondary sulphide assemblages of the four deposits are qualitatively similar but that they vary in their relative proportions, (Tables 5.9.1. to 5.9.4.). Violarite after pentlandite is present as elongate blocky stringers in Lunnon and McMahon ore, (Figs.5.9.1A. and 1B. respectively), but occurs in more massive forms in equivalent material from the Otter and Durkin Shoots, (Figs.5.9.1C. and 1D.).

Fine-grained marcasite occurs as an initial replacement to pyrrhotite in all four deposits, and this mineral commonly forms mimicked pyrrhotite cleavage textures in the Otter, Durkin and McMahon deposits, (Figs.5.9.1E. to 1G.).Large bird's eye structures are however more typically present in Lunnon secondary marcasite, (Fig.5.9.1H.).

Secondary recrystallisation of fine-grained marcasite is a common feature in Otter, Durkin and McMahon secondary ore. Petrographic observations demonstrate that the phase typically recrystallises to massive pyrite, either with or without an intermediate coarse marcasite stage, (Figs.5.9.1G. and 9.2A, respectively). Further, nickel-rich (Bravoitic) zoning is common in Otter Shoot secondary pyrite and likely indicates that the original pyrrhotite contained significant quantities of this metal, (Fig.5.9.2B.).

The likely vertical extent of secondary sulphide development in each of the sampled Kambalda deposits is indicated in Tables 5.9.1. to 4. Petrographic data based on Lunnon and Otter Shoot material indicate that the secondary sulphides commonly exhibit direct replacement by iron oxides at the sulphide-oxide transition horizon. In this respect, pyrite demonstrates a typically progressive replacement by goethite, (Figs.5.9.2C. and 2D.). Violarite is also typically replaced by goethite, but may in addition exhibit an initial part replacement by covellite - probably as a result of supergene enrichment by copper-rich groundwater solutions, (Figs.5.9.2E. and 2F.).

344

Fig. 5.9.1. Petrography of Kambalda Sulphide Ores (1)

Scale length = 500 μ

A. Typical Vpn texture in Lunnon ore (x 40) Air

Violarite; medium-dark grey: Pyrrhotite; medium grey: Voids; black

B. Typical Vpn texture in McMahon ore (x 80) Air

Violarite; light-medium to dark grey, granular: Pyrite; grey-white:
Carbonate; dark grey, vein-like: Spinel; dark grey, rounded

C. Typical Vpn texture in Otter Shoot ore (x 40) Air

Violarite; light to medium grey, granular: Silica; dark grey, vein-like

D. Typical Vpn texture in Durkin Shoot ore (x 40) Air

Violarite; medium grey, granular: Silica; dark grey, vein-like: Pyrite;
light-medium grey (left margin)

E. Fine-grained marcasite mimics after pyrrhotite cleavage at Otter (x 220) Oil

Marcasite; light-medium grey: Covellite; medium-dark grey, elongate:
Carbonate mimicking Vpo fringe texture; dark grey

F. Fine-grained marcasite after pyrrhotite cleavage at Durkin (x 110) Air

Marcasite; light-medium grey, granular: Vpo; dark grey; granular:
Voids; black: Carbonate; grey-black (right margin)

G. Fine-grained marcasite mimics after pyrrhotite cleavage at McMahon (x 220)
Oil

Fine-grained marcasite; medium-dark grey, granular: Coarse marcasite; light-
medium grey (right and centre): Bravoite; medium-dark grey (left of centre):
Pyrite; medium grey (left margin)

H. Marcasite bird's-eye structure typical of Lunnon secondary ore (x 80) Air

Marcasite; medium grey (lower left): Pyrrhotite; medium grey (upper right):
Violarite; medium-dark grey (left centre): Voids; black: Pyrite (fringing
Vpn); white-grey

Fig.5.9.1.

A

B

C

D

E

F

G

H

346
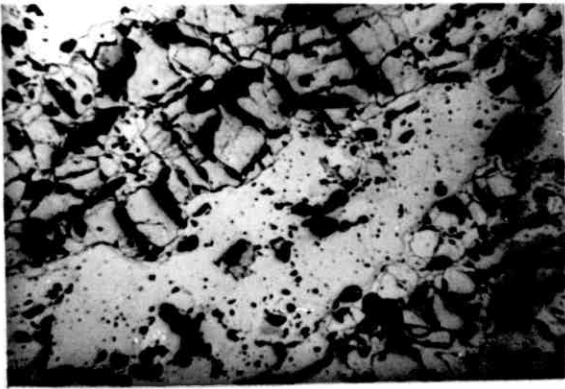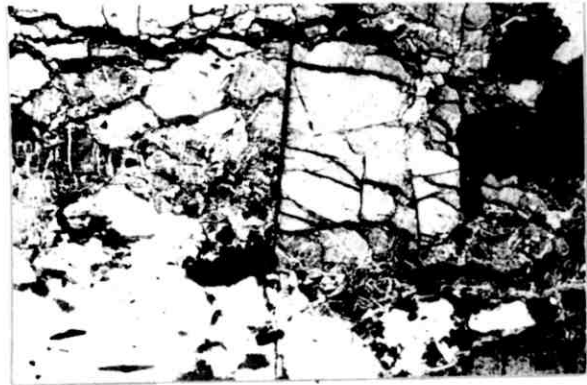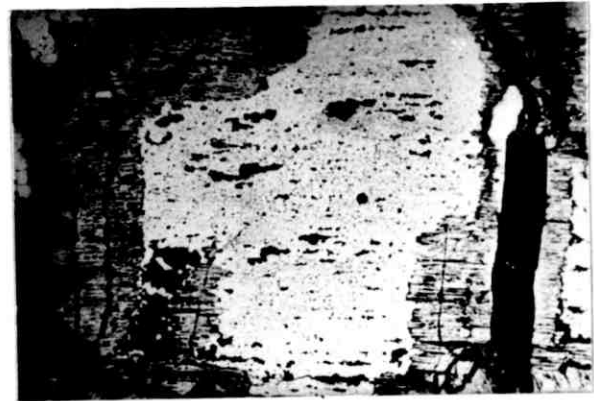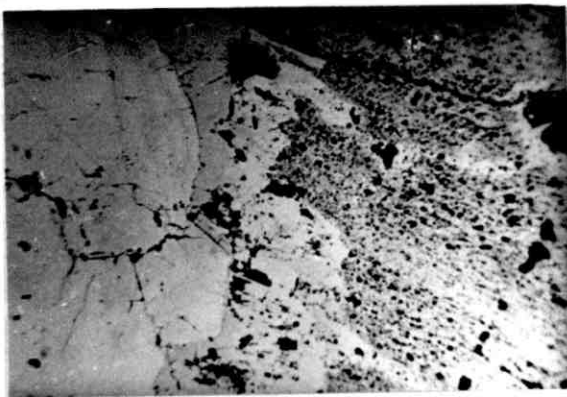
Fig. 5.9.2. Petrography of Kambalda Sulphide Ore (2)

Scale length = 100μ

A.   Direct recrystallisation of fine-grained marcasite to massive pyrite (x 320) Air

F.G. marcasite; light-medium grey, granular: Pyrite; light grey: Vpo;
light-medium grey, granular, fringe-like: Carbonate; grey-black

B.   Bravoitic zoning in secondary massive pyrite (Otter Shoot) (x 220) Oil

Pyrite; light-medium grey, homogeneous: Bravoite; medium-dark grey,
zoned in pyrite: Vpo; light-medium grey, granular: Vpn; dark grey,
granular: Voids; black

C.   In situ replacement of pyrite by goethite (1) (x 220) Air

Pyrite; white-grey: Goethite; medium-dark grey, granular: Voids; black

D.   In situ replacement of pyrite by goethite (2) (x 110) Air

Pyrite; light-medium grey: Goethite; dark grey, granular: Voids; black

E.   Replacement of violarite by covellite (1) (x 320) Air

Covellite; medium-dark grey: Goethite; dark grey, granular: Pyrite;
white: Silicate; grey-black: Silica; medium grey (lower centre)

F.   Replacement of violarite by covellite (2) (x 220) Oil

Covellite/Goethite after violarite; dark grey, mottled: Pyrite; white-grey:
Goethite after pyrite; medium grey (lower centre and top right):   Voids;black

Fig.5.9.2.
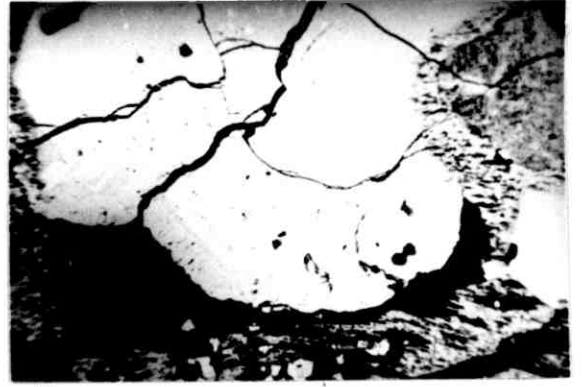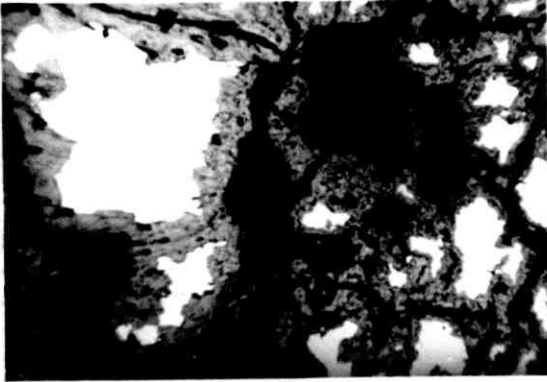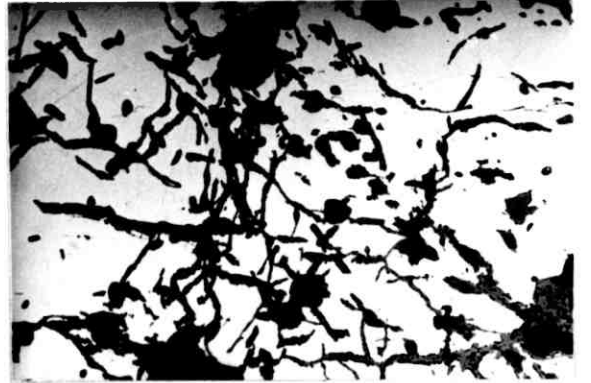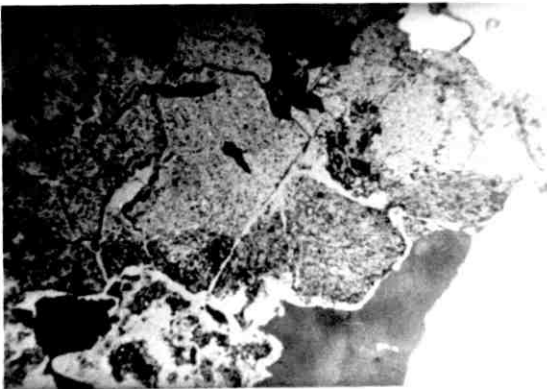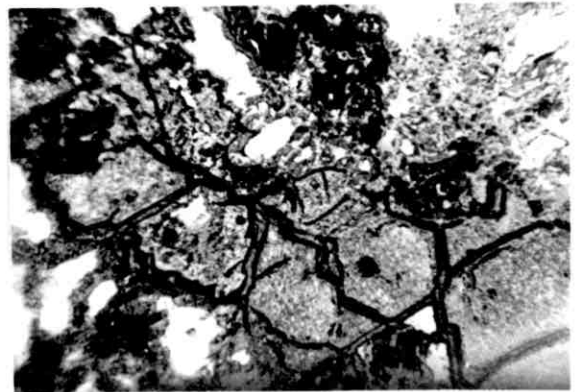
The petrology of the oxide zones

The respective mean mineralogical proportions of the four sampled oxide zones
are indicated in Tables 5.9.1. to 4. Each zone consists principally of goethite
and silica with minor to trace quantities of hematite. Carbonate is an important
constituent of the sampled Otter Shoot oxide zone, (Table 5.9.3.).

Goethite is present as pseudomorphic and/or skeletal replacement textures after
several former ore minerals in all four oxide zones. It occurs as large areas of
boxworks after secondary pyrite, (Figs.5.9.3A. to 3D.), and is also noted as
solid pseudomorphs after this mineral, particularly in the Otter Shoot oxide
zone, (Fig.5.9.3A.). Goethite is similarly observed as quite rare secondary
mimics after pyrrhotite in the S.L.O.B., Otter and Durkin oxide zones, (Figs.
5.9.3F. to 3H.).

Goethite also typically occurs as pseudomorphs after both violarite species in all
four oxide zones. In particular, the textural configurations of original Vpn grains
are generally well-preserved, (Figs.5.9.4A. to 4D.). Violarite after pyrrhotite
mimics are similarly well preserved, (Figs.5.9.4D. to 4G.).

Silica occurs as a major constituent mineral in all deposits except the Otter Shoot,
where it is present only in minor to trace quantities. In the S.L.O.B., McMahon
and Durkin oxide zones it is characteristically present as a pervasive crypto-
crystalline matrix that invests both boxwork structures after sulphide and also
large areas previously affected by wholesale leaching, (Figs.5.9.3A, 3D and
4G.).

Hematite generally occurs in minor but typically variable amounts in each of the
sampled oxide zones, (Tables 5.9.1. to 4.). Where present it commonly forms
rather localised pseudomorphic replacements of secondary pyrite or marcasite,
(Figs.5.9.4A. and 5A. to 5C.). Hematite is also present as rather rare pseudo-
morphs after chalcopyrite in the Otter Shoot oxide zone, (Fig.5.9.5D.).

Carbonate forms a major component of the sampled Otter Shoot oxide zone, (Table
5.9.3.), and is present chiefly as pseudomorphs after both violarite species,
(Fig.5.9.5E.)

Several species of carbonate are present as oxidate minerals in the four oxide
zones, and textural data indicate that these phases have characteristically
formed as precipitants from (groundwater) solutions, (Tables A2/2 to A2/5 ;
Appendix Two).

Magnesite ($MgCO_3$) is noted in oxidising sulphide and in oxide after sulphide in the McMahon and Otter Shoots. The typically ore metal-rich composition of this mineral is a direct indication of its relationship to sulphide leaching, (Table A2/2; Appendix Two). Further, the very high nickel contents of the samples indicate that substantial lattice substitution of magnesium has occurred during its formation.

Huntite ($Mg_3Ca(CO_3)_4$) occurs in a similar locus to magnesite in the S.L.O.B. oxide zone. This mineral is similarly rich in ore metals and appreciable lattice substitution of nickel for magnesium is indicated by the chemistry of analysed samples. In contrast, the metal-poor content of huntite after talcose mafic silicate sampled at Otter Shoot directly reflects the relatively low ore metal content of the parent host rock from which it is directly derived in this instance.

Dolomite ($CaMg(CO_3)_2$) is noted in the S.L.O.B. oxide material. It is typically associated with the sulphide-oxide transition zone, and available chemical data indicate that the mineral exhibits considerable lattice substitution of nickel for magnesium. Dolomite also contains appreciable quantities of other ore metals, (Table A2/4; Appendix Two).

Calcite ($CaCO_3$) is present in surface gossan material in all four sampled oxide zones, (Tables 5.9.1. to 4.). In both the S.L.O.B. and Otter Shoot it also occurs in association with dolomite, (Table A2/5; Appendix Two). Both minerals are typically present as joint or weathered surface coverings, and the generally low metal contents exhibited by analysed samples indicates their derivation from near surface silicate weathering rather than as an indirect result of wholesale sulphide leaching.

Aragonite ($CaCO_3$) occurs as a rather rare fracture lining in deep oxide zone material from Otter Shoot. It is likely that the probable restriction of this mineral to the lower horizons of the oxide zone is related to its long term metastability with respect to calcite.

Mean density and porosity variation within the sampled Kambalda profiles

The likely mean variation in true density and porosity within the SLOB/Lunnon and McMahon sulphide oxidation profiles, (based on sampled material) are

350

Fig. 5.9.3. Petrography of the Kambalda Gossans (1)

Scale length = 300μ   Blue-white filter used throughout

A.   Goethite boxworks after secondary pyrite – Silver Lake/Lunnon (x 110) Air

Goethite; light-medium grey: Silica; dark grey: Voids; black

B.   Goethite mimics after secondary pyrite – Otter Shoot (1) (x 80) Air

Goethite after pyrite; medium grey: Goethite after violarite– grey-black

C.   Goethite boxworks after secondary pyrite – McMahon (x 80) Air

Goethite; medium greys: Silica; grey-black

D.   Goethite boxworks after secondary pyrite – Durkin Shoot (x 320) Air

Goethite; medium greys: Silica; grey-black: Goethite after Vpo; dark grey, granular (right centre)

E.   Goethite mimics after secondary pyrite – Otter Shoot (2) (x 110) Air

Goethite after pyrite; light-medium grey: Goethite after violarite; dark grey: Voids; black

F.   Goethite mimics after secondary mimicked pyrrhotite Silver Lake/Lunnon (x 110) Air

Goethite septae; medium-dark grey: Hematite linings; light grey: Goethite after lamellar violarite; dark grey: Goethite after interstitial violarite; dark grey (left margin): Voids; black

G.   Goethite mimics after secondary mimicked pyrrhotite – Otter Shoot (x 110) Air

Goethite after marcasite/pyrite; medium grey: Goethite after Vpo; dark grey: Voids; black

H.   Goethite mimics after secondary mimicked pyrrhotite – Durkin Shoot (x 110) Air

Goethite after FeS_2; medium grey: Goethite after Vpo; medium-dark grey

Goethite after Vpn; medium greys, granular (top right): Voids; black

Fig.5.9.3.
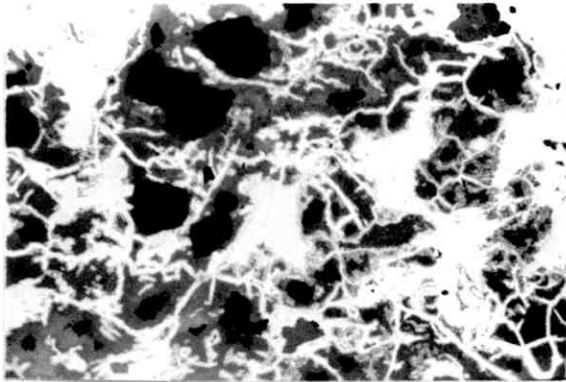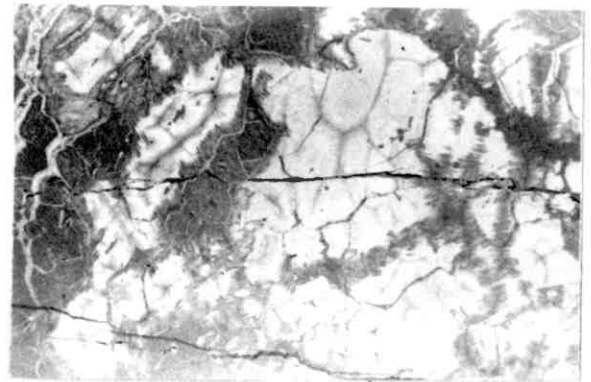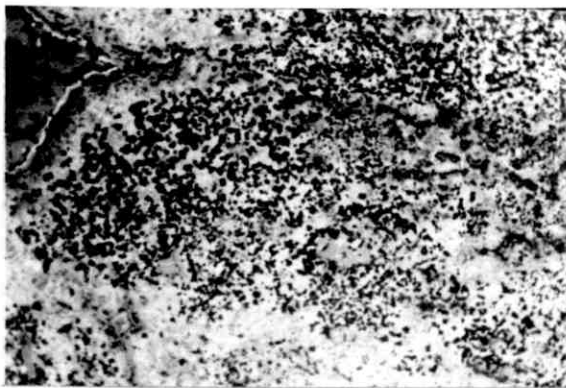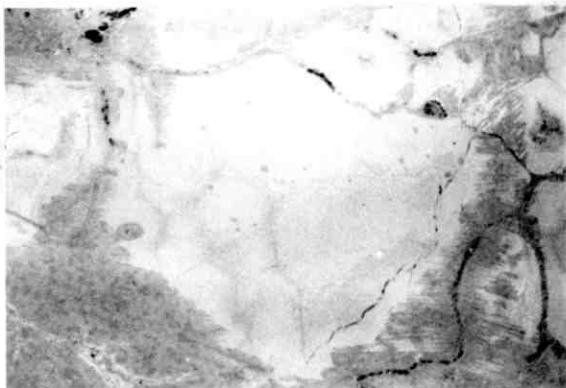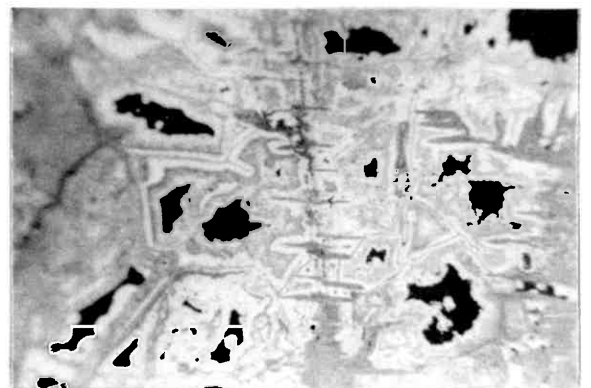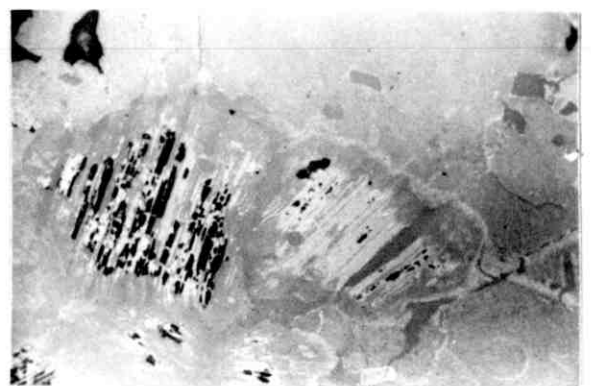
Fig. 5.9.4. Petrography of the Kambalda Gossans (2)

Scale length = 300 μ Blue-white filter used throughout

A.   Goethite mimics after violarite – Silver Lake/Lunnon (x 110) Air

Goethite after violarite; medium-dark grey: Hematite after secondary pyrite; light grey: Voids; black

B.   Goethite mimics after violarite – Otter Shoot (x 80) Air

Silicified goethite after violarite; dark grey: Goethite after Vpn cleavages; light-medium grey

C.   Goethite mimics after violarite – McMahon (x 40) Air

Goethite after Vpn and pyrite (boxworks); light grey: Silica; dark grey: Voids; black

D.   Goethite mimics after violarite (Vpo) – Durkin Shoot (x 80) Air

Silicified goethite after Vpn and Vpo; medium greys: Voids; black

E.   Goethite mimics after violarite (Vpn) – Silver Lake/Lunnon (x 320) Air

Goethite after Vpn and Vpo; medium greys: Silicified goethite after FeS_2; dark grey: Voids; black

F.   Goethite mimics after violarite (Vpo) – Otter Shoot (x 110) Air

Goethite after Vpn and Vpo; dark grey: Goethite after secondary FeS_2; light greys

G.   Goethite mimics after violarite (Vpo); McMahon (x 110) Air

Goethite after Vpn and Vpo; medium grey, mottled: Silica matrix; dark grey

Fig.5.9.4.

354
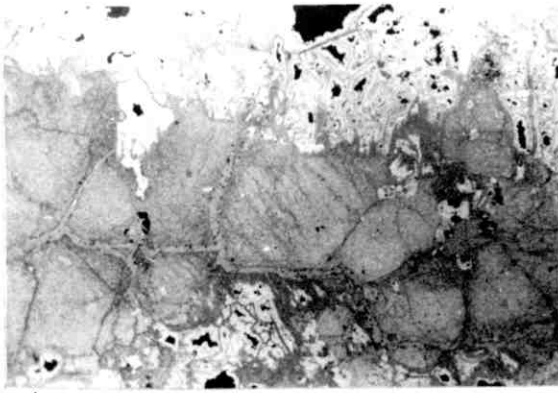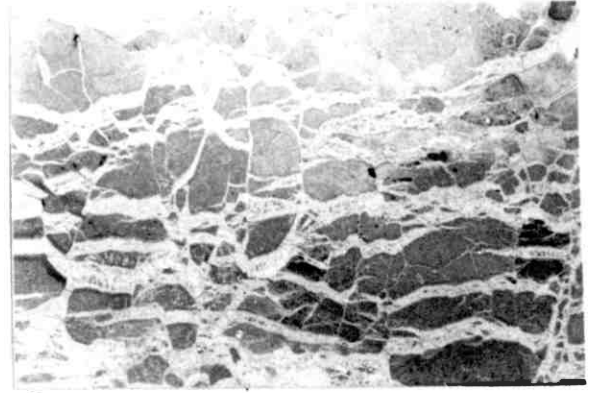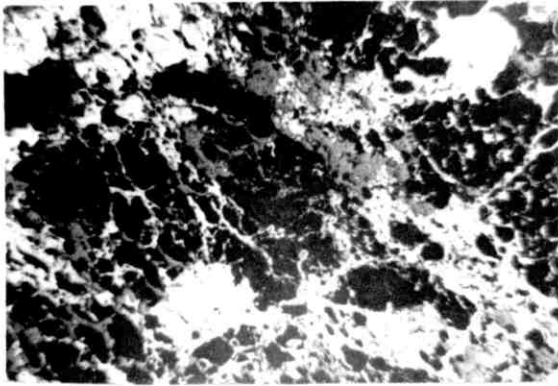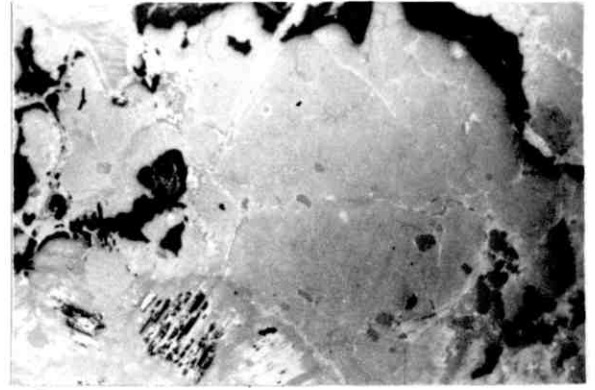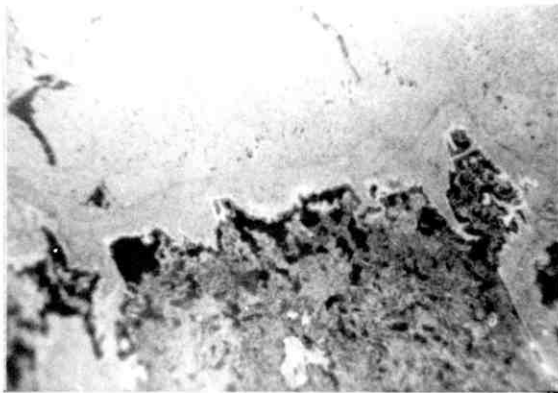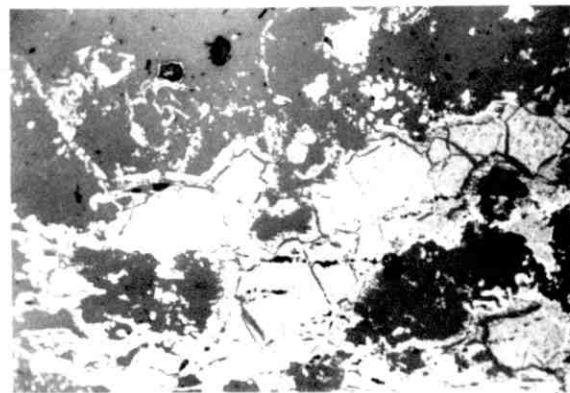
Fig. 5.9.5. Petrography of the Kambalda Gossans (3)

Scale length = 300μ Blue-white filter used throughout

A.   Hematite mimics after secondary iron disulphides - Otter Shoot (x 320) Air

Hematite; light grey: Goethite; medium-dark grey

B.   Hematite mimics after secondary iron disulphides - McMahon (x 80) Air

Hematite after marcasite bird's eyes; light grey: Silica; dark grey
Voids; black

C.   Hematite mimics after secondary iron disulphides - Durkin Shoot (x 80) Air

Hematite after pyrite (mimics and boxworks); white-grey: Silica; dark grey:
Voids; black: Goethite; medium grey

D.   Hematite mimic after chalcopyrite - Otter Shoot   (x 110) Air

Hematite; light grey: Goethite after Vpn; dark grey, granular:
Goethite after Vpn cleavage; light-medium greys

E.   Typical carbonate mimic replacement of violarite species (x 80) Air

Carbonate; dark grey, mottled: Goethite as Vpn cleavages; medium grey:
Hematite after FeS_2; light grey

Fig.5.9.5.
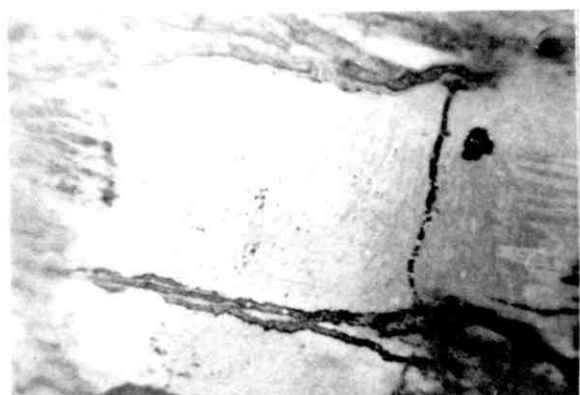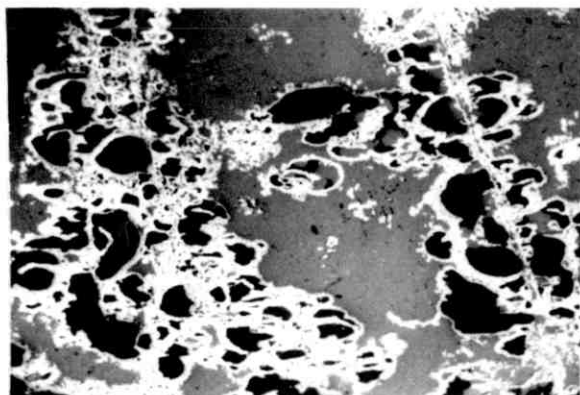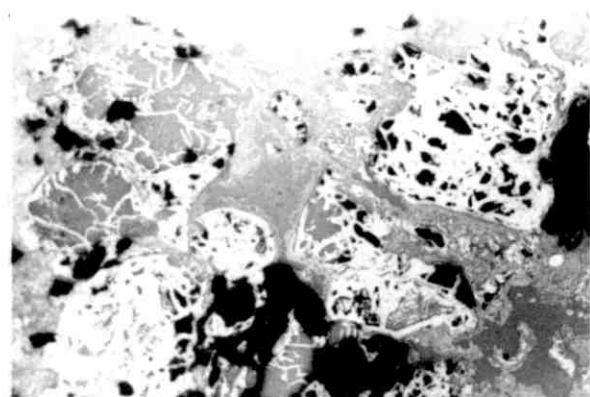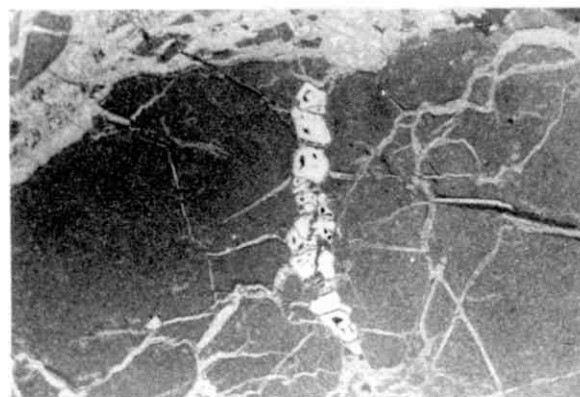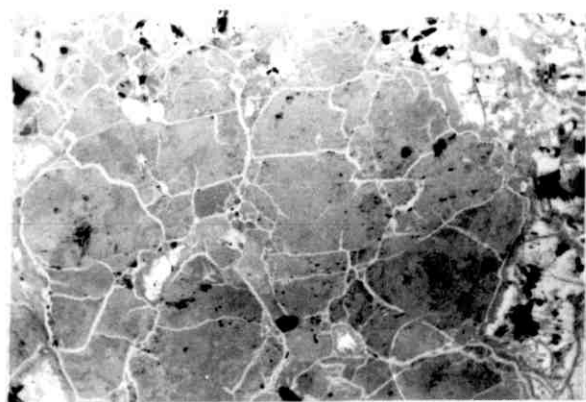
presented in Figs. 5.9.6. and 7 respectively.

The forms of both mean density profiles closely follow the overall sequence of mineralogical changes that occur within each deposit during progressive oxidation of the (primary) sulphide assemblage, and the relatively small change in mean porosity that occurs across the respective sulphide-oxide transition horizons supports petrographic evidence that substantial proportions of the secondary sulphide material is retained as iron oxide pseudomorphs or mimic structures in the overlying oxide zones of these deposits.

Bulk chemical variation within the Lunnon/S.L.O.B. composite oxidation profile

The likely bulk mean chemical variation within the sampled oxidation sequence developed in the Lunnon/SLOB composite ore profile is presented in Fig.5.9.8. The indicated mean constancy of all elements (excepting iron) between the 55m. and 19m. levels indicates that the development of the supergene (secondary) alteration sequence at Lunnon/SLOB probably occurs within an effectively closed chemical system. In contrast, the progressive reduction in mean iron content between the 55m. and 40m. levels reflects the release of iron from altering pentlandite during the development of secondary violarite within the transition zone.

The noted changes in mean iron and sulphur contents that occur across the sulphide-oxide transition (18 metre) horizon are consistent with the chemical behaviour expected of these two elements under such an acid oxidising regime, and the approximately 50 percent retention of iron noted at this level in Fig.5.9.8. supports petrographic evidence of widespread iron oxide development in the S.L.O.B. oxide zone, (Table 5.9.1.). In addition, the observed near three-fold increase in mean silicon content across the 18m. horizon is consistent with the presence of significant quantities of externally derived silica in the overlying oxide zone.

The observed mean depletions of individual trace metals across the sulphide leaching zone are generally consistent with the expected chemical mobilities of the oxidised forms of these elements under low pH-high Eh conditions. The noted near 30 percent retention of nickel is however anomalously high and is most probably related to the in situ fixation of this metal within the significant

Fig. 5.9.6. Mean True Density and Porosity profiles – Lunnon/S.L.O.B.
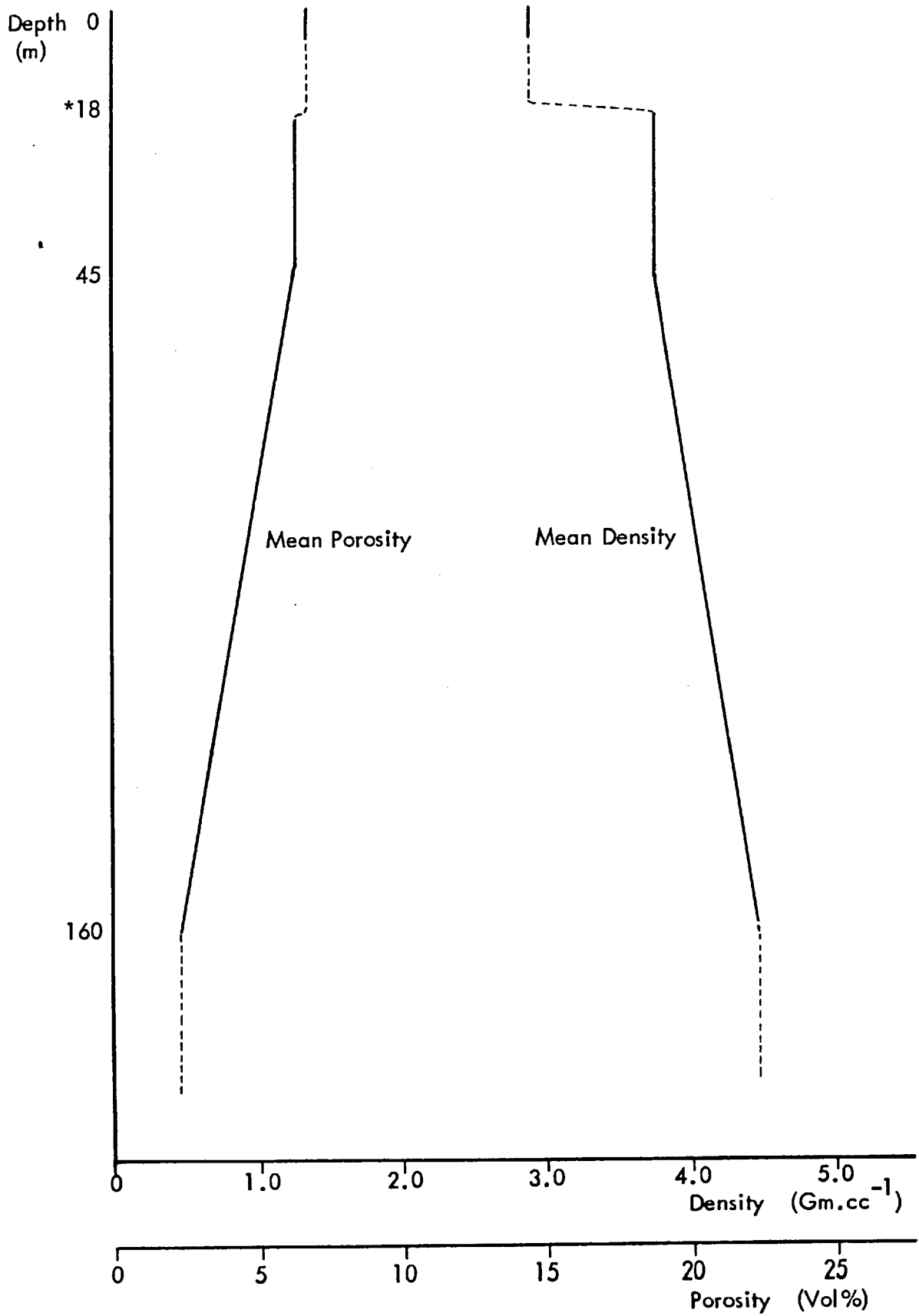
* Approximate position of the water table

Fig. 5.9.7. Mean True Density and Porosity profiles – McMahon

Depth (m)

Mean Porosity

Mean Density

Density (Gm.cc^{-1})

Porosity (Vol%)
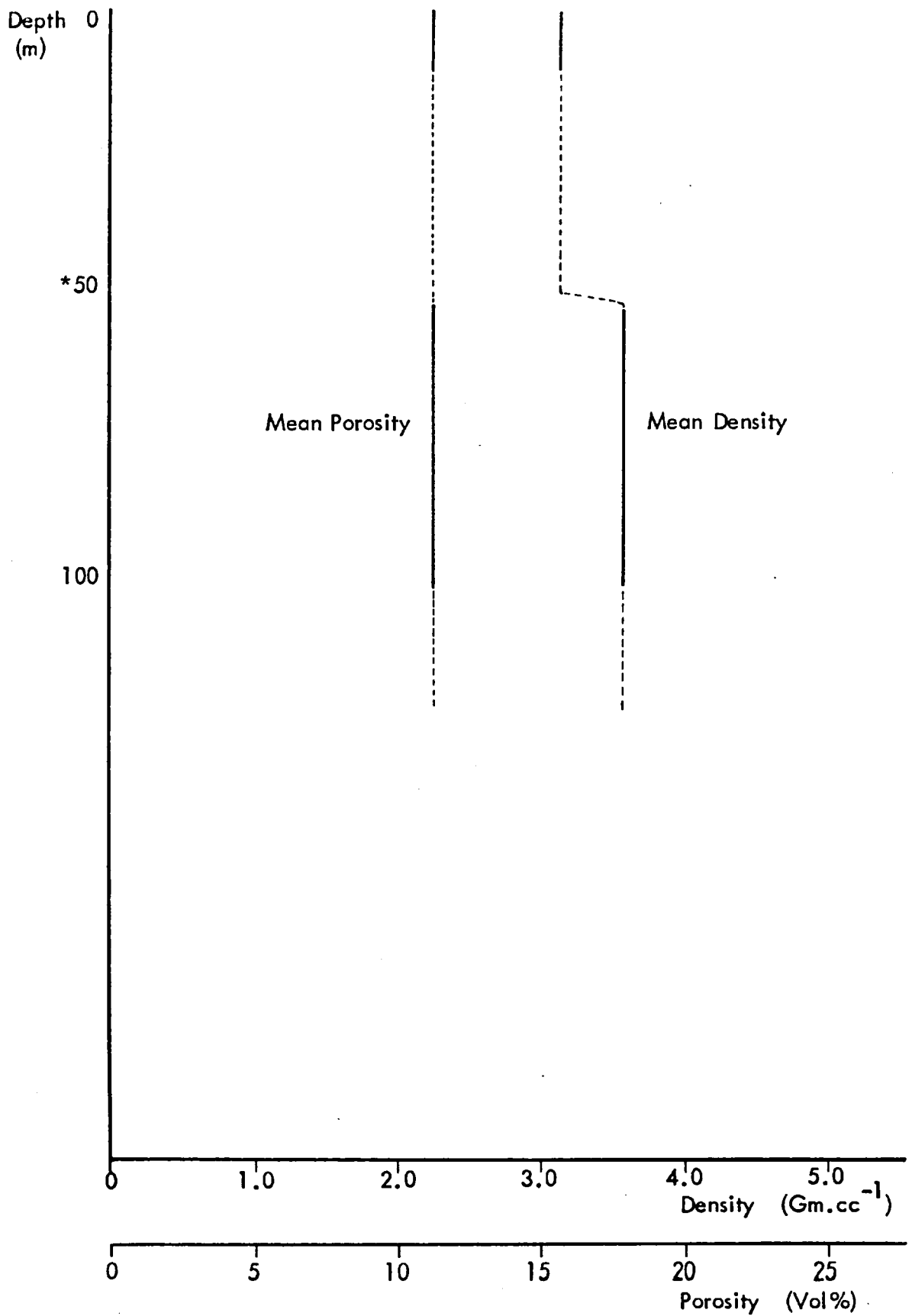
* Approximate position of the water table

Fig. 5.9.8. Chemical Variations in Alteration Profile – Lunnon/S.L.O.B.

TABLE 5.9.1. SUMMARY DATA OF SULPHIDE ALTERATION - LUNNON/S.L.O.B.

Depth (m)	Alteration Zone	No. of Samples (n)	MINERALOGY (Means and ranges) — Volume % Units										Physical data (mean/ranges) Den gm/cc	Por %	GEOCHEMISTRY (Means and ranges) — Wt.% Units: S	Fe	SiO₂	MgO	Al₂O₃	CO₃	p.p.m. Units: Ni	Cu	Mn	Cr	Co	Ti
			Hm	Gt	Sl			Ca	Dol	Hun																	
18	Oxide	6	0.0	30.0	15.0								2.30	1.8		21.41	21.78	0.90	0.10	N/A	2075	455	104	178	90	84
			1.5	60.5	38.5			trace	trace	trace			2.88	6.7		32.68	44.38	1.38	0.23	N/A	3921	3663	147	623	243	170
			5.0	80.0	70.0								3.50	15.1		46.93	63.08	2.10	0.40		7795	6790	215	1156	396	396
				Gt	Vl	Cv				Py		Sil															
	Sulphide-oxide transition	3		35.0	0.0	0.0				17.0		10.0	3.40	2.3	6.99	38.67	13.25	0.00	0.00		833	647	312	9939	1068	192
				50.0	6.8	1.0				25.0		15.0	3.77	4.1	16.29	40.59	15.32	4.10	0.73	N/A	24221	14195	1008	9599	1618	540
				62.5	13.0	3.0				50.0		20.0	4.10	6.2	29.00	42.38	20.29	8.90	1.20		45781	39341	1776	9914	2479	953
					Vl	Cp	Mt			Py	Mc	Sil														
	Violarite - pyrite	2			4.5	1.5	0.0			75.0		0.0	3.00	5.6	26.52	42.57	1.59	0.00	0.00		9862	6598	535	698	844	102
					6.0	3.2	2.5			80.0	-	7.5	3.70	6.3	36.70	44.82	8.90	2.85	1.00	N/A	12809	17574	606	945	2502	447
40-50					7.5	5.0	5.0			85.0	15.0		4.40	7.0	46.89	44.08	16.20	5.70	2.00		15755	28549	676	1191	4159	791
			Po		Vl	Cp	Mt			Py	Mc	Sil														
	Transition	3	11.5		4.0		0.0			0.0	0.0	0.5	4.10	1.7	37.20	49.79	0.85	0.00	0.00		12699	144	230	274	629	78
			42.0		6.5	0.5	0.5			45.0	5.0	2.5	4.47	2.3	42.16	53.41	1.44	0.27	0.10	N/A	19182	418	495	949	1625	100
180			80.0		12.5		1.0			75.0	15.0	7.0	4.70	3.2	47.06	58.58	2.45	0.50	0.30		31330	671	721	1943	2120	132
	Primary	no data																									

TABLE 5.9.2.   SUMMARY DATA OF SULPHIDE ALTERATION - McMAHON

Depth (m)	Alteration Zone	No. of Samples (n)	MINERALOGY (Means and ranges) Volume % Units								Physical data (mean/ranges)		GEOCHEMISTRY (Means and ranges)											
			Hm	Gt	Sl	Carb	FCr	Ca	MgS	Sil	Den gm/cc	Por %	S	Fe	SiO₂	MgO	Al₂O₃	CO₃	Ni	Cu	Mn	Cr	Co	Ti
50	Oxide	6	2.0	33.0	4.0	0.0	0.0	Ca	MgS		2.10	4.6		37.80	3.77	0.10	0.10	0.00	4055	951	67	287	142	72
			3.0	69.0	25.0	3.2	0.2	trace	trace		2.77	11.1		43.94	18.30	3.62	0.12	2.27	23258	6494	951	1441	552	90
			4.0	93.0	65.0	19.0	1.0				3.00	18.7		47.50	31.59	11.00	0.20	7.20	61732	14602	2727	4454	1419	108
90 – 150	Violarite – pyrite	4	Vl 10.0	Cp				Py 0.0	Mc 75.0	Sil 2.0	3.40	7.2	32.68	26.34	3.12	0.60	0.10		34151	30	238	281	30	36
			12.0	0.5				2.5	79.5	6.5	3.58	11.2	42.33	39.17	7.87	0.98	0.11		40510	874	533	606	463	44
			15.0					5.0	82.5	10.0	3.70	14.3	46.05	42.14	12.46	1.53	0.12		44539	2876	1330	766	830	60
	Transition	no data																						
	Primary	no data																						

TABLE 5.9.3. SUMMARY DATA OF SULPHIDE ALTERATION - OTTER SHOOT

Depth (m)	Alteration Zone	No.of Samples (n)	MINERALOGY (Means and ranges) Volume % Units										Physical data (mean/ranges) Den gm/cc	Por %	GEOCHEMISTRY (Means and ranges) Wt.% Units S	Fe	SiO$_2$	MgO	Al$_2$O$_3$	CO$_3$	p.p.m. Units Ni	Cu	Mn	Cr	Co	Ti
18	Oxide	9	Hm	Gt			Dol	MgS	Hun	Sl	Cab														
			0.0	30.0							3.0	2.60	1.4	0.00	41.44	0.61	0.10	0.00	0.00	4644	4226	260	30	30	42
			1.5	75.0			trace	trace	trace	0.0	25.0	2.91	12.5	0.07	51.11	1.79	1.10	0.40	5.85	31786	19269	389	340	563	245
			10.0	95.0							60.0	3.50	23.3	0.41	54.05	11.99	3.00	2.00	15.50	70659	30179	721	1348	1867	1163
	sulphide-oxide transition	4	Gt	Vl	Cp	Cv	Py			Sl	Cab														
			10.0	0.0		0.0	8.0			0.0	0.0	3.00	2.3	0.75	21.73	0.67	2.50	0.00	0.00	10687	4178	126	30	30	36
			49.0	0.8	1.0	1.0	26.4			7.5	16.0	3.33	7.5	17.75	35.64	11.06	3.80	0.08	5.20	19297	25396	275	156	510	48
			85.0	3.0		2.0	75.0			30.0	54.0	3.80	12.5	40.78	47.83	35.79	5.00	0.10	15.00	35047	59662	446	534	1090	66
80-90	Violarite - pyrite	1		Vl	Cp	Cv	Py	Mc		Sl	Cab														
				2.5	1.5	2.5	40.0	35.0		2.5	17.0	3.70	1.2	42.81	36.94	8.57	2.10	0.10	N/A	9076	31784	104	30	134	30
	Transition	no data																							
	Primary	no data																							

TABLE 5.9.4. SUMMARY DATA OF SULPHIDE ALTERATION - DURKIN SHOOT

Depth (m)	Alteration Zone	No. of Samples (n)	MINERALOGY (Means and ranges) Volume % Units							Physical data (mean/ranges) Den gm/cc	Por %	GEOCHEMISTRY (Means and ranges) Wt.% Units S	Fe	SiO₂	MgO	Al₂O₃	CO₃	p.p.m. Units Ni	Cu	Mn	Cr	Co	Ti
25	Oxide	5	Hm 1.0	Gt 15.0	Sl 10.0				Ca	2.60	0.4		19.21	32.34	0.10	0.00		2059	6710	104	30	194	30
			5.5	49.0	46.5				trace	2.80	2.6		29.96	45.06	0.33	0.07		13388	15736	490	13488	699	268
			20.0	90.0	82.5					3.00	6.0		37.33	67.85	0.70	0.20		23755	22614	854	40395	1015	725
55	Violarite – pyrite	1		Sl 10.0	Vl 2.0	Py 57.5	Mc 30.0		Carb 2.0	3.90	1.4	45.75	30.37	22.17	0.30	0.00		6593	1238	52	30	60	36
	Transition	no data																					
	Primary	no data																					

363

quantities of goethite pseudomorphs after Vpn that are present within the S.L.O.B. oxide zone.

The observed high depletion of both titanium and chromium across the 18 metre horizon is similarly anomalous as both metals are typically rather immobile under acid oxidising conditions. This apparent anomaly is, however, more likely caused by a heterogeneous distribution of parent magnetite/ferrochromite within the Lunnon-SLOB ore profile, rather than to an actual mobilisation of these metals during sulphide leaching. This feature indicates that oxide and sulphide material are not strictly equivalent in respect of absolute spinel content in the original sample suite.

5.10. SUMMARY

Chapter five has presented synoptic descriptions of the near surface sulphide alteration profiles that are developed in eleven nickel-copper sulphide deposits in Western Australia.

The alteration sequences present in four of these deposits, (Mt. Edwards, Mt. Monger, Jan Shoot and Ravensthorpe) have not been previously described, and the existence of sulphide alteration has only been indicated, but not previously described in detail at three other deposits; Carr Boyd, Redross and Spargoville 5a. The four sampled Kambalda dome deposits have been well documented by a number of workers.

The alteration profile developed in each deposits has been described in terms of the progressive mineralogical and textural evolution of near-massive to massive primary ore through supergene (secondary) sulphide development to the formation of the overlying oxide zone. The corresponding changes in bulk chemistry within this documented petrological sequence have also been described for each deposit. Further, each alteration profile description has been supplemented by documentation of the corresponding mean density and porosity changes that occur during progressive sulphide ozidation.

The profile descriptions of several deposits have been confined to the secondary sulphide and overlying oxide zones. This has been due to either a lack of adequate sample coverage or because of the absence of primary and partly-altered components from the sulphide alteration sequence.

The results of the profile description work indicate however that the primary sulphide assemblages of all sampled deposits are qualitatively similar, and further that the progressive near-surface alteration of these primary ores occur in a qualitatively similar mode across the deposits suite.

A full inter-deposit descriptive comparison of the 11 sampled Australian profiles together with those developed in the six previously documented southern African deposits is presented in Chapter Six.

CHAPTER SIX

A DESCRIPTIVE COMPARISON OF NEAR SURFACE ALTERATION IN 15

NICKEL SULPHIDE DEPOSITS FROM

SOUTHERN AFRICA AND WESTERN AUSTRALIA

6.1. INTRODUCTION

In chapter six the principal features of progressive near surface sulphide alteration
are descriptively compared across the 15 southern African and Western Australian
nickel sulphide deposits that form the study suite of the present work. Such an
exposition allows the similarities and differences in alteration petrology and
geochemistry that exist across this suite to be brought out. It also however provides
a summary basis on which the genetic studies of nickel sulphide oxidation and
gossan formation that comprise part two of the present work can be developed.

An inter-deposit comparison of sulphide alteration petrology forms the first part
of the present chapter (section 6.2.). In this section the mineralogy, textures and
mineral chemistries of individual primary sulphide assemblages are firstly compared.
A similar treatment is then carried through for the equivalent secondary sulphide
rocks and the section closes with an inter-deposit comparison of the mineralogy
and textural features of associated oxide zones and their related oxidate minerals.

Chapter six continues with summary expositions of inter-deposit density and porosity
profile variation, (section 6.3.), and observed inter-deposit variations in alteration
zone development are treated in section 6.4.

Section 6.5. initially comprises an inter-deposit comparison of the bulk chemistry
of progressive sulphide alteration. Here the chemical similarities and differences
observed in the development of the documented secondary sulphide assemblages are
firstly described.An inter-deposit comparison is then made of the bulk mean chemical
changes that occur as a result of oxide formation within individual alteration profiles.

Chapter six closes with a summary section (section 6.6.) in which the principal
results of the descriptive comparison work are precied.

6.2. A COMPARISON OF SULPHIDE ALTERATION PETROLOGY

Primary sulphide assemblages: mineralogy

A composite summary of the principal features of sampled sulphide alteration
petrology in 15 study deposits is presented in Fig.6.2.1. The data demonstrate
that the primary mineral assemblage: Pyrrhotite-pentlandite-chalcopyrite-spinel-
silicate is present in all 15 study deposits. Spinel is however not observed in the
Jan Shoot or McMahon sulphide ores. Further, the presence of pyrrhotite is
indirectly inferred from the existence of secondary iron disulphide replacements
at Jan, Carr Boyd, Spargoville and McMahon. This is because the primary sulphide
assemblages were not sampled or are absent in these deposits. In addition, the
presence of primary pentlandite is inferred for similar reasons from pseudomorphing
secondary violarite at these four deposits together with Ravensthorpe and Lunnon.

Considerable variation in mean primary mineral proportions occurs across the study
suite, (Fig.6.2.1.). Pyrrhotite mean proportions are however fairly constant in
near-massive to massive sulphide ore, and range between 75 and 85 percent. Carr
Boyd pyrrhotite is an exception in this respect, as it likely averages only about
63 percent of the relevant primary sulphide assemblage, (Fig.6.2.1.).

The mean pentlandite proportions of primary ore exhibit considerable inder-deposit
variation. The majority of primary massive ores contain between 6.5 and 10 percent
pentlandite, but higher mean proportions are exhibited by Phoenix (15%), Mt.
Edwards (14%), and Spargoville and Lunnon (11% each). In contrast, lower mean
contents are characteristic of Carr Boyd (2.5%), Ravensthorpe (4%) and Pikwe (5%),
(Fig.6.2.1.).

Mean chalcopyrite contents of near-massive to massive primary ore also vary across
the study suite, (Fig.6.2.1.). The highest mean contents are displayed by Carr Boyd
and Pikwe (8% each), and Perserverence (about 6.5%). All other primary ore
assemblages contain between 0.5 and two percent chalcopyrite. Less than 0.5 per-
cent is however observed at McMahon, (Fig.6.2.1.). Further, the sampled
southern African deposits generally contain a higher proportion of chalcopyrite in
their massive primary ore assemblages than do the equivalent Western Australian ores.

Magnetite and/or composite magnetite-ferrochromite typically forms between 0.5 and
2.5 percent of the primary massive sulphide assemblages of the study suite, (Fig.
6.2.1.). Higher mean proportions are however present at Selkirk (6%), Redross
(4.5%) and Pikwe (4%). Recognisable ferrochromite has a greater qualitative

Fig.6.2.1. Inter-deposit Comparison of Sulphide Alteration Petrology
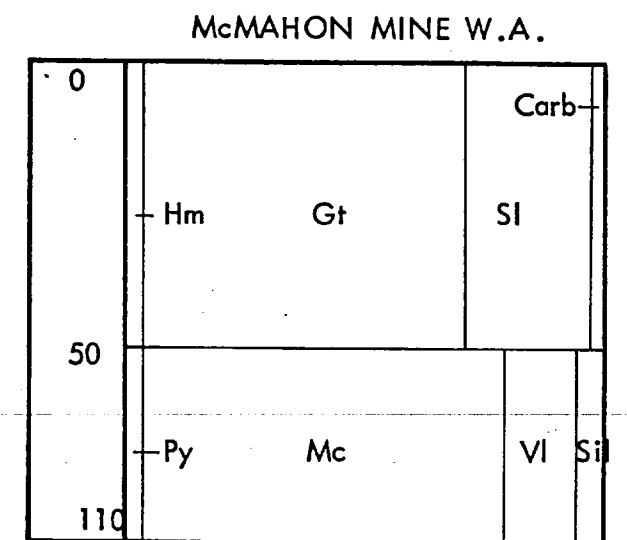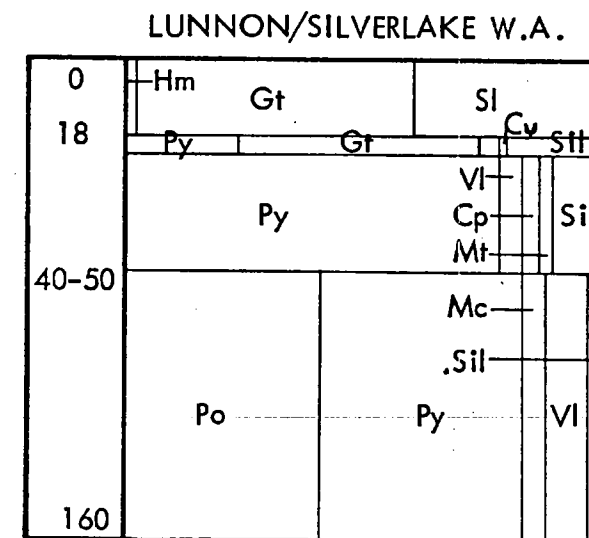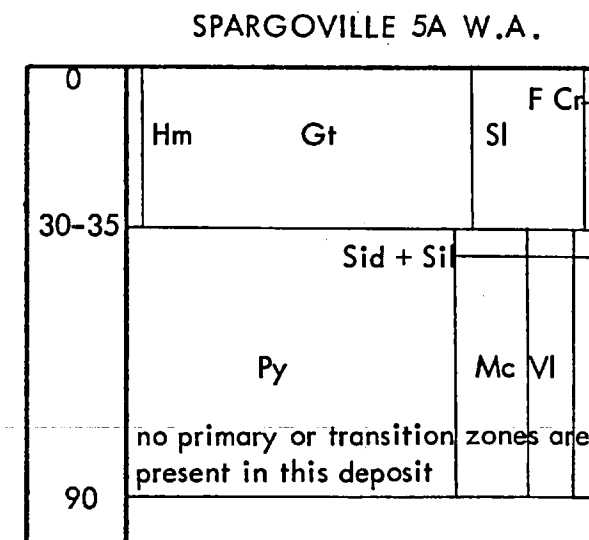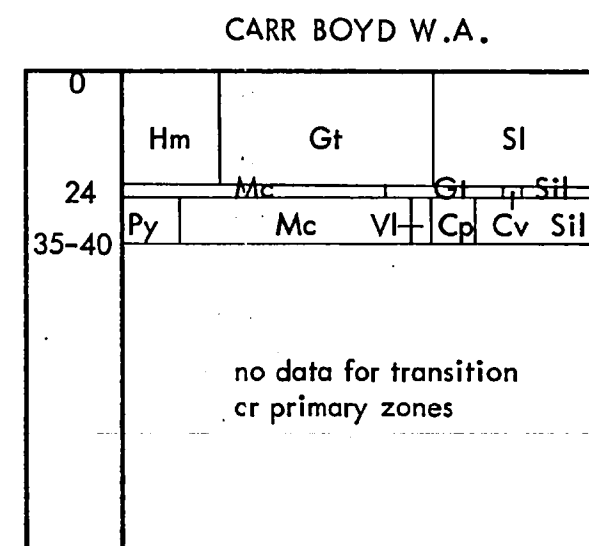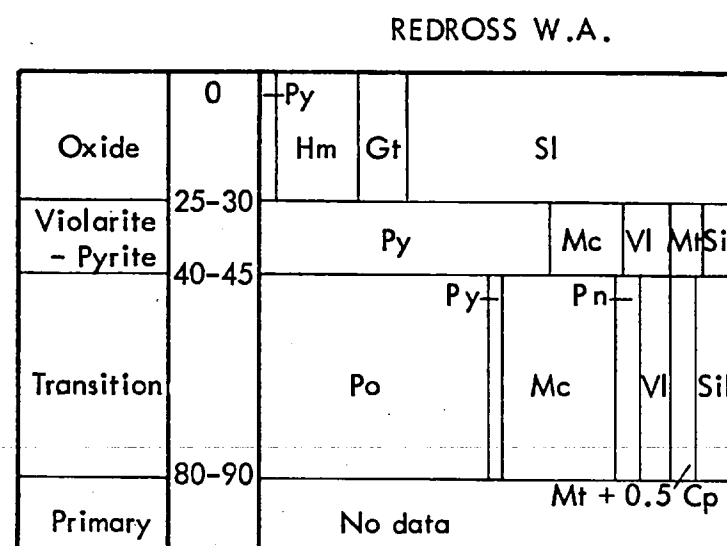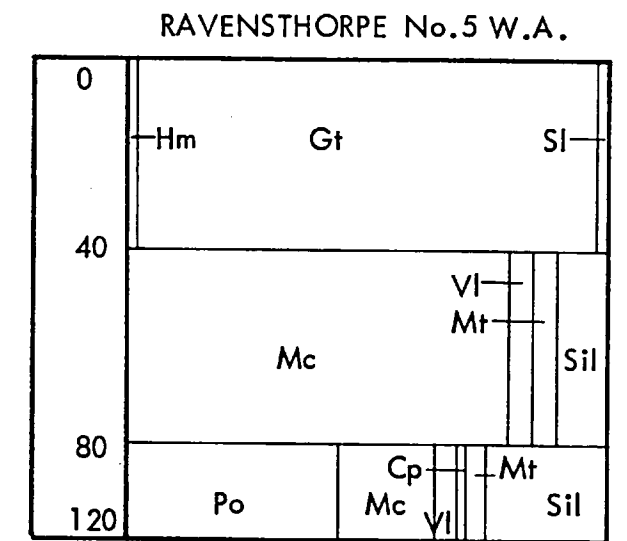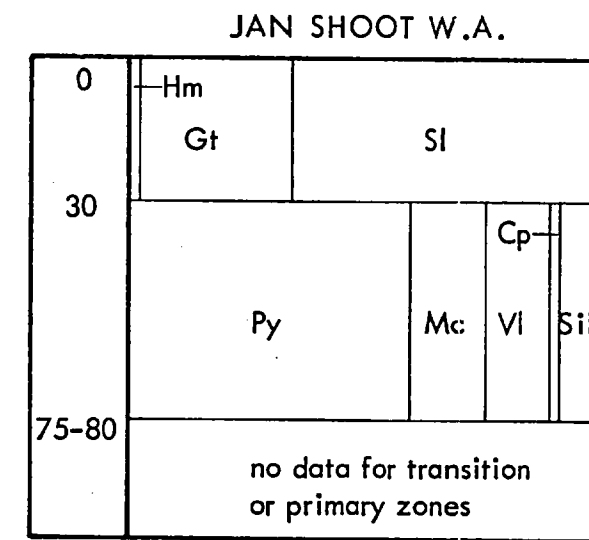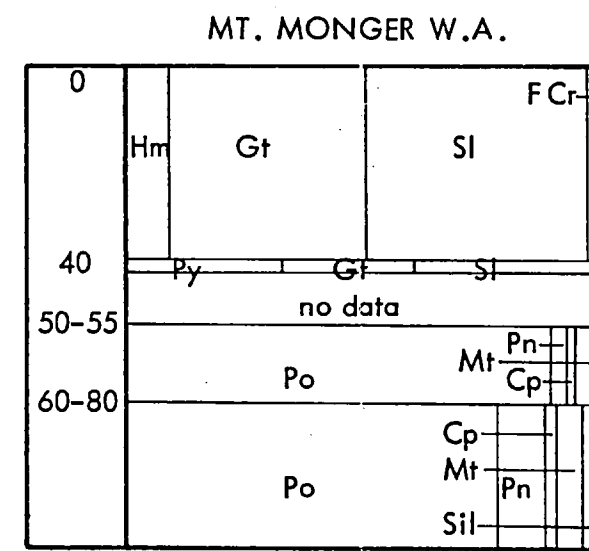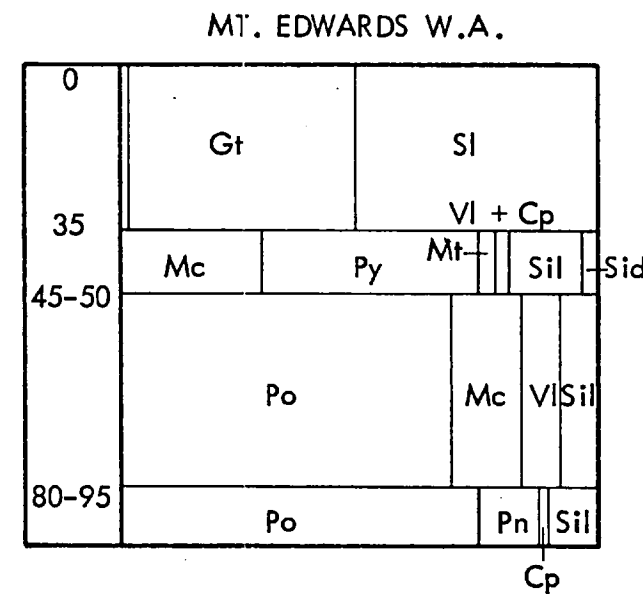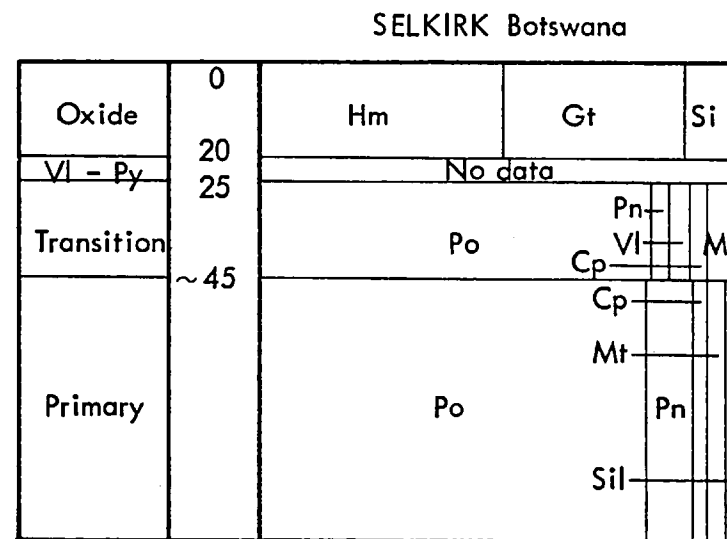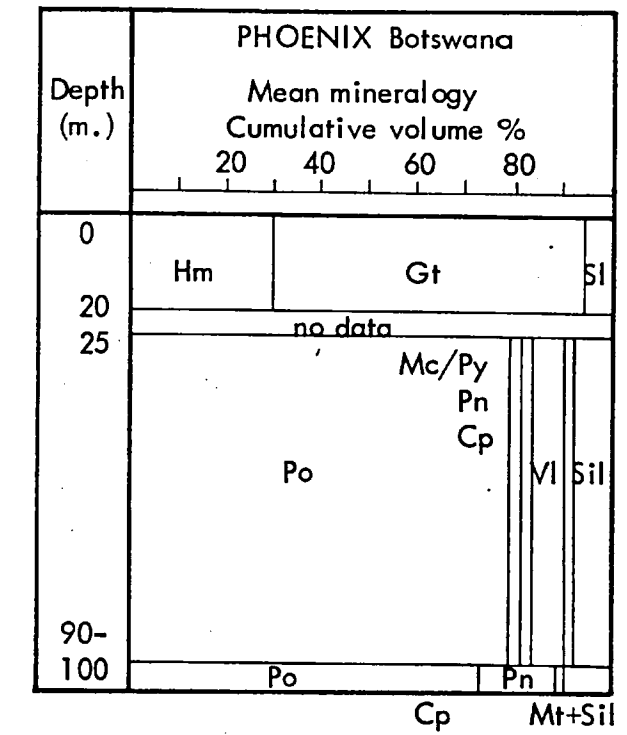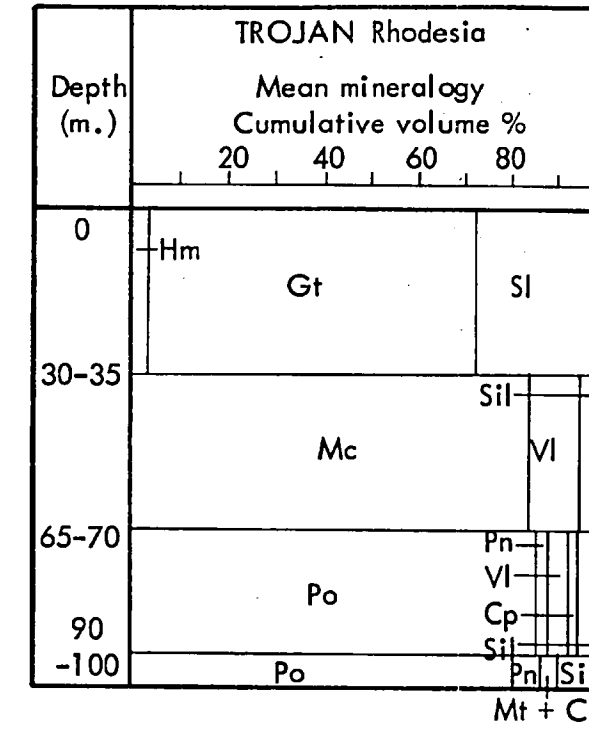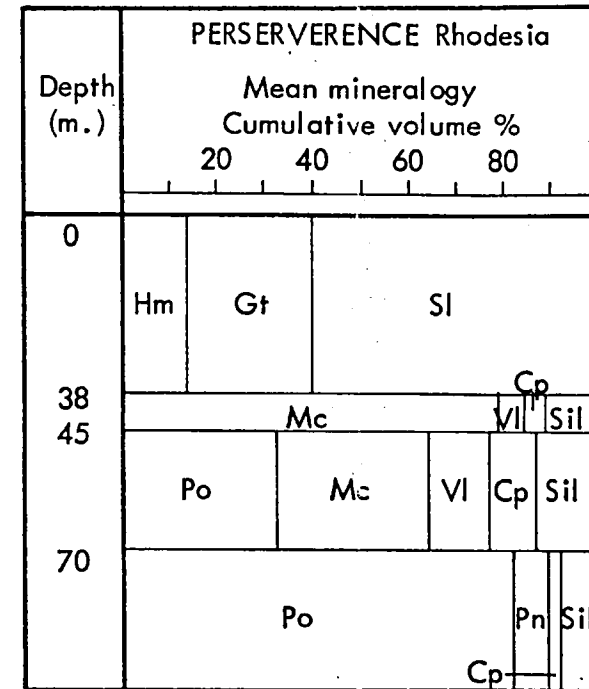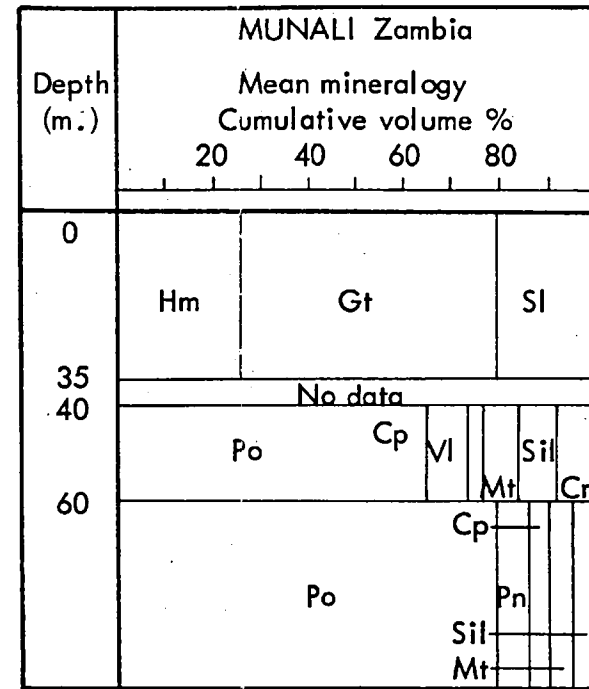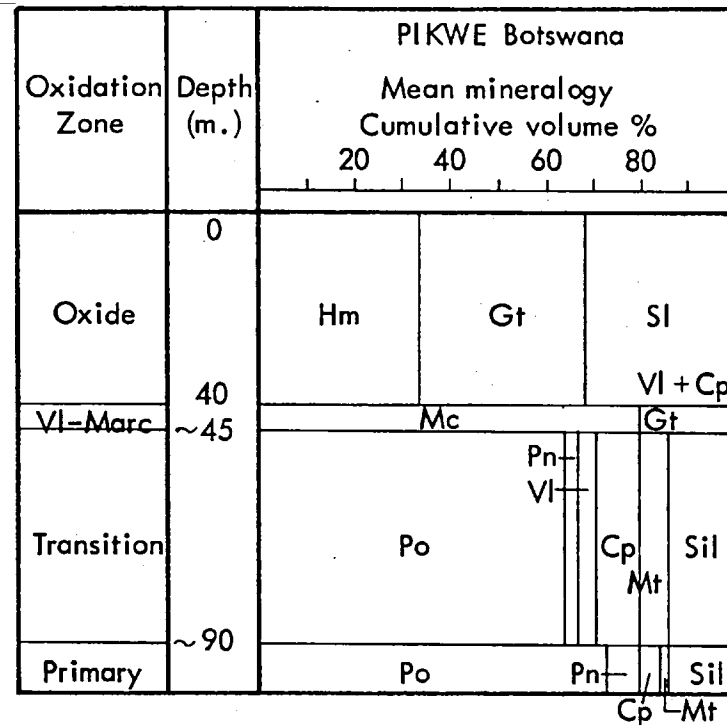
occurrence in the Australian deposits of the suite.

The mean contents of associated silicates exhibit considerable inter-deposit variation, (Fig.6.2.1.). The majority of sampled primary ores carry between 2.5 and eight percent silicate, but higher mean contents are noted at Carr Boyd (25%), Pikwe (about 13%) and at Perserverence (10%). In contrast, the Spargoville massive sulphide assemblage averages only about 1.5 percent silicate.

Primary sulphide assemblages: textures

A brief summary comparison of the ore textures present within the sampled primary ore assemblages is now given in conjunction with Table 6.2.1.

Pyrrhotite forms the matrix of the sulphide ore assemblage in all sampled deposits. It is present in three textural configurations: As an interlocking network of irregular-shaped grains; as polygonal mosaics; and as aggregates of rather equant grains that commonly display mutual boundary textures, (Table 6.2.1.). These textural varieties may occur singly or in combination within individual ores. Further, Table 6.2.1. indicates that the first type is typically more common in Western Australian assemblages, whereas the equivalent African ores are commonly more variable in their pyrrhotite textural compositions. In addition deformation twinning and kink-banding are generally present to some extent in all nickel ores, although the frequency of these phenomena vary between individual assemblages.

Table 6.2.1. indicates that pentlandite is present within sampled nickel sulphide assemblages in two distinct textural forms; namely, as interstitial stringers along pyrrhotite borders, and as flamme lamellar aggregates within pyrrhotite grains. The interstitial variety is characteristic of the sampled Australian nickel ores, but the lamellar form is however (anomalously) present in the Ravensthorpe sulphide assemblage. In contrast, all the sampled southern African nickel ores, with the exception of Munali, contain both pentlandite forms. The interstitial variety predominates in all African assemblages though except that of Perserverence where approximately equal proportions of the two types are noted, (Table 6.2.1.).

Chalcopyrite possesses a typically heterogeneous distribution within the massive ore matricies of all sampled deposits. It is, though, quite commonly associated with spinel. The copper sulphide is typically elongate and irregular in shape, and it commonly demonstrates textural evidence of post-formational re-mobilisation. More

TABLE 6.2.1. TEXTURAL COMPARISON OF PRIMARY ORE ASSEMBLAGES

Deposit	Pyrrhotite			Pentlandite		Chalcopyrite			Magnetite
	Irregular matrix	Polygonal mosaic	Equant matrix	Interstitial forms	Flammes (Po matrix)	Irregular shapes and distrib't'n	Massive forms	Bleb-like forms	Rounded euhedral forms
Pikwe	Ty	Uc	R	C	Fc	C	Fc	Fc	Ty
Munali	R	R	C	Ty	n.o.	Ty	n.o.	n.o.	Ty
Perserverance	n.o.	Ty	n.o.	C	C	Ty	n.o.	n.o.	Ty
Trojan	n.o.	n.o.	Ty	C	Uc	Ty	n.o.	n.o.	Ty
Phoenix	C	Fc	n.o.	C	C	C	Fc	n.o.	Ty
Selkirk	Ty	n.o.	n.o.	C	Uc	Ty	n.o.	n.o.	Ty
Mt. Edwards	Ty	Fc	R	Ty	n.o.	Ty	n.o.	n.o.	Ty
Mt. Monger	Ty	Fc	R	Ty	n.o.	Ty	n.o.	n.o.	Ty
Jan Shoot	Ty*	-	-	Ty	n.o.	Ty	n.o.	n.o.	n.o.
Ravensthorpe	Ty	n.o.	n.o.	C	C	Ty	n.o.	n.o.	Ty
Redross	-	-	C*	Ty	n.o.	Ty	n.o.	n.o.	Ty
Carr Boyd	C	C	n.o.	Ty	n.o.	Ty	n.o.	n.o.	Ty
Spargoville	-	-	C*	Ty	n.o.	Ty	n.o.	n.o.	Ty
Lunnon/S.L.O.B.	-	-	C*	Ty	n.o.	Ty	n.o.	n.o.	Ty
McMahon	C*	-	Fc*	Ty	n.o.	Ty	n.o.	n.o.	n.o.

FREQUENCY SCALE

Ty = Typical

C = Common

Fc = Fairly common

Uc = Uncommon

R = Rare

n.o.= Not observed

- = no data (primary ore not sampled)

* = as indicated by gossan relic textures

370

massive forms are however present at Pikwe and Phoenix, (Table 6.2.1.), and chalcopyrite also occurs as bleb-like inclusions in both sulphide and silicate at Pikwe.

Spinel (magnetite) is typically present as generally equant, commonly idiomorphic grains possessing smooth rounded outlines, (Table 6.2.1.), and the mineral tends to be randomly distributed within the associated sulphide matrix in all deposits. Further, ilmenite lamellae or rims generally occur to some extent in magnetites from all sampled nickel ores.

Ferrochromite is definitely present in Perserverence and Trojan ore, and in several Australian deposits. It has a similar textural configuration to normal magnetite, and where present is commonly rimmed by discrete zones of this iron spinel.

Primary sulphide mineral chemistry

The chemical composition of primary sulphides in a number of unaltered nickel ores are now descriptively compared. In the present study, data are available from five southern African primary nickel ores, and the quoted Western Australian and North American data are drawn from previous work on these deposits by several workers.

Pentlandite

The chemical compositions of analysed pentlandite grains from four southern African deposits are plotted in Fig.6.2.2., and the corresponding mean composition for each deposit are tabulated in Table 6.2.2A. These data indicate that no significant composition differences exist either within or between these four sampled deposits. Pikwe pentlandite is however slightly sulphur-rich and iron-poor compared with equivalent data from the other three orebodies, and analysed Trojan pentlandites are relatively poor in ore metals - principally in cobalt,(Table 6.2.2A.).

A comparison of southern African with available Western Australian and Canadian data indicates that no recognisable inter-regional composition differences exist in pentlandite from pyrrhotite-pentlandite mineral assemblages within these three areas. Further, only relatively minor composition differences are noted across the combined sampled suite. In this respect, iron and the combined ore metals both exhibit composition ranges of about five Atomic % units. Whereas sulphur varies by about three Atomic % units across the combined data set.

Comparison of mean pentlandite compositions from the three areas, (Table 6.2.2A.),

FIG. 6.2.2. PENTLANDITE FROM AFRICA, AUSTRALIA AND CANADA

Fe 30
S 50
Ni, Co, Cu 20

Fe 15
S 50
Ni, Co, Cu 35

S

Fe — Ni

Fe 35
S 45
Ni, Co, Cu 20

Fe 15
S 45
Ni, Co, Cu 40
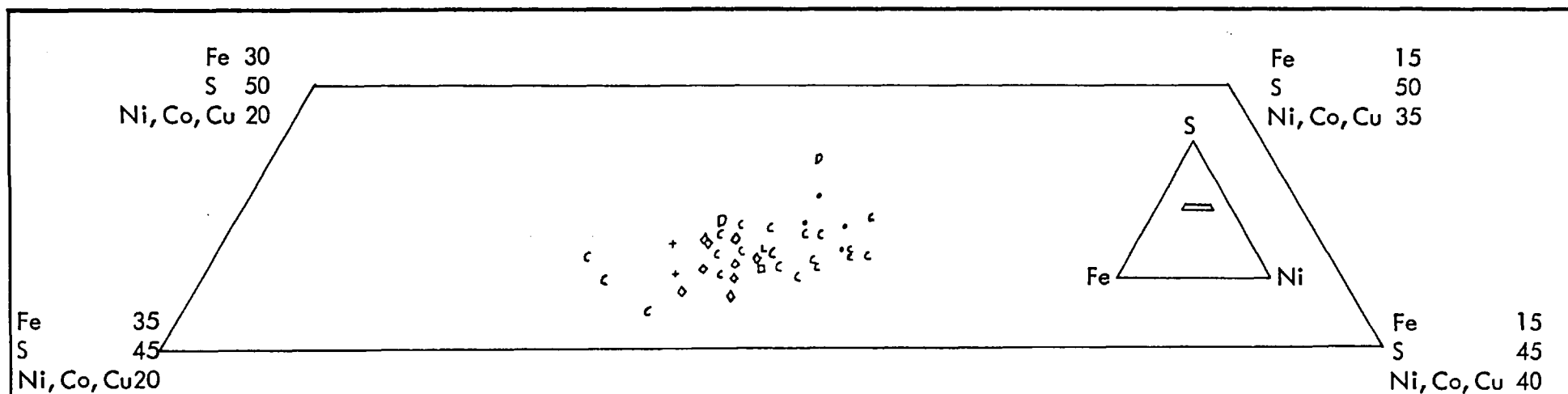
Common Key
(Figs. 6.2.2. to 6.2.5. inclusive)

Southern African Deposits			Supplementary Data			
Deposit	Sample	Mean	Deposit	Sample	Mean	Source
Pikwe (Botswana)	•		Durkin/Lunnon (W.A.)	D, L		Nickel et al 1974
(Lamellar Vpn)	∟					
Perserverance (Rhodesia)	o		Otter Shoot (W.A.)	T		Keele and Nickel 1975
Trojan (Rhodesia)	+		Mt Windarra (W.A.)	w		Watmuff 1975
Phoenix (Botswana)	□		Bloomington (U.S.A.) (Smythite only)	B		Taylor 1970
Selkirk (Botswana)	◊		Canadian deposits (Smythite and Pentlandite)	C		Various workers
(Lamellar Vpn)	◊					

372

Table 6.2.2A. Pentlandite mean compositions from Africa, Australia and Canada

Deposit	Fe	Ni	Co	Cu	S	$\frac{Ni+Co+Cu}{Fe}$
Pikwe	22.62	26.49	2.34	0.27	48.25	1.29
Trojan	25.62	27.10	0.27	0.12	46.86	1.07
Phoenix	24.44	27.39	1.53	0.10	46.54	1.19
Selkirk	25.05	26.05	2.20	0.15	46.55	1.13
Mean of African deposits	24.60	26.37	1.93	0.17	46.93	1.16
Durkin[*]	23.50	28.20	0.30	n.a.	48.00	1.21
Lunnon[*]	24.32	28.34	0.63	n.a.	46.88	1.19
Mean of Australian deposits	23.80	28.20	0.40	n.a.	47.60	1.20
Mean;Creighton -Falconbridge[*] (Canada)	24.52	27.64	0.83	0.01	47.28	1.16

Table 6.2.2B. Chalcopyrite mean compositions from three African deposits

Deposit	Fe	Ni	Co	Cu	S	$\frac{Ni+Co}{Fe}$
Pikwe	25.13	n.d.	n.d.	24.91	49.93	-
Perserverance	25.28	0.72	0.56	23.79	49.62	0.05
Selkirk	25.16	0.01	0.48	24.62	49.72	0.02

* Studies by other workers
All composition data are in Atomic % units

374

indicates that southern African pentlandites differ from documented Australian and Canadian types only in the relative proportions of their individual ore metals. In this respect, the data indicate that the African pentlandites typically contain significantly more cobalt (and copper) and less nickel than analysed grains from the other two regions. Overall proportions of iron, ore metals and sulphur are, however, the same for all three regions.

Pyrrhotite

The chemical compositions of pyrrhotite from five southern African deposits are plotted in Fig.6.2.3. The data indicate that pyrrhotite from Pikwe, Perserverence, Phoenix and Selkirk is principally monoclinic in character, and that variable stoichiometry typifies this iron sulphide at all four deposits. In contrast, Table 6.2.3A. demonstrates that the mean ore metal contents of monoclinic pyrrhotite exhibit recognisable inter-deposit variation. Further, Fig.6.2.3. also indicates that hexagonal pyrrhotite occurs at Trojan, and this finding supports the mineragraphic evidence previously noted in section 4.4.

Monoclinic pyrrhotite data from several previously documented Australian nickel deposits are also plotted in Fig.6.2.3., and a comparison of both means and individual sample data from the two regions indicates that monoclinic pyrrhotite has approximately similar overall compositions in southern Africa and Western Australia. Significantly however, Table 6.2.3A. indicates that the Australian pyrrhotites typically contain more nickel than their African equivalents, but that higher cobalt contents are more common in pentlandite from the latter deposits.

Chalcopyrite

The chemical compositions of a small number of chalcopyrite grains from three southern African deposits are plotted in Fig.6.2.4. These data indicate that there is a fairly close stoichiometric agreement between observed and theoretical composition in the samples, but that almost all chalcopyrite grains are slightly metal-rich and sulphur-poor compared to the ideal composition.

Table 6.2.2B. indicates that differences in trace metal contents appear to typify chalcopyrites from individual deposits. In this respect, Pikwe chalcopyrite does not contain detectable quantities of either nickel or cobalt, whereas that from Selkirk possesses appreciable quantities of cobalt, and Perserverence grains exhibit relatively high contents of both transition metals. Further, an analysis of mean iron and copper values across the three deposits, (Table 6.2.2B.), indicates that both

FIG. 6.2.3.　PYRRHOTITE AND SMYTHITE FROM AFRICA, AUSTRALIA AND N.AMERICA
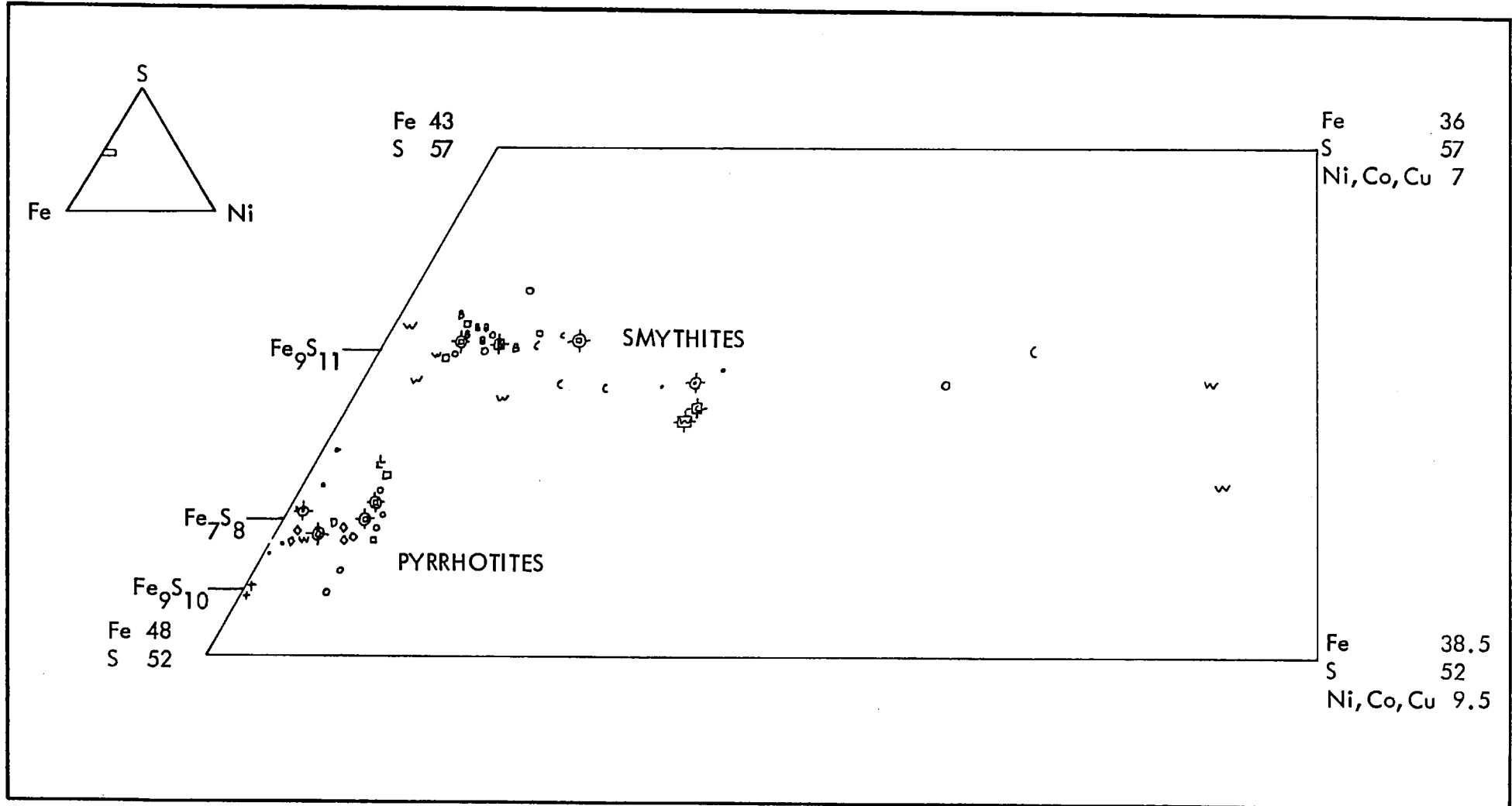
Table 6.2.3A.   Pyrrhotite mean compositions from Africa and Australia

Deposit	Fe	Ni	Co	Cu	S	$\frac{Ni+Co+Cu}{Fe}$
Trojan	47.35	n.d.	n.d.	0.04	52.56	0.001
Pikwe	46.47	n.d.	n.d.	0.09	53.41	0.002
Perserverance	45.92	n.d.	n.d.	0.04	53.35	0.015
Phoenix	45.79	0.11	0.57	0.03	53.48	0.016
Selkirk	46.46	n.d.	0.28	0.05	53.18	0.007
Combined Lunnon/Durkin* (W.Aust.)	45.78	0.45	0.08	n.a.	53.73	0.012
Mt. Windarra*	46.63	0.20	n.a.	n.a.	53.17	0.004

Table 6.2.3B.   Smythite mean compositions from Africa, Australia and N.America

Deposit	Fe	Ni	Co	Cu	S	$\frac{Ni+Co+Cu}{Fe}$
Pikwe	42.50	2.64	n.d.	0.10	54.71	0.065
Perserverance	43.31	0.85	0.70	0.04	55.08	0.037
Phoenix	44.33	n.d.	0.53	0.03	55.08	0.013
Mt.Windarra*	42.78	2.87	n.a.	n.a.	54.36	0.067
Mean of Canadian Ni deposits*	42.72	2.37	n.a.	n.a.	54.92	0.056
Bloomington Indiana*	44.09	0.76	n.a.	n.a.	55.15	0.017

* Studies by other workers
All composition data are in Atomic % units

FIG. 6.2.4.   CHALCOPYRITE FROM THREE AFRICAN NICKEL DEPOSITS
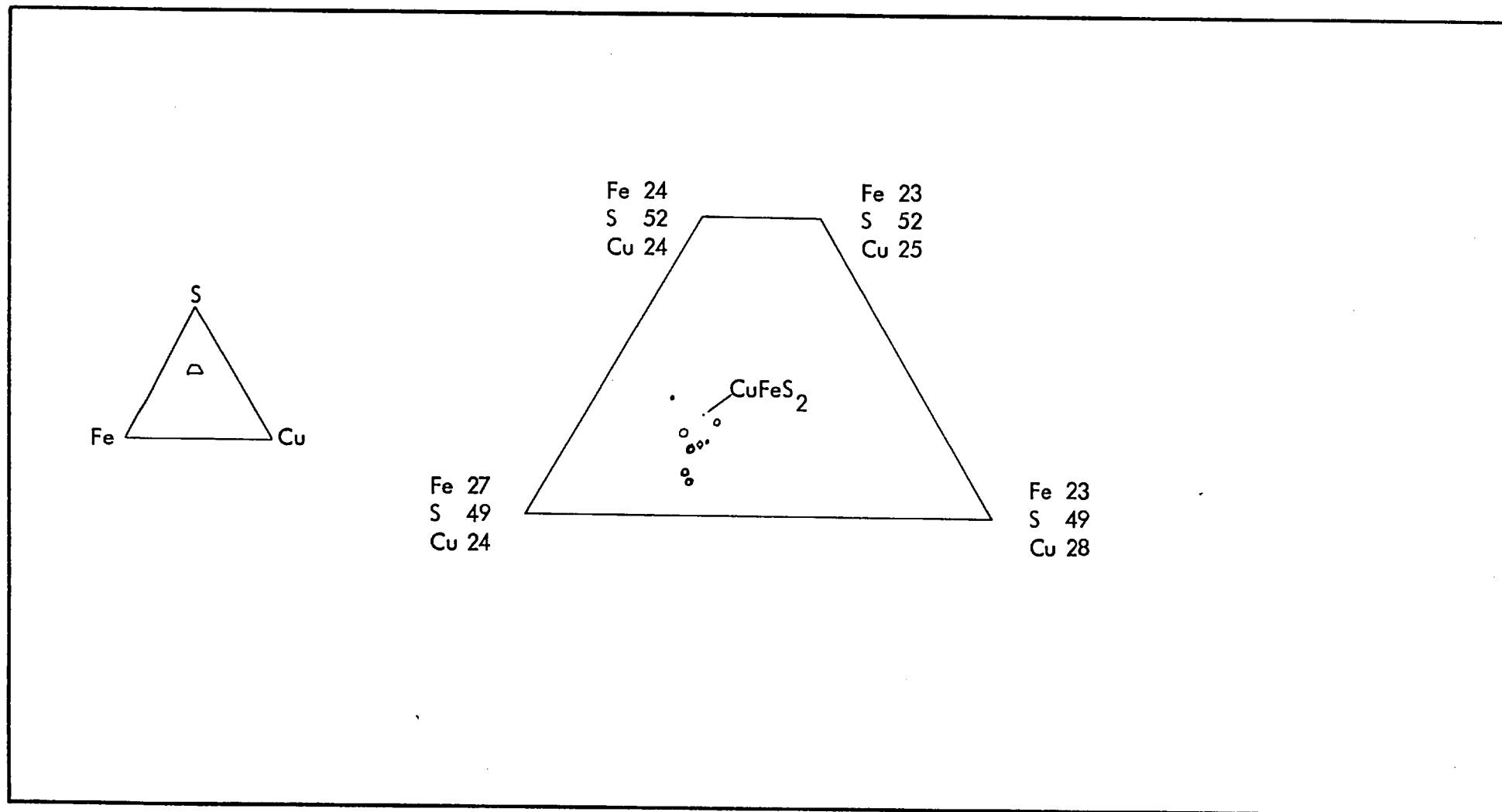
nickel and cobalt substitute copper and not iron in these chalcopyrite species.

A comparison of sulphide alteration petrology: mineralogy

The primary sulphide assemblages of all sampled deposits undergo alteration to secondary (supergene) minerals, (Fig.6.2.1.). In this respect, violarite pseudo-morphically replaces both textural varieties of pentlandite and the proportions of violarite in the secondary assemblage directly reflects the pentlandite content of the parent primary ore.

Violarite also characteristically replaces a proportion of the pyrrhotite in each sample ore, and violarite after pyrrhotite (Vpo) formation constitutes the first stage of pyrrhotite alteration in all investigated deposits. The development of Vpo is however typically preceeded by the genesis of an intermediate iron sulphide mineral-smythite. This phase is definitely not present though at Trojan, and it is not observed at Selkirk, Mt.Edwards and Mt.Monger, although its absence in these three deposits may be due to critical gaps in the sampling coverage. Further, smythite is not observed in the fully-developed secondary assemblages that were the sole material sampled at Jan, Carr Boyd and Spargoville. But it is very likely that smythite is or was present as a transient alteration product of pyrrhotite in the corresponding partly altered primary sulphide assemblages of all three deposits.

Marcasite occurs as a replacement of pyrrhotite in all documented nickel sulphide alteration profiles, and its presence is confirmed by the retention of characteristic relic textures in the oxide zones of deposits where direct observational evidence is absent, (Fig.6.2.1.).

Secondary pyrite after pyrrhotite is definitely present or is inferred from oxide zone textures in all deposits except Pikwe, Perserverence, Trojan and Ravensthorpe. The mineral may occur as a direct replacement of pyrrhotite, (Table 6.2.4.), but more typically forms as a recrystallisation product of secondary marcasite.

The absolute proportions of secondary marcasite and pyrite vary between deposits, (Fig.6.2.1.), but in general, though, the combined absolute proportions of the two iron disulphides correspond quite closely with the mean proportion of pyrrhotite in the equivalent primary ore. Further, the relative proportions of marcasite and pyrite also exhibit considerable inter-deposit variation where both are present. Thus, marcasite predominates at McMahon and Carr Boyd, whereas pyrite is the principal

secondary dimorph at Lunnon. In general though, pyrite is commonly present in greater relative proportions than marcasite within the sampled secondary sulphide assemblages, (Fig.6.2.1.).

Available data on the chalcopyrite, spinel and silicate contents of secondary nickel ores indicate that these minerals are typically present in quantities similar to that of the equivalent primary assemblages, (Fig.6.2.1.).

A comparison of sulphide alteration petrology: textures

As previously indicated, secondary violarite (Vpn) characteristically forms pseudo-morphs after both pentlandite textural varieties. A comparison of secondary Vpn textures across the deposit suite is hence redundant. Similarly, little or no variation in Vpo textural form occurs, and no qualitative comparison of these textures is hence necessary.

Secondary marcasite after pyrrhotite occurs in three textural forms in the investigated deposits, (Table 6.2.4.). Mimic textures after pyrrhotite are present in all secondary ores except Munali and Mt.Monger, although the proportion of marcasite possessing such textures varies considerably between deposits, (Table 6.2.4.). The mimics typically take the form of retained pyrrhotite 001 cleavage structures in fine-grained marcasite, and the outlines of the former parent grains are commonly preserved in these structures. The pseudomorph type at Pikwe differs however from this structure, and direct pseudomorphed replacements after kink-zoned (deformed) pyrrhotite are more typical in this deposit.

Secondary marcasite also occurs in bird's-eye and pseudocolloform structures, (Table 6.2.4.). The occurrence of this textural form is not however universal and it is not present in the Perserverence, Mt.Monger, Jan or Ravensthorpe deposits. Further, the frequency of occurrence of this texture in the remaining deposits is typically variable, (Table 6.2.4.), but it generally occurs both with and without recognisable associated pyrrhotite external grain form structure in all of these secondary ores.

The third type of secondary marcasite textures present is a structureless fine-grained form. This is generally located in ex-pyrrhotite areas and differs from the first textural type described in that no pyrrhotite cleavage mimics are preserved. Further, the texture is not present in seven of the study deposits, (Table 6.2.4.), and occurs in varying proportions across the eight deposits that possess it.

Table 6.2.4.   Inter-deposit comparison of secondary iron disulphide textures

Deposit	Secondary Marcasite			Secondary Pyrite	
	Po mimic textures	Birds-eye and/or colloform textures	fine-grain amorphous forms	fine-grain amorphous or colloform	Massive
Pikwe	Ty	Fc	n.o.	n.o.	n.o.
Munali	n.o.	C	n.o.	n.o.	C
Perserverance	Fc	n.o.	C	n.o.	n.o.
Trojan	Fc	C	n.o.	n.o.	n.o.
Phoenix	Fc	Fc	n.o.	n.o.	Fc
Selkirk	Uc	Fc	Fc	Fc	C
Mt.Edwards	C	Fc	Fc	Fc	C
Mt.Monger	n.o.	n.o.	n.o.	n.o.	Ty
Jan Shoot	Fc	n.o.	n.o.	n.o.	Ty
Ravensthorpe	C	n.o.	n.o.	n.o.	Fc
Carr Boyd	C	Uc	Uc	n.o.	Fc
Redross	C	Fc	Uc	n.o.	Fc
Spargoville	R	Fc	C	n.o.	C
Lunnon/SLOB	R	Fc	R	n.o.	Ty
McMahon	C	R	Uc	n.o.	Fc

All frequency symbols as per Table 6.2.1.

Secondary pyrite after pyrrhotite occurs in two textural forms, (Table 6.2.4.). It exists principally in massive habit as a recrystallisation product after fine-grained secondary marcasite, and in all deposits except Selkirk and Mt.Edwards this massive form is the sole secondary pyrite texture present. Further, the development of massive pyrite typically causes at least the visible obliteration of marcasite and mimicked pyrrhotite structures. Interestingly, bravoitic zoning is present in massive secondary pyrite at Munali, Carr Boyd and Otter Shoot, and probably reflects the incorporation into the pyrite lattice of nickel that was originally present in the parent pyrrhotite.

The second textural form exhibited by secondary pyrite occurs as fine-grained amorphous colloform structures. These are observed as direct replacements of pyrrhotite only at Selkirk and Mt.Edwards, but form only a fairly small proportion of secondary iron disulphide in both deposits, (Table 6.2.4.). Further, these fine-grained structures commonly undergo a secondary recrystallisation to the more massive Pyrite form at both locations.

A comparison of the mineral chemistry of secondary sulphide assemblages

Violarite after pentlandite

The chemical compositions of violarite after interstitial pentlandite grains from five southern African deposits are plotted in Fig.6.2.5. The data indicate that considerable within-deposit variation in Vpn composition is present. In this respect, Pikwe Vpn compositions display considerable variation in Iron, sulphur and combined ore metal contents. Whereas Vpn from Perserverence possess more restricted Iron/ore metal ratios but exhibit considerable Sulphur content variation. Selkirk Vpn compositions however, exhibit reverse trends compared to those of the Perserverence data. Further, the small number of composition data available for both Phoenix and Trojan indicate that variable chemistries probably typify Vpn grains from both deposits.

Available data also indicate that considerable inter-deposit variation in Vpn composition occurs, (Table 6.2.5A.). Thus both Trojan and Pikwe violarites are relatively sulphur-rich, and Selkirk violarite is sulphur-poor. In addition, ore metal/iron ratios vary from relatively high (1.81:1 at Selkirk) through to low (1.21 - 1.23:1 at Perserverence and Phoenix). Further, both the absolute and the relative proportions of individual ore metals exhibit recognisable inter-deposit variation, (Table 6.2.5A.).

FIG. 6.2.5.   VIOLARITE AFTER PENTLANDITE FROM AFRICA AND AUSTRALIA
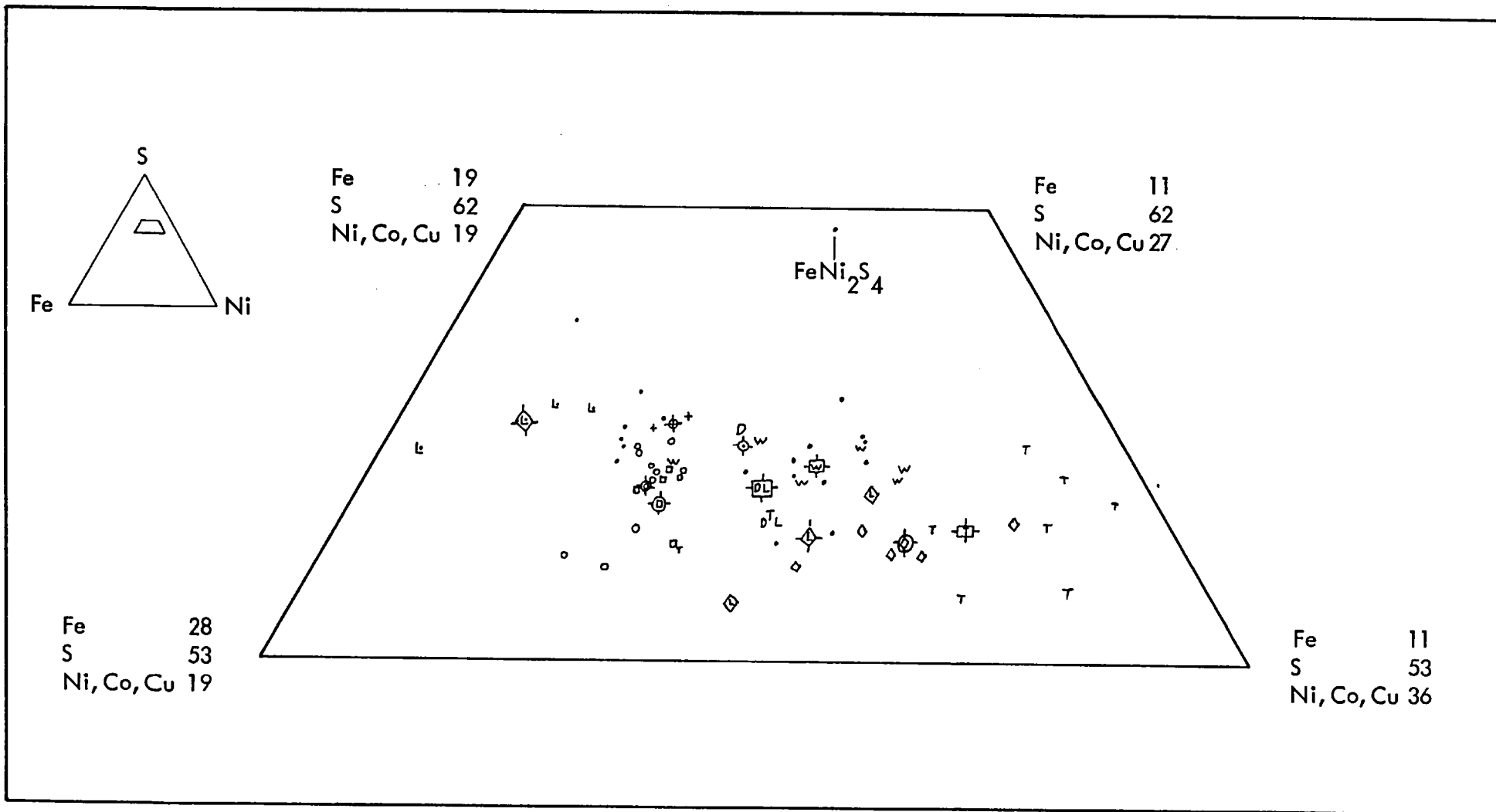
Table 6.2.5A. Violarite (Vpn) mean compositions from Africa and Australia

Deposit	Fe	Ni	Co	Cu	S	$\frac{Ni+Co+Cu}{Fe}$
Pikwe	17.56	22.81	2.09	0.28	57.28	1.43
Perserverance	19.73	21.74	1.95	0.14	56.42	1.21
Trojan	18.60	23.46	0.15	0.09	57.66	1.27
Phoenix	19.69	22.69	1.41	0.08	56.06	1.23
Selkirk	15.88	26.09	2.62	0.10	55.30	1.81
Lunnon/Durkin*	17.77	25.53	0.37	n.a.	56.37	1.46
Mt.Windarra*	16.56	26.31	0.21	0.07	56.88	1.61
Otter Shoot*	14.53	29.54	0.24	n.a.	55.69	2.05
Pikwe lamellar Vpn	21.14	21.14	0.15	0.07	57.68	1.00
Selkirk lamellar Vpn	17.30	24.84	2.28	0.08	55.48	1.57

Table 6.2.5B. Violarite (Vpo) mean compositions from Africa and Australia

Deposit	Fe	Ni	Co	Cu	S	$\frac{Ni+Co+Cu}{Fe}$
Pikwe	20.06	21.16	1.96	0.10	56.70	1.16
Perserverance	22.22	20.26	1.17	0.10	56.22	0.97
Phoenix	21.15	21.47	0.81	0.07	56.47	1.06
Selkirk	18.39	22.44	2.44	1.80	54.96	1.45
Lunnon/Durkin*	21.03	22.33	0.05	n.a.	56.65	1.06
Mt.Windarra*	20.50	22.87	0.10	0.10	56.63	1.18
Otter Shoot*	17.44	26.72	0.07	n.a.	55.77	1.54

* Studies by other workers
All com osition data are in Atomic % units

Thus Pikwe and Perserverence have high absolute and relative amounts of both cobalt and copper. Whereas Selkirk and Phoenix display high and medium cobalt respectively, coupled with low copper contents, and Trojan contains low absolute and relative quantities of both transition metals.

A chemical comparison of violarite after both interstitial and lamellar pentlandite for the Pikwe and Selkirk deposits is also made in Fig.6.2.5. and Table 6.2.5A. Here, available data indicate that the compositions of the two violarite types overlap considerably in both deposits. The lamellar species are however typically iron-rich and have lower absolute and relative ore metal contents compared with the corresponding interstitial pentlandite variety.

The chemical composition data of interstitial Vpn grains from four previously documented Western Australian nickel deposits are also presented in Fig.6.2.5. and Table 6.2.5A. A comparison of these data with the African interstitial violarite data indicates that violarite compositions from both regions plot within the same composition field, and that, further, the Australian Vpn compositions exhibit similar degrees of within – and inter-deposit variation. In contrast however, a comparison of mean Vpn values across the combined regional suites indicates that the African violarites have a distinct tendency to be richer in Iron and poorer in ore metals than the equivalent Australian material.

Pyrrhotite alteration: Smythite

The chemical compositions of smythite after pyrrhotite from three southern African deposits are plotted in Fig.6.2.3. The data indicate that considerable within-deposit variation typifies smythite composition at all three locations. The composition of individual samples, however, all approximate the theoretical metal-to-sulphur ratio of 9:11.

Available data imply that overall composition (metal ratio) variation may be significantly different in each of the three sampled deposits. Hence Table 6.2.3B. indicates that Pikwe smythite has a relatively high; Perserverence a medium; and Selkirk a relatively low ore metal-to-iron ratio.

Further, both absolute and relative proportions of individual ore metals possess considerable inter-deposit variation. In this respect, Pikwe mean smythite is typified by high nickel and very low Cobalt and copper; Perserverence by medium

nickel and cobalt and low copper; and Phoenix by sub-detection levels of nickel, and by medium cobalt and low copper. Interestingly, the occurrence of effectively nickel-free smythite at Phoenix is the first reported instance of this phenomenon.

A comparison of southern African smythite compositions with those from previously recorded Australian, Canadian and American occurrences is also made in Fig.6.2.3. and Table 6.2.3B. These non-African smythite data similarly show considerable within-deposit compositional variations, and a comparison of mean values across the various deposits, (Table 6.2.3B.), indicates that extensive substitution of individual ore metals in place of iron can occur within the Smythite mineral lattice.

A comparison of African smythite compositions with those of parent monoclinic pyrrhotite is also made in Fig.6.2.3. Here, the relevant data indicate that the pyrrhotite-smythite transformation is accompanied by overall mean chemical changes that exhibit considerable inter-deposit variation. In this respect, the relevant composition changes indicate, on available evidence, that smythite formation at Pikwe and Perserverence is accompanied by loss of iron and a significant increase in ore metal content. In contrast, the corresponding alteration phenomenon at Phoenix appears to be caused simply by the expulsion of excess iron from the pyrrhotite lattice. These observed changes may be quantified by reference to the relevant entries in Tables 6.2.3A. and 3B.

Pyrrhotite alteration: Violarite after pyrrhotite

The compositions of Vpo grains from four African nickel deposits are plotted in Fig.6.2.6. These data indicate that considerable inter-deposit variation of Vpo composition occurs, but that violarites from all four sampled deposits plot within the same composition field. Further, a comparison of mean composition values demonstrates that considerable inter-deposit variation does exist, and the occurrence of similar mean metal-to-sulphur ratios across the deposit suite implies that the observed variation in mean Vpo composition is principally governed by the ore metal-to-iron ratio, (Table 6.2.5B.).

A comparison of mean Vpo chemistry for the four deposits, (Table 6.2.5B.) also indicates that significant inter-deposit differences are present in respect of the absolute and relative proportions of individual ore metals.

The composition data for Vpo samples from several previously documented Western

FIG. 6.2.6. VIOLARITE AFTER PYRRHOTITE FROM AFRICA AND AUSTRALIA

Australian deposits are also plotted in Fig.6.2.6. Here, a comparison of African and Australian sample data indicates that violarite after pyrrhotite compositions from these two areas overlap almost completely, and plot within the same composition field. Further, the data demonstrate that mean metal-to-sulphur ratios are relatively constant across this combined deposit suite and that significant mean compositional variation is chiefly governed by ore metal-to-iron ratio as within the African suite alone. No discreet regional bias with respect to this ratio is however noted in available data, (Table 6.2.5B.).

A comparison of absolute and relative proportions between the two area suites, (Table 6.2.5B.), reveals however that Australian Vpo is significantly poorer in cobalt (no copper data are quoted). This lack of cobalt is compensated for though by generally greater nickel (and iron) contents in Australian Vpo samples.

A comparison of Vpo and Vpn mean compositions at the four sampled African deposits is also set out in Fig.6.2.6. These data indicate that the two violarite forms contain very similar proportions of sulphur but that Vpo is characteristically richer in iron and poorer in combined ore metals than its Vpn counterpart. These differences are quantified in Tables 6.2.5A. and 5B. , which data also indicate that the absolute proportions of individual ore metals are significantly lower in Vpo than in the corresponding Vpn.

A comparison of oxide zone petrology: mineralogy

The secondary sulphide assemblages of all study deposits are without exception superceded at the respective water table horizon by an oxidised mineral assemblage that typically extends through to the surface.

The qualitative bulk mineralogy of all sampled oxide zones consists of Goethite, Hematite and Silica, and both the absolute and the relative proportions of these three minerals vary widely between individual occurrences, (Fig.6.2.1.). Further, trace amounts of relic ferrochromite are noted in the Mt.Monger and Spargoville oxide zones, and small quantities of pyrite and carbonate are respectively present in the Redross and McMahon oxide zones. Very small amounts of relic pyrite and/ or spinel are however commonly present in all sampled oxide zones.

Goethite is the principal iron oxide present in all deposits except Pikwe, Selkirk and Redross. The absolute mean proportion of this mineral within individual oxide

zones is however rather variable. In this respect, it ranges from about 6.5 percent
(Redross) to about 98 percent (Ravensthorpe No.5). The majority of deposits fall
though within the 35-70 percent range, and goethite is typically the principal
iron oxide present in Western Australian oxide zones with the exception of Redross.

The absolute mean proportions of hematite vary considerably between individual
oxide zones, (Fig.6.2.1.). In this respect, values range from about one percent
(Mt.Edwards) up to 50 percent (Selkirk). Further, available data demonstrate that
the African oxide zones contain significantly higher absolute proportions of hematite
than do their Australian counterparts. Thus the African deposits average 20-25 percent
hematite, with only Trojan significantly lower at about 3.5 percent. Whereas the
comparable Australian deposits average two percent with significant quantities
exhibited only by Redross and Carr Boyd (20%) and Mt.Monger (9%).

Goethite : hematite relative proportions vary widely between individual deposits.
Thus goethite overwhelmingly predominates (>15:1) at Trojan, Mt.Edwards, Jan,
Ravensthorpe, Spargoville, S.L.O.B. and McMahon, and is the chief iron oxide
present, (15:1<5:1) at Munali, Perserverence, Phoenix, Mt.Monger and Carr Boyd.
Further, the two oxides are present in approximately equal proportions at Pikwe
(0.9:1), with Hematite the principal oxide phase present at Selkirk (0.8:1) and
Redross (0.4:1).

The absolute proportions of silica present within the oxide zone exhibit considerable
inter-deposit variation, (Fig.6.2.1.). In this respect, silica mean contents range
from 1.5 percent (Ravensthorpe) up to 70 percent (Redross). The oxide zones of the
sampled Western Australian deposits are however significantly richer in silica
(average about 40%) than those of the corresponding southern African deposits
(average 20%). In contrast, the sampled African oxide zones exhibit greater inter-
deposit mean silica variation than the corresponding Australian deposits.

A comparison of oxide zone petrology: textures

Recognisable mimic textures after individual secondary ore minerals are present in
all sampled oxide zones. In this respect mimic textural configurations after secondary
violarites, secondary marcasite and pyrite, secondary mimicked pyrrhotite structures,
chalcopyrite and spinel may be variously present within each oxide zone. These
textures may be defined in either goethite or hematite, or by both oxides, either in

combination or separately within the same oxide zone, (Table 6.2.6.). Combinations of mimic textures with respect to the two iron oxides hence vary widely between deposits.

Pseudomorphic and other mimic structures after both Vpn and Vpo typically occur as goethite in all deposits except Perserverence, (Table 6.2.6.), and at the latter deposit these structures are more typically preserved in hematite, although equivalent goethite forms are uncommonly present.

The preservation of mimicked pyrrhotite structures of various types is noted in all sampled oxide zones with the exception of Carr Boyd, Redross and McMahon, (Table 6.2.6.). These textures are typically preserved in goethite at Trojan, Mt. Edwards, Ravensthorpe, Spargoville, S.L.O.B., Otter and Durkin, but occur in both goethite and hematite (either separately or in composite form) in the remaining deposits. Exclusive preservation in goethite is however more common within Western Australian oxide zones, (Table 6.2.6.).

The preservation of relic textures after secondary marcasite - chiefly bird's-eye and colloform structures, occur in all oxide zones except the pyrite-rich Mt.Monger, Redross, S.L.O.B., and Durkin deposits. Further, marcasite relic textures occur solely as goethite replacements at Pikwe, Mt.Edwards, Ravensthorpe and (commonly) at Spargoville, and as both oxides in approximately equal proportions at Perserverence, Phoenix and Carr Boyd. In contrast, hematite predominates or typifies these relic textures at Munali, Selkirk, Jan and McMahon, (Table 6.2.6.).

Relic textures after secondary pyrite - characteristically the massive textural form, are present in all oxide zones except Pikwe, Perserverence and Trojan, (Table 6.2.6.). These textures are typically present in goethite at Mt.Edwards, Jan, Ravensthorpe, Spargoville and at the four sampled Kambalda dome deposits, but in contrast, occur chiefly as hematite structures at Munali, Phoenix and Selkirk. They are noted in equal overall proportions at Mt.Monger, Carr Boyd, and Redross. This inter-deposit distribution of mimicking iron oxide type hence indicates that secondary pyrite relic structures are typically preserved as hematite in southern African oxide zones and as goethite at equivalent Western Australian locations.

Relic textures after chalcopyrite - chiefly boxwork structures, are recognisably preserved only in the six sampled African deposits and at Ravensthorpe, Carr Boyd and Otter Shoot in Western Australia, (Table 6.2.6.). These former chalcopyrite structures occur chiefly as goethite replacements at Pikwe, Ravensthorpe and Carr

Table 6.2.6.   Inter-deposit frequency of relic ore textures in Gossans

Deposit	Iron oxide	Vpn	Vpo	Po mimics	Second. Marc.	Second. Pyrite	Cp	Mag
Pikwe	Goe	Ty	Ty	C	Ty	n.o.	C	n.o.
	Hem	Fc	R	C	Fc	n.o.	Fc	n.o.
Munali	Goe	Ty	Ty	Uc	Uc	Uc	R	C
	Hem	R	R	Ty	Ty	Ty	C	R
Perserverance	Goe	Uc	Uc	C	C	n.o.	Uc	n.o.
	Hem	Fc	Fc	C	C	n.o.	C	Ty
Trojan	Goe	Ty	Ty	Ty	Ty	n.o.	Ty	n.o.
	Hem	R	R	n.o.	R	n.o.	n.o.	n.o.
Phoenix	Goe	Ty	Ty	C	C	n.o.	Fc	n.o.
	Hem	n.o.	n.o.	C	C	C	C	n.o.
Selkirk	Goe	Ty	Ty	Uc	Uc	Uc	n.o.	Uc
	Hem	Uc	Uc	C	C	C	Ty	Ty
Mt. Edwards	Goe	Ty	Ty	Ty	Ty	Ty	n.o.	R
	Hem	R	R	n.o.	n.o.	n.o.	n.o.	Ty
Mt. Monger	Goe	Ty	Ty	C	n.o.	C	n.o.	R
	Hem	R	R	C	n.o.	C	n.o.	Ty
Jan Shoot	Goe	Ty	Ty	C	Uc	C	n.o.	n.o.
	Hem	n.o.	n.o.	R	C	R	n.o.	n.o.
Ravensthorpe	Goe	Ty	Ty	Ty	Ty	Ty	Ty	n.o.
	Hem	n.o.	n.o.	R	R	R	n.o.	n.o.
Carr Boyd	Goe	Ty	Ty	n.o.	C	C	Ty	n.o.
	Hem	R	R	n.o.	C	C	n.o.	Ty
Redross	Goe	Fc	Fc	n.o.	n.o.	C	n.o.	n.o.
	Hem	C	C	n.o.	n.o.	C	n.o.	Ty
Spargoville	Goe	Ty	Ty	Ty	C	Ty	n.o.	n.o.
	Hem	R	R	R	Fc	n.o.	n.o.	n.o.
Lunnon/SLOB	Goe	Ty	Ty	Ty	n.o.	Ty	n.o.	n.o.
	Hem	n.o.	n.o.	n.o.	n.o.	Uc	n.o.	n.o.
McMahon	Goe	Ty	Ty	n.o.	n.o.	Ty	n.o.	n.o.
	Hem	Uc	n.o.	n.o.	Ty	Uc	n.o.	n.o.
Otter Shoot	Goe	Ty	Ty	Ty	n.o.	Ty	n.o.	n.o.
	Hem	n.o.	n.o.	n.o.	n.o.	Uc	Ty	n.o.
Durkin Shoot	Goe	Ty	Ty	Ty	n.o.	Ty	n.o.	n.o.
	Hem	n.o.	n.o.	n.o.	n.o.	n.o.	n.o.	n.o.

Boyd, and predominately as hematite in the remaining five deposits exhibiting these textures. The differential occurrence of chalcopyrite relic textures in the African deposits is likely due at least partly to the relatively high proportions of this mineral in the equivalent sulphide ores, (Fig.6.2.1.).

Relic structures after spinel - principally pseudomorphic and/or boxwork forms are recognisably present in seven deposits, (Table 6.2.6.). These mimic forms occur chiefly as hematite replacements in all deposits except Munali, where they are mostly present as goethite.

A comparison of oxidate mineral petrology and geochemistry

A petrological and geochemical comparison is now made of the oxidate minerals that are present within individual oxide zones and their adjacent weathered host silicate rocks, (Table 6.2.7.). Eleven oxidate minerals have been identified in the present study. These fall into four definite chemical groups: Carbonates; simple and complex sulphates; hydrated chloride; and iron oxide.

Carbonate minerals are associated with oxide after sulphide and weathered silicate rocks in all deposits except Munali, Perserverence, Phoenix, Selkirk and Jan. These minerals are hence typically present in the oxide zones of the sampled Western Australian deposits, but are absent from the corresponding African deposits except Pikwe and Trojan, (Table 6.2.7.).

Calcite is qualitatively the commonest carbonate mineral present across the study suite. It is noted in all carbonate-bearing oxide zones except Trojan, Ravensthorpe and Carr Boyd, and is the sole carbonate recognised at Pikwe, Mt.Edwards, Redross, Spargoville and Durkin, (Table 6.2.7.).

The principal textural and chemical features of sampled oxidate calcite are presented in Table A2/3 ; Appendix Two. The data indicate that the carbonate typically occurs in surface or near-surface rocks as a commonly soft, very fine-grained surficial covering to massive oxide after sulphide. In addition, the corresponding chemical data demonstrate that trace metal contents are rather variable but generally low within the sampled suite. It is hence likely that calcite deposition is a surface weathering phenomenon and is not directly related or influenced by sulphide leaching.

Oxidate magnesite occurs in four oxide zones: Trojan, Carr Boyd, McMahon and

Table 6.2.7. Occurrence of oxidate minerals in sampled Gossans

Deposit / mineral type	CARBONATES				SULPHATES			CO$_3$-ate	IRON OXIDES	
Pikwe		Ca				Nal	Naj		Hm	
Munali										Gt
Perserverance										Gt
Trojan	Mgs									
Phoenix										Gt
Selkirk									Hm	Gt
Mt. Edwards		Ca			Gyp					Gt
Mt. Monger		Ca	Dol							
Jan Shoot										
Ravensthorpe			Dol							
Carr Boyd	Mgs					Nal	Naj	Pact		
Redross		Ca								
Spargoville 5A		Ca								
Lunnon/SLOB		Ca	Dol	Hun						Gt
McMahon	Mgs	Ca								
Otter Shoot	Mgs	Ca	Dol	Hun						
Durkin Shoot		Ca								

Abbreviations

Mgs	Magnesite	Nal	Natroalunite
Ca	Calcite	Naj	Natrojarosite
Dol	Dolomite	Pact	Paratacamite
Hun	Huntite	Hem	Hematite
Gyp	Gypsum	Goe	Goethite

Otter, and is the sole carbonate noted in the first two deposits, (Table 6.2.7. The chief textural and chemical features of sampled magnesite are presented in Table A2/2 ;Appendix Two. These data indicate that magnesite occurs at a wide variety of depths, (70 - 0 m.), in both oxide after sulphide and adjacent weathered silicate.

Table A2/2 also demonstrates that the mineral occurs in a variety of textural forms from veins to cavity linings and that it is typically fine-grained. It is hence very probably formed by precipitation from solution.

The trace metal chemistry of sampled magnesite exhibits considerable within - and between-deposit variation. Typically however, the samples have very high absolute nickel and copper contents together with high relative concentrations of the minor ore metals, (Table A2/2). These chemical features together with the corresponding textural and spatial data indicate that magnesite typically formed from solutions that were rich in ore metals, and it is hence very likely that most of this ore metal component was derived from that released during spatially proximal sulphide leaching.

Dolomite occurs in four oxide zones: Mt.Monger, Ravensthorpe, S.L.O.B. and Otter. It is hence exclusively confined to Western Australian deposits. It is the sole carbonate mineral noted at Ravensthorpe, and occurs in combination with Calcite at Mt.Monger, (Table 6.2.7.).

Available data on oxidate dolomite, (Table A2/4 ;Appendix Two), indicate that the mineral is associated with several rock types across the deposit suite, and, further, that it occurs at various depths. In addition, present evidence suggests that textural configuration is related to depth of occurrence, and in this respect, deep samples are generally present as drusy (precipitation) growths in fractures, whereas surface samples are more commonly present as deposits on weathered surfaces.

These likely genetic differences are supported by the corresponding chemical data. Here, 'deep' dolomites are commonly nickel-rich and chromium-poor, with ore metal contents likely influenced by proximal sulphide leaching. Whereas, 'surface' dolomites exhibit a distinct tendency to be nickel-poor and chromium-rich, indicating that they are most likely derived from the near-surface weathering of adjacent ultramafic rocks. Further, this composition trend is paralleled by variations in grain colour from green (Ni-rich) through to pinks and pink-whites in the

relatively ore metal-free surface specimens, (Table A2/4).

Dolomite also occurs as intergrowths with calcite in the surface gossans of several deposits, (Table A2/5), and available textural and chemical data indicate that these mixtures very probably result from the weathering of proximal silicate rocks.

Oxidate Huntite is a qualitatively rare mineral and is observed only in the Kambalda dome deposits; S.L.O.B. and Otter Shoot, (Table 6.2.7.). Available textural and chemical data indicate that huntite can form both as a precipitant from ore-metal-rich solutions or as an in situ replacement of weathered mafic silicate.

Three sulphate minerals are noted as oxidate phases in the study suite oxide zones. Oxidate sulphate is not widely distributed however and is noted only in three deposits, (Table 6.2.7.). In this respect, gypsum is observed in association with the Mt. Edwards oxide zone, and the complex hydrated sulphates natroalunite and natrojarosite are respectively associated with the oxide zones and weathered silicate host rocks of the Pikwe and Carr Boyd deposits.

Oxidate gypsum from Mt. Edwards occurs in several characteristic groundwater precipitation textures, (Table A2/6 ; Appendix Two), and it is likely that the sulphate component is principally derived from the oxidation of proximal sulphide ore.

Natroalunite occurs as a groundwater precipitant phase at both Pikwe and Carr Boyd, (Table A2/7 ; Appendix Two). These textural relations, coupled with the relatively high trace metal contents of analysed samples and the obvious availability of substantial quantities of sulphate ion indicate that natroalunite development is directly influenced by proximal sulphide leaching.

Similar considerations apply to the formation of natrojarosite. But here the relatively low levels of ore metals associated with this phase underline its principal occurrence in weathered silicate rocks adjacent to the oxidised ore profile, (Table A2/8 ; Appendix Two).

The hydrated copper chloride Paratacamite is observed only at Carr Boyd where it occurs as rather rare dark green botryoids and veinlets in weathered dunitic host, (Table 6.2.7.). No trace chemical data are available on this phase, but its chemical composition indicates that it probably has a mixed silicate/sulphide origin.

The iron oxides goethite and hematite occur as oxidate minerals, as opposed to in situ or early precipitated phases in eight of the 17 study deposits, (Table 6.2.7.). Definite oxidate hematite is restricted to Pikwe and Selkirk. Whereas oxidate goethite is observed in seven deposits, (Table 6.2.7.). Further, both iron oxides are present as oxidate minerals within the Selkirk oxide zone.

Hematite occurs in definite precipitation textures in both oxide after sulphide and weathered silicates, and the variability in trace metal contents exhibited by the analysed samples broadly reflect this diversity of formation locus.

Oxidate goethite similarly occurs as a groundwater precipitant in and adjacent to oxide zone profiles. In contrast to hematite, however, no simple correlation between spatial location and trace metal chemistry appears to be present.

6.3. A COMPARISON OF MEAN DENSITY AND MEAN POROSITY PROFILES

Mean density

The zonal variation of mean true density within the sulphide alteration profiles of the 15 study deposits are set out in Fig.6.3.1. Available data indicate that the mean density of near-massive to massive primary ore likely falls within the range 4.0 to 4.7 gm. cc^{-1} for all 15 examples, and that no systematic regional variation probably exists.

The observed inter-deposit primary ore density variation is most likely caused by differences in pyrrhotite:pentlandite mean ratio between deposits, (Fig.6.2.1.). But it is also influenced by the mean proportions of heavy (spinel) and light (silicate) minerals that are present within each primary ore assemblage.

Partly-altered (Transition) sulphide assemblages exhibit greater inter-deposit density variation than the equivalent primary ores, (Fig.6.3.1.). This phenomenon is partially due to variations in overall pyrrhotite:pentlandite ratios, but is compounded by the individual variation in the ratio of pyrrhotite to (less dense) iron disulphide that occurs across the study suite, (Fig. 6.2.1.).

The mean densities of secondary sulphide (violarite-pyrite) zones also exhibit considerable inter-deposit variation, (Fig.6.3.1.), and a qualitative comparison of secondary zone density and mineralogy across the study suite, (Figs.6.2.1. and

FIG. 6.3.1. INTER-DEPOSIT COMPARISON OF MEAN TRUE DENSITY

(Zonal mean values are indicated by upper boundaries)
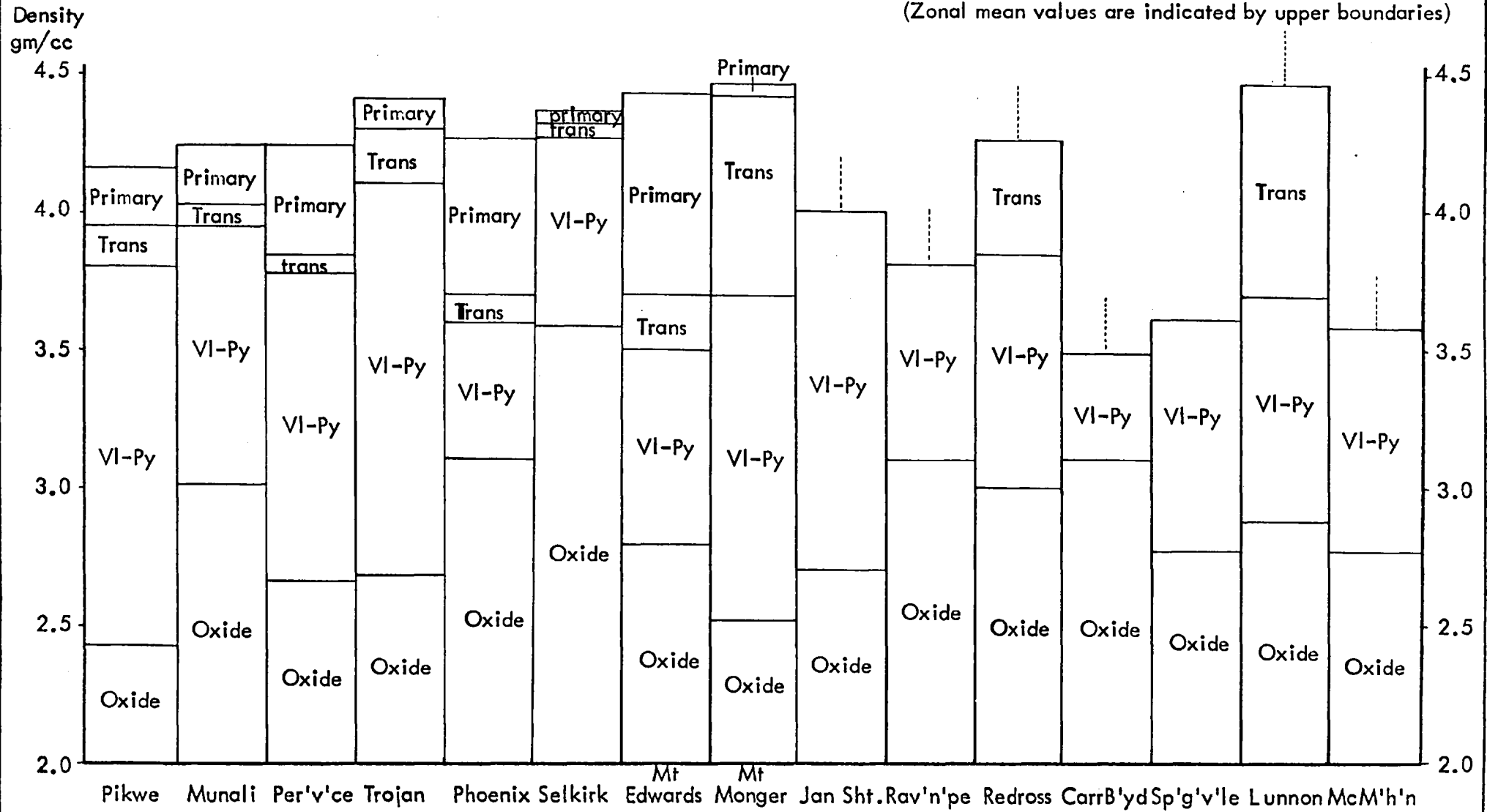
3.1.), infers that two principal factors are probably involved in this phenomenon; namely, sulphide-silicate ratio, and marcasite-pyrite ratio.

The absolute proportion of silicate present is important in this respect as silicate minerals are significantly less dense than sulphides and hence act as important moderators of mean ore density. In contrast, the variation in proportions of (lighter) marcasite to (denser) massive pyrite probably serves as a secondary modifier of the silicate 'density dilution' phenomenon.

The mean true densities of sampled oxide zones exhibit considerable inter-deposit variation, (Fig.6.2.1.). Here a comparison of relevant mineral proportions and density values, (Figs. 6.2.1. and 3.1.), indicates that the principal factor involved in this variation is the absolute mean ratio of total iron oxides to silica within each oxide zone. It is likely however that the density effect of the iron oxide-silica ratio is variously modified in individual deposits by the hematite-goethite ratio. This is because of the relatively large density difference that generally exists between these two oxide minerals.

Mean porosity

The variation in mean porosity within each of the 15 sulphide oxidation profiles is indicated in Fig.6.3.2. Available data demonstrate that small variations in mean porosity exist between individual primary sulphide assemblages. But it is unlikely that these differences are caused by significant variations in either mineralogy or in textural configuration across the study suite.

No simple quantitative relation between porosity and mineralogy exists within the sampled transition zone assemblages. Although it is likely that a recognisable semi-quantitative relation occurs between mean porosity and the absolute combined proportions of the porous minerals violarite and secondary marcasite within each sampled zone, (Figs. 6.2.1. and 3.2.). A similar relationship between porosity and porous mineral proportions appears also to hold for the sampled secondary sulphide zones.

Fig. 6.3.2. also indicates that there is considerable inter-deposit variation in mean porosity across the 15 study oxide zones, but a comparison of mineralogical and porosity variation within the study suite demonstrates that no recognisable simple correlation exists between these variables.

FIG. 6.3.2. INTER-DEPOSIT COMPARISON OF MEAN POROSITY
(Zonal mean values are indicated by upper boundaries)
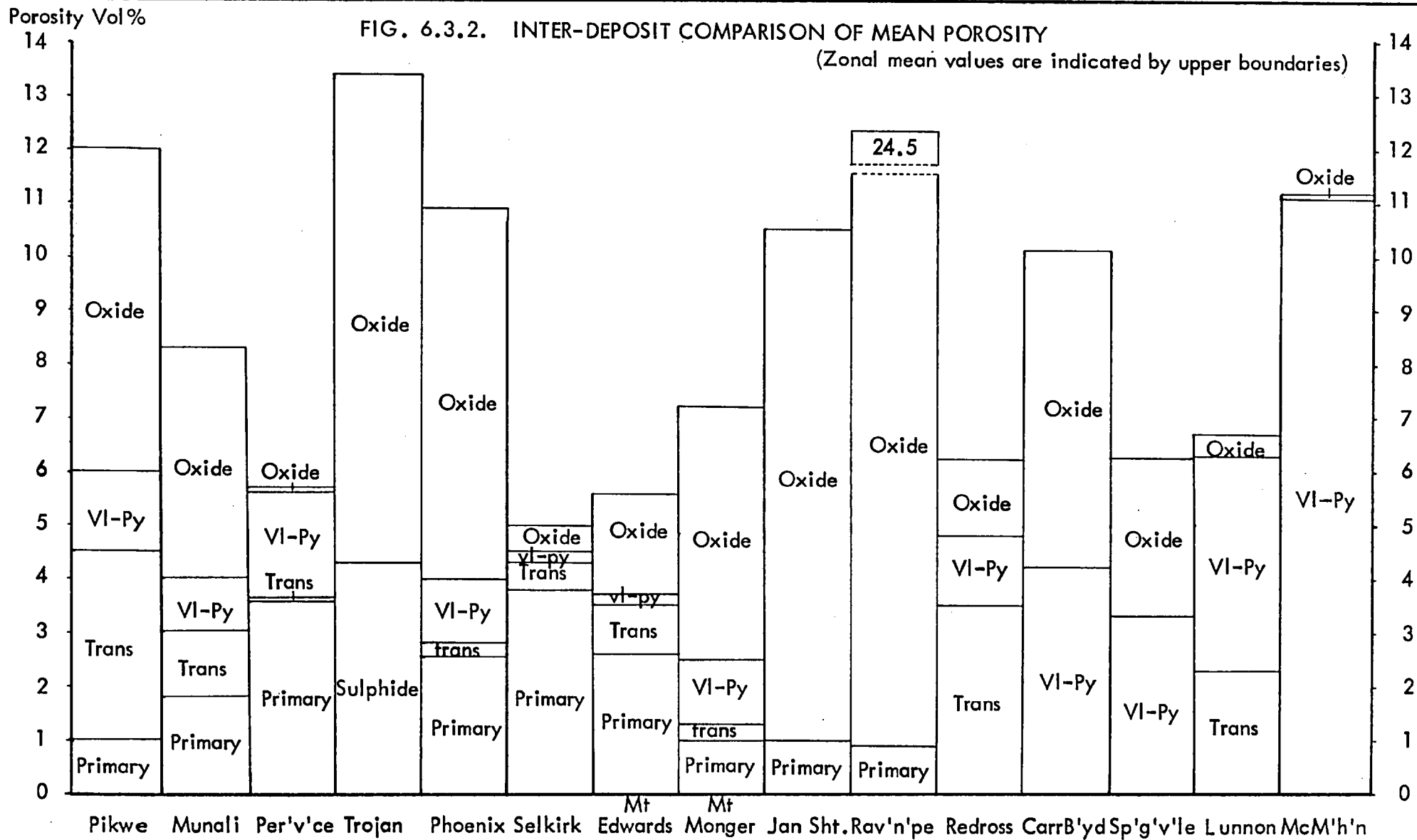
6.4. A COMPARISON OF ZONAL DEVELOPMENT WITHIN THE ALTERATION PROFILE

The quantitative variability in sulphide alteration zone development that exists across the study suite is illustrated in Fig.6.2.1. Available data indicate that considerable inter-deposit variation in initial alteration depth occurs, with extreme values exhibited by Selkirk (45m. level) and Lunnon and McMahon (150-180m. level). Fig.6.2.1. further demonstrates that the majority of primary assemblages start to visibly alter between 110 and 90 metres b.s., and that completely unaltered primary ore tends to occur closer to the surface in the sampled African deposits than in the Western Australian profiles.

The vertical depth range interval over which partly-altered ore is present is widely variable between deposits, and the values are probably quite specific to individual ore profiles. In this respect, sampled transition zone profiles range from 25 metres deep at Selkirk through to 110-120 metres deep at Lunnon, (Fig.6.2.1.). Further, the Australian transition zones generally exhibit greater vertical development than the documented African equivalents, although there is considerable within-region variation, (Fig.6.2.1.). In contrast however, the top of the transition zone generally occurs at a shallower depth in the sampled southern African deposits.

The observed depth ranges of the fully developed secondary sulphide assemblages exhibit considerable inter-deposit variation across the study suite. In this respect, vertical secondary zone development ranges from five metres or less at Pikwe and Phoenix through to at least 60 metres at McMahon, (Fig.6.2.1.). In addition, the relevant data indicate that the African secondary sulphide zones have a typically narrower vertical development than their Australian equivalents.

The oxide zones overlying the documented sulphide alteration sequences exhibit considerable variation in their vertical development, (Fig.6.2.1.). In this respect, depth values range from 18 metres (S.L.O.B.) to 50 plus metres (McMahon). The majority of sampled oxide zones,however, average between 25 and 35 metres in depth and no significant inter-regional differences in vertical oxide zone development are noted.

6.5. A COMPARISON OF BULK GEOCHEMISTRY OF PROGRESSIVE SULPHIDE ALTERATION

The mean contents of combined metals and sulphur, together with the corresponding metal-to-sulphur ratios are set out in Table 6.5.1. for 14 sampled near-massive to massive nickel sulphide ores from southern Africa and Western Australia. The table indicates, with the exception of those deposits sampled exclusively from the (sulphur-rich) secondary sulphide zones, that the metal-to-sulphur ratio of all documented nickel sulphide ores approximate unity. This result infers that each ore deposit originally formed from an immiscible parent monosulphide solid solution (m.s.s.) and is hence very probably the final result of a magmatic segregation of this mss phase from its associated silicate melt of crystal mush.

Available data on profile chemistry indicate that no significant variations in element mean contents occur-with the exception of some iron loss during secondary sulphide development, in any of the 14 study deposits. Further, a small but observable iron loss is observed in only three deposits; Munali, Mt. Edwards and Lunnon. It is therefore likely that progressive secondary (supergene) sulphide alteration effectively takes place as a closed chemical system in all sampled deposits with the exception of these three deposits in respect of iron.

Iron

Fig.6.5.1A. demonstrates that the mean iron contents of sampled massive nickel sulphide ores exhibit considerable inter-deposit variation. Thus, mean iron contents range from 2.8×10^{-2} gm.equv.cc^{-1} at Carr Boyd (11) through to 4.5×10^{-2} gm.equv. cc^{-1} at Selkirk and Mt. Edwards (Nos 6 and 8). Further, values are fairly evenly distributed over this observed range. Mean iron contents tend, however, to be higher in the southern African ores than in the corresponding Australian samples.

The observed changes in iron content across the sulphide-oxide transition (Fig. 6.5.1A.) demonstrate that a wide range of absolute iron depletion occurs across the study suite as a result of wholesale sulphide leaching. Thus, mean depletion values range from about seven percent (Phoenix (6)) to about 75 percent (Redross (12)). Fig.6.5.1A. further indicates, however, that the degree of iron leaching present exhibits a regional bias. Thus four out of six African deposits possess iron depletions of less than 35 percent. Whereas seven out of eight Australian deposits exhibit mean depletions greater than this value.

Table 6.5.1.   Inter-deposit comparison of metal and sulphur mean contents and metal-to-sulphur ratios

Deposit	Combined metal content Massive sulphide	Sulphur content Massive sulphide	Mean Metal:Sulphur ratio
Pikwe	4.574	4.700	0.973
Munali	4.321	4.445	0.972
Perserverance	4.207	4.506	0.933
Trojan	3.807	4.004	0.951
Phoenix	3.984	4.266	0.934
Selkirk	4.798	4.985	0.963
Mt. Edwards	3.612	3.740	0.966
Mt. Monger	4.838	4.690	1.032
Jan Shoot*	3.370	4.740	0.711
Ravensthorpe	4.157	4.100	1.014
Redross*	3.839	4.588	0.837
Carr Boyd*	3.022	4.272	0.708
Spargoville 5a*	3.369	4.569	0.737
Lunnon/SLOB*	3.943	5.103	0.773

All element contents are in (Gram equiv. $cc^{-1} \times 10^2$) units

* Data based on transition and/or secondary sulphides only

Fig. 6.5.1. Inter-deposit Comparison of Sulphide and Gossan Element Mean Contents

Explanation of Figure

For each deposit, the element mean content of the sulphide ore is indicated by the position of the deposit number on the line of zero depletion.

The element mean content of the corresponding gossan is indicated by the position of the larger deposit number.

Deposit Code

1 PIKWE

2 MUNALI

3 PERSERVERANCE

4 TROJAN

5 PHOENIX

6 SELKIRK

7 Mt EDWARDS

8 Mt MONGER

9 JAN SHOOT

10 RAVENSTHORPE

11 CARR BOYD

12 REDROSS

13 SPARGOVILLE 5A

14 LUNNON/S.L.O.B.
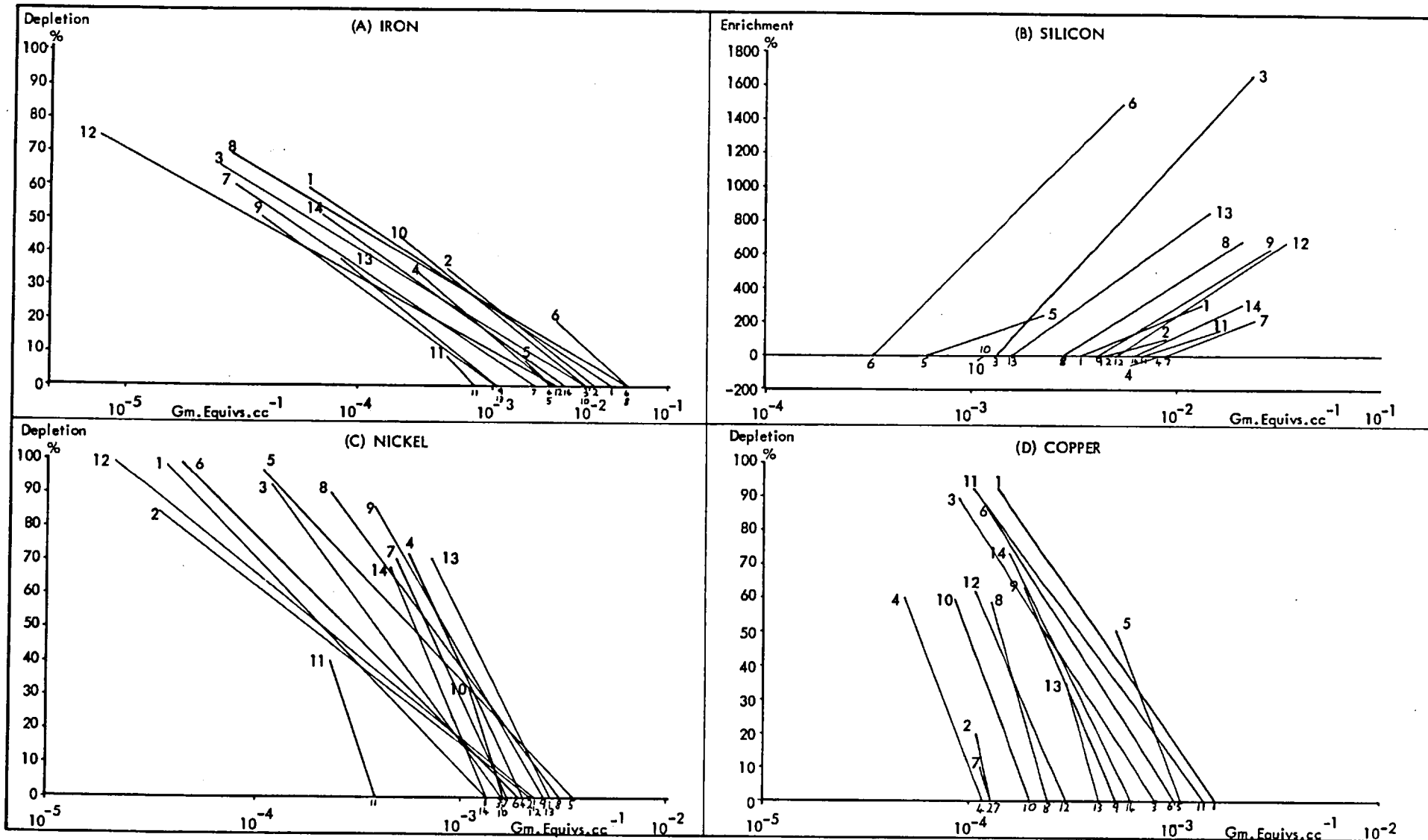
Fig. 6.5.1. Continued
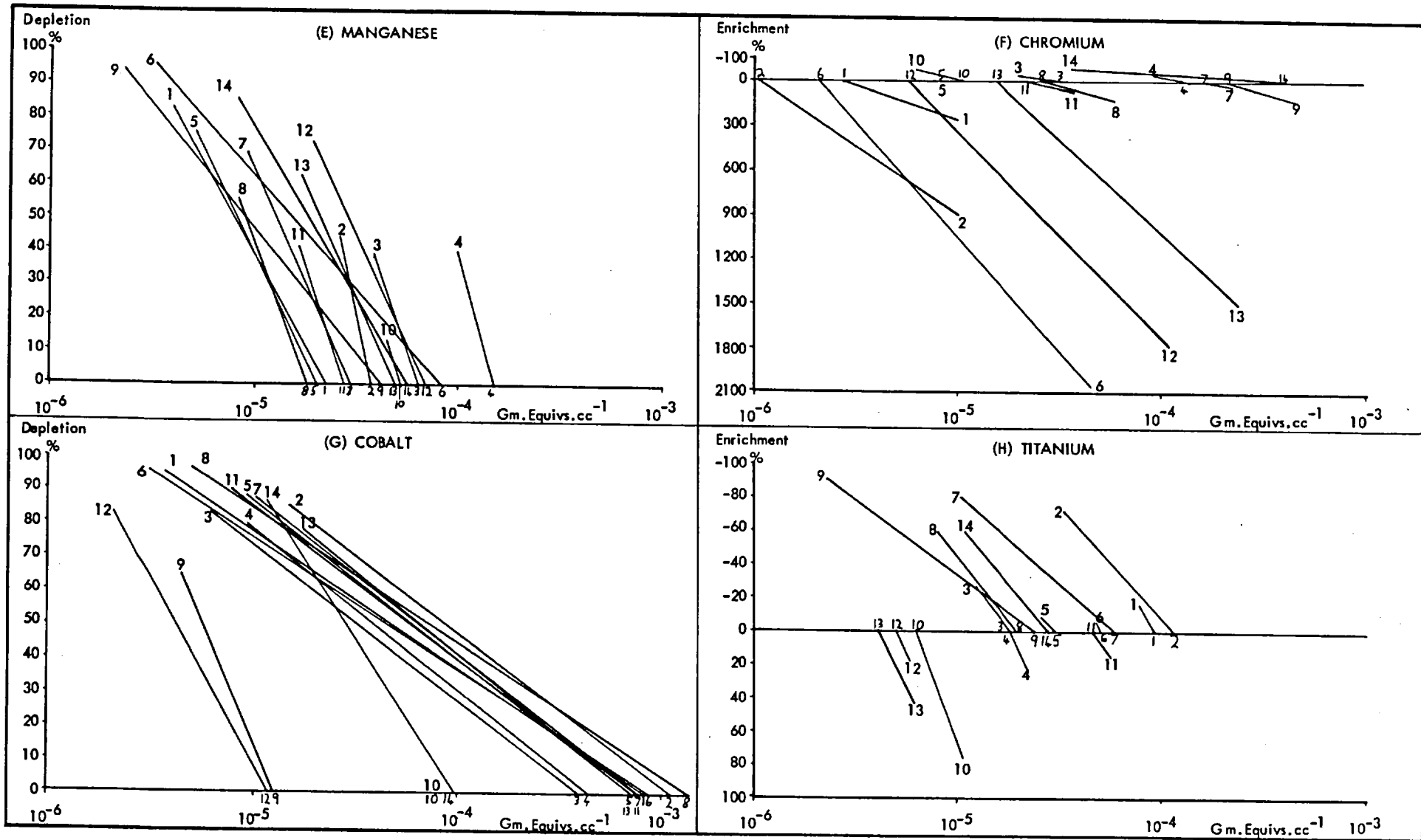
Fig. 6.5.1. Concluded

Fig.6.5.1A. also indicates that a substantial absolute increase in the inter-deposit variance of mean iron contents occurs as a result of sulphide leaching. Further, the data also demonstrate that no simple relationship exists between the mean iron contents of sulphide ores and their corresponding oxide zones.

Silicon

Fig.6.5.1B. indicates that the mean silicon contents of sampled sulphide ores exhibit considerable inter-deposit variability. In this respect values range from $3.4 \times 10^{-4} gm.equv.cc^{-1}$ at Selkirk (6) through to $0.77 \times 10^{-2} gm.equv.cc^{-1}$ at Mt. Edwards (7). Further, the deposits are not evenly distributed across this range, with the result that two rather loose mean content groupings, (respectively high and low) are present. These sub-sets do not exhibit a significant inter-group regional bias, but African ores tend to possess lower mean silicon contents than Australian examples within both sets, (Fig.6.5.1B.).

Tha absolute changes in mean silicon content that occur as a result of oxide zone formation demonstrate considerable inter-deposit variation, (Fig.6.5.1B.). In this respect silicon enrichment occurs in 12 deposits and ranges in value from 100 percent (Munali (2) to 1650 percent (Perserverence (3)). In contrast, silicon depletion occurs only in two deposits; Trojan (4) (17 percent), and Ravensthorpe (10) (Five percent).

Mean enrichment values are quite evenly distributed across the observed range. Although there is a noticeable tendency for members of the 'low silicon' sulphide group to demonstrate relatively higher mean enrichment values than those of the corresponding 'high silicon' set, (Fig.6.5.1B.).

A four-fold absolute increase occurs in the inter-deposit variance of mean silicon contents between sulphide and corresponding oxide material, (Fig.6.5.1B.). Further, the observed distribution of oxide zone silicon values demonstrates that the content-based sub-groupings of the parent sulphide suite are maintained and further different-iated in the equivalent oxide zones. In addition, the composition of these two groups indicate that Australian oxide zones are relatively more enriched in silicon than the equivalent African examples.

Nickel

Fig.6.5.1C. indicates, with the exception of Carr Boyd (11), that the mean nickel contents of sampled nickel sulphide ores exhibit a relatively narrow range. Further,

available data indicate that mean values are evenly distributed across this content range, although the sampled African ores typically occur towards the lower end of the span.

Nickel exhibits a wide range of depletion across the sulphide-oxide transition zones of the 14 study deposits, (Fig.6.5.1C), and values range from 33 percent (Ravensthorpe (10)) to 99 percent (Redross (12)). Three quite distinct depletion ranges are present : High (>85 percent); medium (65> 85percent); and low (30>45 percent). Further, the sampled African deposits characteristically occur in the high depletion sub-group, and hence generally demonstrate relatively low oxide zone nickel mean contents.

Comparison of the range of nickel mean contents across sulphide and oxide suites demonstrates that greater inter-deposit relative variation occurs within the oxide suite than across the parent sulphide suite, (Fig.6.5.1C.). In contrast, however, the absolute range of nickel contents is considerably smaller in the oxide suite in comparison with the corresponding sulphide set because of the overall convergent effect of wholesale nickel leaching.

Copper

Fig.6.5.1D. demonstrates that the mean copper contents of the sampled sulphide deposits exhibit a relatively large overall range. In this respect, mean copper contents run from $1.2 \times 10^{-4} gm.equv.cc^{-1}$ (Trojan (4)) to $1.6 \times 10^{-3} gm.equv.cc^{-1}$ (Pikwe (1)). The deposits are,however, quite homogeneously distributed across this content span, although the sampled African ores characteristically occur towards both the high and the low ends of the range.

Considerable variation in copper depletion occurs across the study suite as a result of sulphide leaching. Thus differences in mean copper values between sulphide and oxide zones range from 11 percent (Mt.Edwards (7)) up to 92 percent (Carr Boyd (11)). In addition, three quite well-defined depletion sub-groups are present : High (>75 percent); medium (50>70 percent); and low (<40 percent), and there is a tendency for African deposits in particular, and for high copper ores in general to exhibit high depletion values across the sulphide-oxide transition. Further, a comparison of copper content ranges across the sulphide and oxide suites indicates that oxide copper values exhibit smaller overall inter-deposit variation both in absolute and relative terms than do their parent sulphide ores.

Manganese

The mean manganese contents of sampled nickel ores exhibit considerable inter-deposit variation, and range from 1.8×10^{-5}gm.equv.cc^{-1} (Mt.Monger (8)) to 1.5×10^{-4}gm.equv.cc^{-1} (Trojan (4)), (Fig.6.5.1E.). The individual deposits are however evenly distributed across this observed range and no regional bias is evident.

Manganese depletion values possess a wide range and run from 14 percent (Ravensthorpe (10)) up to 95 percent (Jan (9)), (Fig.6.5.1E.). Further, individual deposit data are quite evenly distributed within the 35 to 95 percent range, and only Ravensthorpe exhibits a depletion value that is significantly less than this indicated span. No regional bias is apparently present with respect to depletion values, and no observable systematic relationship exists between manganese ore content and degree of depletion.

Manganese mean contents demonstrate a greater relative inter-deposit variance in the oxide suite than in the corresponding sulphide ores, (Fig.6.5.1E.), but available data indicate that the absolute range of mean values is considerably greater in the sulphides.

Cobalt

The mean cobalt content of sampled nickel ores range from 1.2×10^{-5}gm.equv.cc^{-1} at Redross (12) through to 1.3×10^{-3}gm.equv.cc^{-1} at Mt.Monger (8). They hence span two orders of magnitude, (Fig.6.5.1F.). Further, the data are not homogeneously distributed within this range and three rather loosely-defined content groupings are differentiated. Significantly, the high group contains four out of six African deposits and the medium group contains the other two. This obvious regional bias indicates that African nickel ores generally contain more cobalt than equivalent Australian examples.

The range of cobalt depletion values noted across the sulphide-oxide transition zones of the study suite is relatively narrow compared with those of nickel, copper and manganese, (Fig.6.5.1F.). Thus values range from 65 percent (Jan) through to 96 percent (Mt.Monger). Depletion values are, further, quite evenly distributed across this range, but there is noticeable tendency for cobalt depletion to exceed 80 percent in most instances. No significant regional bias is noted in the depletion value distribution, and there is therefore no strong overall correlation between sulphide

and oxide mean cobalt content across the study suite.

A comparison of cobalt content ranges between sulphide and oxide suites indicates
that the latter exhibits significantly less inter-deposit variance in both absolute
and relative terms. Further, a comparison of the two suites shows that mean cobalt
values exhibit significantly greater homogeneity in their range distribution than do
the parent sulphide ores.

Chromium

The mean chromium contents of the sampled nickel sulphide ores exhibit an overall
range of 2.5 orders of magnitude, (Fig.6.5.1G.), and they extend from 1.0×10^{-6} gm.equv.cc^{-1} at Munali to 3.1×10^{-4} gm.equv.cc^{-1} at Lunnon. Further, three
sub-groups are recognisable on the basis of mean chromium content: The high group
comprises Trojan, Mt.Edwards, Jan and Lunnon and has a range of 1.34 to 3.08×10^{-4} gm.equv.cc^{-1}. The medium group comprises Perserverence, Mt.Monger, Carr
Boyd, Ravensthorpe and Spargoville, and ranges between 1.0 and 3.0×10^{-5} gm.
equv.cc^{-1}, and the low group consists of Pikwe, Munali, Phoenix, Selkirk and
Redross, and has a range of 1.0 to 8.0×10^{-6} gm.equv.cc^{-1}. The regional
distribution of deposits within these sub-groups hence indicates that African nickel
sulphide ores are typically chromium-poor in comparison with the equivalent
Australian rocks.

Fig.6.5.1G. also demonstrates that chromium enrichment occurs across the sulphide-
oxide transition in the majority of sampled deposits. In contrast, varying degrees of
mean depletion take place in four deposits, (Perserverence, Trojan, Ravensthorpe
and Lunnon), and one profile (Phoenix) exhibits no net change at all. Of the four
depleted deposits noted, mean chromium losses generally average about 30-40 per-
cent, except at Lunnon where a depletion value of 87 percent is observed.

Present data indicate that mean chromium enrichment shows high inter-deposit
variation, (Fig.6.5.1G.). In this regard, values range from 36 percent (Mt.Edwards)
to 2100 percent (Selkirk). Further, enrichment values are not evenly distributed
across this overall range, and a low sub-set composed of four deposits is present
with mean values ranging between 36 and 130 percent. The five other (higher)
chromium enriched deposits, in contrast, do not form a single coherent sub-group,
but they are fairly evenly distributed within the enrichment range 250 - 2100 percent.

The observed distribution of chromium enrichment values indicates that low chromium

ores tend to exhibit high enrichment values. Thus, inasmuch as the African ores tend to be chromium-poor, a recognisable regional bias exists as regards the mean increase of this metal across the sulphide-oxide transition zones of the study suite.

Titanium

The mean titanium contents of sampled nickel ores exhibit a considerable overall range, (Fig.6.5.1H.). In this respect, values run from 4.0×10^{-6} gm.equv.cc^{-1} at Spargoville to 1.2×10^{-4} gm.equv.cc^{-1} at Munali. Further, mean values are not evenly distributed across this range, but fall into three recognisable sub-groups; high, medium and low.

The high sub-group comprises the deposits; Pikwe, Munali, Selkirk, Mt. Edwards and Carr Boyd. The medium group is composed of Perserverence, Trojan, Mt. Monger, Jan and Lunnon, and the corresponding low group comprises Ravensthorpe, Redross and Spargoville. Further, these three sub-groups have respective titanium content ranges of 4.5 to 11.8×10^{-5}; 1.3 to 2.6×10^{-5}; and 4.8 to 6.0×10^{-6} gm.equv.cc^{-1}, and the distribution of deposits within these sub-groups therefore indicates that African nickel ores are generally richer in titanium than their Australian equivalents, although considerable inter-deposit variation exists within both regional sub-sets.

Fig.6.5.1H. demonstrates that both depletion and enrichment of mean titanium contents commonly occur across the sulphide-oxide transitions of the study suite. Depletion is however the more common phenomenon exhibited, and available data demonstrate that nine deposits exhibit this feature. Mean depletion values in fact range from six percent at Selkirk to 90 percent at Jan, but individual values are not homogeneously distributed across this observed range, and two definite sub-groupings (high and low) are present.

The high depletion sub-group is composed of Munali, Mt. Edwards, Mt. Monger, Jan and Lunnon, and it demonstrates a titanium depletion range of between 60 and 90 percent. In contrast, the corresponding low depletion sub-group consists of Pikwe, Perserverence, Phoenix and Selkirk, and possesses a depletion range of between five and 30 percent. The distribution of deposits between the two groups hence indicates a distinct regional bias, with the Australian deposits exhibiting significantly greater titanium depletion values than the equivalent African profiles.

Titanium enrichment of oxide zones occurs in five out of the 14 sampled nickel deposits, (Fig.6.5.1H.). These five are Trojan, Ravensthorpe, Redross, Carr Boyd

and Spargoville. This phenomenon hence occurs in deposits from all three ore-
content sub-groups, but appears to be typical only of the low titanium type.
Further, mean enrichment values vary considerably across the five deposits. Thus
mean titanium increases of about 20 percent occur in the Trojan, Carr Boyd and
Redross deposits. Whereas enrichment values of 45 and 75 percent are respectively
noted in the Ravensthorpe and Spargoville oxide zones.

A comparison of copper-to-nickel mean ratios in oxide zones and corresponding
sulphide ore is made in Fig.6.5.2. for each member of the study suite of 14 deposits
using the overall ratio of these two variables.

The data indicate that copper typically exhibits a relative increase with respect to
nickel in oxide zones compared with sulphide ore in all sampled deposits except
Ravensthorpe, Carr Boyd and Lunnon. Further, Fig.6.5.2. demonstrates that the
modal value of this copper increase is between three and six times, but that both
significantly smaller and larger mean increases occur within the study suite. No
marked regional bias in relative copper enrichment appears however to be present.

The negative ratios exhibited by the three indicated deposits demonstrate that the
sulphide-oxide transitions in these profiles are characterised by an overall mean
relative depletion of copper with respect to nickel. The value of this copper
depletion is however relatively small compared with the corresponding generally
large increases noted in the other eleven deposits, and available data indicate that
the phenomenon is confined to the Western Australian deposits.

Fig. 6.5.2. Inter-deposit comparison of Cu:Ni ratios in Sulphides and Gossans
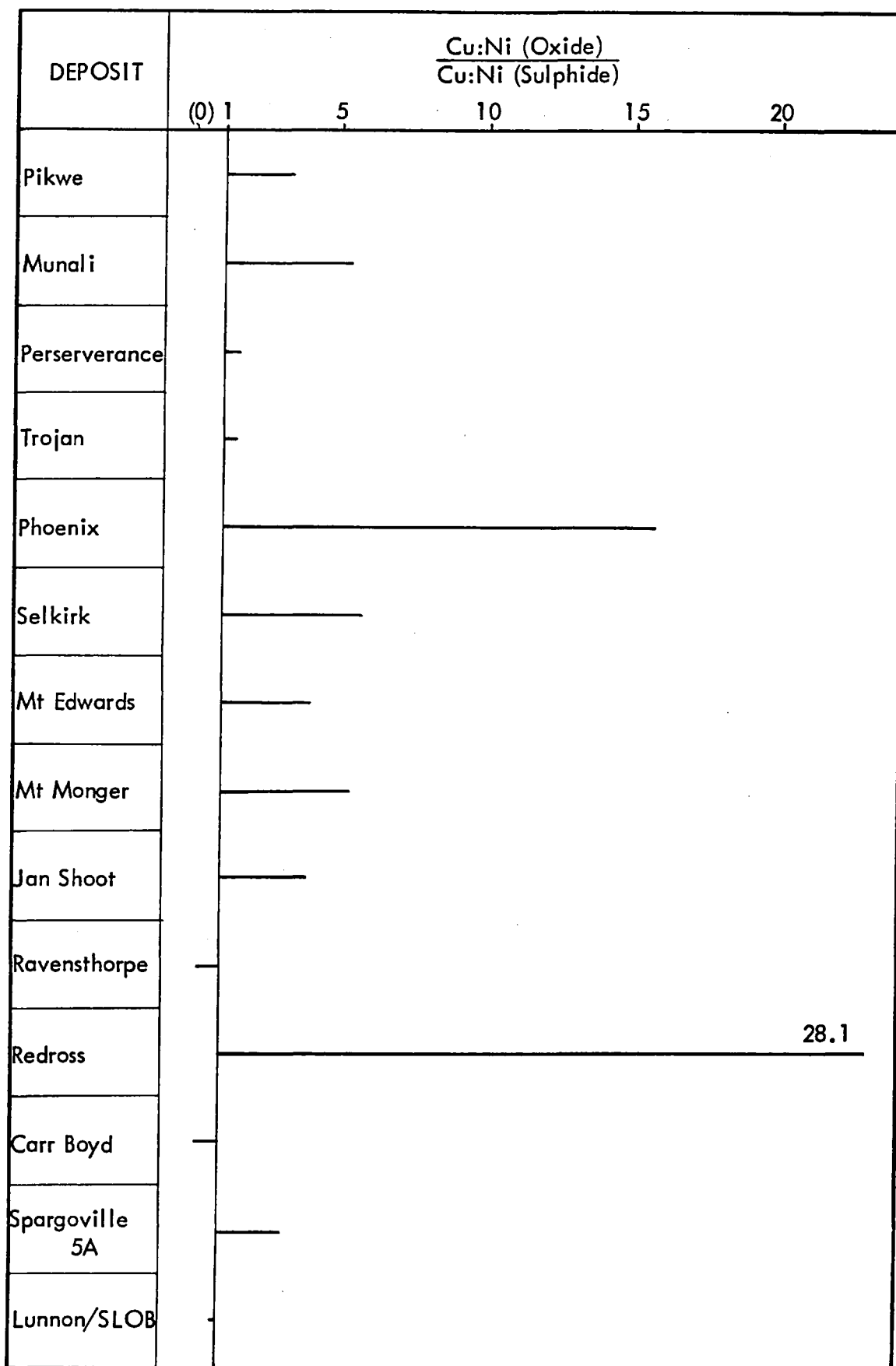
6.6 SUMMARY

Chapter Six has provided a descriptive comparison of near surface alteration across a suite of 15 nickel-copper sulphide deposits in southern Africa and Western Australia. This task has been achieved through the investigation of both the petrology and the geochemistry of progressive sulphide alteration of the study deposits. The chief results of the comparative description are now summarised.

Primary sulphide ore characteristics

(1) The mineralogy of all sampled near-massive to massive primary ores is qualitatively similar, and consists of the assemblage: Pyrrhotite, pentlandite, chalcopyrite, spinel and silicate.

(2) This assemblage exhibits quantitative inter-deposit variation.

(3) Pyrrhotite is the principal matrix sulphide in all deposits, and occurs chiefly as the monoclinic form except at Trojan (Rhod.), where hexagonal pyrrhotite predominates.

(4) Post-formational deformation of primary ore has occurred in all sampled deposits. This is indicated by the presence of pyrrhotite and chalcopyrite deformation textures and by the typically inhomogeneous distribution of chalcopyrite in the ore assemblage.

(5) An overall metal-to-sulphur ratio of unity is typically associated with the sampled primary nickel ores. This feature strongly implies their origin as high temperature silicate-immiscible monosulphide solid solution phases.

(6) Several gross inter-regional differences in primary sulphide chemistry are noted across the ore suite. In this respect, the sampled African ores tend to be richer in iron, copper, cobalt and titanium, and poorer in nickel and chromium than the equivalent Australian examples.

(7) The mineral chemistries of individual phases exhibit recognisable inter-regional and/or inter-deposit variation. Thus, African pyrrhotites are generally nickel-poor and copper-rich compared to Australian pyrrhotites. There is considerable inter-deposit variation in the trace metal contents of African chalcopyrites.

The secondary alteration of nickel ore

i) The supergene sulphide sequence

(1) The alteration sequence: Primary sulphide – secondary (supergene) sulphide – iron oxide-rich gossan is present in all 15 sampled oxidation profiles.

(2) This sequence is qualitatively similar to those developed in the Kambalda deposits in Western Australia.

(3) Broad inter-regional differences exist in alteration zone development. Thus, in the African profiles the primary ore is typically shallower, and transition and secondary zones are generally less vertically developed than in the equivalent Australian alteration sequences.

(4) In all sampled profiles, the primary pentlandite-pyrrhotite assemblage undergoes a phased alteration to one of violarite after pentlandite, violarite after pyrrhotite and secondary iron disulphides after pyrrhotite.

(5) Smythite is characteristically formed as an intermediate product during the formation of violarite after monoclinic pyrrhotite. It is not developed during the formation of violarite after hexagonal pyrrhotite.

(6) Marcasite is the first-formed secondary iron disulphide phase in all sampled profiles.

(7) The mineral is characteristically in a fine-grained near-colloidal form, and in all but four deposits subsequently re-crystallises either directly, or via a coarse marcasite stage, to massive secondary pyrite.

(8) Secondary marcasite displays a range of textures. In this respect, mimic cleavage structures after pyrrhotite, together with Bird's eyes and/or pseudocolloform (de-watering) textures are generally present in all sampled supergene ores.

(9) The formation of the secondary sulphide assemblage typically occurs within a closed chemical system. A loss from the ore profile of iron released in consequence of pentlandite alteration is however noted in several deposits.

(10) Recognisible inter-regional variations occur in the composition of secondary sulphide minerals. African violarite after pentlandite is generally iron-rich and nickel-poor, and African violarite after pyrrhotite is typically nickel-poor and cobalt-rich compared with the respective equivalent Australian phases. Violarite after interstitial pentlandite is typically ore metal-rich and iron-poor compared with that after flamme pentlandite in all sampled ores, and violarites after

pentlandite and pyrrhotite typically differ in that the former is ore metal-rich and iron-poor compared with the latter. Smythite compositions show no recognisible inter-regional variation, but reflect the inter-deposit differences in ore metal-to-iron ratios and ore metal relative proportions that characterise their violarite after pyrrhotite daughter products. Not withstanding these differences though, equivalent secondary phases from all sampled deposits plot in the same mineral composition fields.

ii) The development of gossans

(1) iron oxide-rich mineral assemblages abruptly supercede the secondary sulphides above recent water table levels in all sampled alteration profiles.

(2) The bulk mineralogy of all sampled oxide zones is qualitatively similar and comprises goethite, hematite and silica. However, the mean quantitative proportions of these minerals differ from deposit to deposit.

(3) Goethite is typically the predominant iron oxide present in all oxide zones. It is the principal iron mineral in almost all sampled Australian gossans.

(4) Hematite is present in all sampled gossans, but typically occurs in higher proportions in the African examples. Goethite-hematite mean ratios are typically high.

(5) Secondary dehydration of goethite to hematite is observed in a number of sampled gossans. The phenomenon is however volumetrically significant only in the Pikwe (Botswana) oxide profile.

(6) Higher mean silica contents typically occur in the sampled Australian gossans. In contrast, the African examples show a greater inter-deposit variation in silica content.

(7) Mimic (relic) textures after individual secondary sulphide minerals are noted in all gossans. Violarite pseudomorphs occur in all examples, and are present chiefly as goethite. Secondary mimic textures after pyrrhotite are similarly present in all sampled oxide zones. These may exist as either goethite or hematite replacements. Exclusive preservation in the former is more common in Australian gossans. Secondary marcasite mimics occur in all gossans except for those deposits rich in pyrite. The replacing mineral may be either goethite or hematite or a composite of the two. Mimic secondary pyrite textures are present in the gossans of all deposits but those containing only the marcasite dimorph. These textures are

preserved chiefly in either goethite (Australian gossans) or hematite (African gossans). Chalcopyrite is typically represented as either goethite or hematite boxwork structures in individual gossans.

(8) Silica typically occurs as an amorphous or cryptocrystalline matrix to iron oxide structures. Detailed work on the Pikwe oxide profile indicates that this texture is caused by the precipitation of silica from influxing SiO_2-rich ground waters. The silica is probably derived by the weathering of adjacent silicates.

(9) Several fundamental chemical changes occur at the sulphide-oxide transition in consequence of pervasive sulphide leaching. Sulphur is oxidised to sulphate, and is totally removed from the ore profile by solution in ground water. Iron is similarly mobilised (as ferrous ion) and is also lost through ground water solution. Appreciable, although typically variable quantities are, however, retained within the gossan formation zone, and are oxidised and subsequently precipitated as ferric oxides. Preferential retential of iron oxide within the gossan occurs in the sampled African deposits. All gossans typically exhibit silicon enrichment in comparison with their parent ores.

(10) The transition metals, nickel, cobalt, manganese and copper typically exhibit high levels of depletion across the sulphide-oxide transition. This is probably due to the release of these metals as soluble oxidised mobile species from their parent sulphide lattices during leaching. A proportion of each is however retained - probably as a result of co-precipitation with iron oxides. There is a general rendency for copper to be preferentially retained over nickel within the oxide zone. This is probably due to the principal occurrence of these metals in sulphides of differing chemical stability. A comparison of chromium mean contents between sulphide and gossan indicates that the latter is typically enriched in this metal. The extra chromium is probably derived from the weathering of adjacent ultramafic host silicate rocks.

PART TWO

THE GENESIS OF SUPERGENE SULPHIDE AND GOSSANS

CHAPTER SEVEN

SUPERGENE ALTERATION IN NICKEL SULPHIDE OREBODIES

7.1 Introduction

This chapter provides an interpretative discussion of supergene alteration in nickel sulphide ores based on the results of the descriptive study of 17 oxidising nickel sulphide deposits reported in chapters three to six of this thesis.

The text proper is divided into two sections and is based on the electrochemical and geological model previously developed by Thornber, (1975a, op.cit.), to explain the supergene alteration of the Kambalda deposits in Western Australia.

Section 7.2. presents a review of supergene alteration chemistry in the light of new chemical and mineralogical data generated during the present investigation. This permits the component reactions of the original chemical model to be generalised.

A new conceptual extension of Thornber's original geological alteration model is presented in section 7.3. Here the implications of coeval silicate lateratisation and steady ore profile exhumation for supergene alteration genesis are discussed.

A summary of conclusions of the above discussions is presented in section 7.4.

7.2 Generalised chemical reactions involved in nickel sulphide supergene alteration

Recent studies on the supergene alteration of nickel sulphide orebodies, (Nickel et.al.,1974 and 1977 op.cit.; and Watmuff,op.cit.), have been interpreted in the form of a chemical genetic model by Thornber, (1975a and b, op.cit.).

The principal features of this model are as follows: Galvanic corrosion due to aeration of the top of the ore body at the water table is considered to result in deep anodic oxidation reactions whereby primary sulphides undergo a phased oxidative transition to sulphur-rich violarite-pyrite ore. Further, the galvanic corrosion process also causes shallow oxidative anodic reactions in which secondary violarite-pyrite ore is oxidised to sulphate ion and iron oxides. The electrons resulting from these oxidation processes are conducted through the massive ore profile to the cathode where they are consumed during the reduction of oxygen radicals dissolved in the groundwater.   The electrical continuity of

FIG. 7.2.1.   THE GENERALISED CHEMISTRY OF NICKEL SULPHIDE ALTERATION

A   REACTION PRODUCING THE DRIVING FORCE FOR WEATHERING

Athmospheric Oxygen $\longrightarrow$ Oxygen dissolved in ground water

B   CATHODIC REDUCTION OF OXYGEN RADICALS

1   $O_2 + e^- \xrightarrow{+H2O} HO_2 + OH^- \xrightarrow{+e^-} HO_2^- + OH^- \xrightarrow{+H2O} 2OH^- + H_2O_2 \xrightarrow{+e^-} OH + 3OH^- \xrightarrow{+e^-} 4OH^-$

C   DISCONNECTED SULPHIDE (ANODIC) REACTIONS

1   $FeS_2 + 8H_2O = Fe^{2+} + 2SO_4^{2-} + 16H^+ + 14e^-$
     Marcasite/Pyrite

2   $CuFeS_2 + 4H_2O = CuS + Fe^{2+} + SO_4^{2-} + 8H^+ + 8e^-$
     Chalcopyrite   Covellite

D   CARBONATE EXCHANGE AND ACID BUFFERING REACTIONS

1   $(Ca\,Mg\,Fe\,Ni\,Co\,Cu)^{2+} + OH^- + HCO_3^- = (Ca\,Mg\,Fe\,Ni\,Co\,Cu)CO_3 + H_2O$
                                                              Carbonates

2   $(Mg, Ca)CO_3 + H^+ = (Mg, Ca)^{2+} + HCO_3^-$
   Alkaline Earth Carbonates

3   $4NaCa_2(MgFe)_5AlSi_7O_{22}(OH)_2 + 22H_2O + 56H^+ = 4Na^+ + 8Ca^{2+} + 20(Mg, Fe)^{2+} + 4OH^- + Al_4Si_4O_{10}(OH)_8$
     Amphibole (Edenite)   Kaolinite

$+ 24H_4SiO_4$
Hydrosilicic Acid

E   SHALLOW (ANODIC) WEATHERING REACTIONS

1   $(Ni, Fe)_3S_4 + 16H_2O = 3(Ni, Fe)^{2+} + 4SO_4^{2-} + 32H^+ + 30e^-$
     Violarite

2   $Fe^{2+} + 2H_2O = FeOOH + 3H^+ + e^-$
                         Goethite

3   $2Fe^{2+} + 3H_2O = Fe_2O_3 + 6H^+ + 2e^-$
                         Hematite

F   SUPERGENE ENRICHMENT REACTION

1   $2Ni_xFe_{3-x}S_4 + yNi^{2+} = 2Ni_{x+y}Fe_{3-(x+y/2)}S_4 + yFe^{2+}$
     Violarite   Ni-rich Violarite

G   DEEP (ANODIC) WEATHERING REACTIONS

1   $Fe_9S_{10} = 5FeS_2 + 4Fe^{2+} + 8e^-$
   Hexagonal Po Marcasite/Pyrite

2   $Fe_7S_8 = 4FeS_2 + 3Fe^{2+} + 6e^-$
   Monoclinic Po

3   $Fe_9S_{10} + zNi^{2+} = 2.5(Ni_zFe_{3-z})S_4 + (1.5+2.5z)Fe^{2+} + 2(1.5+2.5z)e^-$
   Hexagonal Po   Violarite (after Po)

4   $0.73(Fe_{9-x}Ni_x)S_{11} + yNi^{2+} = 2(Ni_{x+y}Fe_{3-(x+y)})S_4 + (1+2(x+y))Fe^{2+} + 2(1+2(x+y))e^-$
     Smythite   Violarite (after Po)

4A $Fe_7S_8 + xNi^{2+} = 0.73(Fe_{9-x}Ni_x)S_{11} + (.43+.73x)Fe^{2+} + 2(.43+.73x)e^-$
   Monoclinic Po   Smythite

5   $(Ni, Fe)_9S_8 = 4(Ni, Fe)S_2 + 5(Ni, Fe)^{2+} + 10e^- \xrightarrow{+2(Ni,Fe)^{2+}} 2(Ni, Fe)_3S_4$
     Pentlandite   Bravoite   Violarite (after Pn)

6   $(Ni, Fe)_9S_8 = 2(Ni, Fe)_3S_4 + 3(Ni, Fe)^{2+} + 6e^-$
     Pentlandite   Violarite (after Pn)

7   $4(Ni_{1-v}Fe_v)S + uFe^{2+} = (Ni_{3-(4-(v+u))}Fe_{4v+u})_3S_4 + (1+u)Ni^{2+} + 2e^-$
     Millerite   Polydymite

the corrosion cell is maintained by ionic transport through the groundwater system to the anodic regions of the ore body.

The chemical reactions of supergene sulphide alteration indicated in the above summary of the chemical model are now briefly reviewed on the basis of data generated during the present study.

The chemical reactions constituting the model, (Thornber, 1975a, op.cit.), are partitioned into seven groups, (Table 7.2.1.). The indicated equations of five of these groups that correspond with observed supergene changes in the sulphide assemblage or its host rocks are now each briefly reviewed in turn.

Deep (anodic) weathering reactions, (Group G, Fig.7.2.1.).

Four deep anodic weathering reactions are represented by chemical equations in the model. These are; the direct alteration of pentlandite (Pn) to violarite (Vpn); the alteration, via a smythite intermediate, of pyrrhotite (Po) to violarite (Vpo); the alteration of pyrrhotite to secondary iron disulphide; and the reaction, specific to the Otter Shoot, of the alteration of millerite to polydimite. All four reactions are assumed to take place under constant sulphur conditions.

The direct alteration of pentlandite to violarite is observed in each of the 17 study ores, and although present data, (Tables 6.2.2A. and 6.2.5A.), indicate that there is considerable inter-sample and inter-deposit composition variation in both parent and daughter minerals, they both approximate their theoretical metal-to-sulphur ratios. Because of this fact, it is possible to formulate a general pentlandite-violarite reaction which corresponds to the situation in all 17 of the sampled deposits;

$$(Ni, Fe)_9 S_8 \rightarrow 2(Ni, Fe)_3 S_4 + 3(Ni, Fe)^{2+} + 6e^- \quad \text{Reaction G6}$$
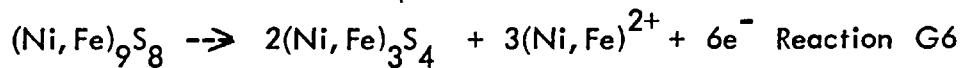
A second, although quite rare, pentlandite alteration reaction is observed at Pikwe. Here pentlandite oxidises to an intermediate nickel-rich bravoite prior to the formation of violarite, (Fig.3.2.5D.). This reaction appears to be specific to the Pikwe deposit;

$$(Ni, Fe)_9 S_8 \rightarrow 4(Ni, Fe)S_2 + 5(Ni, Fe)^{2+} + 10e^- \xrightarrow{\ (Ni, Fe)^{2+}\ } 2(Ni, Fe)_3 S_4 \quad \text{Reaction G5}$$
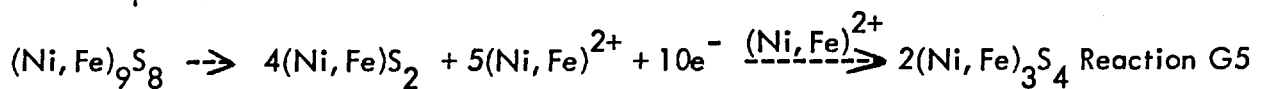
The alteration of pyrrhotite to violarite occurs in the sampled oxidising ores of all 13 non-Kambalda deposits in the study set. Further, smythite, $(Fe, Ni)_9 S_{11}$, is observed or is inferred present in all 12 sulphide assemblages of this suite that have a substantial proportion of their primary pyrrhotite present as the monoclinic variety,

(section 6.2). In consequence, a generalised reaction based on the typically near
theoretical stoichiometries of the three minerals can be formulated:

$$Fe_7S_8 \xrightarrow{xNi^{2+}} 0.73(Fe_{9-x}Ni_x)S_{11} + (.43 + .73x)Fe^{2+} + 2(.43 + .73x)e^-$$

$$\xrightarrow{yNi^{2+}} 2(Ni_{x+y}Fe_{3-(x+y)})S_4 \quad \text{Reaction G4}$$
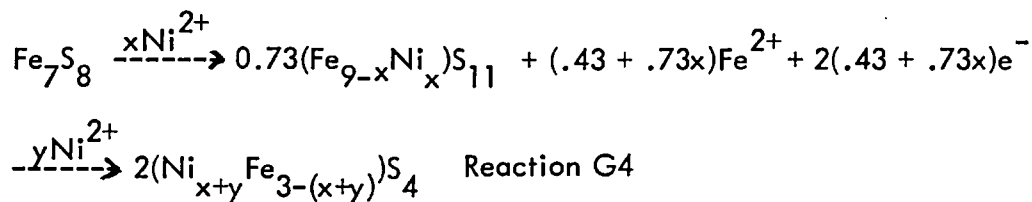
The Trojan deposit is an exception to the above rule. Here, present data indicate
that hexagonal pyrrhotite predominates in the primary sulphide assemblage, (Table
4.4.2.), and that smythite is absent as an intermediate product. The alteration of
(hexagonal) pyrrhotite to violarite apparently involves a direct replacement process
at this deposit;

$$Fe_9S_{10} \xrightarrow{zNi^{2+}} 2.5(Ni_zFe_{3-z})S_4 + (1.5 + 2.5z)Fe^{2+} + 2(1.5 + 2.5z)e^- \quad \text{Reaction G3}$$
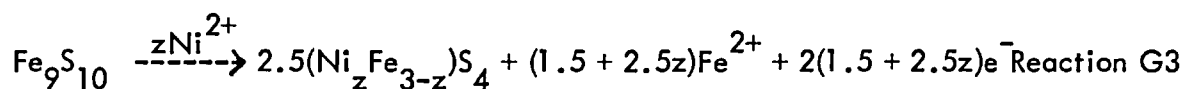
The alteration of unviolarised monoclinic pyrrhotite to secondary iron disulphide
occurs in 16 out of 17 study ores. This feature is represented as reaction G2 and has
exactly the same quantitative form as the corresponding expression in Thornber's
original scheme, (Table 1, Thornber 1975a, op.cit.).

Alteration of pyrrhotite to secondary iron disulphides also occurs in the Trojan deposit.
Hexagonal pyrrhotite is predominately involved in this instance;

$$Fe_9S_{10} \longrightarrow 5FeS_2 + 4Fe^{2+} + 8e^- \quad \text{Reaction G1}$$
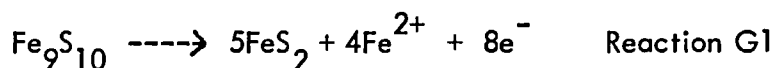
The reaction involved in millerite-polydymite alteration, (reaction G7), is specific
to the millerite-rich Otter Shoot primary assemblage, (Thornber, op.cit.). Present
work demonstrates that is does not significantly occur in any of the other 16 deposits
in the combined study suite.

Supergene enrichment reactions, (Group F, Fig.7.2.1.).

No analytical work was undertaken in the present study to investigate supergene
enrichment of secondary minerals in the sampled ores. It is noteworthy however
that a considerable range of violarite body colour was observed during minera-
graphic study of these rocks. In this respect, bluish-grey hued violarite was
generally noted more frequently in ore specimens from locations proximal to the
likely water table zone in many of the deposits.

It is in consequence probable that this colour indicates ore metal enrichment in

these 'shallow' violarites, and hence implies that their chemical characteristics tend towards polydymite or possibly siegenite;

$$2(Ni_xFe_{3-x}S_4) + yNi^{2+} \longrightarrow 2Ni_{x+y}Fe_{3-(x+y/2)}S_4 + yFe^{2+} \qquad \text{Reaction F1}$$
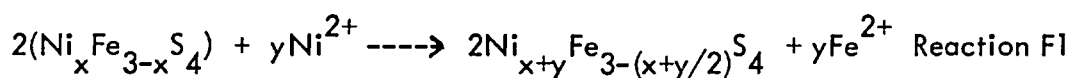
Shallow (anodic) weathering reactions, (Group E, Fig.7.2.1.).

In the original model, several shallow weathering reactions occur at or near the water table zone and are anodic, i.e., oxidising in character. The mineralogical changes that correspond to these reactions are also observed in the oxidising ores of the nickel sulphide study suite.

The oxidative leaching of violarite, (Reaction E1), is observed in all sampled ores for which suitable depth samples are available. Similarly, the precipitation of ferrous iron as goethite is noted in all study profiles, (Reaction E2). In addition, the precipitation of primary hematite observed at Pikwe represents an additional, if rarer, shallow anodic weathering reaction;

$$2Fe^{2+} + 3H_2O \longrightarrow Fe_2O_3 + 6H^+ + 2e^- \qquad \text{Reaction E3}$$
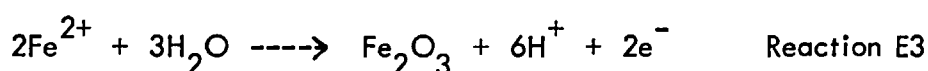
Carbonate exchange and acid buffering reactions, (Group D, Fig.7.2.1.).

Precipitation of carbonates, (Reaction D1), in the chemical environment associated with the cathodic reduction of oxygen at the water table is observed in a number of study deposits, (Tables A2/2 to A2/5;Appendix Two). Present data demonstrate though that acid buffering of carbonate in the vicinity of oxidising secondary ores is restricted to those deposits with carbonate-rich host rock assemblages, (Reaction D2).

In deposits with less deeply-weathered host silicates – chiefly the southern African group, work has demonstrated that silicate hydrolysis largely occurs in place of carbonate buffering;

$$4(NaCa_2(Mg,Fe^{2+})_5AlSi_7O_{22}(OH)_2) + 22H_2O + 56H^+ \longrightarrow 4Na^+ + 8Ca^{2+}$$

$$+ 20(Mg,Fe)^{2+} + 40H^- + Al_4Si_4O_{10}(OH)_8 + 24\ H_4SiO_4 \qquad \text{Reaction D3}$$
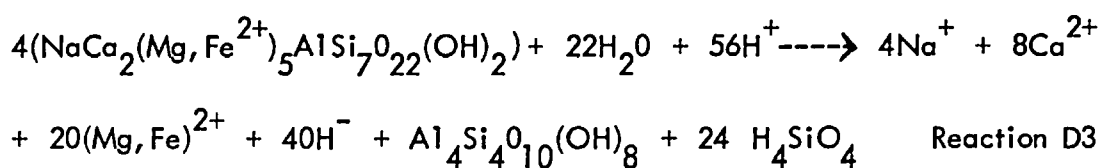
Disconnected sulphide reactions, (Group C, Fig.7.2.1.).

In the model these reactions are assumed to occur at or above the water table level. Further, they are thought to represent an anodic oxidation of the relatively stable sulphide minerals pyrite and chalcopyrite that are present in blocks of material that have become physically separated from the rest of the ore zone. The physical changes corresponding to anodic oxidation of both minerals are ubiquitously observed across the 17 members of the sulphide study suite, (Reactions C1 and C2, Fig.7.2.1.).

Cathodic reduction of oxygen radicals and the driving force of sulphide weathering, (Groups A and B, Fig.7.2.1.).

The electrons produced by both deep and shallow anodic processes are postulated in the model to be consumed in the water table zone by the cathodic reduction of dissolved oxygen radicals, (Reaction B1). Hence, the initial dissolution of atmospheric oxygen in groundwater is inferred as providing the driving force of the whole supergene (anodic) oxidation process in nickel sulphide ores. The veracity of these inferences cannot however be tested on the basis of observed mineralogical relations, and it is hence reasonable to suppose that these phenomena likely fulfil the roles inferred for them by the model.

In summary, the foregoing discussion indicates that very similar chemical reactions occur during the supergene alteration of a significant number of nickel sulphide deposits. These reactions are very much like those postulated by Thornber for the galvanic cell model that is based solely on the Kambalda deposits. It is hence very probable that galvanic corrosion cells of a similar type and form are, on the basis of observed mineralogical, textural and geochemical evidence, operating, or have operated in each of the 17 deposits studied.

7.3 A geological model for the genesis and evolution of nickel sulphide supergene alteration

In view of the overall chemical similarity of the sampled supergene altered profiles, it is probable that the latter all formed under the same qualitative geological conditions.

The genesis of supergene alteration in a nickel sulphide ore profile exhuming under near-surface lateratisation conditions, (Fig.7.3.1.).

Recent work on the Agnew (W.A.) nickel sulphide profile by Nickel et.al., (1977, op.cit.) indicates that the latter's supergene alteration was developed contemporaneously with the Eocene-middle Miocene lateratisation investing the deposit. The formation of supergene alteration profiles in other Western Australian nickel ore bodies invested by Mid-Tertiary laterite therefore probably also occurred coevally with this regional silicate weathering phenomenon.

The deeply kaolinised rock mantles investing all sampled southern African alteration profiles were similarly initiated during the mid-Tertiary, (section 2.2). It is hence very likely that supergene profile development and lateratisation also took place contemporaneously in this region.

Recent work by Blain and Brotherton, (op.cit.), has indicated the importance of long term exhumation in the operation of the electrochemical corrosion cell involved in the development of the supergene alteration profile. It is hence probable that exhumation is similarly involved during both the initial genesis and the subsequent evolution of supergene alteration in all altered nickel sulphide ores.

The implications for supergene alteration development of either contemporary lateratisation or profile exhumation are not, however, indicated in the original alteration model proposed by Thornber, (1975A, op.cit.). The likely sequence of events affecting a nickel sulphide ore profile progressively exhuming under fluctuating water table lateratisation conditions is therefore presented in Fig.7.3.1.

The dry and wet season water table levels are indicated in the figure, together with an associated deeper horizon. This represents a hypothetical minimum depth level associated with the specific water table below which the groundwater Eh is too low to allow the pentlandite-violarite reaction to take place unless a galvanic corrosion cell is operating.

The relatively increased depression of this 'minimum reaction Eh' horizon during the wet season is thought likely because of the greater probable concentration of dissolved oxygen in the groundwater under these conditions. This being due to the increased downward percolation at this season of oxygen-rich surface waters through the aerated upper levels of the weathered rock mantle.

The postulated sequence of events occurring during progressive exhumation of a nickel ore body during an episode of lateratisation is as follows:-

Fig. 7.3.1. The Effects of Lateratisation and Profile Exhumation on Supergene Alteration Development

| A | DRY SEASON | B | WET SEASON | C | DRY SEASON | D | WET SEASON |

| E | DRY SEASON | F | WET SEASON | G | DRY SEASON | H | WET SEASON |

| I | DRY SEASON | J | WET SEASON | K | DRY SEASON | L | WET SEASON |

M POST-LATERATISATION (SEMI- ARID) CONDITIONS
Stable Water Table

LEGEND

——————— Land Surface

----------- Seasonal Water Table Level

.... Idealised level corresponding to the lowest Eh value necessary for Pn → Vpn to occur

O, o   Oxide Zone

S, s   Secondary (Violarite - Pyrite) Zone

T   Transition Zone

P   Primary Zone

A, B, C refers to locations indicated in the text

Fig.7.3.1A. The 'minimum Eh'horizon corresponding to the depressed dry season water table intersects the tip, (A), of a progressively exhuming nickel sulphide ore body. In consequence, the pentlandite in this apical region undergoes incipient alteration to violarite and an embryo transition zone begins to be formed.

Fig.7.3.1B. The corresponding wet season condition. The 'minimum Eh' horizon has moved above the apex of the now incipiently altered primary ore, with the result that violarite formation has ceased.

Fig.7.3.1C. Exhumation has brought the ore body nearer the surface such that, under dry season conditions, its highest part projects above the minimum Eh horizon. The higher Eh environment of the apex (A) now allows the oxidation of pentlandite to violarite to occur at an increased rate. In addition though, the Eh is now high enough in this region for pyrrhotite to begin altering (via smythite) to violarite. In the basal part of the tip, (B), however, the Eh is sufficient only for the continued slow alteration of pentlandite to occur. These activities therefore cause the rather slow downward extention of the transition zone.

Fig.7.3.1D. The corresponding wet season condition. The level of the minimum Eh horizon is low enough relative to the ore body to allow only pentlandite in the apex, (A), to continue slowly altering to violarite. All other activity in the previously altering ore has ceased because of insufficient Eh.

Fig.7.3.1E. The orebody is now structurally high enough to allow its tip to intersect the dry season water table. In consequence, the Eh is high enough in the highest parts of the ore, (A), for both violarite alteration reactions to go rapidly to completion, and for residual pyrrhotite to alter to secondary iron disulphide. An embryo secondary zone is consequently formed. In addition, however, the Eh in this region is now high enough to permit the corresponding shallow anodic reactions to be initiated.

Lower down the profile the formation of secondary sulphides is accelerated at B, and unaltered ore in even deeper levels, (C), begins to alter from pentlandite-pyrrhotite to violarite.

The result of these processes is that both the secondary and transition zones grow downwards at the expense of their respective underlying neighbours. More importantly however, the connection of the profile tip with the water table means that

differential aeration proper is initiated at this stage of profile evolution, and the ore body starts to act as a galvanic corrosion cell of Kambalda type.

Fig.7.3.1F. The corresponding wet season condition. The Eh is now too low for the shallow anodic reactions to continue, (A), and in consequence, the operation of the corrosion cell slows down significantly. The Eh is still high enough at B however for continued, if slower alteration of pentlandite-pyrrhotite to violarite to occur, and, (possibly) for pyrrhotite to continue altering to iron disulphides. Consequently, the secondary zone continues growing downwards but at a very slow rate. The transition zone similarly continues growing at a rate that is slower than in the dry season, but which is faster than that of the secondary zone. It hence starts to become disproportionately long with respect to the latter.

Fig.7.3.1G. Further progressive exhumation of the ore profile has occurred to properly breach the dry season water table. The full operation of the galvanic corrosion cell has thus re-ensued, and has caused both the development of an oxide zone proper, (A), and the continued growth of both the secondary and transition zones at, (respectively) B and C.

Fig.7.3.1H. In the corresponding wet season at this structural level, the Eh is again insufficient for the shallow anodic reactions to continue. Consequently oxide zone formation again ceases, and the activity of the corrosion cell slows down appreciably. The Eh is again high enough however for iron disulphide to form from pyrrhotite at A, and for both pentlandite and pyrrhotite to form violarite at B. In consequence both secondary and transition zones continue to grow, although once more the latter exhibits a disproportionate increase in size over the former.

Figs. 7.3.1I to 1L. Continued progressive profile exhumation under alternate dry and wet seasonal water table regimes produces the same seasonal variation in corrosion cell activity with its associated continued oxide, secondary and transition zone formation during dry seasons, and the cessation of oxide zone formation and reduction in cell activity during wet season.

The growth of both secondary and transition zones continues during the wet season, the latter disproportionately so because of the lower Eh conditions required for its genesis. Eventually however all net zone growth will likely become equilibrated with the mean rate of exhumation exhibited by the ore profile under the imposed

seasonally fluctuating water table level regime.

Fig.7.3.1M. The documented onset of semi-arid climatic conditions by the end of
the Tertiary, (especially in Western Australia and S.W.Rhodesia - N.E. Botswana),
implies that water table levels have likely remained relatively stable ever since
in these areas. Present day profile configurations hence reflect the water table
and exhumation conditions under which they developed, except where small
re-equilibrium adjustments have been necessary due to significantly differing post-
formation conditions involving these two variables.

In the mature alteration profile in Fig.7.3.1M. therefore, the downward growth of
the transition and secondary zones is completely balanced by the upward rate of
profile exhumation. No net zonal growth consequently takes place under these
conditions.

The above qualitative model of supergene alteration genesis demonstrates that
relatively long transition zones, (and to a lesser extent), long secondary zones,
together with deep primary-transition zone boundaries are likely to occur in alteration
profiles that were initiated and developed under the influence of long term seasonally
fluctuating water table levels.

It is also interesting however to discuss the effect on profile configuration of
different exhumation rates and of different inter-seasonal ranges in water table
level. Accordingly, the likely effects of these different formation conditions on
profile development are now briefly described.

The effect of different seasonal ranges of water table level on alteration zone
growth, (Fig.7.3.2A.).

The likely effect on zonal development of different inter-seasonal ranges in water
table level are indicated in Fig.7.3.2A. The dry season condition is shown in Fig.
7.3.2A(I). Here the profile is operating as a galvanic corrosion cell powered by
differential aeration of oxygen species at the water table.

The reaction of the alteration profile to conditions of high wet season rainfall is
illustrated in Fig.7.3.2A(II). Here the water table level has been raised high
enough so that only the uppermost portion of the secondary zone remains within the
lowest part of the minimum Eh region associated with this horizon. In consequence
shallow anodic reactions cease and cell activity drops to a near minimum.

Fig. 7.3.2A. The Effect of Different Wet Season Water Table Levels on Alteration Zone Development

(Figure symbols as for Fig.7.3.1.)

1 DRY SEASON	2 WET SEASON (HIGH)	3 WET SEASON (LOW)
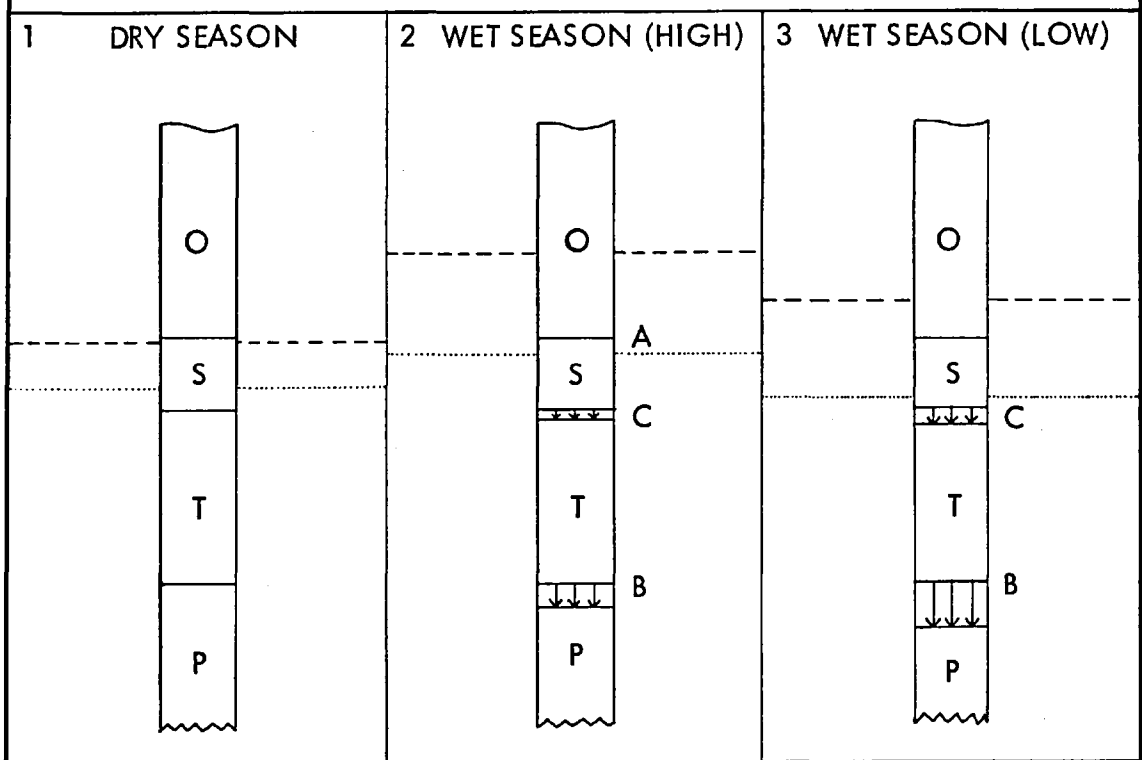
Fig. 7.3.2B. The Effect of Differential Profile Exhumation Rates on Alteration Zone Development

Exhumation Rate of Profile B = Twice that of Profile A

(Figure symbols as for Fig.7.3.1.)

1 FIRST DRY SEASON	2 WET SEASON	3 SECOND DRY SEASON
A B	A B	A B
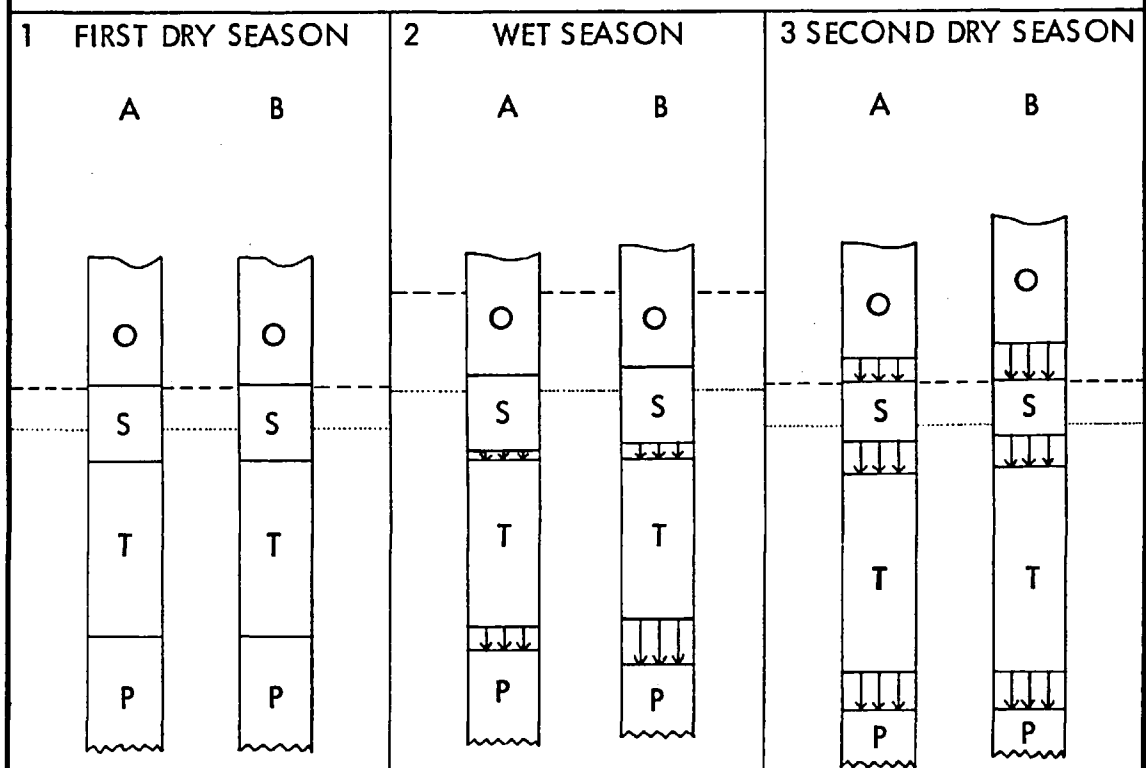
The Eh environment at the top of the secondary zone, (A), is, however still high enough to sustain the continued if relatively slow alteration of pentlandite and pyrrhotite to violarite at the top of the primary zone, (B). And it is also likely to be just high enough to sustain very slow conversion of residual pyrrhotite to iron disulphide at the top of the transition zone, (C).

Consequently, the presence of a high wet season water table implies that the transition zone will continue to grow downwards, but at a slower rate than in the dry season, and that the secondary zone also continued to grow downwards but at a much slower rate compared with the transition zone.

The likely response of the alteration profile in Fig.7.3.2A(I). to a considerably less humid wet season is illustrated in Fig.7.3.2A(III). Here the water table remains deep enough for a substantial proportion of the secondary zone to remain within the minimum Eh region. As a result, although shallow anodic activity ceases due to insufficiently high Eh, the deep anodic reactions of violarite formation continue at reduced rates at B. These rates are however significantly faster than those exhibited under the wetter conditions indicated in Fig.7.3.2A(II). Similarly, the formation of iron disulphides from pyrrhotite occurs at C but at a slower rate than in the dry season. The rate is however significantly faster than that associated with wetter conditions.

These considerations imply therefore that of two nickel sulphide alteration profiles developing under seasonally fluctuating humid conditions, the one which is subject to the smallest seasonal variation in water table level will exhibit the greatest growth of both secondary and transition zones. This result is of course based on the assumption that the mean exhumation rates of both ore profiles are the same or very similar.

The effect of different profile exhumation rates on alteration zone growth, (Fig.7.3.2B.)

The possible consequences for alteration zone development of different rates of profile exhumation are illustrated in Fig.7.3.2B. for two profiles present within the same seasonally fluctuating water table regime. For the purposes of exposition, one profile, (B), is assumed to be exhuming at twice the rate of the other, (A).

In Fig.7.3.2B(I), a hypothetical dry season condition is indicated with both profiles having the same absolute and relative zonal development, and with both at the same level with respect to the associated water table horizon.

The combined effect of differential exhumation and the onset of wet season conditions

are illustrated in Fig.7.3.2B(II). Here the higher elevation of profile B within the Eh zone of the water table causes both secondary and transition zones to grow downwards at greater rates than the equivalent zones in the less exhumed profile A.

On the resumption of dry season conditions however, (Fig.7.3.2B(III).), a greater depth of unoxidised secondary ore now lies above the water table in profile B because of the latters high rate of exhumation. In consequence, a greater relative and absolute proportion of secondary ore is now in disequilibrium with its environment in profile B than in profile A and rapid corrosion ensues. The secondary zones of the two profiles are therefore effectively truncated at their upper ends. The thickness of secondary ore in profile B is however disproportionately reduced with respect to that of profile A.

Zone growth continues in the portion of the ore beneath the water table in both profiles due to the full operation of the corrosion cells and, therefore of deep anodic reactions. Further, it is very likely that the respective rates of secondary and transition zone growth will be similar in the two profiles, as both of these bodies are again altering under the same chemical conditions.

As a result, a comparison of the zonal lengths of the two profiles in Fig.7.3.2B(III) indicates that high profile exhumation rates operating under a seasonally variable water table regime cause the relatively slow growth of secondary zones. In contrast, though, these conditions also lead to the relatively fast growth of transition zones. The reverse consequences hold for profiles exhibiting slow exhumation rates.

The modified model of supergene alteration genesis and development indicated in Figs.7.3.1. to 7.3.2B. has therefore three implications for profile evolution. These are; firstly, that the presence of relatively extensive transition and secondary zones, together with a deep primary-transition zone boundary imply a   quite   long term development of the profile under seasonally variable water table conditions; secondly, that profiles developed under conditions of relatively small seasonal water table level differences will generally possess   quite   extensive secondary and transition zones; and, thirdly, that profiles developed under high rates of exhumation will generally exhibit rather restricted secondary zones, but relatively extensive transition zones.

On this basis, it may hence be inferred that the typically depth-restricted secondary zones, (relatively) restricted transition zones and generally shallow primary-transition bounderies of the sampled southern African alteration profiles, (Fig.6.2.1.), indicate that these ores have generally been only affected for a relatively short time by

seasonally variable water table conditions.

Further, these generalised features also imply that relatively large seasonal water table changes have occurred during this period and that the developing profiles have been exhumed at relatively high rates.

Such data that are available on the climatological and physiographic evolution of the Rhodesian craton and Limpopo mobile belt tend to support these general regional inferences. In this respect, the presence of Jurassic age fault-bounded crustal blocks in the region implies that exhumation may have been fairly continuous in the long term, and (probably) rather rapid in character. This inference in turn helps to explain the implied relative juvenility of the alteration profiles in respect of the persistent seasonally humid climatic conditions still operative over most of the region. Further, the inferred occurrence of markedly differing seasonal water table levels during the development of the profiles is also tentatively supported by the noted seasonal precipitation pattern developed over much of the region at present, (section 2.2).

In contrast, the sampled Australian alteration profiles are more typified, (Fig.6.2.1.), by generally extensive secondary and transition zones, and by relatively deep primary-transition zone boundaries. This infers that these deposits have been more typically subjected to a relatively long term development under a climatic regime character-ised by rather small seasonal fluctuations in water table levels, and, further, by long term near-average exhumation rates. Again, these inferences are generally supported by available data on the climatological and physiographic history of the Yilgarn Shield region, (section 2.2).

Comparison of weathering histories with those predicted by the proposed alteration model

It will be interesting, as a conclusion of the present discussion of nickel sulphide alteration profile development, to now briefly compare the weathering histories of the sampled deposits with those predicted by the proposed geological alteration model.

The narrow secondary zone, fairly extensive transition zone and relatively deep primary-transition zonal boundary of the Pikwe deposit, (Fig.6.2.1.), imply the quite rapid generation of the alteration profile under conditions of significantly large seasonal differences in rainfall coupled with a high profile exhumation rate.

These inferred formation conditions are consistent with both the tectonic setting of the deposit and the known climatological history of N.E.Botswana, (section 2.2).

The narrow secondary and transition zones of the Munali alteration profile, together with the rather shallow primary ore boundary imply that the deposit has only been influenced by lateratisation conditions for a relatively short period of geological time. Further, it is likely that these conditions have been typified by quite large seasonal rainfall variation.

These implications are tentatively supported by the association of the deposit with a likely late intrusive gabbroic stock, and by the long term development of seasonally humid climatic conditions in south-central Zambia, (Chapter two).

A similar profile configuration to that of Munali occurs at Perserverence, (Rhodesia). Here, though, the implied relative juvenility of the altered Archean nickel ore profile might be explained by a relatively recent movement of the deposit into the near-surface environment as a result of gradual epeirogenic uplift. No definite data are however available to either support or invalidate this consideration, although suitable climatic conditions have likely persisted in north-central Rhodesia since the late Tertiary.

The extensive secondary zone development of the Trojan deposit, together with the relatively restricted extent of the transition zone and the presence of a deep primary ore boundary imply that this alteration profile has been generated over a considerable period of time, and with the ore body exhuming at a below average rate.

The profile configuration of the vein-like Phoenix deposit, (Fig.6.2.1.), is indicative of a relatively rapid generation under conditions of marked seasonal changes of precipitation level and of fairly rapid exhumation.

The probable genesis of the deposit as a re-mobilisation phenomenon associated with the (late) intrusion of a granite stock, (section 2.3), may hence semi-quantitatively explain the implied exhumation characteristics, and the presence of a seasonally humid climate in N.E. Botswana prior to the onset of semi-arid conditions in the late Tertiary likewise infers the necessary climate required for the genesis of the observed profile.

The occurrence of a profile configuration in the Selkirk deposit of similar character to that of the Munali deposit, (Fig.6.2.1.), implies that the presence of the former may also be explained in terms of a relatively late exhumation into near-surface lateratisation conditions. In this instance however, the likely formation conditions

are probably due to the association of the deposit with a fault-bounded metatroct-olite stock, (section 2.3).

The alteration profile characteristics of the Mt. Edwards deposit are very similar to those of the Pikwe deposit, (Fig.6.2.1.). It is hence reasonable to assume that the formation of the Mt. Edwards alteration profile also took place under conditions of significantly large seasonal differences in rainfall, and with the assistance of an above average rate of profile exhumation.

The Mt. Monger alteration profile exhibits features that are very much like those of the Munali and Perserverence profiles already indicated, (Fig.6.2.1.). Its configur-ation therefore implies that it was subject to the pre mid-Miocene lateratisation episode that affected the Yilgarn Shield, but for only a relatively short period of time. This contention in turn infers that the Mt. Monger deposit was relatively deeply buried and probably only came under the influence of the near-surface weathering regime during the late Oligocene - early Miocene epoch.

The profile configuration of the Redross deposit is rather similar to the proximal Mt. Edwards deposit. It is hence likely that it also formed under similar climatic conditions, i.e., inferred large seasonal variations in rainfall, and subject to a relatively high exhumation rate. However, the noticeable differences between the two profiles in respect of secondary zone development infer that the rate of ex-humation in the Redross area may not have been as great as at Mt. Edwards.

The extensive development of secondary and transition zones in the three sampled Kambalda deposits - Jan, Lunnon/S.L.O.B., and McMahon, and in the Ravensthorpe deposit, (Fig.6.2.1.), indicates that these profiles were developed over a relatively long period during a lateratisation episode which was probably typified by 'near-normal' seasonal rainfall variations.

No data on the deeper part of the Carr Boyd alteration profile were available for investigation in the present study. It is therefore difficult to even qualititatively infer the likely formation history of this ore body. The presence of a relatively narrow secondary zone suggests however that profile development may have taken place under conditions similar to those previously inferred for either the Mt. Edwards or the Mt. Monger deposits.

The absence of transition and primary zones in the Spargoville 5A profile makes it impossible to infer the overall geological and climatological conditions under which it formed. The deposit, as presently constituted, likely represents

434

the distil end of a now mostly eroded ore shoot, and it can hence be inferred that the original ore body was situated at a relatively higher level than the rest of the sampled Western Australian deposits. Quite considerable uplift and erosion must therefore have occurred since the Spargoville 5A alteration profile was probably first developed in the (? early) middle Tertiary.

7.4. Summary of conclusions

The chemical and geological model proposed by Thornber to explain the occurrence of supergene alteration in the Kambalda (W.A.) nickel deposits has been discussed on the basis of work carried out in the present study on 17 oxidising nickel sulphide deposits from southern Africa and Western Australia.

The conclusions of this work are as follows:

1) That supergene chemical reactions very similar to those at Kambalda occur in all sampled alteration profiles;

2) That, in consequence, electrochemical corrosion cells of the type proposed by Thornber are operating, or have operated during the development of supergene alteration in these deposits;

3) That observed inter-deposit variations in alteration profile configuration can be largely explained by a conceptual model that assumes supergene alteration was first initiated and then subsequently evolved through the steady exhumation of the parent ore profile under seasonally fluctuating water table, (lateratisation), conditions.

CHAPTER EIGHT

THE GENESIS AND POST-FORMATION HISTORY OF NICKEL GOSSANS

8.1 Introduction

The genesis and post-formation maturation of nickel gossans is now investigated.
The work is based on inferences that are drawn from the interpretation of oxide
zone phenomena observed during the present study. It is divided into three major
parts.

The first part, (section 8.2), briefly re-iterates the principal mineralogical and
geochemical features of both nickel gossan formation and of the subsequent history of
these rocks based on work carried out on a suite of 17 study oxide zones. The
second part, (section 8.3), interprets the likely chemical environment of gossan
formation on the basis of observed iron oxide and oxidate mineral phenomena. The
post-formation history of nickel gossans is interpretatively discussed in section 8.4
from the standpoint of three important subsequently acquired features of these rocks.

Previous work in this field is limited to a discussion by Nickel and Thornber (1977),
based chiefly on the Kambalda (W.A.) deposits, of the probable chemical environ-
ment at and above the water table in serpentinite bodies containing nickel sulphides.
The present report complements this previous work through the synthesis of a more
generalised interpretation of gossan formation and post-genetic chemical environ-
ments.

8.2 The mineralogical and geochemical features of gossan formation and development

Mineragraphic and geochemical work on the sulphide ores and equivalent oxide
rocks of 17 nickel deposits from southern Africa and Western Australia indicates
that several features typify oxide zone formation and the latters subsequent
maturation in this ore type. These features are now briefly summarised.

Sulphide dissolution and iron oxide precipitation

Available data, (section 6.2), indicate that the secondary sulphide assemblages
of all 17 sampled nickel ores undergo pervasive oxidative leaching at their
respective water table horizons. The leaching sequence; violarite - iron disulphide/
spinel - chalcopyrite is typically observed, although considerable overlap generally
occurs. Further, pyrite, and, (especially), chalcopyrite mineral relics typically

persist into the overlying oxide zone for a considerable vertical distance above the inferred water table horizon.

The secondary sulphides are replaced at the water table by iron oxides – chiefly by goethite, although hematite replacement is significant in several deposits, viz., at Pikwe, Selkirk and Redross. Further, pseudomorphic and/or other forms of recognisable sulphide mimic textures are generally present in these replacing oxides, with violarite, (Fig.10.2.1A.); secondary pyrite, (Fig.10.2.3C.); secondary marcasite, (Fig.10.2.3A.); chalcopyrite, (Fig.10.2.2C.); and spinel, (Fig.10.2.4F.) all represented by mimicked fine-grained iron oxide structures.

The geochemistry of the sulphide-oxide transition

The major and minor elements constituting the secondary nickel sulphide assemblages respond in different ways to pervasive oxidation at the water table horizon. The relevant data demonstrate that sulphur is almost entirely leached from the sulphides, and is rapidly removed from the oxidising ore profile – most probably in the form of the oxidised water-soluble sulphate radical. The agent responsible for this removal is probably the investing groundwater.

In the case of iron however, a significant proportion is retained within the developing oxide zone as iron oxides. Data, (Fig.6.5.1.), also infer though that a considerable proportion of the sulphide iron content is mobilised and subsequently transported (leached) out of the ore profile by groundwater in response to oxidation. This variation of behaviour is probably due to a corresponding variation in the proportion of liberated ferrous (II) ions that are rapidly oxidised and precipitated as ferric (III) oxides at the water table.

The minor elements associated with the secondary sulphide assemblage – the first row Transition metals, can be divided into two groups on the basis of their response to pervasive sulphide leaching.

The metals; nickel, cobalt, copper and manganese form one group. These elements, which are chemically rather similar, each exhibit extensive depletion in consequence of sulphide degradation at the water table. The extent of this depletion for a given metal however exhibits considerable inter-deposit variation, (Fig.6.5.1.).

These data also indicate though that both copper and manganese tend to be retained within the developing oxide zone to a greater relative extent than do nickel and cobalt, (Fig.6.5.2.). In the instance of copper, this preferential retention

phenomenon is probably due to the almost exclusive occurrence of this metal in relatively stable chalcopyrite, but may also be related to a preferential co-precipitation of this metal with goethite, (Nickel and Thornber, op.cit.). Manganese retention is probably related to the relative immobility of this metal in the sulphide leaching environment.

All four metals are however released into solution as oxidised soluble species as a result of sulphide leaching. The proportion of each metal retained within the developing oxide zone chiefly depends on the proportion co-precipitated with, and/or adsorbed on, coevally precipitating ferric oxides.

The second group of minor (transition) metals comprises titanium and chromium. These metals exhibit, (on available data), little variation across the immediate sulphide-oxide transitions in the sampled deposits. This behaviour corresponds well with their theoretical chemical immobility within the oxidising, acid environment associated with active sulphide leaching. It is however also probably related to their principal respective occurrence in the typically resistate minerals Ilmenite and Chromite/Ferrochromite in the sampled nickel ores.

Associated host silicate alteration

The silicate rocks adjacent to the ore profile are affected by sulphide leaching in the horizon of the water table.

Data, (section 2.2), indicate that deep zones of lateritic weathering overlie the majority of the study ores in both regions. The silicates present within the water table zones of the southern African ore profiles are however typically more mafic in character, and are generally less weathered, (viz., relatively unaltered), compared with the equivalent Western Australian rocks. These are more typically ultramafic and are deeply weathered to Talc-Tremolite or Talc-Carbonate assemblages at the corresponding water table levels.

The differences in mineralogical and chemical characteristics affect the response of the host silicate to the acid released during pervasive sulphide oxidation. The (relatively) carbonate-free African silicate assemblages - notably that of Pikwe, neutralise excess released acid by undergoing pervasive hydrolysis. This phenomenon causes degradation of the silicate lattice with the result that silica is released, together with the constituent alkali and alkaline earth metals, (section 3.2).

The more deeply weathered carbonate-rich assemblages of the Western Australian

host silicates however respond in a different manner. Here, the presence of abundant carbonate means that neutralisation can take place by the chemically simpler phenomenon of hydrogen ion exchange. By this means, the host carbonate is broken down and both its alkaline earth cation content, and the generated bicarbonate anions are released into (groundwater) solution.

Both types of silicate neutralisation response however generally lead to the formation of oxidate minerals in the water table zone by recombination of released species and/or by reaction of these with the soluble metals and acid radicals directly derived from sulphide leaching.

A number of these oxidate minerals have been observed in the basal portions of the developing oxide zone or in laterally equivalent horizons in the adjacent host silicates, (Fig.6.2.7.). Their mineralogy and chemistry appears to be generally related to the character of the specific host silicate rock. Thus, alkaline earth carbonates - considerably substituted by ore metals, (nickel, copper and cobalt), predominate in the water table zones of the oxidising Australian nickel ores. Whereas complex alkali-iron sulphate minerals are more typical of the equivalent horizons of the sampled southern African deposits.

The typical drusy or vein growth textures of oxidate minerals in both African and Australian water table zones however demonstrates that these phases ubiquitously form by precipitation from groundwaters that are rich in their component elements and acid radical species.

Post-formational changes in the oxide zone

Three significant mineralogical and geochemical changes occur within the oxide zone depth profile above the basal (water table) zone. These are; silica enrichment; chromium enrichment; and the dehydration (hematisation) of goethite.

Available data, (Fig.6.5.1B.), indicate that silica enrichment of the developed oxide zone profile occurs in 14 out of 15 deposits of the study suite. The silica is characteristically in the form of an amorphous matrix. Further, a detailed mineralogical study of the Pikwe oxide profile demonstrates, (Fig.3.2.3.), that silica content distribution is inversly proportional to depth.

Chromium enrichment occurs in the majority of the study gossans, (Fig.5.6.1.). A depth profile is available only from the Pikwe oxide zone, (Fig.3.4.2.). This indicates that chromium distribution may be partially related to that of silicon.

The definite alteration, (dehydration), of goethite to hematite is observed in progress in four of the sampled oxide zones; those of Pikwe, Carr Boyd, Spargoville 5A and Ravensthorpe. Moreover, the phenomenon is confined to goethite aggregates at relatively shallow depths in all four deposits. It therefore occurs only among relatively mature goethite structures.

8.3 Oxide zone phenomena as indicators of the nickel gossan formation environment

The principal features of nickel gossans are now utilised to discuss the generalised formation environment of these rocks.

The implications of iron oxide mineralogy

The precipitation of iron oxide minerals in the water table zones of oxidising nickel ores is now interpreted in terms of the Eh/pH of the gossan formation environment.

Goethite is typically formed at the water table in preference to hematite as a result of sulphide leaching. Primary hematite is unequivocally noted only at Pikwe. A comparison of the theoretical Eh-pH stability fields of the two phases, (Fig.8.3.1.), demonstrates however that both are stable under almost identical conditions. By implication, therefore, no direct relationship exists between the specific Eh-pH environment of the oxidising parent sulphide ore and the iron oxide assemblage that directly results from it.

Work by Schellmann, (1959), indicates however that hematite and goethite generally form under different chemical conditions during the ageing of laboratory-precipitated ferric hydroxide gels. Hematite principally forms under low pH conditions, whereas goethite forms under alkaline conditions, $(pH > 11)$, or in neutral conditions in the presence of adsorbed bicarbonate or sulphate ion.

The indicated preferantial formation of goethite at the water table in the study profiles might hence be explained by Schellmann's findings, given the known occurrence of high sulphate ion concentrations in this location during sulphide leaching. Neutral conditions are however very unlikely to exist in close proximity to actively leaching massive sulphides. Moreover, present data on secondary sulphide metal-to-sulphur ratios and on FeS_2 proportions infer that no discernable qualitative

Fig. 8.3.1. Theoretical Eh/pH Stability Fields of Hematite and Goethite

A

B

Hematite Stability Relations
(This Study)

Goethite Stability Relations
(From Nickel and Thornber 1977)
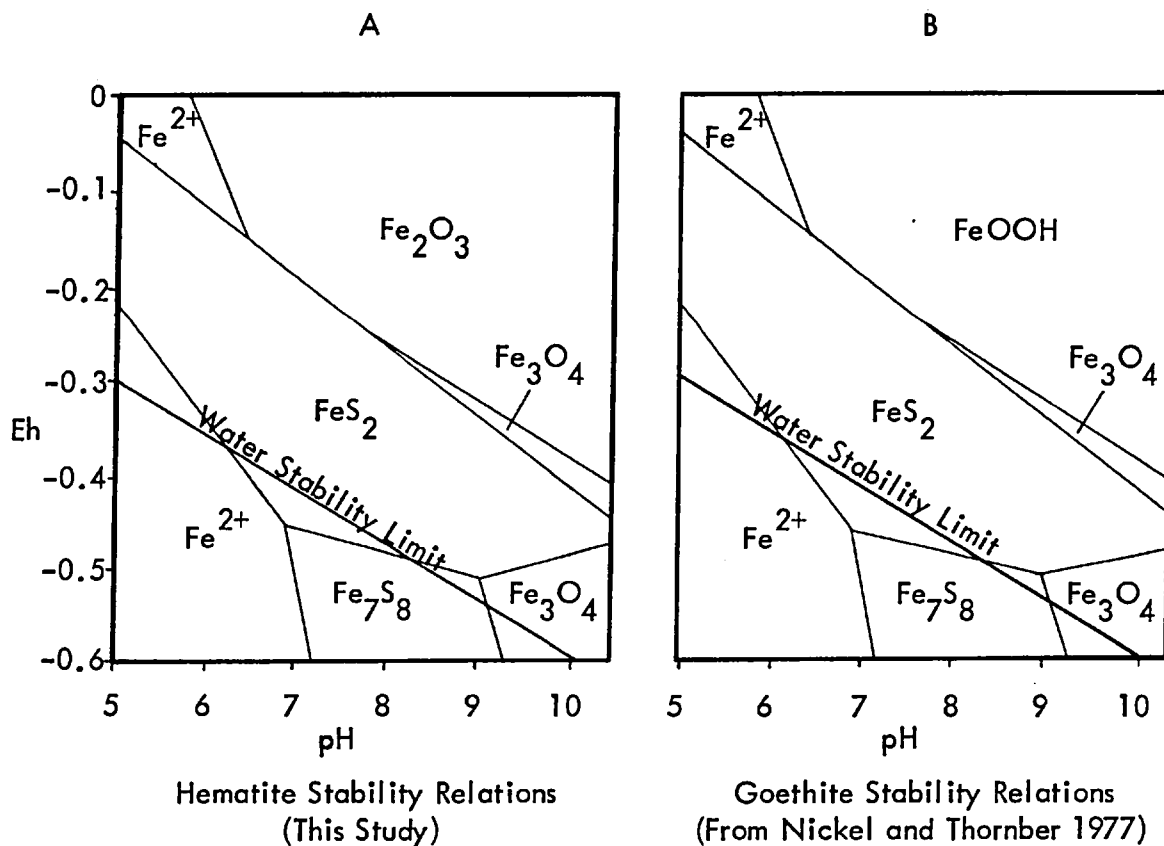
Theoretical Reactions involving Hematite (Fig. 8.3.1A.)

A $2Fe^{2+} + 3H_2O = Fe_2O_3 + 6H^+ + 2e^-$

Eh $= 0.658 - 0.177pH - 0.059 \log (Fe^{2+})$

B $2FeS_2 + 19H_2O = Fe_2O_3 + 4SO_4^{2-} + 38H^+ + 30e^-$
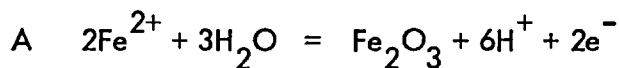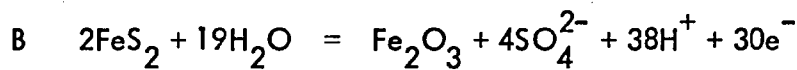
Eh $= 0.391 - 0.075pH + 0.008 \log (SO_4^{2-})$

C $2Fe_3O_4 + H_2O = 3Fe_2O_3 + 2H^+ + 2e^-$
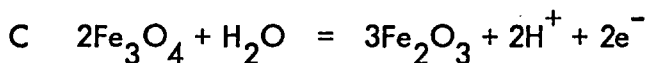
Eh $= 0.214 - 0.059pH$

correlation exists between inferred leaching pH and the type of iron oxide precipitated. pH therefore exerts no direct influence on iron oxide formation in the natural sulphide leaching environment.

A recent study by McAndrew et.al.,(1975), on the solubility of ferric oxide phases in sulphate-rich acid solutions demonstrates that precipitation of goethite and hematite is related to the total content of aqueous ferric species in the parent solution. Fig.8.3.2. indicates that goethite forms in preference to hematite from solutions containing a minimum of $10^{-6.5}$ mole per litre of ferric species at moderately acid to neutral pH values. On this basis, sufficient quantities of aqueous ferric species must be present within the sulphide leaching horizons zones of the majority of the sampled deposits to cause goethite to precipitate instead of hematite.

The formation and maintainence of mobile species is related to the redox characteristics of the environment as ferrous ion oxidation must be involved in these phenomena. Iron oxide formation must therefore be influenced by the Eh conditions of the sulphide leaching environment.

A theoretical relationship between Eh and iron oxide precipitation mode is presented in Fig.8.3.3. for a range of Ferric/Ferrous equilibrium concentrations at one mole per litre sulphate ion activity. These relations infer - Ferric species concentration notwithstanding, that goethite likely forms at a higher Eh than does hematite. In this respect, Fig.8.3.3. shows that goethite forms at Eh values greater than about +0.35 V, whereas hematite forms within the range +0.1 to +0.45 V.

Assuming McAndrew's results to be applicable to the natural nickel sulphide oxidation environment, these relations indicate that the Eh environment of a typical nickel sulphide leaching horizon is likely to be in the region of at least +0.35 V.

The occurrence of hematite mimics after secondary marcasite at Pikwe indicates the rapid precipitation of this iron oxide phase. This phenomenon could be caused by the presence in this deposit of a water table Eh environment at the higher end of the + 0.1 to + 0.45 volt range inferred from Fig. 8.3.3.

Fig. 8.3.2. Thermodynamic Solubility Curves of Hematite and Goethite at $25^{\circ}C$

(After McAndrew et.al.,1975)
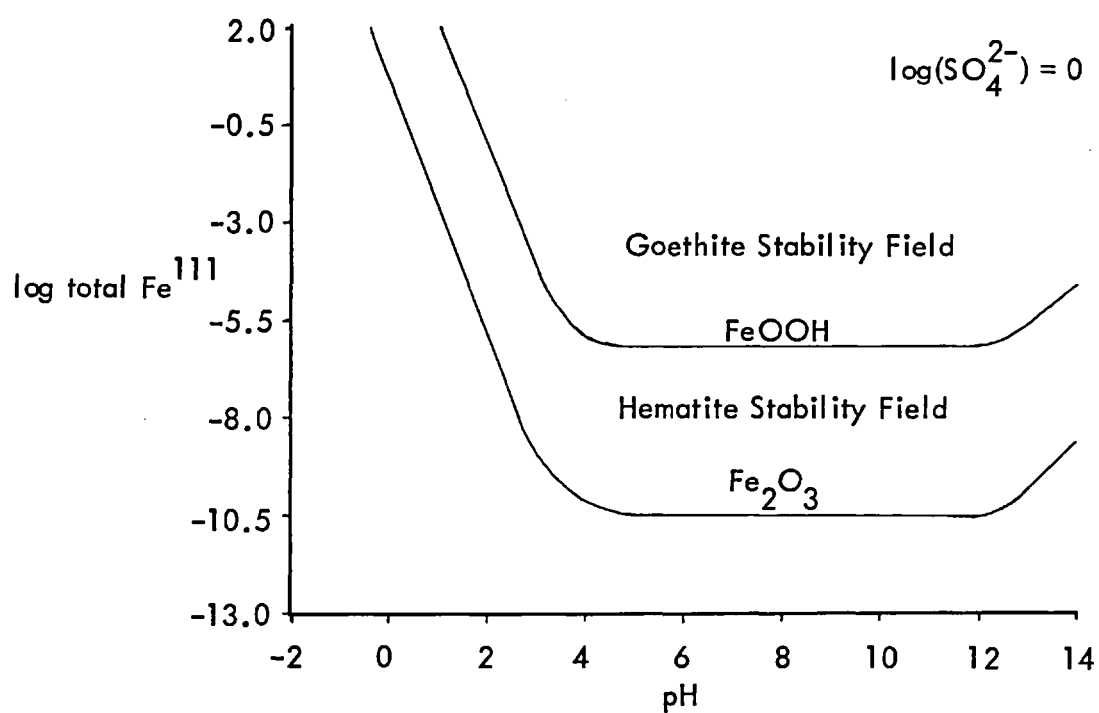
FIG. 8.3.3. THEORETICAL RELATIONSHIP BETWEEN Eh AND TOTAL FERRIC SPECIES ACTIVITY
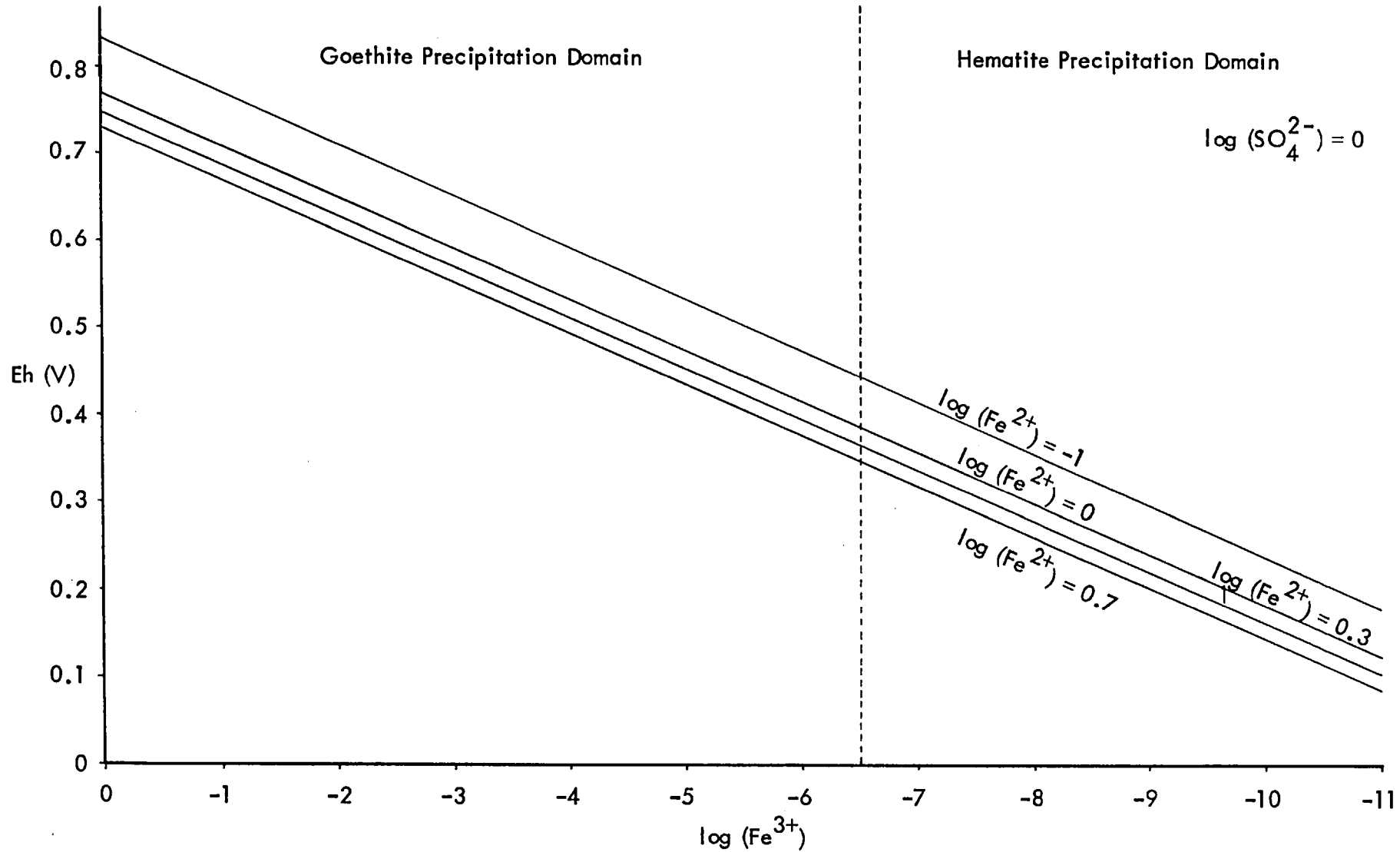
The implications of oxidate mineral formation

Work in this study, (section 6.2), has shown that several types of oxidate minerals may be precipitated in the basal region of the developing oxide zone and/or in the neighbouring silicate wallrocks. These phases result from the precipitation of soluble oxidised species released from both sulphide and adjacent silicate as a result of the sulphide leaching process. Inferences about the formation environment of nickel gossans that such minerals provide are now indicated. The carbonates, magnesite and dolomite are dealt with first.

Magnesite

Magnesite is noted as a non-surficial oxidate mineral within the oxide profiles of three sampled deposits; McMahon, Otter Shoot and Carr Boyd. It is present as a precipitant phase within internal cavities in both gossans and adjacent silicates. Further, the characteristic ore metal substitution of these samples, (Table A2/2; Appendix Two), indicates a strong genetic association with sulphide leaching.

The majority of the sampled magnesites are situated within the oxide profile above the present-day sulphide-oxide transition. This phenomenon represents the result of earlier episodes of sulphide leaching that took place before the ore profile was exhumed to its present position. The aqueous insolubility of magnesite and the recent semi-arid climatic regimes affecting the sample deposits support this inference.

Recent experimental work on the metal composition of siderites precipitating within the nickel supergene alteration environment has been carried out by Thornber and Nickel, (1976, op.cit.). These workers have been able to qualitatively indicate the likely co-precipitation preference of iron for magnesium and a number of ore metals in siderite. Further, Thornber has been able, through the concept of a Distribution Coefficient, to qualitatively indicate both the probable concentration levels of these metals in the corresponding solution and the formation pH of the precipitating siderite.

Thornber's results have been adapted in the present study in order to investigate these parameters for the oxidate ferroan magnesites noted in the three sample deposits. Some insight into the formation environment of nickel oxide zones has been gained as a result.

The concentration of metal in the parent solution is computed from the relation:

$$Metal_{(solution)} = \frac{Fe_{(solution)}}{55.85} \times \frac{At.Wt.(Metal)}{Atomic\ Ratio_{(Solution)}}$$

Here, iron is assumed to be present in solution at a total concentration of 10^{-3} moles per litre. Thornber considers that this value is probable assuming that carbonate ions precipitate to maintain a partial pressure of about 10^{-3} athmospheres of CO_2. Atomic ratio (solution) data are computed from data in Thornber and Nickel's paper.

In the present study, the inferred formation pH of the magnesite is estimated on the assumption that magnesium (Mg^{2+}) is the principal ion in equilibrium with the solid phase. It is calculated by substitution in the relation:

$$pH = \frac{10.59 - \log P_{CO2} - \log Mg^{2+}}{2}$$, which is based on equation A3 of Thornber's 1976 paper.

The results of these computations for a total of seven oxidate magnesites from the three sample deposits are given in Fig.8.3.4. However, because of the assumptions made in the computation of these data, they must be regarded as providing only a qualitative indication of the soluble metal concentration and the formation pH of the magnesite.

These calculated data infer however that considerable quantities of ore metals – especially nickel and cobalt, are present within the basal portions of the oxide zone during or soon after sulphide leaching. This region also appears typified by considerable variations in aqueous metal content, as is indicated by the data for the two closely coincident basal oxide magnesites from Carr Boyd, (1279A and C). Further, the distribution of aqueous magnesium – principally derived from adjacent weathering silicates, bears little or no relationship, (Fig.8.3.4.), to immediate host rock type. These observations are indicative of the complex geochemical environment that exists at the top of the oxidising ore body.

Nickel and cobalt appear though to be preferentially concentrated within the oxide zone samples. These metals have probably percolated through the newly-formed iron oxide matrix from sulphide leaching sites to become trapped by co-precipitation with magnesium and bicarbonate ion.

The very low(inferred) aqueous concentrations of both copper and manganese in Fig. 8.3.4. is probably caused by the high co-precipitant affinity of magnesium for these metals.

The data on formation pH values in Fig.8.3.4. are interesting in that they typically infer the existence of a slightly acid environment during magnesite precipitation.

FIG. 8.3.4.   INFERRED FORMATION ENVIRONMENTS OF SEVEN OXIDATE MAGNESITES

Assume: $\log pCO_2 = -3.5$; $(Fe^{2+}) = 10^{-3}M$

DEPOSIT/ SAMPLE No.	HOST ROCK	PRESENT DEPTH (m)	ATOMIC RATIOS (* = SOLID; ( ) = SOLUTION)					INFERRED METAL CONCENTRATIONS OF PARENT SOLUTION (PPM UNITS)					INFERRED FORMATION pH
			$\frac{Fe}{Mg}$	$\frac{Fe}{Ni}$	$\frac{Fe}{Co}$	$\frac{Fe}{Mn}$	$\frac{Fe}{Cu}$	Mg	Ni	Co	Mn	Cu	
McMahon 01155	Massive Gossan	20	1.83×10^{-1} / (2.80×10^{-3})	5.60×10^{-1} / (7.30×10^{-2})	2.81×10^{1} / (2.20×10^{2})	3.93×10^{1} / (3.10×10^{2})	4.48×10^{0} / (2.10×10^{3})	8.69×10^{3}	805	0.27	0.18	0.03	7.3
Otter Shoot 01165	Talcose Mafic Silicate	20	2.70×10^{-2} / (3.60×10^{-6})	1.99×10^{0} / (2.20×10^{-1})	1.54×10^{2} / (4.75×10^{2})	1.08×10^{2} / (7.50×10^{2})	6.94×10^{0} / (1.52×10^{3})	6.75×10^{5}	267	0.01	0.07	0.04	6.3
Otter Shoot 01178	Massive Gossan	16	3.20×10^{-2} / (4.30×10^{-5})	6.52×10^{-1} / (7.90×10^{-2})	4.67×10^{0} / (3.50×10^{2})	8.71×10^{1} / (1.80×10^{2})	7.84×10^{0} / (1.53×10^{3})	5.66×10^{5}	744	16.9	0.10	0.04	6.4
Carr Boyd 01278A	Serpentinised Dunite	20.5	7.50×10^{-2} / (1.00×10^{-4})	2.10×10^{-1} / (2.40×10^{-1})	3.40×10^{0} / (2.20×10^{0})	1.18×10^{1} / (7.70×10^{1})	1.14×10^{0} / (2.30×10^{2})	2.43×10^{5}	2449	26.8	0.71	0.28	6.6
Carr Boyd 01278C	Serpentinised Dunite	20.5	2.90×10^{-2} / (4.20×10^{-5})	2.60×10^{-1} / (3.10×10^{-1})	3.53×10^{0} / (2.50×10^{0})	1.70×10^{1} / (1.00×10^{2})	3.97×10^{0} / (8.10×10^{2})	5.79×10^{5}	190	23.6	0.55	0.08	6.4
Carr Boyd 01279A	Basal Gossan	25.8	2.60×10^{-2} / (4.10×10^{-5})	1.18×10^{0} / (0.50×10^{-1})	2.24×10^{0} / (1.60×10^{0})	1.13×10^{1} / (7.20×10^{1})	8.50×10^{-1} / (2.05×10^{2})	5.94×10^{5}	1175	36.9	0.08	0.31	6.4
Carr Boyd 01279B	Basal Gossan	25.8	3.70×10^{-2} / (5.40×10^{-5})	9.20×10^{-2} / (1.10×10^{-2})	1.38×10^{0} / (1.00×10^{0})	5.90×10^{0} / (3.50×10^{1})	7.24×10^{0} / (1.40×10^{3})	4.51×10^{5}	5343	60	1.57	0.45	6.4

The exact spatial relationship between ore leaching and magnesite deposition is however unknown except for the Carr Boyd samples. These are located at a minimum distance of about three centimetres from visibly oxidising ore. The slightly acid pH values inferred for these magnesites are therefore indicative of the dramatic neutralisation effect of carbonated silicates on the acid released from proximal oxidising sulphides.

In addition, the indication of essentially similar acidity levels in host rocks immediately adjacent to the oxidising ore profile demonstrates that the effects of sulphide leaching are localised where ore zones are invested by carbonate-rich silicate assemblages.

The occurrence of oxidate magnesite in the basal portions of the oxide zone therefore broadly indicates that the pH conditions in this locus are, allowing for the buffering effect of carbonate-rich silicates, moderately acid of neutral.

Dolomite

Non-surficial oxidate dolomite is noted only in oxide material from the Silver Lake Ore Body, (S.L.O.B.). The sampled material occurs within about 1.5 to Two centimetres of actively oxidising massive sulphide. Magnesium is extensively substituted by ore metals - principally by nickel, (Table A2/4 ; Appendix Two).

Little data is currently available on the low temperature formation conditions of dolomite. A study by Garrells et.al., (1960), on the stability of several carbonates indicates however that the equilibrium pH of Dolomite is 5.72.

This finding infers that the oxidate dolomite noted at S.L.O.B. probably precipitated at about this pH value. It is not known however if the formation of these oxidate dolomites occurred under equilibrium conditions. But this is probable as the formation of the ordered dolomite structure cannot occur very rapidly, (Goldsmith, 1959).

It may be broadly inferred therefore that the immediate base of the oxide zone is in general moderately acidic in character. This implication supports that derived from the oxidate magnesite study.

Other dolomite formation parameters are difficult to deduce due to the current failure to synthesise low temperature dolomite. Garralls, et.al. indicate however that, under athmospheric levels of CO_2 partial pressure, the ratio of Calcium to

magnesium ions required to form dolomite ranges from 4.4×10^{-4} to 3×10^{2}. Considerable quantities of both calcium and magnesium species, together with bicarbonate ion must therefore be locally available in order to precipitate the double carbonate.

Gypsum

Oxidate gypsum is observed only within the oxide zone of the Mt. Edwards deposit, (section 6.2, and Table A2/6 ; Appendix Two). It is probable that the chief cationic and anionic components are respectively derived from adjacent silicates and leaching sulphides.

Partington, (1931), indicates that gypsum may be artificially precipitated by the addition of sulphuric acid to calcium chloride solution. Little or no work has apparently been done however on the natural formation conditions of this phase. It is probable though that Gypsum formation takes place within a low pH environment.

The formation of oxidate gypsum within the (former) water table zone of the Mt. Edwards deposit hence appears to be very broadly commensurate with the acid conditions that likely existed within that locus.

Natrojarosite

This phase occurs as an oxidate mineral chiefly in the altered host silicates immediately adjacent to the Pikwe and Carr Boyd oxide zone profiles, (section 6.2, and Table A2/8 ; Appendix Two). The mineral has formed in this location in consequence of the mixing of solutions derived from silicate weathering, (sodium and some iron) and sulphide leaching, (iron and oxidised sulphur species). It is therefore formed as a direct result of silicate buffering of locally produced highly acidic sulphate-rich solutions.

Work by Brown on the theoretical stability field of the potassium analogue, jarosite, indicates (1970 and 1971), that this mineral is stable at $pH \leqslant 3$ and $Eh \geqslant +0.4$ V. It is therefore probable that the sampled natrojarosite formed under essentially similar chemical conditions. This conclusion broadly supports the leaching zone Eh environment inferred from the iron oxide mineralogy discussion.

Further, Brown's results infer that the slow acid hydrolysis buffering response of the Pikwe silicates, (section 3.2.), is conducive to the persistence of highly acid

conditions in the adjacent wallrock. These conditions allow natrojarosite to
readily precipitate out of a solution that is rich in its components. The metas-
table persistence of natrojarosite within the exhumed oxide profile is likely due
to its very low aqueous solubility, (Dana, 1951).

By direct analogy, a sequence of events similar to those inferred for Pikwe
natrojarosite must have occurred within the Carr Boyd host silicates.

Natroalunite

This phase also occurs as an oxidate mineral at both Pikwe and Carr Boyd. It is
however more common at the former deposit. At both locations it is chiefly
confined to the oxide zone, (section 6.2 and Table A2/7 ; Appendix Two).

No work on alunite stability relations comparable to that previously indicated
for jarosite has been done. Brophy et.al., (1962), have however synthesised a
complete solid-solution series between these two end members. These workers
indicate that at a given pH iron is preferentially incorporated into the alum lattice.
This is due to the larger hydrolysis constant of the hydrated ferric ion, as opposed
to the hydrated Al^{3+} ion. Brophy's work infers that Al-rich (alunite) alums only
form under relatively alkaline conditions in the presence of ferric ion.

The insolubility of Al^{3+} ion complexes with respect to solid phases such as gibbsite,
(Garralls and Christ, p.354, (1965)), indicates however that sufficient quantities
of these mobile species are unlikely to be available unless a pH regime of about
three or less is prevalent. It is therefore likely that natroalunite formed within the
basal oxide zone as a result of an influx of aqueous aluminium and sodium after
much of the iron had been precipitated out as iron oxides. The pH environment
of the basal oxide zone must therefore have remained acid long enough for this
phenomenon to occur. The slow buffering response of the Pikwe wallrock silicates
is almost certainly responsible for this condition.

Paratacamite

The hydrated copper chloride paratacamite occurs as an oxidate mineral in the
serpentinised dunite host of the Carr Boyd deposit at a level that is slightly higher than
the present sulphide-oxide transition horizon, (section 6.2). Recent work on the
solution geochemistry of copper, (Mann and Deutscher, 1977), indicates that
the orthorhombic dimorph atacamite is stable within environments defined by

chloride and sulphate ion activities respectively greater than 10^{-2} and 10^{-3} moles per litre. These workers note that atacamite, (and, presumably, paratacamite), is stable within the pH range 2 to 8 under these conditions.

Summary of implications for the gossan formation environment

The principal mineralogical and chemical features of nickel gossans have been qualitatively interpreted in terms of the pH, Eh and aqueous metal concentrations of the gossan formation environment. A chemical interpretation of iron oxide mineralogy infers that the precipitation of individual phases depends on the available concentration of intermediate ferric ion species. Further, iron oxide formation probably occurs at Eh values equal to or greater than +0.35 Volts. This latter conclusion is supported by an interpretation of the formation environment of oxidate natrojarosite in former basal levels of the Pikwe and Carr Boyd oxide profiles.

Interpretation of oxidate natrojarosite and natroalunite formation environments in these deposits infers the presence of laterally extensive highly acidic conditions, (pH $\leqslant$ 3), in carbonate-poor host silicate rocks that exhibit slow acid hydrolytic buffering responses.

In contrast, interpretation of oxidate carbonate formation environments indicates that moderately acidic conditions, (pH 5.5 to 6.5), typify those sulphide leaching zones having adjacent carbonated host silicates.

These results broadly agree with the generalised nickel sulphide leaching environment proposed by both Blain and Brotherton, and Nickel and Thornber. The inferred water table Eh value is however considerably higher than the latter workers value of - 0.2 Volts, which is similarly at variance with the results of work by Bass Becking et.al., (1960).

8.4 The post-formational history of nickel gossans

The mineralogical and geochemical changes that subsequently affect nickel gossans (section 8.2) are now briefly discussed as indicators of profile maturation.

Silica enrichment

The majority of nickel gossans sampled in the present study, (section 8.2), are enriched in silica. Nickel and Thornber, (op.cit.), attribute this phenomenon in the Agnew (W.A.) oxide zone to the effects of lateratisation-the silification occurring at depth as a result of near-surface lateritic leaching of the adjacent ultramafic silicates. These workers interpret the occurrence of silicified surface gossans to a subsequent erosional stripping of the profile down to this deep silicified zone.

Secondary silicification in ultramafic-derived laterite profiles however typically occurs both at and below the basal levels of the mottled zone - viz. in the assumed dry season water table horizon, (Smith 1977; Van Schulenborgh, 1969). Now, on the basis of the supergene alteration model developed in section 7.4 of the present study, oxide zone formation can only occur at this indicated horizon. It is therefore unlikely that silicification of a complete oxide profile could have taken place, as this could only have occurred at or below the dry season water table. It is hence more feasible to intimate that silicification occurred in increments during the gradual upward growth of the oxide zone as it slowly exhumed above the water table during lateratisation of the surface silicate host rocks.

This postulated state of affairs can be more readily visualised by reference to a simple developmental model, (Fig.8.4.1.).

Figs.8.4.1A. and 1B. indicate the 'start' conditions of oxide zone formation. The exhumed sulphide profile has reached the level of the dry season water table. The corresponding laterite zonation and zone of secondary silica deposition of the adjacent ultramafic host silicate are shown.

Fig.8.4.1C: The sulphide orebody is exhumed above the dry season water table with the consequent formation of an incipient oxide zone. This is as yet unsilicified.

Fig.8.4.1D: The consequences of the ensuing wet season. Here, silica-rich ground-waters derived from the leaching of the upper near surface levels of the host ultra-mafic percolate down to be deposited in the upper portion of the pallid (saprolite) zone. In consequence, the protruding incipient oxide zone is bathed in these waters and silica is precipitated within and in place of the porous iron oxide matrix.

Fig.8.4.1E: Subsequent exhumation - the next dry season. An additional unsilified increment of oxide zone has been formed beneath the oxide that was silicified during the previous wet season.

FIG. 8.4.1.   PROGRESSIVE SILICIFICATION OF NICKEL GOSSANS UNDER LATERATISATION CONDITIONS
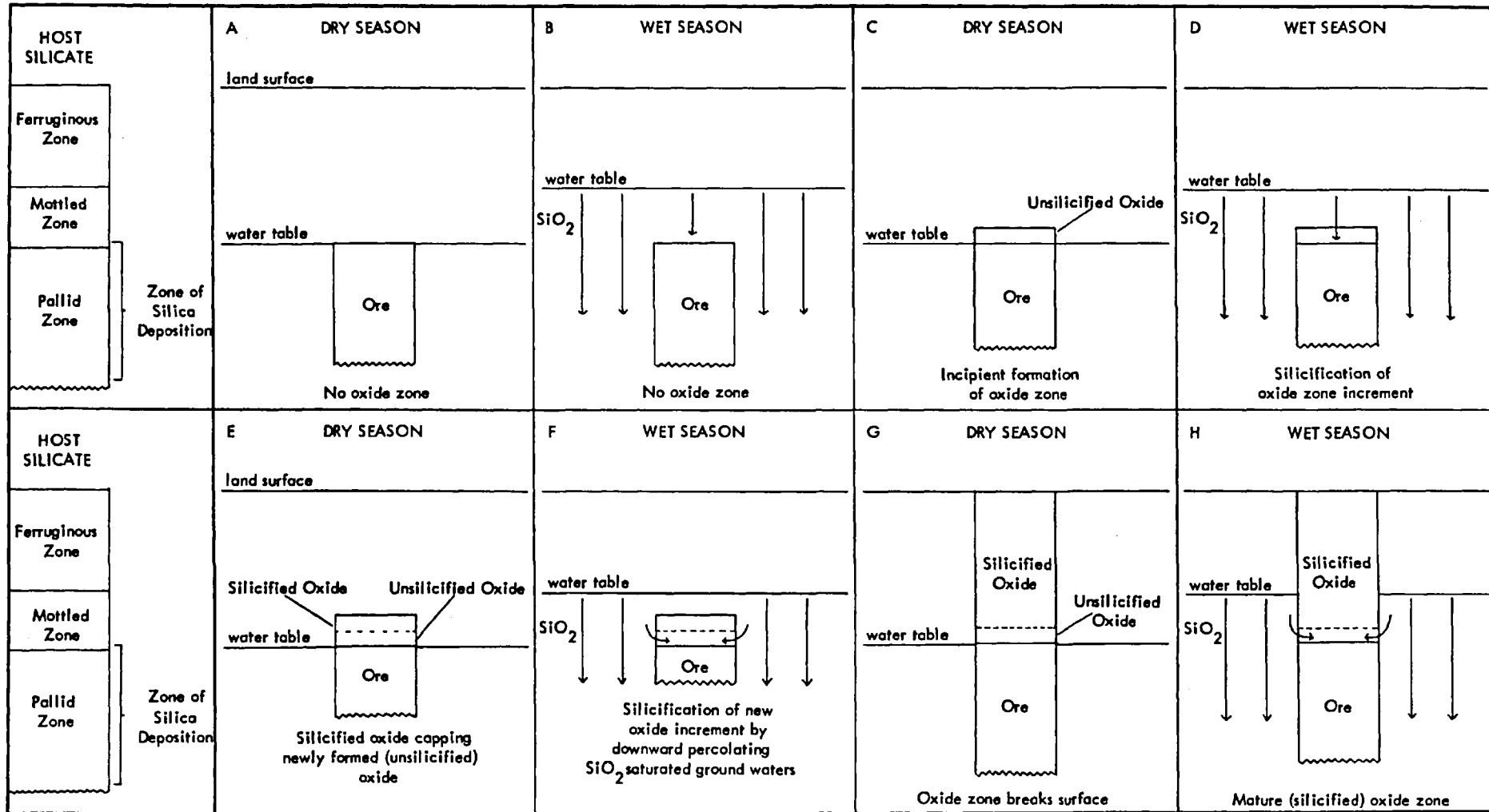
Fig.8.4.1F: The consequences of the next wet season. The oxide zone is again bathed in descending silica-rich groundwaters, and the newly-formed oxide zone increment is consequently silicified.

Fig.8.4.1G: the oxidation profile has been further exhumed so that the oxide zone now crops out. Under dry season conditions however the newly-formed basal oxide segment is, as before, unsilicified.

Fig.8.4.1H: The corresponding wet season condition. The basal oxide zone is now silicified by silica-rich groundwaters. Steady exhumation under constant lateratisation conditions results in the continued existence of this steady-state oxide profile condition.

The simple model illustrated in Fig.8.4.1. infers that silicification took place progressively as the oxide zone was formed. It indicates, in constrast to Nickel and Thornber's conclusions that silicification occurred very shortly after the development of each oxide zone increment in what was effectively a large number of annual pulses.

It is well known, (section 2.2), that lateratisation conditions gradually ceased at the end of the Tertiary, and coincided with the onset of semi-arid conditions in both the Yilgarn Shield and the western portion of the Rhodesian Shield. In the present study, an adequately depth sampled oxide zone profile is available only for the Pikwe, (Botswana), deposit. The present day configuration of this zone with respect to silica distribution is now therefore briefly interpreted. This work permits the general sequence of events that have affected silicified nickel oxide profiles during this post-lateratisation period to be outlined.

Silica content in the Pikwe oxide zone follows a recognisable depth distribution, (Fig.3.2.3.). Mean silica content decreases progressively from about 80 percent in surface samples down to about 50 percent at the 17.5 to 18 metre level. It then remains constant at about this average value down to about 27-28 metres, and then progressively decreases again down to one or two percent at the present-day water table level, (40 metres b.s.).

An idealised sequence of post-lateratisation events is outlined in Fig.8.4.2. in order to relate this phenomenon to the onset of semi-arid conditions in the late Tertiary.

Fig.8.4.2A: The steady-state conditions developed during the late Tertiary lateratis-ation regime. The oxide zone is completely silicified throughout its vertical

FIG. 8.4.2. DEVELOPMENTAL HISTORY OF THE PRESENT PIKWE GOSSAN

A

HOST
SILICATE

Depth (m)

GOSSAN
SiO_2 (wt%)

5   80(+)

Fully developed
(silicified) oxide zone
Active laterite formation

0

-10

Ferruginous
Zone

-20

-30

Wet season water table

Mottled
Zone

-40

Dry season water table

Pallid
Zone

Ore

B

HOST
SILICATE

GOSSAN
SiO_2 (wt%)

5   80

Ferruginous
Zone

Onset of semi-arid climate in
late Tertiary:
Progressive reduction in
water table fluctuation range

SiO_2 deposition progressively
reduced

Inactive
Mottled
Zone

mottled zone

wet
dry

Pallid
Zone

Ore

C

HOST
SILICATE

GOSSAN
SiO_2 (wt%)

5   80

Temporary phase of water table
fluctuation range stability

SiO_2 deposition relatively stable

Inactive
Mottled
Zone

mottled zone

wet
dry

Pallid
Zone

Ore

D

HOST
SILICATE

GOSSAN
SiO_2 (wt%)

5   80

Further progressive reduction
in water table fluctuation range

SiO_2 deposition tapers off

Inactive
Mottled
Zone

Mottled zone

wet

dry

Pallid
Zone

Ore

E

HOST
SILICATE

Depth (m)

GOSSAN
SiO_2 (wt%)

5   80

0

Present configuration in pre-
vailing semi-arid climate

10

Inactive
Mottled
Zone

20

30

Recent water table level

40

Pallid
Zone

Ore

The Relationship of Silica Texture to Profile Depth

Typical active replacement
of iron oxides by Silica

Typical passive addition of
Silica as pervasive matrix

Typical cavity-filling Silica textures

454

development. The full laterite depth sequence of Ferruginous zone;Mottled zone and Pallid zone is developed in the adjacent mafic-ultramafic host silicate.

Fig.8.4.2B: The effects of exhumation under a progressively declining seasonal fluctuation in water table levels. The quantity of silica deposited within the newly-formed oxide zone gradually decreases as a result of diminishing silicate leaching. The vertical extent of the active portion of the mottled zone becomes progressively restricted as the laterite profile is slowly exhumed.

Fig.8.4.2C: A temporary phase of water table fluctuation stability. Silica deposition becomes relatively uniform during continued exhumation and oxide formation. The vertical extent of the active mottled zone remains approximately constant.

Fig.8.4.2D: Further progressive reduction in seasonal water table fluctuations as semi-arid climatic conditions begin to (permenently) re-assert themselves. The silica content of forming oxide zone gradually drops away to near-zero as a result of, firstly, progressive diminution and, then, termination of silicate lateritic leaching. The active mottled zone is progressively restricted and eventually disappears altogether.

Fig.8.4.2E: The present oxide profile configuration with respect to silica distribution. The laterite sequence that generated both the original oxide zone, (Fig.8.4.1.), and its silica content is now represented by the remaining kaolinised portions of the former (inactive) mottled and pallid zones.

The relation of silica replacement textures to depth in the present Pikwe oxide profile is also indicated. The upper levels of the oxide profile, (0 - 28m.), are characterised by the replacement of iron oxides by amorphous silica. This is indicative of active silicification taking place under the control of a still active lateratisation regime.

In contrast, the lower-middle levels of the profile, (28 - 36m.) are more typified by the presence of silica as a pervading amorphous matrix to the generally unreplaced iron oxide assemblage. This is indicative of a more passive introduction of siliceous ground waters, probably as a result of progressively declining near-surface leaching.

The lowest oxide zone levels, (36 - 40m.), are typified by silica in a number of cavity-filling textures. These features demonstrate that little or no silica was available from lateritic leaching during the most recent stages of oxide zone

formation. It is likely that these textures result from the 'normal' semi-arid near-surface weathering of the adjacent lateratised silicates.

The above interpretation indicates that the present top of the Pikwe oxide zone roughly corresponds with the final full episode of laterite-induced silicification. This in turn implies that approximately 40 metres of overburden has been eroded off since lateratisation began to wane.Thus on the assumption of a mean rate of profile exhumation of 0.003 cm. per year, (Blain and Brotherton, op.cit.), the lateratisation episode entered its final stages about 2 million years B.P. - i.e., at the end of the Tertiary. This result accords well with the progressive change in climatic conditions that occurred in the western part of the Rhodesian Shield at the end of the Tertiary.

Chromium enrichment

Nickel gossans are typically chromium enriched compared with the corresponding massive sulphide ore, (Fig.6.5.1.). Available data on the aqueous chemistry of chromium, (Stumm and Morgan, 1970); (Hawkes and Webb,op.cit.), indicate that the metal is mobile only in alkaline oxidising environments. Under these conditions chromium probably exists as the moderately mobile chromate ion, (CrO_4^{2-}). The presence of chromium enrichment in nickel gossans indicates therefore that the metal has probably been transported into the oxide zone from an external source in this form.

The principal source available is the mafic to ultramafic silicates that typically invest the ore zones of these deposits. Further, statistical data generated in the present study indicate that significant positive correlation typically exists between chromium and silica in nickel gossans. The inference is therefore that chromium is co-evally released from host silicate as a result of lateratisation and that it passes into the oxide zone with silica.

The observed statistical correlation also infers that chromium is brought out of solution as a result of silica deposition. No data are currently available on the mechanism involved in this phenomenon. However, as the silica is characteristically present as aggregates of near colloidal sized particles, surface adsorption would appear to be more likely involved than direct co-precipitation.

The relative proximity of leaching sulphides during silica deposition, (Fig.8.4.2.), may however also contribute to chromium deposition. This is because the mildly acid environment associated with the basal oxide zone would probably cause the chemical destabilisation of chromate ion, bringing it out of solution independently

457

Fig. 8.4.3. Silicon and Chromium Distributions in the Pikwe Gossan Profile
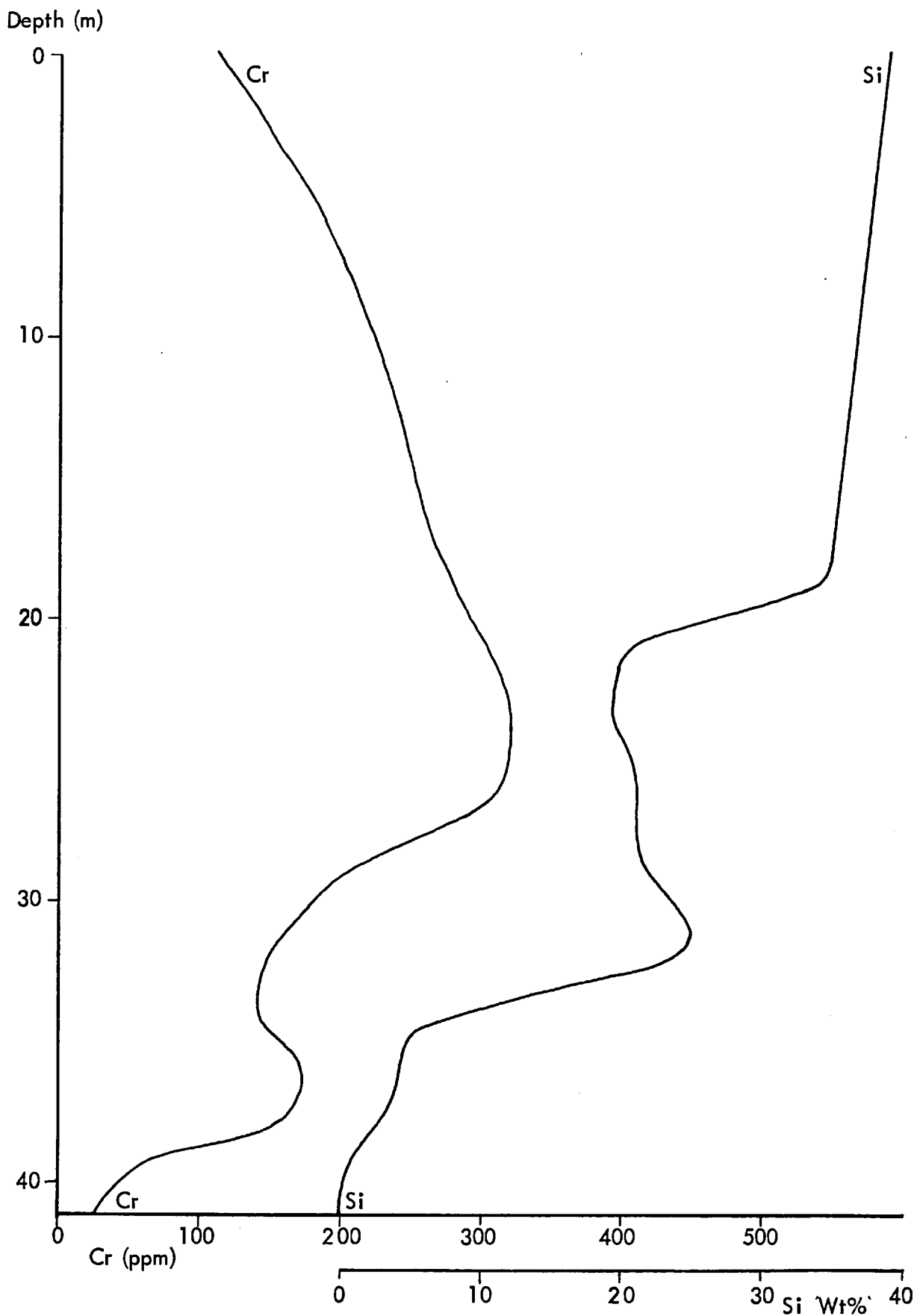
of any silica precipitation.

Oxide zone profiles of silicon and chromium are currently available for Pikwe,
(Fig.8.4.3., this study), and for Agnew (W.A.), (Nickel et.al.,1977,op.cit.).The
Agnew data show a very close semi-quantitative relationship, with silicon and
chromium contents, (Wt% units), decreasing progressively from surface down to the
present water table.

This feature infers that leaching of both elements from adjacent ultramafic progress-
ively decreased as a result of the postulated gradual (late Tertiary) cessation of
laterite formation. The closely sympathetic relationship also strongly implies
however that chromium fixation was chiefly due to the scaveging effects of silica
precipitation.

The relationship of chromium to silicon in the Pikwe oxide profile is however
rather more erratic, (Fig.8.4.3.). The two elements show an apparent divergence
in the top 20 metres of the profile. But exhibit a generally sympathetic variation
in the bottom 20 metres. This feature may indicate a rather heterogenous chromium
distribution in the parent host silicates, which, in turn give rise to a variable
content of aqueous chromium in the groundwaters bathing the developing oxide zone.

It may be however that the relationship in the top half of the profile infers that
pH destabilisation of chromate ion was more prevalent during the initial waning
of lateratisation at Pikwe.Whereas the subsequent greater importance of silica ex-
solution as a chromium fixant during the latter stages of profile silification is
manifested by the distribution patterns of the bottom 20 metres.

Goethite dehydration

The dehydration of goethite to hematite observed in a number of the study deposits,
(section 8.2), indicates that goethite is unstable with respect to the latter mineral
in the near-surface environment. Berner, (1969), has shown that this relationship
is supported by thermodynamic considerations in that the free energy change in-
volved in the reaction is negative in character. Secondary hematite formation in
nickel gossans is therefore indicative of the essential metastability of typically
first-formed (hydrous) goethite.

Present data indicate that goethite alteration generally occurs at relatively shallow
depths in the oxide zone, (section 8.2). From this it can be inferred that a consider-

able time lag – of the order of several million years at least, is generally required for the stable hematite phase to begin forming. However, secondary hematite formation at Pikwe is initiated in the basal levels of the oxide profile, (section 3.2). This divergence of behaviour is probably explained by the numerous potential nucleation loci provided by the significant quantities of primary hematite present in this deposit.

The generally slow goethite conversion rate inferred in the majority of sampled oxide zones implies therefore that these rocks never become hematite-rich during their slow exhumation from water table to surface outcrop. In contrast, the primary mineralogical characteristics of the Pikwe basal oxide zone imply that the lower levels of this profile will have been substantially converted into a hematite-rich or even a monominerallic hematite assemblage by the time that they eventually break surface.

8.5 Summary of conclusions

Present work on the interpretation of observed oxide zone phenomena in terms of nickel gossan genesis has yielded the following results:

One) The precipitation of specific iron oxide phases at the water table is probably related to the quantity of free ferric species present in solution.

Two) In consequence, iron oxide formation is indirectly related to the Eh of the immediate environment, with likely values of +0.35 Volts or higher inferred for the water table zone.

Three) The interpreted formation environments of associated oxidate minerals indicate that the pH of gossan formation is largely modified by wall rock reaction, and ranges from moderately acid, (carbonate-rich host silicate), to strongly acid, (carbonate-poor host silicate).

Four) Considerable quantities of aqueous ore metals are available for incorporation in these oxidate phases.

Parallel work on the implications of post-formation oxide zone phenomena for the subsequent maturation of nickel gossans indicates the following:

One) The typical occurrence of silica enrichment in present-day nickel gossan profiles can be explained by a simple development model which relates silica influx to the slow progressive formation of the oxide zone

above the dry season water table associated with active lateratisation of adjacent silicates.

Two)   The observed content and textural distributions of silica in the Pikwe oxide zone profile can be explained in terms of a general cessation of laterite formation in the late Tertiary that was coupled with a concommitant progressive onset of semi-arid climatic conditions.

Three)   A parallel enrichment of chromium in nickel gossans is due to the mobilisation of this element during the moderately alkaline oxidising conditions associated with the lateratisation of typically ultramafic host silicates.

Four)   Chromium is subsequently immobilised in the oxide zone by surface adsorption on precipitating silica and/or by chemical destabilisation of its mobile aqueous species within the relatively low pH environment of the newly-formed iron oxide assemblage.

Five)   Significant dehydration of (metastable) primary goethite to secondary hematite does not generally occur within the oxide zone profile unless primary hematite is available as a nucleation locus.

PART THREE

THE EVALUATION OF NICKEL GOSSANS IN MINERAL EXPLORATION

CHAPTER NINE

THE USE OF MINERALOGY IN THE RECOGNITION
AND SULPHIDE POTENTIAL EVALUATION OF
NICKEL GOSSANS

9.1. INTRODUCTION

The third major part of the present work deals with the utilisation of surface gossan characteristics in the evaluation of buried nickel sulphide ore. It commences with Chapter Nine, which gives the results of work on the application of mineralogy to the recognition of nickel gossan outcrops, and to the subsequent evaluation of these rocks in terms of their underlying parent sulphide mineralisation.

Chapter Nine is divided into two major parts. Section 9.2. presents the results of a study in which oxidate mineral characteristics are utilised in the recognition of nickel gossan outcrops. Section 9.3. subsequently details a new statistics-based evaluation technique in which nickel gossan bulk mineralogy is used to predict the mean economic metal contents of underlying sulphide ore.

Chapter Nine ends with a brief summary of conclusions, (section 9.4).

9.2. THE USE OF OXIDATE MINERALS IN NICKEL GOSSAN RECOGNITION

The use of oxidate minerals in the recognition of nickel gossan outcrops is now described. The origin, distribution and genetic significance of oxidate minerals associated with nickel gossans has already been indicated in the relevant parts of Chapters Three, Six and Eight, to which the interested reader is referred.

In summary, oxidate minerals form as precipitates from groundwater solutions that are rich in chemical species released as a result of near-surface weathering processes. In sulphide mineralisation environments, these species include ore metals released as a direct result of sulphide leaching. Recognition of oxidate minerals associated with possible nickel gossans, together with interpretation of the most likely provenence of their major and minor chemical components may, hence, provide initial evidence of the presence of underlying sulphide mineralisation prior to the initiation of a more detailed outcrop investigation programme.

The present study documents the principal features of those oxidate minerals that occur in the surface gossan material of the study suite. Further, it indicates how the presence of these phenomena may be interpreted as gossan recognition criteria.

The section of each mineral commences with an indication of its qualitative inter-deposit distribution. This is followed by a brief genetic interpretation of the corresponding trace metal geochemistry.

Recognition criteria for field use are subsequently indicated. These include textural features, and the use of mineral body colours both as mineral indentifiers and as indicators of ore metal concentration, where such features are present. Simple chemical tests are then indicated by which visually similar minerals, (viz.carbonates) may be differentiated. Chemical tests for the detection of the principal ore metals nickel and copper are then given.

Confirmatory tests for both mineralogy and geochemistry are indicated where these are either necessary or advisable in order to characterise the mineral or to quantify its ore metal content.

Magnesite

Oxidate magnesite has been observed in the surface gossans of two deposits in the study suite - Dordie North and Widgiemooltha No.3, (both from Western Australia).

Table A2/2 , (Appendix Two) demonstrates that considerable inter-sample variation characterises the geochemistry of oxidate magnesite. In this respect, iron, calcium and aluminium, together with nickel and the other ore metals substitute directly for magnesium in varying proportions in each of the samples. The extent and variability of this substitution can be observed in the summary of surface magnesite chemistry presented in Table 9.2.1.

A comparison of available data on the ore metal contents of magnesites from non-mineralised environments, (Dana, op. cit.) , and those associated with nickel gossans, indicate that the latter contain anomalously high levels of these metals. A proportion of this ore metal component may, however, be derived from the weathering of adjacent ultramafic rocks, as these may contain up to 2400 ppm nickel, (De Waal, 1976), and considerable quantities of copper, cobalt and manganese, (Hawkes and Webb, op.cit.). These considerations are particularly important since the major chemical components of oxidate magnesite, (magnesium and carbonate radical), are almost certainly derived from weathering of adjacent ultramafic silicate rocks.

It seems unlikely however that the concentration levels of ore metals indicated in Table 9.2.1. could be derived solely as a result of host serpentinite weathering because of the gross silicate degradation and subsequent metal concentration that such an origin would require . It is therefore thought more reasonable to consider that a substantial proportion of the ore metal complement of these oxidate surface magnesites originates either directly or indirectly as components of underlying nickel sulphide ore. In consequence, it is important to be able to identify oxidate magnesite associated with possible nickel gossans, and to obtain semi-quantitative indications of its ore metal content in order that the significance of its presence can be fully realised.

Table A2/2 , (Appendix Two), indicates that oxidate magnesite occurs as either joint surface coverings or as veinlets in gossan material. Identification of individual oxidate minerals in the hand specimen is, however, generally difficult because of the characteristic fine-grained habit of the mineral in these textural forms. Simple chemical tests are therefore utilised in order to make initial indications of the nature of individual specimens prior to confirmatory analysis using standard X-Ray powder diffraction techniques. Suspected carbonates are identified using the Alizarin Red staining technique devised by Warne (1962). Oxidate magnesite samples are readily recognised by this means.

The ore metal content of magnesite - importantly the nickel content, is noted to be semi-quantitatively related to the body colour of the sample. In this respect, a scan of the relevant data in Table A2/2 , (Appendix Two), indicates that magnesites containing less than about five mole percent nickel generally possess body colours within the range white to buff. Whereas, those containing higher nickel contents are more typically greenish in colour.

Positive indentification of magnesite nickel contents below about five percent cannot therefore be made by visual inspection alone. However, if enough material is available, the qualitative presence of both nickel and copper may be respectively indicated by Dimethyl-glyoxime and Cupron tests upon suitable solutions of the specimen. Confirmation and quantification of these results can, if necessary, be obtained by subsequent analysis of the magnesite sample by Atomic Absorption Spectroscopy.

Bearing in mind the proviso about mixed ore metal provenences, it is apparent that the identification at outcrop of ore metal-rich oxidate magnesites by simple chemical techniques provides a rapid field method for the recognition of probable nickel

Table 9.2.1. Simple Statistics : Surface magnesite chemistry

N = 6 Metal	Mean $\bar{X}$ (WT%)	Standard Dev. S	Coeff. of Variation $S/\bar{X}$	Std. Error of Mean $S/\sqrt{N}$	Min. Value (WT%)	Max. Value (WT%)	Range
Ca	1.197	1.040	0.868	0.424	0.500	3.000	2.500
Mg	18.045	7.040	0.390	2.874	7.000	26.000	19.000
Fe	8.713	4.272	0.490	1.744	3.920	14.000	10.080
Al	1.150	1.161	1.009	0.474	0.100	2.300	2.200
Ni	4.593	5.240	1.141	2.139	0.480	13.680	13.200
Cu	0.345	0.288	0.835	0.118	0.130	0.760	0.630
Co	0.121	0.163	1.350	0.067	0.001	0.400	0.399
Mn	0.081	0.055	0.680	0.022	0.008	0.150	0.142
Cr	0.176	0.183	1.035	0.075	0.028	0.500	0.472
Zn	0.021	0.016	0.793	0.007	0.003	0.044	0.041

Table 9.2.2. Simple Statistics : Surface calcite chemistry

N = 9 Metal	Mean $\bar{X}$ (WT%)	Standard Dev. S	Coeff. of Variation $S/\bar{X}$	Std. Error of Mean $S/\sqrt{N}$	Min. Value (WT%)	Max. Value (WT%)	Range
Ca	34.037	3.426	0.400	1.142	30.969	39.960	8.991
Mg	2.423	1.779	0.734	0.593	1.000	6.625	5.625
Fe	3.675	1.597	0.435	0.532	1.400	6.000	4.600
Al	1.874	1.561	0.833	0.520	1.000	5.000	4.000
Ni	0.205	0.153	0.747	0.051	0.047	0.433	0.386
Cu	0.076	0.055	0.728	0.081	0.030	0.196	0.166
Co	0.021	0.037	1.703	0.012	0.001	0.100	0.099
Mn	0.058	0.028	0.480	0.009	0.025	0.100	0.075
Cr	0.225	0.150	0.669	0.050	0.006	0.500	0.494
Zn	0.034	0.028	0.827	0.009	0.003	0.093	0.090

gossans during detailed outcrop assessment programmes.

Calcite

Oxidate calcite has been recognised in the surface gossans of ten sampled nickel sulphide deposits; nine in Western Australia and one in southern Africa, (Table A2/3 ,Appendix Two).

The summary chemical data of nine specimens of surface calcite, (Table 9.2.2.), indicate that extensive, though variable, substitution of calcium by other metals typifies oxidate calcites associated with nickel gossans. In this respect, iron, magnesium and aluminium all replace calcium in significant quantities. More importantly however, the ore metals – particularly nickel, also substitute for calcium to some extent.

The indicated ore metal contents of sampled oxidate calcites are not large in absolute terms, but they are anomalous relative to those associated with calcites from un-mineralised environments, (Dana,p152, op.cit.). The incidence of anomalously high quantities of ore metals, (chiefly nickel) in oxidate calcites associated with nickel gossans is hence useful as a likely qualitative indicator of proximal buried sulphide mineralisation. Similar provenence considerations apply to calcite as to magnesite, however, as the calcium and carbonate components of the former mineral are similarly derived from the weathering of adjacent ultramafic silicate rocks that may themselves contain appreciable quantities of 'ore' metals.

Table A2/3 , (Appendix Two) indicates that oxidate calcite typically occurs as a surficial covering on nickel gossans. The mineral is however very difficult to identify positively in the hand specimen due to its characteristic fine-grained crystal habit. It is though readily characterised using the Warne carbonate staining scheme. Alternatively, or in addition, an X-Ray diffraction analysis of the mineral identifies it with certainty.

The use of anomalous body colour to identify high nickel concentrations is not possible with oxidate calcite because of the low absolute contents of nickel within the mineral lattice, (Table 9.2.2.). Qualitative identification of nickel and copper can however be made by the reaction of suitably prepared material with specific metal indicating reagents. Further, these results may subsequently be confirmed and quantified, if required, by A.A. analysis of the calcite sample.

The above results together indicate that calcite is not as straightforward an indicator

of probable nickel sulphide mineralisation as is magnesite. The relevant data do demonstrate however that calcite has a more extensive qualitative occurrence in surface nickel gossans than magnesite and, hence, its use is probably of more widespread applicability in this respect than that of the magnesium carbonate.

Dolomite

Oxidate dolomite has been identified in the surface gossans of four nickel sulphide deposits - all from Western Australia, (Table A2/4 , Appendix Two). Reliable chemical data are available though, from only two specimens, (Table 9.2.3.). These data infer that the ore metal contents of oxidate surface dolomite associated with nickel gossan outcrops is anomalously high compared to that from un-mineralised localities, (Dana, p212, op.cit.).

This anomalous ore metal geochemistry hence implies the likely presence, subject to the established provenence considerations, of underlying nickel sulphide mineralisation.

Table A2/4 , (Appendix Two) shows that oxidate dolomite typically occurs as joint plane or surface coverings in the host gossans. In practice however, the identification of the mineral in hand specimen is generally hampered by its typically small grain size. Dolomite is easily recognised though, using the Warne staining technique.

Oxidate dolomite displays a tendency to be pinkish in colour - a feature that may aid initial identification, (Table A2/4 , Appendix Two), but which sometimes is also shown by oxidate calcite, (Table A2/3 ,Appendix Two). The distinct lack of green colouration in sampled surface dolomites, (cf. deep samples), is, though, a primary indication that these minerals contain relatively low, (?$\leqslant$5 mol%), quantities of nickel.

The treatment of solutions of suitable material with Dimethyl-glyoxime and Cupron reagents however typically yield positive results for (respectively) nickel and copper, and these data therefore indicate that the two base metals are definitely present in anomalous concentrations in surface oxidate dolomite. This result thus allows a positive inference to be made concerning the likely presence of buried sulphide ore.

Calcite/Dolomite composite mixtures

Composite mixtures of oxidate calcite and dolomite are observed in the surface gossan material from five (Western Australian) study deposits, (Table A2/5 ,

Table 9.2.3. Simple Statistics : Surface dolomite chemistry

N =2 Metal	Mean $\bar{X}$ (WT%)	Standard Dev. S	Coeff. of Variation $S/\bar{X}$	Std. Error of Mean $S/\sqrt{N}$	Min. Value (WT%)	Max. Value (WT%)	Range
Ca	12.000	5.000	0.417	3.536	9.500	14.500	5.000
Mg	9.750	3.500	0.359	2.475	8.000	11.500	3.500
Fe	5.550	-	-	-	5.550	5.550	-
Al	1.000	-	-	-	1.000	1.000	-
Ni	0.538	0.875	1.628	0.619	0.100	0.975	0.875
Cu	0.482	0.637	1.322	0.450	0.163	0.800	0.637
Co	0.063	0.124	1.968	0.088	0.001	0.125	0.124
Mn	0.237	0.275	1.158	0.194	0.100	0.375	0.275
Cr	0.300	0.400	1.333	0.283	0.100	0.500	0.400
Zn	0.024	0.012	0.500	0.008	0.018	0.030	0.012

Table 9.2.4. Simple Statistics : Surface calcite/dolomite chemistry

N = 2 Metal	Mean $\bar{X}$ (WT%)	Standard Dev. S	Coeff. of Variation $S/\bar{X}$	Std. Error of Mean $S/\sqrt{N}$	Min. Value (WT%)	Max. Value (WT%)	Range
Ca	19.900	8.600	0.432	6.081	15.600	24.200	8.600
Mg	7.795	2.830	0.363	2.001	6.380	9.210	2.830
Fe	2.760	1.120	0.406	0.792	2.200	3.320	1.120
Al	1.036	0.928	0.896	0.656	0.572	1.500	0.928
Ni	0.139	0.087	0.624	0.062	0.096	0.183	0.087
Cu	0.079	0.036	0.456	0.025	0.061	0.097	0.036
Co	0.014	0.006	0.429	0.004	0.011	0.017	0.006
Mn	0.026	0.014	0.539	0.010	0.019	0.033	0.014
Cr	0.073	0.121	1.669	0.086	0.012	0.133	0.121
Zn	0.006	0.004	0.667	0.003	0.004	0.008	0.004

Appendix Two). Available chemical data, (Table 9.2.4.), indicate that these carbonate mixtures exhibit anomalously high ore metal contents, even though such values are low in absolute terms. Further, from lattice substitution considerations, it is likely that much of this ore metal component is substituted for magnesium in the dolomite portion of each composite mixture, and it is hence probable that the ore metal content due to dolomite is effectively 'diluted' by the calcite component of the mixture.

In practice, the presence of an intimate fine-grained mixture of the two carbonates renders qualitative identification in the hand specimen very difficult. The existence of at least the dolomite component may however by initially suspected as all mixtures sampled during the present work are pinkish in hue, (Table A2/5 , Appendix Two). Further, the Warne staining technique is not definitive for calcite-dolomite mixtures because only calcite stains with Alizarin Red S. Calcite-dolomite mixtures are therefore difficult both to identify and to resolve unless X-Ray powder patterns are made. These mixtures are consequently of less value than single carbonates as field indicators of likely nickel gossans. A qualitative indication of the presence of both nickel and copper is obtainable though from such composites using the indicated standard test reagents.

9.3. THE PREDICTION OF METAL CONTENTS OF NICKEL SULPHIDE ORES FROM THE BULK MINERALOGY OF THEIR CORRESPONDING SURFACE GOSSANS

Introduction

A new statistics-based technique is now described in which the sampled mean bulk mineral compositions of nickel gossan outcrops are used to predict the ore metal contents of underlying parent sulphide mineralisation.

The exposition commences with a preliminary summary, in geological terms, of the statistical relations of the individual mineralogical variables measured within the gossans making up the study suite. The statistical relations of these variables to the geochemistry of nickel gossans are then briefly stated.

The objective of this initial study is to indicate both the statistical and the geological basis on which the final evaluation technique is founded. The work then continues with a brief description of the devised evaluation technique. This is followed by

summary descriptions of the several ways in which the technique is applied to the problems of nickel sulphide ore evaluation.

The bulk mineralogy of nickel gossans

The bulk mineralogy of nickel gossans comprises goethite, silica and hematite, although observed void content was additionally used in the present study. These data were obtained from a visual estimation of the mineral proportions present within individual polished sections of gossan material. The accuracy of this technique, (between 90 and 95 relative percent), was subsequently checked by point counting on a ten percent random sample drawn from the combined suite of 151 gossans.

The mutual statistical relations of bulk mineralogy in nickel gossans

The Pearson correlation matrix for the combined suite of Australian and African gossans samples, (Fig.9.3.1.), indicates that the bulk mineralogy of these rocks exhibits several distinctive features. In this respect, goethite content exhibits significant negative statistical correlations with both silica and hematite contents, and similar relations are noted between hematite and silica content, and between silica and void content.

The relationship between bulk mineralogy and geochemistry in nickel gossans

The likely distribution of major and minor elements – particularly ore metals, across the bulk mineral assemblage of nickel gossans is now briefly indicated. This work is based on the statistical relationships observed in the correlation matrix comprising Fig.9.3.1. It provides the necessary geological framework on which any evaluation of gossan mineralogy in terms of sulphide ore metal contents must properly be based. This is because the geochemistries of nickel sulphide ores and of their equivalent gossans are directly linked, (section 6.4).

Fig.9.3.1. indicates that several economically-important metals exhibit significant positive statistical correlations with the goethite content of nickel gossans. Each of these metals hence varies sympathetically with goethite content across the study suite of gossans, and it is therefore probable that each metal is primarily associated with this iron oxide in these rocks.

FIG. 9.3.1. CORRELATION MATRIX FOR THE COMBINED GOSSAN SUITE

Sample size = 151

Critical value for (r) is ± .150 at the 95% confidence level and with 149 degrees of freedom (d.f.)

	Fe	Si	Ni	Cu	Mn	Cr	Co	Ti	GOE	HEM	SILICA	VOIDS
GOE	.420	-.455	.318	.156	(.074)	.180	.344	(0.000)	1.000			
HEM	.405	-.373	-.211	(.086)	(-.128)	-.185	-.212	(.037)	-.436	1.000		
SILICA	-.912	.942	-.151	-.208	(-.026)	(.029)	-.244	(-.049)	-.549	-.355	1.000	
VOIDS	.228	-.222	(.063)	(-.047)	(.142)	(-.099)	.199	(-.003)	-.151	(-.082)	-.219	1.000

The significant negative statistical correlation noted between silica and the ore metals nickel, copper and cobalt, (Fig.9.3.1.), has no real geological basis. It occurs simply because iron and silica contents exhibit a strong, geologically demonstrable, antipathetic relationship in nickel gossans and the three ore metals show significant positive statistical and geological correlations with iron content in these rocks.

The evaluation of nickel gossan mineralogy in terms of sulphide metal content: a statistical study

Introduction

The results of the above statistical correlation study indicate that the economically important trace metals nickel, copper and cobalt are preferentially associated with goethite in nickel gossans. Further, the petrographic observation of commonly preserved pseudomorphic and boxwork structures in goethite after parent violarite and chalcopyrite strongly implies that substantial proportions of these elements are likely associated with these textural phenomena.

The formation and presence of relic violarite and chalcopyrite structures in nickel gossans hence provides an important physico-chemical link between the geochemistry of nickel sulphide ores and the bulk mineralogy of their overlying oxide zones and gossans. It is this relationship which provides the geological framework on which any statistical method devised to predict sulphide ore metal contents from gossan bulk mineralogy is likely to be based.

In the present study, the statistical relations that exist between gossan bulk mineralogy and sulphide metal contents are investigated using the technique of multiple linear regression analysis, (Koch and Link, 1971, p.87). The method examines how a single (dependent) variable is related to a number of other (independent) variables, and performs a regression of the specified dependent variable on the independent variable set in order to quantify the statistical relationship that exists between them.

In fact, the method produces a linear regression equation in the independent variables which gives the best "least-square" regression of the dependent variable on these parameters. This linear regression equation hence provides a measure by which the independent variables can be used to predict the value of the corresponding dependent variable.

For the present investigation, a data matrix was erected in which four independent variables were initially utilised. These correspond to the mean values of the four indicated mineralogical variables for a number of nickel gossan occurrences. The dependent variable corresponding to these data was then set up, and comprised the mean metal values (defined below) of the sulphide ore corresponding to each of these specific nickel gossans. In this way a linear regression function was produced by which nickel gossan bulk mineralogical data could be used to predict the corresponding mean nickel or copper contents of parent sulphide ore for a suite of nickel sulphide deposits.

In practice the data set is run initially in a step-wise multiple linear regression computer programme in order to determine which independent variables are statistically significant with respect to the specific dependent variable under consideration. The results of this preliminary run are then assessed and the data set run on a single-step regression analysis programme in order to obtain the best fitting linear regression (predictor) equation for that particular dependent variable.

The derived equation is then used to predict the values of the dependent variable for each of the deposits comprising the test data set. The closeness of the actual and predicted values of the   dependent variable in individual deposits in the test set hence provides an empirical measure of the overall accuracy of the derived predictor equation.

In addition though, an independent assessment of the predictive accuracy of the derived equation is made by comparison of the real and computed values of the specific dependent variable for several deposits that were not used in the derivation of the original equation.

Four measures of sulphide metal contents are used as dependent variables in the present study; firstly, the mean nickel or copper content of analysed near-massive to massive sulphide ore; and, secondly, the overall mean contents of these metals within the orebody as indicated by published nickel and copper grade data.

Four different dependent variables are hence utilised and the mineralogical evaluation study consequently consists of four separate sub-studies. The same four independent (gossan mineralogical) variables are however used throughout the study, even though the composition of the test data set varies between sub-studies.

The results of the four evaluation sub-studies are now described in turn.

The prediction of massive sulphide mean nickel contents

The equation of best fit derived from the linear regression of mean massive sulphide nickel content on an optimum combination of independent (gossan) variables is presented in Fig.9.3.2A. The expression indicates that the best overall prediction of mean sulphide nickel values for the test set is achieved by a linear combination of functions involving mean goethite and mean silica contents. In addition, the accompanying analysis of variance data and F-statistic test indicate that the equation explains a significant proportion of the variability of the original data with approximately 90 percent confidence. Further, the associated coefficient of determination (R^2) value indicates that this proportion is about 52 percent of the total variability exhibited.

An analysis of residuals and relative percentage differences derived from the comparison of actual and predicted mean sulphide nickel values for each of the ten member deposits in the test set is presented in Fig.9.3.2B. These data indicate that the predictive accuracy of the derived equation varies considerably across the test set. It also demonstrates however that, overall, the mean sulphide nickel contents of all the test deposits are predicted to within about 25 percent of their actual values with about 90 percent confidence.

The maximum and minimum values indicated in the percentage difference column represent the 95 percent confidence precision limits of the predicted sulphide nickel content value. For each deposit, the simple statistics of goethite and silica data in the parent gossan sample set are used to compute the corresponding maximum and minimum expected mean goethite and mean silica values. The respective mean and standard error of the mean data are used in this work, (section 10.3). These data are then run through the sulphide nickel predictor equation and the equivalent extreme values of sulphide nickel mean content that correspond to the 95 percent confidence precision level range are computed.

An independent assessment of the accuracy of the derived predictor equation is presented in Fig.9.3.2C. This evaluation consists of an analysis of residuals arising from the computation of predicted sulphide nickel mean contents for three deposits that were not part of the original test set of ten. The mean sulphide nickel contents of all three deposits are known and the computation of their corresponding predicted values therefore provides an unbiased independent estimate of the accuracy of the derived predictor equation. Further, the indicated maximum and minimum percentage difference data represent the 95 percent confidence precision range of

Fig.9.3.2. Results of the Sulphide Nickel Tenor Prediction Study

A THE DERIVED PREDICTOR EQUATION

Mean Ni tenor = 0.377 + 0.054 mean goethite content + 0.022 mean silica content

Vol % units
Tenor data = Wt%

The corresponding analysis of variance and F test data

Source of variation	d.f.	Sum of Squares	Mean Squares	F Value	F-Statistic at 90% C.L
Due to regression	2	3.50225	1.75112	3.7434	3.2574
Deviation from regression	7	3.27451	0.46779		
Total	9	6.77676			

Proportion of total variation explained by the equation (R^2) = 0.5168

B AN ANALYSIS OF TEST SET RESIDUALS

Deposit	Observed Mean Value (WT%)	Predicted Mean Value (WT%)	Residual	Accuracy (Rel %)	Precision Range at 95% C.L.
Pikwe	2.45	2.66	+ 0.21	+ 8.6	26.5
Perserverance	2.30	2.61	+ 0.31	+ 13.5	53.9
Munali	3.11	3.13	+ 0.02	+ 0.6	46.4
Phoenix	4.93	3.71	- 1.22	- 24.8	29.4
Selkirk	2.49	2.57	+ 0.08	+ 3.2	52.2
Jan Shoot	3.45	3.32	- 0.13	- 3.8	42.3
Mt. Monger	3.76	3.12	- 0.64	- 17.0	22.6
McMahon	3.93	3.78	- 0.15	- 3.8	25.9
Ravensthorpe 5	2.50	3.42	+ 0.92	+ 36.8	30.0
Spargoville 5A	3.96	4.56	+ 0.60	+ 15.2	18.9

C AN INDEPENDENT ASSESSMENT OF PREDICTIVE ACCURACY

Deposit	Observed Mean Value (WT%)	Predicted Mean Value (WT%)	Residual	Accuracy (Rel %)	Precision Range at 95% C.L.
Trojan	2.82	3.87	+ 1.05	+ 37.2	81.5
Mt. Edwards	3.52	3.89	+ 0.37	+ 10.5	23.6
SLOB/Lunnon Shoot	4.40	4.42	+ 0.02	+ 0.5	45.4

ESTIMATED WORKING ACCURACY OF THE EQUATION = $\pm$ 30% AT 90% C.L.

the predicted sulphide nickel mean content values.

The above results indicate that the absolute predictive accuracy of the derived equation varies considerably between the three deposits. On the basis of the indicated results however, it seems likely that the predictor equation has on estimated overall accuracy of about $\pm$ 30 percent at the 90 percent confidence level.

The likely precision level of results computed by the predictor equation cannot however be ignored in any realistic assessment of the latters overall applicability to sulphide evaluation work. In the present instance, this quantity is estimated by averaging the 95 percent confidence precision values of the test set deposits, and computes as $\pm$ 38 percent (at the 95 percent confidence level).

Thus estimated accuracy and precision levels of $\pm$ 30 percent and 35 percent respectively are associated with the predicted nickel content values of any nickel deposit whose gossan mineralogical data are run through the predictor equation. The relative positions of the computed accuracy and precision values and of their related probability ranges will, however, be unknown for all deposits not involved in the original test suite.

Two extreme conditions are possible in the latter instance. At one extreme, that of complete superposition, the mean predicted value will correspond exactly with the mean observed value, and a combined accuracy/precision working range of $\pm$ 38 percent will be applicable. Alternatively, the occurrence of the mean predicted value at either end of the accuracy range will cause the ranges of the two parameters to add algebraically and will result in a combined working range of $\pm$ (30 + 38) or 68 percent.

The actual combined closeness fit or predictability value for a given deposit will hence lie at some definite, but undeterminable position between these two extreme cases.

The prediction of massive sulphide mean copper contents

A statistical study involving the prediction of massive sulphide mean copper contents from nickel gossan bulk mineralogy is now presented. This work similarly involves the derivation of a linear regression (predictor) equation based on a test set of sample deposits. In the present study however, the equation that was initially derived from a test suite of 13 available deposits was not good enough to give acceptably accurate results at any reasonable level of confidence.

Fig.9.3.3. Results of the High Sulphide Copper Tenor Prediction Study

A   THE DERIVED PREDICTOR EQUATION

Mean Cu tenor = 2.340 − 0.013 mean Silica content

Volume % units
Tenor data = Wt %

The corresponding analysis of variance and F test data

Source of variation	d.f.	Sum of Squares	Mean Squares	F Value	F–Statistic at 90% C.L
Due to regression	1	0.44039	0.44039	3.3692	5.5383
Deviation from regression	3	0.39213	0.13071		
Total	4	0.83252			

Proportion of total variation explained by the equation $(R^2) = 0.5290$

B   AN ANALYSIS OF TEST SET RESIDUALS

Deposit	Observed Mean Value (WT%)	Predicted Mean Value (WT%)	Residual	Accuracy (Rel %)	Precision Range at 95% C.L.
Phoenix	2.57	2.33	− 0.24	− 9.3	0.4
Selkirk	2.00	2.18	+ 0.18	+ 9.0	5.0
Jan Shoot	1.96	1.55	− 0.41	− 20.9	9.7
S.L.O.B. / Lunnon Shoot	1.64	1.78	+ 0.14	+ 8.5	22.0
Perserverance	1.35	1.69	+ 0.34	+ 25.2	21.5

C   AN INDEPENDENT ASSESSMENT OF PREDICTIVE ACCURACY

Deposit	Observed Mean Value (WT%)	Predicted Mean Value (WT%)	Residual	Accuracy (Rel %)	Precision Range at 95% C.L.
Pikwe	2.26	1.83	− 0.43	− 19.0	5.7

ESTIMATED WORKING ACCURACY OF THE EQUATION = $\pm$ 25 % AT 90% C.L.

In consequence, the test suite was split into two sub-suites based on observed sulphide copper content. Two deposits were however randomly removed from the combined suite prior to this treatment in order to provide some degree of independent assessment of the derived predictor equations.

The designated 'high-copper' evaluation sub-suite consists of five deposits. These have massive sulphide mean copper contents that range from 1.35 percent to 2.57 percent.

The derived 'high-copper' predictor equation is presented in Fig.9.3.3A. The function indicates that mean silica content is the only significant gossan variable involved in the regression equation, which, by the results of the corresponding analysis of variance computation provides an only relatively poor statistical fit to the original data. This lack of fit is at least partly due to the low number of deposits present in the high-copper sub-suite. The value of the corresponding determination coefficient indicates however, that the equation accounts for nearly 53 percent of the total variability exhibited by the original data.

The corresponding analysis of residuals for the high copper sub-set, (Fig.9.3.3B.), also reflects the relatively poor statistical fit of the equation. The related mean percent difference values of the test deposits indicate though that the high copper equation is accurate to within ± 25 percent at about the 90 percent confidence level. This accuracy level is supported by the result of the independent assessment of the Pikwe deposit that is set out in Fig.9.3.3C.

The overall mean precision of the predicted sulphide copper mean content values is computed from the extreme range data presented in the percent difference column. It is estimated as about ± 10.5 percent at the 95 percent confidence level. The corresponding overall working predictability value for the high copper equation is, hence ± 35 percent at the 90 percent level of confidence.

The low copper evaluation sub-suite is composed of six deposits. These have massive sulphide mean copper contents that range from 1900 ppm to 7700 ppm.

The derived predictor equation for the low copper sub-suite further demonstrates this significant inter-suite difference in quantitative gossan mineralogy as mean void content is the sole mineralogical variable expressed in the linear regression function, (Fig.9.3.4A.). As with the high copper case, the corresponding analysis of variance computation indicates that the low copper predictor equation provides only a relatively poor fit to the original input data. This point is further demonstrated b the relativel low value of the determination coefficient, '.4939).

Fig.9.3.4. Results of the Low Sulphide Copper Tenor Prediction Study

A   THE DERIVED PREDICTOR EQUATION

Mean Cu tenor = 0.635 - 0.012 mean void content

Vol % units
Tenor data = Wt%

The corresponding analysis of variance and F test data

Source of variation	d.f.	Sum of Squares	Mean Squares	F Value	F-Statistic at 90% C.L
Due to regression	1	0.12719	0.12719	3.9028	4.5448
Deviation from regression	4	0.13036	0.03259		
Total	5	0.25755			

Proportion of total variation explained by the equation $(R^2) = 0.4938$

B   AN ANALYSIS OF TEST SET RESIDUALS

Deposit	Observed Mean Value (WT%)	Predicted Mean Value (WT%)	Residual	Accuracy (Rel %)	Precision Range at 95% C.L.
Spargoville	0.77	0.59	- 0.18	- 23.4	1.3
Mt. Edwards	0.59	0.56	- 0.03	- 5.1	6.8
Ravensthorpe 5	0.34	0.15	- 0.19	- 55.9	50.0
Munali	0.31	0.40	+ 0.09	+ 29.0	32.3
McMahon	0.23	0.37	+ 0.14	+ 60.9	69.5
Trojan	0.19	0.37	+ 0.18	+ 94.7	26.4

C   AN INDEPENDENT ASSESSMENT OF PREDICTIVE ACCURACY

Deposit	Observed Mean Value (WT%)	Predicted Mean Value (WT%)	Residual	Accuracy (Rel %)	Precision Range at 95% C.L.
Mt. Monger	0.34	0.44	+ 0.10	+ 29.4	35.3

ESTIMATED WORKING ACCURACY OF THE EQUATION = $\pm$ 60 % AT 90% C.L.

The analysis of residuals for the low copper sub-suite is given in Fig.9.3.4B., and the mean percent difference data values indicate that a working accuracy of about ± 60 percent is associated with the low copper equation. The corresponding estimated mean precision of the predicted sulphide copper mean values is calculated from the maximum and minimum percent difference data on the combined test and independent deposit suites. Its value is ± 31.5 percent at the 95 percent confidence level. The overall closeness of prediction of the low copper equation is hence ± 90 percent at approximately the 90 percent confidence level.

This estimated range of workable predictability borders on the limit of practical usefulness, even though the mean copper content of Mt.Monger ore is correctly predicted to within 30 percent of its measured value by the low copper equation, (Fig.9.3.4C.).

The allocation of previously unclassified gossan data to the correct copper ore predictor equation is obviously necessary if the copper content of the equivalent ore is to be predicted with any accuracy. In practice, however, rational allocation of previously unclassified gossans to the correct equation is very difficult as even the approximate copper tenor of the corresponding ore is not known.

This problem has been at least partly overcome in the present study by the development of an allocation technique based on multivariate discriminant analysis, (Koch and Link, p102, op.cit.). By this means a linear function is derived which allows an unclassified gossan to be allocated to one or other of the copper evaluation equations on the basis of its mean bulk mineralogy. The discriminant function is itself derived from an analysis of the multivariate differences in mean gossan bulk mineralogy that exist between the two groups of deposits that separately comprise the high and low copper evaluation test sub-suites.

The allocation (discriminant) function derived from the copper test sub-suites is presented in Fig.9.3.5A. The value of the associated F - statistic shows that the function gives a significant separation of the two constituent multivariate (sub-suite) data clusters at the 95 percent level of confidence.

The indicated cutting grade is defined as that value of the derived function (L) that falls exactly halfway between the mean values of L for the two sub-suite data clusters. In the present instance this means that gossans that have a computed L value more positive than - 9.900   are allocated to the high copper predictor equation, and those with L values more negative than this figure are allocated to

Fig.9.3.5. Results of the Sulphide Copper Sub-set Allocation Study

A THE DERIVED ALLOCATION (DISCRIMINANT) FUNCTION

$L = -4.420 \log(\text{mean Goethite content}) - 0.833 \log(\text{mean Silica content})$
$- 1.559 \log(\text{mean Void content})$

All variables = Vol %

CUTTING GRADE, $L = -9.900$: Range $(L \pm 2.5\%) = -9.650$ to -10.150

MAHALANOBIS D^2 STATISTIC $= 9.0802$

F TEST : $F_{(3,7)} = 6.4204$; $F_{(3,7;0.05)} = 4.3468$

B THE ALLOCATION OF THE TEST SET

High Test Sub-Set L Scores	Low Test Sub-Set L Scores	High Sub-Set Deposit	Low Sub-Set Deposit
- 9.084		Selkirk	
- 9.284		Perserverance	
- 9.418		Jan Shoot	
- 9.589		Phoenix	
- 9.604		S.L.O.B. / Lunnon Shoot	
	- 9.929		Mt. Edwards
	- 10.189		Spargoville 5A
	- 10.225		Ravensthorpe 5
	- 10.283		Munali
	- 10.869		McMahon
	- 10.935		Trojan

C AN INDEPENDENT ASSESSMENT OF THE ALLOCATION FUNCTION

Deposit	Computed L Score	Allocated Predictor Equation	Known Correct Sub-Set Affinity
Pikwe	- 8.825	high	high sub-set
Mt. Monger	- 9.915	low	low sub-set

ESTIMATED MISALLOCATION RATE (at 95% C.L.) <5 percent

the low copper predictor equation.

It is highly unlikely however that this allocation procedure is totally accurate, and a certain proportion of unclassified gossans are likely to be misallocated as a result of its use. An empirical measure of the misallocation rate likely to be associated with the derived discriminant function can though be obtained by computation of the L scores of each member of the high and low copper sub-suites, (11 deposits), and by subsequent comparison of these values with that of the cutting grade.

The results, (Fig.9.3.5B.), indicate that the function correctly allocates all 11 deposits to their parent evaluation sub-suite. An empirical misallocation rate of no more than about five percent at approximately the 95 percent confidence level is hence deemed likely to be applicable in this instance.

A further (independent) measure of the accuracy of the allocation technique is demonstrated in Fig.9.3.5C. Here data from two deposits that were not part of either copper evaluation sub-suite are run through the discriminant function and the results tabulated. The results indicate that the Pikwe and Mt.Monger gossans are correctly assigned to the sub-set equation that best represents their actual mean sulphide copper contents.

Further to the above however, the misallocation of an unknown nickel gossan occurrence will almost certainly lead to a totally misleading ore copper content value being predicted for its parent sulphide. Under real conditions, therefore, the allocation method is better served is a zone of L-scores either side of the cutting grade is demarcated in order to indicate the presence of possible misclassified (borderline) gossans.

In the present study, this border zone is selected at $\pm$ 2.5 percent of the cutting grade value, i.e. from -9.65000 to -10.15000. Thus, under real conditions, both the Mt.Edwards and the Mt.Monger gossans, (Figs.9.3.5B. and 5C. respectively), would fall under suspicion of being possibly misallocated to the low copper sub-set. The results of the predicted copper ore contents for these two deposits would hence in an actual evaluation programme be treated more cautiously than would otherwise be generally necessary.

The prediction of overall nickel grade

Details of a statistical study involving the prediction of the overall nickel grade of an orebody from the bulk mineralogy of the overlying near-massive to massive gossan are now presented. The technique used in this study is exactly analogous to that employed in the prediction of massive sulphide nickel and copper mean contents. It differs only in the nature of the dependent (predicted) variable, which consists, in this instance, of the published nickel grade data for the eight individual deposits comprising the specific test suite.

The linear regression (nickel grade predictor) equation derived using the test set of eight deposits is presented in Fig.9.3.6A. The function indicates that mean gossan hematite content, and more importantly, mean gossan void content are significant variables in the prediction of sulphide nickel grade. Further, the accompanying analysis of variance results indicate that the equation explains about 60 percent of the total variability exhibited by the original data.

This relative poorness of fit of the derived equation is further illustrated in the associated analysis of residuals data set out in Fig.9.3.6B. These results infer that the equation is able to predict the overall nickel grade of a sulphide orebody from the bulk mineralogy of its equivalent surface gossan to within ± 50 percent with about 90 percent confidence.

This indicated level of accuracy is supported by the results of an independent assessment of the predictor equation based on two deposits, (Pikwe and Redross), that were randomly removed from the test suite before the equation was derived, (Fig.9.3.6C.).

The estimated overall precision of the mean predicted nickel grade value, as calculated from the percent difference maxima and minima of the combined test and independent deposit suite, is ± 50 percent at the 95 percent confidence level, (Fig.9.3.6C.). Hence the estimated range of workable predictability associated with the nickel grade equation, based on available data, is ± 100 percent. This is because, as previously indicated, the predictability value depends on the relative dispositions of the mean accuracy range associated with the equation and the precision range value computed from the test and independent deposits.

The significance of the mean nickel grade data for the four deposits in Table 9.3.1. must therefore be understood in this context. Hence, one may state that the mean nickel grade value predicted for each deposit lies within at least ± 50 percent of

Fig.9.3.6. Results of the Nickel Grade Prediction Study

A THE DERIVED PREDICTOR EQUATION

Ni grade = 3.326 - 0.030 mean Hematite content - 0.086 mean Void content

Vol % units
Tenor data = Wt%

The corresponding analysis of variance and F test data

Source of variation	d.f.	Sum of Squares	Mean Squares	F Value	F-Statistic at 90% C.L
Due to regression	2	5.48042	2.74021	3.6261	3.7797
Deviation from regression	5	3.77847	0.75569		
Total	7	9.25889			

Proportion of total variation explained by the equation $(R^2) = 0.5919$

B AN ANALYSIS OF TEST SET RESIDUALS

Deposit	Observed Mean Value (WT%)	Predicted Mean Value (WT%)	Residual	Accuracy (Rel %)	Precision Range at 95% C.L.
S.L.O.B./ Lunnon Shoot	4.29	3.11	- 1.18	- 27.5	3.0
Spargoville 5A	2.40	2.94	+ 0.54	+ 22.5	5.0
Mt. Edwards	2.20	2.78	+ 0.58	+ 26.5	14.0
Phoenix	2.10	1.54	- 0.56	- 26.5	56.0
Carr Boyd	1.65	0.81	- 0.84	- 51.0	49.0
Perserverence	0.92	1.36	+ 0.44	+ 48.0	121.0
Selkirk	0.90	1.36	+ 0.46	+ 51.0	81.2
Trojan	0.83	1.41	+ 0.58	+ 70.0	43.3

C AN INDEPENDENT ASSESSMENT OF PREDICTIVE ACCURACY

Deposit	Observed Mean Value (WT%)	Predicted Mean Value (WT%)	Residual	Accuracy (Rel %)	Precision Range at 95% C.L.
Pikwe	1.45	1.89	+ 0.44	+ 30.5	31.6
Redross	3.50	1.70	- 1.80	- 51.5	44.1

ESTIMATED WORKING ACCURACY OF THE EQUATION = $\pm$ 50 % AT 90% C.L.

TABLE 9.3.1. PREDICTED NICKEL GRADE VALUES FOR FOUR
PREVIOUSLY UNCLASSIFIED NICKEL DEPOSITS

DEPOSIT	PREDICTED NICKEL GRADE (Wt %)	THE CORRESPONDING EXTREME VALUES EXPECTED WITH 95% CONFIDENCE (PRECISION)	
		MINIMUM	MAXIMUM
MUNALI (Zambia)	1.10	0.09	2.10
JAN SHOOT (W.A.)	2.61	1.79	3.43
Mt.MONGER (W.A.)	1.77	0.86	2.68
McMAHON (W.A.)	1.40	0.30	2.51

the actual grade figure, and at worst is within $\pm$ 100 percent of this latter quantity.

The prediction of overall copper grade

A parallel study of copper grade prediction in terms of bulk gossan mineralogy was also undertaken during the course of the present work. The combined predictability value associated with the best derived predictor equation was however only $\pm$ 150 percent at the 90 percent level of confidence. This low predictability level is of little or no practical use in outcrop evaluation work, and a description of the results of the copper grade prediction study is therefore omitted from the present report.

9.4 SUMMARY OF CONCLUSIONS

The principal results of the mineralogical evaluation work on nickel gossans described in Chapter Nine are now summarised.

Oxidate mineralogy

(1) The carbonates, magnesite, calcite and dolomite occur as oxidate minerals in the surface nickel gossans of a number of deposits – especially those in Western Australia.

(2) These minerals are readily identified using a staining technique devised by Warne.

(3) They are characterised by anomalously high ore metal contents – especially nickel and copper, which are qualitatively identifiable using standard element tests.

(4) The presence of ore metal-rich oxidate carbonate in surface ironstone outcrops hence infers the local presence of buried ore mineralisation. This feature is therefore proposed as a useful recognition aid for nickel gossans.

Gossan bulk mineralogy

(1) The bulk mineralogy of nickel gossans is used as a predictor of sulphide ore metal tenor through the application of the multivariate statistical technique of multiple linear regression analysis. Three measures of sulphide metal content are studied. In each instance a regression equation relating ore metal content or grade to a linear combination of significant bulk mineralogical (gossan) variables is derived. A

specific test set of documented deposits is used in each study. In this way, each derived expression can be used to predict the likely mean value of the corresponding sulphide metal parameter from equivalent surface gossan data.

(2) The massive sulphide copper study is divided into two sub-studies on the basis of indicated ore copper test data. Unclassified gossan data are allocated to the most suitable predictor equation by use of a derived discriminant function.

(3) The estimated closeness of predictive fit of the derived sulphide predictor equations (at the 90 percent confidence level) are as follows;

Prediction Study	Closeness of Predictive Fit (Accuracy)
Massive sulphide nickel:	± 30 percent
Massive sulphide high copper:	± 25 percent
Massive sulphide low copper:	± 60 percent
Nickel ore body grade:	± 50 percent

(4) These results indicate that the copper contents of high-copper nickel ores can be predicted with workable accuracy from the mean bulk mineralogy of the equivalent surface gossan. Similarly, the nickel contents of near-massive to massive nickel ores can be quite accurately estimated from surface gossan bulk mineralogy.

(5) In contrast, the technique is of less use in both low-copper massive ore and nickel grade prediction. Here only broad ranges of probable values can be estimated for these two ore parameters using surface gossan bulk mineralogical data.

CHAPTER TEN
THE PREDICTION OF NICKEL SULPHIDE METAL TENOR
FROM GOSSAN RELIC ORE TEXTURES

10.1 INTRODUCTION

Chapter ten deals with the use of sulphide relic textures in nickel gossans as indicators of ore metal grade in corresponding buried sulphide mineralisation. The work is based on an investigation of these textures that was carried out on the present study suite of southern African and Western Australian nickel gossans.

The chapter is divided into two major sections. In the present (introductory) section, (10.1), the scope of the chapter is indicated, and previous work on nickel gossan textural evaluation is briefly reviewed. The introduction is followed by section 10.2., which comprises a summary re-iteration of the relic textural forms present in the investigated suite of nickel gossan occurrences, (chapter six).

An investigation of sulphide mimic textures in nickel gossans as quantitative metal tenor indicators in underlying sulphide ore is presented in section 10.3. The exposition is divided into two parts. In the first part, the results of a direct evaluation of violarite mimic textures in terms of sulphide nickel tenor are firstly presented, and the quantitative differences in predicted and measured sulphide nickel contents that follow from this direct texture evaluation are then interpreted in terms of likely causative factors. The results of a second study of violarite mimic textures are then set out in which linear regression analysis is used to derive an equation which allows a much improved prediction of sulphide nickel tenor to be made.

In the second part of section 10.3., the results of a direct evaluation study of chalcopyrite mimic textures in terms of sulphide copper tenor are presented. The quantitative differences between predicted and measured sulphide copper tenor values across the study deposit suite are then interpreted in terms of likely causative factors.

Chapter ten concludes, (section 10.4), with a summary of conclusions of the work detailed in section 10.3.

As indicated in chapter one, very little work has been published on the evaluation of relic sulphide textures in nickel gossans. Such reports of the technique that have been made in the literature, (Whittle, op.cit.; Roberts and Travis, op.cit.; Groves

and Whittle, op.cit.), are confined exclusively to the Western Australian nickel province.

The work of these authors indicates however that the technique is a potentially useful tool in the prediction of minimum sulphide metal grades from surface gossan outcrops in this region. No work has been published on the application of the technique to nickel gossan outcrop investigations in southern Africa.

10.2 MINERAL TEXTURES IN NICKEL GOSSANS: A SHORT REVIEW

A brief illustrated review of nickel gossan textures as determined during the present study is now presented. The object of this exposition is both to re-iterate the petrographic background data on which the textural evaluation study (section 10.3.) is based, and to visually indicate the types of textures that have necessarily to be recognised and assessed during this type of investigation.

Petrographic work has demonstrated that four basic classes of iron oxide textures exist in nickel gossans: Replacement textures after both economic and non-economic sulphide minerals; replacement textures after non-sulphide ore minerals; and non-specific textures whose provenence is not visually apparent.

Replacement textures after the economically-important sulphides violarite and chalcopyrite exist in two forms; as direct pseudomorphic replacements; and as skeletal (boxwork) structures. Iron oxide pseudomorphs after interstitial violarite (Vpn) are present in all members of the study gossan suite, and they occur in goethite in all the gossans investigated, (chapter six).

Some variation of internal structure is however present in goethite pseudomorphs after Vpn, particularly in regard to the preservation form of the octahedral cleavage network. In this respect, violarite octahedral cleavage may be defined as goethite, (Fig.10.2.1A.), as hematite, (Fig.10.2.1B.), or as elongate voids, (Fig.10.2.1C). Not uncommonly however, little or no indication of the former cleavage network is preserved, (Fig.10.2.1D.).

490

Fig. 10.2.1. Mimic Replacement Textures after Economic Sulphides

Scale length = 200 μ Blue-white filter used throughout

A. Goethite mimic after interstitial violarite (Vpn) (x 320) Air

Goethite; light to medium grey: Silica; medium-dark grey:
Voids; grey-black

B. Goethite mimics after interstitial violarite (Vpn) (x 600) Oil

Goethite; dark grey: Hematite; light grey. Hematite defines the relic
pentlandite cleavage

C. Goethite mimics after Vpo (x 220) Oil

Outline of interstitial Vpn. Vpn internal cleavage structure. Fringing
Vpo mimic in goethite

D. Goethite mimic after interstitial violarite (Vpn) (x 80) Air

Goethite (after Vpn); dark grey, mottled: Hematite after magnetite; white-
grey: Silicified goethite matrix; medium greys, mottled: Silica; dark grey

E. Hematite mimic after interstitial violarite (x 110) Air

Hematite; light-medium grey: Silica; dark grey: Voids; grey-black

F. Typical carbonate mimic replacement of violarite species (x 80) Air

Carbonate; dark grey, mottled: Goethite as Vpn cleavages; medium grey:
Hematite after FeS_2; light grey

G. Silica mimicking interstitial violarite grain form (x 110) Air

Silica; dark grey: Voids; black: Goethite; medium grey: Hematite;
light grey

H. Hematite mimic after chalcopyrite (x 110) Air

Hematite; light grey: Goethite after Vpn; dark grey, granular:
Goethite after Vpn cleavage; light-medium greys

491
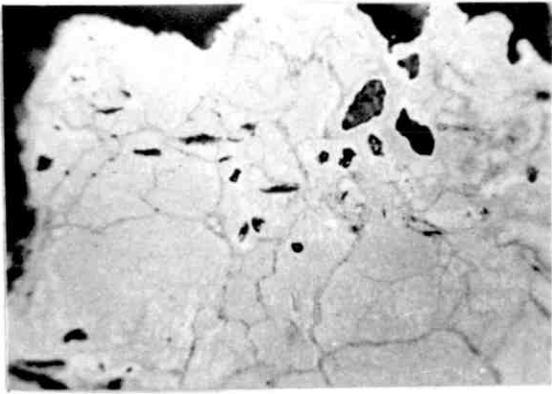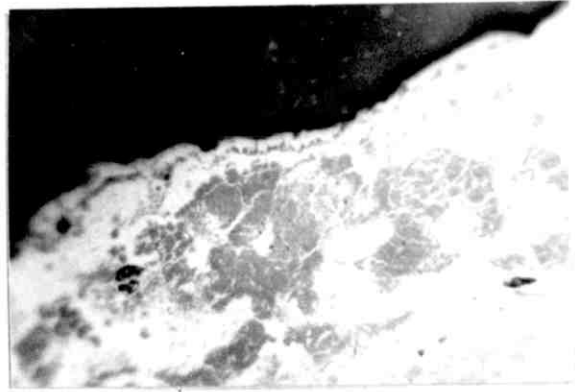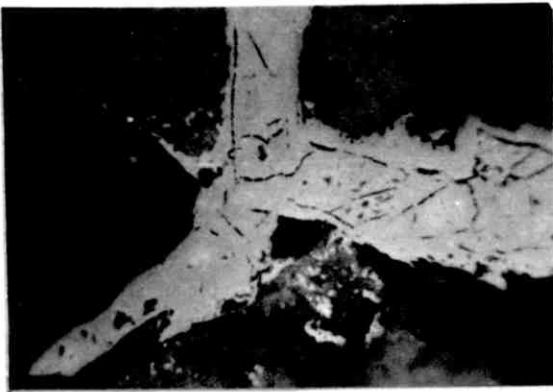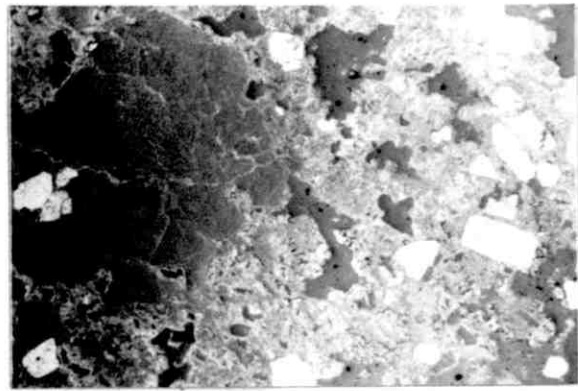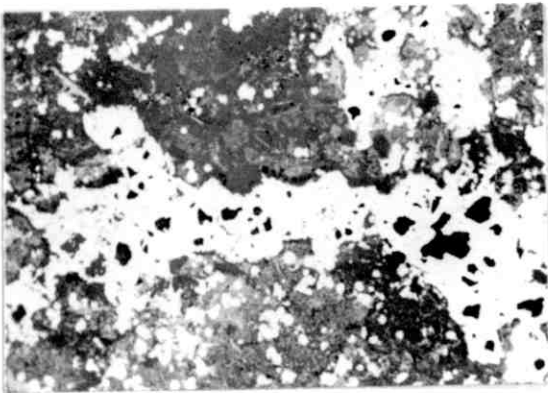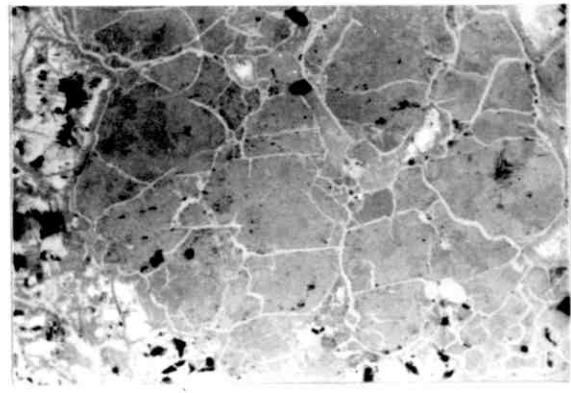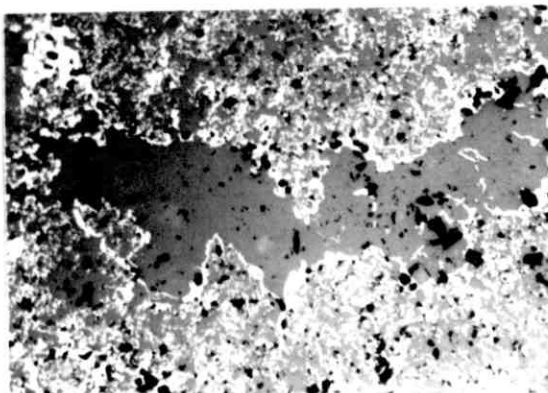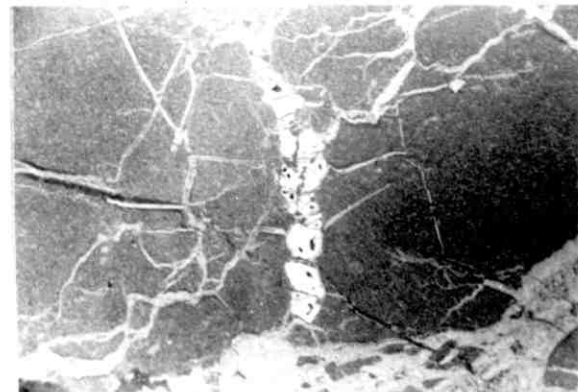
Fig.10.2.1.

Interstitial violarite pseudomorphs also occur in hematite, (Fig.10.2.1E.). Available data indicate however that this phenomenon is largely confined to southern African gossan occurrences and to one or two Australian examples, (Table 6.2.6.). Further, petrographic studies, (i.e. on Pikwe and Carr Boyd), indicate the likelihood of the hematite occuring as a secondary, post-formation replacement of goethite in these structures.

Interstitial violarite is also replaced by carbonate in several gossan occurrences, (Fig. 10.2.1F.). This phenomenon is not common though, and occurs principally in the gossans of the sampled Kambalda Dome (W.A.) deposits.

Silica mimics after interstitial violarite occur in several gossans, (Fig.10.2.1G.). They are, though, significantly more common in highly siliceous examples, and hence tend to occur preferentially in the Australian members of the study suite.

Iron oxide pseudomorphs of violarite after pyrrhotite also occur in all members of the study gossan suite. These structures are typically defined in goethite, (Fig.10. 2.1C.), but secondary hematite forms are by no means rare, (Table 6.2.6.). Where present Vpo pseudomorphs are in general spatially associated with those after interstitial Vpn. Although petrographic data indicate that they may not necessarily be preserved along with the latter structures.

Recognisable pseudomorphic mimics after the economically important copper mineral chalcopyrite are rather rare in the study nickel gossans. Where present, however, they typically occur as hematite structures, (Fig.10.2.1H.).

Boxwork structures after violarite species, (chiefly interstitial Vpn), are quite rare. Where they do occur however, they usually manifest themselves as thin hematite septae after octahedral cleavage, (Fig.10.2.2A.). Further, violarite boxwork structures may be invested in cryptocrystalline silica, (Fig.10.2.2B.).

In contrast to violarite, chalcopyrite typically occurs as boxwork structures in the gossans of the study suite. These structures do not however exhibit a universal inter-deposit distribution, and are confined mostly to the southern African gossans and to three Australian examples, (Table 6.2.6.). This distribution reflects the quantitative occurrence of chalcopyrite in the parent sulphide ores.

The former presence of the copper sulphide is easily recognised as its boxwork form typically manifests the tetragonal symmetry of the parent mineral in a more or less regular rectangular ladder structure , (Fig.10.2.2C.). This skeletal structure,

Fig. 10.2.2. Boxwork Replacement Textures after Economic Sulphides

Scale length = 100μ Blue-white filter used throughout

A.   Hematite boxworks after interstitial violarite (Vpn) (x 320) Air

Hematite (light-medium grey) defines the retained blocky octahedral cleavage of the original pentlandite

B.   Hematite boxwork after interstitial violarite (Vpn) (x 110) Air

Hematite; light grey: Silica; dark grey: Voids; black

C.   Goethite as chalcopyrite boxworks (x 220) Oil

Boxworks defined in goethite (med-dark grey), rimmed by hematite (light grey). Cp grain outline well preserved.   A small goethite mimic after bird's eye marcasite is also present.   Boxwork intersticies filled with hematite or as voids (dark grey)

D.   Goethite as chalcopyrite boxworks (x 110) Air

Goethite; medium grey, mottled: Peripheral hematite; light grey: Silica; dark grey, mottled: Voids; black

E.   Composite goethite/hematite boxwork after chalcopyrite (x 220) Oil

Goethite; medium grey: Hematite; light grey: Voids; black.   A small Cp relic is present (left centre).. Cell walls are goethite sheathed in hematite.

F.   Hematite boxwork after chalcopyrite (x 220) Oil

Hematite; light-medium grey: Chalcopyrite relics; white: Voids; black

G.   Hematite boxwork after chalcopyrite (x 110) Air

Hematite; light-medium grey: Silica matrix; dark grey: Voids; grey-black

H.   Goethite boxwork after chalcopyrite (x 110) Air

Silica; medium to dark-medium grey: Voids; dark grey: Goethite; light grey

494
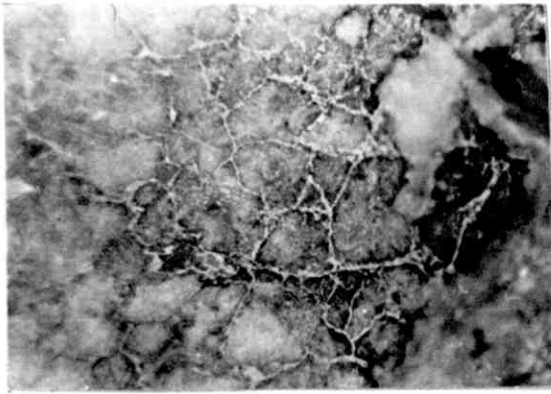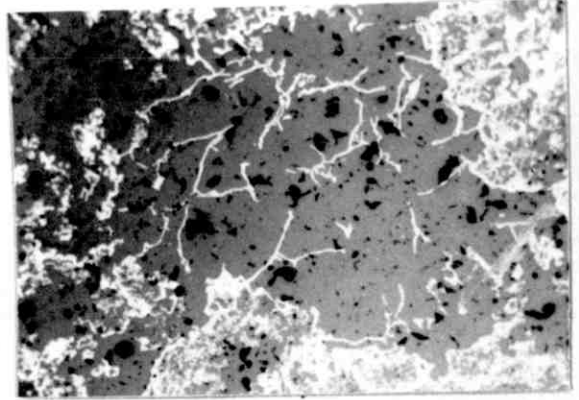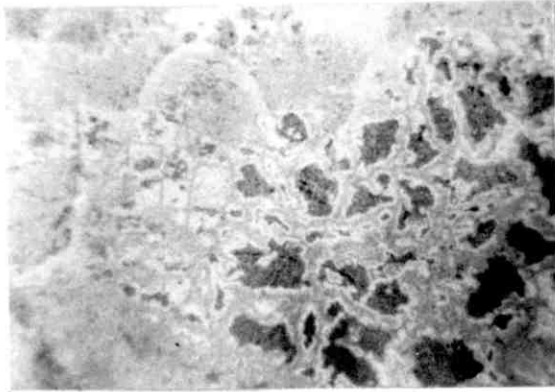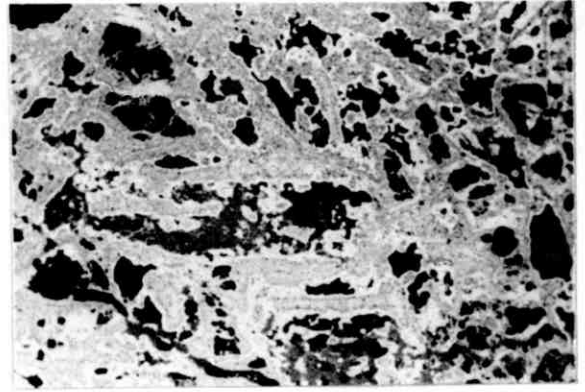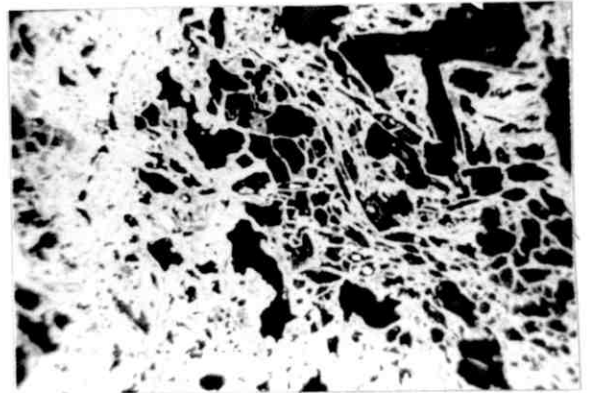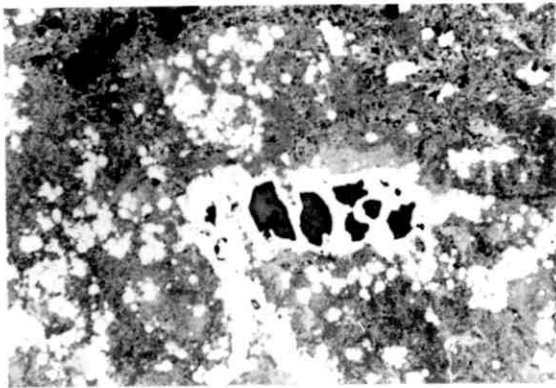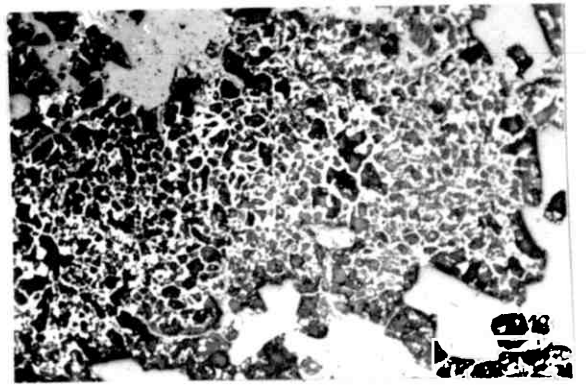
Fig.10.2.2.

which is defined by the cleavage pattern of the parent grain, may occur as goethite, (Fig.10.2.2C. and 2D.), as (quite rare) goethite/hematite composites, (Fig.10.2.2E.), or as hematite structures, (Figs. 10.2.2F. to 2H.). Hematite forms tend,however, to be quantitatively more common.

Relic textures after non-economic sulphide minerals - principally marcasite and pyrite after pyrrhotite, together with pyrrhotite secondary mimic forms, occur as a class in all members of the gossan study suite. In common with the economic sulphides, the relic textures of these phases occur both as solid (pseudomorphic) replacements and as skeletal boxwork structures. Both relic types are character- istically defined in iron oxides.

Pseudomorphic structures after secondary marcasite occur in the majority of the study gossans, (Table 6.2.6.). These structures typically take the form of goethite mimics of colloidal bird's eye structures, (Fig.10.2.3A.), although they are less commonly defined in hematite, (Table 6.2.6.). Rather rarer pseudomorphs of recrystallised coarse-grained marcasite, (section 6.2.), are also however, observed in several gossan occurrences, (Fig.10.2.3B.).

Solid pseudomorphs after secondary pyrite are observed in the majority of gossans whose equivalent secondary sulphide ore demonstrates a recrystallisation of secondary marcasite to massive pyrite. These replacement structures, which can be defined in either goethite or (less commonly) in hematite, may be in the form of massive cubiform features, (Fig.10.2.3C.). Alternatively, and more commonly, massive pyrite pseudomorphs occur as areas of iron oxide that contain numerous small cube-like leached cavities, (Fig.10.2.3D.).

Pseudomorphic replacement textures after secondary mimicked pyrrhotite structures are present in the majority of gossans whose secondary sulphide assemblages exhibit these textures. These structures are present in several forms; as polygonal-shaped configurations defined in goethite, (Fig.10.2.3E.), or hematite, (Fig.10.2.3F.), and as mimic replacements that exhibit details of original internal structures such as deformation twinning, (Figs. 10.2.3G. and 3H.).

Boxwork textures after pyrrhotite derivatives occur to some extent in all study gossans. In this context, boxwork forms after massive secondary pyrite exist in the majority of all gossans with this phase in their parent secondary sulphide assemblages. Where present, the boxwork takes the form of a network of relatively large cube- like cells whose walls are defined either in goethite, (Fig.10.2.4A.), or else in

496

Fig. 10.2.3. Mimic Replacement Textures after Non-Economic Sulphides
Scale length = 100μ

A.   Goethite mimic after marcasite bird's-eye structure (x 220) Oil
     Goethite; medium grey: Hematite; light grey

B.   Hematite mimics after coarse bladed marcasite (x 110) Air Blue-white filter
     Hematite; light-medium grey: Silica; dark grey: Voids; black

C.   Goethite mimic after massive secondary pyrite (x 220) Oil Blue-white filter
     Zoned structure well shown. Small pyrite relic (light grey) at upper right

D.   Hematite boxwork after secondary pyrite (x 320) Air   Blue-white filter
     Hematite; light-medium grey: Silica; dark grey. Cube-like boxwork form

E.   Goethite mimics after original pyrrhotite polyhedra (x 110) Air Blue-white
     filter
     Goethite; light to medium greys: Silica; medium-dark grey: Voids; black

F.   Hematite mimics after secondary marcasite (x 110) Air
     Hematite; grey-white: Goethite; medium grey: Silica; dark grey:
     Voids; black. Relic pyrrhotite cleavage structure is preserved

G.   Composite goethite/hematite mimic after pyrrhotite scissor twinning
     (x 220) Oil   Blue-white filter
     Goethite; medium-dark grey: Hematite; light-medium grey

H.   Hematite mimics after mimicked pyrrhotite twinning (x 220) Oil   Blue-white
     filter
     Hematite; light grey: Goethite; medium grey: Voids; black

Fig.10.2.3.
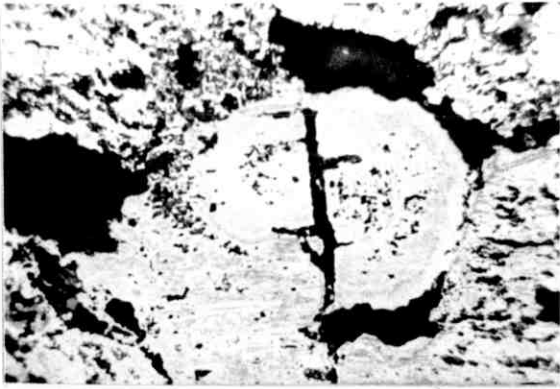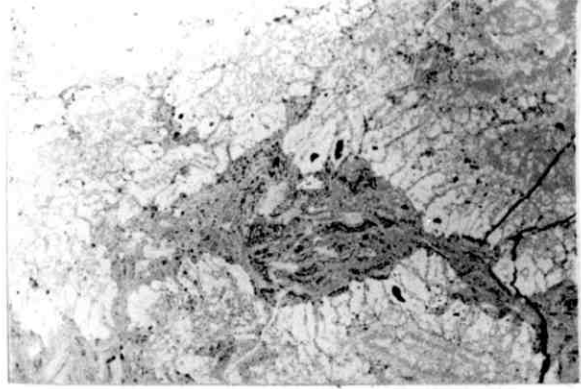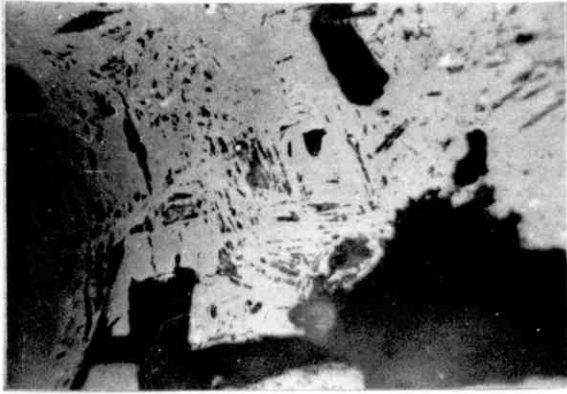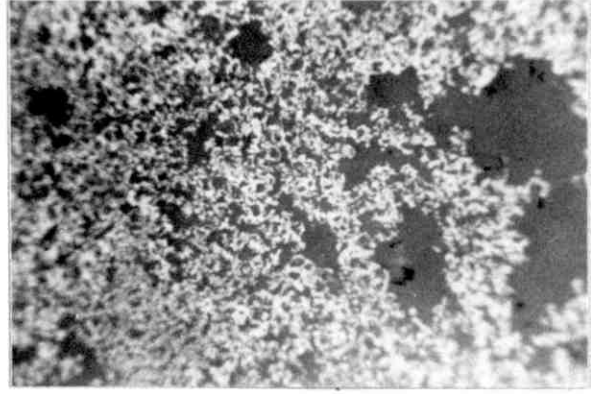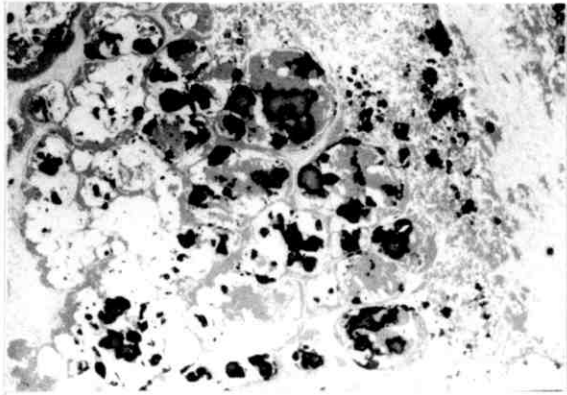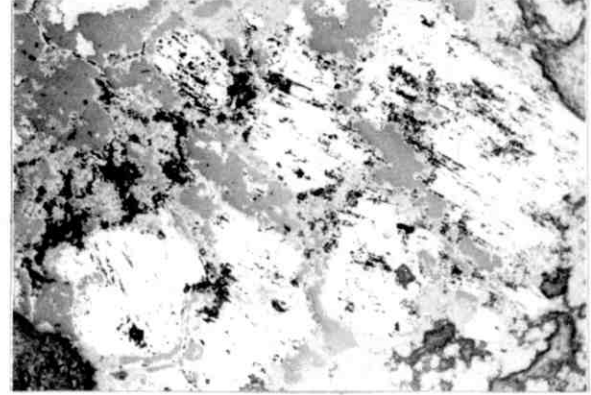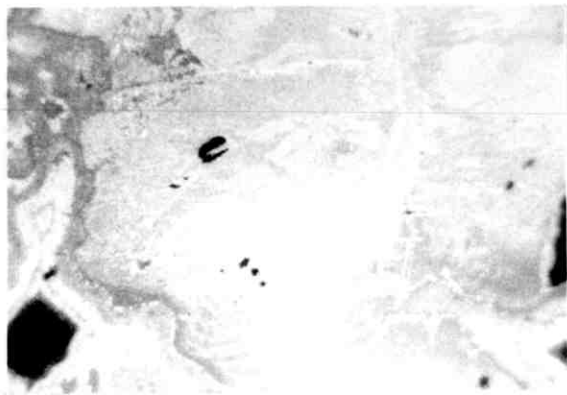
hematite, (Fig.10.2.4B.). No definitive boxwork forms after secondary marcasite are, in contrast, observed in the gossan study suite.

Skeletal structures after secondary mimicked pyrrhotite are present in a majority of gossans whose secondary ores possess this textural form. These structures typically occur as closely-spaced sub-parallel iron oxide lamellae that commonly possess cross-connecting septae. The lamellae themselves may be present as either goethite, (Fig.10.2.4C.), or as hematite, (Fig.10.2.4D.). In contrast, hexagonal pyrrhotite mimics predominate in the Trojan gossan, as the primary pyrrhotite in this deposit is exclusively hexagonal in character, (Fig.10.2.4E.).

Relic textures after non-sulphide ore minerals in the study gossans are confined to those after spinel. Pseudomorphic replacement forms predominate, and hematite is the typical iron oxide involved in these structures, (Fig.10.2.4F.). In contrast, goethite pseudomorph forms after spinel are relatively uncommon, (Fig.10.2.4G.). Boxworks after spinel are quite rare, (Fig.10.2.4H.), and are observed in only a very few gossan occurrences. In addition, though, several of the Australian gossans contain significant quantities of relic ferrochromite.

The fourth class of iron oxide textures observed in the study nickel gossans are those which do not appear to correspond with any one member of the secondary sulphide assemblage. They may hence be termed non-specific textures.

Two kinds of non-specific textures are observed in the study gossans. Non-specific precipitation textures occur as a result of iron oxide formation at the water table. They exist because the movement of iron out of the sulphide lattice prior to oxidation has resulted in the (delayed) precipitation of insoluble ferric oxides as amorphous fine-grained aggregates.

This mode of iron oxidation is hence in direct contrast to that which results in the formation of iron oxide pseudomorph structures, (chapter eight). Non-specific precipitation textures can occur as either goethite or hematite fine-grained aggregates, (Figs. 10.2.5A. and 5B. respectively).

The second type of non-specific iron oxide texture exhibited is that due to secondary recrystallisation processes. It occurs in two forms; firstly, and more commonly, as a secondary replacement of goethite by hematite. In this recrystallisation type, the parent goethite structure - be it pseudomorph or amorphous aggregate, is progressively replaced by fine-grained spherulitic hematite, (Fig.10.2.5C.).

Fig. 10.2.4.   Textures after Non Economic Sulphides and Non-Sulphide Ore Minerals

Scale length = 100µ   unless otherwise indicated.

Blue-white filter used throughout

A.   Goethite boxworks after secondary pyrite (x 110) Air

Goethite; medium grey: Hematite; light grey: Voids; black

B.   Hematite boxwork after secondary pyrite (x 110) Air

Hematite; light grey: Silica; dark grey: Voids; black

C.   Goethite mimic after mimicked pyrrhotite structure (x 110) Air

Goethite; light-medium grey: Silica; medium-dark grey: Hematite; light grey.   Pyrrhotite cleavage lineations are well-preserved

D.   Goethite mimics after secondary mimicked pyrrhotite (x 110) Air

Goethite after marcasite/pyrite; light-medium grey: Goethite after Vpo; dark grey: Voids; black

E.   Goethite boxworks after hexagonal pyrrhotite (x 40) Air

Voids; black: Goethite; light-medium grey

F.   Hematite mimics after magnetite (x 600) Oil

Hematite (light grey) defines the octahedral spinel cleavage.   Relic magnetite (medium-dark grey) is present in inter-cleavage blocks.   Matrix (dark grey) is colloidal silica

G.   Hematite mimics after magnetite (x 80) Air

Hematite (after magnetite); white-grey: Goethite; dark grey, mottled: Silicified goethite matrix; medium greys, mottled: Silica; dark grey

H.   Hematite boxwork after magnetite (x 110) Air

Hematite; light grey: Silica; dark grey: Voids; black

Fig.10.2.4.

A

B

C

D

E   1000 μ
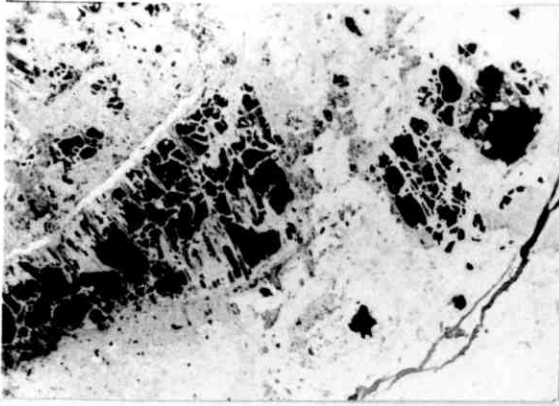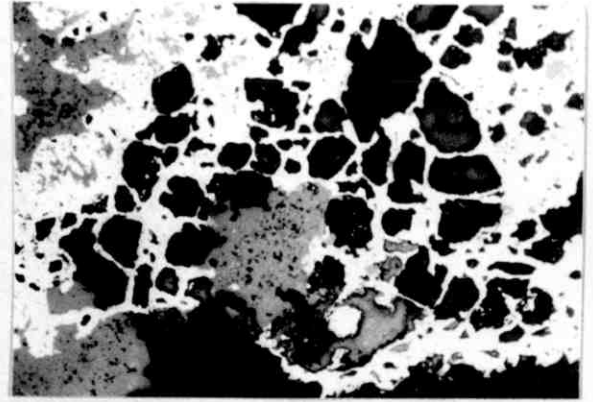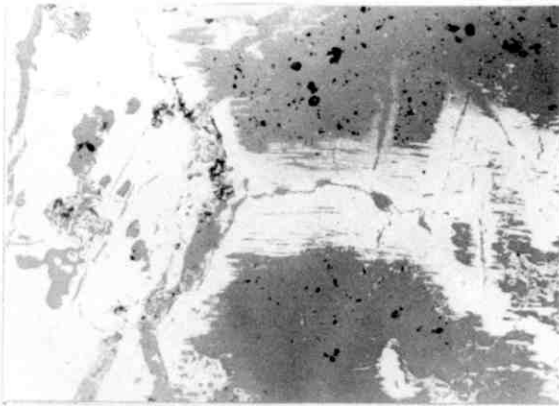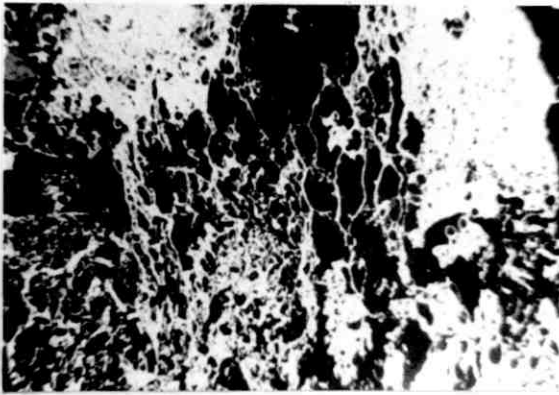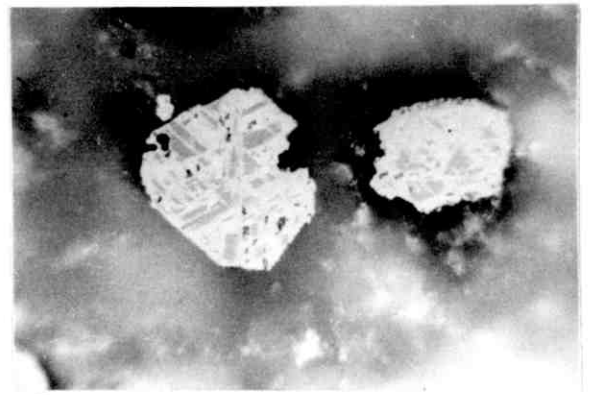
F
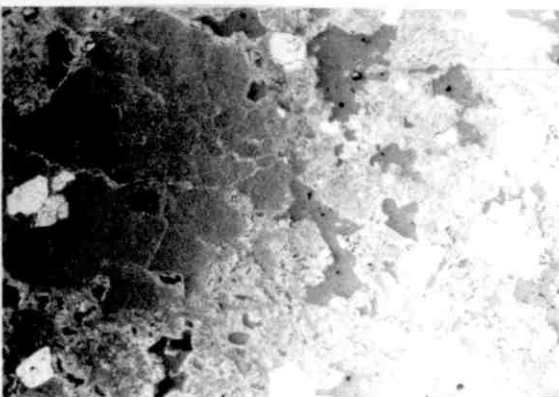
G
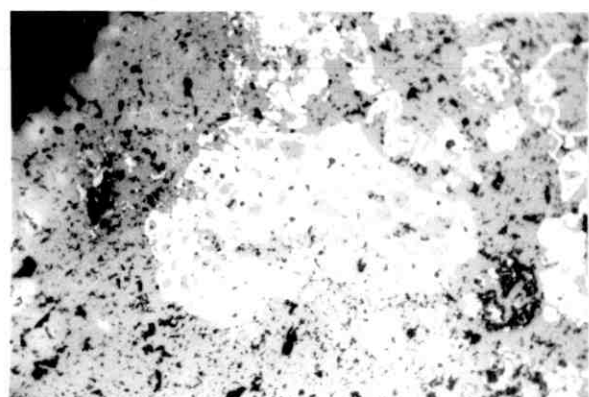
H

Fig. 10.2.5. Non-Specific Mineral Textures in Nickal Gossans

Scale length = 100 μ

A. Goethite as late-stage drusy growth on hematite (x 320) Air
    Partly crossed nicols

    Goethite (dark grey) precipitated on hematite (light-medium grey)
    Voids; black

B. Hematite as late drusy growth (x 220) Oil   Blue-white filter

    Hematite (light grey) precipitated on goethite mimics after violarite (dark grey)

C. In situ replacement of goethite by hematite (x 320) Air   Blue-white filter

    Goethite; medium-dark grey: Hematite; light-medium grey, spherulitic
    Voids; grey-black

D. Goethite recrystallisation texture (x 100) Oil

    Goethite; medium grey, spherulitic: Silica matrix; grey-black:
    Relic marcasite; white-grey

E. Typical form of silica matrix (1) (x 80) Air

    Silica; dark grey: Goethite; light-medium to medium-dark greys

F. Typical form of silica matrix (2) (x 110) Air

    Silica; dark grey: Goethite; white-grey to light grey: Voids; black

G. Silica as interstitial filling to leached cavities (x 220) Oil

    Silica; dark grey, blotchy: Goethite; medium grey

H. Interstitial silica mimicking magnetite (x 110) Air

    Silica; dark grey: Hematite; light grey: Goethite; medium grey (centre)

Fig.10.2.5.
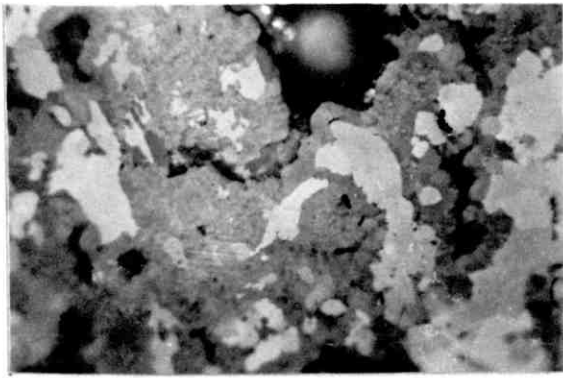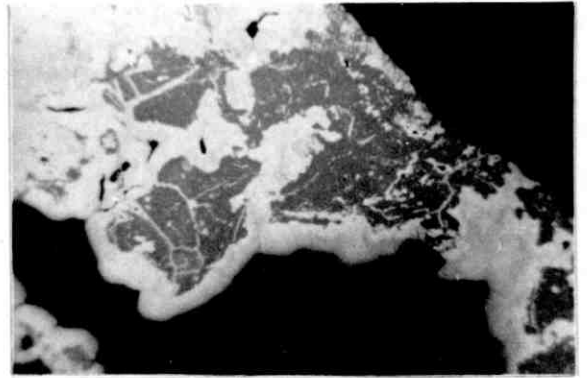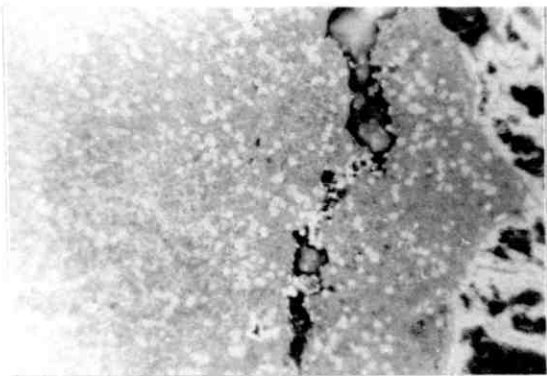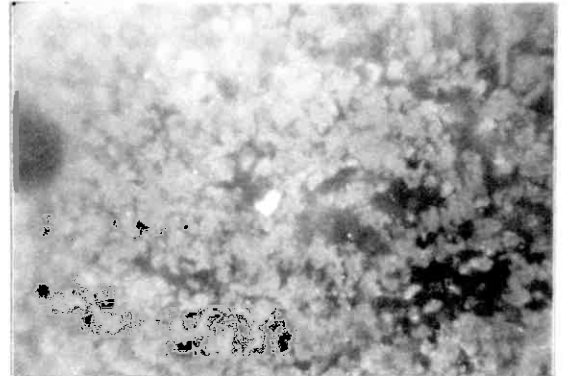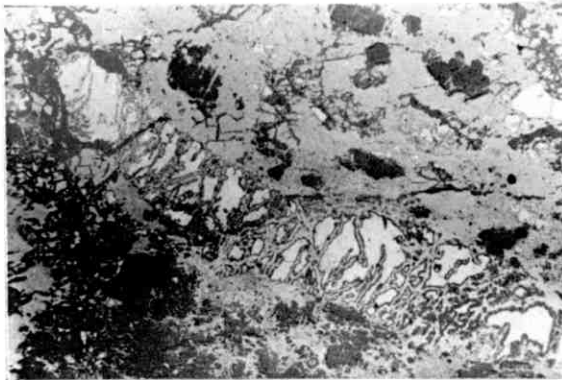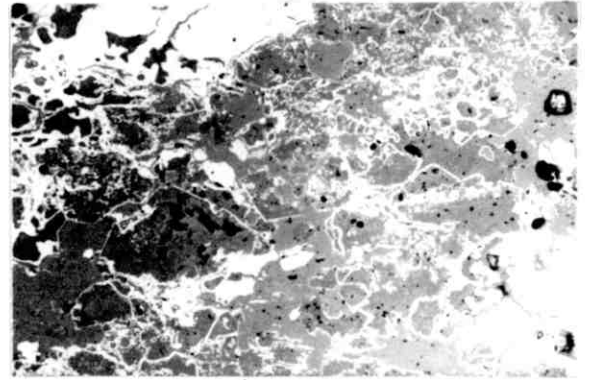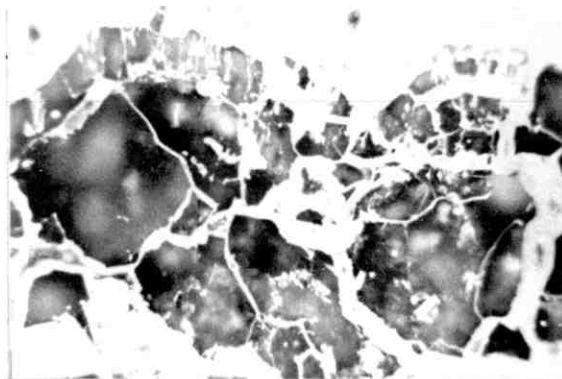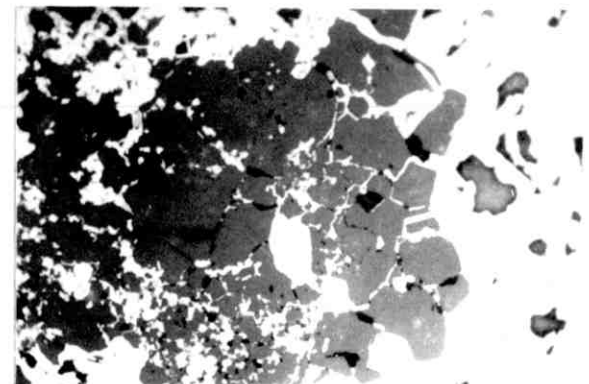
The second form of recrystallisation texture is quite rare except at Pikwe. It typically occurs as fine-grained, commonly spherulitic oxide grains nucleated within the cryptocrystalline silica that pervades the iron oxide assemblage above the 35 metre level in this deposit, (chapter three), and it is likely that the iron oxides represent a re-precipitated residuum of the iron oxide assemblage that is likely removed as a result of the associated large-scale influx of silica-saturated groundwater, (Fig.10.2.5D.).

Externally-derived silica also forms several types of non-specific textures in the study gossans. In this respect, it is present as a pervasive matrix to the developed iron oxide assemblage,(Figs. 10.2.5E. and 5F.). It is also noted however, as a filling of leached cavities in various types of pseudomorph structures, (Figs. 10.2.5G. and 5H.).

10.3 THE EVALUATION OF SULPHIDE MIMIC TEXTURES IN NICKEL GOSSANS

The results of an evaluation study of economic sulphide mineral textures in nickel gossans are now presented. The first part of the work details the findings of an investigation of violarite textural proportions as quantitative predictors of sulphide nickel tenor. The second part indicates the results of a parallel study of chalcopyrite mimic texture proportions as quantitative predictors of sulphide copper tenor.

The nickel evaluation study is based on a visual estimation of the mean proportion of violarite mimic textures in the sample suite of a given gossan occurrence. These data are used to calculate the mean nickel content of an equivalent volumetric proportion of primary pentlandite on the basis of the relation: one volume percent of mimic violarite texture equals 0.35 weight percent of nickel. This latter quantity is therefore the direct sulphide nickel equivalent of the mean proportion of relic nickel sulphide texture preserved in the gossan.

The results of a direct evaluation of violarite mimic textural proportions in terms of directly equivalent ore nickel content are presented in Table 10.3.1. for a suite of 15 test nickel gossan occurrences. Column two of this table contains the observed mean nickel content values of parent near-massive to massive nickel sulphide ore. Whereas the mean volumetric proportions of observed violarite textures in the corresponding gossans are noted in column three. The predicted ore nickel mean contents equivalent to these latter data are displayed in column

Table 10.3.1.

The direct relation of violarite mimic proportions to sulphide nickel content

Deposit (n)	Observed mean Ni tenor (Wt%)	Mean proportion violarite relic texture in gossan (vol%)	Corresponding predicted Ni content (Wt%)	Accuracy of predicted value (Rel%)	95% c.l. range of predicted v'l'e (± Rel%)
Pikwe 66	2.45	2.67	0.94	– 61.6	21.6
Pers'v'an'e 10	2.30	1.70	0.60	– 73.9	14.3
Munali 9	3.11	3.80	1.33	– 57.2	17.0
Phoenix 9	4.94	2.20	0.77	– 84.4	5.2
Selkirk 17	2.49	5.50	1.93	– 22.5	11.7
Trojan 3	2.82	9.00	3.15	+ 11.7	94.0
Mt Edwards 17	3.52	11.20	3.92	+ 11.4	48.5
Jan Shoot 7	3.45	7.33	2.57	– 25.5	33.9
Mt Monger 15	3.76	11.77	4.12	+ 9.6	19.9
McMahon 7	3.93	8.30	2.91	– 26.0	58.5
Redross 7	3.35	2.60	0.91	– 72.8	20.0
Carr Boyd 5	3.30	11.00	3.85	+ 16.7	103.9
Ravenst'pe 3	2.50	5.30	1.86	– 25.6	24.8
Sparg'v'lle 15	3.96	15.20	5.32	+ 34.3	86.7
SLOB/ Lunnon 7	4.40	7.90	2.77	– 37.1	50.6

(n) = no.of samples

four.

The results of a comparison of observed ore nickel contents and those predicted by the direct textural evaluation of the corresponding gossans are presented in the form of predictive accuracy values in column five. These latter data are computed by the relation:

$$\text{ACCURACY (\%)} = \frac{\text{PREDICTED VALUE} - \text{OBSERVED VALUE}}{\text{OBSERVED VALUE}} \times 100 \text{ (\%)}$$

and they indicate that the sulphide nickel mean contents of ten out of 15 test deposits are predicted to within $\pm$ 40 percent of their likely values by the direct gossan evaluation method.

The predicted nickel contents of these test deposits are, however, typically lower than their observed values. In practice therefore, the mimic violarite mean proportions of near-massive to massive nickel gossans indicate only the minimum likely nickel mean content of the corresponding buried ore.

These typically low predicted values are   due chiefly to the non-preservation of a significant proportion of violarite grain textures across the sulphide-oxide transition at each deposit. But it is also probable that a proportion of those textures that are preserved may subsequently be obliterated due to a later influx and precipitation of externally-derived silica in the oxide zone.

The presence of these likely 'textural dilutants' therefore indicates that a direct evaluation of mimic violarite textures in nickel gossans is very inefficient as a means of quantitatively predicting the nickel content of the corresponding ore.

In addition, the typically wide precision ranges of the predicted test set results, (column six, Table 10.3.1.), computed as they are in each instance from the data statistics of the individual sample sets, further reduce the effective fit of the computed nickel tenor data.

In order to circumvent these difficulties and, hence to improve both the accuracy and the precision of the textural evaluation method, a prediction technique based on linear regression analysis was devised. This approach was adopted both on geological and statistical grounds because data were available from a significant number of major nickel sulphide deposits in the investigation.

In this study, a linear regression equation is devised in which measured sulphide nickel mean content is erected as the dependent variable against an independent variable formed by the mean mimic violarite content of the corresponding gossan.

The function itself is developed from the relevant data of a test set of 12 out of the original suite of 15 deposits. The three remaining deposits, which are withdrawn at random prior to the production of the regression equation, are subsequently used in an independent accuracy assessment of the final equation.

The derived linear regression (predictor) equation quantitatively relating sulphide nickel and violarite mimic mean contents is presented in Fig.10.3.1A. The accompanying analysis of variance table indicates that a significant proportion of the total variability of the sulphide nickel data is explained by the regression of the latter on violarite mimic mean content. Hence violarite mimic texture content can be used as a workable predictor of sulphide nickel content through the agency of the equation.

A more readily visualised indication of the equations applicability to textural evaluation studies is, however, demonstrated in Fig.10.3.1B. This figure shows an analysis of residuals computed from an application of the equation to each member of the parent test set of 12 deposits. The corresponding predictive accuracy values indicate, when compared with the data in column five, (Table 10.3.1.), that a substantial improvement in this important quantity is gained through the use of the equation for all deposits with the exception of Selkirk.

Further, a comparison of the size of the values in column six of Table 10.3.1. and Fig.10.3.1B. demonstrates that the relative precision of the mean predicted sulphide nickel content value is substantially improved in all instances through the use of the derived predictor equation.

The results of an independent assessment of the predictor equation using the three unutilised test deposits are presented in Fig.10.3.1C. These data indicate that the equation predicts the mean sulphide nickel mean content of the parent ore from the mean violarite mimic data of the corresponding gossan within workably accurate limits for each deposit. Further, the precision range of these results similarly exhibit considerable improvement over those of the equivalent direct evaluation study, (Table 10.3.1.).

The above results therefore allow the overall working accuracy of the predictor equation to be estimated at about $\pm$ 25 percent at (approximately) the 90 percent level of confidence.

The results of a parallel evaluation study of chalcopyrite mimic textures in nickel gossans for the test suite of 15 deposits are set out in Table 10.3.2. These results,

Fig.10.3.1. Results of the Sulphide Nickel Content Prediction Study

A THE DERIVED PREDICTOR EQUATION

Mean Ni tenor = 2.436 + 0.113 mean Violarite mimic proportions

The corresponding analysis of variance and F test data

Source of variation	d.f.	Sum of Squares	Mean Squares	F Value	F-Statistic at 90% C.L
Due to regression	1	2.4545	2.4545	8.4960	3.2850
Deviation from regression	10	2.8886	0.2889		
Total	11	5.3431			

Proportion of total variation explained by the equation (R^2) = .4594

B AN ANALYSIS OF TEST SET RESIDUALS

Deposit	Observed Mean Value (WT%)	Predicted Mean Value (WT%)	Residual	Accuracy (Rel %)	Precision Range at 95% C.L.
Pikwe	2.45	2.74	+ 0.29	+ 11.8	7.0
Perserverence	2.30	2.63	+ 0.33	+ 14.4	4.7
Selkirk	2.49	3.06	+ 0.57	+ 22.9	3.6
Mt. Edwards	3.52	3.70	+ 0.18	+ 5.1	15.6
Jan Shoot	3.45	3.26	- 0.19	- 5.5	10.5
Mt. Monger	3.76	3.76	0.0	0.0	6.4
McMahon	3.93	3.37	- 0.56	- 14.3	18.8
Redross	3.35	2.73	- 0.62	- 18.5	6.6
Carr Boyd	3.30	3.67	+ 0.37	+ 11.2	33.3
Ravensthorpe 5	2.50	3.03	+ 0.53	+ 21.2	8.0
Spargoville 5A	3.96	4.15	+ 0.19	+ 4.8	27.8
S.L.O.B./Lunnon	4.40	3.33	- 1.07	- 24.3	16.1

C AN INDEPENDENT ASSESSMENT OF PREDICTIVE ACCURACY

Deposit	Observed Mean Value (WT%)	Predicted Mean Value (WT%)	Residual	Accuracy (Rel %)	Precision Range at 95% C.L.
Munali	3.11	2.86	- 0.25	- 8.0	5.7
Trojan	2.82	3.45	+ 0.63	+ 22.3	30.2
Phoenix	4.94	2.68	- 2.26	- 45.8	1.9

ESTIMATED WORKING ACCURACY OF THE EQUATION = ± 25% AT 90% C.L.

expressed as the data values in column six, indicate that a wide range of predictive accuracy occurs across the test deposit suite. In this respect, differences between predicted and observed sulphide copper mean contents range from + 38.2 percent (Mt. Monger) through to - 96.1 percent (Phoenix). There is, however, a fundamental and recognisable bias towards low (negative) accuracy values across the test suite.

The principal geological causes of this low accuracy are in part essentially the same as those affecting violarite mimic textures; namely, the non-preservation of parent (chalcopyrite) grain textures across the sulphide-oxide transition, and the subsequent likely obliteration of a proportion of these preserved textures by an ensuing episode of silicification in the oxide zone.

Two additional factors though also likely contribute to this phenomenon. These are; firstly, the low absolute chalcopyrite mean content of many of the sampled parent ores - typically those from Western Australia; and, secondly, the well-documented typically heterogeneous distribution of chalcopyrite within the sampled parent nickel sulphide mineral assemblages.

The first of these factors is reflected in very low chalcopyrite relic texture proportions in the gossan, and hence renders accurate estimation of these data rather difficult with the visual technique employed in the study. The second factor contributes to inaccuracy in the computed mean chalcopyrite mimic content value where this quantity is derived from a relatively small number of gossan samples.

It is therefore probable that a combination of geological, statistical and methodological factors combine to produce the typically low predictive accuracy that is noted across the chalcopyrite mimic texture evaluation suite, (Table 10.3.2.).

A linear regression study relating sulphide copper mean content and mimic chalcopyrite mean proportions, and analogous to that developed in the nickel study was, however, subsequently attempted in order to effect an improvement in this situation. Preliminary work on the relations of these two indicated variables demonstrated, though, that there was insufficient statistical correlation between them to permit a workably accurate linear regression equation to be derived.

On present data, therefore, chalcopyrite mimic textures in nickel gossans are useful as qualitative indicators of buried chalcopyrite, but they cannot be evaluated with sufficient accuracy to merit their adoption as quantitative predictors of underlying sulphide copper content.

Table 10.3.2.

The direct relation of chalcopyrite mimic proportions to sulphide copper content

Deposit (n)	Observed mean Cu tenor (Wt%)	Mean proportion chalc'py relic texture in gossan (vol%)	Corresponding predicted Cu content (Wt%)	Accuracy of predicted value (Rel%)	95% c.l. range of predicted v'l'e (± Rel%)
Pikwe 66	2.26	5.89	2.06	- 8.9	60.1
Pers'v'an'e 10	1.35	0.45	0.16	- 88.2	11.1
Munali 9	0.31	0.93	0.33	+ 6.5	45.1
Phoenix 9	2.57	0.28	0.10	$>$- 96.1	2.3
Selkirk 17	2.00	<0.5	<0.18	- 91.0	-
Trojan 3	0.19	<0.5	<0.18	$>$- 52.6	-
Mt Edwards 17	0.59	<0.5	<0.18	$>$- 69.5	-
Jan Shoot 7	1.96	1.25	0.44	- 77.6	15.3
Mt Monger 15	0.34	1.33	0.47	+38.2	70.6
McMahon 7	0.23	<0.5	<0.18	$>$- 21.7	-
Redross 7	0.63	0.71	0.25	- 60.3	38.1
Carr Boyd 5	3.30	1.80	0.63	- 80.9	12.4
Ravenst'pe 3	0.35	0.5	0.18	- 48.6	-
Sparg'v'lle 15	0.77	<0.5	<0.18	$>$- 76.6	-
SLOB/ Lunnon 7	1.64	0.71	0.25	- 84.6	4.7

(n) = no.of samples

10.4 SUMMARY OF CONCLUSIONS

The principal results of the textural evaluation work on nickel gossans described in chapter ten are now summarised.

(1) A direct evaluation of gossan relic violarite textures in terms of the mean nickel content of equivalent near-massive to massive sulphide has associated with it a mean closeness of predicted fit of ± 70 per cent.

(2) The derivation, using a test set of 12 deposits, of a linear regression equation relating gossan mean violarite mimic content and massive sulphide nickel content is a significantly more accurate sulphide predictor technique. The derived equation permits massive sulphide nickel content to be predicted from the violarite mimic content of the overlying gossan to within ± 25 percent at the 90 percent confidence level.

(3) A direct evaluation of relic chalcopyrite textures in terms of the copper content of near-massive to massive ore has associated with it a mean closeness of predictive fit of about ± 90 percent. Further, no improvement in the predictive accuracy of chalcopyrite mimics is possible through the development of a linear regression (predictor) equation on the basis of present data.

(4) The mean nickel tenor of near-massive to massive nickel ores can hence be accurately predicted from the relic violarite texture content of the corresponding surface gossan by use of a derived regression (predictor) equation. In contrast, relic chalcopyrite textures are unusable as accurate quantitative predictors of sulphide copper tenor. Their use is restricted to that of qualitative indicators of copper mineralogy in the buried sulphide ore.

CHAPTER ELEVEN

THE QUANTITATIVE GEOCHEMICAL EVALUATION OF NICKEL GOSSANS

11.1 INTRODUCTION

The present chapter deals with the use of nickel gossan bulk geochemistry as a quantitative predictor of ore metal tenor in underlying sulphide mineralisation.

Previously published work in this field has been limited to the investigation of platinum group metals carried out by Travis et.al., (1976, op.cit.), and the results of this latter study demonstrate that the iridium content of nickel gossans can be used as a semi-quantitative predictor of nickel tenor in equivalent massive sulphide ore, (chapter one).

The present study is based on an investigation of transition metal geochemistry in nickel gossans and their equivalent near-massive to massive sulphide ores from 15 deposits in southern Africa and Western Australia. It is divided into five sections for the purposes of exposition.

The present (introductory) section (11.1) indicates the structure of the work by briefly outlining the content of each succeeding part. The results of preliminary work on both the individual and the combined geochemical features of sampled nickel ores and gossans are then described, (sections 11.2 and 11.3). This provides the necessary conceptual background on which the prediction study proper is based.

The main work of the study is described in section 11.4. This concerns both the development and the results of an evaluation technique, based on Multiple Linear Regression Analysis, that allows a number of important measures of sulphide nickel and copper tenor to be quantitatively predicted with accuracy from the transition metal geochemistry of the corresponding surface gossan outcrop. The significance of this prediction technique in mineral exploration is then briefly indicated.

The chapter closes with a short summary of the chief results of the study, (section 11.5).

11.2 THE GEOCHEMISTRY OF NICKEL SULPHIDE ORES

Introduction

In this section, the bulk geochemistry of the study nickel sulphide ores are investigated on both an individual and a combined basis. This work is carried out as necessary background to the geochemical evaluation study that is presented in section 11.4.

The bulk geochemistry of individual ores is firstly investigated. This work is based on the data generated in the oxidation profile study reported in chapters three to six of the present work. The object of the investigation is to indicate the inter-deposit variation in geochemical signature that exists across the ore suite.

The bulk geochemistry of the combined ore suite is then presented. This work takes the form of a description of sample population statistics in these rocks. An indication of the overall geochemical characteristics of nickel ores is thereby gained.

An inter-deposit comparison of ore geochemistry

The inter-deposit variations of sulphide ore geochemistry are investigated through a statistical comparison of sampled mean values for a suite of nine major, minor and trace elements, (Fig.11.2.1.). The individual element comparisons are made through the agency of t-tests, (Till, 1974), which in the present context indicate the degree of equality of the sample mean values of an individual ore with that of the combined sulphide data suite of 15 deposits.

Degrees of difference between the two mean values are then semi-quantitatively indicated by indexation of the confidence level value at which they can be considered to be   equal. In this way, the differences between the sampled means of individual deposits are standardised against the corresponding suite mean value for each element, thus allowing inter-deposit comparisons to be made on a simple, standardised basis.

The results of this statistical comparison of sample means for the 15 study ores are indicated   in Fig.11.2.1. The inter-deposit comparison of these data may be performed in two ways; firstly on an element-suite basis; and secondly on an individual element basis. In this respect, a visual scan of the element indicies for each sulphide ore in the study suite indicates that individual ores are

Fig. 11.2.1.   Inter-deposit comparison of Sulphide and Oxide Geochemistries

DEPOSIT	Fe(Oxide) / Fe(Ore)	— / S(Ore)	Si(Oxide) / Si(Ore)	Ni(Oxide) / Ni(Ore)	Cu(Oxide) / Cu(Ore)	Co(Oxide) / Co(Ore)	Cr(Oxide) / Cr(Ore)	Mn(Oxide) / Mn(Ore)	Ti(Oxide) / Ti(Ore)
PIKWE (Botswana)	0	—	0	-4	0	-3	-2	-1	0
	0	0	0	0	+2	0	0	0	0
PERSERVERANCE (Rhodesia)	-2	—	+3	0	-2	0	0	0	0
	+1	0	-1	-1	0	0	0	+3	0
MUNALI (Zambia)	+2	—	-2	0	0	0	0	0	+4
	0	0	0	0	0	0	0	0	+4
PHOENIX (Botswana)	+4	—	-4	0	+4	0	0	0	0
	-1	-2	+4	+4	+4	0	0	-2	0
SELKIRK (Botswana)	+4	—	-4	-2	-1	-1	0	0	0
	+3	0	-4	0	+2	0	0	0	0
TROJAN (Rhodesia)	-4	—	+3	0	0	0	+3	0	0
	0	0	+1	0	0	0	0	-1	0
Mt EDWARDS (W.Aust)	+4	—	+3	0	0	0	+3	0	0
	0	0	+1	0	0	0	0	-1	0
JAN SHOOT (W.Aust)	-3	—	+3	0	0	0	+3	0	0
	-4	0	0	0	+1	0	+4	0	0
Mt MONGER (W.Aust)	-2	—	+3	0	0	-1	0	0	0
	0	0	0	0	0	0	0	0	0
McMAHON (W.Aust)	0	—	0	+4	0	+1	0	0	0
	-4	+3	0	0	0	0	0	0	0
RAVENSTHORPE (W.Aust)	+2	—	-2	+4	0	+4	0	0	0
	0	0	0	0	0	0	0	0	0
REDROSS (W.Aust)	-4	—	+4	0	0	0	0	+2	0
	0	+4	0	0	0	-1	0	+1	0
SPARGOVILLE 5A (W.Aust)	0	—	0	+4	+4	+4	+3	0	0
	-1	+4	0	+1	0	0	0	0	0
SILVER LAKE/ LUNNON (W.Aust)	0	—	0	0	0	0	0	0	0
	0	+4	-1	+4	0	0	0	0	0
CARR BOYD (W.Aust)	0	—	+1	0	0	0	0	0	0
	-4	0	+4	-4	+3	0	0	0	0

Comparison of t-statistics $H_o : \mu_{deposit} = \mu_{overall}$

$t_{deposit}$ vs $t_{overall}$

Confidence level value for t (overall) at which Ho is accepted	Index value for individual deposits
<90	0
90<95	(+) 1
95<97.5	(+) 2
97.5<99	(+) 3
99	(+) 4

distinguishable from one another by the possession of semi-quantitatively distinct mean geochemical assemblages.

This latter finding is important as it effectively demonstrates that the mean ore metal (viz. nickel and copper) content of each sampled deposit has associated with it a quantitatively distinct geochemical signature. Further, it is possible that this latter phenomenon may, at least in part, be preserved into the overlying oxide zone at each ore location. It is hence realistic to investigate methods that would potentially allow such likely attenuated geochemical signatures to be used as predictors of ore metal tenor in parent sulphide ore.

The overall geochemical features of nickel sulphide ores

The overall geochemical characteristics of the combined study suite of 15 nickel sulphide ores are now investigated. This work takes the form of an elucidation of the sample population distributions of each of the nine constituent elements across the study suite.

This work permits the shape of the sample probability distribution for each element to be interpreted in terms of the likely presence of single or of multiple parent populations. These latter results, when compared with parallel work on oxide zone probability distributions allow inferences to be made as to whether oxide formation promotes or works against the overall homogenisation of element populations. This is important because the presence of approximately single probability distributions for individual elements in the combined oxide suite is essential for the potential development of sulphide ore prediction methods based on multivariate statistics.

The distribution of individual sample data for each of the nine constituent elements in the combined ore suite are now presented in histogram form, (Fig.11.2.2.). These diagrams, together with the associated goodness- of- fit (chi-square) statistic values computed from the individual metal sample values, permit inferences to be made about the likely overall character of individual metal populations in nickel sulphide ores.

In summary, the sample population distributions of the nine elements across the nickel sulphide suite, (Fig.11.2.2.), indicate that Iron likely approximates a single negatively-skewed population, and that sulphur and nickel probably both occur as single, normally-distributed populations in these rocks.

In contrast, each of the five indicated trace metals, together with silicon are likely

FIG. 11.2.2. DISTRIBUTION OF INDIVIDUAL ELEMENTS ACROSS THE COMBINED SULPHIDE SAMPLE SUITE

Associated χ^2 statistic with 15 degrees of freedom = 22.30 at the 90% confidence level; n = 63

A IRON $\chi^2 = 79.17$
Interval Width = 1.3 wt%

B SULPHUR $\chi^2 = 23.98$
Interval Width = 1.2 wt%

C SILICON ($\log_{10}$) $\chi^2 = 130.09$
$\log_{10}$ Interval Width = 0.21

D NICKEL $\chi^2 = 20.39$
Interval Width = 0.3 wt%

E COPPER ($\log_{10}$) $\chi^2 = 62.32$
$\log_{10}$ Interval Width = 0.195

F COBALT ($\log_{10}$) $\chi^2 = 163.25$
$\log_{10}$ Interval Width = 0.150

G CHROMIUM ($\log_{10}$) $\chi^2 = 153.62$
$\log_{10}$ Interval Width = 0.135

H MANGANESE ($\log_{10}$) $\chi^2 = 28.90$
$\log_{10}$ Interval Width = 0.078

I TITANIUM ($\log_{10}$) $\chi^2 = 29.80$
$\log_{10}$ Interval Width = 0.117
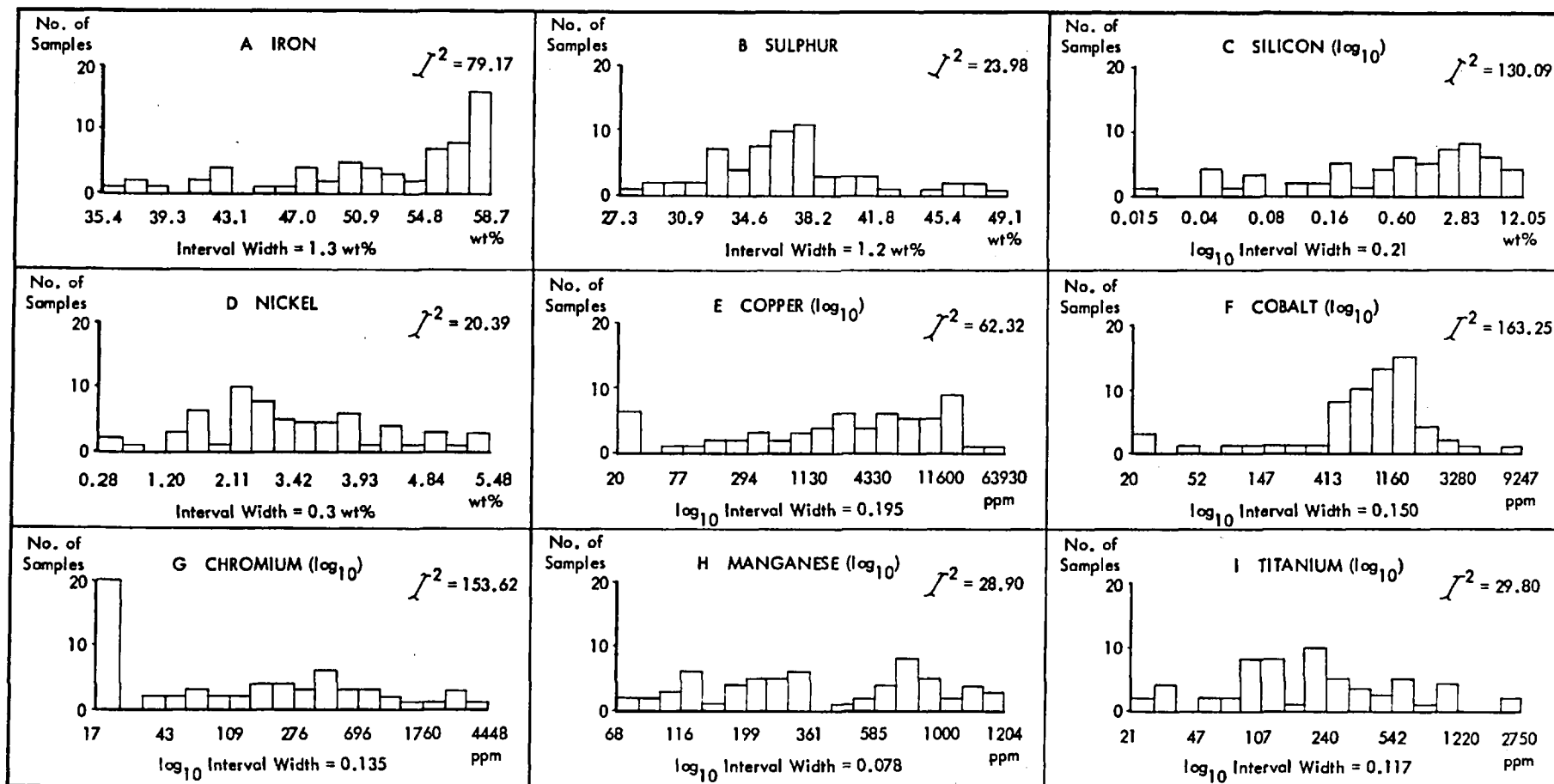
present as multiple or otherwise poorly defined statistical populations that may represent combinations of various sub-groups of nickel ores.

11.3 THE GEOCHEMISTRY OF NICKEL GOSSANS

Introduction

An investigation of the bulk geochemistry of the gossans associated with the 15 study ores is now presented. This work is divided into two parts; namely, an investigation of the inter-deposit variation of the individual gossans; and an indication of sample population distributions in the combined suite of 15 gossan occurrences.

These studies are made in order to complement the work carried out on the parent sulphide ores (section 11.2), and their results provide the conceptual basis on which the developed evaluation technique is founded (section 11.4).

An inter-deposit comparison of nickel gossan geochemistry

The results of a study of inter-gossan geochemical variation are indicated in Fig.11.2.1. for the 15 study gossan occurrences. The data for individual elements are obtained in an analogous manner to that of the corresponding sulphide data (section 11.2). In the present instance however the inter-deposit differences are standardised against the sample mean of the combined oxide suite data for each of the eight constituent major and trace elements in the study set.

In summary, an inter-deposit comparison of the geochemistry of sampled nickel gossans indicates that each is characterised by a specific quantitative suite of element mean content values.

This finding is important as it indicates that the geochemical signatures of individual ores indicated in section 11.2 are represented by other parallel and individually distinct geochemical signatures in the corresponding oxide zones. In consequence of this outcome, the investigation of a method to relate sulphide ore metal tenor and gossan geochemistry is placed on a realistic geological footing.

The overall geochemical features of nickel gossans

The overall geochemical characteristics of the combined study suite of 15 nickel gossans are now described. The work takes the form of an investigation of sample

population distributions for the eight constituent elements in the gossan geochemical suite.

The distribution of individual sample data for each of the eight constituent elements analysed in the combined gossan suite are presented in histogram form in Fig.11.3.1. As with the parallel sulphide study, these diagrams, together with their corresponding chi-square statistic values allow the likely character of individual element populations in nickel gossans to be indicated.

The sample histogram plots and chi-square data for all trace elements except cobalt, (Fig.11.3.1G.), demonstrate that the sample distributions of these metals probably represent single log-normal populations. Bearing the cobalt sample distribution in mind, it is, therefore, probably reasonable to state that the data in Figs. 11.3.1C. to 1H. indicate that the formation of gossans from nickel sulphide ores leads to the homogenisation of transition metal populations into single log-normal element distributions.

This finding is of critical importance for the development of a sulphide evaluation technique based on gossan trace metal chemistry.This is because only if such an homogenisation of element populations occurs in these rocks can statistically powerful multivariate analysis techniques be properly employed in the elucidation and solution of the nickel sulphide evaluation problem using gossan trace element geochemistry.

In summary, the results of an inter-deposit geochemical comparison of nickel gossans indicate that these rocks are characterised by specific quantitative assemblages of element mean contents. It is therefore established that the geochemical signatures of individual nickel sulphide ores are paralleled by the existence of individually discreet parallel geochemical signatures in their respective gossans. This latter conclusion thus provides a firm geological basis on which an attempt at the evaluation of nickel gossan geochemistry in terms of sulphide metal contents can be pursued.

Further, work on the sample distribution of a suite of major and trace elements across the combined nickel gossan suite has demonstrated that the six most important transition metal constituents of nickel ores approximate single log-normally distributed populations in their oxide (gossan) equivalents.

This result indicates that an overall homogenisation of individual transition metal

populations occur in nickel gossans, and this phenomenon in turn allows multi-variate statistical methods to be properly considered as a means of resolving the problem of sulphide ore metal content prediction through the use of gossan trace metal geochemistry.

The results of these two investigations hence firmly establish the overall geological and statistical feasibility of, firstly, the quantitative investigation of nickel gossan geochemistry in terms of parent ore metal content; and, secondly, the potential feasibility of applying multivariate statistical techniques in the execution of this work.

FIG. 11.3.1. DISTRIBUTION OF INDIVIDUAL ELEMENTS ACROSS THE COMBINED GOSSAN SAMPLE SUITE

Associated χ^2 statistic with 15 degrees of freedom = 22.30 at the 90% confidence level; n = 151
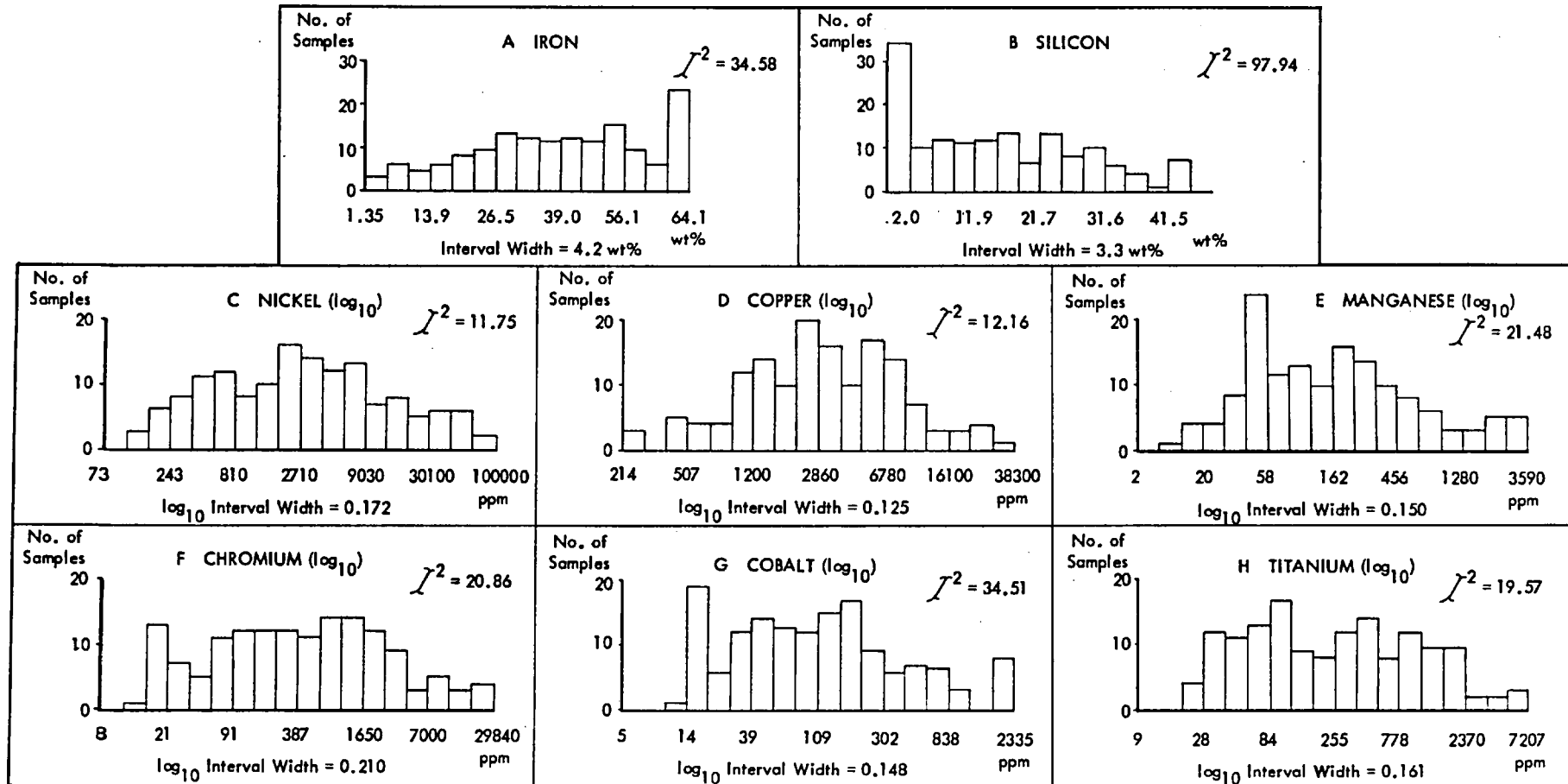
11.4 THE PREDICTION OF SULPHIDE METAL TENOR FROM NICKEL GOSSAN GEOCHEMISTRY

Introduction

The results of the geochemical evaluation study proper are now presented. The work is in the form of four separate sub-studies, and each investigation is based on the multivariate statistical method of multiple linear regression analysis, (section 9.3). In this technique, a set of independent variables, in this instance significant gossan element mean contents, is used to predict the mean nickel and copper contents of equivalent near-massive to massive nickel sulphide ore. The gossan data are also used however to predict the overall nickel and copper grade values of the parent sulphide mineralisation.

These investigations are carried out through the agency of linear regression equations that are derived by the running together of the relevant ore metal and gossan element data for sets of test deposits in each sub-study.

In the present study it is necessary, for reasons of predictive accuracy, to split each of the four test deposit sets into high and low sub-sets. These sub-sets are based on the known ore metal contents or grade values of the individual test deposits. This treatment consequently necessitates the derivation of a (discriminant) function to permit unclassified gossans to be correctly allocated to the most suitable predictor equation in each instance. These functions are based on the multivariate statistical differences that exist between the combined gossan geochemical data of the two relevant test sub-sets.

Prior to the initiation of the evaluation study however, the gossan geochemical data for each deposit are screened to remove chemically anomalous samples. This treatment consists of an exclusion of individual samples from each gossan occurrence set whose nickel content falls outside the range: 650 to 8000 ppm. This spread of values corresponds to the range: nickel mean $\pm$ approximately one standard deviation for the 230 samples present in the combined suite of 28 sampled gossan occurrences.

This preliminary work is carried out in order to reduce the inter-sample variability of the data to within manageable, although still representative limits.

In addition, however, the numbers of gossan samples used to compute the element mean data in each of the 19 deposits used across the four evaluation sub-studies are standardised at a maximum of eight. This is done in order to eliminate bias potentially

due otherwise to gross inter-deposit variation in original gossan sample size. A maximum of eight samples per gossan is chosen, as this figure allows similar numbers of gossan samples to be utilised from each of the 19 test deposits. However, where more than this number of suitable gossan samples were present for any deposit, eight samples are randomly selected from those available in order to compute the mean chemical data for that particular gossan.

On the completion of this preliminary work, the arithmetic mean values of the iron, silicon, nickel, copper, manganese, chromium, cobalt and titanium contents of each of the 19 test gossan occurrences are computed. These data are then punched onto computer cards in a suitable format, together with the corresponding observed sulphide nickel and copper mean content or published nickel and copper grade values for the deposit. This data set forms the basis of the four sulphide metal prediction sub-studies that are now described.

The sulphide metal content evaluation study

The prediction of sulphide nickel mean content from surface gossan geochemistry

An investigation of surface gossan geochemistry as a predictor of nickel mean content in near-massive to massive nickel sulphide ores is now presented. The test set for this study comprises 14 deposits, (Figs.11.4.1B., and 11.4.2B.), and as indicated above, this is split into two sub-sets on the basis of observed nickel ore content. Prior to this splitting operation, however, two deposits, (Redross and Munali), are randomly withdrawn from the test set in order to provide some measure of unbiased assessment for the derived predictor equations.

The derived high nickel predictor equation is indicated in Fig.11.4.1A. The function indicates that manganese, titanium and iron mean contents are the significant independent (gossan) variables involved in the prediction of high ore nickel mean contents.Further, the corresponding analysis of variance and F-test data demonstrate that the predictor equation explains a high proportion of the original variation of the observed nickel ore mean contents. In other words, it accurately predicts the nickel contents of the parent ores from the indicated mean geochemistry data of the equivalent surface gossans.

The close predictive accuracy of the high nickel equation is further illustrated

Fig.11.4.1. Results of the High Sulphide Nickel Tenor Prediction Study

A THE DERIVED PREDICTOR EQUATION

Mean Ni Tenor = 42583.4 - 5.893 mean Mn gossan + 5.581 mean Ti gossan + 54.560 mean Fe gossan

$$Fe = Wt\%$$
$$All\ other\ variables = ppm$$

The corresponding analysis of variance and F test data

Source of variation	d.f.	Sum of Squares	Mean Squares	F Value	F-Statistic at 90% C.L
Due to regression	4	162432582	40608146	292.61	9.2434
Deviation from regression	2	277561	138781		
Total	6	162710143			

Proportion of total variation explained by the equation $(R^2) = .9983$

B AN ANALYSIS OF TEST SET RESIDUALS

Deposit	Observed Mean Value (WT%)	Predicted Mean Value (WT%)	Residual	Accuracy (Rel %)	Precision Range at 95% C.L.
Phoenix	4.935	4.930	- 0.005	- 0.10	6.5
Silver Lake / Lunnon Shoot	4.400	4.404	+ 0.004	+ 0.10	5.5
Spargoville 5A	3.963	3.962	- 0.001	- 0.01	28.4
McMahon	3.931	3.946	+ 0.015	+ 0.40	18.0
Mt. Monger	3.758	3.732	- 0.026	- 0.70	27.8
Mt. Edwards	3.524	3.560	+ 0.036	+ 1.00	10.9
Jan Shoot	3.451	3.428	- 0.023	- 0.70	30.0

C AN INDEPENDENT ASSESSMENT OF PREDICTIVE ACCURACY

Deposit	Observed Mean Value (WT%)	Predicted Mean Value (WT%)	Residual	Accuracy (Rel %)	Precision Range at 95% C.L.
Redross	3.351	4.021	+ 0.670	+ 20.00	9.4

ESTIMATED WORKING ACCURACY OF THE EQUATION = ± 15 % AT 90% C.L.

in the analysis of test set residuals table presented in Fig.11.4.1B. The residual values indicated in column four consists of the algebraic difference between the observed (input) sulphide nickel mean data and that predicted from the equation. These data hence demonstrate that the difference between observed and predicted values across the test set are very small - generally less than 200 ppm. In addition, the corresponding accuracy values (column five) which are computed using the formula:

$$\text{ACCURACY (\%)} = \frac{\text{PREDICTED VALUE} - \text{OBSERVED VALUE}}{\text{OBSERVED VALUE}} \times 100\%,$$

provide further indications of the predictive efficiency of the derived equation.

The results of an independent assessment of the predictive accuracy of the high nickel equation are given in Fig.11.4.1C. Here, the relevant element mean data of the Redross gossan have been used to compute a predicted value of the nickel mean content of the equivalent near-massive to massive sulphide ore. This computed value is then compared with that obtained from the chemical analysis of a representative suite of near-massive to massive sulphide samples of Redross ore, (columns one and two). This operation permits an unbiased assessment of the general applicability of the derived predictor equation to be made.

In this instance, the relevant data indicate that the mean nickel content of Redross near-massive to massive sulphide is predicted to within 20 percent of its likely real value. This result, combined with that of the individual test set members allows a likely working accuracy value of ± 15 percent at the 90 percent confidence level to be assigned to the high nickel equation.

The associated precision range values, (column six, Fig.11.4.1B.) are specific to individual deposits within the test set. These data are derived from the likely extreme mean values of each constituent gossan element used in the computation of the predicted nickel ore mean value. The size of the precision range value probably has, within reasonable limits, however, no direct effect on the accuracy level that is associated with the specific deposit.

As previously explained in section 9.3 though, imprecisions in the input (gossan) data cannot be ignored in assessing the overall level of predictive closeness of fit, (predictability) of the computed ore metal result for any given deposit. This is because the super-positional relationship of the accuracy value associated with the predictor equation to the precision range value associated with the deposit is not, in reality, known.

It is hence sound methodological practice to summate these two values in order to arrive at an approximate, if likely rather pessimistic closeness of fit value for the predicted ore metal mean content figure. In this respect, it is therefore over 90 percent likely that the predicted sulphide nickel mean content value of Redross ore, (Fig.11.4.1C.), falls within $\pm$ (20.0 + 9.4), or 29.4 percent of the actual mean value of this metal in near-massive to massive sulphide ore.

The derived predictor equation for the corresponding low nickel ore evaluation study is set out in Fig.11.4.2A. Here, the form of the expression indicates that manganese, titanium and silicon mean contents are the significant independent (gossan) variables involved in the prediction of low mean sulphide nickel contents. Further, both the accompanying statistical data, and the analysis of test set residuals in Fig.11.4.2B. demonstrate the high level of predictive accuracy associated with the equation.

The result of an independent accuracy assessment of the derived equation is given in Fig.11.4.2C. Here, a comparison of observed and predicted sulphide, nickel mean contents for near-massive to massive Munali (Zambia) ore indicates that the former quantity is predicted with an accuracy of 20.8 percent by the equation. This result means that an estimated working accuracy value of about $\pm$ 15 percent at the 90 percent level of confidence can be assigned to the low sulphide nickel predictor equation.

In addition, however, a summation of the indicated accuracy and precision levels for the Munali result demonstrate that, in practical terms, the predicted ore content of this deposit, based on available gossan data, very probably falls within $\pm$ (20.8 + 7.5) or 28.5 percent of the corresponding observed (real) value.

The derivation of two predictor equations based on different ranges of sulphide nickel contents implies that some practical method is required in order to allocate previously unclassified gossan data to the most suitable sub-set equation of the pair. In the mineralogical evaluation study described in section 9.3, this allocation problem was overcome by the development of a discriminant function based on the multivariate statistical differences existing between the gossan data of the two relevant test sub-sets. This method is similarly employed in this context in the present study.

The derived allocation function for the nickel ore evaluation study, together with

Fig.11.4.2. Results of the Low Sulphide Nickel Tenor Prediction Study

A THE DERIVED PREDICTOR EQUATION

Mean Ni Tenor = 22807.5 + 1.580 mean Mn gossan + 3.155 mean Ti gossan − 54.646 mean Si gossan

Si = Wt% units
All other variables in ppm units

The corresponding analysis of variance and F test data

Source of variation	d.f.	Sum of Squares	Mean Squares	F Value	F-Statistic at 90% C.L
Due to regression	3	14557437.0	4852479.0	13672.8	53.593
Deviation from regression	1	354.9	354.9		
Total		14557791.9			

Proportion of total variation explained by the equation (R^2) = .9998

B AN ANALYSIS OF TEST SET RESIDUALS

Deposit	Observed Mean Value (WT%)	Predicted Mean Value (WT%)	Residual	Accuracy (Rel %)	Precision Range at 95% C.L.
Trojan	2.822	2.823	+ 0.001	+ 0.01	19.7
Ravensthorpe	2.500	2.499	− 0.001	− 0.01	2.6
Selkirk	2.489	2.490	+ 0.001	+ 0.01	5.5
Pikwe	2.450	2.449	− 0.001	− 0.01	8.7
Perserverance	2.301	2.301	0.000	0.00	9.4

C AN INDEPENDENT ASSESSMENT OF PREDICTIVE ACCURACY

Deposit	Observed Mean Value (WT%)	Predicted Mean Value (WT%)	Residual	Accuracy (Rel %)	Precision Range at 95% C.L.
Munali	3.113	2.465	− 0.648	− 20.8	7.5

ESTIMATED WORKING ACCURACY OF THE EQUATION = $\pm$ 15% AT 90% C.L.

Fig.11.4.3. Results of the Sulphide Nickel Sub-set Allocation Study

A   THE DERIVED ALLOCATION (DISCRIMINANT) FUNCTION

$$L = 3.046 \log (\text{mean Ni gossan}) + 3.954 \log (\text{mean Cu gossan})$$
$$- 3.232 \log (\text{mean Co gossan}) - 1.479 \log (\text{mean Ti gossan})$$

All variables in ppm units

CUTTING GRADE, L = 13.920 : Range (L ± 2.5%) = 13.572 to 14.268

MAHALANOBIS D^2 STATISTIC = 16.5727

F TEST : $F_{(4,7)}$ = 8.4590; $F_{(4,7;\ 0.05)}$ = 4.1203

B   THE ALLOCATION OF THE TEST SET

High Test Sub-Set L Scores	Low Test Sub-Set L Scores	High Sub-Set Deposit	Low Sub-Set Deposit
15.544		Jan Shoot	
15.009		Spargoville 5A	
14.719		Mt. Monger	
14.684		McMahon	
14.632		Phoenix	
14.602		Mt. Edwards	
14.049		Silver Lake / Lunnon Shoot	
	13.532		Pikwe
	13.348		Trojan
	12.921		Perserverance
	12.835		Selkirk
	12.820		Ravensthorpe 5

C   AN INDEPENDENT ASSESSMENT OF THE ALLOCATION FUNCTION

Deposit	Computed L Score	Allocated Predictor Equation	Known Correct Sub-Set Affinity
Redross	16.852	high	high sub-set
Munali	12.891	low	low sub-set

ESTIMATED MISALLOCATION RATE (at 95% C.L.) < 5 percent

Table 11.4.1.

Predicted sulphide nickel content values for 14 previously unclassified nickel deposits

Deposit	Discriminant function L-score	Predictor equation allocated	Predicted Ni content (p.p.m.)	95% c.l. ·precision of predicted value (+ Rel%)	Closeness of fit of result to actual value + (A + Prec)%
W.A. Carr Boyd	12.58738	LOW	29371	20.0	35.0
Dordie North	13.02382	LOW	23997	9.8	24.8
Durkin Shoot	16.39961	HIGH	31517	89.0	104.0
Nepean	11.50196	LOW	26772	13.9	28.9
Otter Shoot	18.25867	HIGH	44266	7.1	22.1
Scotia	16.02630	HIGH	42870	7.0	22.0
Widgiemootha No 3	14.58738	HIGH (Borderline)	45111 (23194)	13.0 (12.4)	28.0 (27.4)
Mt. Windarra	10.23684	LOW	26037	6.6	21.6
RHODESIA Damba	24.66997	HIGH	44457	3.0	18.0
Empress	16.98689	HIGH	46553	11.0	26.0
Epoch	15.98177	HIGH	43399	5.0	20.0
Fibre	8.81458	LOW	26357	28.8	43.8
Shangani	15.53644	HIGH	44707	4.9	19.9
BOTSWANA Selibi	17.29473	HIGH	46615	3.1	18.1

A = Working accuracy value of the corresponding predictor equation

Values in brackets correspond to predicted values based on an assumed misallocation of the gossan data

a listing of the individual test-set deposit L-scores is presented in Fig.11.4.3A. and 3B. respectively, and the results of an independent assessment of the accuracy of the derived function are set out in Fig.11.4.3C. The significance of the associated statistics, of the cutting grade value and the latters indicated ± 2.5 percent border zone are exactly similar to those previously displayed in Fig.9.3.6.

In the present instance, the test set results in Fig.11.4.3B., and the independent accuracy assessment data in Fig.11.4.3C. both indicate that the derived nickel ore discriminant function is likely to allocate less than five percent of all unknown gossan occurrence data to the wrong predictor equation. The technique hence represents a simple, rapid and accurate method of data allocation.

The results of the complete evaluation procedure of initial data allocation through to subsequent prediction of likely sulphide nickel mean contents are presented in Table 11.4.1. for the 14 previously unused nickel sulphide deposits in the overall study set of 28. The gossan data of these deposits have, (where possible) been standardised both with respect to nickel content range and to sample size prior to this treatment.

Further, the 95 percent confidence precision range associated with the predicted result, as computed from the corresponding extreme mean values of the individual element data, is also displayed in each instance. In addition, the likely overall closeness of fit of each predicted result to the (unknown) corresponding real nickel mean content value is presented as the sum of the predicted value precision range and the accuracy value associated with the specific predictor equation utilised.

The results of this work demonstrate that the mean nickel contents of the majority of sampled near-massive to massive sulphide ores are likely predicted to within ± 25 percent of their actual values using the derived statistical functions outlined above. Further, the relatively wide indicated discrepancies between predicted and actual ore nickel values shown by a minority of deposits are likely due principally to an important lack of sample data precision in those gossan elements significant in the predictor equations for those occurrences.

The results of the above work therefore indicate that the devised technique represents a significant advance in the accurate quantitative prediction of nickel contents of buried nickel sulphide ores from the geochemical characteristics of their surface gossans.

Further, the use of elements in this method that can be analysed on a rapid, accurate

and routine basis similarly represents a dramatic decrease in both analytical time and unit cost over presently available methods that exhibit lower levels of predictive accuracy and which rely on time consuming and expensive neutron activation techniques.

The prediction of sulphide copper mean content from surface gossan geochemistry

A parallel study of sulphide copper mean content prediction is also carried out as part of the present investigation. The test set of 14 deposits involved in this work is initially run in a multiple linear regression program as a single unit. The low predictive accuracy of the derived equation however precluded the latters practical use, and the deposit data were consequently split into two sub-sets (high and low) based on observed sulphide copper mean contents. Two test deposits, (Redross and Mt.Monger), are first randomly removed from the test set however to enable independent accuracy assessments of the derived sub-set predictor equations to be later made.

The results of the high copper prediction study are presented in Fig.11.4.4. The developed regression (predictor) equation and its attendant statistics are set out in Fig.11.4.4A. The form of the equation indicates that the optimum prediction of high copper ore mean contents is achieved by a linear combination of the gossan metal means; copper, manganese, chromium and cobalt. The statistical data demonstrate however that the fit of the equation to the original sulphide metal data values is relatively poor.

An analysis of test set residuals, (Fig.11.4.4B.), indicates, in contrast, that the equation very accurately predicts the sulphide copper mean contents of these deposits. The corresponding precision ranges of these results are however rather wide, (column six). This latter feature is even more marked in the companion low copper sub-set results, and it is probably caused by relatively wide between-sample variations in significant (predictor) element contents in these gossan occurrences. These rather wide precision values are however considered to fall within generally acceptable limits in the context of the present study.

The lack of data in Fig.11.4.4C. indicates that no independent assessment of predictive accuracy is possible for the high copper equation on the basis of available data. This is because neither of the randomly removed test deposits has an observed sulphide copper mean content that falls within or close to the range of values indicated in column two of Fig.11.4.4B. The estimated working

Fig.11.4.4 Results of the High Sulphide Copper Tenor Prediction Study

A THE DERIVED PREDICTOR EQUATION

Mean Cu Tenor = 19024.9 + 1.043 mean Cu gossan − 6.020 mean Mn gossan
+ 0.281 mean Cr gossan − 27.757 mean Co gossan

All variables in ppm units

The corresponding analysis of variance and F test data

Source of variation	d.f.	Sum of Squares	Mean Squares	F Value	F-Statistic at 90% C.L
Due to regression	4	93732140	23433035	43.48	55.833
Deviation from regression	1	538941	538941		
Total	5	94271081			

Proportion of total variation explained by the equation (R^2) = .9943

B AN ANALYSIS OF TEST SET RESIDUALS

Deposit	Observed Mean Value (WT%)	Predicted Mean Value (WT%)	Residual	Accuracy (Rel %)	Precision Range at 95% C.L.
Phoenix	2.570	2.591	+ 0.021	+ 0.8	45.4
Pikwe	2.263	2.203	− 0.060	− 2.7	17.9
Selkirk	1.999	2.036	+ 0.037	+ 1.9	10.8
Jan Shoot	1.955	1.955	0.000	0.0	47.3
Silver Lake / Lunnon Shoot	1.635	1.635	0.000	0.0	51.4
Perserverance	1.351	1.353	+ 0.002	+ 0.2	31.5

C AN INDEPENDENT ASSESSMENT OF PREDICTIVE ACCURACY

Deposit	Observed Mean Value (WT%)	Predicted Mean Value (WT%)	Residual	Accuracy (Rel %)	Precision Range at 95% C.L.

ESTIMATED WORKING ACCURACY OF THE EQUATION = ± 15% AT 90% C.L.

accuracy of the high sulphide copper predictor equation is hence set at a plausible figure of $\pm$ 15 percent at the 90 percent level of confidence.

The results of the parallel study of low sulphide copper mean content prediction are set out in Fig.11.4.5. The developed predictor equation presented in Fig.11.4. 5A. indicates that nickel, cobalt, titanium and iron are the significant gossan variables involved in the linear function. Further, the associated statistical data indicate the close fit of the equation to the observed sulphide copper data of the six test deposits.

This closeness of fit of the test set results is further demonstrated by the analysis of residuals displayed in Fig.11.4.5B. These data show that the sulphide copper mean contents of the test deposits are perfectly predicted by the derived equation. A more realistic level of predictive accuracy is however provided by the results of the independent prediction assessment of the two un-utilised deposits, (Fig.11.4.5C.). These indicate that a likely working accuracy value of about $\pm$ 20 percent may be attached to the low sulphide copper predictor equation at the 90 percent level of confidence.

The problem of allocating unclassified gossan data to the most suitable predictor equation is in the sulphide copper evaluation study also solved by the development of a suitable discriminant function, (Fig.11.4.6A.). The attendant statistics of this expression indicate that a wide and therefore efficient separation of the test sub-sets is achieved by this means, and the expression itself demonstrates that this separation is made through a linear combination of $\log_{10}$ transformed arithmetic means of the gossan metals; nickel, copper, manganese and titanium.

The wide separation of sub-set data is further illustrated in Fig.11.4.6B. Here, the computed L-scores for the individual members of both copper evaluation sub-sets are listed in descending order of value. Unfortunately, the estimated misallocation rate of the derived allocation function cannot be set at a neglegible level on this basis because of the observed misallocation of both independent test deposits, (Fig.11.4.6C.). It is hence more plausible to assign a misallocation rate of approximately 12 percent (at about the 95 percent level of confidence) to the derived sulphide copper allocation function.

The results of an equation allocation and subsequent prediction of copper ore mean values for the 14 un-utilised members of the overall nickel sulphide study set are presented in Table 11.4.2.

Fig.11.4.5. Results of the Low Sulphide Copper Prediction Study

A   THE DERIVED PREDICTOR EQUATION

Mean Cu Tenor = 10204.5 + 0.003 mean Ni gossan + 2.325 mean Co gossan
+ 5.893 mean Ti gossan - 222.901 mean Fe gossan

Fe = Wt% units
All other data in ppm units

The corresponding analysis of variance and F test data

Source of variation	d.f.	Sum of Squares	Mean Squares	F Value	F-Statistic at 90% C.L
Due to regression	4	26002810	6500703	2132650.6	55.833
Deviation from regression	1	3.048	3.048		
Total	5	26002813			

Proportion of total variation explained by the equation $(R^2) = 1.000$

B   AN ANALYSIS OF TEST SET RESIDUALS

Deposit	Observed Mean Value (WT%)	Predicted Mean Value (WT%)	Residual	Accuracy (Rel %)	Precision Range at 95% C.L.
Spargoville 5A	0.772	0.772	0.000	0.0	77.8
Mt. Edwards	0.594	0.594	0.000	0.0	59.6
Ravensthorpe	0.344	0.344	0.000	0.0	63.0
Munali	0.311	0.311	0.000	0.0	210.0
McMahon	0.228	0.228	0.000	0.0	80.2
Trojan	0.192	0.192	0.000	0.0	200.0

C   AN INDEPENDENT ASSESSMENT OF PREDICTIVE ACCURACY

Deposit	Observed Mean Value (WT%)	Predicted Mean Value (WT%)	Residual	Accuracy (Rel %)	Precision Range at 95% C.L.
Redross	0.634	0.671	+ 0.037	+ 5.8	45.7
Mt. Monger	0.341	0.434	+ 0.093	+ 27.3	98.7

ESTIMATED WORKING ACCURACY OF THE EQUATION = $\pm$ 20 % AT 90% C.L.

Fig.11.4.6. Results of the Sulphide Copper Sub-set Allocation Study

A THE DERIVED ALLOCATION (DISCRIMINANT) FUNCTION

$$L = - 7.428 \log(\text{mean Ni gossan}) + 7.362 \log(\text{mean Cu gossan}) + 3.130 \log(\text{mean Mn gossan}) - 4.911 \log(\text{mean Ti gossan})$$

All variables in ppm units

CUTTING GRADE, $L = - 6.688$: Range $(L \pm 2.5\%) = -6.521$ to -6.855

MAHALANOBIS D^2 STATISTIC $= 56.1696$

F TEST : $F_{(4,7)} = 29.4890$; $F_{(4,7: .05)} = 4.1203$

B THE ALLOCATION OF THE TEST SET

High Test Sub-Set L Scores	Low Test Sub-Set L Scores	High Sub-Set Deposit	Low Sub-Set Deposit
- 2.990		Phoenix	
- 3.303		Pikwe	
- 3.754		Perserverance	
- 3.779		Jan Shoot	
- 4.605		Selkirk	
- 4.844		Silver Lake / Lunnon Shoot	
	- 8.511		Mc Mahon
	- 8.883		Munali
	- 9.189		Mt. Edwards
	- 9.805		Trojan
	- 9.980		Spargoville 5A
	- 10.609		Ravensthorpe 5

C AN INDEPENDENT ASSESSMENT OF THE ALLOCATION FUNCTION

Deposit	Computed L Score	Allocated Predictor Equation	Known Correct Sub-Set Affinity
Redross	+ 2.385	high	low
Mt. Monger	- 5.458	high	low

ESTIMATED MISALLOCATION RATE (at 95% C.L.) $\approx$ 12 percent

Table 11.4.2.

Predicted sulphide copper content values for 14 previously unclassified nickel deposits

Deposit	Discriminant function L-score	Predictor equation allocated	Predicted Cu content (p.p.m.)	95% c.l. ·precision of predicted value ($\pm$ Rel%)	Closeness of fit of result to actual value $\pm$ (A + Prec)%
W.A. Carr Boyd	- 10.99207	LOW (Borderline)	11553 (16425)	99.6 (40.7)	119.6 (55.7)
Dordie North	- 4.54468	HIGH	10497	251.0	266.0
Durkin Shoot	- 3.47667	HIGH	19692	189.0	204.0
Nepean	- 7.31981	LOW	3087	42.4	62.4
Otter Shoot	- 5.74226	HIGH	23562	106.0	121.0
Scotia	- 8.34477	LOW	10068	28.3	48.3
Widgiemooltha No 3	- 8.89530	LOW	7789	96.3	116.3
Mt. Windarra	- 11.62323	LOW	7055	90.2	110.2
RHODESIA Damba	- 9.53668	LOW	2012	134.0	154.0
Empress	- 4.80055	HIGH	24747	42.4	57.4
Epoch	- 8.74976	LOW	1367	189.0	209.0
Fibre	- 12.49741	LOW	10051	107.0	127.0
Shangani	- 4.49686	HIGH	8045	258.0	273.0
BOTSWANA Selibi	0.69015	HIGH	38748	33.9	48.9

A = Working accuracy value of the corresponding predictor equation

Values in brackets correspond to predicted values based on an assumed misallocation of the gossan data

The relevant results indicate that no anomalous (borderline) allocation of gossan data occur across this deposit suite. This is in spite of the 12 percent misallocation rate likely associated with the allocation function. In this respect however the relatively anomalous predicted copper mean values of the Carr Boyd, Dordie North and Shangani deposits may be significant.

The very large precision ranges of the majority of the predicted values (column five) are almost certainly due to the effects of significant inter-sample element distribution within each gossan sample set, and this feature is in turn probably related to the small sample numbers that typically make up these gossan suites.

It is highly likely however that such variation could be minimised by the presence of larger numbers of suitably representative gossan samples from each occurrence. It is possible in that case though that the mean element values from which the sulphide copper content is predicted would alter slightly, although probably not by a significant amount. The subsequent improvement in precision that would likely result from such a development would however bring about a corresponding improvement in the closeness of predictive fit for the majority of the unclassified deposits in Table 11.4.2.

However, even allowing for the relative imprecision of the present unclassified nickel gossan data, the evaluation method outlined above is capable of producing a rapid, workably accurate quantitative prediction of likely sulphide copper mean content from the geochemistry of the corresponding surface gossan.

The development of this technique therefore represents a significant advance in the quantitative geochemical evaluation of nickel sulphide ores from their equivalent surface gossans.

The deposit metal grade evaluation study

The application of nickel gossan geochemistry to the prediction of overall metal grades in parent sulphide mineralisation is now described. The study is split into two parts; namely a prediction first of nickel grade and then one of copper grade. Multiple linear regression analysis is again used to derive suitable predictor equations. In this instance however, the published values of nickel or copper grade are erected as dependent variables against the independent variables of the gossan element mean content suite for each of the 19 test deposits utilised in the study.

The overall metal grade value of a deposit and the mean geochemistry of its

gossan after near-massive to massive sulphide are not though directly related –
either geochemically or conceptually. This is because the published grade value,
although (hopefully) a representative index of metal content is generally a
weighted composite mean of the ore metal contents of the massive, near-massive
and disseminated components of the orebody. As such it represents a quantitatively
distinct though similar geochemical population to that of the near-massive to
massive sulphide component alone. This is because it additionally takes account of
the disseminated ore component of the orebody.

The equations relating metal grade and gossan geochemistry that are derived in the
present study are hence rather more directly based on statistical relationships
rather than on geochemical ones. This relative lack of conceptual linkage appears
not, in practical terms to matter significantly however as useful working accuracies
are associated with each of the predictor equations developed during the grade
evaluation study.

The prediction of nickel grade from surface gossan geochemistry

The nickel grade evaluation study and its results are now described. The work is
based on a test set of 19 nickel sulphide deposits for which both published nickel
grade and representative gossan geochemical data were available.

These deposits are split into two sub-groups based on grade value subsequent to
an initial combined evaluation run which produced only a very inaccurate and
hence unusable predictor equation. Prior to the split however the data for three
test deposits were randomly removed and were later used as independent assessors
of predictive accuracy for the developed equations.

The results of the high nickel grade prediction study are presented in Fig.11.4.7.,
and the derived equation and its attendant statistical fit data are indicated in Fig.
11.4.7A. The form of the equation demonstrates that, based on available data,
a linear function involving the $\log_{10}$ transformed arithmetic means of gossan chromium,
titanium, iron and silicon content provides the most efficient predictive combination
of high nickel grade. Further, the accompanying statistical data indicate that the
equation explains almost all of the total inter-deposit variation exhibited by the
observed nickel grade values of the test set.

The corresponding analysis of test set residuals, (Fig.11.4.7B.) additionally
demonstrates this closeness of statistical fit through the small values of both the

Fig.11.4.7. Results of the High Nickel Grade Prediction Study

A THE DERIVED PREDICTOR EQUATION

Ni grade = 70316.9 - 16342.9 log(mean Cr gossan) - 6649.3 (mean Ti gossan)
+ 9820.3 log(mean Fe gossan) + 13150.4 log(mean Si gossan)
Fe, Si = Wt% units
All other variables in ppm units

The corresponding analysis of variance and F test data

Source of variation	d.f.	Sum of Squares	Mean Squares	F Value	F-Statistic at 90% C.L
Due to regression	4	367077723	91769430.9	60.0475	9.2434
Deviation from regression	2	3056562	1528281.1		
Total	6	370134285			

Proportion of total variation explained by the equation (R^2) = .9917

B AN ANALYSIS OF TEST SET RESIDUALS

Deposit	Observed Mean Value (WT%)	Predicted Mean Value (WT%)	Residual	Accuracy (Rel %)	Precision Range at 95% C.L.
Silver Lake / Lunnon Shoot	4.290	4.201	- 0.091	- 2.1	28.3
Redross	3.500	3.595	+ 0.095	+ 2.7	30.0
Scotia	3.070	3.051	- 0.019	- 0.6	24.8
Nepean	3.000	3.044	+ 0.044	+ 1.5	14.8
Spargoville 5A	2.400	2.464	+ 0.064	+ 2.7	39.6
Mt. Edwards	2.200	2.115	- 0.085	- 3.9	33.9
Phoenix	2.100	2.091	- 0.009	- 0.4	54.3

C AN INDEPENDENT ASSESSMENT OF PREDICTIVE ACCURACY

Deposit	Observed Mean Value (WT%)	Predicted Mean Value (WT%)	Residual	Accuracy (Rel %)	Precision Range at 95% C.L.
Otter Shoot	3.500	3.164	- 0.336	- 9.6	34.3

ESTIMATED WORKING ACCURACY OF THE EQUATION = $\pm$ 10% AT 90% C.L.

residual and predicted accuracy values that occur for each test deposit. And an independent assessment of overall predictive accuracy based on the predicted grade value of the Otter Shoot indicates that a workable accuracy level of about ± 10 percent at the 90 percent confidence level is likely to be associated with the high nickel grade equation.

Fig.11.4.7B. also indicates however that the precision ranges of the predicted test set and independent deposit results are in general quite wide, although they are within reasonable limits in the context of the present work. This feature is again most probably related to the relatively small numbers of samples that had of necessity to be utilised in the computation of the majority of the gossan mean data values used in this study. The relative imprecision of the test set data does not in reality detract from the accuracy of the derived equation as the gossan mean values are generally considered to be representative of the populations from which they are drawn.

The results of the companion evaluation study of the low nickel grade test set are presented in Fig.11.4.8., and, the derived predictor equation is set out in Fig.11.4.8A. The form of the function indicates that $\log_{10}$ transformed arithmetic means of gossan copper, chromium and titanium are the significant independent variables involved in the linear regression function.

In contrast to the high nickel grade equation however the associated statistical data demonstrate that a relatively low level of data fit characterises the low grade equation. This phenomenon is further reflected in the relatively wide predictive accuracy values noted across the test deposit suite and the two independent assessor deposits, (Figs. 11.4.8B. and 8C.). In addition these latter data imply that a working accuracy value of about ± 35 percent at the 90 percent confidence level is likely to be associated with the derived predictor equation.

The precision range values for the test deposits are, as in the high grade study rather wide and, in this instance, likely border on acceptable limits. Bearing this point in mind however the results of the low nickel grade prediction study indicate that the derived equation is capable of reasonable levels of predictive fit. This is especially true if the input data for a previously unclassified deposit is derived from a relatively large number of suitable gossan samples.

The derivation of two predictor equations based on separate nickel grade value ranges again raises the problem of allocating previously unclassified nickel gossan

Fig.11.4.8. Results of the Low Nickel Grade Prediction Study

A THE DERIVED PREDICTOR EQUATION

Ni grade = -3213.6 - 2849.0 log(mean Cu gossan) + 3123.8 log(mean Cr gossan)
+ 5883.1 log(mean Ti gossan)

All variables in ppm units

The corresponding analysis of variance and F test data

Source of variation	d.f.	Sum of Squares	Mean Squares	F Value	F-Statistic at 90% C.L
Due to regression	3	57032641.6	19010880.5	3.1633	3.6195
Deviation from regression	5	30049580.6	6009916.1		
Total	8	87082222.2			

Proportion of total variation explained by the equation (R^2) = .6549

B AN ANALYSIS OF TEST SET RESIDUALS

Deposit	Observed Mean Value (WT%)	Predicted Mean Value (WT%)	Residual	Accuracy (Rel %)	Precision Range at 95% C.L.
Carr Boyd	1.650	1.547	- 0.103	- 6.2	69.1
P ikwe	1.450	1.098	- 0.352	- 24.3	28.6
Widgiemooltha 3	1.230	1.130	- 0.010	- 8.1	34.8
Dordie North	1.200	1.378	+ 0.178	+ 14.8	30.0
Shangani	0.920	0.822	- 0.098	- 10.7	39.5
Perserverance	0.920	0.933	+ 0.013	+ 1.4	41.3
Selkirk	0.900	1.120	+ 0.220	+ 24.4	75.2
Empress	0.700	0.957	+ 0.257	+ 36.7	58.6
Selibi	0.700	0.685	- 0.015	- 2.1	65.7

C AN INDEPENDENT ASSESSMENT OF PREDICTIVE ACCURACY

Deposit	Observed Mean Value (WT%)	Predicted Mean Value (WT%)	Residual	Accuracy (Rel %)	Precision Range at 95% C.L.
Mt. Windarra	1.910	1.677	- 0.233	- 12.2	7.3
Trojan	0.830	1.186	+ 0.356	- 42.9	21.6

ESTIMATED WORKING ACCURACY OF THE EQUATION = ± 35 % AT 90% C.L.

Fig.11.4.9. Results of the Nickel Grade Sub-set Allocation Study

A   THE DERIVED ALLOCATION (DISCRIMINANT) FUNCTION

$L = 0.361$ log(mean Ni gossan) $- 0.088$ log (mean Cu gossan) $+ 0.186$ log (mean Cr gossan) $- 0.350$ log(mean Co gossan) $- 0.431$ log (mean Ti gossan) $- 0.261$ log (mean Si gossan)

Si = Wt% units
All other variables in ppm units

CUTTING GRADE, $L = - 0.646$: Range $(L \pm 2.5\%) = -0.630$ to -0.662

MAHALANOBIS D^2 STATISTIC $= 4.1303$

F TEST : $F_{(6,9)} = 1.7425$; $F_{(6,9;.10)} = 2.5509$

B   THE ALLOCATION OF THE TEST SET

High Test Sub-Set L Scores	Low Test Sub-Set L Scores	High Sub-Set Deposit	Low Sub-Set Deposit
- 0.144		Mt. Edwards	
- 0.492		Redross	
- 0.509		Scotia	
- 0.524		Nepean	
	- 0.543		Shangani
- 0.565		Phoenix	
- 0.617		Spargoville 5A	
- 0.635		Silver Lake / Lunnon Shoot	
	- 0.726		Perserverance
	- 0.742		Selkirk
	- 0.762		Widgiemooltha 3
	- 0.776		Dordie North
	- 0.826		Carr Boyd
	- 0.879		Empress
	- 0.884		Selibi
	- 1.002		Pikwe

C   AN INDEPENDENT ASSESSMENT OF THE ALLOCATION FUNCTION

Deposit	Computed L Score	Allocated Predictor Equation	Known Correct Sub-Set Affinity
Otter Shoot	- 0.315	high	high
Mt. Windarra	- 0.650	low (borderline)	low (borderline)
Trojan	+ 0.137	low	low

ESTIMATED MISALLOCATION RATE (at 95% C.L.) $\approx$ 8 percent

Table 11.4.3.

Predicted nickel grade values for nine previously unclassified nickel deposits

Deposit	Discriminant function L-score	Predictor equation allocated	Predicted Ni grade (p.p.m.)	95% c.l. ·precision of predicted value (± Rel%)	Closeness of fit of result to actual value ± (A + Prec)%
W.A. Durkin Shoot	- .49768	HIGH	1.859	77.0	87.0
Jan Shoot	- .06515	HIGH	2.663	33.0	43.0
Mt. Monger	- .35391	HIGH	2.613	59.0	69.0
McMahon	- .12056	HIGH	3.410	73.0	83.0
Ravensthorpe No 5	- .91476	LOW	0.779	14.0	49.0
RHODESIA Damba	- .23274	HIGH	4.838	31.0	41.0
Fibre	- 1.32632	LOW	1.442	34.0	69.0
Epoch	- .22708	HIGH	2.711	39.0	49.0
BOTSWANA Selibi	- .88361	LOW	0.685	40.0	75.0

A = Working accuracy value of the corresponding predictor equation

data to the most suitable predictor equation. In the present instance, this problem is also solved by the development of an allocation (discriminant) function based on the multivariate statistical differences that exist between the combined gossan geochemical data of the two test sub-suites.

This function is presented in Fig.11.4.9A., and its form indicates that the $\log_{10}$ transformed arithmetic means of nickel, copper, chromium, titanium and silicon are the significant gossan variables involved in this instance. Both the accompanying statistics and the visual presentation of computed test deposit L-scores, (Fig.11.4.9B.), indicate though that the separation of the two sub-sets is not perfect. But, in spite of this, the correct allocation of all three independent test deposits in Fig.11.4.9C. demonstrates that a working misallocation rate of about eight percent (at the 95 percent confidence level) is likely to be applicable to the indicated function.

The practical application of the above nickel grade evaluation procedure is illustrated in Table 11.4.3. for a suite of nine previously unclassified nickel deposits. The results are based on suitable nickel gossan data from each deposit and as such the majority exhibit the effects of relatively small sample numbers on the precision of their predicted grade values. Much improved levels of overall predictive fit should however be possible with input gossan mean data drawn from suitably sized sample numbers.

Even allowing for these existing levels of data imprecision it can be stated though, that the outlined prediction technique still allows rapid, workably accurate assessments of likely grade levels to be made from the geochemistry of the surface gossan outcrop. It therefore represents a considerable advance in the field of nickel sulphide ore evaluation.

The prediction of copper grade from surface gossan geochemistry

The results of a parallel prediction study of copper ore grade from gossan geochemistry are now presented. In common with the other reported investigations, the test set deposits used for the copper grade study were split into two sub-set on the basis of observed grade values after initial work on the combined suite failed to produce a useable predictor equation.

The derived high copper grade predictor equation is set out in Fig.11.4.10A., and its form indicates that the arithmetic mean values of copper, chromium, cobalt and titanium form the significant gossan predictor variables in the expression.

Fig.11.4.10 Results of the High Copper Grade Prediction Study

A   THE DERIVED PREDICTOR EQUATION

Mean Cu grade = − 229.728 + 0.635 mean Cu gossan + 27.737 mean Cr gossan
− 63.130 mean Co gossan + 5.139 mean Ti gossan

All variables in ppm units

The corresponding analysis of variance and F test data

Source of variation	d.f.	Sum of Squares	Mean Squares	F Value	F-Statistic at 90% C.L
Due to regression	4	92799999	23199998	9.570	9.243
Deviation from regression	2	4848581	2424290		
Total	6	97648571			

Proportion of total variation explained by the equation (R^2) = .9503

B   AN ANALYSIS OF TEST SET RESIDUALS

Deposit	Observed Mean Value (WT%)	Predicted Mean Value (WT%)	Residual	Accuracy (Rel %)	Precision Range at 95% C.L.
Selibi	1.560	1.543	− 0.017	− 1.1	106
Pikwe	1.140	1.059	− 0.081	− 7.1	123
Phoenix	0.800	0.827	+ 0.027	+ 3.4	313
Selkirk	0.800	0.924	+ 0.124	+ 15.5	132
Trojan	0.650	0.543	− 0.107	− 16.5	838
Perserverence	0.460	0.408	− 0.052	− 11.3	466
Silver Lake / Lunnon Shoot	0.410	0.516	+ 0.106	+ 25.9	554

C   AN INDEPENDENT ASSESSMENT OF PREDICTIVE ACCURACY

Deposit	Observed Mean Value (WT%)	Predicted Mean Value (WT%)	Residual	Accuracy (Rel %)	Precision Range at 95% C.L.
Carr Boyd	0.490	2.127	+ 1.637	+ 334	174

ESTIMATED WORKING ACCURACY OF THE EQUATION = $\pm$ 40 % AT 90 % C.L.

Fig.11.4.11. Results of the Low Copper Grade Prediction Study

A   THE DERIVED PREDICTOR EQUATION

Cu grade = - 2506.12 + 872.05 log(mean Cu gossan) + 1407.86 log(mean
Mn gossan) - 1367.00 log (mean Co gossan) + 555.05 log (mean
Si gossan)

Si in Wt% units
All other variables in ppm

The corresponding analysis of variance and F test data

Source of variation	d.f.	Sum of Squares	Mean Squares	F Value	F-Statistic at 90% C.L
Due to regression	4	4713212.1	1178303.0	15.9404	4.1073
Deviation from regression	4	295676.8	73919.2		
Total	8	5008888.9			

Proportion of total variation explained by the equation $(R^2) = .9410$

B   AN ANALYSIS OF TEST SET RESIDUALS

Deposit	Observed Mean Value (WT%)	Predicted Mean Value (WT%)	Residual	Accuracy (Rel %)	Precision Range at 95% C.L.
Empress	0.300	0.305	+ 0.005	+ 1.7	49.0
Redross	0.270	0.265	- 0.005	- 1.9	85.6
Scotia	0.250	0.260	+ 0.010	+ 4.0	34.0
Spargoville 5A	0.210	0.168	- 0.042	- 20.0	57.2
Nepean	0.200	0.215	+ 0.015	+ 7.5	40.0
Mt. Edwards	0.200	0.184	- 0.016	- 8.0	46.0
Dordie North	0.120	0.143	+ 0.023	+ 19.2	317.0
Widgiemooltha 3	0.100	0.104	+ 0.004	+ 4.0	200.0
Shangani	0.070	0.077	+ 0.007	+ 10.0	163.0

C   AN INDEPENDENT ASSESSMENT OF PREDICTIVE ACCURACY

Deposit	Observed Mean Value (WT%)	Predicted Mean Value (WT%)	Residual	Accuracy (Rel %)	Precision Range at 95% C.L.
Otter Shoot	0.350	0.112	- 0.238	- 68.0	56.3
Mt. Windarra	0.190	0.213	+ 0.023	+ 12.1	92.0

ESTIMATED WORKING ACCURACY OF THE EQUATION = $\pm$ 20 % AT 90% C.L.

Further, both the associated statistical data and the results of an analysis of test set residuals, (Fig.11.4.10B.) demonstrate that the statistical fit of the equation to the input grade data is relatively poor. In addition however the totally unacceptable predictive accuracy value for the independent Carr Boyd deposit, (Fig.11.4.10C.), implies that an estimated minimum working accuracy of at least ± 40 percent or possibly more is probably associated with the derived equation.

Under normal circumstances this accuracy value would allow a reasonable, if semi-quantitative estimation of copper grade to be made from surface gossan geo-chemistry. However, the typically huge precision range values associated with the test set results properly preclude further serious consideration of the equation as a useful predictor of ore copper grade. This is because these levels of precision are incompatable with the relatively high accuracy levels achieved by the linear combination of gossan metal mean data for each deposit, and they indicate the likelihood that the gossan mean data are, in the context of the equation, likely to be unrepresentative of their parent populations.

These considerations unfortunately also apply to the results of the corresponding low copper grade evaluation study, (Fig.11.4.11.). Here, sample imprecision in the combination of statistically significant gossan variables utilised in the equation has been large enough in the majority of cases to produce very high precision range values in the corresponding predicted copper grade data.

These levels of precision in the test set data are hence realistically incompatable with the relatively small predictive accuracy values demonstrated by these deposits. Consequently the derived equation cannot be utilised as a generally applicable grade evaluation tool. And in this context, the results of the study are presented in Fig.11.4.10. for the sake of completeness.

In conclusion therefore it can be stated that the workable prediction of overall copper grades in nickel sulphide ores cannot, on presently available data, be made from the geochemistry of surface gossans after near-massive to massive sulphide ore.

The significance of the prediction technique in mineral exploration

The investigation of surface nickel gossan geochemistry as an accurate quantitative tool in the prediction of economic metal tenor in underlying sulphide mineralisation has, on the basis of the above results, been successfully accomplished.

Significantly, the derived evaluation technique is based on gossan chemical (element) data that are generally available from routine geochemical studies of gossan outcrops. In consequence, the technique represents a considerable quantitative advance on previous nickel gossan outcrop evaluation techniques that utilise trace levels of difficult-to analyse platinum group metals (PGM), and which only furnish wide indications of likely ore nickel contents.

In addition though, use of the devised method enables results to be rapidly computed from the relevant gossan data by pocket electronic calculator, and is achieved by substitution of values in the appropriate discriminant function and predictor equation for each specific measure of sulphide metal tenor that is required to be known.

The technique is therefore significantly more rapid to use, is much cheaper and is more convenient than the neutron activation techniques required for PGM evaluation work. Further, in the instance of the sulphide copper mean content and nickel grade prediction work, the results form a significant qualitative advance in this field. This is because neither of these paramenters has previously been able to be quantitatively predicted from the surface gossan.

However, not only is the method accurate, rapid and simple to use, its derivation from a significant number of well-documented oxidising nickel sulphide deposits that are located within the semi-arid Archean shield regions of southern Africa and Western Australia indicates that the derived equations very probably have a wide application in similar deposits in these two major nickel provinces of the world. Further, this contention similarly infers the likelihood that the derived equations may also be applicable in other semi-arid Archean shield regions where oxidising, magmatic segregation deposits of nickel sulphide ores are found.

In conclusion therefore, the derived sulphide metal prediction technique represents a significant advance in the field of rapid, accurate, quantitative evaluation of surface nickel gossan outcrops in terms of their buried parent sulphide mineralisation. It is not seriously suggested however that application of the technique should supplant a well-organised prospect evaluation programme based on percussion and diamond drilling, but rather that the utilisation of the developed equations at the post-discovery, pre-drilling stage should be seriously considered as a very useful means of rapidly assessing the economic potential of a newly-discovered nickel gossan prospect. Its adoption in these circumstances would thereby enable more efficient use to be made of expensive drill footage in the proper detailed evaluation of buried nickel sulphide mineralisation.

11.5 SUMMARY OF CONCLUSIONS

The principal results of the geochemical evaluation work on nickel gossans described in chapter 11 are now summarised.

(1) Near-massive to massive nickel sulphide ores and their equivalent gossans possess geochemical signatures that are quantitatively distinct from each other and from rocks of similar type in other nickel sulphide orebodies.

(2) Multiple distributions typify the population statistics of major and minor elements across a combined suite of 15 nickel sulphide ores.

(3) Single distributions characterise the population statistics of these elements across an equivalent suite of surface nickel gossans.

(4) These features enable a series of multiple linear regression (predictor) equations to be developed that allow three important measures of sulphide metal content to be accurately predicted from the mean geochemistry of the equivalent surface gossan. These measures are; i) massive sulphide nickel content; ii) massive sulphide copper content; iii) nickel ore body grade.

(5) Each study is split into two separate sub-studies on the basis of known sulphide metal contents. The estimated closeness of predictive fit, at the 90 percent confidence level, of the derived predictor equations for each of the six sub-studies are as follows:

The sulphide nickel prediction study;	High equation:	± 15 percent
	Low equation:	± 15 percent
The sulphide copper prediction study;	High equation:	± 15 percent
	Low equation :	± 20 percent
The nickel grade prediction study;	High equation:	± 10 percent
	Low equation :	± 35 percent

(6) Allocation of previously unclassified gossan data to the most suitable predictor equation in each study is effected by the derivation of a sub-set allocation (discriminant) function. These functions are developed from the multivariate statistical differences that exist between the gossan input data of the relevant high and low test sub-sets. The estimated misallocation rates of the three functions derived in this way are as follows:

Prediction Study	Misallocation rate (95% c.l.)
Massive sulphide nickel:	Less than five percent
Massive sulphide copper:	Not more than 12 percent
Nickel ore body grade:	Not more than eight percent

(7) The results of ore tenor prediction trials involving available unclassified gossan data indicate the following;

i) The likely massive sulphide nickel content of the parent ore is typically predicted to within at least ± 30 percent.

ii) The likely massive sulphide copper content of the parent ore is typically predicted to within ± 60 percent on available data.

iii) The likely nickel ore body grade of the parent ore is generally predicted to within ± 70 percent on available data.

The results of trials ii and iii show generally low levels of predictability. This is in all instances due to the relatively high sample imprecision value associated with each predicted result. This is, in turn, due to the relatively small numbers of individual samples that were available for computation of the necessary gossan input data in each instance. Use of larger gossan sample suites would substantially improve the precision of the corresponding predicted ore tenor values.

(8) The derived technique has several major advantages over the neutron activation technique currently used in the semi-quantitative prediction of nickel ore tenor. It is more accurate. It is more rapid to use. It is much cheaper. It is more convenient. In addition, it also enables the previously unavailable parameters of massive sulphide copper content and nickel ore body grade to be accurately predicted from the surface gossan. Further, the technique is generally applicable to evaluation of nickel sulphide ores in the Archean Shield regions of both southern Africa and Western Australia. It may also be tentatively applied to oxidised mineralisation of this type at present cropping out in such Shield regions that have been recently affected by semi-arid climatic regimes.

CHAPTER TWELVE

SUMMARY, CONCLUSIONS AND RECOMMENDATIONS FOR FURTHER WORK

12.1 Summary

This thesis has reported a recent study of near-surface alteration in a number of Archean nickel sulphide ore bodies at present outcropping in semi-arid terrains. The work is divided into three principal parts, each of which is concerned with a major aspect or implication of this alteration phenomenon in nickel sulphide ores.

Part 1 describes the near-surface alteration present in 17 nickel sulphide ore profiles from southern Africa and Western Australia. The recognition and description of secondary alteration in the majority of these deposits has not previously been reported.

The descriptive work, (chapters three to five), takes the form of a documentation of the mineralogical, textural and geochemical changes that occur in each ore profile during the progressive alteration of massive primary ore. The principal features of each developed alteration sequence are subsequently compared, (chapter six).

In Part Two of the study, (chapters seven and eight), these descriptive data are utilised in an interpretative discussion of both supergene sulphide and oxide zone genesis in nickel sulphide ores. The post-formation history of the oxide zone is also discussed on this basis. These investigations are undertaken against the general conceptual background of a supergene genetic model previously developed by another worker.

The third part of the study comprises work on the utilisation of surface nickel gossan characteristics as sulphide ore prediction tools in mineral exploration programmes.

In chapter nine the bulk mineralogical compositions of surface nickel gossans are developed as quantitative predictors of sulphide ore metal tenor through the application of multivariate statistics. In addition, the oxidate minerals associated with these surface rocks are utilised as aids to nickel gossan outcrop recognition.

The well-established qualitative use of nickel gossan relic ore textures as sulphide metal predictors is further developed in chapter ten. Here, the application of

multivariate statistics permits these phenomena to be employed as quantitative predictors of parent sulphide nickel tenor.

In chapter eleven, the observed geochemical characteristics of surface nickel gossans are utilised, through the application of multivariate statistics, as quantitative predictors of a number of important sulphide ore metal parameters.

12.2 Conclusions

The principal conclusions of the above work programme are now presented. These results are set out in three parts, each part corresponding to a major sub-division of the study.

12.2.1 The principal features of secondary alteration in nickel sulphide ores

Petrological and geochemical work on 17 oxidised nickel sulphide deposits from southern Africa and Western Australia has produced the following conclusions.

(A) Primary sulphide ore characteristics

(1) The mineralogy of all sampled near-massive to massive primary ores is qualitatively similar, and consists of the assemblage: Pyrrhotite, pentlandite, chalcopyrite, spinel and silicate.

(2) This assemblage exhibits quantitative inter-deposit variation.

(3) Pyrrhotite is the principal matrix sulphide in all deposits, and occurs chiefly as the monoclinic form except at Trojan (Rhod.), where hexagonal pyrrhotite predominates.

(4) Post-formational deformation of primary ore has occurred in all sampled deposits. This is indicated by the presence of pyrrhotite and chalcopyrite deformation textures and by the typically inhomogeneous distribution of chalcopyrite in the ore assemblage.

(5) An overall metal-to-sulphur ratio of unity is typically associated with the sampled primary nickel ores. This feature strongly implies their origin as high temperature silicate-immiscible monosulphide solid solution phases.

(6) Several gross inter-regional differences in primary sulphide chemistry are noted across the ore suite. In this respect, the sampled African ores tend to be richer in iron, copper, cobalt and titanium, and poorer in nickel and chromium than the

equivalent Australian examples.

(7) The mineral chemistries of individual phases exhibit recognisable inter-regional and/or inter-deposit variation. Thus, African pyrrhotites are generally nickel-poor and copper-rich compared to Australian pyrrhotites. There is considerable inter-deposit variation in the trace metal contents of African chalcopyrites.

(B) The secondary alteration of nickel ore

i) The supergene sulphide sequence

(1) The alteration sequence: Primary sulphide - secondary (supergene) sulphide - iron oxide-rich gossan is present in all 17 sampled oxidation profiles.

(2) This sequence is qualitatively similar to those developed in the Kambalda deposits in Western Australia.

(3) Broad inter-regional differences exist in alteration zone development. Thus, in the African profiles the primary ore is typically shallower, and transition and secondary zones are generally less vertically developed than in the equivalent Australian alteration sequences.

(4) In all sampled profiles, the primary pentlandite-pyrrhotite assemblage undergoes a phased alteration to one of violarite after pentlandite, violarite after pyrrhotite and secondary iron disulphides after pyrrhotite.

(5) Smythite is characteristically formed as an intermediate product during the formation of violarite after monoclinic pyrrhotite. It is not developed during the formation of violarite after hexagonal pyrrhotite.

(6) Marcasite is the first-formed secondary iron disulphide phase in all sampled profiles.

(7) The mineral is characteristically in a fine-grained near-colloidal form, and in all but four deposits subsequently re-crystallises either directly, or via a coarse marcasite stage, to massive secondary pyrite.

(8) Secondary marcasite displays a range of textures. In this respect, mimic cleavage structures after pyrrhotite, together with Bird's Eyes and/or pseudocolloform (de-watering) textures are generally present in all sampled supergene ores.

(9) The formation of the secondary sulphide assemblage typically occurs within a closed chemical system. A loss from the ore profile of iron released in consequence

of pentlandite alteration is however noted in several deposits.

(10) Recognisable inter-regional variations occur in the composition of secondary sulphide minerals. African violarite after pentlandite is generally iron-rich and nickel-poor, and African violarite after pyrrhotite is typically nickel-poor and cobalt-rich compared with the respective equivalent Australian phases. Violarite after interstitial pentlandite is typically ore metal-rich and iron-poor compared with that after flamme pentlandite in all sampled ores. And violarites after pentlandite and pyrrhotite typically differ in that the former is ore metal-rich and iron-poor compared with the latter. Smythite compositions show no recognisable inter-regional variation, bur reflect the inter-deposit differences in ore metal-to-iron ratios and ore metal relative proportions that characterise their violarite after pyrrhotite daughter products. Notwithstanding these differences though, equivalent secondary phases from all sampled deposits plot in the same mineral composition fields.

ii) The development of gossans

(1) Iron oxide-rich mineral assemblages abruptly supercede the secondary sulphides above recent water table levels in all sampled alteration profiles.

(2) The bulk mineralogy of all sampled oxide zones is qualitatively similar and comprises goethite, hematite and silica. However, the mean quantitative proportions of these minerals differ from deposit to deposit.

(3) Goethite is typically the predominant iron oxide present in all oxide zones. It is the principal iron mineral in almost all sampled Australian gossans.

(4) Hematite is present in all sampled gossans, but typically occurs in higher proportions in the African examples. Goethite-hematite mean ratios are typically high.

(5) Secondary dehydration of goethite to hematite is observed in a number of sampled gossans. The phenomenon is however volumetrically significant only in the Pikwe (Botswana) oxide profile.

(6) Higher mean silica contents typically occur in the sampled Australian gossans. In contrast, the African examples show a greater inter-deposit variation in silica content.

(7) Mimic (relic) textures after individual secondary sulphide minerals are noted in all gossans. Violarite pseudomorphs occur in all examples, and are present chiefly as goethite. Secondary mimic textures after pyrrhotite are similarly present

in all sampled oxide zones. They may exist as either goethite or hematite re-placements. Exclusive preservation in the former is more common in Australian gossans. Secondary marcasite mimics occur in all gossans except for those deposits rich in pyrite. The replacing mineral may be either goethite or hematite or a composite of the two. Mimic secondary pyrite textures are present in the gossans of all deposits but those containing only the marcasite dimorph. These textures are preserved chiefly in either goethite (Australian gossans) or hematite (African gossans). Chalcopyrite is typically represented as either goethite or hematite boxwork structures in individual gossans.

(8) Silica typically occurs as an amorphous or cryptocrystalline matrix to iron oxide structures. Detailed work on the Pikwe oxide profile indicates that this texture is caused by the precipitation of silica from influxing SiO_2-rich ground waters. The silica is probably derived by the weathering of adjacent silicates.

(9) Several fundamental chemical changes occur at the sulphide-oxide transition in consequence of pervasive sulphide leaching. Sulphur is oxidised to sulphate, and is totally removed from the ore profile by solution in ground water. Iron is similarly mobilised (as ferrous ion) and is also lost through ground water solution. Appreciable, although typically variable quantities are, however, retained within the gossan formation zone, and are oxidised and subsequently precipitated as ferric oxides. Preferential retention of iron oxide within the gossan occurs in the sampled African deposits. All gossans typically exhibit silicon enrichment in comparison with their parent ores.

(10) The transition metals, nickel, cobalt, manganese and copper typically exhibit high levels of depletion across the sulphide-oxide transition. This is probably due to the release of these metals as soluble oxidised mobile species from their parent sulphide lattices during leaching. A proportion of each is however retained – probably as a result of co-precipitation with iron oxides. There is a general tendency for copper to be preferentially retained over nickel within the oxide zone. This is probably due to the principal occurrence of these metals in sulphides of differing chemical stability. A comparison of chromium mean contents between sulphide and gossan indicates that the latter is typically enriched in this metal. The extra chromium is probably derived from the weathering of adjacent ultramafic host silicate rocks.

12.2.2. The origin of secondary alteration in nickel sulphide ores

(A) The genesis of supergene sulphide alteration

An interpretative discussion of Thornber's chemical and geological model of supergene sulphide alteration made in the light of data generated by the present study has produced the following conclusions.

(1) Supergene chemical reactions very similar to those at Kambalda occur in all sampled nickel sulphide alteration profiles.

(2) In consequence, electrochemical corrosion cells of the type proposed by Thornber are operating, or have operated during the development of supergene alteration in these deposits.

(3) Quantitative inter-deposit variation in supergene alteration zone development is explained by a conceptual model that relates the initiation and subsequent growth of secondary alteration to a progressive exhumation of the parent ore profile under a seasonally fluctuating water table (lateratisation) regime.

(B) The formation of gossans and their subsequent maturation

i) The chemical environment of gossan formation

Present work on the interpretation of observed oxide zone phenomena in terms of the formation environment of nickel gossans indicates the following.

(1) The precipitation of specific iron oxide phases at the water table is probably related to the quantity of free ferric species present in solution.

(2) In consequence, iron oxide formation is indirectly related to the oxidation potential (Eh) of the immediate environment, with likely values of +0.35 Volts or higher inferred for the water table zone.

(3) The inferred formation environments of associated oxidate minerals imply that the low pH conditions generated by wholesale sulphide leaching may be modified by the chemical influence of adjacent wall rocks:Moderately acidic conditions are associated with carbonate-rich assemblages.Whereas strongly acid conditions persist in the locale of carbonate-poor wall rocks.

(4) Considerable quantities of aqueous ore metals are available for incorporation in these oxidate phases.

ii) The post-formation maturation of nickel gossans

Work on the implications of post-formation oxide zone phenomena for the subsequent

maturation of nickel gossans indicates the following.

(1) The typical occurrence of silica enrichment in present-day nickel gossan profiles can be explained by a simple development model which relates silica influx to the slow progressive formation of the oxide zone above the dry season water table associated with the active lateratisation of adjacent silicates.

(2) The observed content and texture distributions of silica in the Pikwe (Botswana) oxide profile can be explained in terms of a general cessation of laterite formation in the late Tertiary that was coupled with a concommitant progressive onset of semi-arid climatic conditions.

(3) The enrichment of chromium in nickel gossans is due to the mobilisation of this element as a result of the moderately alkaline oxidising conditions associated with the lateratisation of typically ultramafic host silicates.

(4) Subsequent immobilisation of chromium within the oxide zone probably occurs by surface adsorption on precipitating silica and/or by chemical destabilisation of mobile aqueous chromium species within the relatively low pH environment of the newly-formed iron oxide assemblage.

(5) Significant dehydration of (metastable) primary goethite to secondary hematite does not generally occur within the oxide zone profile unless primary hematite is available as a nucleation locus.

12.2.3 The utilisation of nickel gossan characteristics in ore tenor prediction

(A) The use of gossan mineralogy

i) Oxidate mineralogy

(1) The carbonates, magnesite, calcite and dolomite occur as oxidate minerals in the surface nickel gossans of a number of deposits - especially those in Western Australia.

(2) These minerals are readily identified using a staining technique devised by Warne.

(3) They are characterised by anomalously high ore metal contents - especially nickel and copper, which are qualitatively identifiable using standard element tests.

(4)The presence of ore metal-rich oxidate carbonate in surface ironstone outcrops hence infers the local presence of buried ore mineralisation. This feature is therefore proposed as a useful recognition aid for nickel gossans.

ii) Gossan bulk mineralogy

(1) The bulk mineralogy of nickel gossans is used as a predictor of sulphide ore metal tenor through the application of the multivariate statistical technique of multiple linear regression analysis. Three measures of sulphide metal content are studied. In each instance a regression equation relating ore metal content or grade to a linear combination of significant bulk mineralogical (gossan) variables is derived. A specific test set of documented deposits is used in each study. In this way, each derived expression can be used to predict the likely mean value of the corresponding sulphide metal parameter from equivalent surface gossan data.

(2) The massive sulphide copper study is divided into two sub-studies on the basis of indicated ore copper test data. Unclassified gossan data are allocated to the most suitable predictor equation by use of a derived discriminant function.

(3) The estimated closeness of predictive fit of the derived sulphide predictor equations (at the 90 percent confidence level) are as follows;

Prediction Study	Closeness of Predictive Fit (Accuracy)
Massive sulphide nickel:	± 30 percent
Massive sulphide high copper:	± 25 percent
Massive sulphide low copper:	± 60 percent
Nickel ore body grade:	± 50 percent

(4) These results indicate that the copper contents of high-copper nickel ores can be predicted with workable accuracy from the mean bulk mineralogy of the equivalent surface gossan. Similarly, the nickel contents of near-massive to massive nickel ores can be quite accurately estimated from surface gossan bulk mineralogy.

(5) In contrast, the technique is of less use in both low-copper massive ore and nickel grade prediction. Here only broad ranges of probable values can be estimated for these two ore parameters using surface gossan bulk mineralogical data.

(B) The use of relic sulphide mineral textures

Work on the prediction of ore metal tenor from the relic sulphide textures present in a suite of 15 study gossans indicates the following.

(1) A direct evaluation of gossan relic violarite textures in terms of the mean nickel content of equivalent near-massive to massive sulphide has associated with it a mean closeness of predicted fit of ± 70 percent.

(2) The derivation, using a test set of 12 deposits, of a linear regression equation relating gossan mean violarite mimic content and massive sulphide nickel content is a significantly more accurate sulphide prediction technique. The derived equation permits massive sulphide nickel content to be predicted from the violarite mimic content of the overlying gossan to within $\pm$ 25 percent at the 90 percent confidence level.

(3) A direct evaluation of relic chalcopyrite textures in terms of the copper content of near-massive to massive ore has associated with it a mean closeness of predictive fit of about $\pm$ 90 percent. Further, no improvement in the predictive accuracy of chalcopyrite mimics is possible through the development of a linear regression (predictor) equation on the basis of present data.

(4) The mean nickel tenor of near-massive to massive nickel ores can hence be accurately predicted from the relic violarite texture content of the corresponding surface gossan by use of a derived regression (predictor) equation. In contrast, relic chalcopyrite textures are unusable as accurate quantitative predictors of sulphide copper tenor. Their use is restricted to that of qualitative indicators of copper mineralogy in the buried sulphide ore.

(C) The use of gossan geochemistry

Present work on the prediction of sulphide nickel and copper tenor from the geochemistry of the corresponding surface gossan indicates the following.

(1) Near-massive to massive nickel sulphide ores and their equivalent gossans possess geochemical signatures that are quantitatively distinct from each other and from rocks of similar type in other nickel sulphide orebodies.

(2) Multiple distributions typify the population statistics of major and minor elements across a combined suite of 15 nickel sulphide ores.

(3) Single distributions characterise the population statistics of these elements across an equivalent suite of surface nickel gossans.

(4) These features enable a series of multiple linear regression (predictor) equations to be developed that allow three important measures of sulphide metal content to be accurately predicted from the mean geochemistry of the equivalent surface gossan. These measures are; i) massive sulphide nickel content; ii) massive sulphide copper content; iii) nickel ore body grade.

(5) Each study is split into two separate sub-studies on the basis of known sulphide

metal contents. The estimated closeness of predictive fit, at the 90 percent confidence level, of the derived predictor equations for each of the six sub-studies are as follows:

The sulphide nickel prediction study;   High equation $\pm$ 15 percent

                                         Low equation $\pm$ 15 percent

The sulphide copper prediction study;   High equation $\pm$ 15 percent

                                         Low equation $\pm$ 20 percent

The nickel grade prediction study;   High equation $\pm$ 10 percent

                                         Low equation $\pm$ 35 percent

(6) Allocation of previously unclassified gossan data to the most suitable predictor equation in each study is effected by the derivation of a sub-set allocation (discriminant) function. These functions are developed from the multivariate statistical differences that exist between the gossan input data of the relevant high and low test sub-sets. The estimated misallocation rates of the three functions derived in this way are as follows:

Prediction Study	Misallocation rate (95% c.l.)
Massive sulphide nickel:	Less than five percent
Massive sulphide copper:	Not more than 12 percent
Nickel ore body grade:	Not more than eight percent

(7) The results of ore tenor prediction trials involving available unclassified gossan data indicate the following;

i) The likely massive sulphide nickel content of the parent ore is typically predicted to within at least $\pm$ 30 percent.

ii) The likely massive sulphide copper content of the parent ore is typically predicted to within $\pm$ 60 percent on available data.

iii) The likely nickel ore body grade of the parent ore is generally predicted to within $\pm$ 70 percent on available data.

The results of trials ii and iii show generally low levels of predictability. This is in all instances due to the relatively high sample imprecision value associated with each predicted result. This is, in turn, due to the relatively small numbers of individual samples that were available for computation of the necessary gossan input data in each instance. Use of larger gossan sample suites would substantially improve the precision of the corresponding predicted ore tenor values.

(8) The derived technique has several major advantages over the neutron activation

technique currently used in the semi-quantitative prediction of nickel ore tenor. It is more accurate. It is more rapid to use. It is much cheaper. It is more convenient. In addition, it also enables the previously unavailable parameters of massive sulphide copper content and nickel ore body grade to be accurately predicted from the surface gossan. Further, the technique is generally applicable to evaluation of nickel sulphide ores in the Archean Shield regions of both southern Africa and Western Australia. It may also be tentatively applied to oxidised mineralisation of this type at present cropping out in other such Shield regions that have been recently affected by semi-arid climatic regimes.

12.3 Recommendations for further work

The following recommendations for further work are now made.

1) Detailed studies on other Archean nickel ores presently cropping out within semi-arid climatic terrains, and on their enclosing host silicates, would enable the secondary alteration of these deposits to be documented. This work would allow comparison with currently available data, and would consequently permit testing of the geological models of alteration profile genesis and of secondary (gossan) silicification developed in part two of this thesis.

2) Detailed work on these additional deposits might also permit the ore tenor prediction studies (part three of this thesis), to be updated. The incorporation of data from these deposits – perhaps including some from Archean Shield regions other than the Rhodesia and Yilgarn blocks, could potentially lead to greater predictive accuracy and regional applicability for these derived gossan evaluation techniques.

3) Further investigations of currently available sample material could, however, also be usefully performed. More detailed mineral chemical work on supergene alteration could be done – especially for the sampled Australian profiles, as no such studies were made on these deposits in the present investigation. This work would allow a more detailed documentation of alteration chemistry to be made for the sampled Australian deposits. It would also permit better inter-regional and inter-deposit comparisons of alteration phenomena to be made. Similarly, knowledge of trace metal distributions in the gossans of all sampled profiles – data presently unavailable, would significantly aid further work on the natural formation environments of nickel gossans.

APPENDIX ONE: TECHNIQUES

This appendix provides details of the various techniques employed in the present study. It is divided into seven sections. Each section briefly describes the techniques developed and/or used in one principal area of research activity.

1A   Field sampling technique

Field sampling was carried out at 28 nickel sulphide mineral occurrences in southern Africa and Western Australia. Detailed spatially controlled sampling of surface gossan, oxide profile and supergene sulphide sequence was carried out at each deposit as far as was practicable. Surface gossan and shallow depth oxide samples were respectively taken at outcrop and in costeans (where present). The equivalent sulphide ore including supergene altered and actively leaching material, together with the lower portions of the oxide profile, were sampled from either spatially located drillcore and/or at relevant levels in the mine or open pit developed over the ore body. All samples were numbered prior to bagging, and brief details made of the assigned number and of the relevant spatial co-ordinates – especially depth, in a field notebook.

1B   Subsequent handling and sample preparation techniques

i) Cataloguing

All samples were catalogued on arrival in the laboratory. The essential details of each were recorded, including field sample number, locality co-ordinates and a brief petrological description. Brief indications of laboratory work subsequently performed on individual specimens were added in due course.

ii) Sample preparation

A) Polished section material

All sampled oxide, sulphide and silicate specimens (about 650) were individually examined. Each was then cut into two equal halves in a direction normal to any observed mineralogical or textural banding. One half was then re-examined more closely and an area or areas marked out for polished section preparation. Polished thin sections were indicated where the sulphide or oxide material was obviously silicate-rich. Details of individual sectioning decisions were noted in the appropriate entries in the sample catalogue, and the material was then submitted for sectioning.

B) Specimens for bulk chemical analysis

Bulk chemical analysis of the study sample suite was carried out by X-Ray
Fluorescence, (section 1C). This required the pulverisation of all samples and
their subsequent pelletisation. Prior to this operation however, the sample
suite was split into two portions - oxides, and sulphides/silicates. This was done
in order to limit contamination of oxide material by metal-rich sulphides during
sample preparation. Further limitation of random error was effected by adopting
a randomised preparation sequence within each of the two sample sub-suites.
Each specimen was allocated a random number and each subsequent stage of
crushing pelletisation and analysis was carried out in this imposed treatment
order.

Each cut specimen was inspected for homogeneity and for obvious late mineral
growths. It was then crushed down to 6 mesh size using a tungsten carbide pestle
and mortar, coned and quartered, and two opposing portions were bagged. The
remaining material was subsequently further pulverised for about one to two
minutes in a agate Tema mill.

The resulting homogenised powder was bagged and approximately five grams was
later withdrawn for pelletisation. This process was performed in a bench press.
The powder was firstly consolidated by light pressure on a sleeve and piston
arrangement within a stainless steel cylinder. The sleeve was then removed and
about five grams of borax was carefully added around the sides and on top of the
powder lozenge so formed. A steel plunger was then carefully inserted into the
cylinder and was pressed on top of the borax/powder lozenge for two minutes at
a pressure of eight tons.

The prepared lozenge was subsequently ejected into a small sample cup and its
sides were immediately bound with adhesive tape to prevent unloading expansion.
This technique was also used to prepare the pellets of the primary compositional
standards used in the X.R.F. analysis, (section 1C).

C) Oxidate minerals

Oxidate minerals present in oxide material were prepared for X-Ray Diffraction
analysis by the following method. The parent hand specimen was first lightly
dusted with a camel hair brush to remove extraneous surficial material. A sample
of the oxidate mineral was then carefully removed from its site using a fine steel
needle and was deposited onto a clean glass slide. Any obvious contaminant

fragments (typically iron oxides) were then carefully removed. A second slide
was then placed on top and the specimen was crushed by slow rotation of this
upper slide. The pulverised material was then collected together and the tip
region of a thin glass fibre lightly coated with cow gum was rolled through it.
The resulting powder-impregnated glass fibre was then carefully mounted in a
Plasticene base on a glass slide, given an identification number, and carefully
stored until required for X.R.D. analysis.

1C Analytical Methods

i) Bulk Chemical Analysis

X-Ray Fluorescence was used for the bulk chemical analysis of the sample suite of
sulphides, oxides and silicates. This method was principally employed because it
enables highly siliceous oxide material to be analysed on a routine basis. The
machine used for the work was a Philips 1212 Automatic X-Ray Spectrometer.
Major and minor element analysis was carried out on compressed powder samples,
(section 1B). The following elements were analysed for: Fe, Si, S, Mg, Al, Ni, Cu,
Mn, Cr, Ti, Co.

A) Primary Standards

Two series of primary standards were employed in the analytical work. These were
based on the known compositional ranges of major and minor elements in nickel
sulphides and their equivalent oxide-rich rocks. 'Specpure' oxides were used to
prepare all standards.

A 'Major element' series gave variation in the relative proportions (from zero to
80 wt.%) of three major components; Iron oxide, silica and iron monosulphide.
A minor and trace element tail of constant absolute and relative proportions was
present in each standard of this series.

A 'Minor element' standard series was also produced that was composed of four
discrete sub-series; High iron oxide - low silica, low iron oxide - high silica,
FeS-iron oxide-silica, and FeS. These four consisted of fixed relative proportions
of these major components and also of Mg and Al. Variation was confined to a
trace element block of fixed relative proportions that was mixed with these major
elements in varying quantities. In this way a wide range of standard trace
element compositions was generated within each of the four sub-series.

The compositional ranges covered by the Major and Minor standard series gave

useable analytical totals for the majority of study samples. The total number of primary standard employed was approximately 60.

B) Raw data treatment – Preliminary work

Due to the lack of suitable software for sulphide/oxide data handling on the utilised X.R.F. system, preliminary dead time and drift correction of both standards and samples had to be determined by individual computations. The individual element true peak count (Tpk) data for each standard and sample were firstly computed using desk calculator programmes developed in this study, (A1 and A2, section 1F). Drift corrections to the Tpk values were then calculated for all standards and samples using the drift data generated by a continuously analysed standard, (Programme A3, section 1F). Slope factor (background) corrections for Ni and Cr Tpk values, made on the basis of data from a continuously run spectrosil plate, were respectively calculated using programmes A4 and A5, (section 1F).

C) Raw data treatment – Standard matching and matrix absorbance corrections

The corrected count data of all samples were punched onto computer cards and run in a combined standard matching/matrix absorbance correction programme that was expressly derived for this purpose, (Programme B1, section 1F). Output data were in the form of oxide weight percent units, (Fig.B1, section 1F). The trace metal data of all samples were then converted to p.p.m. units, true density and porosity data were added, and the modified data were re-punched in free format onto computer cards. These data were subsequently run in a specially devised data handling programme, (B2, section 1F). This converted all oxide data into elemental contents. It also computed weight equivalent content per unit volume data for all elements in each sample, (Fig.B2, section 1F). These latter units are independent of density/porosity considerations and were utilised in studies of bulk chemical migration.

D) The Precision and Accuracy of the X.R.F. analytical technique

The quality of the overall X.R.F. procedure was tested in two ways. The precision of the method was assessed by running randomly selected duplicate samples through the complete analytical and matching/correction procedure. Additionally an indication of the combined accuracy and precision of the devised procedure was gained by comparison of analytical results obtained by X.R.F. and by Atomic

Absorption Spectroscopy for a randomly selected suite of sulphide, oxide and silicate samples. The closeness of fit of these data, at the 90 percent confidence level, is as follows:

ELEMENT	X.R.F. Precision (%)	Combined Precision/ Accuracy of X.R.F. (%)	Implied Accuracy X.R.F. (%)
Iron	$\pm$ 15	$\pm$ 18	$\pm$ 3
Nickel	$\pm$ 16	$\pm$ 20	$\pm$ 4
Copper	$\pm$ 11	$\pm$ 25	$\pm$ 14
Cobalt	$\pm$ 10	$\pm$ 20	$\pm$ 10
Titanium	$\pm$ 8	-	-
Manganese	$\pm$ 13	$\pm$ 15	$\pm$ 2
Chromium	$\pm$ 20	$\pm$ 30	$\pm$ 10

ii) Carbonate Analysis

Routine carbonate analyses were performed on the oxide and silicate members of the sample suite as part of the bulk chemical investigation programme. The technique involved isothermal measurement of the volume of carbon dioxide released from a known weight of sample by a known volume of hydrochloric acid of given strength. This method, which is in routine use in the Sedimentology Laboratories at Imperial College, London, enables rapid, quite accurate indications of carbonate content to be made. It cannot however be used on sulphide material as this typically reacts with strong HCl to give hydrogen sulphide gas.

iii) X-Ray Diffraction Analysis

X-Ray Diffraction techniques were utilised for two principal lines of investigation. Both studies employed the Philips stabilised diffraction set present in the Geology Department of Imperial College. Routine mineral identifications – chiefly of iron oxides, were carried out on a powder diffractometer set-up using cobalt K_α radiation and a scan speed of 1° 2θ per minute. The principal use of X.R.D. was however in the identification of oxidate minerals. This work was performed on fibre-mounted specimens (section 1B) mounted within an 11.483 mm. diameter Debije-Scherrer powder camera and irradiated with either cobalt K_α or, less commonly, iron K_α radiation.

iv) Atomic Absorption Spectroscopy

Atomic Absorption Spectroscopy was utilised for the routine chemical analysis of oxidate minerals and for a quality control investigation of the X.R.F. analytical technique developed in this study. Oxidate mineral specimens were prepared for analysis using a standard nitric acid/perchloric acid leach technique. This preparation method was also used for rock samples in the quality control study. However in the latter work siliceous material was prepared using a standard hydrofluoric acid leach technique. All samples were analysed by Imperial College Geology Department analytical staff on a Perkin-Elmer 403 model Atomic Absorption Spectrometer.

v) Electron Microprobe Analysis

A limited amount of mineral chemical work - chiefly on sulphide material, was performed on the Cambridge Microscan 5 set-up of the Geochemical Division, Institute of Geological Sciences, London. This machine is fitted with solid-state detectors and with an integral mini digital computer that allows rapid generation of results.

1D Density and Porosity Measurement

True density and porosity determinations were performed using a technique based on the Walker's Steelyard and devised by Dr.C.F.Blain. The method allows these two properties to be determined for porous non-friable materials. The balance point (A) on the steelyard is firstly determined with the specimen in air. The specimen is then immersed in water for two minutes and the steelyard is then re-balanced, (B). The specimen is then removed from water, its surface is carefully dried and the steelyard re-balanced, (C). Simple calculations indicate that the true specific gravity of the specimen, i.e., that of solid plus included voids, is given by the expression $\dfrac{\frac{1}{A}}{\frac{1}{C} - \frac{1}{B}}$. Similarly, the porosity of the specimen is found by substitution in the expression $\dfrac{\frac{1}{C} - \frac{1}{A}}{\frac{1}{C} - \frac{1}{B}}$ x 100%. Devised calculator routines that permit these two quantities to be determined are respectively presented in Programmes A6 and A7, section 1F.

1E Microscopy

The programme of mineragraphic work executed in the present study was done on a Reichert research reflected light microscope in the Division of Mining Geology, Imperial College. Photomicrographic work on polished section material was carried out using an attached Reichert KAM-ES apparatus. Monochrome photography was executed with either Kodak Pan-X or equivalent Ilford film. Colour work was done with either Kodak High-speed Ektachrome or Ilfrachrome film.

1F Computational and Computer-based Methods

i) Devised desk calculator programmes

A Casio Al-1000 programmable desk calculator was used to make routine computations in several areas of the present study. This work was executed using a number of devised programmes. The form of these programmes is now indicated.

The following code is used in compiling programmes with the Casio Al-1000

CODE NUMBER	EQUIVALENT KEY	FUNCTION
1	–	minus
2	* (white key)	add, command key
3	(*) (grey key)	subtract, command key
4	I	calls memory I
5	II	calls memory II
6	III	calls memory III
7	IV	calls memory IV
8	X	multiply
9	÷	divide
2.	AC	clear all memories
3.	KC	clear display entry
4.	√	square root
6.	ST	stop – allows variables to be entered
7.	RT	returns programme to the beginning

Memories are set in either K-mode – if they contain constants for use in the calculation, or in M-mode if they are used to store intermediate results. + mode is used where an accumulation of data is required.

Preliminary treatment of X.R.F. raw count data

A1) Dead time calculation for element data in counts per second (c.p.s.) form

$b = \dfrac{a}{1 - (ak)}$, where b = dead time corrected sample value (c.p.s. units)

a = uncorrected sample value (c.p.s.)

k = dead time constant = 2×10^{-6}

CODE   8 4 2 7 3 8 7 2 5 3. 6 9 5 2 7.

PROGRAMME X I * IV (*) X IV * II KC III ÷ II * RT

Memories   IV   III   II   I

         K   M   M   K   Function mode

       (1.0) ( )   ( ) (2×10^{-6}) Initial content

OPERATING SEQUENCE: a; III; *

A2) Dead time calculation for fixed count element data (10^6 counts) – Iron

$b = \dfrac{10^6}{(a - 2)}$, where b = dead time corrected sample value (seconds)

a = uncorrected value (seconds)

CODE   2 3. 7 3 2 6 3. 4 9 6 2 7.

PROGRAMME * KC IV (*) * III KC I ÷ III * RT

Memories   IV   III   II   I

         K   M   M   K   Function mode

       (2.0) ( )   – (10^6) Initial content

OPERATING SEQUENCE: a; *

A3) Drift correction of sample count data (c.p.s. or second units).

$b = a\left(\dfrac{c}{d}\right)$, where b = drift corrected sample value

a = uncorrected sample value

c = mean dead time corrected value for running standard

d = dead time corrected value of running standard on specific sample run

CODE   4 2 3. 7 8 6. 2 9 4 2 7.

PROGRAMME I * KC IV X ST * ÷ I * RT

Memories   IV   III   II   I

         K   M   M   M   Function mode

       (c)   –   –   ( )   Initial content

OPERATING SEQUENCE: d; *; a; *

A4) Calculation of slope factor correction for nickel

$$c = \frac{ak - b}{k}$$, where c = slope factor corrected nickel peak count data

a = uncorrected nickel peak count data

b = background nickel count data

k = slope factor

CODE		8	7	2	6.	3	9	7	2	7
PROGRAMME	X	IV	*	ST	(*)	$\div$	IV	*	RT

Memories	IV	III	II	I	
	K	M	M	M	Function mode
	(k)	–	–	–	Initial content

OPERATING SEQUENCE: a; *; b; *

A5) Calculation of slope factor correction for chromium

c = a - (bk), where c = slope factor corrected chromium peak count data

a = uncorrected chromium peak count data

b = background chromium count data

k = slope factor

CODE		4	3	6.	8	7	2	5	3.	4	1	5	3	7.
PROGRAMME	I	KC	ST	X	IV	*	II	KC	I	–	II	(*)	RT

Memories	IV	III	II	I	
	K	M	M	M	Function mode
	(k)	–	–	–	Initial content

OPERATING SEQUENCE: a; *; b; *

True density and porosity calculations (Walker's Steelyard Method)

A6) True density (solid + voids)

$$d = \frac{\frac{1}{a}}{\frac{1}{c} - \frac{1}{b}} \ ,$$ where

d = true density of sample

a = balance point in air

b = balance point in water

c = balance point in air with absorbed water

CODE	4	7	9	3	4	7	9	6.	3	1	4	7	9	6.	3	9	4	3	7.
PROGRAMME	I	IV	÷	(*)	I	IV	÷	ST	(*)	-	I	IV	÷	ST	(*)	÷	I	(*)	RT

Memories	IV	III	II	I	
	K	M	M	+	Function mode .
	(1)	( )	( )	( )	Initial content

OPERATING SEQUENCE: c; *; b; *; a; *

A7)Porosity

$$\frac{p}{100} = \frac{\frac{1}{c} - \frac{1}{a}}{\frac{1}{c} - \frac{1}{b}} \ ,$$ where

p = porosity of sample

a = balance point in air

b = balance point in water

c = balance point in air with absorbed water

CODE	4	7	9	4	3	4	7	9	6.	3	1	4	7	9	6.	3	6	7	9	6.
PROGRAMME	I	IV	÷	I	(*)	I	IV	÷	ST	(*)	-	I	IV	÷	ST	(*)	ST	IV	÷	ST

	3	1	6	3.	4	9	6	3	7
	(*)	-	III	KC	I	÷	III	(*)	RT

Memories	IV	III	II	I	
	K	+	M	+	Function mode
	(1)	( )	( )	( )	Initial content

OPERATING SEQUENCE: c; *; a; *; c; *; b; *

ii) Devised computer programmes

Two major computer programmes were written during the present study. The first, listed in Fig.A1/1, was written as part of the X.R.F. bulk analytical study. It has two major functions. The first is to match the count data of individual samples to a

primary standard so that sample compositions can be calculated. This is done by matching each sample to the standard having the closest major element composition. Subsequently, both the nominal and the true (matrix absorbance-corrected) compositions of each sample are computed using the data of the matched standard. The results are printed out in weight percent oxide units. A comprehensive documentation of this program is given in the listing, (Fig.Al/1). Typical output results are illustrated in Fig.Al/2.

The second programme, listed in Fig.Al/3, has a data handling function. It has three principal parts: One, to round bulk chemical analytical totals to 100 percent on the basis of major element contents - where this is necessary; two, to recompute Wt% oxide data as the equivalent Wt% element data; and, three, to compute the corresponding weight equivalent per unit volume data for all elements in each sample. These results are also written by the programme, (Fig.Al/4).

1G Statistical Methods

Several statistical methods were employed in the present study. The principal use of these techniques was however in the gossan evaluation work reported in part three of the thesis.

The univariate statistical methods chiefly used in the delineation of sample statistics were carried out using programmes available in the GEOLIB statistical library devised by the Applied Geochemistry Research Group at Imperial College, London. The multivariate methods subsequently employed in further investigation of the various gossan evaluation problems were performed using suitable programmes from the University of California Bio-Medical Statistics package similarly available at Imperial College. All computing work was executed using the CDC 6400 facility in the Imperial College Computing Centre.

571

FIG. A1/1   LISTING OF X.R.F. SAMPLE MATCHING AND MATRIX

ABSORBANCE CORRECTION PROGRAMME

```
C      PROGRAM TO MATCH X.R.F. SAMPLE DATA TO MOST APPROPRIATE STANDARD
C      AND THEN TO CALCULATE NOMINAL AND TRUE (ABSORPTION-CORRECTED)
C      CONCENTRATIONS
C      THE PROGRAM WORKS AS FOLLOWS.EACH STANDARD IS TAKEN IN TURN,AND
C      THE FOLLOWING SEQUENCE IS EXECUTED.THE FIRST SAMPLE COUNT DATACARD
C      IS TAKEN.IT IS SEQUENTIALLY COMPARED WITH THE COUNT DATACARDS OF
C      ALL STANDARDS.THE CRITERION USED IS D=SQRT((A*A)+(B*B)+(C*C)),
C      WHERE A,B AND C ARE THE RESPECTIVE ORTHOGONAL DISTANCES BETWEEN
C      SAMPLE AND STANDARD COUNT DATA FOR THE MAJOR ELEMENTS IRON,SILICON
C      AND SULPHUR.THE PROGRAM FINDS TO THE STANDARD GIVING THE SMALLEST
C      D VALUE WITH THE SAMPLE.IF THIS STANDARD IS THE SAME AS THAT
C      ORIGINALLY TAKEN,THEN THE SAMPLE DATA ARE STORED IN AN ARRAY
C      ASSOCIATED WITH THAT STANDARD AND THE PROGRAM GOES BACK AND READS
C      THE SECOND SAMPLE CARD.IF THE STANDARDS ARE DIFFERENT THE PROGRAM
C      GOES DIRECTLY BACK AND TAKES THE SECOND SAMPLE CARD.THIS SEQUENCE
C      IS FOLLOWED THROUGH TO THE N TH SAMPLE CARD AND ALL SAMPLES IN
C      THE INPUT SET THAT MATCH THE FIRST STANDARD ARE STORED IN A
C      SPECIAL ARRAY.WHEN ALL SAMPLE/STANDARD COMBINATIONS HAVE BEEN
C      TESTED,ALL SAMPLES MATCHED TO THE FIRST STANDARD HAVE THEIR
C      NOMINAL AND TRUE OXIDE CONCENTRATIONS COMPUTED.THESE DATA ARE THEN
C      PRINTED,TOGETHER WITH THOSE OF THE FIRST STANDARD.THE PROGRAM THEN
C      RETURNS TO THE BEGINNING AND REPEATS THIS COMPLETE PROCEDURE WITH
C      THE SECOND STANDARD IN THE SET,AND THEREON SUCCESSIVELY THROUGH TO
C      THE N TH STANDARD.BY THIS MEANS ALL SAMPLES ARE MATCHED TO THE
C      STANDARD OF CLOSEST MAJOR ELEMENT AFFINITY.
       PROGRAM NAME (INPUT,OUTPUT,TAPE5=INPUT,TAPE6=OUTPUT)
       COMMON ZS(150,16),ZU(200,16),RARRAY(200,2),NN,COC(150,16),NC,NS,NU
      2,ZUPAY(200,16),ENC(200,16),Z(17),AO(17,16),ASD(17),E(17),X(17)
       EQUIVALENCE (FER,Z(3)),(SI,Z(4)),(S,Z(5)),(NI,Z(6)),(MG,Z(7)),(AL,
      2Z(8)),(CU,Z(9)),(MN,Z(10)),(CR,Z(11)),(CO,Z(12)),(TI,Z(13)),(CO3,Z
      3(14)),(K,Z(15)),(V,Z(16))
C      READ THE NUMBER OF MATRIX ABSORPTION FACTOR CARDS
       READ(5,8000)MX
C      READ THE NUMBER OF STANDARD CONCENTRATION DATA CARDS
       READ(5,8000)NC
C      READ THE NUMBER OF STANDARD COUNT DATA CARDS
       READ(5,8000)NS
C      READ THE NUMBER OF SAMPLE COUNT DATA CARDS
       READ(5,8000)NU
C      READ THE MATRIX ABSORPTION FACTOR CARDS
       READ(5,2000)((AO(MX,MY),MY=1,16),MX=1,17)
C      READ THE STANDARD CONCENTRATION DATA CARDS
       READ(5,8900)((COC(IS,I),I=1,16),IS=1,NC)
C      READ THE STANDARD COUNT DATA CARDS
       READ(5,4500)((ZS(J,I),I=1,16),J=1,NS)
C      READ THE SAMPLE COUNT DATA CARDS
       READ(5,4500)((ZU(K,I),I=1,16),K=1,NU)
       DO 3000 L=1,NS
       NN=0
       IDUM=IFIX(ZS(L,1))
       DO 4000 K=1,NU
       TEST=0.0
       DO 5000 J=1,NS
       A=ZS(J,3)-ZU(K,3)
       B=ZS(J,4)-ZU(K,4)
       C=ZS(J,5)-ZU(K,5)
       D=SQRT((A*A)+(B*B)+(C*C))
       IF(J.EQ.1)GO TO 9
       IF(TEST.LT.D)GO TO 5000
9      TEST=D
       NSAV=IFIX(ZS(J,1))
5000   CONTINUE
       IF(IDUM.NE.NSAV)GO TO 4000
       NN=NN+1
       RARRAY(NN,1)=ZU(K,1)
       RARRAY(NN,2)=TEST
       DO 1000 IN=1,16
       ZURAY(NN,IN)=ZU(K,IN)
1000   CONTINUE
4000   CONTINUE
       IF(NN.EQ.0)GO TO 3000
       DO 9060 LLL=1,NN
       DO 9070 IN=1,16
       IF(IN.EQ.1)GO TO 9070
       IF(IN.EQ.14)GO TO 900
       GO TO 950
900    IF(ZURAY(LLL,14).GT.0.0)GO TO 1010
950    IF(ZURAY(LLL,IN).EQ.0.0.OR.COC(L,IN).EQ.0.0.OR.ZS(L,IN).EQ.0.0)GO
      2TO 9077
```

FIG. A1/1 CONTINUED

```
      ENC(LLL,IN)=(ZURAY(LLL,IN)*COC(L,IN))/ZS(L,IN)
      GO TO 9070
 9077 ENC(LLL,IN)=0.0
      GO TO 9070
 1010 ENC(LLL,14)=ZURAY(LLL,14)
 9070 CONTINUE
      IF(L.GT.1)GO TO 14
C     WRITE ABSORPTION COEFFICIENT MATRIX HEADING FORMAT
      WRITE (6,1070)
C     WRITE ABSORPTION COEFFICIENT MATRIX
      WRITE(6,1150)((AO(MX,MY),MY=2,16),MX=1,17)
   14 ST=0.0
      DO 240 IN=2,16
  240 ST=ST+COC(L,IN)
   15 IF(LLL.GT.1)GO TO 16
C     WRITE STANDARD IDENTIFICATION FORMAT
      WRITE(6,1155)(ZS(L,1))
C     WRITE STANDARD HEADING FORMAT
      WRITE (6,1070)
C     WRITE STANDARD CONCENTRATION DATA
      WRITE(6,1150)(COC(L,IN),IN=3,16),ST
   16 DO 255 MX=2,16
      ASD(MX)=0.0
      DO 250 MY=2,16
  250 ASD(MX)=AO(MX,MY)*COC(L,MY)+ASD(MX)
  255 CONTINUE
      IF(LLL.GT.1)GO TO 20
C     WRITE SUM OF MATRIX ABSORDANCE COEFFICIENTS FOR ALL CONSTITUENT
C     OXIDES (STANDARD)
      WRITE(6,1021)(ASD(MX),MX=3,16)
C     WRITE SAMPLE IDENTIFICATION FORMAT
   20 WRITE (6,1060)(ZURAY(LLL,1))
      SUMNC=0.0
      DO 25 IN=2,16
   25 SUMNC=SUMNC+ENC(LLL,IN)
C     WRITE COMPUTED NOMINAL CONCENTRATIONS FOR SAMPLE PLUS THEIR TOTAL
      WRITE(6,1080)(ENC(LLL,IN),IN=2,16),SUMNC
      DO 55 MX=2,16
      E(MX)=0.0
      DO 57 MY=2,16
   57 E(MX)=AO(MX,MY)*ENC(LLL,MY)+E(MX)
   55 CONTINUE
      DO 60 MX=2,16
      IF(ASD(MX).LE.0.0) ASD(MX)=1.0
      IF(E(MX).LE.0.0) E(MX)=1.0
      Z(MX)=(ENC(LLL,MX)*E(MX))/ASD(MX)
   60 IF(E(MX).EQ.1.0) Z(MX)=ENC(LLL,MX)
      SUMX=0.0
      DO 65 IN=3,16
      X(IN)=Z(IN)
   65 SUMX=SUMX+X(IN)
C     WRITE SUM OF MATRIX ABSORDANCE COEFFICIENTS FOR ALL CONSTITUENT
C     OXIDES (SAMPLE)
      WRITE(6,1090)(E(MX),MX=3,16)
C     WRITE COMPUTED TRUE COMPOSITIONS FOR SAMPLE PLUS THEIR TOTAL
      WRITE (6,1092)((X(IN),IN=3,16),SUMX)
 9060 CONTINUE
 3030 CONTINUE
 4500 FORMAT (10F8.1/6F8.1)
 8000 FORMAT(I4)
 8900 FORMAT(1X,F7.3,12F6.3/3F6.3)
 1021 FORMAT (12X,14F8.3)
 1060 FORMAT (50X,F8.1)
 1070 FORMAT(6X,*N3*,6X,*FE*,6X,*SIO2*,4X,*S*,7X,*NIO*,6X,*MGO*,5X,*AL20
     2**,3X,*CUO*,3X,*MNO*,5X,*CR2O3*,3X,*CO3O4*,3X,*TIO2*,4X,*CO3*,5X,*
     3K2O*,6X,*V2O5*,4X,*TOTAL*)
 1080 FORMAT (4X,16F8.3)
 1090 FORMAT (12X,14F8.3)
 1092 FORMAT (12X,15F8.3)
 1150 FORMAT (12X,15F8.3)
 1155 FORMAT (50X,*STANDARD IS*,F8.1)
 2000 FORMAT (3X,11F7.3/5F7.3)
      STOP
      END
```

FIG. A1/1 CONCLUDED

```
MX              (THE NUMBER OF MATRIX ABSORBANCE CORRECTION CARDS)
NC              (THE NUMBER OF STANDARD CONCENTRATION DATA CARDS)
NS              (THE NUMBER OF STANDARD COUNT DATA CARDS)
NU              (THE NUMBER OF SAMPLE COUNT DATA CARDS)
                (MATRIX CORRECTION DATA)
(FORMAT.OXIDE IDENT,THEN CORRECTION FACTORS IN THE FOLLOWING SEQUENCE.
FE203,SIO2,S,NIO,MGO,AL203,CUO,MNO,CR203,CO304,TIO2,CO3)
                                      (DUMMY CARD)
    111.999

                             (DUMMY CARD)
    111.111

                             (FE203)
    222.222       .714   .669  1.674   .759   .547   .609   .848   3.313   .547
  1.914  2.361  .214
                             (SIO2)
    333.333     25.021  6.676  5.175 26.833               29.925 16.403 19.412
 10.725 12.803  8.436
                             (S)
    444.444     11.575 11.431  2.394 12.396  9.477 10.484 12.438  8.956  7.553
 10.741  5.878  3.864
                             (NIO)
    555.555      3.796   .435  1.092   .497   .355   .395   .555   2.169  2.697
  1.253  1.546  .128
                             (MGO)
    666.666     61.207 16.706 12.658 65.792 12.451 14.705 73.344 46.352 47.647
 25.494 31.603 21.271
                             (AL203)
    777.777     33.406 10.360  7.943 41.233 32.362  9.118 45.975 25.235 29.844
 15.209 19.738 13.140
                             (CUO)
    888.888      3.111   .356   .892   .407   .289   .489   .455   2.210  1.776
  2.539  1.266  .112
                             (MNO)
    999.999       .894   .843  2.101   .951   .689   .766  1.062   .575   .686
  2.395  2.957  .894
                             (CR203)
    111.222      1.133  1.069  2.661  1.202   .874   .974  1.342   .727   .867
  3.028  3.737  .343
                             (CO304)
    111.333      3.564   .408  1.024   .466   .333   .371   .521  2.532  2.036
   .403  1.451  .129
                             (TIO2)
    111.444      1.856  1.772  4.396  1.978  1.455  1.607  2.207  1.198  1.427
  4.975   .926  .538
                             (DUMMY CARD)
    111.555

                             (DUMMY CARD)
    111.666

                             (DUMMY CARD)
    111.777

                             (DUMMY CARD)
    111.888
```

FIG. A1/2 TYPICAL OUTPUT RESULTS OF SAMPLE MATCHING PROGRAMME

FE	SIO2	S	NIO	MGO	AL2O3	CUO	MNO	CR2O3	CO3O4	TIO2	CO3	K2O	V2O5	TOTAL
-C	-C	-0	-C	-C	-0	-J	-0	-0	-0	-0	-0	-0	-0	-0
-0	-0	-0	-0	-0	-0	-0	-0	-0	-0	-0	-0	-0	-0	-0
-0	.714	.669	1.674	.759	.547	.603	.848	3.313	.547	1.914	2.361	.214	-C	-0
-C	25.031	6.676	5.175	26.833	-0	-0	29.925	16.403	19.412	10.725	17.803	8.436	-0	-0
-0	11.575	11.431	2.394	12.390	9.477	13.484	12.438	8.956	7.553	10.741	5.876	3.804	-0	-0
-C	3.706	.435	1.092	.497	.355	.395	.555	2.169	2.697	1.253	1.546	.128	-0	-0
-0	61.217	16.706	12.658	65.792	12.451	14.705	73.344	40.352	47.647	25.404	31.603	21.271	-0	-0
-0	33.416	10.350	7.943	41.233	32.362	9.118	45.975	25.235	29.844	16.209	19.738	13.140	-0	-0
-C	3.111	.356	.892	.407	.289	.489	.455	2.210	1.776	2.539	1.266	.112	-0	-0
-0	.894	.643	2.101	.951	.689	.766	1.062	.575	.686	2.396	2.957	.894	-0	-0
-0	1.133	1.069	2.661	1.202	.874	.974	1.342	.727	.867	3.028	3.737	.343	-0	-0
-0	3.564	.408	1.024	.466	.333	.371	.521	2.532	2.036	.403	1.451	.129	-0	-0
-0	1.856	1.772	4.396	1.978	1.455	1.607	2.207	1.198	1.427	4.976	.926	.598	-0	-0
-0	-0	-0	-0	-0	-0	-0	-0	-0	-0	-0	-C	-0	-0	-0
-0	-0	-0	-0	-0	-0	-0	-0	-0	-0	-0	-0	-0	-0	-0
-0	-0	-0	-0	-0	-0	-0	-0	-0	-0	-C	-0	-0	-0	-0

STANDARD IS   8.0

FE	SIO2	S	NIO	MGO	AL2O3	CUO	MNO	CR2O3	CO3O4	TIO2	CO3	K2O	V2O5	TOTAL
60.000	20.000	-0	1.273	10.000	7.228	.250	.633	.292	.068	.169	-0	-0	-0	99.913
70.056	1695.364	1122.149	243.144	4385.951	2994.194	203.140	85.630	108.557	231.205	177.705	C	0	0	

1022.0

60.443	13.792	0	.530	4.207	.566	.699	.081	13.746	.010	.052	0	0	0	99.124
67.293	1941.829	1380.440	277.332	4820.310	3124.738	221.435	84.109	106.573	253.575	174.911	1.000	1.000	1.000	
58.062	21.534	0	.597	4.623	.590	.761	.080	13.495	.011	.051	0	0	0	99.794

STANDARD IS   9.0

FE	SIO2	S	NIO	MGO	AL2O3	CUO	MNO	CR2O3	CO3O4	TIO2	CO3	K2O	V2O5	TOTAL
40.000	40.000	-C	1.273	10.000	7.223	.250	.633	.292	.068	.169	-0	-0	-0	99.913
69.156	1328.464	1119.269	178.933	3495.931	2433.374	148.040	84.610	107.277	168.085	176.025	0	0	0	

1013.0

43.035	49.273	0	1.063	.761	.246	.357	.057	.346	.045	.087	0	0	95.267	
66.032	1454.144	1092.854	187.133	3589.006	2264.540	153.321	82.745	104.892	175.496	172.440	1.000	1.000	1.000	
41.091	53.931	0	1.112	.781	.229	.370	.055	.339	.047	.085	0	0	0	98.040

STANDARD IS   12.0

FE	SIO2	S	NIO	MGO	AL2O3	CUO	MNO	CR2O3	CO3O4	TIO2	CO3	K2O	V2O5	TOTAL
5.000	75.000	-0	1.273	10.000	7.228	.250	.633	.292	.068	.169	-0	-0	-C	99.413
67.581	686.389	1114.229	61.233	1930.390	1451.564	51.615	82.825	105.037	57.625	173.085	0	0	0	

1071.0

5.429	85.440	0	.239	5.102	.460	0	.098	.137	.010	.030	0	0	0	96.944
64.777	717.389	1097.830	69.535	1857.313	1280.120	49.624	81.238	103.014	56.762	170.500	1.000	1.000	1.000	
5.203	89.298	0	.236	4.689	.406	0	.096	.134	.010	.030	C	0	0	100.302

FIG. A1/3   LISTING OF CHEMICAL DATA HANDLING PROGRAMME

```
C     THIS PROGRAM FIRSTLY RECOMPUTES X.R.F. ANALYTICAL TOTALS TO 100 WT
C     PERCENT BY ROUNDING MAJOR ELEMENT DATA.IT THEN CONVERTS ANALYTICAL
C     DATA INTO EQUIVALENT ELEMENT CONCENTRATIONS.FINALLY IT COMPUTES
C     WEIGHT EQUIVALENT PER UNIT VOLUME DATA FOR ALL ELEMENTS IN ALL
C     SAMPLES
      PROGRAM NAME (INPUT,OUTPUT,TAPE 5=INPUT,TAPE 6=OUTPUT)
      REAL MO
      DIMENSION BB(70,22),MATA(5J,21),MATV(50,21)
      COMMON MO(70,22),AO(70,22),AWT(22),N,NO,B(70,22),L,GRAV(22),C(20),
     2O(21),E(21),F(50,21),NX,NUM,CC(21),DO(21),EE(21),DATA(50,21),AVE(1
     30,21),FE(50,21),SI(50,21),G(50,21),GO(50,21),CU(50,21),AFE(15,21),
     4ASI(15,21),AS(15,21),AGO(15,21),ACU(15,21),DATV(50,21),DUMMY(15,21
     5),MDUM(10),NDAT(10),NATV(1J),NCC(21),NEE(21),NFE(10),NAFE(10),FC(5
     60,21)
      EQUIVALENCE (B(70,22),BB(70,22)),(DATA(50,21),MATA(50,21)),(DATV(5
     20,21),MATV(50,21))
C     READ THE NUMBER OF GRAVIMETRIC PROPORTIONS CARDS TO BE USED
      READ (5,1000)L
C     READ THE NUMBER OF ATOMIC/MOLECULAR WEIGHT CARDS TO BE USED
      READ (5,1000)M
C     READ THE NUMBER OF DATA CARDS IN THE INPUT SET
      READ (5,1000) NO
C     READ THE GRAVIMETRIC PROPORTIONS CARDS
      READ (5,2800)(GRAV(K),K=1,L)
C     READ THE ATOMIC/MOLECULAR WEIGHT CARDS
      READ (5,2900)(AWT(M),M=1,M)
C     READ THE SAMPLE DATA CARDS
      READ(5,1500)((MO(ID,I),I=1,18),(MO(ID,IN),IN=20,22),MO(IO,19),ID=1
     2,10)
      JJ=1
      DO 100 ID=1,NO
C     WRITE THE SAMPLE HEADING INFORMATION
      WRITE(6,4500)
      WRITE(6,2000)
      DO 205 IA=8,20
      IF(MO(ID,IA).EQ.0)GO TO 204
      GO TO 208
  204 MO(ID,IA)=0.0J01
  208 IF(IA.EQ.19) GO TO 205
      IF(IA.GT.8) GO TO 206
      TOT=MO(ID,IA)
      GO TO 205
  206 TOT=TOT+MO(ID,IA)
  205 CONTINUE
C     ROUND MAJOR ELEMENT COMPOSITION DATA TO GIVE TOTALS OF 100 PERCENT
      FACT=100.0/TOT
      DO 210 IC=7,14
      MO(ID,IC)=MO(ID,IC)*FACT
  210 CONTINUE
      IF(MO(ID,22).LT.15.0) GO TO 105
C     CONVERT OXIDE DATA INTO ELEMENT COMPOSITION DATA FOR ALL CHEMICAL
C     VARIABLES EXCEPT MGO AND AL2O3 - NICKEL GOSSAN SAMPLES
      DO 120 I=1,22
      IF(I.EQ.7.OR.I.EQ.9.OR.I.EQ.11.OR.I.EQ.14.OR.I.EQ.15.OR.I.EQ.16.OR
     2.I.EQ.17.OR.I.EQ.18.OR.I.EQ.19) GO TO 109
      AO(ID,I)=MO(IJ,I)
      IF(I.NE.10)GO TO 120
      IF(AO(ID,10).GT.0.0)GO TO 120
      AO(ID,10)=0.0J1
      GO TO 120
  109 IF(MO(ID,9).GE.0.001)GO TO 110
      MO(ID,9)=0.001
  110 AO(ID,I)=MO(ID,I)*GRAV(I)
  120 CONTINUE
C     WRITE DETAILS OF SAMPLE VARIABLES (NICKEL GOSSAN SAMPLES)
      WRITE(6,2100)
C     WRITE SAMPLE VARIABLE (ELEMENT) DATA IN WT PC/PPM UNITS
      WRITE(6,2500)(AO(ID,I),I=1,22)
      GO TO 125
C     CONVERT OXIDE DATA INTO ELEMENT COMPOSITION DATA FOR ALL CHEMICAL
C     VARIABLES EXCEPT MGO AND AL2O3 - NICKEL SULPHIDE SAMPLES
  105 DO 130 III=1,22
  108 IF(III.EQ.9.OR.III.EQ.11.OR.III.EQ.14.OR.III.EQ.15.OR.III.EQ.16.OR
     2.III.EQ.17.OR.III.EQ.18.OR.III.EQ.19) GO TO 107
      AO(ID,III)=MO(ID,III)
      IF(III.NE.10)GO TO 130
      IF(AO(ID,10).GT.0.0)GO TO 130
      AO(ID,10)=0.001
      GO TO 130
```

FIG. A1/3 CONTINUED

```
  107 IF(MD(ID,9).GE.0.001)GO TO 106
      MD(ID,9)=0.001
  106 AJ(ID,III)=MD(ID,III)*GRAV(III)
  130 CONTINUE
C     WRITE DETAILS OF SAMPLE VARIABLES (NICKEL SULPHIDE SAMPLES)
      WRITE(6,4500)
      WRITE(6,2100)
C     WRITE SAMPLE VARIABLE (ELEMENT) DATA IN WT PC/PPM UNITS
      WRITE(6,2500)(AD(ID,III),III=1,22)
C     COMPUTE THE GRAM EQUIVALENT PER CC VALUES OF ALL ELEMENTS IN THE
C     SAMPLE (OXIDE AND SULPHIDE SAMPLES)
  125 DO 250 II=4,22
      IF(II.GT.6)GO TO 126
      E(ID,II)=AD(ID,II)
      GO TO 250
  126 IF(II.EQ.21)GO TO 251
      IF(II.EQ.22)GO TO 252
      A=AD(ID,II)/AWT(II)
      B(ID,II)=A*AD(ID,5)
      IF(B(ID,II).GE.0.0001) GO TO 250
      B(ID,II)=0.0001
      GO TO 250
  251 B(ID,21)=AD(ID,21)
      GO TO 250
  252 B(ID,22)=AD(ID,22)
  250 CONTINUE
      JJ=JJ+1
C     WRITE THE SAMPLE HEADING INFORMATION - GM.EQ.PER CC DATA
C     (ALL SAMPLES)
      WRITE(6,4500)
      WRITE(6,3000)
C     WRITE DETAILS OF SAMPLE VARIABLES
      WRITE(6,3050)
C     WRITE SAMPLE VARIABLE DATA IN (GM.EQ.PER CC X 100) UNITS
      WRITE(6,3100)(B(ID,II),II=7,22)
      WRITE(6,4500)
  100 CONTINUE
 2000 FORMAT (*WEIGHT PERCENT MAJOR ELEMENTS TO 3 SIG. FIGS. WITH TRACES
     2 AND FE TO 5 SIG. FIGS.*)
 2100 FORMAT (2X,*SAMNO*,1X,*TYPE*,1X,*LOC*,1X,*DENS*,2X,*APPDEN PORS*,2
     2X,*FE*,5X,*FEOOH*,2X,*SI   *,3X,*S*,6X,*NI*,5X,*MGO*,3X,*AL203*,2X,
     3*CU*,5X,*MN*,5X,*CR*,5X,*JO*,5X,*TI*,5X,*V(DR)CO3 DEP SI*)
 2500 FORMAT (1X,F5.0,1X,F2.0,2X,F2.0,4X,F4.2,2X,F4.2,3X,F4.1,1X,4F7.3,F
     27.4,2F7.3,3F7.4,F7.5,F6.4,F6.4,F3.,F4.0,F3.0)
 3000 FORMAT (*VALUE IN GRAM MOLES PER CC X 100 (MAJORS) OR GRAM EQUIVS.
     2PER CC X 100 (IRON(FE) AND TRACE METALS)*)
 3050 FORMAT (36X,*FE*,5X,*FEO))1*,2X,*SI  *,3X,*S*,6X,*NI*,5X,*MGO*,3X,*
     2AL203*,2X,*CU*,5X,*MN*,5X,*CR*,5X,*CO*,5X,*TI*,5X,*V(DR)CO3 DEP SI
     3*)
 3100 FORMAT (35X,3F7.3,2F7.4,2F7.3,3F7.4,F7.5,F6.4,F6.4,F3.0,F4.0,F3.0)
 4500 FORMAT(1H0)
 1000 FORMAT (I4)
 1500 FORMAT (F5.0,2F2.0,2F3.2,5F3.1,F5.4,2F3.1,3F5.4,F4.4,F5.4,F3.1,F5.
     21,F2.0,F5.4)
 2800 FORMAT(F6.4)
 2900 FORMAT (F6.2)
      STOP
      END
```

```
  22                  (THE NUMBER OF GRAVIMETRIC PROPORTIONS CARDS)
  22                  (THE NUMBER OF ATOMIC/MOLECULAR WEIGHT CARDS)
  ND                  (THE NUMBER OF SAMPLE DATA CARDS)
                      (GRAVIMETRIC PROPRTIONS DATA)
                      DUMMY CARD
                      DUMMY CARD
                      DUMMY CARD
                      DUMMY CARD
                      DUMMY CARD
                      DUMMY CARD
  .6296              GRAV.  PROP.  FE IN FEOOH
                      DUMMY CARD
  .4675              GRAV.  PROP.  SI IN SIO2
                      DUMMY CARD
  .7858              GRAV.  PROP.  NI IN NIO
                      DUMMY CARD
                      DUMMY CARD
  .7988              GRAV.  PROP.  CU IN CUO
  .6319              GRAV.  PROP.  MN IN MNO
  .6842              GRAV.  PROP.  CR IN CR203
  .7342              GRAV.  PROP.  CO IN CO304
  .5995              GRAV.  PRUP.  TI IN TIO2
```

FIG. A1/3 CONCLUDED

```
1.0090              VANADIUM PROP DATA (UNUSED)
                    DUMMY CARD
                    DUMMY CARD
                    DUMMY CARD
                    (ATOMIC/MOLECULAR WT. DATA)
                    DUMMY CARD
                    DUMMY CARD
                    DUMMY CARD
                    DUMMY CARD
                    DUMMY CARD
                    DUMMY CARD
  55.85             ATOMIC WT. FE
  88.85             MOLE.  WT. FEOOH
  28.09             ATOMIC WT. SI
  32.06             ATOMIC WT. S
  58.71             ATOMIC WT. NI
  40.31             MOLE.  WT. MGO
 101.96             MOLE.  WT. AL2O3
  63.54             ATOMIC WT. CU
  54.94             ATOMIC WT. MN
  52.00             ATOMIC WT. CR
  58.93             ATOMIC WT. CO
  47.90             ATOMIC WT. TI
  50.54             ATOMIC WT. V
  60.01             ATOMIC WT. CO3
                    DUMMY CARD
                    DUMMY CARD
```

FIG. A1/4   TYPICAL OUTPUT RESULTS OF DATA HANDLING PROGRAMME

```
WEIGHT PERCENT MAJOR ELEMENTS TO 3 SIG. FIGS. WITH TRACES AND FE TO 5 SIG. FIGS.
  SAMNO TYPE LOC DENS APPDEN PORS  FE     FEOOH  SI     S     NI     MGO    AL2O3  CU     MN     CR     CO     TI     V(OR)CO3 DEP SI
2057. -0  -0   3.30  3.10   4.1  50.061 79.512 3.060  6.060  .0644  .200   5.900  2085  .0051 .03.1 .00J73 .0042 .00.1 .. -015.

VALJE IN GRAM MOLES PER CC X 100 (MAJORS) OR GRAM EQUIVS.PER CC X 100 (IRON(FE) AND TRACE METALS)
                                  FE     FEOOH  SI     S     NI     MGO    AL2O3  CU     MN     CR     CO     TI     V(OR)CO3 DEP SI
                                 2.779  2.774   .336  .5860  .0034  .015   .179   :102  .0003 .0018 .0001C .0003 .0001 .. -015.


WEIGHT PERCENT MAJOR ELEMENTS TO 3 SIG. FIGS. WITH TRACES AND FE TO 5 SIG. FIGS.
  SAMNO TYPE LOC DENS APPDEN PORS  FE     FEOOH  SI     S     NI     MGO    AL2O3  CU     MN     CR     CO     TI     V(OR)CO3 DEP SI
2058. -0  -0   3.50  3.10   8.7  61.440 97.586  .057   .000   .3316  .300   .700  0919  .0215 .0069 ..1982 .1619 .0001 C. 34.15.

VALUE IN GRAM MOLES PER CC X 100 (MAJORS) OR GRAM EQUIVS.PER CC X 100 (IRON(FE) AND TRACE METALS)
                                  FE     FEOOH  SI     S     NI     MGO    AL2O3  CU     MN     CR     CO     TI     V(OR)CO3 DEP SI
                                 3.410  1.405   .006  .0001  .0175  .023   .021   0045  .0012 .00 5 .0011 .0105 .001 .. 34.15.


WEIGHT PERCENT MAJOR ELEMENTS TO 3 SIG. FIGS. WITH TRACES AND FE TO 5 SIG. FIGS.
  SAMNO TYPE LOC DENS APPDEN PORS  FE     FEOOH  SI     S     NI     MGO    AL2O3  CU     MN     CR     CO     TI     V(OR)CO3 DEP SI
2060. -0  -0   3.50  3.50   1.2  51.368 81.589 5.503  .000   .0057  .200   5.100  0008  .0057 .0368 .00147 .1379 .0001 C. -015.

VALUE IN GRAM MOLES PER CC X 100 (MAJORS) OR GRAM EQUIVS.PER CC X 100 (IRON(FE) AND TRACE METALS)
                                  FE     FEOOH  SI     S     NI     MGO    AL2O3  CU     MN     CR     CO     TI     V(OR)CO3 DEP SI
                                 3.219  3.214   .686  .0001  .0051  .017   .175   .001  .0004 .0021 .0010 .0101 .0001 C. -015.


WEIGHT PERCENT MAJOR ELEMENTS TO 3 SIG. FIGS. WITH TRACES AND FE TO 5 SIG. FIGS.
  SAMNO TYPE LOC DENS APPDEN PORS  FE     FEOOH  SI     S     NI     MGO    AL2O3  CU     MN     CR     CO     TI     V(OR)CO3 DEP SI
2075. -0  -0   3.40  2.60   22.6 61.199 97.202  .052   .006   .1540  .300   .900  7229  .0057 .0014 ..2570 .0378 .0001 C. 39.15.

VALJE IN GRAM MOLES PER CC X 100 (MAJORS) OR GRAM EQUIVS.PER CC X 100 (IRON(FE) AND TRACE METALS)
                                  FE     FEOOH  SI     S     NI     MGO    AL2O3  CU     MN     CR     CO     TI     V(OR)CO3 DEP SI
                                 2.849  2.844   .005  .0001  .0066  .019   .023   6296  .0003 .0001 .0113 .0021 .0001 C. 39.15.
```

TABLE A2/1 THE CHEMICAL DATA OF 28 NICKEL GOSSANS FROM SOUTHERN AFRICA AND WESTERN AUSTRALIA

MUNALI (ZAMBIA)

SAMP	APON	DENS	POR	FE	SI	S	NI	MGO	ALOX	CU	MN	CR	CO	TI
2104.	3.50	3.10	12.6	60.075	.001	.100	.7842	.800	1.800	.2604	.0436	.0025	.0558	.0114
2105.	3.10	2.70	13.4	59.769	.001	.100	1.0200	.600	2.300	.2229	.0291	.0041	.0065	.0162
2108.	2.60	2.50	9.4	16.839	31.982	.100	.3206	3.100	.200	.4130	.0164	.0025	.0147	.0641
2109.	2.90	2.60	12.1	57.710	.001	.100	1.5441	2.300	2.600	.1733	.0708	.0766	.0951	.0276
2112.	3.30	3.10	3.5	53.486	2.232	.100	.8031	.400	.300	.0559	.0417	.0185	.0272	3.8794
2113.	3.30	3.20	5.0	61.727	.001	.100	.3316	.400	.700	.0919	.0215	.0089	.0198	.0162
2114.	3.00	3.00	5.2	60.738	.001	.100	.5760	.500	.900	.1438	.0322	.0369	.0323	.2050
2115.	3.00	2.90	5.0	28.584	24.879	.100	.1053	.200	.100	.6095	.0063	.0025	.4466	.0426

PERSERVERENCE (RHODESIA)

SAMP	APON	DENS	POR	FE	SI	S	NI	MGO	ALOX	CU	MN	CR	CO	TI
2286.	3.20	3.20	2.6	36.348	18.092	.100	.2538	.200	2.400	.2404	.0701	.0151	.0081	.0036
2287.	2.50	2.40	5.3	2.559	44.327	.130	.1422	.100	.500	.1669	.0796	.0096	.0169	.0042
2288.	2.30	2.20	8.2	5.593	41.376	.100	.2098	.200	1.400	.1598	.1434	.0116	.0242	.0048
2289.	2.40	2.30	4.2	4.338	42.686	.100	.2106	.100	.900	.2029	.1169	.0089	.0154	.0024
2291.	3.00	2.90	5.0	42.670	10.777	.100	.5100	6.000	1.100	.3099	.0645	.1970	.0162	.0528
2292.	3.00	2.90	3.0	30.833	23.192	.100	.2499	.300	.300	.2668	.0310	.0171	.0044	.0036
2293.	2.80	2.70	2.3	24.942	27.576	.100	.1462	.600	.200	.1326	.0537	.0178	.0029	.0054
2294.	3.20	2.70	14.0	61.589	.001	.100	.2483	.500	.700	.0034	.0082	.0205	.0176	.1025

TROJAN (RHODESIA)

SAMP	APON	DENS	POR	FE	SI	S	NI	MGO	ALOX	CU	MN	CR	CO	TI
2252.	3.30	3.00	12.0	59.909	.001	.100	.8557	.400	2.100	.1430	.1510	.1567	.0162	.0330
2253.	2.80	2.40	15.0	46.492	8.015	.100	1.4467	1.800	1.700	.1134	1.1058	.0048	.0367	.0414
2254.	2.90	2.60	11.5	42.670	10.040	.100	1.4412	1.900	1.900	.0879	1.6006	.0025	.0053	.0426

FIBRE (RHODESIA)

SAMP	APON	DENS	POR	FE	SI	S	NI	MGO	ALOX	CU	MN	CR	CO	TI
2173.	2.60	2.50	4.3	17.829	29.838	.100	.7190	1.500	.200	.0655	.4392	.0198	.1299	.0054
2174.	3.10	2.70	13.6	60.521	.000	.100	.5721	.300	1.500	.0871	.0227	.0965	.0139	.2973
2176.	2.90	2.80	5.3	28.320	25.234	.100	.3159	.200	.200	.0248	.0284	.0287	.0095	.0312
2177.	3.00	2.90	4.6	28.411	25.306	.100	.0864	.100	.300	.0040	.0145	.0062	.0007	.1085
2178.	3.60	3.10	13.6	41.715	15.104	.100	.5516	.200	.100	.0431	.1024	.0014	.0462	.0168
2179.	3.10	2.10	33.2	16.159	34.336	.100	.0079	.100	.500	.0104	.0076	.0103	.0007	.1355

PIKWE (BOTSWANA)

SAMP	APON	DENS	POR	FE	SI	S	NI	MGO	ALOX	CU	MN	CR	CO	TI
2002.	3.40	3.10	11.5	59.913	.055	.100	.2805	.400	2.100	.5663	.0316	.0192	.0272	.2056
2005.	3.00	2.70	9.7	37.527	18.204	.100	.1022	.200	.300	.3890	.0088	.0116	.0103	.1439
2017.	3.30	2.80	14.9	35.107	19.176	.100	.0668	.200	1.700	.6007	.0057	.0520	.0051	.0270
2018.	2.80	2.50	11.9	37.975	16.254	.100	.2145	.300	2.300	1.0592	.0070	.0431	.0125	.0809
2019.	3.30	3.10	8.0	41.709	14.247	.100	.0833	.500	1.400	.5703	.0076	.0479	.0073	.0414
2031.	3.10	2.70	19.5	31.305	22.516	.310	.0951	.200	.400	.4889	.0057	.0068	.0073	.0462
2072.	2.90	2.20	23.2	47.980	6.989	3.147	.0799	.300	3.700	.6362	.0032	.0801	.0018	.0270
2074.	3.90	3.10	22.9	62.010	.051	.110	.0440	.400	.400	.1717	.0051	.0096	.0051	.0426
2001.	1.90	1.60	15.7	7.672	40.383	.100	.0330	.100	.300	.1366	.0032	.0034	.0020	.4994
2013.	2.70	2.20	18.6	23.548	28.541	.100	.0707	.200	.400	.3746	.0152	.0910	.0426	.1145
2021.	2.40	2.10	5.2	45.658	11.692	.100	.1210	.300	.600	.7053	.0063	.0452	.0059	.1439
2022.	2.20	2.00	5.3	23.954	27.971	.100	.0346	.200	.900	.5727	.0057	.0445	.0191	.0456
2024.	2.30	1.20	47.3	22.731	28.820	.100	.0401	.200	1.200	.5000	.0057	.0041	.0020	.0528
2028.	2.40	1.50	39.9	30.057	21.686	.456	.0354	.300	.800	.2189	.0057	.0123	.0029	1.2601
2038.	2.70	2.60	7.3	51.602	6.987	.100	.0393	.200	1.700	.1885	.0057	.0253	.0022	.1739
2043.	2.30	2.10	7.3	32.424	21.303	.100	.0401	.500	1.800	.2436	.0126	.0212	.0029	.1535
2045.	3.10	2.80	5.8	40.238	15.188	.100	.0338	.200	2.600	.2844	.0063	.0068	.0020	.0959
2046.	3.50	3.00	14.5	52.849	5.504	.100	.0495	.200	2.600	.6263	.0063	.0137	.0029	.1499
2050.	2.90	2.80	3.2	29.749	23.358	.100	.0223	.200	1.500	.2141	.0101	.0192	.0020	.4358
2051.	2.70	2.40	13.2	45.403	11.955	.100	.0668	.500	1.100	.2364	.0088	.0458	.0022	.0588
2056.	3.30	3.10	5.0	53.344	4.895	.100	.0471	.200	3.100	.2724	.0063	.0096	.0020	.1577
2062.	2.80	2.20	21.4	49.202	6.943	.100	.2090	.300	3.900	.9538	.0063	.0192	.0037	.0971
2066.	3.10	2.30	25.7	52.928	6.660	.100	.0593	.300	.600	.3371	.0051	.0025	.0026	.0863
2067.	2.70	2.10	21.9	53.859	5.508	.100	.1485	.300	.800	.7700	.0057	.0025	.0026	.0863
2068.	3.80	3.40	11.6	61.963	.055	.100	.0338	.300	.500	.2916	.0051	.0041	.0044	.0078
2070.	3.80	3.10	19.0	61.032	.056	.100	.4353	.300	.500	.6790	.0120	.0025	.0477	.0594
2012.	2.70	2.50	19.4	24.495	18.188	5.711	.3127	.200	11.300	1.3827	.0051	.0479	.0162	.0725
2026.	2.00	1.80	9.4	19.203	30.301	.100	.0676	.100	3.200	.4074	.0070	.0109	.0029	.2974
2029.	2.90	2.50	12.0	31.330	22.873	.100	.0668	.100	.400	.4705	.0038	.0062	.0059	.0360
2033.	2.30	2.10	8.8	14.914	35.236	.100	.0473	.100	.200	.3651	.0025	.0021	.0051	.0510
2036.	2.20	2.10	3.0	15.343	35.096	.100	.0346	.100	.300	.0030	.0030	.0055	.0030	.0516
2048.	2.00	1.80	8.7	6.041	41.955	.100	.0102	.100	.400	.0783	.0025	.0030	.0030	.0396
2055.	3.40	2.90	13.6	59.509	.520	.100	.0597	.300	3.100	.7517	.0057	.0130	.0029	.1565
2057.	3.30	3.10	4.1	50.001	3.060	6.060	.0644	.200	.590	.2085	.0051	.0301	.0030	.0042
2058.	3.50	3.10	8.7	61.440	.057	.100	.3316	.300	.700	.0919	.0215	.0089	.0198	.1619
2060.	3.50	3.50	1.2	51.368	5.503	.100	.0857	.200	5.100	.0030	.0057	.0308	.0030	.1379
2075.	3.40	2.60	21.0	61.110	.052	.100	.1540	.300	.900	.7229	.0057	.0030	.0257	.0378
2081.	2.20	1.90	12.2	14.396	34.325	.100	.0526	.100	1.000	.3682	.0044	.0157	.0051	.1697
2082.	2.10	1.80	10.2	7.114	39.258	.100	.0526	.100	2.600	.2173	.0038	.0103	.0030	1.1253
2083.	2.00	1.90	2.7	5.226	41.908	.100	.0259	.100	1.100	.1574	.0025	.0048	.0030	.3981

DAMBA (RHODESIA)

SAMP	APDN	DENS	POR	FE	SI	S	NI	MGO	ALOX	CU	MN	CR	CO	TI
2183.	3.00	2.80	5.9	48.845	6.754	.100	4.2873	.200	.100	.7828	.0183	.0212	.0007	.0072
2185.	3.10	2.70	11.0	38.395	12.380	.100	5.3269	3.400	.600	.4274	.0133	.0301	.0007	.0174
2186.	2.90	2.50	15.3	36.278	16.630	.100	1.0278	1.700	1.200	.6023	.0177	.0096	.0007	.0168

MT.MONGER (W.A.)

SAMP	APDN	DENS	POR	FE	SI	S	NI	MGO	ALOX	CU	MN	CR	CO	TI
1184.	2.60	2.30	11.5	36.422	19.254	.100	.4408	.100	.100	.0559	.0010	.0356	.0088	.0072
1185.	3.20	3.10	4.0	59.198	.001	.100	2.3393	1.000	.300	.5112	.0177	.0602	.0308	.0048
1190.	2.60	2.40	5.7	17.650	32.933	.100	.0684	.100	.200	.3555	.0025	.4215	.0020	.0090
1193.	2.30	1.90	15.8	16.796	33.340	.100	.2460	.400	.200	.3123	.0019	.4003	.0051	.0060
1197.	2.80	2.40	14.5	44.326	12.062	.100	.3638	1.400	.400	.6638	.0088	.2080	.0242	.0162
1199.	2.60	2.40	5.0	30.784	22.326	.100	.3953	.500	.200	.0975	.0278	1.2049	.0125	.0552
1200.	2.80	2.50	8.1	34.525	19.004	.100	.3520	.500	.200	.1134	.3475	1.6058	.0117	.0354
1201.	2.70	2.50	5.4	27.652	24.957	.100	.3261	.500	.200	.1006	.0145	.8163	.0117	.0366
1186.	3.20	3.00	9.0	60.739	.001	.100	1.5488	.100	.200	.5911	.0171	.0062	.0264	.0036
1187.	2.80	2.80	1.4	13.942	35.862	.100	.3065	.100	.200	.2189	.0303	.0821	.0066	.0042
1188.	2.80	2.60	5.5	5.656	42.380	.100	.1234	.100	.100	.0775	.0051	.0185	.0029	.0054
1192.	2.20	2.20	.1	2.056	44.860	.100	.0251	.300	.200	.0951	.0044	.0924	.0022	.0072
1194.	3.10	2.90	3.9	44.523	10.290	.100	.4165	4.200	.600	.5584	.0512	.0274	.0073	.0312
1196.	2.50	2.30	8.9	39.653	16.415	.100	.1304	.600	.300	.4322	.0044	.0677	.0029	.0126
1198.	2.60	2.50	1.9	5.234	42.606	.100	.0110	.100	.300	.0479	.0013	.0164	.0037	.0072

MT.EDWARDS (W.A.)

SAMP	APDN	DENS	POR	FE	SI	S	NI	MGO	ALOX	CU	MN	CR	CO	TI
1284.	2.40	1.90	29.5	4.075	41.399	.100	.1226	2.300	2.500	.0104	.0215	.1471	.0037	.0462
1285.	3.00	3.00	4.5	53.161	3.588	.100	.7481	.700	4.000	.1278	.0164	.6370	.0020	.0677
1286.	2.90	2.70	6.9	34.364	20.671	.100	.1996	.100	.100	.0967	.0044	.3790	.0020	.0030
1288.	2.90	2.90	1.7	16.705	32.369	.100	.1634	.100	.200	.1877	.0013	2.2900	.0020	.0024
1289.	2.90	2.80	1.3	19.712	31.908	.100	.0959	.100	.100	.1270	.0019	.0192	.0020	.0030
1290.	3.00	2.80	4.5	29.652	23.808	.100	.4424	.100	.400	.0863	.0038	.3811	.0022	.0030
1305.	3.30	3.10	8.2	21.434	26.588	.100	.2742	.600	.100	.1526	.0297	4.5205	.0037	.0102
1310.	3.30	3.10	4.1	28.090	24.660	.100	.6554	.100	.100	.0847	.0082	.0048	.0037	.0228
1287.	2.90	2.70	4.4	12.633	35.436	.100	1.4883	.100	.200	.7820	.0010	.7437	.0020	.0024
1304.	2.90	2.70	3.6	41.500	11.517	.100	5.4794	.200	.100	.7493	.0114	.0629	.1263	.0132
1306.	2.80	2.60	4.3	34.815	16.003	.100	1.6533	6.000	.100	.9697	.0373	.1697	.0947	.0060
1307.	3.00	2.90	3.7	27.438	23.072	.100	1.1795	2.800	1.000	.2564	.0392	.2032	.0110	.0028
1308.	2.90	2.90	3.4	30.956	22.329	.100	.9532	.900	.200	.0959	.0158	.0766	.0206	.0144
1309.	3.00	2.90	6.4	26.759	25.444	.100	.7779	.700	.200	.1558	.0221	.2826	.0279	.0192

TABLE A2/1 CONTINUED

JAN SHOOT (W.A.)

SAMP	APON	DENS	POR	FE	SI	S	NI	MGO	ALOX	CU	MN	CR	CO	TI
1134.	2.80	2.80	.5	12.057	35.285	.100	.8887	.100	.100	.5624	.0025	2.1805	.0088	.0054
1135.	3.10	3.00	2.8	32.042	22.056	.100	.6357	.200	.100	.3802	.0032	.0698	.0499	.0030
1136.	2.90	2.80	2.7	21.827	29.870	.100	.2742	.100	.100	.2860	.0044	.2313	.0264	.0036
1221.	3.20	3.10	2.0	19.368	31.544	.100	.3693	.100	.100	.1973	.0107	.5255	.0088	.0036
1222.	3.10	2.20	25.4	25.009	24.766	.100	.7811	.400	.100	.2261	.0177	2.3051	.0162	.0024

SPARGOVILLE 5A (W.A.)

SAMP	APON	DENS	POR	FE	SI	S	NI	MGO	ALOX	CU	MN	CR	CO	TI
1245.	2.70	2.60	5.9	43.950	8.743	.100	.5964	.400	.900	.2995	.0487	5.3648	.0132	.1193
1248.	3.20	3.00	6.5	40.841	14.613	.100	.3874	.400	.600	.3379	.0278	.8771	.0095	.0246
1254.	3.10	2.80	6.8	32.515	17.065	.100	4.3918	.900	.800	.6342	.1415	.0274	.0382	.2206
1255.	2.80	2.70	5.0	38.913	12.348	.100	4.4319	.600	.700	.7916	.2730	.0274	.1505	.1876
1257.	2.90	2.80	5.0	40.376	9.387	.100	5.2735	1.100	.300	.8004	.0600	.1115	.1373	.0114
1258.	3.00	2.90	5.0	52.039	.848	.100	7.1201	.400	.300	.8555	.0632	.0356	.0940	.0072
1260.	2.90	2.80	5.0	40.192	12.674	.100	3.0497	.300	.100	.8427	.0689	.0698	.1593	.0078
1261.	3.00	2.60	14.0	39.600	14.286	.100	1.0954	.700	.100	.6470	.0284	.6917	.1322	.0222
1249.	2.90	2.90	.7	34.468	18.242	.100	2.8289	.500	.100	.7029	.0221	.0294	.0764	.0060
1250.	2.90	2.80	3.8	35.994	16.945	.100	2.1169	.300	.200	1.2062	.0152	.3325	.0338	.0156
1256.	3.00	2.90	5.0	45.609	5.268	.100	5.8754	1.700	.500	1.0265	.0701	1.2432	.1395	.0444
1263.	2.90	2.60	19.9	24.971	17.256	.100	1.7060	2.800	.800	.7708	.0942	.3277	.0976	.0528

REDROSS (W.A.)

SAMP	APON	DENS	POR	FE	SI	S	NI	MGO	ALOX	CU	MN	CR	CO	TI
1348.	2.80	2.70	4.3	17.553	33.438	.100	.0629	.100	.200	.0975	.0101	.0294	.0029	.0036
1349.	3.10	2.90	2.3	13.649	36.087	.100	.1611	.100	.100	.1941	.0367	.2737	.0029	.0030
1350.	3.10	2.90	5.7	5.723	41.899	.100	.0173	.100	.200	.6950	.0234	.1129	.0051	.0090
1351.	2.90	2.40	17.5	34.687	20.141	.100	.0401	.800	.100	.2173	.0739	.1970	.0059	.0108
1352.	3.10	3.10	1.1	21.854	30.014	.100	.0424	.300	.100	.0935	.0221	.3257	.0037	.0222

CARR BOYD (W.A.)

SAMP	APON	DENS	POR	FE	SI	S	NI	MGO	ALOX	CU	MN	CR	CO	TI
1268.	2.90	2.70	7.2	49.919	6.110	.100	.3701	1.500	4.000	.4929	.0329	.1526	.0264	.1055
1269.	3.20	3.10	4.3	55.795	1.517	.100	.6522	3.700	.300	.0631	.0436	.0541	.0162	.2626
1270.	3.70	3.40	8.2	43.616	6.158	1.854	.4220	.100	.100	.3251	.0152	.0089	.0022	.0629
1273.	3.10	2.40	20.5	49.565	5.757	3.408	.4078	.200	3.400	.1238	.0051	.0657	.0191	.3867
1277.	2.90	2.50	15.2	36.014	11.263	17.208	.0762	.600	.100	.0120	.0057	.0554	.0044	.2128

TABLE A2/1   CONTINUED

WIDGIEMOOTHA NO. 3 (W.A.)

SAMP	APON	DENS	POR	FE	SI	S	NI	MGO	ALOX	CU	MN	CR	CO	TI
1346.	1.40	1.10	21.4	.0J1	44.816	.100	.1234	1.800	1.800	.1062	.0044	.0315	.0015	.1906
1340.	2.50	2.40	5.J	35.410	18.358	.100	1.3154	.400	.5JJ	1.0089	.0088	.0445	.J338	.0J30
1341.	3.00	2.90	4.1	49.187	8.264	.100	1.3932	.300	.800	.5384	.0044	.0369	.0492	.0030
1342.	2.60	2.3J	10.1	28.8i2	24.037	.100	.9610	.6JJ	.2JJ	.2740	.0335	.0848	.C330	.0336
1344.	2.60	2.5J	5.8	28.3J2	24.1i71	.1J0	.8353	.800	.3JJ	.2852	.0360	.2360	.0330	.05.22
1347.	2.50	2.40	4.5	19.849	3C.504	.100	.8424	.40J	.700	.4361	.0051	.0691	.0286	.0C48

SCOTIA (W.A.)

SAMP	APON	DENS	POR	FE	SI	S	NI	MGO	ALOX	CU	MN	CR	CO	TI
1204.	2.70	2.70	2.9	14.378	31.433	.100	.7221	5.700	1.100	.4353	.0272	.1163	.0007	.0510
1205.	2.70	2.50	4.3	17.3J2	28.275	.100	.5563	7.500	1.0JJ	.4305	.J373	.0972	.00C7	.0498
1207.	2.6J	2.60	3.J	3.5J8	41.196	.100	.1878	5.100	.500	.J008	.0619	.0937	.0073	.0180
1202.	2.70	2.2J	18.1	29.481	13.941	.100	1.4419	14.7JJ	1.30J	.5815	.0708	.0985	.0139	.0689
1203.	2.8C	2.60	5.2	24.036	24.725	.10J	.9414	4.400	1.000	.4992	.0347	.1888	.0007	.0599
1206.	2.70	2.70	1.J	19.571	24.593	.100	.8102	9.8JJ	1.700	.J399	.0310	.1430	.G037	.0689
1208.	2.60	2.40	5.9	12.6J3	2i.428	.100	1.3288	19.0JJ	1.60J	.1909	.0493	.3592	.0029	.1C19

NEPEAN (W.A.)

SAMP	APON	DENS	POR	FE	SI	S	NI	MGO	ALOX	CU	MN	CR	CO	TI
1359.	3.10	3.00	2.4	41.136	14.493	.1J0	.3622	.400	1.700	.C679	.2035	.2313	.0191	.0330
1360.	3.30	3.10	4.4	44.851	11.138	.100	.6208	1.100	1.400	.1198	.2610	.1642	.0316	.0300

TABLE A2/1 CONTINUED

EMPRESS (RHODESIA)

SAMP	APON	DENS	POR	FE	SI	S	NI	MGO	ALOX	CU	MN	CR	CO	TI
2257.	2.80	2.10	24.8	21.579	17.505	.100	.7866	17.100	2.900	2.1983	.0575	.0212	.0066	.1259
2260.	3.40	3.10	6.9	58.318	.000	.100	.3756	2.000	2.100	1.3907	.0322	.0239	.0008	.0516
2263.	2.80	2.00	25.1	46.815	9.503	.100	.7646	1.900	1.600	.3187	.0284	.0089	.0007	.0701
2265.	2.70	2.40	7.7	14.353	32.527	.100	.4424	2.000	3.200	.7229	.0550	.0327	.0088	.0731
2268.	2.80	2.70	1.2	15.327	29.888	.100	.6632	3.100	5.400	.4162	.0872	.0082	.0081	.1673
2255.	3.60	3.10	14.6	49.458	6.145	.100	1.3036	4.700	.900	.3938	.1087	.0062	.0440	.0162
2256.	3.40	3.10	10.2	47.325	7.520	.100	1.2306	2.000	3.800	.6454	.0234	.0068	.0095	.0522
2258.	3.20	2.90	4.8	55.607	.000	2.054	1.2856	1.600	1.800	.3563	.0581	.0007	.0044	.0252
2261.	3.30	2.60	24.4	29.199	23.885	.100	.0456	.300	.800	1.1079	.0177	.0109	.0037	.0228
2262.	2.60	2.40	7.3	21.019	20.951	.100	1.2086	4.400	7.000	2.2007	.1674	.0513	.0338	.4220
2269.	3.50	3.30	2.7	51.104	5.569	.100	1.1386	1.100	2.000	.7892	.0512	.0055	.0117	.0857
2274.	2.70	2.50	6.1	25.075	18.449	.100	.8880	6.900	7.100	.8443	.1119	.1471	.0352	.2260

EPOCH (RHODESIA)

SAMP	APON	DENS	POR	FE	SI	S	NI	MGO	ALOX	CU	MN	CR	CO	TI
2201.	3.20	2.90	9.3	30.489	15.931	.100	.7441	15.100	.200	.0847	.0145	.1143	.0008	.0234
2194.	2.10	1.50	29.3	36.012	12.356	.100	1.8458	12.400	.300	.3523	.0158	.1745	.0235	.0330
2195.	2.70	2.20	14.6	58.484	.000	.100	1.8906	1.500	.700	1.2341	.0360	.0260	.0793	.0078
2196.	3.00	2.80	7.7	37.436	11.156	.100	1.6494	13.100	.700	.2708	.0227	.2805	.0125	.0426
2199.	3.80	3.60	4.7	57.709	.000	.100	2.8627	1.100	1.600	.3938	.0139	.0759	.0250	.0090
2200.	2.50	2.20	12.1	48.314	6.367	.100	2.1672	2.700	2.500	.4937	.0297	.1786	.0022	.0210
2202.	2.60	2.30	11.4	58.335	.000	.100	.8408	3.500	.400	.4665	.0177	.5179	.0396	.0222
2203.	3.00	2.40	18.9	58.470	.000	.100	1.6305	3.100	.300	.3315	.0145	.1642	.0426	.0096
2204.	3.20	2.90	7.7	51.929	5.494	.100	1.4734	2.000	.300	.3403	.0139	.3592	.0184	.0192

SHANGANI (RHODESIA)

SAMP	APON	DENS	POR	FE	SI	S	NI	MGO	ALOX	CU	MN	CR	CO	TI
2229.	3.20	2.90	7.0	57.957	.000	.100	.9964	.400	1.600	2.5586	.0253	.0924	.1997	.0180
2230.	2.80	2.50	5.9	59.378	.000	.100	1.0978	.900	1.200	1.0033	.0366	.0267	.0338	.0228
2231.	3.00	2.80	6.1	56.800	.000	.100	1.4191	.700	3.800	1.3987	.0385	.0527	.1138	.0557
2232.	3.10	2.80	8.2	59.315	.300	.100	1.3516	.700	.700	.9098	.0133	.0335	.0492	.0096
2233.	3.20	3.00	5.8	49.413	7.960	.100	1.1166	.300	1.000	.7724	.0575	.0431	.0778	.0198
2234.	3.10	2.80	8.2	50.823	6.448	.100	1.6604	.300	1.100	.7716	.0221	.1286	.0617	.0390

SELKIRK (BOTSWANA)

SAMP	APON	DENS	POR	FE	SI	S	NI	MGO	ALOX	CU	MN	CR	CO	TI
2142.	3.50	3.40	3.3	48.385	9.729	.100	.0173	.300	1.500	.0511	.0057	.0712	.0020	.0935
2146.	3.30	3.20	4.7	44.286	13.102	.100	.0173	.200	.600	.1725	.0051	.0931	.0029	.1733
2148.	4.10	3.80	4.0	61.738	.001	.100	.0802	.300	.600	.2508	.0063	.0931	.0029	.1733
2149.	4.00	3.70	7.6	61.036	.001	.100	.2365	.300	1.200	.5296	.0101	.0034	.0162	.0090
2150.	4.20	4.10	.1	62.163	.001	.100	.0550	.300	.400	.2516	.0063	.0025	.0037	.0066
2151.	3.90	3.70	1.6	61.574	.001	.100	.1422	.300	.800	.4457	.0070	.0025	.0037	.0072
2152.	4.00	4.00	3.8	62.004	.001	.100	.0597	.300	.500	.2860	.0063	.0021	.0051	.0114
2153.	3.60	3.60	2.7	61.824	.001	.100	.1124	.300	.500	.3802	.0057	.0151	.0044	.0282
2143.	3.80	3.40	9.0	49.009	8.784	.100	.0141	.200	2.400	.0399	.0057	.1362	.0022	.0797
2144.	3.70	3.50	9.5	60.674	.001	.100	.0181	.300	2.300	.0495	.0063	.1581	.0044	.0989
2145.	3.50	3.10	9.3	45.633	11.591	.100	.0126	.200	1.600	.0495	.0038	.2600	.0022	.0623
2154.	3.70	3.70	.9	61.854	.100	.100	.0566	.300	.400	.5016	.0051	.0030	.0037	.0090

PHOENIX (BOTSWANA)

SAMP	APON	DENS	POR	FE	SI	S	NI	MGO	ALOX	CU	MN	CR	CO	TI
2126.	3.20	2.80	15.9	59.261	.001	.100	.0841	.300	1.800	1.9898	.0076	.0944	.0051	.1876
2127.	3.40	3.00	13.0	59.116	.001	.100	.0676	.300	1.700	2.5186	.0076	.0554	.0073	.0174
2128.	3.70	3.40	9.8	58.037	.001	.100	.0699	.400	4.000	1.5425	.0063	.0595	.0044	.1643
2129.	3.10	2.90	5.8	60.147	.001	.100	.1925	.400	1.200	1.4235	.0076	.0027	.0073	.1145
2130.	3.60	3.10	9.8	59.509	.001	.100	.2059	.400	3.400	.3299	.0107	.0025	.0095	.0342
2131.	3.60	3.50	4.9	60.521	.001	.100	.6051	.300	1.700	.2788	.0082	.0055	.0734	.0312
2132.	3.50	2.90	15.3	61.434	.001	.100	.2043	.400	2.200	.3826	.0101	.0027	.0132	.0270
2133.	3.50	3.20	3.6	58.453	2.058	.574	.1697	.300	.400	.1286	.0063	.0025	.0059	.0246

SELIBI (BOTSWANA)

SAMP	APON	DENS	POR	FE	SI	S	NI	MGO	ALOX	CU	MN	CR	CO	TI
2095.	3.10	3.00	3.6	37.036	18.334	.100	.2491	.300	.500	.5056	.0126	.0445	.0059	.0330
2097.	2.80	2.80	3.1	43.230	12.760	.100	.5524	.500	.700	1.3164	.0120	.0239	.0250	.0743
2098.	2.80	2.70	3.4	30.998	21.030	.415	.1265	.400	.600	3.1089	.0145	.0178	.0037	.0420
2099.	2.70	2.40	7.0	26.677	25.056	.100	.1249	.300	.500	2.3165	.0120	.0027	.0015	.0617
2100.	2.80	2.70	2.3	28.016	23.327	.100	.1501	.400	.600	3.4915	.0076	.0034	.0044	.0120
2101.	2.70	2.60	3.6	23.688	28.189	.100	.1414	.200	.200	1.1702	.0057	.0048	.0044	.0180
2094.	2.60	2.30	9.4	20.435	6.987	.151	.0409	1.300	1.800	1.3428	.0120	.0007	.0059	.0528
2096.	2.70	2.60	5.5	27.615	24.606	.100	.0448	.200	.400	2.2542	.0101	.0082	.0007	.0773

TABLE A2/1 CONTINUED

RAVENSTHORPE NO.5 (W.A.)

SAMP	APDN	DENS	POR	FE	SI	S	NI	MGO	ALOX	CU	MN	CR	CO	TI
1387.	2.90	2.40	15.5	56.797	1.531	.100	3.0740	.300	.700	.2061	.1131	.0123	.2144	.0186
1388.	3.10	2.10	39.4	59.529	.001	.100	2.2772	.500	.500	.2836	.0904	.0144	.1593	.0240
1389.	2.80	2.30	27.6	58.368	.001	.100	3.5062	.500	.500	.2468	.0752	.0144	.2349	.0282

MT. WINDARRA (W.A.)

SAMP	APDN	DENS	POR	FE	SI	S	NI	MGO	ALOX	CU	MN	CR	CO	TI
1225.	2.60	2.30	11.1	9.939	26.858	.100	.4620	16.600	2.600	.0008	.2572	.2401	.0191	.0677
1226.	2.60	2.40	5.9	9.148	28.114	.100	.3960	14.600	3.000	.1598	.0727	.1676	.0103	.0911
1227.	2.40	2.10	9.9	7.542	29.046	.100	.3662	15.800	2.700	.0831	.0215	.3099	.0088	.0599
1228.	2.40	2.30	6.4	7.764	29.573	.100	.3520	14.900	2.600	.0216	.0215	.3380	.0103	.0743
1229.	2.50	2.40	4.8	11.593	26.062	.100	.4550	16.600	2.300	.0136	.2686	.2114	.0176	.0569
1230.	2.40	2.00	15.3	11.308	25.730	.100	.4707	16.500	2.700	.0112	.2869	.2703	.0228	.0647
1231.	2.60	2.40	19.0	14.928	30.340	.100	.4660	3.500	2.400	.0240	.2351	.3086	.0198	.0725
1232.	2.50	2.40	7.9	11.432	26.238	.100	.4754	16.500	2.400	.0272	.0992	.2778	.0095	.0839
1223.	2.50	2.20	11.5	24.494	17.145	.100	1.5802	6.100	5.800	3.9325	.0057	.3503	.0440	.1768
1233.	3.00	2.30	20.3	30.659	13.079	.100	5.5399	6.700	3.100	.3027	1.6252	.0007	.0294	.0516
1234.	3.20	2.40	25.8	30.009	11.797	.100	5.4754	7.600	4.600	.2484	1.6398	.0007	.0220	.0773
1235.	3.00	2.80	5.4	28.131	16.147	.100	3.1888	6.300	3.100	.6694	.2945	.1416	.0228	.0971
1236.	2.90	2.60	10.9	27.370	15.603	.421	1.1669	7.600	5.000	.4250	.5175	.1450	.1270	.2332

DORDIE NORTH (W.A.)

SAMP	APDN	DENS	POR	FE	SI	S	NI	MGO	ALOX	CU	MN	CR	CO	TI
1327.	2.70	2.40	9.7	45.695	10.847	.100	.6648	2.000	.200	.2963	.0291	.2039	.0360	.0156
1328.	2.90	2.60	7.6	39.587	16.943	.100	.1391	.200	.100	.1430	.0076	.0452	.0345	.0168
1331.	2.60	2.50	3.8	33.374	19.974	.100	.4856	2.300	.200	.2077	.0322	.1601	.0220	.0246
1333.	3.40	3.10	2.3	36.154	4.337	.100	.4345	10.000	2.000	1.5385	.0986	1.8555	.1226	.1445
1332.	2.90	2.70	5.7	22.071	30.037	.100	.0558	.200	.100	.1302	.0069	.0465	.0272	.0078
1334.	3.10	3.00	3.5	38.373	2.374	8.153	3.2233	6.100	.200	.4945	.0404	.1587	.0485	.0210
1335.	3.40	2.80	12.0	47.702	2.266	7.203	5.2531	.100	.800	.6582	.0556	.0978	.0962	.0150
1336.	3.10	2.40	21.7	50.784	4.094	.100	6.3972	.500	.100	.1446	.0581	.0705	.0257	.0186
1337.	3.10	2.90	4.0	43.037	4.151	.705	1.5590	.100	.100	.1709	.1131	1.1549	.0272	.0899
1338.	3.20	2.70	15.8	40.382	3.015	.358	5.1486	6.000	.400	.9753	.0575	.2244	.1366	.0282
1339.	3.10	3.00	3.8	37.909	5.334	.254	3.3884	7.800	1.500	.3730	.1333	.2976	.0184	.0827

TABLE A2/1 CONCLUDED

OTTER SHOOT (W.A.)

SAMP	APON	DENS	POR	FE	SI	S	NI	MGO	ALOX	CU	MN	CR	CO	TI
1163.	3.70	3.50	2.2	46.812	1.781	.100	.9155	2.300	.100	1.1103	.0101	.0025	.0020	.0066
1167.	3.60	3.50	1.4	47.043	.248	.354	.4644	3.000	.100	.4226	.0613	.0025	.1836	.0042
1171.	3.30	3.00	19.0	54.129	1.440	.100	3.7915	.300	.100	1.9611	.0221	.0025	.0668	.0042
1172.	3.50	2.60	23.3	51.527	.738	.100	7.0659	.100	.100	2.5825	.0360	.0561	.0206	.0102
1173.	3.30	2.80	18.5	53.820	.589	.100	5.8393	.100	.100	3.0179	.0385	.0041	.0147	.0054
1177.	3.00	2.60	15.1	28.180	3.304	.100	.9948	.800	2.000	2.4667	.0303	.1348	.0433	.1163

MCMAHON (W.A.)

SAMP	APON	DENS	POR	FE	SI	S	NI	MGO	ALOX	CU	MN	CR	CO	TI
1150.	3.00	2.80	6.3	44.447	12.673	.100	.5689	.600	.100	.3698	.0063	.0390	.0176	.0072
1151.	3.10	3.00	4.8	41.725	14.763	.100	.4055	.400	.200	.0951	.0057	.4454	.0139	.0108
1152.	3.20	2.90	13.8	45.093	1.762	.100	5.0975	11.000	.100	.8731	.0297	.1211	.0558	.0096
1153.	3.10	2.90	4.6	37.804	8.849	.100	1.0538	5.600	.100	1.4602	.2319	.1266	.1013	.0084
1155.	3.60	2.90	18.7	47.504	2.187	.100	6.1732	4.000	.100	.9410	.2041	.1040	.1182	.0096
1156.	2.70	2.10	18.1	47.036	11.082	.100	.6561	.100	.100	.1574	.0076	.0287	.0191	.0084

DURKIN SHOOT (W.A.)

SAMP	APON	DENS	POR	FE	SI	S	NI	MGO	ALOX	CU	MN	CR	CO	TI
1146.	2.80	2.60	5.0	37.388	15.112	.100	2.3755	.700	.100	2.2614	.0436	.0025	.0999	.0048
1147.	3.00	3.00	.4	33.378	16.345	.100	1.4349	.100	.100	1.7885	.0727	4.0395	.0874	.0725
1148.	2.90	2.80	1.4	19.242	31.704	.100	.2059	.200	.100	.6710	.0088	.0041	.0191	.0030

LUNNON/S.L.O.B. (W.A.)

SAMP	APON	DENS	POR	FE	SI	S	NI	MGO	ALOX	CU	MN	CR	CO	TI
1108.	3.10	3.10	1.8	34.832	19.280	.100	.7795	1.400	.400	.0455	.0088	.0903	.0088	.0396
1109.	3.60	3.50	3.3	47.009	10.179	.100	.3513	.900	.300	.0911	.0183	.1156	.0389	.0084
1112.	3.10	2.90	5.7	21.446	29.477	.100	.2075	1.100	.100	.6494	.0101	.0253	.0301	.0096
1115.	2.60	2.30	15.1	27.642	24.011	.100	.2302	2.100	.100	.6790	.0126	.0178	.0176	.0102

TABLE A2/2 INDIVIDUAL OXIDATE MINERAL DATA : MAGNESITES

TRACE ELEMENT CHEMISTRY (PPM)						COLOUR	FORM AND RELATION TO HOST ROCK TYPE	DEPTH (m.) b.s.	ASSOCIATED HOST ROCK	(DEPOSIT) SAMPLE No
Ni	Cu	Co	Mn	Cr	Zn					
7.99 %	10.32 %	1665	333	4662	1032	Pea Green	Botryoidal forms lining solution cavities	2	Oxidising massive sulphide	(McMahon) 01152A
9.00 %	12.20 %	1800	1200	400	3240	Pale Green	Joint surface capping and cleavage plane covering	20	Oxide after massive sulphide	01155
7714	240	<10	133	400	200	White to Pink – Orange	Botryoidal crusts on joint planes	20	Talcose mafic silicate	(Otter) 01165
20.50 %	2.50 %	7500	500	1500	300	Green	Bladed, in drusy cavities	20	Oxide after massive sulphide	01169
16.65 %	4.00 %	2665	333	1000	233	Pale Pea-Green	Joint and fracture surface cover	20	Oxidising massive sulphide	01170A
8.33 %	12.99 %	1332	<10	1000	<10	Dark Green	Vein filling	20	Oxidising massive sulphide	01170B
2.20 %	1980	3080	154	88	18	Medium Green	Siliceous acicular vein-filling	16	Oxide after sulphide	01178

TABLE A2/2 ·CONTINUED

TRACE ELEMENT CHEMISTRY (PPM)						COLOUR	FORM AND RELATION TO HOST ROCK TYPE	DEPTH (m.) b.s.	ASSOCIATED HOST ROCK	(DEPOSIT) SAMPLE No
Ni	Cu	Co	Mn	Cr	Zn					
13.00 %	1750	500	10	1500	100	Pea Green	Acicular or fingerlike encrustations on drusy quartz	18.8	Oxidising massive sulphide	(Otter) 01181
5.94 %	9900	1782	1518	198	198	Green	Botryoidal forms on drusy fracture linings and as drusy fillings	1.2	Oxide after massive sulphide	(Scotia) 01203
15.00 %	3.00 %	9300	2500	500	350	White	Along cleavage planes and on joint faces	20.5	Serpentinised dunite	(Carr Boyd) 01278A
6.40 %	4500	4700	910	60	190	Pale Orange	Massive podiform stringers	20.5	Serpentinised dunite	01278C
1.08 %	1.62 %	5700	1050	40	290	Pea green	Vein filling	25.8	Oxidising disseminated sulphide	01279A
15.84 %	2178	1.06 %	2310	165	389	White	Joint and fracture cover Also as intrusive in host silicate	25.8	Oxidising disseminated sulphide	01279B
3.60 %	2200	10	1000	5000	300	White	Cavity and fissure filling	0	Oxide after sulphide	(Dordie N) 01334A

590

TABLE A2/2 CONTINUED

TRACE ELEMENT CHEMISTRY (PPM)						COLOUR	FORM AND RELATION TO HOST ROCK TYPE	DEPTH (m.) b.s.	ASSOCIATED HOST ROCK	(DEPOSIT) SAMPLE No
Ni	Cu	Co	Mn	Cr	Zn					
2.30 %	2450	1000	2500	2500	250	Buff–Yellow	On weathered joints	0	Oxide after sulphide	(Dordie N) 01334B
1.86 %	1615	430	715	858	128	Buff–Brown	Joint and fracture surface covering	0	Oxide after sulphide	01335A
2.60 %	1440	600	1000	1600	220	Buff	Patchy covering on joints and fracture surfaces	0	Oxide after msaaive sulphide	01336A
1.60 %	1300	400	1500	900	400	Buff–Brown	Joint and fracture surface covering	0	Oxide after massive sulphide	01338A
4.10 %	2600	1000	$\triangleleft$10	6000	600	White	Veining	0	Oxide after massive sulphide	01338B
5.60 %	7600	1200	80	280	28	Pea green	Silicified veining	0	Oxide after massive sulphide	01338C
13.68 %	5845.	1425	855	1710	171	Pale Green	Silicified botryoidal covering to joint faces	0	Oxide after disseminated sulphide	01339C

TABLE A2/2 CONCLUDED

TRACE ELEMENT CHEMISTRY (PPM)						COLOUR	FORM AND RELATION TO HOST ROCK TYPE	DEPTH (m.) b.s.	ASSOCIATED HOST ROCK	(DEPOSIT) SAMPLE No
Ni	Cu	Co	Mn	Cr	Zn					
4800	2300	<10	400	1100	80	Chocolate Brown	Surface covering	0	Oxide after disseminated sulphide	(Widgie 3) 01346A
924	61	69	3388	115	246	Light brown to White	Massive crystalline veining with drusy structure	70	Argillite	(Trojan) 02251B
NO DATA						White to Pale green	Joint surface covering	1	Oxide after massive sulphide	(McMahon) 01152B
NO DATA						Pea green	Botryoidal joint and fracture surface covering	3	Silified oxide after sulphide	(Otter) 01166
NO DATA						Buff- Brown	Surface coating	0	Massive oxide after sulphide	(Dordie N) 01338A
NO DATA						Pea green	Silicified veins in host	0	Massive oxide after sulphide	01338B
NO DATA						Blue-green	Joint and fracture covering	0	Oxide after disseminated sulphide	01339A

TABLE A2/3   INDIVIDUAL OXIDATE MINERAL DATA : CALCITES

TRACE ELEMENT CHEMISTRY (PPM)						COLOUR	FORM AND RELATION TO HOST ROCK TYPE	DEPTH (m.) b.s.	ASSOCIATED HOST ROCK	(DEPOSIT) SAMPLE No
Ni	Cu	Co	Mn	Cr	Zn					
360	1.26 %	50	120	160	28	Pale pink – buff	Joint/fracture surface covering	0	Silicified oxide after massive sulphide	(S.L.O.B.) 01108B
411	152	28	241	185	40	Pink	Thin surficial covering	0	Oxide after massive sulphide	01109
4329	1964	<10	333	1000	932	White to Orange-Pink	Surficial covering	0	Oxide after massive sulphide	(Durkin) 01147
800	180	<10	400	1200	100	Pink	Surficial covering	2	Talcose mafic silicate	(Mt Monger) 01189
1000	800	<10	500	3000	250	Pale pink to White	Surficial covering	2	Silified oxide after massive sulphide	01190
332	285	66	133	400	40	Pink	Surficial layering on silica	2	Silified oxide after massive sulphide	01193
500	600	500	500	5500	750	White	Surficial crust	0	Silicified oxide after massive sulphide	01198B

TRACE ELEMENT CHEMISTRY (PPM)						COLOUR	FORM AND RELATION TO HOST ROCK TYPE	DEPTH (m.) b.s.	ASSOCIATED HOST ROCK	(DEPOSIT) SAMPLE No
Ni	Cu	Co	Mn	Cr	Zn					
1000	300	1000	1000	5000	500	White	Surficial covering	0	Silicified oxide after disseminated sulphide	(Spargoville) 01246A
4000	400	1000	1000	5000	400	Light Brown	Weathered surface of 01246A	0	Silicified oxide after disseminated sulphide	01246B
2500	1200	<10	500	1500	250	White	Surficial covering	0	Silicified oxide after massive sulphide	(Mt Edwards) 01304B
1332	1100	333	1000	1665	300	White	Surficial covering	0	Silicified oxide after massive sulphide	01305C
500	400	500	500	3000	450	White	Surficial layering	0	Silicified oxide after massive sulphide	01306A
3500	1200	<10	1000	2500	300	White	Surface patches	0	Oxide with remnant sulphide	(Dordie N) 01326A
3000	1200	<10	2000	5000	500	Orange-Buff	Surficial covering and crack filling	0	Ochreous oxide after massive sulphide	01330

TRACE ELEMENT CHEMISTRY (PPM)						COLOUR	FORM AND RELATION TO HOST ROCK TYPE	DEPTH (m.) b.s.	ASSOCIATED HOST ROCK	(DEPOSIT) SAMPLE No
Ni	Cu	Co	Mn	Cr	Zn					
2000	800	<10	800	2400	280	Pale pink – buff	Surface covering	0	Ochreous oxide after massive sulphide	(Dordie N) 01332
3000	800	1000	1000	5000	300	Pink-White	Flaky surficial covering	0	Oxide after disseminated sulphide	01333A
4000	600	<10	500	2500	250	Pink-White	Patchy crust on goethite	0	Silicified oxide after massive sulphide	(Widgie 3) 01342C
10	300	<10	1000	4000	700	Pinky-White	Joint surface covering	0	Silicified oxide after massive sulphide	(Redross) 01349
2664	600	333	666	1665	233	Mid Brown	Weathered joint covering	0	Silicified oxide after massive sulphide	(Spargoville) 01250A
2000	500	<10	1000	2500	150	White	Surficial coating	0	Silicified oxide after massive sulphide	01250B
470	3850	46	246	62	30	White	Thick surficial covering	2.5	Breccia of silicified oxides and carbonate	(Selibi) 02094

TRACE ELEMENT CHEMISTRY (PPM)						COLOUR	FORM AND RELATION TO HOST ROCK TYPE	DEPTH (m.) b.s.	ASSOCIATED HOST ROCK	(DEPOSIT) SAMPLE No
Ni	Cu	Co	Mn	Cr	Zn					
		NO DATA				Pink-White	patchy joint surface cover	0	Oxide after massive sulphide	(Durkin) 01146
		NO DATA				White	Joint surface covering	0	Silicified oxide after massive sulphide	(McMahon) 01151B
		NO DATA				Pinky-Orange	Thick surficial layering	2	Oxide after sulphide	(Mt Monger) 01191
		NO DATA				Orange	Joint surface covering	0	Silicified oxide after massive sulphide	01198A
		NO DATA				Medium Brown	Joint surface covering	0	Silicified oxide after massive sulphide	(Spargoville) 01250A
		NO DATA				White	Joint surface coating and layering	0	Silicified oxide after massive sulphide	01250B
		NO DATA				Pinky-White	Botryoidal cavity lining	0	Silicified laterite	(Mt Edwards) 01298B

TRACE ELEMENT CHEMISTRY (PPM)						COLOUR	FORM AND RELATION TO HOST ROCK TYPE	DEPTH (m.) b.s.	ASSOCIATED HOST ROCK	(DEPOSIT) SAMPLE No
Ni	Cu	Co	Mn	Cr	Zn					
		NO DATA				Chocolate Brown	Patchy surficial covering	0	Silicified oxide after massive sulphide	(Mt Edwards) 01306B
		NO DATA				Medium Brown	Patchy cavity lining	0	Silicified oxide after massive sulphide	01308A
		NO DATA				White	cavity lining	0	Silicified oxide after massive sulphide	01308B
		NO DATA				Pink-Brown	Weathered surface cover.	0	Oxide after massive sulphide	01309A
		NO DATA				White	Patchy joint surface cover	0	Silicified oxide after massive oxide	(Redross) 01350A
		NO DATA				Pink-White	Surficial layering	0	Silicified oxide after massive sulphide	01350B
		NO DATA				Mid to dark green	Thin varnish on silicified joint surfaces	23	Silicified oxidised mafic silicate	(Pikwe) 02001D

TABLE A2/4   INDIVIDUAL OXIDATE MINERAL DATA : DOLOMITES

TRACE ELEMENT CHEMISTRY (PPM)						COLOUR	FORM AND RELATION TO HOST ROCK TYPE	DEPTH (m.) b.s.	ASSOCIATED HOST ROCK	(DEPOSIT) SAMPLE No
Ni	Cu	Co	Mn	Cr	Zn					
6.27 %	750	643	2680	495	69	Light Green	Drusy growths in fractures	24	Oxidising sulphide	(S.L.O.B.) 01103A
3.25 %	950	1050	1400	125	25	Leaf Green	Surficial covering	24	Oxidising sulphide	01105A
9750	1625	1250	3750	1000	175	Red-Pink	Joint/fracture surface covering	1.5	Oxide after disseminated sulphide	(Scotia) 01202B
1000	800	<10	1000	5000	300	Light Buff	Surficial coating on exposed surfaces	3	Oxide after massive sulphide	(Dordie N) 01329A
2000	1200	<10	1000	4000	500	Orange-Pink	Surficial coating on joint faces	0	Silicified oxide after massive sulphide	(Widgie 3) 01343B
5000	1100	<10	1000	5000	300	Pinky-White	Patchy surface coating	0	silicified oxide after massive sulphide	01345
2.20 %	2300	1000	2000	7000	800	Buff-Yellow	Joint surface covering	0	Oxide after massive sulphide	(Ravenst'pe) 01389A

TABLE A2/5   INDIVIDUAL OXIDATE MINERAL DATA : CALCITE / DOLOMITE MIXTURES

TRACE ELEMENT CHEMISTRY (PPM)						COLOUR	FORM AND RELATION TO HOST ROCK TYPE	DEPTH (m.) b.s.	ASSOCIATED HOST ROCK	(DEPOSIT) SAMPLE No
Ni	Cu	Co	Mn	Cr	Zn					
957	970	110	190	121	43	pink-white	Thin joint surface layering	0	Silicified oxide after massive sulphide	(S.L.O.B.) 01112
1425	570	◁10	712	1140	171	Buff-pink	Weathered surface cover	0	Oxide after massive sulphide	(Mt Monger) 01186
2700	1035	135	315	855	67	Pink-buff	Joint surface covering	0	Silicified oxide after massive sulphide	(Spargoville) 01245
1826	614	166	332	1328	83	Pink-white	Crustiform joint surface covering	0	silicified oxide after massive sulphide	01267
NO DATA						Pale pink	Botryoidal fillings in crack and fracture linings	0	Laterite	(Mt Edwards) 01294
NO DATA						Pinky-brown	Botryoidal surface covering	0	Oxide after massive sulphide	(Otter) 01163A

599

TABLE A2/6   INDIVIDUAL OXIDATE MINERAL DATA : GYPSUMS

TRACE ELEMENT CHEMISTRY (PPM)						COLOUR	FORM AND RELATION TO HOST ROCK TYPE	DEPTH (m.) b.s.	ASSOCIATED HOST ROCK	(DEPOSIT) SAMPLE No
Ni	Cu	Co	Mn	Cr	Zn					
1881	188	57	57	171	946	Colourless	Transparent layering on joint surfaces: 120° twins	60	Supergene sulphide	(Lunnon) 01131B
9120	142	<10	570	855	228	Colourless	Tabular books on joints and cavities	50	Supergene sulphide	(Redross) 01358B
NO DATA						White	Botryoidal cavity filling	10	Oxide/laterite	(Mt. Edwards) 01293A
NO DATA						Colourless	Translucent joint surface covering	10	Oxide/laterite	01293B

TABLE A2/7   INDIVIDUAL OXIDATE MINERAL DATA : NATROALUNITES

TRACE ELEMENT CHEMISTRY (PPM)						COLOUR	FORM AND RELATION TO HOST ROCK TYPE	DEPTH (m.) b.s.	ASSOCIATED HOST ROCK	(DEPOSIT) SAMPLE No
Ni	Cu	Co	Mn	Cr	Zn					
2000	4900	90	20	170	16	Pale Green	Podiform	23.5	Talcose mafic silicate	(Pikwe) 02004
9332	8032	1000	1.00 %	4000	200	white to pale green	Patches on fracture surface and in veinlets	28	Massive silicified ochre complex	02012B
2500	1.28 %	<10	<10	2000	150	Pale Blue-green	Botryoidal or fingerlike in cavities	28	Oxide after sulphide	02019A
150	645	<10	15	169	10	White to Pale green	Massive replacements along rock cleavage	33.5	Partly silicified oxidised mafic silicate	02053
2943	5566	227	2012	126	77	Pale green	Joint/fracture surface covering	34	Silicified oxide after disseminated sulphide	02060A
		NO DATA				Pale Yellow-green	Massive on weathered surfaces	4.5	Oxidised Mafic silicate	(Carr Boyd) 01272
		NO DATA				Blue-green	Botryoids on cavity walls and joint faces	23	Silicified oxidised mafic silicate	(Pikwe) 02001A

TRACE ELEMENT CHEMISTRY (PPM)						COLOUR	FORM AND RELATION TO HOST ROCK TYPE	DEPTH (m.) b.s.	ASSOCIATED HOST ROCK	(DEPOSIT) SAMPLE No
Ni	Cu	Co	Mn	Cr	Zn					
		NO DATA				White	Patches on unsilicified cavity walls	23	Ochreous oxide after massive sulphide	(Pikwe) 0 2002D
		NO DATA				White	Patches on joints and cavities	24	Silicified oxide after massive sulphide	02008
		NO DATA				Yellow-buff	Cavity lining	30	Silicified oxidised mafic silicate	02032
		NO DATA				White	Patches on fracture surfaces	28.5	Silicified oxide after sulphide	0 2038C

TABLE A2/8 INDIVIDUAL OXIDATE.MINERAL DATA : NATROJAROSITES

TRACE ELEMENT CHEMISTRY (PPM)						COLOUR	FORM AND RELATION TO HOST ROCK TYPE	DEPTH (m.) b.s.	ASSOCIATED HOST ROCK	(DEPOSIT) SAMPLE No
Ni	Cu	Co	Mn	Cr	Zn					
142	31	29	<10	1515	10	Yellow-green	Massive intrusive	19	Highly weathered ultramafic silicate	(Carr Boyd) 01277A
1144	57	<10	<10	3146	42	medium brown	Patchy on cavity and joint surfaces	19	Highly weathered ultramafic silicate	01277D
NO DATA						Bright green	Patches on weathered surfaces and in cavities	19	Highly weathered ultramafic silicate	01277B
NO DATA						Medium brown	individual spheroids on silicified joint surfaces	30	Oxidised silicified mafic silicate	(Pikwe) 02030
NO DATA						Yellow	Thin patchy joint/fissure covering	30	Partly silicified oxidised mafic silicate	02035
NO DATA						Pale Yellow-buff	Botryoidal clusters on cavity walls and joints	30	Silicified oxidised mafic silicate	02001C

BIBLIOGRAPHY

ANDERSON, C.A., 1955 Oxidation of copper sulphides and secondary sulphide enrichment. Economic Geology. 50th.Anniversary vol.1905-1955. Bateman, A.M., (Ed.). Lancaster, Penn.,Economic Geology, p.324 - 340

ANDREWS, P.B. 1975 Spargoville nickel deposits. In Economic Geology of Australia and Papua New Guinea Metals vol.Australasian Inst.Min.Metall.Mon. Ser. No.5, p.89 - 91

ANHAEUSSER, C.R., 1976 Archean Metallogeny in Southern Africa . Econ. Geol., v 71, p.16 - 43

BAAS BECKING, L.G.M., KAPLAN,I.R., and MOORE, D.,1960 Limits of the natural environment in terms of pH and oxidation - reduction potentials. Jour. Geol., v 68, p.243 - 284

BALDOCK, J.W., HEPWORTH, J.V., and MARENEWA, B.S., 1976 Gold, Base metals, and Diamonds in Botswana. Econ. Geol., v 71, p.139 - 156

BALME, B.E., and CHURCHILL, D.M., 1959 Tertiary sediments at Coolgardie, Western Australia. Jour. Roy. Soc. W.Aust., v 42 (2), p.37 - 43

BERNER, R.A., 1969 Goethite stability and the origin of red beds. Geochem. Cosmochim Acta, v 33, p.267 - 273

BETTANAY, E., BLACKMORE, A.V., and HINGSTON, F.G., 1964 Aspects of the hydrologic cycle and related salinity in the Belka Valley, Western Australia. Aust. Jour. Soil. Res., v 2, p.187 - 210

BLAIN, C.F., and ANDREW, R.L., 1977 Sulphide weathering and the evaluation of gossans in mineral exploration. Minerals Sci. Engng., v 9, No.3, p.119 - 150

BLAIN, C.F., and BROTHERTON, R.L., 1975 Self potentials in relation to oxidation of nickel sulphide bodies within semi-arid climatic terrains. Trans. Instn. Min. Metall. v 84, p.B123 - B127

BLANCHARD, R., 1939 Interpretation of leached outcrops. J. Chem.Soc.S.Afr., v 39, p.344 - 372

BLANCHARD, R., 1942 Leached derivations of arsenopyrite and chromite. Econ. Geol., v 37, p.596 - 626

BLANCHARD, R., 1944 Chemical and mineralogical composition of twenty typical limonites. Am. Mineral., v 29, p.111 - 114

BLANCHARD, R., 1968 Interpretation of leached outcrops. Nevada State Bur. Mines, Bull.66

BLANCHARD, R., and BOSWELL, P.F., 1925 Notes on the oxidation products derived from chalcopyrite. Econ. Geol., v 20, p.613 - 638

BLANCHARD, R., and BOSWELL, P.F., 1930 Limonite types from borite and tetraheorite. Econ. Geol., v 25, p.557 - 580

BLANCHARD, R., and BOSWELL, P.F., 1934 Additional limonite types of galena and sphalerite derivation. Econ.Geol., v 29, p.671 - 690

BLANCHARD, R., and BOSWELL, P.F., 1935 Limonite of molybdenite derivation. Econ.Geol., v 30, p.313 - 319

BOSWELL, P.F., and BLANCHARD, R., 1927 Oxidation products derived from sphalerite and galena. Econ. Geol., v 22, p.413 - 453

BOSWELL, P.F., and BLANCHARD, R., 1929 Cellular structure in limonite. Econ. Geol., v 24, p.791 - 796

BREWER, R., and BETTENAY, E., 1973 Further evidence concerning the origin of the Western Australian sand plains. Jour. Geog. Soc. Aust., v. 19 (4), p.533 - 541

BROPHY, G.P., SCOTT, E.S., and SNELLGROVE, R.A., 1962 Sulfate Studies II. Solid solution between alunite and jarosite. Am. Mineral., v 47, p.112 - 126

BROWN, J.B., 1970 A chemical study of some synthetic potassium-hydronium jarosites. Can. Mineral., v 10, p.696 - 703

BROWN, J.B., 1971 Jarosite - Goethite stabilities at $25^{o}C$, 1 ATM. Min. Dep. v 6, p.245 - 252

BROWN, J.S., 1936 Supergene sphalerite, galena and willemite at Balmat, New York. Econ. Geol., v 31, p.331 - 354

BUEHLER, H.A., and GOTTSCHALK, V.H., 1910 Oxidation of sulphides. Econ. Geol., v 5, p.28 - 35

BULL, A.J., and MAZZUCHELLI, R.H., 1975 Application of discriminant analysis to the geochemical evaluation of gossans. In Geochemical Exploration 1974, Elliott, I.L., and Fletcher, W.K., (Eds.).Amsterdam, Elsevier, 1975, p.219 - 226

CHRISTIE, D., 1975 Scotia nickel sulphide deposit. In economic geology of Australia and Papua New Guinea metals vol: Australasian Inst.Min.Metall.Mon. Ser.No.5. p.121 - 125

CLEMA, J.M., and STEVENS-HOARE, N.P., 1973 A method of distinguishing nickel gossans from other ironstones on the Yilgarn Shield, Western Australia. J.Geochem.Explor., v 2, p.393 - 402

COCHRANE, R.H.A., 1973 A guide to the geochemistry of nickeliforous gossans and related rocks from the eastern goldfields. Rep. Geol. Surv. W.Aust.1972, p.69 - 75

COX, K.G., JOHNSON, R.L., MONKMAN, L.J., STILLMAN, C.J., VAIL,J.R., and WOOD, D.N., 1965 The geology of the Nuanetsi Igneous province. Phil.Trans. Roy.Soc. (A), 257, p.71 - 218

DALGARNO, C.R., 1972 Geochemistry of the Redross nickel prospect, Widgie-mooltha area, Western Australia. Jt.spec.group meet.,Canberra,(Abstr.): Geol. Soc.Aust., p.B12 - B14

DALGARNO, C.R., 1975 Nickel deposits of the Widgiemooltha dome - Redross, Wannaway, Widgiemooltha, Dordie. In economic geology of Australia and Papua New Guinea metals vol: Australasian Inst.Min.Metall.Mon.Ser.No.5, p.82 - 86

DANA, J.S., 1951 The system of mineralogy. Volume two. Palache C.,Berman H., and Frondel C., New York; Wiley and Sons

DAVID, T.W.E., 1950 The geology of the Commonwealth of Australia, Vol.2 London: Arnold

DESBOROUGH, G.A., and CZAMANSKE,G.K.,1973. Sulphides in eclogite nodules from a Kimberlite pipe, South Africa, with comments on violarite stoichio-metry: Am. Mineral. v 58, p.195 - 202

De WAAL, S.A., 1971 South African nickeliferous serpentinites Minerals Sci. Engng.,v 3, p.32 - 45

EMMONS, S.F., 1901 The secondary enrichment of ore deposits. Trans. Am. Inst. Min.Eng., v 30, p.177 - 217

EMMONS, S.F., 1917 The enrichment of ore deposits. U.S.Geol.Surv.Bull., 625, p.1 - 530

GARRELS, R.M., and CHRIST, C.L., 1965 Solutions, minerals and equilibria. New York: Harper and Row

GARRELS, R.M., THOMPSON, M.E., and SIEVER, R., 1960 Stability of some carbonates at 25° and one Athmosphere Total Pressure. Am.Jour.Sci., v 258, p.402 - 418

GEE, R.D., 1975. Regional geology of the Archean nucleii of the Western Australian Shield. In economic geology of Australia and Papua New Guinea metals vol: Australasian Inst.Min.Metall. Mon.Ser.No.5, p.43 - 55

GOLDSMITH, J.R., 1959 Some aspects of the geochemistry of carbonates. In Abelson, P.H., Ed., Researches in Geochemistry; Wiley, New York

GORDON, P.S.L., 1973 The Selibi - Pikwe nickel-copper deposits, Botswana In Spec.Publ.Geol.Soc.S.Afr.3, p167 - 187

GROVES,D.I., BARRETT, F.M., BINNS, R.A., and McQUEEN, K.G., 1977 Spinel phases associated with metamorphosed volcanic-type iron-nickel sulphide ores from Western Australia. Econ.Geol., v72,p.1224 - 1244

GROVES, D.I., BARRETT, F.M., and BROTHERTON, R.L., 1979 Relict zinci-ferous ferrochromites in the evaluation of gossans after massive nickel sulphide ore (in preparation)

GROVES, D.I., and WHITTLE, A.W.G., 1976 Mineragraphy applied to mineral exploration and mining, Workshop Course (unpubl.). Adelaide: Aust.Miner. Fdn., p.94 - 111

HANCOCK, W., and WILMSHURST, J.R., 1972 Geochemical observation on some nickel-copper gossans. Jt.spec.group meet. Canberra, (Abstr): Geol.Soc.Aust., p.B10 - B11

HAWKES, H.E., and WEBB, J.S., 1962 Geochemistry in mineral exploration. New York, Harper and Row. 162pp

HEYL, A.V., and BOZION, C.N., 1962 Oxidized zinc deposits of the United States: Pt.1 General Geology. U.S. Geol.Surv.Bull. 1135 - A, p.A1 - A52

INAL STAFF, 1975 BHP/INAL nickel sulphide occurrences of the Widgiemooltha area. In economic geology of Australia and Papua New Guinea metals vol: Australasian Inst.Min.Metall.Mon.Ser. No.5, p.86 - 89

JOHNSTONE, M.H., LOWRY, D.C., and QUILTY, P.G., 1973 The geology of south western Australia - a review. Jour. Royal Soc.W.Aust., v 56, p.5 - 15

JOYCE, A.S., and CLEMA, J.M., 1974 An application of statistics to the chemical recognition of nickel gossans in the Yilgarn Block, Western Australia. Proc.Australas.Inst.Min.Metall., 252, p.21 - 24

KEAYS, R.R., 1972 Platinoids as discriminators of gossans derived from nickeliferous sulphides. Jt.Spec.Group Meet., Canberra, (Abstr.): Geol.Soc.Aust.,1972, p.B11

KEELE, R.A., and NICKEL, E.H., 1974 The geology of a primary millerite - bearing sulphide assemblage and supergene alteration at the Otter Shoot, Kambalda, Western Australia. Econ.Geol., v 6, p.1102 - 1117

KELLEY, W.C., 1958 A topical study of lead - zinc gossans. New Mex.Bur.Mines Min.Res. Bull.46

KELLEY, W.C., TAKAHASHI, T., BEHRE, C.H.Jr., DUREK, J.J., STOERTZ, G.E. and FELBER, B.E.Jr., 1958 Progress in leached outcrop studies. (Abstr). Econ.Geol., v 53, p.9211

KEMP, J.R. 1906 Secondary enrichment in ore-deposits of copper. Econ.Geol., v 1, p.11 - 25

KNIGHT, C.W., 1975 The nickel sulphide province of the Yilgarn Block - An Introduction. In economic geology of Australia and Papua New Guinea, metals. vol: Australasian Inst.Min.Metall.Mon.Ser.No.5, p65.

KOCH, G.S., and LINK, R.F., 1971 Statistical analysis of geological data. Volume II. New York: Wiley and Sons

KRAUSKOPF, K.B., 1967 Introduction to Geochemistry. New York: McGraw - Hill

Le ROEX, H.D., 1964 Nickel deposit on the Trojan claims, Bindura district, Southern Rhodesia. In Haughton, S.H.(Ed.): The Geology of some ore deposits in southern Africa, v 2, p.509 – 520. Johannesburg, The Geogolical Society of South Africa

LOCKE, A. 1926 Leached outcrops as guides to copper ore. Baltimore; Williams and Wilkins

LOVERING, T.S., 1923 The leaching of iron protores: solution and precipitation of silica in cold water. Econ.Geol. v 18, p.523 – 540

MANN, A.W., and DEUTSCHER R.L., 1977 Solution geochemistry of copper in water containing carbonate, sulphate and chloride ions. Chem.Geol., v 19, p.253 – 265

MAUFE, H.B., 1935 Some factors in the geographical evolution of southern Rhodesia and neighbouring countries. S.Afr.Geol.Jour., v 18

McANDREW, R.T., WANG, S.S.,and BROWN, W.R. 1975 Precipitation of iron compounds from sulphuric acid leach solutions. Can.Min.Metall.Bull., v 68 p.101 – 110

MOESKOPS, P.G., 1977 Yilgarn nickel gossan geochemistry – a review with new data. J.Geochem. Explor. v 8, p.267 – 258

MOORE, E.S., and MAYNARD, J.E., 1929 Solution, transportation and precipitation of iron and silica I. Econ.Geol. v 24, p.272 – 303

MORSE, H.W., and LOCKE, A., 1924 Recent progress with leached ore capping. Econ.Geol.,v 19, p.249 – 258

MULCAHY, M.J., 1964 Laterite residuals and sand plains. Aust.Jour. Sci., v 27, p.54 – 55

MULCAHY, M.J., 1973 Landforms and soils of south western Australia. Jour. Roy.Soc. W.A., v 56, p.16 – 22

NELSON, A., and NELSON, K.D., 1967 Dictionary of Applied Geology, Mining and Civil Engineering. London: Newnes. pp164

NICKEL, E.H., 1972 Nickeliferous smythite from some Canadian occurrences. Can.Mineral.,v 11, p.514 – 519

NICKEL, E.H., 1973 Violarite – a key mineral in the supergene alteration of nickel sulphide ores. Western Australian Conference, Perth, May 1973: Aust. Inst.Min.Metall. p.111 – 116

NICKEL, E.H., ALLCHURCH, P.D., MASON, M.G., and WILMSHURST, J.R., 1977 Supergene alteration at the Perserverance nickel deposit, Agnew, Western Australia. Econ.Geol., v 72, p.184 – 203

NICKEL, E.H., ROSS, J.R., and THORNBER, M.R., 1974 The supergene alteration of pyrrhotite-pentlandite ore at Kambalda, Western Australia. Econ. Geol., v 69, p.93 - 107

NICKEL, E.H., and THORNBER, M.R., 1977 Chemical constraints on the weathering of serpentinites containing nickel-iron sulphides. Jour.Geochem. Explor., v 8, p.235 - 245

OWEN, H.B., 1954 Bauxite in Australia. Bull. Bur. Min. Resour. Aust., v 24: 234pp.

PARTINGTON, J.R., 1931 A text-book of inorganic chemistry. London: Macmillan

PEACOCK, M.A., 1942 On goethite and lepidocrocite. Trans. Roy. Soc. Canada, Ser 3, v 36, p.107 - 118

PENROSE, R.A.F., 1894 The superficial alteration of ore deposits. Jour.Geol., v 2, p.288 - 317

PHAUP, A.E., 1973 The granitic rocks of the Rhodesian Craton. In Geol.Soc. South Africa Spec. Pub.3, p.59 - 67

PONTIFEX, I.R., 1972 The mineralogy and geochemistry of some Western Australian gossans and pseudogossans. Jt.Spec.Group.Meet. Canberra (Abstr): Geol.Soc.Aust., p.B16 - B17

POSNJAK, E., and MERWIN, H.E., 1919 The hydrated ferric oxides. Amer. Jour.Sci., v 47, p.311 - 348

POSNJAK, E., and MERWIN, H.E., 1922 The system Fe_2O_3 - SO_3 - H_2O J.Am.Chem.Soc., v 44, p.1965 - 1995

PRESCOTT, J.A., and PENDLETON, R.L., 1952 Laterite and lateritic soils. Commonwealth Bureau of Soil Science, Technical Communication No.47

PRIDER, R.T., 1966 The laterized surface of Western Australia. Aust.Jour.Sci., v 28, p.443 - 451

PURVIS, A.C., NESBITT, R.W., and HALLBERG, J.A., 1972 The geology of part of the Carr-Boyd rocks complex and its associated nickel mineralization, Western Australia. Econ.Geol., v 67, p.1076 - 1093

RAMDHOR, P. 1960 Die Erzmineralein und ihre Verwachsungen. Akademie Verlag, Berlin. 1089 pp.

RANSOME, F.L., 1910   Criteria of downward sulphide enrichment. Econ.Geol., v 5, p.205 - 220

ROBERTS, D.E., and TRAVIS, G.A., 1974 Textural evaluation of nickel sulphide gossans. Western Australian Conference, Perth, 1973. Abstracts. Parkville; Australas. Inst. Min. Metall. p. 97

ROBERTS, J.B., 1975 Windarra nickel deposits. In economic geology of Australia and Papua New Guinea metals vol: Australasian Inst. Min. Metall. Mon. Ser. No.5, p.129 - 143

ROSS, J.R., and HOPKINS, G.M.F., 1975 Kambalda nickel sulphide deposits. In economic geology of Australia and Papua New Guinea Metals vol: Australasian Inst. Min. Metall. Mon. Ser. No.5, p.100 - 121

ROY, C.J., 1945 Silica in natural waters. Am. Jour. Sci., v 243, p.393 - 403

SATO, M., and MOONEY, H.M., 1960 The electrochemical mechanism of sulfide self - potentials. Geophysica, v 25, p.226 - 249

SCHELLMANN, W., 1959 Experimentelle untersuchungen uber die sedimentare bilung von goethit und hamatit. Chem. Erde, v 20, p.104 - 135

SCHMITT, H.A., 1939 Outcrops of ore shoots. Econ. Geol., v 34, p.654 - 673

SCHULTZ, K., 1975 Carr-Boyd rocks nickel-copper deposits. In economic geology of Australia and Papua New Guinea Metals vol: Australasian Inst.Min. Metall.Ser. No.5, p.125 - 128

SHARPE, J.W.N., 1964 The Empress nickel-copper deposit, Southern Rhodesia. In (Haughton, S.H. (Ed.) :) The geology of some ore deposits in southern Africa, vol.2, p.497 - 508. Johannesburg; The Geological Society of South Africa

SHEPPY, N.R., and ROWE, J., 1975 Nepean nickel deposit. In economic geology of Australia and Papua New Guinea Metals vol: Australasian Inst. Min. Metall. Mon. Ser. No.5, p.91 - 98

SILLITOE, R.H., and CLARK, A.H., 1969 Copper and copper-iron sulfides as the initial products of supergene oxidation, Copiapo Mining District, Northern Chile. Am. Mineral.,v 54, p.1684 - 1710

SIVARAJASINGHAM, S., ALEXANDER, L.T., CADY, J.G., and CLINE, M.G. 1962 Laterite. Adv. Agron., v 14, p.1 - 60

SMITH, A.G., 1964 The geology of the country around Mazabuka and Kafue. Northern Rhodesia Ministry of Labour and Mines: Report of the geological survey, No.2

SMITH, B.H., 1977 Some aspects of the use of geochemistry in the search for nickel sulphides in lateritic terrain in Western Australia. Jour.Geochem.Explor., v 8, p.259 - 281

STEPHENS, C.G., 1971 Laterite and silcrete in Australia: A study of the genetic relationships of laterite and silcrete and their companion materials, and their collective significance in the formation of the weathered mantle, soils, relief and drainage of the Australian continent. Geoderma, v 5, p.5 - 52

STUMM, W., and MORGAN, J.J., 1970 Aquatic chemistry. An introduction emphasising chemical equilibria in natural waters. New York: Wiley - Interscience

TAKAHASHI, T., 1960 Supergene alteration of zinc and lead deposits in limestone. Econ. Geol., v 55, p.1083 - 1115

TAYLOR, J.H., 1958 Formation of supergene galena at Broken Hill, N.Rhodesia. Mineral. Mag., v 31, p.908 - 913

TAYLOR, L.A., 1970 Smythite, $Fe_{3+x}S_4$, and associated minerals from the Silver Fields Mine, Cobalt, Ontario. Am. Mineral, v 55, p.1650 - 1658

TAYLOR, L.A., and WILLIAMS, K.L., 1972 Smythite, $(Fe, Ni)_9S_{11}$ - A redefinition. Am.Mineral., v 57, p.1571 - 1577

THORNBER, M.R., 1972 Pyrrhotite - the matrix of nickel sulphide mineralization. Newcastle Conf. May - June 1972: Australian Inst.Min.Metall., p.51 - 58

THORNBER, M.R., 1975A Supergene alteration of sulphides, I. A chemical model based on massive nickel sulphide deposits at Kambalda, Western Australia. Chem. Geol., v 15, p.1 - 14

THORNBER, M.R., 1975B Supergene alteration of sulphides, II. A chemical study of the Kambalda nickel deposits. Chem.Geol., v 15, p.117 - 144

THORNBER, M.R., and NICKEL, E.H., 1976 Supergene alteration of sulphides, III. The composition of associated carbonates. Chem. Geol., v 17, p.45 - 72

TILL, R., 1974 Statistical methods for the earth scientist. London: MacMillan 154pp.

TRAVIS, G.A., KEAYS, R.R., and DAVISON, R.M., 1976 Palladium and iridium in the evaluation of Ni gossans in Western Australia. Econ. Geol., v 71, p.1229 - 1243

TRUTER, F.C., 1945 Geology of a post-karoo fault trough in the Zoutpansberg District, Transvaal. Trans.Geol.Soc. S.Afr., v 68

VAN BREEMAN, O., and DODSON, M.H., 1972 Metamorphic chronology of the Limpopo belt, Southern Africa. Geol. Soc.America Bull., v 84, p.2005 - 2018

VAN HISE, C.R., 1901 Some principles controlling the deposition of ores. Trans. Am.Inst.Min.Eng., v 30, p.127 - 177

VAN SCHUYLENBORGH, J., 1969 Weathering and soil-forming processes in the tropics. In: Natural resources research, XI. Soils and tropical weathering. UNESCO, Paris. 57pp.

VILJOEN, M.J., BERNASCONI, A., VAN COLLER, N., KINLOCH, E., and VILJOEN, R.P., 1976 The geology of the Shangani nickel deposit, Rhodesia. Econ. Geol., v 71, p.76 - 95

WAKEFIELD, J., 1974 The geology of the Pikwe Ni - Cu province. Unpubl. PhD thesis, Leeds University

WAKEFIELD, J., 1976 The structural and metamorphic evolution of the Pikwe Ni - Cu sulphide deposit, Selebi - Pikwe, Eastern Botswana. Econ. Geol., v 71, p.988 - 1005

WARNE, S., St.J., 1962 A quick field or laboratory staining scheme for the differentiation of the major carbonate minerals. Jour. Sed. Pet., v 32, p.29 - 38

WATMUFF, I. G., 1974 Supergene alteration of the Mount Windarra nickel sulphide ore deposit. Western Australia. Mineral. Deposita, v 9, p.199 - 211

WEED, W.H., 1901 The enrichment of gold and silver veins. Trans. Am. Inst. Min. Eng., v 30, p.424 - 448

WELLINGTON, J.H., 1955 Southern Africa, a geographical study. Vol.1, Physical Geography: Cambridge University Press

WELLS, R.C., 1914 Electrical activity in ore deposits. U.S. Geol. Surv., Bull., 548, 74pp.

WHITTEN, G. 1966 Leached outcrops. Proc. 8th. Commonwealth Conf.Min. Metall., vol 2, p.193 - 204. Exploration and mining geology, Melbourne, Australas. Inst.Min. Metall.

WHITTLE, A.W.G., 1972 Gossan interpretation as a method in exploration. Jt. Spec.Group.Meet. Canberra, (Abstr.): Geol.Soc.Aust., p.B1 - B4

WILMSHURST, J.R., 1975 The weathering products of nickeliferous sulphides and their associated rocks in Western Australia. In: I.L. Elliott and W.K.Fletcher (Eds.), Geochemical Exploration, 1974. Elsevier, Amsterdam, p.417 - 436

WILMSHURST, J.R., 1976 The recognition of gossans and related rocks. 25th. International Geological Society,Congress, Sydney, 1976: Abstracts, v 2, sect. 10B, p.464 - 465

WINCHEL, H.V., 1903 Synthesis of chalcocite and its genesis at Butte, Montana. Bull.Geol.Soc.Amer., v 14, p.269 - 276

WOODALL, R., and TRAVIS, G., 1969 The Kambalda Nickel Deposits, Western Australia. Proc. 9th. Commonw. Min. Metall. Congr., London, Pap. 26, p.513 - 533

ZIES, E.G., ALLEN, E.T., and MERWIN, H.E., 1916 Some reactions involved in secondary copper sulphide enrichment. Econ. Geol., v 11, p.407 - 503